

GEOTECHNICAL SPECIAL PUBLICATION NO. 128

# SOIL CONSTITUTIVE MODELS

## *EVALUATION, SELECTION, AND CALIBRATION*

---

---

January 24–26, 2005  
Austin, Texas

SPONSORED BY  
Soil Properties and Modeling Committee of  
The Geo-Institute of the American Society of Civil Engineers

EDITED BY  
Jerry A. Yamamuro, Ph.D., P.E.  
Victor N. Kaliakin, Ph.D.



Published by the American Society of Civil Engineers

@Seismicisolation

Library of Congress Cataloging-in-Publication Data

Geo-Frontiers Conference (2005 : Austin, Tex.)

Soil constitutive models : evaluation, selection, and calibration : January 24-26, 2005, Austin, Texas / sponsored by Soil Properties and Modeling Committee, the Geo-Institute of the American Society of Civil Engineers ; edited by Jerry A. Yamamuro, Victor N. Kaliakin.

p.cm. -- (Geotechnical special publication ; no. 128)

Includes bibliographical references and index.

ISBN 0-7844-0771-1

1. Soil mechanics--Mathematical models--Congresses. I. Yamamuro, Jerry A. II. Kaliakin, Victor N. III. American Society of Civil Engineers. Geo-Institute. Soil Properties and Modeling Committee. IV. Title. V. Series.

TA710.A1G344 2005

624.1'5136'015118--dc22

2004062791

American Society of Civil Engineers  
1801 Alexander Bell Drive  
Reston, Virginia, 20191-4400

[www.pubs.asce.org](http://www.pubs.asce.org)

Any statements expressed in these materials are those of the individual authors and do not necessarily represent the views of ASCE, which takes no responsibility for any statement made herein. No reference made in this publication to any specific method, product, process, or service constitutes or implies an endorsement, recommendation, or warranty thereof by ASCE. The materials are for general information only and do not represent a standard of ASCE, nor are they intended as a reference in purchase specifications, contracts, regulations, statutes, or any other legal document. ASCE makes no representation or warranty of any kind, whether express or implied, concerning the accuracy, completeness, suitability, or utility of any information, apparatus, product, or process discussed in this publication, and assumes no liability therefore. This information should not be used without first securing competent advice with respect to its suitability for any general or specific application. Anyone utilizing this information assumes all liability arising from such use, including but not limited to infringement of any patent or patents.

ASCE and American Society of Civil Engineers—Registered in U.S. Patent and Trademark Office.

*Photocopies:* Authorization to photocopy material for internal or personal use under circumstances not falling within the fair use provisions of the Copyright Act is granted by ASCE to libraries and other users registered with the Copyright Clearance Center (CCC) Transactional Reporting Service, provided that the base fee of \$25.00 per article is paid directly to CCC, 222 Rosewood Drive, Danvers, MA 01923. The identification for this book is 0-7844-0771-1/05/ \$25.00. Requests for special permission or bulk copying should be addressed to Permissions & Copyright Dept., ASCE.

Copyright © 2005 by the American Society of Civil Engineers.

All Rights Reserved. ISBN 0-7844-0771-1

Manufactured in the United States of America.

@Seismicisolation

## Geotechnical Special Publications

- 1 *Terzaghi Lectures*
- 2 *Geotechnical Aspects of Stiff and Hard Clays*
- 3 *Landslide Dams: Processes, Risk, and Mitigation*
- 7 *Timber Bulkheads*
- 9 *Foundations & Excavations in Decomposed Rock of the Piedmont Province*
- 11 *Dynamic Response of Pile Foundations—Experiment, Analysis and Observation*
- 14 *Geotechnical Aspects of Karst Terrains*
- 15 *Measured Performance Shallow Foundations*
- 16 *Special Topics in Foundations*
- 17 *Soil Properties Evaluation from Centrifugal Models*
- 18 *Geosynthetics for Soil Improvement*
- 19 *Mine Induced Subsidence: Effects on Engineered Structures*
- 21 *Hydraulic Fill Structures*
- 22 *Foundation Engineering*
- 23 *Predicted and Observed Axial Behavior of Piles*
- 24 *Resilient Moduli of Soils: Laboratory Conditions*
- 25 *Design and Performance of Earth Retaining Structures*
- 27 *Geotechnical Engineering Congress*
- 28 *Detection of and Construction at the Soil/Rock Interface*
- 29 *Recent Advances in Instrumentation, Data Acquisition and Testing in Soil Dynamics*
- 32 *Embankment of Dams—James L. Sherard Contributions*
- 33 *Excavation and Support for the Urban Infrastructure*
- 34 *Piles Under Dynamic Loads*
- 35 *Geotechnical Practice in Dam Rehabilitation*
- 37 *Advances in Site Characterization: Data Acquisition, Data Management and Data Interpretation*
- 39 *Unsaturated Soils*
- 40 *Vertical and Horizontal Deformations of Foundations and Embankments*
- 41 *Predicted and Measured Behavior of Five Spread Footings on Sand*
- 42 *Serviceability of Earth Retaining Structures*
- 43 *Fracture Mechanics Applied to Geotechnical Engineering*
- 44 *Ground Failures Under Seismic Conditions*
- 45 *In Situ Deep Soil Improvement*
- 46 *Geoenvironment 2000*
- 47 *Geo-Environmental Issues Facing the Americas*
- 48 *Soil Suction Applications in Geotechnical Engineering*
- 49 *Soil Improvement for Earthquake Hazard Mitigation*
- 50 *Foundation Upgrading and Repair for Infrastructure Improvement*
- 51 *Performance of Deep Foundations Under Seismic Loading*
- 52 *Landslides Under Static and Dynamic Conditions—Analysis, Monitoring, and Mitigation*
- 53 *Landfill Closures—Environmental Protection and Land Recovery*
- 54 *Earthquake Design and Performance of Solid Waste Landfills*
- 55 *Earthquake-Induced Movements and Seismic Remediation of Existing Foundations and Abutments*
- 56 *Static and Dynamic Properties of Gravelly Soils*
- 57 *Verification of Geotechnical Grouting*
- 58 *Uncertainty in the Geologic Environment*
- 59 *Engineered Contaminated Soils and Interaction of Soil Geomembranes*
- 60 *Analysis and Design of Retaining Structures Against Earthquakes*
- 61 *Measuring and Modeling Time Dependent Soil Behavior*
- 62 *Case Histories of Geophysics Applied to Civil Engineering and Public Policy*
- 63 *Design with Residual Materials: Geotechnical and Construction Considerations*
- 64 *Observation and Modeling in Numerical Analysis and Model Tests in Dynamic Soil-Structure Interaction Problems*
- 65 *Dredging and Management of Dredged Material*
- 66 *Grouting: Compaction, Remediation and Testing*
- 67 *Spatial Analysis in Soil Dynamics and Earthquake Engineering*
- 68 *Unsaturated Soil Engineering Practice*
- 69 *Ground Improvement, Ground Reinforcement, Ground Treatment: Developments 1987-1997*
- 70 *Seismic Analysis and Design for Soil-Pile-Structure Interactions*
- 71 *In Situ Remediation of the Geoenvironment*
- 72 *Degradation of Natural Building Stone*
- 73 *Innovative Design and Construction for Foundations and Substructures Subject to Freezing and Frost*

- 74 *Guidelines of Engineering Practice for Braced and Tied-Back Excavations*  
75 *Geotechnical Earthquake Engineering and Soil Dynamics III*  
76 *Geosynthetics in Foundation Reinforcement and Erosion Control Systems*  
77 *Stability of Natural Slopes in the Coastal Plain*  
78 *Filtration and Drainage in Geotechnical/Geoenvironmental Engineering*  
79 *Recycled Materials in Geotechnical Applications*  
80 *Grouts and Grouting: A Potpourri of Projects*  
81 *Soil Improvement for Big Digs*  
82 *Risk-Based Corrective Action and Brownfields Restorations*  
83 *Design and Construction of Earth Retaining Systems*  
84 *Effects of Construction on Structures*  
85 *Application of Geotechnical Principles in Pavement Engineering*  
86 *Big Digs Around the World*  
87 *Jacketed Tunnel Design and Construction*  
88 *Analysis, Design, Construction, and Testing of Deep Foundations*  
89 *Recent Advances in the Characterization of Transportation Geo-Materials*  
90 *Geo-Engineering for Underground Facilities*  
91 *Special Geotechnical Testing: Central Artery/Tunnel Project in Boston, Massachusetts*  
94 *Performance Confirmation of Constructed Geotechnical Facilities*  
95 *Soil-Cement and Other Construction Practices in Geotechnical Engineering*  
96 *Numerical Methods in Geotechnical Engineering: Recent Developments*  
97 *Innovations and Applications in Geotechnical Site Characterization*  
98 *Pavement Subgrade, Unbound Materials, and Nondestructive Testing*  
99 *Advances in Unsaturated Geotechnics*  
100 *New Technological and Design Developments in Deep Foundations*  
101 *Slope Stability 2000*  
102 *Trends in Rock Mechanics*  
103 *Advances in Transportation and Geoenvironmental Systems Using Geosynthetics*  
104 *Advances in Grouting and Ground Modification*  
105 *Environmental Geotechnics*  
106 *Geotechnical Measurements: Lab & Field*  
107 *Soil Dynamics and Liquefaction 2000*  
108 *Use of Geophysical Methods in Construction*  
109 *Educational Issues in Geotechnical Engineering*  
110 *Computer Simulation of Earthquake Effects*  
111 *Judgment and Innovation: The Heritage and Future of the Geotechnical Engineering Profession*  
112 *Soft Ground Technology*  
114 *Soils Magic*  
115 *Expansive Clay Soils and Vegetative Influence on Shallow Foundations*  
116 *Deep Foundations 2002: An International Perspective on Theory, Design, Construction, and Performance*  
117 *Discrete Element Methods: Numerical Modeling of Discontinua*  
118 *A History of Progress: Selected U.S. Papers in Geotechnical Engineering*  
119 *Soil Behavior and Soft Ground Construction*  
120 *Grouting and Ground Treatment*  
121 *Probabilistic Site Characterization at the National Geotechnical Experimentation Sites*  
122 *Sinkholes and the Engineering and Environmental Impacts of Karst*  
123 *Recent Advances in Materials Characterization and Modeling of Pavement Systems*  
124 *GeoSupport 2004: Drilled Shafts, Micropiling, Deep Mixing, Remedial and Specialty Foundation Systems*  
125 *Current Practices and Future Trends in Deep Foundations*  
126 *Geotechnical Engineering for Transportation Projects*  
127 *Recycled Materials in Geotechnics*  
128 *Soil Constitutive Models: Evaluation, Selection, and Calibration*

# Foreword

## Purpose

Today, advanced numerical methods are increasingly being utilized by engineers for evaluation of deformations in geotechnical structures. At the heart of this analysis is the soil constitutive model. Knowledge of strengths and weaknesses of different constitutive model is a prerequisite for proper selection of one that matches the needs of the particular geotechnical application. To achieve this goal, this volume has brought together invited papers from a large number of well-known constitutive modelers from around the world. The presented models range from the most simple to the most complex. Proper calibration of constitutive models is also necessary to ensure that a model gives accurate results. Thus, emphasis was placed on describing how to calibrate the different models. This Geotechnical Special Publication (GSP) is intended for both practitioners and researchers who are looking for a single source to assist them in the proper selection and calibration of a soil constitutive model.

## Acknowledgements

This Geotechnical Special Publication is an outgrowth of activity at the Geo-Frontiers Conference at Austin, Texas held in January 24-26, 2005. We would like to thank the organizers of Geo-Frontiers.

This GSP was sponsored by:

- The Geo-Institute of the American Society of Civil Engineers
- Soil Properties and Modeling Committee of ASCE Geo-Institute
- Geo-Frontiers Conference, Austin, Texas, January 24-26, 2005

We would also like to thank Professor Poul V. Lade for authoring the overview paper in this GSP and for providing timely advice throughout the process. We would also like to thank him for creating the cover figure. Thanks also to Professor Don J. Degroot, who as Chair of The Soil Properties and Modeling Committee, initially suggested that a document of this type be developed.

# Contents

## *Overview Paper*

<b>Overview of Constitutive Models for Soils .....</b>	<b>1</b>
Poul V. Lade	

## *Invited Papers*

<b>ANISOFT—Constitutive Model for Undrained Loading of Anisotropic and Strain-Softening Clay .....</b>	<b>35</b>
Lars Andresen and Hans Petter Jostad	
<b>Unconstrained Optimization and Calibration of a Kinematic-Cyclic Plasticity Model.....</b>	<b>45</b>
Yu Bao, Yu-Ning Ge, and Stein Sture	
<b>Selection of Soil Models and Parameters for Geotechnical Engineering Application .....</b>	<b>69</b>
Ronald B. J. Brinkgreve	
<b>Review of the Structured Cam Clay Model.....</b>	<b>99</b>
John P. Carter and Martin D. Liu	
<b>Incrementally Non-Linear Constitutive Relations: New Challenges .....</b>	<b>133</b>
Félix A. Darve and Cédric G. Lambert	
<b>Unified Yet Simplified Disturbed State Constitutive Models for Soils and Interface/Joints .....</b>	<b>159</b>
Chandrakant S. Desai	
<b>Geotechnical Constitutive Models in an Explicit, Dynamic Solution Scheme .....</b>	<b>184</b>
Roger D. Hart and Christine Detournay	
<b>NorSand: Features, Calibration, and Use.....</b>	<b>204</b>
Michael G. Jefferies and Dawn A. Shuttle	
<b>Parameter Estimation for Time-Dependent Bonding Surface Models for Cohesive Soils .....</b>	<b>237</b>
Victor N. Kaliakin	
<b>Hypoplasticity as a Constitutive Framework for Granular Soils.....</b>	<b>257</b>
D. Kolymbas and I. Herle	
<b>Single Hardening Model for Soils: Parameter Determination and Typical Values .....</b>	<b>290</b>
Poul V. Lade	
<b>Selection and Calibration of Soil Constitutive Model Parameters Using Genetic Algorithms.....</b>	<b>310</b>
Emir José Macari, Prasad Samarajiva, and Wije Wathugala	
<b>SMP Criterion-Based Unified Constitutive Model for Geomaterials .....</b>	<b>333</b>
Hajime Matsuoka, Yang-Ping Yao, and De' An Sun	

<b>A Simple Elastoplastic Model for Geomaterials Based on <math>T_i</math>-Concept and its Calibration by Various Test Data .....</b>	<b>358</b>
Teruo Nakai and Masaya Hinokio	
<b>A Simple Elastoplastic Model for Soils and Soft Rocks.....</b>	<b>380</b>
Roberto Nova	
<b>Calibration of Elasto-Viscoplastic Models for Cohesive Soils .....</b>	<b>400</b>
Fusao Oka, Sayuri Kimoto, and Toshihisa Adachi	
<b>Calibration of a Simple Anisotropic Plasticity Model for Soft Clays.....</b>	<b>415</b>
Achilleas G. Papadimitriou, Majid T. Manzari, and Yannis F. Dafalias	
<b>Selection of Material Parameters for Sands using the MIT-S1 Model.....</b>	<b>425</b>
Juan M. Pestana, Maria Nikolinakou, and Andrew J. Whittle	
<b>Parameters for Average Gulf Clay and Prediction of Pile Set-Up in the Gulf of Mexico .....</b>	<b>440</b>
Andrew J. Whittle and Twarath Sutabutr	
<b>Hierarchical Critical State Models.....</b>	<b>459</b>
David Muir Wood and Alessandro Gajo	
<b>Calibration of a Generalized Plasticity Model and Its Application to Liquefaction Analysis.....</b>	<b>483</b>
Songtao Yang and Hoe I. Ling	
<b>Subject Index.....</b>	<b>495</b>
<b>Author Index .....</b>	<b>497</b>

## OVERVIEW OF CONSTITUTIVE MODELS FOR SOILS

Poul V. Lade<sup>1</sup>, Member, Geo-Institute

**ABSTRACT:** Numerous constitutive models have been developed over the past forty years for modeling the stress-strain behavior of soils. These models are to be used with finite element and/or finite difference calculations of soil structures and soil/structure interaction problems under axisymmetric, plane strain, and/or general three-dimensional conditions. Simple as well as advanced models have been formulated on the basis of principles of mechanics, some more rigorous than others, some based on experimental evidence, and others based on theoretical principles. The capabilities and the shortcomings of these models are not always easy to ascertain, and the requirements for determination of parameters are not uniform. It is consequently difficult to determine which model to select for a particular task.

Presented here is an overview of the principles, main characteristic features, and components of existing, widely available constitutive models. Their requirements in terms of experimental data for calibration are presented, and their capabilities are reviewed.

### INTRODUCTION

With the development of numerical methods such as finite element and finite difference methods it has become feasible to analyze and predict the behavior of complex soil structures and soil/structure interaction problems. Such analyses depend considerably on the representation of the relations between stresses and strains for the various materials involved in the geotechnical structure. In numerical computations the relations between stresses and strains in a given material are represented by a so-called constitutive model, consisting of mathematical expressions that model the behavior of the soil in a single element, as indicated in Fig. 1. Because soils are most often the weakest materials involved in common geotechnical problems, they

---

<sup>1</sup> Professor, Department of Civil Engineering, The Catholic University of America, Washington, D.C. 20064, U.S.A., Lade@cua.edu



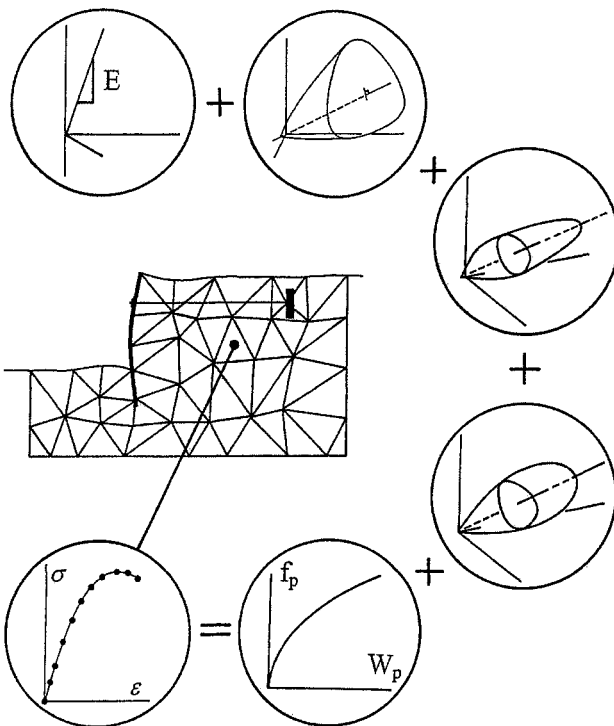


**FIG. 1.** Soil structure divided into a finite number of elements each of which is represented by a constitutive model based on elasticity and plasticity theories.

determine the deformations and the possibility of failure of the structure, and it is therefore important to characterize these materials accurately over the entire range of stresses and strains to which they will become exposed. Other construction materials such as concrete and steel may remain stiff in comparison with the soils, and it may be sufficient to characterize these materials as elastic or as elastic-perfectly plastic. Thus, the purpose of a constitutive model is to simulate the soil behavior with sufficient accuracy under all loading conditions in the numerical computations.

Significant developments of constitutive models have occurred over the past four decades. Naturally, the initial models were relatively simple, and a progression in complexity and capabilities of the models have lead to much improved abilities to capture the behavior of soil structures under complex loading conditions. Simple as well as advanced models have been formulated on the basis of principles of mechanics, some more rigorous than others, some based on experimental evidence, and others based on theoretical principles. Characterization of soil behavior can become quite involved, because the stress-strain relations are nonlinear in nature, the

@Seismicisolation

soils are fundamentally frictional materials, and volume changes occur during drained shearing.

It is clear that constitutive models have already gone through substantial improvements, and more will come. Thus, development of new and improved constitutive models is a continuing endeavor over a foreseeable future. However, the principles, main characteristic features, and components in the constitutive models for soils that are currently widely available to practitioners and researchers in packaged numerical software and in the technical literature are briefly presented and reviewed here. Important aspects of these models are the requirement for experimental data for calibration and the ease with which material parameters are determined.

This presentation is not intended as a highly in-depth discussion of each model. Virtually no particular models are mentioned in the text other than when used as examples in general discussions of e.g. the number of parameters in the models. Simple comparisons of the major components and capabilities of models are all presented in tables with no further comments.

## **CONSIDERATIONS IN MODEL DEVELOPMENT**

Soils are complex materials consisting of a solid skeleton of grains in contact with each other and voids filled with gas (air) and/or water or other fluid. The soil skeleton transmits normal and shear forces at the grain contacts, and this skeleton of grains behaves in a very complex manner that depends on a large number of factors, void ratio and confining pressure being among the most important. However, the overall behavior of the soil skeleton may be captured within principles of continuum mechanics (solid mechanics). Interspersed in the voids is water (incompressible fluid) and gas (compressible fluid), each of which obeys its own physical laws. The mixture of grains, water, and air produces a material that, in comparison with other engineering materials, is one of the most difficult to characterize.

### **The Effective Stress Principle**

A key principle in the behavior of soils was realized by Terzaghi (1923), namely that soils deform in response to changes in effective stresses, and these are calculated from:

$$\sigma' = \sigma - \gamma \cdot u \quad (1)$$

in which  $\sigma'$  is the effective stress,  $\sigma$  is the total stress,  $u$  is the pore pressure, and  $\gamma$  is a coefficient whose value depends on the compressibilities of the grain skeleton and the grains themselves. For all common geotechnical problems the value of  $\gamma$  can be taken as unity. Only for extremely high stresses, encountered under very exceptional circumstances, does the value of  $\gamma$  become smaller than unity (Lade and de Boer 1997).

Since soils deform in response to changes in effective stresses, theoretically sound constitutive models are expressed in terms of effective stresses. Nevertheless, models have also been expressed in terms of total stresses, but they suffer from the same shortcomings as any total stress analysis of a soil structure: They are only valid for the



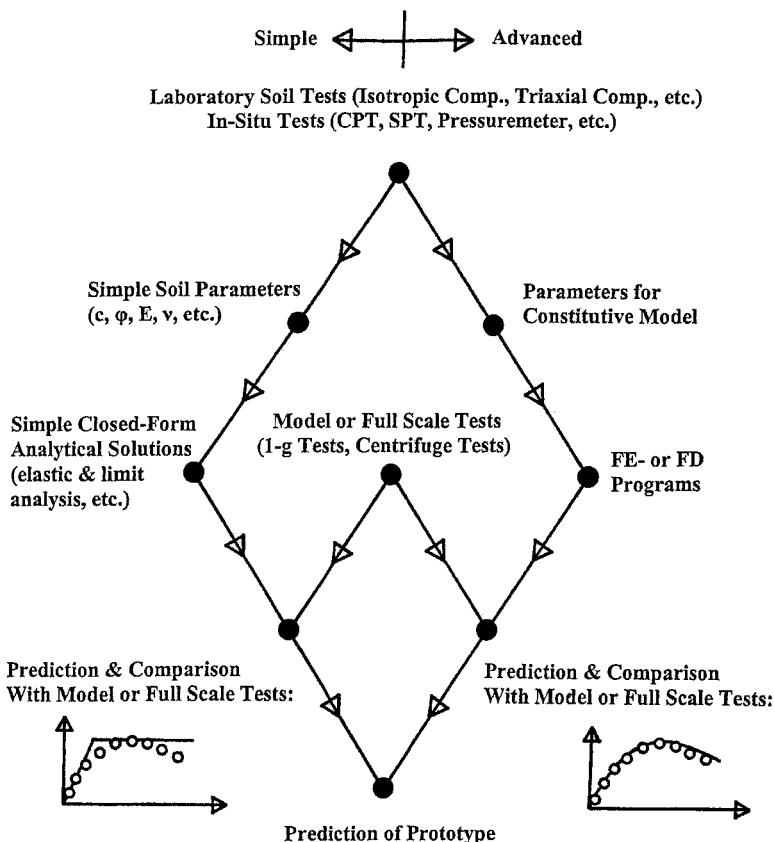


**FIG. 2. Simple and advanced procedures for predicting the behavior of prototype structures.**

particular conditions for which they have been calibrated. Variations in pore pressure or drainage conditions, different from those developing in the experiment from which parameter values are determined, cannot be modeled (see any textbook in geotechnical engineering, e.g. Lambe and Whitman 1969), so their usefulness is limited.

#### Simple versus Advanced Analysis - What is Gained?

Fig. 2 shows a simplified diagram of the analysis procedures generally used in geotechnical engineering. In the simple procedures, represented on the left hand side, simple and easily recognizable soil parameters (e.g.  $c$ ,  $\phi$ ,  $E$ ,  $v$ ) are derived from laboratory and/or in-situ tests and utilized in closed-form solutions for the particular boundary value problem under consideration. Figs. 3 and 4 illustrate some simple

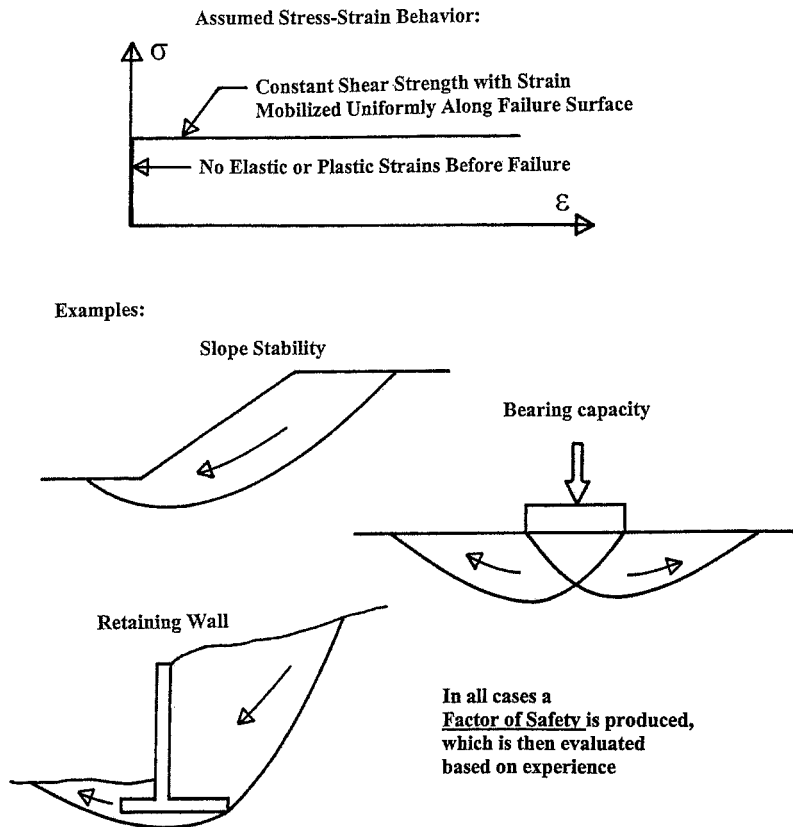


**FIG. 3. Examples of failure or stability of soil structures for which closed-form solutions are available.**

cases for which closed-form solutions are readily available. Usually considerations of failure or stability are made first using formulas from which the factor of safety may be calculated from solutions for slope stability, bearing capacity, and/or stability of retaining walls, as shown in Fig. 3. In these analyses strains are not considered, which corresponds to an assumed stress-strain relation as shown in the upper part of Fig. 3.

Once the stability is ensured, the deformations or settlements may be evaluated using closed-form solutions based on elasticity theory, such as that indicated in Fig. 4 for the settlement of a footing. No matter how high the bearing pressures used in the elastic formulation, failure considerations are not part of the calculations from such formulas.

The results of these classical procedures may be verified by prediction and comparison with model or full scale tests of elements of the prototype structure (e.g.,

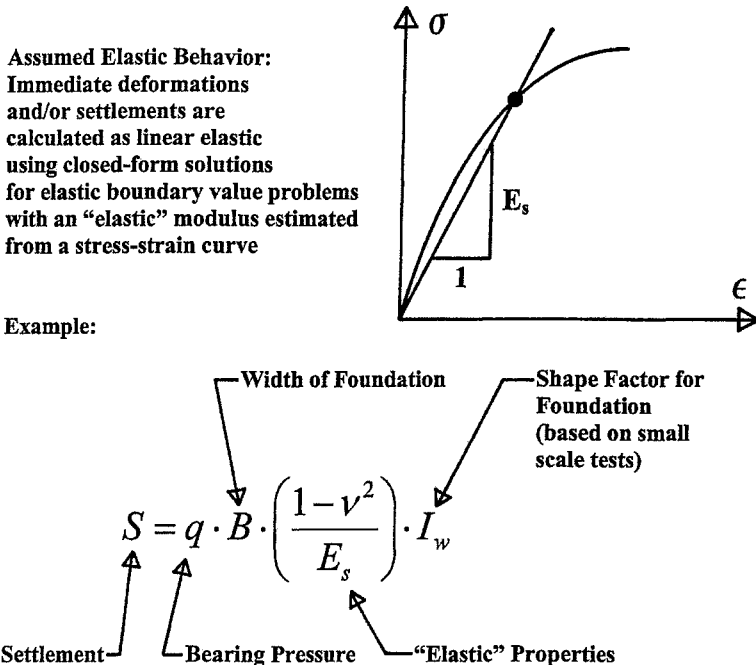


**FIG. 4.** Example of deformation consideration represented by settlement calculation of a footing for which a closed-form solution is available.

one pile). Finally, prediction of the behavior of the prototype may be performed. The simple procedures predict simplified responses such as linear elastic settlements and failure, but prediction of the entire load-deformation relation for a prototype structure is often inaccurate if not impossible to perform, especially in the load range where failure is a distinct possibility.

The real behavior of a footing is indicated in Fig. 5. As loading progresses, the stresses in soil elements located along the potential failure surface in the ground, shown in the upper part of Fig. 5, advance along the stress-strain curve as indicated in the lower part of Fig. 5. The initial state of stress in the ground may be characterized by a  $K_0$ -condition, and as loading progresses, the stresses increase up to peak failure and beyond into the softening region of the stress-strain curve. Thus, a highly nonlinear relation between stresses and strains are encountered in the real behavior of the footing.

In the advanced procedure, indicated on the right hand side of Fig. 2, a constitutive model is used to capture the entire stress-strain relation obtained from laboratory and/or in-situ tests. Incorporating the constitutive model in numerical methods, the behavior of model or full-scale tests may be predicted and serve to verify the

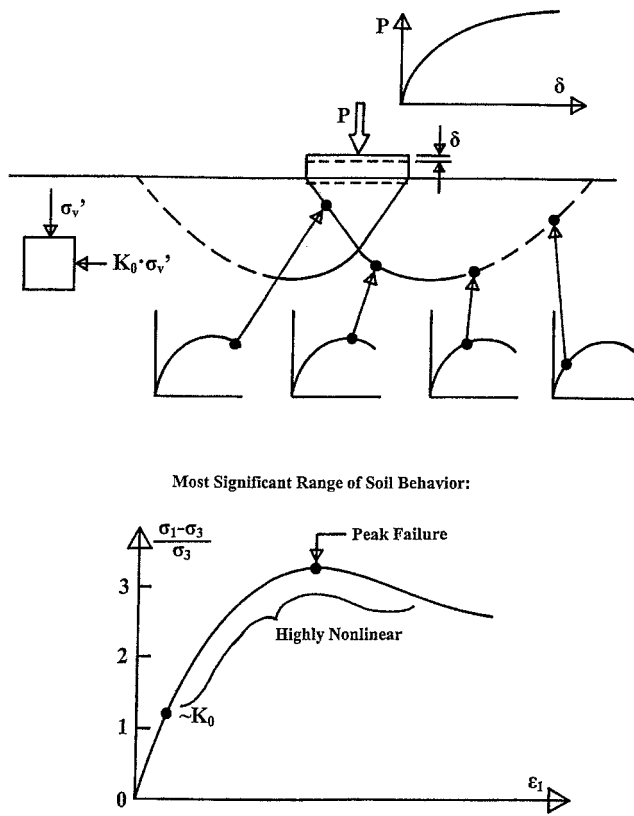


**FIG. 5. Real behavior of a footing involving highly nonlinear soil stress-strain behavior.**

capability of the constitutive model and the numerical method. Finally, the behavior of the prototype may be calculated with better overall accuracy.

Using finite element (or finite difference) methods, a geotechnical structure of any axisymmetric, plane, or three-dimensional shape may be divided into a finite number of elements (nodes), as indicated in Fig. 1. A constitutive model for each element then simulates the soil behavior, and the numerical method ensures equilibrium and compatibility between the soil elements. Thus, much more complex earth structures and soil/structure interaction problems can be analyzed, and their behavior in the form of deformations and stress conditions everywhere in the structure may be obtained for the entire loading history. Such results could not be obtained with closed-form solutions, which are typically only developed for rather simple boundary value problems.

### Requirements of Constitutive Models

One of the critical elements in the advanced procedure is the constitutive model. It is paramount to employ realistic constitutive models that can reproduce the important aspects of the soil stress-strain behavior under various loading conditions. To develop such models requires advanced experiments to study the soil behavior under various loading conditions, and it requires employment of mathematical tools based on sound theoretical frameworks such as, e.g., elasticity and plasticity theories.

Some of the advanced experiments available today are the torsion shear, directional shear, and true triaxial tests. These are suitable for studying soil behavior under three-dimensional stress conditions with and without stress reversals and with and without rotation of principal stresses. While the model should be able to simulate the soil behavior observed in these tests, they should not be required for calibration of the constitutive models. The constitutive model should be such that the required soil parameters can be obtained from relatively simple tests.

### Sequential Development of Models

Most practical models, applicable in numerical methods, are formulated in terms of some form of theories of elasticity and plasticity. They have been developed based on observed behavior in laboratory experiments, and it is the responsibility of the research community to demonstrate that they do, in fact, capture the behavior of soils as they are purported to do. Thus, as realization about the complex behavior of soils is expanding, the models are continuously being improved and new modeling principles have been developed.

For example, the following sequence of observations of soil behavior have lead to improved models: Effects of virgin (primary) loading and unloading-reloading, confining pressure, stress path (stress history), intermediate principal stress, instability (leading to shear banding in dense sand and overconsolidated soils and to liquefaction in loose silty sands), anisotropy, and stress rotation (note: this list of phenomena is not exhaustive). While all of these (and many more) effects have been known to exist for some time, some of them are still to be researched and understood in detail before they may be modeled correctly. Thus, the simple models can only handle the first mentioned phenomena, while the more advanced models may handle additional phenomena. It is difficult to say that any one of these phenomena has definitively been researched, understood, and included in any given model. The latter two topics (effects of anisotropy and effects of stress rotation) are in the forefront of current research, and practically applicable models that correctly capture these effects are still to be developed.

### Shortcomings of Elasticity Theory

The behavior of soils may be predicted with reasonable accuracy by models based on elasticity for stress states not approaching failure. However, phenomena such as irreversibility of a portion of the strains, stress-path dependency, coupling effects such as volume changes due to shear stresses, referred to as shear-dilatancy, rotation of principal stress axes, and most behavior patterns near and beyond failure cannot be



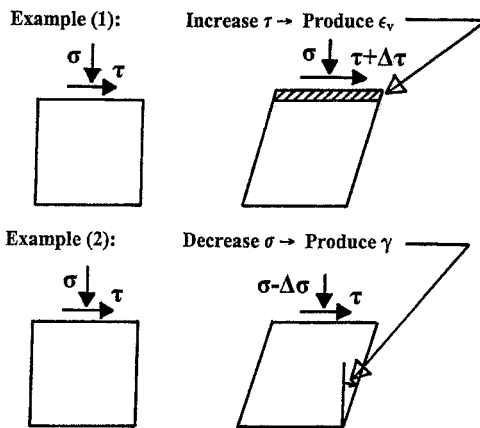
handled by elasticity theory. Two simple examples will illustrate the shortcomings of Hooke's law for elastic behavior.

Fig. 6 shows that zeroes occupy the sub-matrices (1, 2) and (2, 1) of the elastic material matrix that relates plastic strain increments to stress increments. The zeroes in sub-matrix (1, 2) imply that there are no relations between normal strains and shear stresses. However, Example (1) in Fig. 6 shows a dense sand specimen acted upon by a normal stress and a shear stress, as for example in a simple shear test. If the shear stress is increased, then increments in shear strains will result, but observations of real soil indicates that the soil will also dilate such that the specimen height increases.

$$\begin{Bmatrix} \Delta\epsilon_x \\ \Delta\epsilon_y \\ \Delta\epsilon_z \\ \Delta\gamma_{yz} \\ \Delta\gamma_{zx} \\ \Delta\gamma_{xy} \end{Bmatrix} = \begin{Bmatrix} \frac{1}{E} & -\frac{\nu}{E} & -\frac{\nu}{E} & 0 & 0 & 0 \\ -\frac{\nu}{E} & \frac{1}{E} & -\frac{\nu}{E} & 0 & 0 & 0 \\ -\frac{\nu}{E} & -\frac{\nu}{E} & \frac{1}{E} & 0 & 0 & 0 \\ 0 & 0 & 0 & \frac{1}{G} & 0 & 0 \\ 0 & 0 & 0 & 0 & \frac{1}{G} & 0 \\ 0 & 0 & 0 & 0 & 0 & \frac{1}{G} \end{Bmatrix} \begin{Bmatrix} \Delta\sigma_x \\ \Delta\sigma_y \\ \Delta\sigma_z \\ \Delta\tau_{yz} \\ \Delta\tau_{zx} \\ \Delta\tau_{xy} \end{Bmatrix}$$

? (1)

? (2)



**FIG. 6.** Examples to indicate that Hooke's law for elastic behavior does not correctly handle coupling effects: (1) normal (and volumetric) strain increments due to changes in shear stress, and (2) shear strain increments due to changes in normal stress.

Thus, normal strain increments result from increments in shear stress. Since zeroes are present in sub-matrix (1, 2) of the elastic material matrix, no normal strain increments can be predicted from increments in shear stress. Therefore, Hooke's law is not able to model this behavior of soils. The zeroes in sub-matrix (2, 1) of the elastic material matrix may be checked by the experiment in Example (2) in Fig. 6. Here the initial condition is the same as in Example (1), but now the normal stress on the specimen is reduced. Observations of real soil behavior shows that the specimen will produce shear strain increments for such a reduction in normal stress, and sufficient reduction will result in failure. However, the zeroes in sub-matrix (2, 1) preclude any prediction of shear strain increments due to increments in normal stresses. These two examples clearly demonstrate some serious shortcomings of elasticity theory for modeling behavior of soils for stress conditions approaching failure. In fact, all frictional materials exhibit behavior of the types exemplified in Fig. 6.

### Why Using Hardening Plasticity Theory?

Models based on hardening plasticity have the potential to predict the behavior reviewed above. In addition, elasticity and plasticity also differ in predictions of material behavior during gradual stress rotation, as indicated in Fig. 7. The theoretical framework for incremental elasticity implies that the increment of elastic strain coincides in direction with the increment of stress, as shown in Fig. 7(a). This differs clearly from the predictions of isotropic hardening plasticity theory, which has built into its framework the condition that the increment of plastic strain coincides in direction with the total stress, as shown in Fig. 7(b). Observations of soil behavior show that far away from failure the behavior favors the elastic predictions, while the behavior observed closer to failure resembles the behavior simulated by plasticity theory.

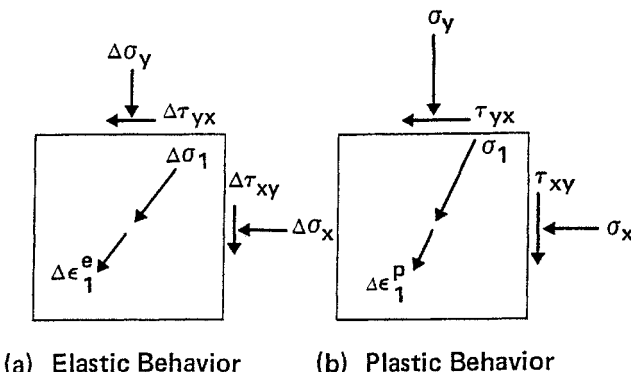


**FIG. 7. (a) Elastic, and (b) plastic behavior of soil element during rotation of stress axes.**

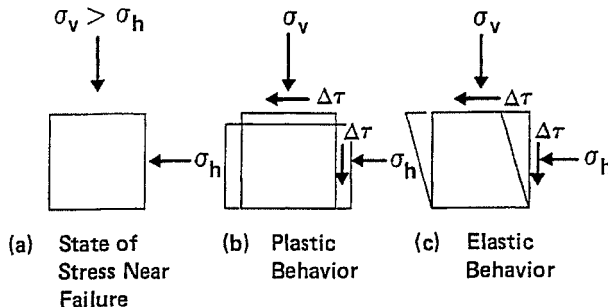


**FIG. 8. (a) Stresses on a soil element near failure, its (b) plastic behavior (Saint Venant's principle), and its (c) elastic behavior.**

Another way of indicating the difference between elasticity and plasticity theories is shown in Fig. 8. A soil specimen is acted upon by vertical and horizontal normal stresses such that  $\sigma_v > \sigma_h$ , but failure has not been reached, as shown in Fig. 8(a). An increment in shear stress is added to the soil element, as shown in Figs. 8(b) and (c). Plastic behavior, shown in Fig. 8(b), entails vertical compression of the specimen, because the direction of the much larger total stress determines the direction of the plastic strain increment, independent of whether the stress increment is a normal or a shear stress increment. In comparison, elastic behavior results in strain increments in proportion to the applied stress increment and is independent of the already existing stress state.

These two types of behavior are both observed in soils. The elastic type behavior is observed at low stress levels near the isotropic stress state and immediately upon unloading and/or reloading where plastic behavior is absent or minimal, while plastic behavior is observed at higher stress levels closer to failure. Elastic strain increments are always present when the state of stress changes, while plastic strain increments may be present or completely absent.

Thus, realistic constitutive models require both elastic and hardening/softening plastic behavior in their framework. All realistic constitutive models for soils involve these two components of deformation.

#### Associated versus Nonassociated Plastic Flow

Early considerations in development of plasticity theory required the relative magnitudes of the plastic strain increments to be such that the direction of the plastic strain increment vector, when superimposed on stress space, would be normal to the plastic yield surface. That implied that this direction (or the relative magnitudes of the plastic strain increments) could be determined from the derivative of the mathematical expression for the yield surface, which was therefore also referred to as the plastic potential surface. Thus, the plastic flow rule (i.e. the expressions for the plastic strain increments) could be derived from the expression for the yield surface,

i.e. plastic flow was associated with the plastic yield surface. A constitutive model based on this concept was using an “associated flow rule.”

Employing “associated flow” resulted in a great advantage, because knowing either the yield surface (from experimental determination of stress conditions at plastic yielding) or knowing the plastic potential surface (from experimental determination of the relative magnitudes of plastic strain increments and therefore the direction of the plastic strain increment vector at different stress points) would automatically result in knowing both surfaces. This simplified the mathematical framework for the model of the plastic behavior. Besides, violation of the “normality rule” was considered to have serious implications in terms of stability of the material, and constitutive models based on so-called nonassociated plastic flow rules, for which the plastic potential surface would be different from the yield surface, could result in unstable material behavior.

The concept of associated plastic flow works well for solid metals, but frictional materials do not seem to fit well with this concept. Much too high rates of volume dilation are predicted if associated flow is used in connection with models for frictional materials. The difference between observed soil behavior and behavior predicted on the basis of associated flow is most pronounced for frictional materials with high effective friction angles (e.g. dense sand), while materials with less pronounced frictional characteristics, such as clays with lower effective friction angles, may be modeled with some approximation by associated flow rules.

Later theoretical considerations have shown that the normality rule does not have to be fulfilled, and observations of sand behavior clearly indicate that experimentally determined plastic strain increment vectors are not perpendicular to the yield surface. Further, the instabilities that might occur in materials that exhibit nonassociated flow actually have been observed in the form of shear bands occurring in the hardening regime (the ascending branch of the stress-strain relation) under plane strain conditions and in the form of instability (decrease in load bearing capacity) leading to liquefaction of loose silty sand.

While it is generally understood at this time that frictional materials obey nonassociated flow rules, some constitutive models developed for clay are still based on associated plastic flow. The characteristics of frictional materials are less pronounced for these materials.

### Prediction of Pore Water Pressures

Pore water pressures are rigorously determined from a constitutive model on the basis that a fully saturated soil element cannot change volume during shearing. Thus, the sum of all volumetric strain components must add up to zero during any change in stress. This requires that for each increment in loading, plastic dilation is balanced by an equal and opposite amount of elastic contraction or vice versa: plastic contraction is balanced by an equal and opposite amount of dilation. This results in a unique effective stress path from which the pore pressure can be obtained as the difference between the total stresses and the effective stresses for each increment of loading.

In case that only one component of volumetric strain is present, e.g. the elastic component inside the yield surface, then the effective stress path will remain in one



octahedral plane corresponding to a constant mean normal stress until the yield surface is reached again.

If a constitutive model contains only one component of volumetric strain, then realistic pore pressures cannot be predicted from the model. On occasion, a separate pore pressure generation model has then been employed to predict pore pressures under undrained conditions. However, such models are usually not compatible with the performance of the constitutive model.

### WHICH PROBLEMS CAN BE SOLVED?

Many different types of geotechnical problems may be analyzed using advanced constitutive models and numerical methods. Duncan (1994) reviewed the literature ten years ago to study the variety of problems that had been investigated using the advanced approach, and to look into the constitutive models that had been employed in the numerical analyses. He organized the review into sections and pointed out that the following types of geotechnical applications had been encountered: Soil structure interaction, soil reinforcement and anchorage, dams, embankments and settlement due to fluid extraction, tunnels, and natural and unbraced cut slopes. Thus, a large variety of problems benefit from insight provided by advanced analyses of stresses and deformations in the soil structures. In fact, it has become feasible to analyze and predict the behavior of any type of complex soil structure and soil/structure interaction problem.

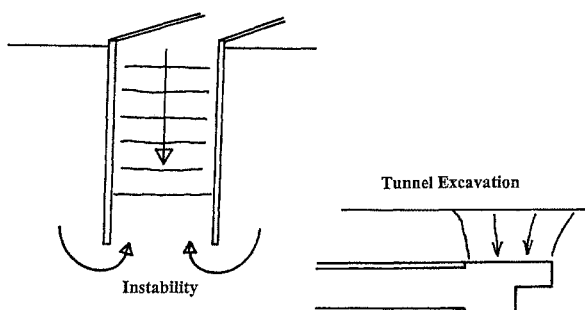
The greatest advantages and insights are obtained for problems in which the soil behavior plays an important role. These include problems in which the interaction between stresses and soil volume changes plays a dominant role. Fig. 9 gives some examples of soil/structure interaction in which the interaction between confinement and volume changes, i.e. the real soil behavior is essential in prediction of the behavior of the structure.

Another type of problem demonstrating the importance of understanding and capturing the soil behavior correctly is shown in Fig. 10. Here the rockfill material in the upstream shell of a rockfill dam may collapse during first wetting due to filling of the water reservoir. This produces displacements of the crest that resemble those observed due to imminent upstream slope failure. Is the dam failing or are these displacements to be expected? An advanced analysis with appropriate modeling of the soil behavior can answer the question.

Fig. 11 illustrates some problems in which the self-weight of the soil plays an important role in the stability analyses of the soil structure. For example, in slope stability analyses, the weight of the soil is the direct cause of potential instability. A classical slope stability analysis produces an accurate estimate of failure, because the normal stresses on the failure plane are proportional to the weight of the soil and independent of the soil behavior. Thus, the normal stress, and therefore the shear strength available along the failure plane, does not change due to e.g. a tendency for the soil to change volume. The normal stress remains proportional with the soil weight, even if the soil tends to dilate. Thus, the calculated factor of safety remains unaffected in any advanced analyses that may include more accurate soil modeling. In such problems, there is limited advantage in an advanced analysis for the purpose of

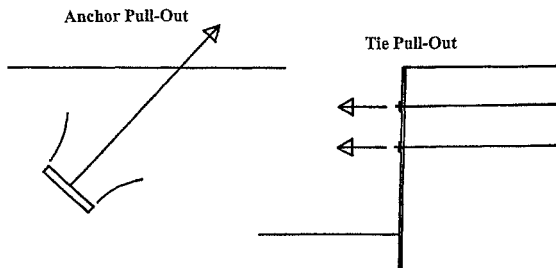


Excavation of Vertical Shaft or Sinking of Caisson



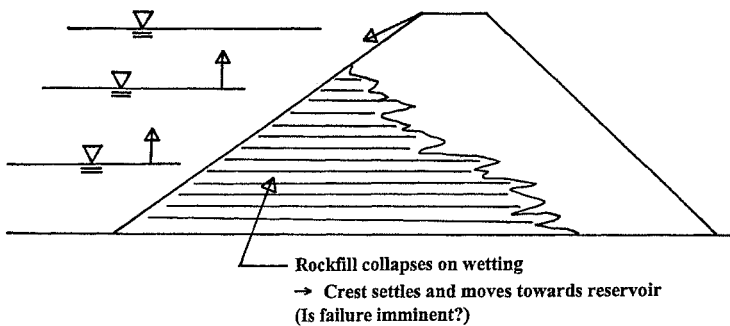
Anchor Pull-Out

Tie Pull-Out



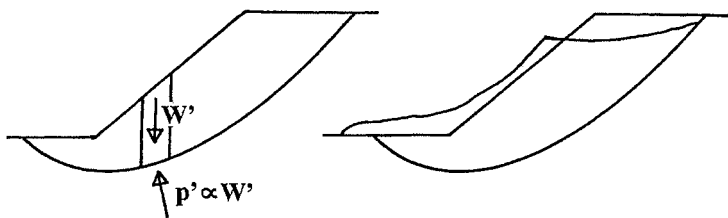
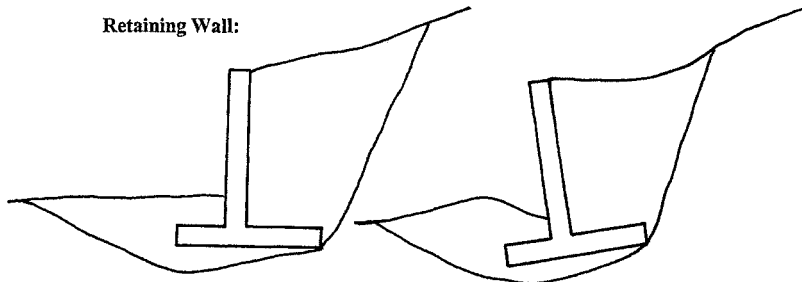
**FIG. 9. Examples of soil/structure interaction in which the soil behavior plays an important role in the deformation and stability of the structure.**

Filling Reservoir Behind Rockfill Dam:



**FIG. 10. Filling of water reservoir behind a rockfill dam with resulting crest displacement due to first wetting and collapse of rockfill material in upstream shell.**

@Seismicisolation

**Natural, Cut and Fill Slopes:****Retaining Wall:**

Stability considerations produce accurate estimate of failure, because normal stresses on failure plane are proportional to weight of soil and independent of soil behavior, .....  
 but deformations are not elastic  
 → simple procedures cannot be used to calculate deformations

**FIG. 11. Examples of slope and retaining wall problems in which soil self-weight plays a dominant role in their stability.**

determining the stability. However, deformations cannot be obtained from a classical slope stability analysis, while an advanced numerical analysis will be able to produce such deformations.

### IMPLEMENTATION IN NUMERICAL COMPUTER PROGRAMS

Many of the commercially available finite element and finite difference programs, e.g. ABAQUS, PLAXIS, and FLAC, allow implementation of most simple as well as advanced constitutive models. Many of these programs have become increasingly user-friendly, and some have been specialized for geotechnical engineering problem solving. Unfortunately, the perception that advanced models may be too complicated for implementation and for easy parameter determination reduces the usefulness of such numerical programs. Therefore, the present exposure of constitutive models for soils should be useful for more frequent applications of advanced analysis procedures in the future.

## PARAMETER DETERMINATION

### Testing Requirements

To predict deformations as well as strengths of soils, the constitutive model should include expressions for the soil behavior observed during compression and during shearing. The modes of deformation are different under these two loading conditions: One involves continuous compression with no failure, while the other leads to failure and beyond. Consequently, the model should contain components that simulate the corresponding two modes of deformation, and experiments that contain information regarding these two modes of deformation should be available for determination of the material parameter values (calibration) that characterize the particular soil in question.

In principle, the parameters for a given model should be derivable from any set of experiments that contains information regarding compression and shearing behavior. This is because the mathematical expressions in the ideal constitutive model may be specialized to correspond to the particular tests available for parameter determination. But most often, the simplest and most convenient experimental results that contain the required information are those from conventional triaxial compression tests and isotropic compression tests.

Typically the results of three triaxial compression tests and one isotropic compression test contain the minimum required information, and such test results are often available for parameter determination. It may be possible to use the results from uniaxial compression tests ( $K_0$ -consolidation) in place of isotropic compression tests. However, it becomes much more complicated if a model requires results from shear tests that cannot be performed in a triaxial apparatus, because more advanced equipment is seldom available for soil testing. On the other hand, results from simpler shearing tests such as those performed in a direct shear box may not be appropriate for parameter determination for any but the most simple models.

The three triaxial compression tests and the isotropic compression test should be performed with the following important points in mind:

- 1) The specimens are tested with the assumption that they represent the average soil behavior at the location of the soil samples in the ground (there is no interest in the lowest ("safe") strength for the advanced analysis).
- 2) The tests are performed by simulating the conditions in the ground as closely as possible. This includes
  - a) range of stresses (due to variable, nonlinear behavior)
  - b) drainage conditions in the field (but typically drained tests are performed on sands and undrained tests are performed on clays)
  - c) density and soil fabric (undisturbed soil specimens are required in most cases)
- 3) The test performance should include primary loading as well as unloading-reloading cycles (to evaluate the elastic parameters), and all physical quantities such as loads, pressures, deformations, volume changes or pore pressures must be measured for a complete characterization of the stress-strain behavior of the soil. Every portion of the experiments is required for parameter determination.

Because the results of advanced tests such as true triaxial tests and torsion shear tests are not available on a routine basis, the constitutive model must have built-in effects of the intermediate principal stress, anisotropy, and stress rotation for which necessary parameters, if any, must come from conventional triaxial tests.

Once the parameters for a model have been determined, they do not change value during the computations, and they should apply to all types of geotechnical problems in which the soil is present. With regard to the latter point, there are two types of constitutive models in existence: For the first and most common type, samples are taken out of the ground and parameters are determined for the particular void ratio present in the soil sample. The constitutive model is then calibrated to this particular initial void ratio, and volume changes (or changes in void ratio) as well as strength can be predicted without updating the parameter values during the computations. For example, the friction angle for a sand at a given void ratio may be one of the parameter values in a model of the first type. While the friction angle for a sand is known to vary considerably with the void ratio, the value determined for the given initial void ratio (e.g. the void ratio of the soil sample recovered from the ground) is assumed to apply at failure for the sand being loaded from that initial void ratio, even though the void ratio changes during shearing. This type of model is suitable for the particular problem at hand for which the parameters have been determined and associated with the particular initial void ratio. Most geotechnical analysis procedures have been worked out for this approach. Clearly, if a different initial void ratio is present in the soil sample, then another set of parameter values is obtained, including that for the friction angle.

For the second type of constitutive model, the parameters are not associated with any particular initial void ratio. These parameters may be used to calculate changes due to variation in void ratio during loading, and this type of model does not change parameter values with initial void ratio. While such a model may seem advantageous, only relatively simple models have been devised with these attributes. Examples of this type of model are the Critical State models such as the Modified Cam Clay Model and the Nor-Sand model.

### What is the Physical Significance of the Parameters?

Advanced models may contain parameters that are not immediately recognizable or do not have immediate physical meaning. These parameters may be constants in mathematical expressions that describe, e.g., the curved three-dimensional failure envelope expressed in terms of stress invariants. The friction angle, which decreases with increasing normal stress, a phenomenon that is well known in geotechnical engineering, is not directly recognizable in such equations. Nevertheless, the parameters express the same phenomenon, namely that the shear strength increases almost (but not quite) linearly with the normal stress. Thus, equations used in advanced constitutive models to express phenomena such as the curvature of failure envelopes, dependence on the third stress invariant, and volume dilation may contain parameters whose physical meaning are not immediately recognizable in a similar manner as the familiar Young's modulus, Poisson's ratio, friction angle, and

cohesion. Such parameters are in all cases simply curve-fitting parameters whose usefulness is similar to the well-known parameters.

The Single Hardening Model (Kim and Lade 1988, Lade and Kim 1988a and b) is an elasto-plastic constitutive model that includes the various necessary components typical of these types of models, as indicated in Table 1. The function of each component and their physical significance are described in this table (where possible). The parameters occurring in the Single Hardening Model are employed to characterize these components, as shown in Table 2, and while the components have functions and physical significance in the overall model, it may not be possible to assign physical significance to each individual parameter. Rather, these parameters are curve-fitting parameters.

### Number of Model Parameters

The number of parameters in a model is often mentioned as a consideration and a concern in relation to employment of this model. But should it really be a concern, or are there other considerations that are more important for employment of advanced constitutive models? To answer this question, three analyses methods are discussed in view of the number of parameters involved, their role in the models, and the capabilities of the methods.

Parameters are listed in Table 2 for the simple analysis approach (SA) described above in which a stability analysis is followed by a deformation or settlement analysis. The parameters used in the Modified Cam Clay (MCC) model are also listed, since this model is well known to geotechnical engineers. Finally, Table 2 contains the parameters employed in the Single Hardening (SH) model.

For the SA approach, the elastic properties are represented by one value of Poisson's ratio,  $\nu$ , and one value of Young's modulus,  $E$ . Similarly, the MCC model involves two constant, elastic parameters,  $\kappa$  and  $G$ , such that the elastic bulk modulus,  $K = p'/\kappa$ , i.e.  $K (= E/[3(1-2\nu)])$  is proportional with the mean normal stress  $p'$ , and the shear modulus  $G (= E/[2(1+\nu)])$  is constant. In the SH model, Poisson's ratio is constant, and Young's modulus increases linearly with the modulus number  $M$ , and it increases according to a power function that contains the stress state to the power  $\lambda$ .

Failure is described by the well-known parameters  $c$  and  $\phi$  in the SA approach, while the MCC model involves the parameter  $M$  that indicates the straight-line critical state ( $=$  failure for normally consolidated clay). The MCC model does not involve effective cohesion (or tensile strength) unless another parameter is added. The SH model includes a curved failure surface for which  $\eta_1$  indicates the opening angle (similar to the friction angle),  $m$  is the curvature parameter, and the parameter "a" characterizes the effective cohesion (or the tensile strength). For sand  $a = 0$ , i.e. one less parameter than indicated in Table 2.

In the MCC model  $\Gamma$  indicates the void ratio for which the critical state line passes through  $p' = 1$ , and  $\lambda$  relates to the slope of the compressibility line and the critical state line (which is parallel to the compressibility line) on an  $e-\ln(p')$  diagram. These two parameters are used to calculate the magnitude of the plastic strain increments. In the SH model the magnitude of the plastic strain increments are controlled by the

**TABLE 1. Components and Their Physical Significance in Elasto-Plastic Models.**

	<b>Component</b>	<b>Function</b>
Elastic Behavior	Hooke's Law	Produces elastic strains whenever the stresses change
Plastic Behavior	Failure Criterion	Imposes limits on stress states that can be reached
	Plastic Potential Function	Produces <u>relative magnitudes</u> of plastic strain increments (similar function as Poisson's ratio for elastic strains)
	Yield Criterion	Determines when plastic strain increments occur: Only when yield surface is pushed out/in (hardening/softening)
	Hardening/Softening Relation	Determines magnitudes of plastic strain increments (similar function as Young's modulus for elastic strains)

**TABLE 2. Components and Number of Parameters in Elasto-Plastic Models.**

<b>Component</b>	Parameters for Simple Elastic-Perfectly Plastic Approach	Parameters for Modified Cam Clay Model	Parameters for Single Hardening Model
Hooke's Law	$\nu, E$	$\kappa, G$	$\nu, M, \lambda$
Failure Criterion	$c, \phi$	$M$	$\eta_1, m, a$
Plastic Potential Function		-	$\mu, \psi_2$
Yield Criterion		-	$h, \alpha$
Hardening/Softening Relation		$\Gamma, \lambda$	$C, p$

parameters  $C$  and  $p$ , which are both curve-fitting parameters used in a power function relating plastic work to the state of stress. Thus,  $C$  and  $p$  serve the same purpose in the SH model as  $\Gamma$  and  $\lambda$  in the MCC model.

Four more parameters are present in the SH model. Two of these,  $h$  and  $\alpha$ , are used to describe the shape of the yield surface in three dimensions. In the MCC model, this is done by the value of  $M$ , which therefore controls failure as well as the shape of the yield surface. While this is very practical and reduces the number of parameters, it does not provide the same flexibility in the MCC model as found in the SH model.

Finally, two parameters,  $\mu$  and  $\psi_2$ , are used in the SH model to describe the plastic potential, which is different from the yield surface, thus providing for non-associated plastic flow, as found from experiments on real soils. Associated plastic flow is assumed in the MCC model, i.e. the yield surface acts as the plastic potential, and no additional parameters are therefore required in this model.

If these three analysis procedures and models are evaluated on an equal basis, then for soils without effective cohesion, the SA approach involves 3 parameters (for  $c = 0$ ), the MCC model requires 5 parameters, and the SH model requires 11 parameter values (for  $a = 0$ ). However, the SA approach clearly has its shortcomings in analysis capabilities as described in a previous section, while the MCC model primarily works for "well-behaved, insensitive" clays. Analyses performed with the SA and the MCC procedures do not provide the flexibilities presented by the SH model, which works equally well for sand and clay, involves non-associated plastic flow, models 3D failure correctly, and can handle contractive as well as dilative volume changes for soils in the normally consolidated range. The SH model has also been shown to work well for materials with effective cohesion such as cemented soils, concrete, and rock (for which  $a \neq 0$ ).

Thus, models with larger number of parameters are typically more versatile and provide more flexibility than models with fewer parameters. In addition, determination of parameters for a given model does really not represent the greatest limitation on the use of the model, because the parameter values can typically be found by computer programs or by some computer program-assisted method.

The real limitation in the employment of advanced analysis methods lies in the expense for performing the required experiments. Although the isotropic compression and the triaxial compression tests are relatively simple to perform, they most often require undisturbed samples as well as a laboratory with the necessary equipment and know-how to perform these tests. Determination of parameters represents a small effort compared to the effort and expense involved in obtaining the experimental results.

## OVERVIEW AND EVALUATION OF CONSTITUTIVE MODELS

To compare many of the well-known models available today, their attributes are listed and compared in tabular form, and an evaluation of the models is attempted. Several models occur in many different versions in the literature. To the extent possible, a representative version has been used for comparison with the other models. No discussion is presented in connection with the comparison of the models.



Tables 3-6 contain the models divided into different groups with similar frameworks and each model is given a name, usually the name under which they are generally known. However, many models could fit under different frameworks, because they include approaches and/or components from different frameworks. Key references to the literature where each model has been presented first or in which it has been explained particularly well are also given. The types of soil for which the model has been developed and shown to work are listed along with the key attributes such as the shapes of the failure, yield, and plastic potential surfaces as well as the hardening parameter(s) employed.

The capabilities of each model (as well as they could be discerned from the publications) are given along with the experiments required for calibration of the model parameters. In particular, it has been noted whether difficult, non-standard experiments are required for calibration. Here it has been assumed that conventional triaxial compression tests, isotropic compression tests, and conventional  $K_0$ -compression tests (conventional oedometer tests) can be performed on a routine basis. However, experiments such as  $K_0$ -compression tests with measurements of lateral stresses and triaxial extension tests as well as other experiments usually performed for purposes of research are considered here to be relatively complex and beyond conventional testing expertise.

Finally, the tables contain the number of parameters required in each model (although this should not be of primary concern, as discussed above) along with an overall evaluation of the model.

The evaluations listed in the tables are given with the intent of providing some guidance towards realistic, practically useful, and applicable constitutive models for soils. In this evaluation it has been kept in mind that “a model should be as simple as possible, but not simpler.” Thus, included in the tables are some of the early, simple models along with the most advanced models available today. Several models are “experimental” in nature, and some of them are still under development. Thus, the evaluation, which aims to indicate practically useful models, reflects these conditions.

Only three categories are used in the evaluation. These categories and the conditions for a model to fit in each of these categories are summarized as follows:

Category 1: Model includes (1) theoretically sound framework that is (2) sufficiently transparent and accessible to anticipate and evaluate the model performance; (3) model includes effects of confining pressure, (4) model can handle 3D conditions; (5) it is straight forward to find the parameters; (6) these may be determined from conventional experiments (difficulty not beyond conventional triaxial compression tests, isotropic compression tests and  $K_0$ -compression tests (conventional oedometer tests)); and (7) the model exhibits an overall high quality of fit with the observed behavior. Note that each model is only applicable as indicated in the other columns, but within these limitations it performs well.

Category 2: Model lacks one or more of the conditions mentioned above.

Category 3: Model is deficient in several of the conditions mentioned above.

**TABLE 3(a). Constitutive Models, Their Attributes and Their Capabilities.**

Type of Model	Model	References	Types of Soil	Failure Surface	Curved Failure Surface in Triaxial Plane?	Yield Surface	Plastic Potential: Associated or Nonassociated?	Hardening Parameter
Elastic	Hooke's Law	Textbook	Yes Sand Clay Cemented Soil	Yes Yes Yes	NA Mohr-Coulomb Extended von Mises	NA NA No = Failure surface	NA NA Associated = Failure surface	NA NA None
	Hyperbolic	Duncan and Chang (1970)	Yes	Yes	Mohr-Coulomb Yes, see Duncan et al. (1980)	NA	NA	NA
	Drucker-Prager	Drucker and Prager (1952)	Yes	Yes	Extended von Mises	No	Associated	None
	Drucker's Cap	Drucker et al. (1957)	Yes	Yes	Extended von Mises	No Spherical Cap	Associated	Plastic Work
	Stress-Dilatancy	Rowe (1962)	Yes	No	Mohr-Coulomb +Dilation Effect	Yes Mohr-Coulomb	Nonassociated = Failure Surface	NA
	Mohr-Coulomb	Smith & Griffitts (1982) Brinkgreve and Vermeer (1997)	Yes	Yes	Mohr-Coulomb Curved Extended von Mises	No Elliptical Cap	Nonassociated Associated	None
	DiMaggio-Sandler	Dimaggio and Sandler (1971) Sandler et al. (1976)	Yes	Yes	Mohr-Coulomb	No Elliptical Cap	Plastic Volumetric Strain	
	PLAXIS Soft Soil	Brinkgreve and Vermeer (1997)	No	Yes	Mohr-Coulomb	No Smooth Triangular, Conical	Plastic Shear & Vol. Strain	
	Lade and Duncan	Lade and Duncan (1975)	Yes	Yes	No	Smooth Triangular, Conical	Nonassociated	Plastic Work
	Simple Elastic Plastic							

**TABLE 3(b). Constitutive Models, Their Attributes and Their Capabilities.**

Model	Does Model Predict/Include	Drained Softening	Large Stress Reversals	Cyclic Loading	Realistic Pore Pressures	Realistic 3D Behavior	Experiments for Parameter Determination	Difficult, Non-Standard Experiments Required	Number of Parameters	Model Category
Hooke's Law	No	No	No	No	No	Yes, away from Failure	Any Comp. Test	No	2	3
Hyperbolic	No	No	No	No	No	Yes, away from Failure	3 Triax. Comp.	No	7	3
Drucker-Prager	No	No	No	No	No	No	Triax. Comp.	No	4	3
Drucker's Cap	No	No	No	No	No	No	Triax. Comp.	No	NA	3
Stress-Dilatancy	Yes	No	No	No	No	No, works only for Discrete Conditions	Triax. Comp., Pl. Strain Comp., or Triax. Ext.	Yes	NA	3
Mohr-Coulomb	No	No	No	No	No	No	3 Triax. Comp.	No	5	2
DiMaggio-Sandler	No	No	No	No	No	No	3 Triax. Comp., 1 Iso. Comp.	No	10	2
PLAXIS Soft Soil	No	No	No	No	Yes		3 Triax. Comp.	No	7	2
Lade and Duncan	No	No	No	No	Yes		3 Triax. Comp.	No	9	2

**TABLE 4(a). Constitutive Models, Their Attributes and Their Capabilities.**

Type of Model	Model	References	Types of Soil			Failure Surface	Curved Failure Surface in Triax. Plane?	Yield Surface	Plastic Potential: Associated or Nonassociated?	Hardening Parameter
			Sand	Clay	Cemented Soil					
Modified Cam Clay	Roscoe and Burland (1968)	No	Yes	No	Extended von Mises	No	Elliptical Cap	Associated	Plastic Volumetric Strain	
Elasto-Viscoplastic	Adachi and Oka (1982)	No	Yes	No	Smooth Triangular, Conical	No	Bullet-shaped (Orig. Cam Clay)	Associated	Plastic Volumetric Strain	
Structured Cam Clay	Liu and Carter (2002)	No	Yes	No	Extended von Mises	No	Elliptical Cap	Associated	Plastic Volumetric Strain	
Anisotropic Cam Clay	Sekiguchi and Ohta (1977)	No	Yes	No	Extended von Mises	No	Bullet-shaped (Orig. Cam Clay)	Associated	Plastic Volumetric Strain	
Anisotropic Plasticity	Dafalias et al. (2003)	No	Yes	No	Rotated, Extended von Mises	No	Distorted Ellipse	Nonassociated	Plastic Vol. & Shear Strain	
Nor-Sand	Jefferies (1993)	Yes	Yes	No	Smooth Triangular, Conical	No	Bullet-shaped (Orig. Cam Clay)	Associated	Plastic Work	
Unified SMP	Matsuoka et al. (1999)	Yes	Yes	No	Smooth Triangular, Conical	No	Modified Elliptical Cap	Associated	Product of Stress Funct. & Plastic Vol. Strain	
$t_{ij}$ -Concept	Nakai and Matsuoka (1986) Nakai (1989)	Yes	Yes	No	Smooth Triangular, Conical	No	Modified Bullet-shape (Mod. Orig. Cam Clay)	Associated in $t_{ij}$ -Space (Nonassoc.)	Plast. Vol. "Plastic Work" in $t_{ij}$ Space (sand)	

**TABLE 4(b). Constitutive Models, Their Attributes and Their Capabilities.**

Model	Does Model Predict/Include				Experiments for Parameter Determination	Difficult, Non-Standard Experiments Required	Number of Parameters	Model Category
	Drained Softening	Large Stress Reversals	Cyclic Loading	Realistic Pore Pressures				
Modified Cam Clay	Yes, for OC clay	No	No	Yes	No	3 Triax. Comp. & 1 Iso. Comp.	5	2
Elasto-Viscoplastic	Yes, for OC clay	No	No	Yes	Yes	3 Triax. Comp. & 1 Iso. Comp.	10	1
Structured Cam Clay	Yes, for OC clay	No	No	Yes	No	3 Triax. Comp. & 1 Iso./K <sub>0</sub> Comp.	10	2
Anisotropic Cam Clay	Yes, for OC clay	No	No	Yes	Yes	3 Triax. Comp. & 1 Iso. Comp.	6	2
Anisotropic Plasticity	Yes, for OC clay	No	No	Yes	No	3 CU Triax. Comp. & Ext. & 1 Iso./K <sub>0</sub> -Comp. with Meas. Lateral Stress	8	2
Nor-Sand	Yes, for OC soil	No	Yes, Undrained	Yes	Yes	2 CD Triax. Comp. & 2 CU Triax. Comp. with Iso. Comp.	7	1
Unified SMP	Yes, for OC soil	No	No	Yes	Yes	1 Triax. Comp. & 1 Iso. Comp.	5	2
t <sub>f</sub> -Concept	Yes, for OC soil	No	No	Yes	Yes	1 Triax. Comp. & 1 Iso. Comp.	5 (clay) 6 (sand)	2

**TABLE 5(a). Constitutive Models, Their Attributes and Their Capabilities.**

Type of Model	Model	References	Types of Soil	Failure Surface	Curved Failure Surface in Triax. Plane?	Yield Surface	Plastic Potential: Associated or Nonassociated?	Hardening Parameter
		Sand	Clay	Cemented Soil				
Hypoplastic	Darve	Darve (1982)	Yes	Yes	Yes	Mohr-Coulomb	No	NA
Hypoplastic	Kolymbas (1991) Gudehus (1996) Bauer (1996)	Yes	No	No	Smooth Triangular, Conical	No	NA	NA
Nondeformable Micromechanics Nonlinear	Iwan (1967) Mroz (1967) Prevost (1978)	Yes	Yes	Yes	Rotated, Extended von Mises	No	Rotating, Extended von Mises	Associated
Nested Surfaces	Klisinski et al. (1987) Klisinski (1988)	Yes	Yes	Yes	Smooth Triangular, Conical	No	Smooth	Plastic Vol. &/or Shear Strain
Fuzzy Set Plasticity	Lade (1977)	Yes	Yes	No	Smooth Triangular, Conical	Yes	Nonassociated and Associated	Plastic Work
Multiple Surfaces	Brinkgreve and Vermeer (1997)	Yes	Yes	Yes	Mohr-Coulomb	No	Smooth Triangular, Conical & Oct. Plane	Nonassociated and Associated
Double Hardening	PLAXIS Hardening						Smooth Triangular, Conical & Spher. Cap	Plastic Work
MONOT	Molenkamp (1981) Griffiths et al. (1982) Hicks (2003)	Yes	Yes	Yes	Smooth Triangular, Conical	Yes	Smooth Triangular, Conical & Spher. Cap	Plastic Vol. & Shear Strain

@Seismicisolation

**TABLE 5(b). Constitutive Models, Their Attributes and Their Capabilities.**

Model	Does Model Predict/Include					Experiments for Parameter Determination	Difficult, Non-Standard Experiments Required?	Number of Parameters	Model Category
	Drained Softening	Large Stress Reversals	Cyclic Loading	Realistic Pore Pressures	Realistic 3D Behavior				
Darve	No	Yes	Yes	No	No	Triax. Comp. & Ext., Cyclic Tests	Yes, Depends on Conditions to be Modeled	16	2
Hypoplastic	Yes	Yes	Yes	Yes	Yes	Triax. Comp. & K <sub>0</sub> -Comp.	Yes, Depends on Conditions to be Modeled	8	2
Nested Surfaces	No	Yes	Yes	Yes	No	Iso. & Triax. Comp. & Ext., Cyclic Tests	Yes, Depends on Conditions to be Modeled	Many Discrete Values (Prevost 1979)	2
Fuzzy Set Plasticity	Yes	Yes	Yes	Yes	Yes	Triax. Comp. & Iso. Comp.	Yes, Depends on Conditions to be Modeled	13-20	2
Lade	Yes	No	No	Yes	Yes	3 Triax. Comp. & 1 Iso-Comp.	No	14	1
PLAXIS Hardening	No	No	No	Yes	Yes	3 Triax. Comp. & 1 Iso-Comp	No	11	2
MONOT	No	Yes	Yes	Yes	Yes	3 Triax. Comp. & 1 Iso-Comp	No	21	1

**TABLE 6(a). Constitutive Models, Their Attributes and Their Capabilities.**

Type of Model	Model	Reference(s)	Types of Soil			Failure Surface	Curved Failure Surface in Triaxial Plane?	Yield Surface	Plastic Potential: Associated or Nonassociated?	Hardening Parameter
			Sand	Clay	Cemented Soil					
Dafalias	Dafalias et al. (1982) Kaliakin and Dafalias (1989)	No Yes	No Yes	No Yes	Smooth Triangular, Conical	No	Elliptical Cap	Associated	Plastic Volumetric Strain	
MIT-E3	Whittle (1993) Ganendra and Potts (1995)	No Yes	No Yes	No Yes	Rotated, Extended von Mises	No	Rotated, Elliptical Cap	Nonassociated	Plastic Volumetric Strain	
MIT-S1	Pestana and Whittle (1999) Pestana et al. (2002a) Pestana et al (2002b)	Yes	Yes	No	Smooth Triangular, Conical	No	Distorted Lemniscate	Nonassociated	Plastic Vol. & Shear Strain	
Single Hardening	Kim and Lade (1988) Lade and Kim (1988a) Lade and Kim (1988b)	Yes	Yes	Yes	Smooth Triangular, Conical	Yes	Tear-Drop Shaped	Nonassociated	Plastic Work	
Sinfonietta Classica	Nova (1988) Nova et al. (2003)	Yes	Yes	Yes	Smooth Triangular, Conical	No	Tear-Drop Shaped	Nonassociated	Plastic Vol. & Shear Strain	
Disturbed State Concept/ Hierarchical Generalized Plasticity	Desai et al. (1986) Desai (2001) Pastor et al. (1990) Ling and Liu (2003)	Yes	Yes	Yes	Smooth Triangular, Conical	No	Tear-Drop Shaped	Associated or Nonassociated	Plastic Vol. & Shear Strain	

@Seismicisolation

**TABLE 6(b). Constitutive Models, Their Attributes and Their Capabilities.**

Model	Does Model Predict/Include						Experiments for Parameter Determination	Difficult, Non-Standard Experiments Required	Number of Parameters	Model Category
	Drained Softening	Large Stress Reversals	Cyclic Loading	Realistic Pore Pressures	Realistic 3D Behavior	Realistic 3D Behavior				
Dafalias	Yes, for OC clay	Yes	Yes	Yes	Yes	Yes	3 CU Triax. Comp. 3 CU Triax. Ext. 1 Iso/K <sub>0</sub> -Comp.	Yes	12	2
MIT-E3	Yes, for OC clay	Yes	Yes	Yes	Yes	Yes	2 CK <sub>0</sub> U Triax. Comp. 1 CK <sub>0</sub> U Triax. Ext. 1 CD Triax. Comp. K <sub>0</sub> -Comp.	Yes	15	2
MIT-S1	Yes	Yes	Yes	Yes	Yes	Yes	CU Triax. Comp. (Iso/K <sub>0</sub> ) CD Triax. Comp. (Iso/K <sub>0</sub> ) Iso/K <sub>0</sub> -Comp.	Yes	13	2
Single Hardening	Yes, see: Lade and Ingr Ingr and Lade (1997)	Yes	Yes	Yes	Yes	Yes	K <sub>0</sub> -Comp. with Meas. Lateral stresses Resonant Column/Bender Element	No	12	1
Sinfonieta Classica	No	No	No	Yes	Yes	Yes	3 Triax. Comp. & 1 Iso. Comp.	No	17	1
Disturbed State Concept/ Hierarchical Generalized Plasticity	Yes	No	No	Yes	Yes, requires 3D Tests	Yes	3 Triax. Comp. & 1 Iso. Comp.	Yes	15	1

The early models were developed at the time when only the simplest, classical 3D failure criteria were available, experimental results of 3D tests had not been performed, concepts in hardening plasticity were still being formulated, and conditions for plastic yielding were not yet fully discovered. These models appear in category 3. The models in category 1 fulfill all the points listed above, while those in category 2 are clearly missing one or more of the important qualities given above.

It should be noted that some of the most advanced and capable models have been placed in category 2, because they require difficult, non-standard experiments for calibration. However, if performance of such experiments is not considered to be a impediment to employment of such models, then the models clearly belong in category 1.

The writer is responsible for placement of each model within one of the three categories, and he apologizes for errors to the extent that misunderstandings have resulted in incorrect evaluation of the models.

## SUMMARY

Presented here is a short review of many of the considerations involved in decisions to use advanced methods in analyses and design of geotechnical structures. This includes the requirements of the models, and why the models have been developed in terms of elasticity and hardening plasticity theories. An attempt has been made to answer some of the frequently asked questions regarding the use of constitutive models in advanced numerical analyses. Tables are presented with comparison of the main characteristic features and components of existing, widely available constitutive models. Key references are given to publications in which the models are first presented or particularly well explained. The requirements of the models in terms of experimental data for calibration are presented and compared in tables, and the capabilities of the models are reviewed. To provide some guidance in selecting realistic, practically useful, and applicable constitutive models for soils to employ in advanced numerical analyses, each model has been placed in one of three categories, the conditions for which are clearly stated.

## Acknowledgment

The writer has benefited from countless invaluable discussions with Dr. Jerry A. Yamamuro over many years regarding experimental techniques, soil behavior, and constitutive modeling. Much appreciation is expressed for the assistance extended in connection with producing the present article.

## REFERENCES

- Adachi, T., and Oka, F. (1982) "Constitutive equation for normally consolidated clays based on elasto-viscoplasticity," *Soils and Foundations*, 22: 57-70.
- Bauer, E. (1996) "Calibration of a comprehensive hypoplastic model for granular materials," *Soils and Foundations*, 36(1), 13-26.
- Brinkgreve, R.B.J., and Vermeer, P.A. (1997) "PLAXIS finite element code for soil and rock analysis – Version 7," Balkema, Rotterdam.

- Dafalias, Y.F., Herrmann, L.R., and DeNatale, J.S. (1982) "The bounding surface plasticity model for isotropic cohesive soils and its application at the Grenoble Workshop," *Proc. Int. Workshop on Constitutive Relations for Soils*, Grenoble, 273-287.
- Dafalias, Y.F., Papadimitriou, A.G., and Manzari, M.T. (2003) "Simple anisotropic plasticity model for soft clays," *Proc. Int. Workshop on Geotechnics of Soft Clays: Theory and Practice*, P.A. Vermeer et al. (eds.), 189-195.
- Darve, F. (1982) "An incrementally non-linear constitutive law: Assumptions and predictions," *Proc. Int. Workshop on Constitutive Relations for Soils*, Grenoble, 385-403.
- Desai, C.S. (2001) *Mechanics of Materials and Interfaces: The Disturbed State Concept*, CRC Press, Boca Raton, FL, USA.
- Desai, C.S., Somasundaram, S., and Frantziskonis, G. (1986) "A hierachial approach for constitutive modeling of geologic materials," *Int. J. Numer. Anal. Meth. Geomech.*, 10(3), 225-257.
- DiMaggio, F.L., and Sandler, I.S. (1971) "Material Model for Granular Soils," *J. Engr. Mech. Div.*, ASCE, 97(EM3), 935-950.
- Drucker, D.C., and Prager, W. (1952) "Soil Mechanics and Plastic Analysis or Limit Design," *Quart. Appl. Math.*, 10(2), 157-165.
- Drucker, D.C., Gibson, R.E., and Henkel, D.J. (1957) "Soil Mechanics and Work-Hardening Theories of Plasticity," *J. Soil Mech. Found. Engr. Div.*, ASCE, 122, 338-346.
- Duncan, J.M. (1994) "The Role of Advanced Constitutive Relations in Practical Applications," *Proc. 13<sup>th</sup> Int. Conf. Soil Mech. Found. Engr.*, New Delhi, India, 5, 31-48.
- Duncan, J.M., and Chang, C.Y. (1970) "Non-linear analysis of stress and strain in soils," *J. Soil Mech. Founds Div.*, ASCE, 96(SM5) 1629-1653.
- Duncan, J.M., Byrne, P., Wong, K.S., Mabry, P. (1980) "Strength, Stress-Strain and Bulk Modulus Parameters for Finete Element Analyses of Stresses and Movements in Soil Masses," *Report No. UCB/GT/80-01*, University of California, Berkeley, 77 pages.
- Ganendra, D, and Potts, D.M. (1995) Discussion of 'Evaluation of constitutive model for overconsolidated clays,' by A.J. Whittle, *Geotechnique*, 45(1), 169-173.
- Griffiths, D.V., Smith, I.M., and Molenkamp, F. (1982) "Computer implementation of a double-hardening model for sand," *Proc. IUTAM Conf. on Deformation and Failure of Granular Materials*, Delft, 213-221.
- Gudehus, G. (1996) "A comprehensive constitutive equation for granular materials," *Soils and Foundations*, 36(1), 1-12.
- Hicks, M.A. (1995) "MONICA – a computer algorithm for solving boundary value problems using the double hardening constitutive law MONOT: I. Algorithm development" *Int. J. Num. Anal. Meth. Geomech.* 19: 1-27.
- Hicks, M.A. (2003) "Experience in calibrating the double-hardening constitutive model Monot," *Int. J. Numer. Analyt. Meth. Geomech.*, 27(13), 1123-1151.

- Inel, S., and Lade, P.V. (1997) "Rotational Kinematic Hardening Model for Sand, Part II. Characteristic Work Hardening Law and Predictions," *Computers and Geotechnics*, Elsevier, 21(3), 217-234.
- Iwan, W.D. (1967) "On a Class of Models for the Yielding Behavior of Continuous and Composite Systems," *J. Appl. Mech., Trans. ASME*, 34(E3) 612-617.
- Jefferies, M.G. (1993) "Nor-Sand: a simple critical state model for sand," *Geotechnique*, 43(1), 91-103.
- Kaliakin, V.N. and Dafalias, Y.F. (1989) "Simplifications to the bounding surface model for cohesive soils," *Int. J. Numer. Analyt. Meth. Geomech.*, 13, 91-100.
- Kim, M.K., and Lade, P.V. (1988) "Single Hardening Constitutive Model for Frictional Materials, I. Plastic Potential Function", *Computers and Geotechnics*, 5(4), 307-324.
- Klisinski, M. (1988) "Plasticity theory based on fuzzy sets," *J. Engr. Mech., ASCE*, 114(4), 563-582.
- Klisinski, M., Alawi, M.M., Sture, S., Ko, H.-Y., and Muir Wood, D. (1987) "Elasto-plastic model for sand based on fuzzy sets," *Proc. Int. Workshop on Constitutive Equations for Granular Non-Cohesive Soils*, A. Saada and G. Bianchini (eds.), Case Western Reserve University, Cleveland, 325-347.
- Kolymbas, D. (1991) "Computer-aided design of constitutive models, *Int. J. Numer. Analyt. Meth. Geomech.* 15, 593-604.
- Lade, P.V., (1977) "Elasto-Plastic Stress-Strain Theory for Cohesionless Soil with Curved Yield Surfaces," *Int. J. Solids Structures*, 13, 1019-1035.
- Lade, P.V., and de Boer, R. (1997) "The concept of effective stress for soil, concrete and rock," *Geotechnique*, 47(1), 61-78.
- Lade, P.V., and Duncan, J.M. (1975) "Elastoplastic Stress-Strain Theory for Cohesionless Soil," *J. Geotech. Engr. Div., ASCE*, 101(GT10), 1037-1053.
- Lade, P.V., and Inel, S. (1997) "Rotational Kinematic Hardening Model for Sand, Part I. Concept of Rotating Yield and Plastic Potential Surfaces," *Computers and Geotechnics*, Elsevier, 21(3), 183-216.
- Lade, P.V., and Kim, M.K. (1988a) "Single Hardening Constitutive Model for Frictional Materials, II. Yield Criterion and Plastic Work Contours", *Computers and Geotechnics*, 6(1), 13-29.
- Lade, P.V., and Kim, M.K. (1988b) "Single Hardening Constitutive Model for Frictional Materials, III. Comparisons with Experimental Data", *Computers and Geotechnics*, 6(1), 31-47.
- Lambe, T.W., and Whitman, R.V. (1969) "Soil Mechanics," John Wiley & Sons, New York.
- Ling, H.I., and Liu, H. (2003) "Pressure-level dependency and densification behavior of sand through a generalized plasticity model," *J. Engr. Mech., ASCE*, 129(8), 851-860.
- Liu, M.D., and Carter, J.P. (2002) "Structured Cam Clay Model," *Can. Geotech. J.*, 39(6), 1313-1332.
- Matsuoka, H. and Nakai, T. (1974) "Stress-deformation and strength characteristics of soil under three different principal stresses," *Proc. JSCE*, 232, 59-70.

- Matsuoka, H., Yao, Y.P., and Sun, D.A. (1999) "The Cam-clay models revised by the SMP criterion," *Soils and Foundations*, 39(1), 81-95.
- Molenkamp, F. (1981) Elasto-plastic double hardening model MONOT," *LGM Report CO-218595*, Delft Soil Mechanics Laboratory.
- Mroz, Z. (1967) "On the Description of Anisotropic Work Hardening," *J. Mech. Phys. Solids*, 15, 163-175.
- Nakai, T. (1989) "An isotropic hardening elastoplastic model for sand considering the stress path dependency in three-dimensional stresses," *Soils and Foundations*, 29(1), 119-137.
- Nakai, T., and Matsuoka, H. (1986) "A generalized elastoplastic constitutive model for clay in three-dimensional stresses," *Soils and Foundations*, 26(3), 81-98.
- Nova, R. (1988) "Sinfonietta classica: an exercise on classical soil modeling," *Proc. Symp. Constitutive Equations for Granular Non-Cohesive Soils*, Cleveland, A. Saada & G. Bianchini, (eds.), Balkema, Rotterdam, 501-519.
- Nova, R., Castellanza, R., and Tamagnini, C. (2003) "A constitutive model for bonded geomaterials subject to mechanical and/or chemical degradation," *Int. J. Num. Anal. Meth. Geomech.* 27(9), 705-732.
- Pastor, M., Zienkiewicz, O.C., and Chan, A.H.C. (1990) "Generalized plasticity and the modeling of soil behavior," *Int. J. Numer. Analyt. Meth. Geomech.*, 14(3), 151-190.
- Pestana, J.M., and Whittle, A.J. (1999) "Formulation of a unified constitutive model for clays and sands," *Int. J. Numer. Analyt. Meth. Geomech.*, 23(12), 1215-1243.
- Pestana, J.M., Whittle, A.J., and Salvati, L.A. (2002) "Evaluation of a constitutive model for clays and sands: Part I – sand behaviour," *Int. J. Numer. Analyt. Meth. Geomech.*, 26(11), 1097-1121.
- Pestana, J.M., Whittle, A.J., and Gens, A. (2002) "Evaluation of a constitutive model for clays and sands: Part II – clay behaviour," *Int. J. Numer. Analyt. Meth. Geomech.*, 26(11), 1123-1146.
- Prevost, J.H. (1978) "Plasticity Theory for Soil Stress-Strain Behavior," *J. Engr. Mech. Div.*, ASCE, 104(EM5), 1177-1194.
- Prevost, J.H. (1979) "Mathematical modeling of soil stress-strain-strength behavior," *Proc. Third Int. Conf. Numerical Methods in Geomechanics*, 1, 347-361.
- Roscoe, K.H. and Burland, J.B. (1968) "On the generalized behaviour of 'wet' clay," *Engineering Plasticity*, 48: 535-609.
- Rowe, P.W. (1962) "The stress-dilatancy relation for static equilibrium of an assembly of particles in contact," *Proceedings of the Royal Society*, 269, 500-527.
- Sandler, I.S., DiMaggio, F.L., and Baladi, G.Y. (1976) "Generalized Cap Model for Geologic Materials," *J. Geotech. Eng. Div.*, ASCE, 102(GT7), 683-699.
- Sekiguchi H., and Ohta, H. (1977) "Induced anisotropy and time dependency in clays," Constitutive aequations of Soils, *Proc. Specialty Session 9, Ninth Int. Conf. Soil Mech. Found. Engr.*, Tokyo, 1: 229-238.
- Smith, I.M., and Griffiths, D.V. (1982) *Programming the finite element method – Second edition*, John Wiley & Sons.

- Terzaghi, K. (1923) "Die Berechnung der Durchlässigkeitssiffer des Tones aus dem Verlauf der Hydrodynamischen Spannungsscheinungen," *Sitzungber. Akad. Wiss. Wien*, 132, 125-138.
- Whittle, A.J. (1993) "Evaluation of a constitutive model for overconsolidated clays," *Geotechnique*, 43(2), 289-313.
- Wood, D.M. (1990) "*Soil Behaviour and Critical State Soil Mechanics*," Cambridge University Press.

## **ANISOFT - CONSTITUTIVE MODEL FOR UNDRAINED LOADING OF ANISOTROPIC AND STRAIN-SOFTENING CLAY**

Lars Andresen<sup>1</sup> and Hans Petter Jostad<sup>2</sup>

**ABSTRACT:** An elastoplastic constitutive model is presented. The model is developed in order to study the effects of anisotropy and post-peak softening in problems of saturated clay subjected to monotonic undrained loading. The non-linear stress-strain relationship depends on the orientation of the major principal stress relative to the vertical. The model is demonstrated by simulation of an undrained simple shear deformation where the direction of the principal stresses rotates.

### **INTRODUCTION**

The stress-strain response of clay subjected to undrained loading is in general non-linear, stress path dependent (anisotropic) and displays post-peak softening. This behaviour is well recognised when the same clay is tested under undrained conditions in triaxial compression, direct simple shear and triaxial extension. Results from laboratory tests (Lacasse et al. 1985) on sensitive clay from Ellingsrud, Norway are shown in Figure 1. The maximum shear stress  $\tau$  from triaxial testing and the shear stress  $\tau_{xz}$  from the DSS testing have been normalised with the in-situ vertical effective stress  $\sigma'_{v0}$ . These light overconsolidated ( $OCR=1.4$ ) specimens were anisotropically consolidated to their in-situ effective stresses prior to undrained loading.

---

<sup>1</sup> Dr., Norwegian Geotechnical Institute, Geomechanics, P.O.Box 3930 Ullevaal Stadion, N-0806 Oslo, la@ngi.no

<sup>2</sup> Dr., Norwegian Geotechnical Institute, Geomechanics, P.O.Box 3930 Ullevaal Stadion, N-0806 Oslo, hpj@ngi.no

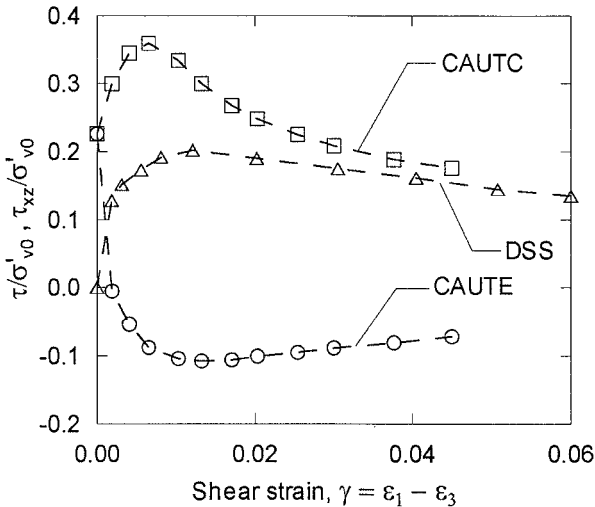


**FIG. 1. Laboratory stress-strain curves for sensitive Ellingsrud clay (Lacasse et al. 1985).** CAUTC/E - Consolidated Anisotropically Un-drained Triaxial Compression and Extension. DSS - Geonor direct simple shear.

Höeg (1972), Nayak & Zienkiewicz (1972), Sture & Ko (1976) pioneered the modelling of strain-softening material within the frame of elastoplasticity, however only isotropic softening was considered. Failure criteria for the anisotropic variation of the peak undrained shear strength have been proposed by several authors, e.g. Casagrande & Carillo (1944), Bishop (1966) and Davis & Christian (1971). The effective stress MIT-3 model (Whittle & Kavadas 1994) does simulate both anisotropic and softening behaviour of clays and utilises the criterion of Davis & Christian as the bounding surface for undrained peak strength. However, there is no simple way of controlling the stress-strain relationship by specifying the rate of softening and the residual strengths. The modified Cam Clay model (Roscoe & Burland 1968) does also account for softening for OC clays but again the degree of softening can not be controlled. Simple isotropic linear elastic-linear softening constitutive models have been used to demonstrate regularisation techniques (Brinkgreve & Vermeer 1995), (Larsson et al. 1993), softening instability and bifurcation (de Borst 1987).

Failure of a soil body involving softening material is most often governed by structural instability in the sense of Hill (1958) preceding the development of a kinematically admissible failure mechanism. Because failure of softening materials is governed by structural instability, the complete stress path dependent stress-strain relationship must be taken into account in stability problems. The anisotropy not only in peak strengths but also in pre- and post-peak stiffness affects the peak load (capacity) significantly.

A constitutive model denoted NGI-ANISOFT is presented herein which takes the aforementioned effects of clay behaviour into account. The model is developed with the objective of including effects of anisotropy and post-peak strain softening in stability analyses of sensitive clays. The main interest is of normally- or light-overconsolidated saturated clay subjected to monotonic undrained loading. Such clays are most often horizontally deposited and develop cross-anisotropy due to a preferred particle orientation and the geological stress history. Typical applications of the model could be bearing capacity, retaining wall (Andresen & Jostad 1999) and the cut-slope stability problems. Time dependent (rate) effects may also affect the structural response but is not included in the NGI-ANISOFT model. The model is formulated for plane-strain conditions.

In an accompanying paper (Jostad & Andresen 2002), the NGI-ANISOFT model is used together with a strong discontinuity regularisation of the shear-band where the localisation of deformation is modelled by interface elements. A finite element formulation with an arc-length based solution procedure (Jostad 1995) is used to trace the most critical load-displacement curve and calculate the peak-load for a bearing capacity problem.

## FORMULATION OF MODEL

The ANISOFT model is formulated in the frame of isotropic strain hardening/softening incremental elastoplasticity. The elastic strain increments during loading and unloading are given by a plane-strain generalisation of Hooke's law. The direction of plastic strain increments are given by an associated flow rule.

The undrained clay response is governed by total stresses. An effective mean stress independent yield function based on the Tresca criterion is used:

$$f(\sigma, \gamma^p) = \tau - F(\alpha, \gamma^p) \cdot \tau_p(\alpha) \dots \dots \dots (1)$$

where  $\tau = 1/2(\sigma_1 - \sigma_3)$  is the maximum shear stress,  $\tau_p(\alpha)$  is the anisotropic representation of undrained peak shear strength (Eq. 3) and  $F$  is a hardening/softening function of the principal stress orientation  $\alpha$  (Eqs. 4,5) and the hardening/softening parameter  $\gamma^p$  given in Equation 2.

A vector representation of the relevant stress and strain components is given by  $\sigma = [\sigma_{xx}, \sigma_{zz}, \tau_{xz}]^T$  and  $d\epsilon = [\epsilon_{xx}, \epsilon_{zz}, \gamma_{xz}]^T$  with the engineering strain measure  $\gamma_{xz} = 2 \cdot \epsilon_{xz}$  and where the superscript T denotes the transpose of the vector. A x-z reference with z being in the vertical direction is used.

The maximum plastic shear strain  $\gamma^p$  is used as the hardening/softening parameter,

$$\gamma^p = \int d\gamma^p = \int \sqrt{(d\epsilon^p_{xx} - d\epsilon^p_{zz})^2 + (d\gamma^p_{xz})^2} \dots \dots \dots (2)$$

where the integral is to be taken along the strain path.

The hardening/softening function  $F$  is defined by the following strength and strain characteristics:

The peak undrained shear strength .....  $\tau_p(\alpha)$

The residual undrained shear strength .....  $\tau_r(\alpha)$



The plastic maximum shear strain at peak state .....	$\gamma_p^p(\alpha)$
The plastic maximum shear strain where the residual state is reached .....	$\gamma_r^p(\alpha)$

The anisotropic variation of these characteristics are in the model represented by an interpolation function (Eq. 3) of the angle  $\alpha$ , where  $\alpha$  is the angle between the vertical ( $z$ -axis) and the major compressive principal stress  $\sigma_1$ .

$$q(\alpha) = S_0 + S_1 \cdot \cos(2\alpha) + S_2 \cdot \cos(4\alpha) \dots \dots \dots (3)$$

where the function  $q(\alpha)$  represents either  $\tau_p(\alpha)$ ,  $\gamma_p^p(\alpha)$ ,  $\tau_r(\alpha)$  or  $\gamma_r^p(\alpha)$  and

$$\begin{aligned} S_0 &= 1/4(\mu^0 + 2\mu^{45} + \mu^{90}) \\ S_1 &= 1/2(\mu^0 - \mu^{90}) \\ S_2 &= 1/4(\mu^0 - 2\mu^{45} + \mu^{90}) \end{aligned}$$

are constants with the strength or strain characteristics  $\mu^0$ ,  $\mu^{45}$ ,  $\mu^{90}$  being known values of  $\tau_p$ ,  $\gamma_p^p$ ,  $\tau_r$  and  $\gamma_r^p$  at three orientations of the principal stresses  $\alpha = 0^\circ$ ,  $45^\circ$  and  $90^\circ$ . These input parameters must be obtained from laboratory testing of the clay in question.

The hardening/softening function is given by

$$F(\alpha, \gamma^p) = F_0 + \kappa(\alpha, \gamma^p) \cdot (1 - F_0) \dots \dots \dots (4)$$

where  $F_0 = \tau_0 / \tau_p(\alpha_0)$ ,  $\tau_0$  is the initial (i.e. prior to undrained loading) maximum shear stress and  $\alpha_0$  is the initial orientation of principal stresses. An initial stress state  $\sigma_0 = [\sigma_{xx}^0, \sigma_{zz}^0, \tau_{xz}^0]^T$  (e.g. consolidation stresses) can be given as input to the model and then defines  $\tau_0$  and  $\alpha_0$ . The function  $\kappa(\alpha, \gamma^p)$  defines the hardening  $\kappa_1$ , softening  $\kappa_2$  and residual  $\kappa_3$  part of the relationship between shear stress  $\tau$  and plastic shear strain  $\gamma^p$ :

$$\begin{aligned} \kappa_1 &= 2 \cdot \frac{\sqrt{\gamma^p / \gamma_p^p}}{1 + \gamma^p / \gamma_p^p} && \text{when } \gamma^p \leq \gamma_p^p \dots \dots \dots (5) \\ \kappa_2 &= 1 - \frac{1}{2} \left( 1 - \cos \left( \pi \cdot \frac{\gamma^p - \gamma_p^p}{\gamma_r^p - \gamma_p^p} \right) \right) \left( 1 - \frac{\tau_r - F_0 \tau_p}{\tau_p - F_0 \tau_p} \right) && \text{when } \gamma_p^p < \gamma^p \leq \gamma_r^p \\ \kappa_3 &= \frac{\tau_r - F_0 \tau_p}{\tau_p - F_0 \tau_p} && \text{when } \gamma^p > \gamma_r^p \end{aligned}$$

The function  $\kappa_1$  proposed by Vermeer & de Borst (1984) is used to establish a smooth transition from the initial mobilised shear stress  $\tau_0$  to the peak maximum shear stress  $\tau_p$ . A smooth hardening curve around the peak may be important to reduce numerical difficulties in the global solution algorithm. A cosine function  $\kappa_2$  is

**@Seismicisolation**

used for the softening branch. In Figure 2 the shape of the hardening/softening function is plotted for a constant  $\alpha$  stress path. The shape of these functions generally fit laboratory data quite well, but other functions that fit laboratory data or even a discrete fitting using the laboratory points directly can be used within the same framework as the proposed model.

The anisotropic representation of the peak shear strength  $\tau_p$  is compared with experimental results for Drammen clay (Soydemir 1976) in Figure 3. The results of Soydemir is obtained by constant volume direct simple shear tests (DSS-CCV) with measurements of the radial stress and where the specimens were cut in different directions and consolidated to in-situ effective stresses prior to shearing. Results from  $K_0$  consolidated undrained triaxial compression (CK<sub>0</sub>UTC) and extension (CK<sub>0</sub>UTE) tests on the same clay are also shown. All stresses are normalised by the in-situ vertical effective stress  $\sigma'_{vo}$ . It is seen that the function (Eq. 3) representing  $\tau_p$  fits quite well to the experimental data. The same function is used also to represent the anisotropic variation of  $\tau_r$ ,  $\gamma_p^P$  and  $\gamma_r^P$ . The experimental support for this is still lacking but other interpolation functions that fits experimental data can be used within the frame presented.

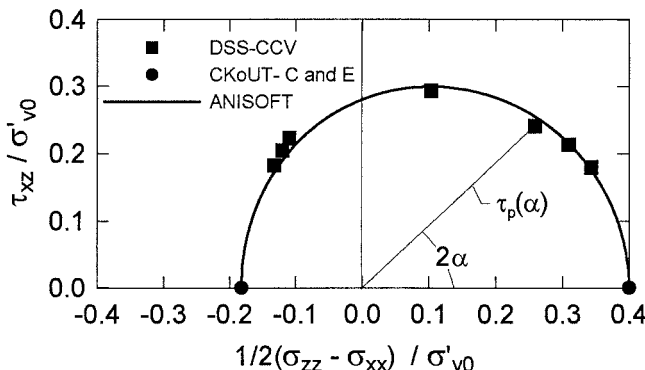


**FIG. 2. Variation of undrained peak shear strength  $\tau_p$  with orientation of principal stresses  $\alpha$  for Drammen clay (Soydemir, 1976). The peak shear strength representation of the NGI-ANISOFT model is shown by the solid line.**

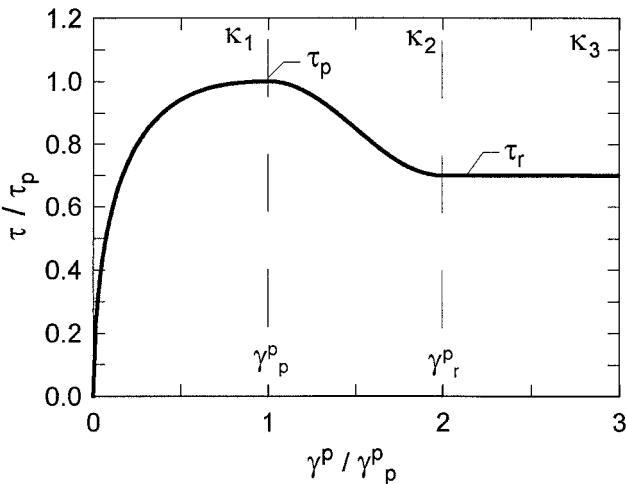


**FIG. 3. Shape of the hardening/softening curve in the NGI-ANISOFT model for  $F_0 = 0$ ,  $\alpha = \text{constant}$ ,  $\tau_r/\tau_p = 0.7$  and  $\gamma_r^p/\gamma_p^p = 2$**

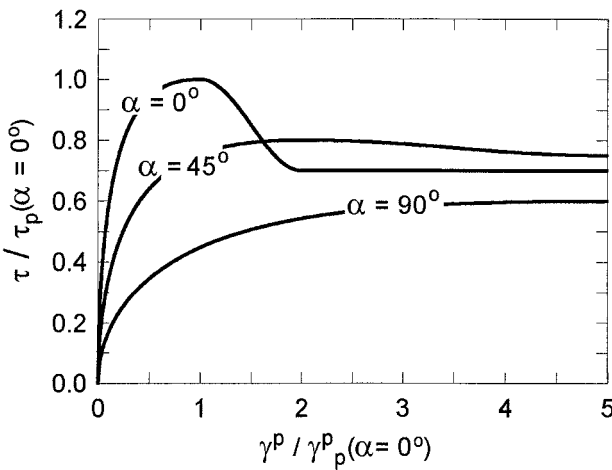


**FIG. 4. The three input hardening/softening curves of the NGI-ANISOFT model for  $\alpha = 0^\circ$ ,  $45^\circ$  and  $90^\circ$  and with  $F_0 = 0$**

The input parameters  $\mu^0$ ,  $\mu^{45}$  and  $\mu^{90}$ , the interpolation function (Eq. 3) and the hardening/softening function (Eqs. 4,5) defines the relationship between shear stress and plastic shear strain for all  $\alpha$  values. Figure 3 shows the predicted response of a normally-consolidated clay for  $\alpha = 0^\circ$ ,  $45^\circ$  and  $90^\circ$ . The input parameters have been

@Seismicisolation

normalised with the peak strength  $\tau_p^0$  for  $\alpha = 0^\circ$  and the corresponding strain  $\gamma_p^{p0}$ . The expected behaviour with highest peak strength and rate of softening in compression ( $\alpha = 0^\circ$ ) and lowest peak strength with little or no softening in extension ( $\alpha = 90^\circ$ ) is reproduced.

## THE INPUT PARAMETERS

In the general case of full anisotropy and softening a total of 13 input parameters defines the ANISOFT model.

This is the shear modulus: ..... G

and the stress - strain characteristics for  $\alpha = 0^\circ, 45^\circ, 90^\circ$ :

Peak undrained shear strengths .....	$\tau_p^0, \tau_p^{45}, \tau_p^{90}$
Residual undrained shear strengths .....	$\tau_p^0, \tau_p^{45}, \tau_p^{90}$
Peak plastic shear strains .....	$\gamma_p^{p0}, \gamma_p^{p45}, \gamma_p^{p90}$
Residual plastic shear strains.....	$\gamma_r^{p0}, \gamma_r^{p45}, \gamma_r^{p90}$

For a given clay these input parameters should be obtained by fitting the constitutive model to results from undrained laboratory shear tests. Such tests could be the triaxial or plane strain compression ( $\alpha = 0^\circ$ ) and extension ( $\alpha = 90^\circ$ ) tests and the direct simple shear (DSS) test. Specimens in these tests should be reconsolidated to the in-situ effective stresses prior to undrained loading (Berre, 1981) in order to obtain realistic parameters.

Special attention must be devoted to the interpretation of the post-peak rate of softening (i.e. the  $\gamma_r^p$  characteristic) from triaxial or plane strain compression testing. Specimens of softening clay usually displays a highly non-homogeneous post-peak deformation mode in such tests, (Read & Hegemier 1984), (Andresen & Jostad 1998). The interpretation of rate of softening must be connected to the chosen regularisation method such that the post-peak energy dissipation becomes the same in finite element simulations as in the laboratory tests, irrespective of the discretization used.

## SIMULATION OF DSS TEST

The application of the model is demonstrated by the simulation of a direct simple shear (DSS) test. It is assumed that the specimen in DSS deforms according to an ideal simple shear displacement mode in which the direction of the applied principal strains is fixed at  $45^\circ$  to the vertical z-axis. Thus, the measured  $\gamma_{xz}$  shear strain will be the maximum shear strain  $\gamma$ . The direction of principal stresses  $\alpha$  rotates during shearing and the measured  $\tau_{xz}$  shear stress is not equal to the maximum shear stress  $\tau = 1/2(\sigma_1 - \sigma_3)$ .

Figure 5 shows the stress path in the deviatoric plane predicted by the NGI-ANISOFT model for the DSS simulation. The stress path starts from an anisotropically consolidated initial stress state with  $K_0 < 1$  and initial principal stress



orientation  $\alpha_0 = 0^\circ$ . The principal stresses rotates such that the peak shear strength curve  $\tau_p$  is reached in the point where  $\tau_{xz}$  attains the maximum value for  $\alpha = 27^\circ$ . Whittle et. al. (1994) reports  $\alpha = 29^\circ$  for the peak state in DSS obtained by numerical simulation of normally consolidated Boston blue clay using the MIT-3 model.

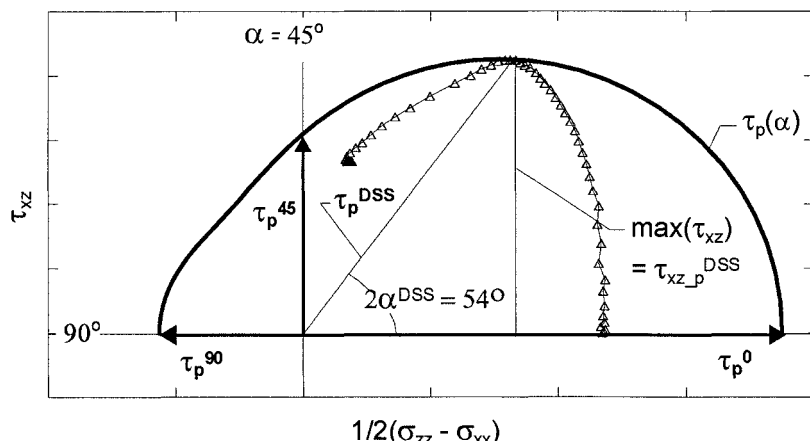


**FIG. 5. Deviatoric stress path predicted by NGI-ANISOFT model for simulation of DSS test. The  $\tau_p^0$ ,  $\tau_p^{45}$  and  $\tau_p^{90}$  characteristics define the anisotropic variation of peak strength  $\tau_p$**

It can be seen from Figure 5 that the peak value from the DSS stress path ( $\tau_{xz-p}^{DSS}$ ) corresponds to the state where the  $\tau_{xz}$  component of  $\tau_p$  attains maximum. Further rotation of principal stresses is predicted by the model in the post-peak softening regime. It is assumed that in real testing the residual state is reached for a principal stress rotation  $\alpha$  close to  $45^\circ$ .

In Figure 6 the  $\tau_{xz}$  versus  $\gamma_{xz}$  model prediction for the DSS test is compared with laboratory DSS results for the Ellingsrud clay presented in Figure 1. The testing were done on specimens obtained from high quality 300 mm diameter cylindrical block samples. For the DSS testing the Geonor apparatus (Bjerrum & Landva, 1966) was used and the vertical stress was reconsolidated to the in-situ effective stress with zero horizontal strain. In this case this gives an initial (prior to undrained shearing) maximum shear stress  $\tau_0$  equal to about 24 kPa for  $K'_0 = 0.6$ .

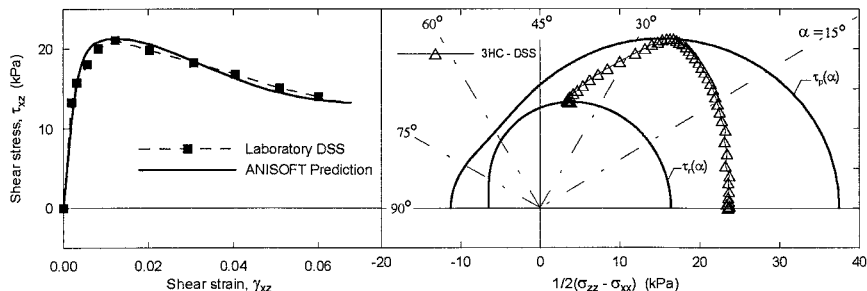


**FIG. 6. Comparison of ANISOFT model prediction and DSS laboratory data (Lacasse et. al., 1985) for Ellingsrud clay (left). The stress path simulated by the ANISOFT model is shown together with the anisotropic representation of peak  $\tau_p$  and residual  $\tau_r$  strength (right).**

The input parameters to the NGI-ANISOFT model for simulation of the DSS test were obtained by fitting the model to the results from these laboratory tests.

## CONCLUSION

An elastoplastic model NGI-ANISOFT with three hardening/softening curves is presented. The model is developed to study the effects of anisotropy and post-peak strain softening in problems of saturated sensitive clay subjected to monotonic undrained loading. The model is limited to plane-strain conditions and does not account for strain rate effects. The model accounts for important features of undrained clay behaviour such as non-linear hardening, anisotropy, principal stress rotation and non-linear softening.

By simulation of direct simple shear deformation it is demonstrated that the model fits to DSS laboratory test data very well. Application to a boundary value problem is demonstrated by the authors (Jostad & Andresen 2002).

## REFERENCES

- Andresen, L. & Jostad, H.P. 1999. "Application of an anisotropic hardening model for undrained response of saturated clay." *Proc. Numerical Models in Geomechanics - NUMOG VII*, pp. 581-585
- Andresen, L. & Jostad, H.P. 1998. "Effect of strain softening in interpretation of laboratory compression tests." *Proc. of Fourth European Conf. On Num. Meth. in Geotech. Eng. - NUMGE98*, pp. 223-232
- Berre, T. 1981. "Triaxial testing at the Norwegian Geotechnical Institute." *Norwegian Geotechnical Institute, Publ. 134*, pp. 7-23
- Bishop, A.W. 1966. "The strength of Soils as Engineering Materials." *Géotechnique*, 16(2), pp. 89-130
- Bjerrum, L. & Landva, A. 1966. "Direct simple shear tests on Norwegian quick clays." *Géotechnique*, 16(1), pp. 1-20
- Brinkgreve, R.B.J., Vermeer, P.A. 1995. "A new approach to softening plasticity." *Proc. Numerical Models in Geomechanics - NUMOG V*, pp. 193-202

- Cassagrande, A. & Carillo, N. 1944. "Shear Failure of Anisotropic Soils." *Contributions to Soil Mech., BSCE*, 1941-1953, pp. 122-135
- Davis, E.H. & Christian, J.T. 1971. "Bearing Capacity of Anisotropic Cohesive Soil." *J. Soil Mech. and Found. Div.*, 97(SM5), pp. 753-769
- de Borst, R. 1987. "Computation of post-bifurcation and post-failure behaviour of strain-softening solids." *Computers & Structures*, 25(2), pp. 211-224
- Hill, R. 1958. "A general theory of uniqueness and stability in elastic-plastic solids." *J. Mech. Phys. Solids*, 6, pp. 236-249
- Høeg, K. 1972. "Finite element analysis of strain softening clay." *J. Soil. Mech. and Found. Div.*, 98(SM1), pp. 43-59
- Jostad, H.P. 1995. "Bifurcation analysis of frictional materials." *Proc. Numerical Models in Geomechanics - NUMOG V*, pp. 173-179
- Jostad, H.P., Andresen, L. 2002. "Capacity analysis of clay with anisotropic softening behaviour using interface elements." *Numerical Models in Geomechanics - NUMOG VIII*
- Lacasse, S., Berre T. & Lefebvre G. 1985. "Block Sampling of Sensitive Clays." *Proc. of 11th Int. Conf. on Soil Mech. and Found. Eng.*, Vol. 2, pp. 887-892
- Larsson, R., Runesson, K., Ottosen, N.S. 1993. "Discontinuous displacement approximation for capturing plastic localisation." *Int. J. Num. Meth. Eng.*, 36, pp. 2087-2105
- Nayak, G.C. & Zienkiewicz, O.C. 1972. "Elasto-plastic stress analysis. A generalization for various constitutive relations including strain softening." *Int. J. Num. Meth. in Eng.*, 5
- Read H.E. & Hegemier G.A. 1984. "Strain Softening of Rock, Soil and Concrete - a review Article." *Mechanics of Materials*, 3, pp. 271-294
- Roscoe, K.H., Burland, J.B. 1968. "On the Generalized Stress-Strain Behaviour of "Wet" clay." *Engineering Plasticity. Heyman, Leckie (eds). Cambridge University Press*. pp. 535 - 609
- Soydemir, C. 1976. "Strength Anisotropy Observed Through Simple Shear Tests." *Laurits Bjerrum Memorial Volume - Contributions to Soil Mechanics*. Janbu, N., Jørstad, F. & Kjærnsli, B. (eds). NGI, Oslo
- Sture, S. & Ko, H.Y. 1976. "Stress analysis of strain softening clay." *Proc. 2nd Int. Conf. Num. Meth. in Geomech.*, Blachsburg VA, USA, 1, pp. 580-589
- Vermeer, P.A. & de Borst R. 1984. "Non-associated plasticity for soil, concrete and rock." *HERON* 29(3), pp. 1-64
- Whittle, A.J., DeGroot, D.J., Ladd, C.C. & Seah, T. H. 1994. "Model Prediction Of Anisotropic Behaviour of Boston Blue Clay." *J. Geo. Eng.*, 120(1), pp. 199-224
- Whittle, A.J. & Kavvadas, M.J. 1994. "Formulation of MIT-E3 Constitutive Model for Overconsolidated Clays." *J. Geo. Eng.*, 120(1), pp. 173-199

## UNCONSTRAINED OPTIMIZATION AND CALIBRATION OF A KINEMATIC-CYCLIC PLASTICITY MODEL

Yu Bao<sup>1</sup>, Member, ASCE, Yu-Ning Ge<sup>2</sup>, Member, ASCE,  
and Stein Sture<sup>3</sup>, Fellow, ASCE

### ABSTRACT:

In this paper, a mixed kinematic and isotropic cyclic plasticity model based on the concept of Fuzzy Set Plasticity, which is a versatile technique for modeling a range of complex phenomena observed in non-proportional loading in soil-structure interaction, is implemented. It is followed by a discussion of associated model parameters and model parameter sensitivity analysis. The use of zero-order numerical optimization techniques is discussed and its application in calibrating the Fuzzy Set Plasticity Model is presented. The performance and comparison among these numerical optimization schemes are also examined and discussed.

---

<sup>1</sup> Graduate Research Assistant, Department of Civil, Environmental, and Architectural Engineering, Campus Box 428, University of Colorado, Boulder, CO 80309-0428.  
yu.bao@colorado.edu

<sup>2</sup> Research Associate, Department of Civil, Environmental, and Architectural Engineering, Campus Box 428, University of Colorado, Boulder, CO 80309-0428.  
gey@colorado.edu

<sup>3</sup> Associate Dean for Research, College of Engineering and Applied Science, and Professor, Department of Civil, Environmental, and Architectural Engineering, Campus Box 428, University of Colorado, Boulder, CO 80309-0428.  
stein.sture@colorado.edu



## INTRODUCTION

Strong ground motion induces a tendency for volume change, especially contraction in medium to loose sandy soils, which may cause a cyclic pore pressure variation as well as a progressive pore pressure buildup depending on the drainage condition and soil permeability. Even if liquefaction were not to take place, the development of excess pore pressures may lead to excessive soil softening or to partial loss of stability and even to bearing capacity failures. Rational analysis of the development of earthquake induced pore pressures requires a fundamental description of the soil's constitutive relations.

In this paper, an effective stress based constitutive model based on fuzzy set theory, which can describe the nonlinear volumetric changes, is presented. The formulation offers a simpler geometrical and mathematical interpretation and simplifies the computer programming of the constitutive driver. We motivate this development by modern mixture theory (Biot) analysis, which require realistic cyclic constitutive descriptions in order to provide accurate simulations.

A wide range of advanced constitutive models includes mixed kinematic and isotropic plasticity, and cyclic degradation concepts, which add to the complexity of model calibration and validation. Conventional methods, such as linear regression, are limited in their use, since many model parameters cannot be determined directly from experimental results and conventional fitting techniques. Therefore, there is a need to develop a method for calibrating advanced constitutive models, and numerical optimization is adopted for this purpose. Numerical optimization algorithms can be categorized into three groups according to the type of information needed in searching for the minimum of the objective function. The simplest way to minimize the function is to randomly choose a sufficiently large number of candidate vectors  $\mathbf{x}$  and evaluate the objective function for each of them. Typical approaches in this category are often referred to as zero-order methods, which include Random Search Methods, Rosenbrock Methods, Complex Methods, and Powell's Methods.

## MODEL FOR PORE PRESSURE GENERATION

In saturated soil, when the loading rate is much higher than the diffusion rate, no flow of the pore fluid can take place, and the fluid follows the motion of the soil skeleton. This response is said to be undrained. Under real seismic loading conditions, some



flow can take place and there is an interaction between the soil skeleton volumetric strains, interstitial fluid pressure and the pore fluid flow. Solving these problems requires that the porous media be analyzed by incorporating the effect of the transient flow of the pore fluid through the soil skeleton voids. Therefore, a multiphase continuum formulation for the coupled field is required. In this paper, in order to simplify the solution technique, only undrained conditions are considered for earthquake loading, therefore, the pore pressure generation is directly related to the soil skeleton volumetric changes. In the following development, we follow conventional coupled analysis concepts. (Arduino, 1999)

The balance of mass expressions for a saturated porous medium can be written as:  
Solid phase:

$$\frac{\partial \rho^{(s)}}{\partial t} + \mathbf{v}^{(s)} \cdot (\nabla \rho^{(s)}) + \rho^{(s)} (\nabla \cdot \mathbf{v}^{(s)}) = 0 \quad (1)$$

Fluid phase:

$$\frac{\partial \rho^{(f)}}{\partial t} + \mathbf{v}^{(f)} \cdot (\nabla \rho^{(f)}) + \rho^{(f)} (\nabla \cdot \mathbf{v}^{(f)}) = 0 \quad (2)$$

Assuming that the solid particles are incompressible in comparison with the soil skeleton, i.e.  $\frac{D^{(s)} \rho_s}{Dt} = 0$ , and there exists an initial homogeneous distribution of porosity, i.e.  $\nabla n = 0$ . Adding (1) and (2) and rearranging the terms, the balance of mass for the saturated soil-fluid mixture implies the following relation:

$$\frac{n}{\rho_f} \frac{D^{(f)} \rho_f}{Dt} + (1-n)(\nabla \cdot \mathbf{v}^{(s)}) + n(\nabla \cdot \mathbf{v}^{(f)}) = 0 \quad (3)$$

where  $n$  represents the porosity as defined in classical soil mechanics;  $\rho_f$  is the density of pore fluid;  $\rho_s$  is the density of soil particles;  $\rho^{(f)} = n\rho_f$ ;  $\rho^{(s)} = (1-n)\rho_s$ ;  $\mathbf{v}^{(s)}$  is the velocity of the soil skeleton and  $\mathbf{v}^{(f)}$  is the velocity of the

pore fluid;  $\frac{D^{(f)} \rho_f}{Dt} = \frac{\partial \rho_f}{\partial t} + \mathbf{v}^{(f)} \cdot (\nabla \rho_f)$  and  $\frac{D^{(s)} \rho_s}{Dt} = \frac{\partial \rho_s}{\partial t} + \mathbf{v}^{(s)} \cdot (\nabla \rho_s)$ .



The first term in (3) can be considered as the storage of fluid mass due to the compressibility of the fluid. If we denote the bulk modulus of the fluid by  $K_f$ , then (3) can be formulated as:

$$\frac{n}{K_f} \frac{\partial u}{\partial t} + (1-n)(\nabla \cdot \mathbf{v}^{(s)}) + n(\nabla \cdot \mathbf{v}^{(f)}) = 0 \quad (4)$$

where  $u$  is the pore pressure magnitude.

For undrained conditions,  $\mathbf{v}^{(s)} = \mathbf{v}^{(f)}$ , then equation (4) can be simplified to:

$$\frac{n}{K_f} \frac{\partial u}{\partial t} + \nabla \cdot \mathbf{v}^{(s)} = 0 \quad (5)$$

$$\begin{aligned} &\Rightarrow \frac{n}{K_f} \frac{\partial u}{\partial t} + \frac{d\varepsilon_v}{dt} = 0 \\ &\Rightarrow du = -\frac{K_f}{n} d\varepsilon_v \end{aligned} \quad (6a)$$

where  $d\varepsilon_v$  is the volumetric strain increment of the soil skeleton,  $d\varepsilon_v > 0$ , dilation; while  $d\varepsilon_v < 0$ , contraction. If we use standard soil mechanics sign, such that  $d\varepsilon_v > 0$  represents contraction; while  $d\varepsilon_v < 0$  represents dilation, then (6a) can be written as:

$$du = \frac{K_f}{n} d\varepsilon_v \quad (6b)$$

According to (6b), pore pressure can be directly calculated from soil skeleton volumetric strain, which also follow for standard compatibility concepts.

## FUZZY SET ELASTO-PLASTICITY CONSTITUTIVE MODEL FOR CYCLIC MOBILITY

Fuzzy-set plasticity theory was first proposed by Klisinski (1988). Due to its



transparency and simplicity, this concept has received increased attention recently. The model is capable of simulating all essential nonlinear characteristics of soils, including nonlinear stress-strain and volume change behavior during unloading and reloading cycles. In fuzzy-set plasticity, it is assumed that there exists an ultimate yield surface where the material behavior is entirely plastic. In addition, the material behavior inside an initial yield surface is purely elastic. The main difference in the formulation is that the elasto-plastic response between the initial and the ultimate yield surfaces is not characterized in the conventional sense but by a fuzzy set representing conditions between the elastic and plastic states. Instead of determining plastic moduli from classical plasticity theory, they are defined in terms of the value of a membership function  $\gamma(s) \in (0,1)$ , such that  $\gamma = 1$  for the purely elastic behavior, whereas  $\gamma = 0$  when the stress point is on the ultimate yield surface. (Klisinski, 1988; Klisinski, Alawi, Sture & Ko, 1987)

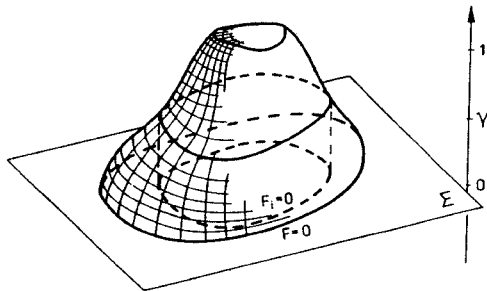


**FIG. 1. The “Fuzzy” Yield Surface Specified by a Given Constant Value of the Membership Function**

Volumetric changes are essential to pore pressure generation. In this paper, we describe a new development to the fuzzy-set constitutive model in order to describe volumetric strains more realistically. The basic idea is introducing the critical state concept, state parameter and phase transform surface into the model.

### Kinematic Mechanisms of Membership Functions

Two types of membership functions are introduced to account for deviatoric and locking kinematic mechanism, respectively. With the assistance of the membership functions  $\gamma_d$  and  $\gamma_l$ , we can readily construct reversal plastic loading without resorting to kinematic hardening rules. Fig. 2 shows an example of the kinematic mechanism of the deviatoric membership function  $\gamma_d$ , which represents plastic loading from point a to b, follow by elastic unloading from point b to c. After point c is reached, unloading with associated decrease of the value of the membership function results in plastic deformation. The degree of material memory can be simulated by predetermining the location of point c. The opposite mechanism of the deviatoric membership function describes the kinematic mechanism of the locking membership function  $\gamma_l$ , shown in Fig. 3. It increases linearly to unity as the mean stress level  $p$  reaches  $p_e$ . Beyond this stress level, the locking membership function remains unity. Points a, b, c, and d correspond to the situation described for the deviatoric membership function mechanism above.

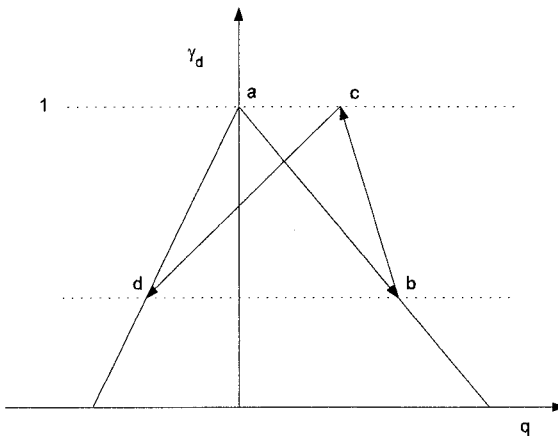


**FIG. 2. Pictorial Illustration of Kinematic Mechanics for the Deviatoric Membership Function**

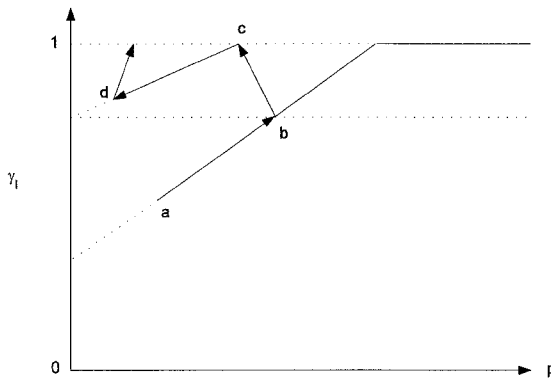


**FIG. 3. Pictorial Illustration of Kinematic Mechanics for the Locking Membership Function**

### Stress Control Formulation

A stress control formulation of the fuzzy set plasticity model is straightforward to implement. The stress control incremental stress strain relation in the  $p - q$  space can be formulated as follows:

Additive strain decomposition:

$$d\mathbf{e} = d\mathbf{e}^e + d\mathbf{e}^p = d\mathbf{e}^e + d\mathbf{e}_d^p + d\mathbf{e}_l^p = \begin{Bmatrix} d\mathbf{\varepsilon}_v \\ d\mathbf{\varepsilon}_d \end{Bmatrix} \quad (7)$$

Hooke's law that characterizes elastic strain increments:

$$d\mathbf{\varepsilon}^e = \mathbf{C}^e d\mathbf{s} = \begin{bmatrix} \frac{1}{K} & 0 \\ 0 & \frac{1}{3G} \end{bmatrix} \begin{Bmatrix} dp \\ dq \end{Bmatrix} \quad (8)$$

where  $d\mathbf{s}$  is the stress increment vector,  $p$  is the effective mean stress and  $q$  is the deviatoric stress.

Incremental plastic strain increment-strain increment relation:

$$d\mathbf{e}_d^p = \mathbf{C}_d^p d\mathbf{s} = \frac{1}{H_d} \mathbf{m}_d \mathbf{n}_d^T d\mathbf{s} \quad (9)$$

where  $H_d = H_d^* + \frac{M_d \cdot \gamma_d^{s_d}}{1 - \gamma_d^{s_d+1}}$ , is the deviatoric plastic modulus;  $H_d^*$  is the hardening modulus of the deviatoric ultimate yield surface;  $\gamma_d$  is the deviatoric membership function;  $M_d$  and  $s_d$  are model parameters;  $\mathbf{n}_d$  is the normal to the deviatoric loading surface and  $\mathbf{m}_d = \mathbf{T}\mathbf{n}_d$  is the flow direction. The transformation matrix  $\mathbf{T}$  is introduced here to apply a non-associated flow rule of the deviatoric portion of the plastic deformation, which essentially models dilatancy.

$\mathbf{T} = \begin{bmatrix} B & 0 \\ 0 & 1 \end{bmatrix}$ , where  $B$  is the dilatancy parameter. The parameter  $B$  determines the dilatancy behavior, such that  $B = 0$  represents no dilatancy at all.

$$d\mathbf{e}_l^p = \mathbf{C}_l^p d\mathbf{s} = \frac{1}{H_l} \mathbf{n}_l \mathbf{n}_l^T d\mathbf{s} \quad (10)$$

where  $H_l = H_l^* + \frac{M_l \cdot \gamma_l^{s_l}}{1 - \gamma_l^{s_l+1}}$ , is the locking plastic modulus;  $H_l^*$  is the hardening modulus of the locking ultimate yield surface;  $\gamma_l$  is the locking membership function;  $M_l$  and  $s_l$  are model parameters; and  $\mathbf{n}_l$  is the normal to the locking loading surface. An associated flow rule is used to characterize the locking portion of the plastic deformation.

$$d\mathbf{e} = \mathbf{C}^{ep} d\mathbf{s} = \left( \begin{bmatrix} 1 & 0 \\ K & 1 \\ 0 & 3G \end{bmatrix} + \frac{1}{H_d} \mathbf{T} \mathbf{n}_d \mathbf{n}_d^T + \frac{1}{H_l} \mathbf{n}_l \mathbf{n}_l^T \right) \begin{Bmatrix} dp \\ dq \end{Bmatrix} \quad (11)$$

### Critical States and State Parameter

Traditionally, void ratio and stress are the primary state variables used to describe the physical condition of soils. The conventional concept of critical state can be expressed as follows (Wood, 1990):

 @Seismicisolation

$$\frac{dq}{d\varepsilon_q} = \frac{dp}{d\varepsilon_q} = \frac{d\varepsilon_v}{d\varepsilon_q} = 0 \quad (12)$$

The state parameter  $\psi$  is the difference between the current void ratio and the critical void ratio, i.e.  $\psi = e - e_c$ . For loose soil,  $\psi > 0$ ; and for dense soil,  $\psi < 0$ . (Been & Jefferies, 1985)

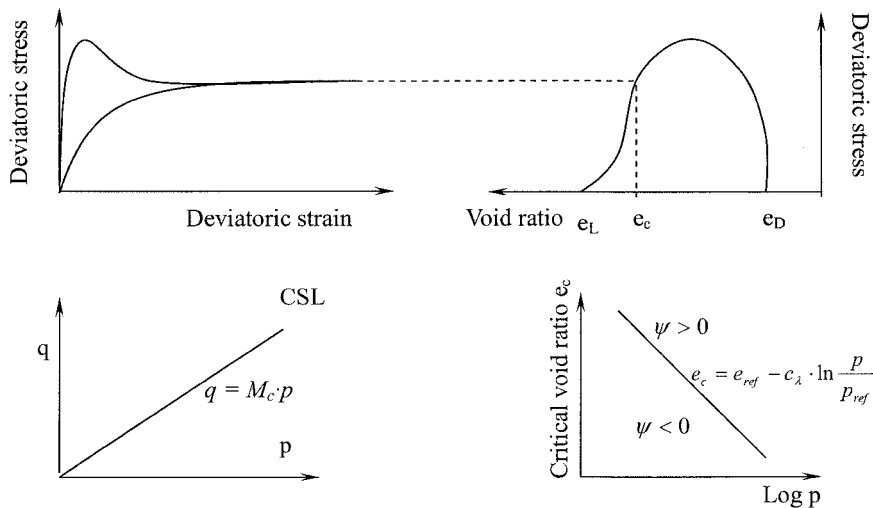


**FIG. 4. Critical States and Critical Void Ratio**

In the enhanced fuzzy-set model, the deviatoric ultimate yield surface can be described as

$$F_d = g(\theta)q - a_0 - a_1p \quad (13)$$

where  $a_1 = M_c + \kappa\langle -\psi \rangle$ ;  $a_0$  is a material constant; and  $\theta$  is the Lode angle. The “elliptical” function  $g(\theta)$  determines the shape of the trace of the ultimate yield surface in any deviatoric plane.

$$e_c = e_{ref} - c_\lambda \ln \frac{p}{p_{ref}} \quad (14)$$

Assuming that  $\varepsilon_v^e$  is insignificant compared to overall volume change, the plastic volumetric strain is related to the void ratio  $e$  as follows.

$$\varepsilon_v^p \approx \varepsilon_v = \frac{\Delta V}{V_o} = \frac{-\Delta e}{1+e_0} = \frac{e_0 - e}{1+e_0}$$

and the incremental plastic volumetric strain is,

$$d\varepsilon_v^p = d\varepsilon_v = -\frac{de}{1+e_0} \quad (15)$$

1) For loose soil,  $e > e_c$ ,  $-\psi < 0$

$$a_1 = M_c \quad (16)$$

$$H_d^* = -\frac{\partial F_d}{\partial a_1} \frac{\partial a_1}{\partial \psi} \frac{\partial \psi}{\partial \varepsilon_v^p} \frac{\partial \varepsilon_v^p}{\partial \varepsilon_{v,d}^p} \frac{\partial F_d}{\partial p} = 0 \quad (17)$$

2) For dense soil,  $e < e_c$ ,  $-\psi > 0$

$$a_1 = M_c - \kappa\psi$$

$$\psi = e - e_c = e_0 - (1+e_0)\varepsilon_v^p - e_c$$

$$\Rightarrow a_1 = M_c - \kappa[e_0 - (1+e_0)\varepsilon_v^p - e_c] \quad (18)$$

$$H_d^* = -\frac{\partial F_d}{\partial a_1} \frac{\partial a_1}{\partial \psi} \frac{\partial \psi}{\partial \varepsilon_v^p} \frac{\partial \varepsilon_v^p}{\partial \varepsilon_{v,d}^p} \frac{\partial F_d}{\partial p} \quad (19)$$

$$H_d^* = -(-p)(-\kappa)[-(1+e_0)]l(-a_1) = -p\kappa \cdot (1+e_0)a_1$$

### Phase Transformation Surface (PTS)

The existence of the phase transformation surface is the key to understanding cyclic mobility, which is a liquefaction related phenomenon that is triggered by cyclic loading. Deformations due to cyclic mobility develop incrementally.

The phase transformation surface (PTS), as shown in Fig. 5, is the locus of stress points at which the volumetric changes of sands transform from contraction to dilation.

The effective stress ratio is defined as  $\eta = \frac{q}{p}$ .

Below PTS, i.e.  $\eta < \eta_{PT}$ : contraction takes place, and the pore pressure  $u$  increases and the mean effective confining stress  $p$  decreases.

On PTS, i.e.  $\eta = \eta_{PT}$ : no volumetric change takes place, and  $p$  remains constant.

Above PTS, i.e.  $\eta > \eta_{PT}$ : dilation takes place,  $u$  decreases and  $p$  increases.

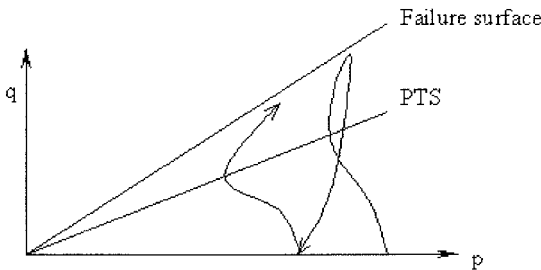


**FIG. 5. Effective Stress Path under Undrained Cyclic Loading**

### DILATANCY BEHAVIOR UNDER CYCLIC LOADING

In this paper, we focus on a more realistic dilatancy formulation for the fuzzy-set model under cyclic loading. Based on experimental results and observations, dilatancy is mainly related to: 1) Current effective stress ratio  $\eta$ ; 2) State parameter  $\psi$ ; 3) Loading, unloading and reloading conditions.

Here the term “loading” refers to “deviatoric loading”. If  $\eta_i$  is the effective stress

ratio at time step  $i$  and  $\eta_{i+1}$  is the effective stress ratio at step  $i+1$ , then the conditions for loading are expressed as,

$$|\eta|_{i+1} \geq |\eta|_i \text{ and } \mathbf{s}_{i+1} : \mathbf{s}_i \geq 0 \quad (20)$$

where  $\mathbf{s}$  is the deviatoric stress vector.

Dilatancy behavior is determined by the model parameter  $B$ . In view of the previous discussion, we have devised the following feasible expressions for  $B$ ,

Loading:

$$\text{Below PTS: } B = \alpha_1 |\psi| \left[ \exp\left(1 - \frac{|\eta|}{|\eta_{PT}|}\right) - 1 \right] \quad (21)$$

$$\text{Above PTS: } B = \alpha_2 |\psi| \left[ \exp\left(1 - \frac{|\eta_F| - |\eta|}{|\eta_F| - |\eta_{PT}|}\right) - 1 \right] \quad (22)$$

Unloading:

$$B = \beta |\psi| \exp\left(\frac{|\eta|}{|\eta_F|}\right) \quad (23)$$

where  $\alpha_1$ ,  $\alpha_2$  and  $\beta$  are model parameters needed to be determined.

Under cyclic loading, the volumetric change behavior from laboratory experiments, as illustrated in Fig.5, can be described as follows:

Loading:

- 1)  $0 \leq |\eta| < |\eta_{PT}|$ : contraction
- 2)  $|\eta_{PT}| < |\eta| \leq |\eta_F|$ : dilation
- 3)  $|\eta| = |\eta_{PT}|$ : no volume change

Unloading:

 @Seismicisolation

1)  $|\eta_{PT}| \leq |\eta| \leq |\eta_F|$ : contraction

2)  $0 \leq |\eta| < |\eta_{PT}|$ : contraction

Reloading: Follow the same rule as loading.

## MODEL RESPONSE UNDER CYCLIC LOADING

The parameters of the constitutive model are calibrated by assisting the constitutive driver with an optimization program that determines the interactive variation of the model parameters and their effects on the predictive capability of the constitutive driver. The optimization scheme adapted to the “fuzzy set” model will be described in detail in the next section. The experimental data used to calibrate the model are provided by a laboratory program described by Perkins (1985). The model responses are shown in Fig. 6 through Fig. 9.

The simulation responses are consistent with a large number of undrained laboratory experiments conducted to study the cyclic behavior of sands. Fig. 6 illustrates a cycle-by-cycle degradation in strength (soil softening) as manifested by the occurrence of increasingly larger strain excursions for the same level of applied deviatoric stress. It shows clearly in Fig. 7 that cyclic shear loading causes a progressive pore water pressure build-up as well as a cyclic pore water pressure variation. Fig. 8 and Fig. 9 show that under undrained conditions, the dilation-induced increase in volume results in an immediate reduction in pore pressures and associated increase in effective confinement.

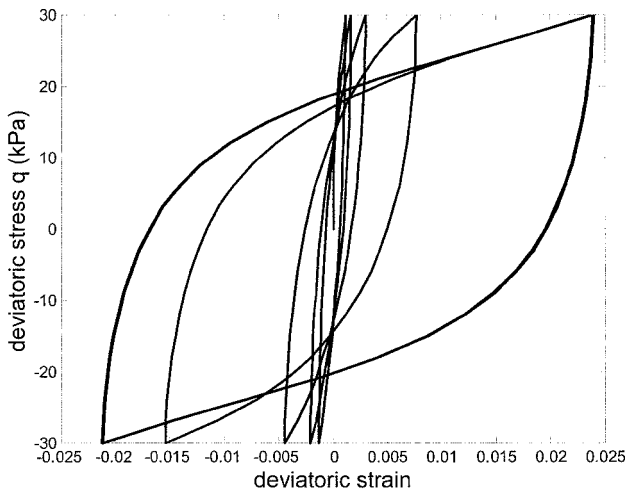


**FIG. 6. Deviatoric Stress-Strain Response Curve**

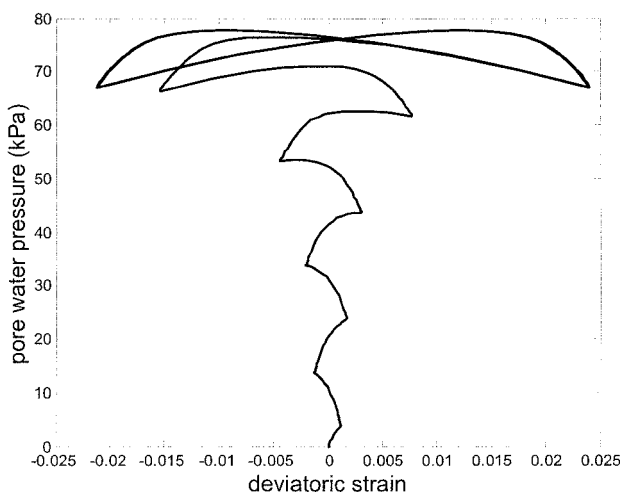


**FIG. 7. Pore Water Pressure-Deviatoric Strain Response Curve**

@Seismicisolation

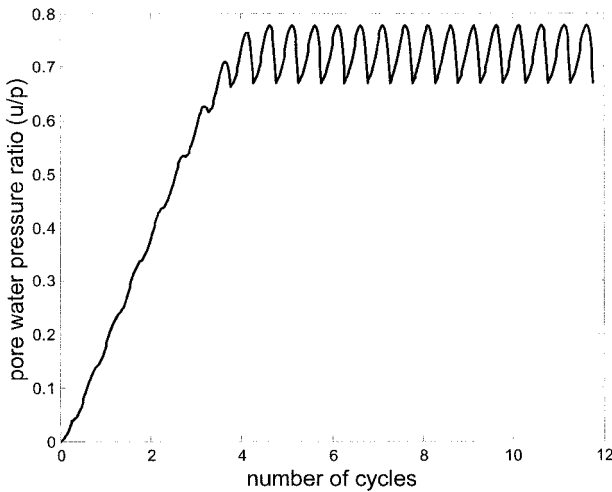


**FIG. 8. Pore Water Pressure Build-Up Curve**

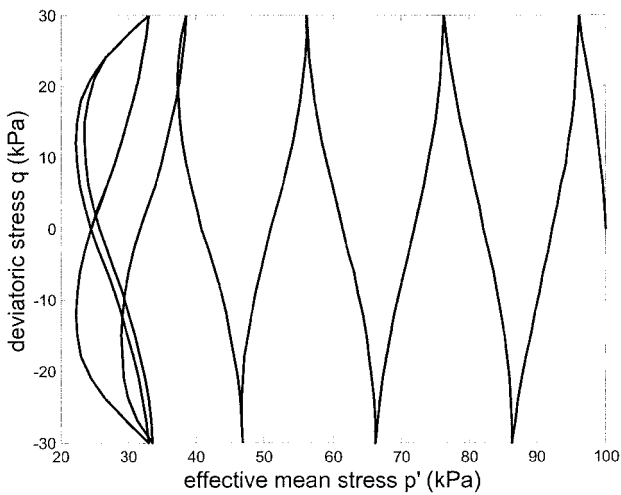


**FIG. 9. Deviatoric Stress-Effective Mean Stress Response Curve**

@Seismicisolation

## MODEL CALBRATION

Typically, a large number of model parameters and constants are needed to describe nonlinear constitutive models for soils. Most of the parameters in these models are not physically well-defined such as cohesion and frictional angle in traditional soil mechanics. Nonlinear phenomenon and dilatancy frequently require more elaborate information, which often have their origins in plasticity theory. Therefore, conventional model fitting and calibration methods such as linear regression are ill-suited of calibrating advanced constitutive models. Since the early 1990's, researchers have been working on developing systematic and efficient methodologies including applying numerical optimization techniques to constitutive model calibration (Anadarajah and Agarwal, 1990, Mattsson, Klisinski, and Axelsson, 1997, and Yang and Elgamal, 2002).

Briefly, these techniques involve comparison between laboratory data (stress-strain response curves) and numerical simulation. A function, normally called objective function, is constructed by summing the distance norm between laboratory and numerical simulation. Numerical optimization schemes are then employed to find a set of constitutive model parameters and constants which generate the numerical simulation and minimize the objective function.

### Unconstrained Numerical Optimization

Generally speaking, optimization problems are defined as follows.

$$\begin{aligned} & \text{Minimize } f(\mathbf{x}) \\ & \text{Subject to } \mathbf{x} \in \Omega \end{aligned} \tag{24}$$

where the function  $f$  is called the objective function or cost function, and the vector  $\mathbf{x}$  consists of  $n$  independent variables, which are called decision variables. The set  $\Omega$  is a subset of  $\mathbb{R}^n$  called the constraint set or feasible set. The "best" vector  $\mathbf{x}$  or  $\mathbf{x}^*$ , is called the minimizer. We will focus on unconstrained optimization in calibration constitutive models, i.e.  $\Omega = \mathbb{R}^n$ .

Numerical optimization algorithms can be categorized into three groups according to the type of information needed in searching for the minimum of the objective function. The simplest way to minimize the objective function is to randomly choose a



sufficiently large number of candidate vector  $x$  and evaluate the objective function for each of them. This approach is often referred to as a zero-order method, where the Random Search method, Rosenbrock methods, Complex methods, and Powell's methods are techniques that fall into this category (Rosenbrock, 1960, Spendley et al., 1962, Powell, 1964, and Nelder and Mead, 1965).

If the information of the gradient of the objective function is implemented into the optimization algorithm, it is referred to first-order-methods. The gradient of the objective function can be obtained by either finite difference computations or analytical solutions. First-order-methods are usually more efficient than zero-order-methods; however, they can perform poorly for objective functions having discontinuous first derivatives. Steepest Descent Methods, Conjugate Direction Methods (or Fletcher and Reeves Methods), Variable Metric Methods (Davidon-Fletcher-Powell or Broydon-Fletcher-Goldfarb-Shanno Methods) belong to this category.

Second-order-methods, also called Newton's Methods, use information related to the second derivative of the objective function (Hessian matrix  $\mathbf{H}$ ) throughout the optimization process. If the Hessian matrix can be calculated relatively easy, Newton's Method is usually the most preferred approach due to its efficiency and stability.

Due to the nature of incremental format of most elasto-plasticity constitutive drivers, such as the fuzzy set model, the objective functions are not explicitly well-defined. This causes the difficulty in calculating the first and second derivatives of the objective functions when first-order-methods and second-order-methods are used. Therefore, only zero-order-methods are considered when calibrating fuzzy set constitutive models.

**Rosenbrock Method:** Rosenbrock (1960) developed an algorithm for finding the greatest or least value of a function. Its strategy is to check the value of the objective function in all possible search directions. If the search direction successfully minimizes the objective function, the step length is increased in that particular direction. On the other hand, if the search direction fails to do so, a smaller step length in the opposite direction will be used to evaluate the objective function. The process is repeated until the search is considered to be ineffective when a success followed by a failure has been recorded at some time during the iteration for every direction.

**Powell's Method:** Powell's method (1964) is based on the concept of conjugate directions. Each iteration begins with a search of  $n$  linearly independent



directions  $\xi_1, \xi_2, \dots, \xi_n$ , starting from the best known approximation to the minimum  $\mathbf{x}^*$ . The coordinate directions are used initially and then the conjugate directions generated by making each iteration define a new direction  $\xi$ , and choosing the linearly independent directions for the next iteration to be  $\xi_2, \xi_3, \dots, \xi_n, \xi$ .

**Simplex Method:** Originally introduced by Spendley et al. (1962), the search for the minimum of the objective function proceeds by comparing its value at the vertices of a geometric figure called a simplex. Nelder and Mead (1965) improved the original algorithm by relaxing the constraint of knowing the relative steps in varying the factors. The simplex method can be described as follows. Let  $x_i$  for  $i = 0 \sim n$  be points in  $n$ -dimensional space defining the current “simplex”.  $f_i$  is the value of the objective function at point  $x_i$ ;  $f_h = \max(f_i)$  and  $f_l = \min(f_i)$  are the maximum and minimum values of the objective function for  $x_i$ . Also,  $x_c$  denotes the centroid of the point with  $i \neq h$ .

At each stage in the process,  $x_h$  is replaced by a new point obtained by the operations of reflection, contraction, or expansion.

The reflection of  $x_h$  is defined by the relation

$$x^{ref} = (1 + \alpha)x_c - \alpha x_h \quad (25)$$

where  $\alpha$  is the reflection coefficient with a positive value.

The expansion  $x^{exp}$  is obtained by the expression

$$x^{exp} = \gamma x_h + (1 - \gamma)x_c \quad (26)$$

where  $\gamma$  is the expansion coefficient greater than 1.

The contraction  $x^{con}$  is defined as

$$x^{con} = \beta x_h + (1 - \beta)x_c \quad (27)$$

where  $\beta$  is the contraction coefficient between 0 and 1.

## Numerical Optimization in Constitutive Model Calibration

### Random Search Method

Random search method is considered to be the most inefficient but most easily implemented among the zero-order methods. The ease of implementation is the reason that random search method was adopted to calibrate the fuzzy set model in this study. Moreover, the inefficiency can be overcome by the aid of modern high-speed



computers. Assume the minimizer  $\mathbf{x}^* = x_i$  for  $i = 1$  to  $n$  lies between its lower bound  $\mathbf{x}^l$  and upper bound  $\mathbf{x}^u$  values, there must exist a  $\mathbf{R}$  such that

$$\mathbf{x}^* = \mathbf{x}^l + \mathbf{R}(\mathbf{x}^u - \mathbf{x}^l) \quad (28a)$$

or

$$x_i^* = x_i^l + R_i(x_i^u - x_i^l) \quad (28b)$$

and minimize the objective function  $f$ .

### Objection Function

Since we are calibrating constitutive models, it is intuitive to use stress and strain as variables in the objective function. It is then straightforward to formulate the objective function as the sum of distances from computed points to their adjacent experimental points in the stress strain space.

For each computed strain lies between  $\varepsilon_j^{\text{exp}}$  and  $\varepsilon_{j+1}^{\text{exp}}$ , the distances between the computed and experimental strains can be calculated. The objective function is constructed as follows. It is noted that we ignore the computed point  $(\sigma_i^{\text{num}}, \varepsilon_i^{\text{num}})$

when  $\varepsilon_i^{\text{num}} = \varepsilon_j^{\text{exp}}$  or  $\varepsilon_i^{\text{num}} = \varepsilon_{j+1}^{\text{exp}}$ .

$$f = \sum_{i=1}^n \frac{1}{2} \left( \sqrt{\left(1 - \frac{\sigma_j^{\text{exp}}}{\sigma_i^{\text{num}}}\right)^2 + \left(1 - \frac{\varepsilon_j^{\text{exp}}}{\varepsilon_i^{\text{num}}}\right)^2} + \sqrt{\left(1 - \frac{\sigma_{j+1}^{\text{exp}}}{\sigma_i^{\text{num}}}\right)^2 + \left(1 - \frac{\varepsilon_{j+1}^{\text{exp}}}{\varepsilon_i^{\text{num}}}\right)^2} \right) \quad (29)$$

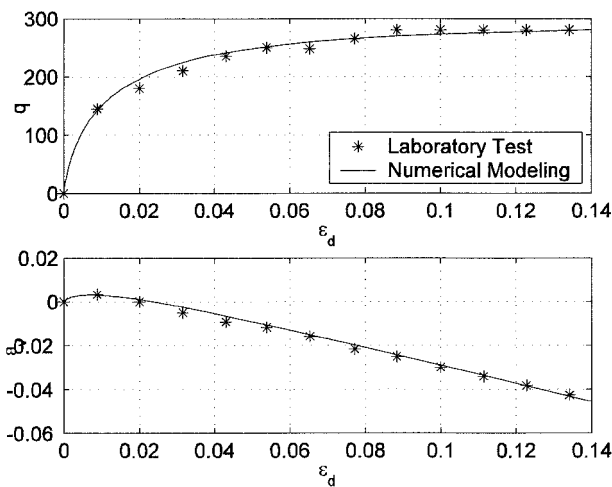
for  $\varepsilon_i^{\text{num}} > \varepsilon_j^{\text{exp}}$  and  $\varepsilon_i^{\text{num}} < \varepsilon_{j+1}^{\text{exp}}$ , and  $n$  is the number of computed strains.

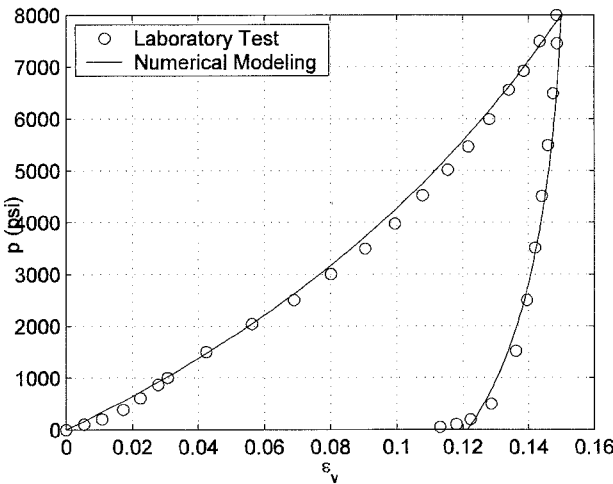
### Optimization Results

Table 1 displays the lower bound, upper bound, and optimized value of the fuzzy set model parameters and constants. Fig. 10 and Fig. 11 show the comparison between laboratory data and numerical simulation for conventional triaxial and isotropic compression tests.

**TABLE 1. Lower, Upper Bounds, and Optimized Values of the Fuzzy Set Model**

	Lower Bound	Upper Bound	Optimized Value
Locking Part			
$K$	1330000	1360000	1345396
$P_e$	44200	44700	44432
$M_l$	750000	800000	778090
$s_l$	1.9	2.0	1.951
$\gamma_{l0}$	0.18	0.20	0.188
Deviatoric Part			
$a_l$	1.4	1.5	1.486
$G$	650000	660000	658750
$M_d$	55000	56000	55385
$s_d$	1.6	1.9	1.787

**FIG. 10. Model Calibration for a CTC Test**



**FIG. 11. Model Calibration for an Isotropic Compression Test**

## IMPLICIT INTEGRATION

Implicit integration schemes such as the closest point method (CPPM) are often discussed in the context of classical plasticity model such as J2 plasticity model with nonlinear isotropic and kinematic hardening. Several applications of the CPPM have been further discussed in relation to some isotropic plasticity models for pressure-sensitive materials. In particular, Borja (1990, 1991), Jeremic and Sture (1997), and Macari et al (1997) presented the works for geomaterials.

Compared to the isotropic/kinematic hardening models, the loading surfaces of the fuzzy set model are not explicit defined, which the consistent condition can not be applied, and the values of the loading surfaces at their corresponding stress states always keep zero. Therefore, a mixed control strain-based implicit integration scheme is developed for the fuzzy set model, and described as follows.

### Elastic Trial Stress State

At time step  $t_n$ , given a prescribed strain increment  $\Delta\epsilon$ , and assuming no plastic strain increment for the first iteration, the stress state at time step  $t_{n+1}$  is calculated from:

$$\mathbf{s}^{trial} = \mathbf{s}_n + \mathbf{E} : \Delta \mathbf{e} \quad (30)$$

### Return to the Fuzzy Surface

If the trial stress state at time step  $t_{n+1}$  is outside the fuzzy surfaces, which is not allowable, returning the stress state to the fuzzy surface is necessary.

### Update the Stress States

It is obvious that the stress state at time step  $t_{n+1}$  should fall between the stress state at time step  $t_n$ ,  $\sigma_n$ , and the first iterated stress state, which is located on the fuzzy surface,  ${}^1\sigma_{n+1}$ . The second iterated stress state is chosen as

$${}^2\mathbf{s}_{n+1} = \frac{1}{2}(\mathbf{s}_n + {}^1\mathbf{s}_{n+1}) \quad (31)$$

## CONCLUSIONS

The “fuzzy set” formulation of the plasticity theory is transparent and simplifies the computer programming of the constitutive driver. Traditional concepts related to critical state, state parameter and phase transformation surface are employed in the enhanced “fuzzy set” model to describe nonlinear volumetric changes in granular soils under cyclic loading. The simulation results show that the enhanced “fuzzy set” constitutive model is proper to capture the strongly dilative/contractive behaviors beneath the failure surface during unloading-reloading cycles, which are necessary to evaluate the consequences of soil liquefaction. The numerical optimization results show that the random search method is suitable for calibrating the “fuzzy set” constitutive model.

## REFERENCES

- Anandarajah, A. and Agarwal, D. (1990). "Computer-aided calibration of a soil plasticity model." *International Journal for Numerical and Analytical Methods in Geomechanics*, 15, 835-856.
- Arduino, P. (1999). "Multiphase description of deforming porous media by the finite element method." Ph.D Thesis, Georgia Institute of Technology.
- Been, K., and Jefferies, M. G. (1985). "A state parameter for sands." *Geotechnique*, 35(1), 99-112.
- Been, K., Jefferies, M. G., and Hachey, J. (1991). "The critical state of sands." *Geotechnique*, 41(3), 365-381.
- Borja, R. I. (1990). "Cam-clay plasticity, part i: Implicit integration of constitutive relations." *Computer Methods in Applied Mechanics and Engineering*, 78, 49-72.
- Borja, R. I. (1991). "Cam-clay plasticity, part ii: Implicit integration of constitutive equation based on a nonlinear elastic stress predictor." *Computer Methods in Applied Mechanics and Engineering*, 88, 225-240.
- Gajo, A., and Muir Wood, D. (1999). "Severn-Trent sand: a kinematic-hardening constitutive mode: the q-p formulation." *Geoteknique*, 49(5), 595-614.
- Ge, Y. N. (2003). "Cyclic constitutive modeling of granular materials." Ph.D Thesis, University of Colorado at Boulder.
- Jeremic, B. and Sture, S. (1997). "Implicit integrations in elastoplastic Geotechnics." *Mechanics of Cohesive-Frictional Materials*, 2(2), 165-183.
- Klisinski, M. (1988). "Plasticity theory based on fuzzy sets." *Journal of Engineering Mechanics*, ASCE, 114(4), 563-582.
- Klisinski, M., Abifadel, N., Runesson, K., and Sture, S. (1991). "Modeling of the behavior of dry sand by an elasto-plastic 'fuzzy set' model." *Computers and Geotechnics*, 11, 229-261.
- Klisinski, M., Alawi, M.M, Sture, S., Ko, H.-Y., and Muir Wood, D. (1987). "Elasto-plastic model for sand based on fuzzy sets." *International Workshop on Constitutive Equations for Granular Non-Cohesive Soils*, Case Western Reserve University.
- Macari, E. J., Weihe, S., and Arduino, P. (1997). "Implicit integration of elastoplastic constitutive models for frictional materials with highly non-linear hardening functions." *Mechanics of Cohesive-Frictional Materials*, 2(1), 1-29.

- Mattsson, H., Klisinski, M., and Axelsson, K. (1997). "Optimization routine for identification of model parameters in soil plasticity." *International Journal for Numerical and Analytical Methods in Geomechanics*, 25, 437-472.
- Nelder, J. A. and Mead, R. A. (1965). "A simplex method for function minimization." *The Computer Journal*, 7, 308-313.
- Perkins, S. W. (1985). "High pressure multiaxial testing and modeling of compacted Nellis Baseline sand." M.S. Thesis, University of Colorado at Boulder.
- Powell, M. J. D. (1964). "An efficient method for finding the minimum of a function of several variables without calculating derivatives." *The computer Journal*, 7, 155-162.
- Prevost, J. H. (1982). "Nonlinear Transient Phenomena in Saturated Porous Media." *Computer Methods in Applied Mechanics and Engineering*, 20, 3-18.
- Prevost, J. H. (1985). "Wave propagation in fluid-saturated porous media: an efficient finite element procedure." *Soil Dynamics and Earthquake Engineering*, 4, 183-202.
- Rosenbrock. H. H. (1960). "An automatic method for finding the greatest or least value of a function." *The Computer Journal*, 3, 175-184.
- Spendley, W., Hext, G. R., and Hinsworth, F. R. (1962). "Sequential application of simplex designs in optimization and evolutionary operation." *Technometrics*, 4, 441-461.
- Yang, Z. (2000). "Numerical modeling of earthquake site response including dilation and liquefaction." Ph.D Thesis, Columbia University.
- Yang, Z. and Elgamal, A. (2003). "Application of unconstrained optimization and sensitivity analysis to calibration of a soil constitutive model." *International Journal for Numerical and Analytical Methods in Geomechanics*, 27, 1277-1297.

## SELECTION OF SOIL MODELS AND PARAMETERS FOR GEOTECHNICAL ENGINEERING APPLICATION

Ronald B.J. Brinkgreve<sup>1</sup>

**ABSTRACT:** The mechanical behaviour of soils may be modelled at various degrees of accuracy. Hooke's law of linear, isotropic elasticity may be thought of as the simplest available stress-strain relationship, but this is generally too crude to capture essential features of soil behaviour. On the other hand, a large number of constitutive models have been proposed by several researchers to describe various aspects of soil behaviour in detail. However, the more sophisticated a soil model is, the more parameters have to be selected on the basis of soil investigation data. For geotechnical engineering applications soil data is usually limited to results obtained from basic field tests. There is often insufficient data to accurately select all parameters of fancy models. As a result, some parameters should be 'estimated' and it can be argued whether such models deliver in practice the accuracy that they pretend. In between Hooke's law and fancy models there is a range of existing models that could be used within the finite element method for geotechnical engineering applications. In this contribution possibilities and limitations of such models are discussed with the purpose to give geotechnical engineers (rather than researchers) guidelines to properly select soil models and their corresponding parameters to be used in the finite element method for engineering applications.

### INTRODUCTION

Well before the introduction of the finite element method, researchers have already tried to formulate the behaviour of materials in mathematical models. In this respect we are talking about relationships between stresses (or stress increments) and strains (or strain increments) that represent to some extend material properties as stiffness and strength.

Regarding strength, there is the well-known relationship by Coulomb (1776) who related the maximum shear stress,  $\tau$ , to a cohesive term,  $c$ , and a friction term,  $c \tan \varphi$ ,

---

<sup>1</sup> Delft University of Technology, Delft, The Netherlands

where the latter term depends on the applied normal stress,  $\sigma$ . Considering material as a continuum, Coulomb's equation was used and generalised into the Mohr-Coulomb criterion to describe failure in frictional materials for three-dimensional states of stress.

Regarding the stiffness of a material as a continuum, there is Hooke's law as a first order approximation involving isotropic linear elastic behaviour. The combination of Hooke's law and the Mohr-Coulomb criterion, formulated in a plasticity framework, is known as the Mohr-Coulomb model (e.g. Smith & Griffith, 1982). This model can be conceived as a first order model for soil behaviour in general.

In the second half of the 20<sup>th</sup> century, several researchers succeeded to formulate the non-linear behaviour of soils in more detail using different modelling concepts like non-linear elasticity (e.g. Duncan & Chang, 1970), hardening plasticity, Critical State theory (e.g. Schofield & Wroth, 1968) and hypoplasticity (Kolymbas, 1985). However, the application of non-linear models was, for some time, limited to analytical solutions of rather simple problems.

Several models already existed when in the sixties the finite element method was introduced as a general method to simulate physical processes in continua, in particular deformations due to loading. However, the implementation of non-linear soil models in the finite element method was not straightforward and involved the development of numerical procedures. Due to its additional complexity, the use of the finite element method for geotechnical applications was, for a long time, limited to special numerical groups within the research community, but at the end of the eighties 'friendly' finite element programs with robust numerical procedures became available for geotechnical engineering applications. The first programs were quite limited in the models they had available to simulate soil behaviour. Meanwhile, a number of 2D and 3D computer programs are available with advanced soil models and features to realistically simulate loading, excavation and construction processes of geotechnical projects (see for example Fig. 1).

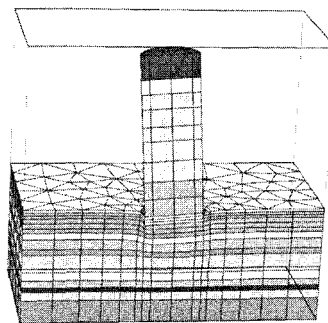


**FIG. 1.** Three-dimensional finite element calculation of time-dependent behaviour of the Pisa tower (after Vermeer et. al., 2002)

Although the geotechnical design of a project is still mostly based on conventional design methods, the finite element method plays an increasingly important role in the

**@Seismicisolation**

analysis of deformations, stability and the influence on surrounding structures. The number of users of finite element programs working in engineering and contracting firms has increased dramatically over the last 15 years. It is important that these (often young) engineers know how to select the right models and their parameters for a certain application. Therefore, they need to understand the possibilities and limitations of the models in order to create the right input data, to correctly interpret the computational results and to translate these into a proper geotechnical design.

Before going into more details on constitutive soil models, attention is first focused on aspects of real soil behaviour. This information is used as a basis to evaluate the possibilities and limitations of some existing models for geotechnical engineering applications, which is done in the third section. The fourth section is devoted to the selection of model parameters. The final section five contains the main conclusions of this contribution.

## ASPECTS OF REAL SOIL BEHAVIOUR

Soil is a complex material that shows a highly non-linear and often anisotropic and time-dependent behaviour when subjected to stresses and stress changes. In this section some characteristic aspects of soil behaviour are described, with the purpose to evaluate to what extend constitutive soil models are capable of describing those aspects.

The first aspect is the influence of water on the behaviour of soil. Total stresses in the soil can be divided into effective stresses,  $\sigma'$ , and pore pressures,  $u$ . The mechanical behaviour of soil is dominated by the effective stresses. Hence, in order to get the effective stresses, it is essential to know the pore pressure distribution in addition to the total stress state in the soil. As a first estimate, pore pressures may be determined from the phreatic level as hydrostatic water pressures. A non-hydrostatic pore pressure distribution causes groundwater flow to occur. If the soil is rather impermeable and saturated, the pore pressure distribution is influenced by quick loading resulting in excess pore pressures (undrained behaviour). A change in the pore pressure distribution without a change in the external loading conditions, for example a change of hydraulic conditions or the decay of excess pore pressures in time (consolidation), causes a complementary change in effective stresses, which will also result in deformations.

The second aspect is the fact that soil stiffness is not a constant, but it depends on various influences. The main influences are listed below:

- *Stress level:* In general: the higher the confining stress level, the larger the stiffness; as a result, the deeper the soil (= higher stress level), the larger the stiffness. On the other hand, the larger the shear stress level (i.e. the more shear strength is mobilised), the smaller the stiffness.
- *Stress path:* Unloading is stiffer than primary loading; also: compression vs. shearing.
- *Strain level:* In general: the smaller the strain level, the larger the stiffness; in this respect, the stiffness against small vibrations (<0.05%) is much higher than the stiffness at the larger ‘engineering’ strain levels (~0.5%).



- *Time (duration)*: In general: the shorter the time, the larger the stiffness.
- *Density*: The denser the soil, the stiffer it is.
- *Water/permeability*: Undrained saturated soils are stiffer than drained or unsaturated soils.
- *Over-consolidation*: Over-consolidated soils are stiffer than normally consolidated soils.
- *Direction*: Some soils have a highly directional-dependent stiffness (stiffness anisotropy)

The third aspect relates to irreversible deformation as a result of loading, i.e. the fact that a part of the deformations will not disappear after removal of the load. Most soils only have a very small elastic region and show irreversible deformation almost from the onset of loading. This is one of the aspects that makes the modelling of soil behaviour such a difficult job. Irreversible deformation should not be confused with failure. For example: when a soil sample is loaded in an oedometer test, it will show irreversible deformations due to one-dimensional compression, but the soil sample will never fail under such conditions.

The fourth aspect relates to the strength of soil. Soil strength is usually expressed in terms of shear strength. Since soil is a frictional material, the shear strength depends on the confining effective stress level. In addition, there are several other influences on the soil shear strength, such as:

- *Loading speed*: The higher the speed, the higher the shear strength.
- *Time (duration)*: Shear strength may increase in time (for example: cementation) or decrease in time (degradation).
- *Density*: The denser the soil is, the higher the (peak) shear strength, but dense soils may show softening behaviour after the peak, i.e. strength reduction towards a residual strength after the peak strength was reached (see Fig. 2).

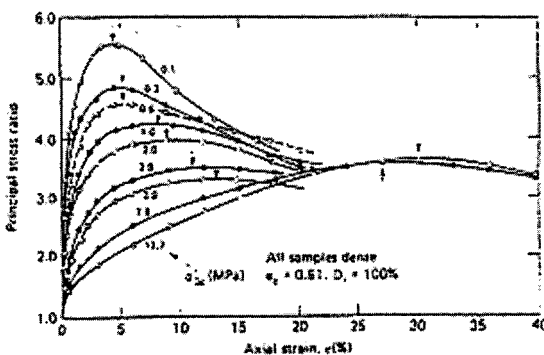


**FIG. 2. Results from standard drained triaxial test on dense sand, indicating peak strength and softening.**

- *Undrained behaviour*: At the short term, the shear strength of undrained soils seems to be constant, but care must be taken with longer periods.
- *Over-consolidation*: Over-consolidation may lead to a high peak shear strength, followed by softening.

- *Direction:* Some soils have a highly directional-dependent shear strength (strength anisotropy).

Regarding soil strength it should also be mentioned that soils hardly show any tensile strength or no tensile strength at all. This certainly applies to dry frictional soils, but also cohesive soils have a tensile strength that is low compared to their cohesive strength.

The fifth aspect relates to the time-dependency of soil behaviour. It was indicated before that the soil stiffness and strength are influenced by time. Even when loading conditions remain unchanged, time can play an important role in the mechanical behaviour of soil. As an example, especially for soft soils, when excess pore pressures have occurred due to undrained loading, these will decay in time (consolidation) and cause additional settlement. In addition, after all excess pore pressures have disappeared, the settlement process may continue in time due to creep. If, on the other hand, the soil is constrained when a certain over-stress has been applied, then the over-stresses will gradually decrease in time due to relaxation. In fact, relaxation is similar as creep; the difference is only in the type of boundary condition. A final type of time-dependent behaviour is swelling. Swelling could be seen as inverse consolidation, i.e. time-dependent expansion of soil as a result of the decay of tensile pore stresses due to removal of load. However, problematic swelling of soils is often caused by additional effects, like de-saturation or chemical processes.

Finally, there are a few other aspects that are typical for soil or particular types of soil, as listed below:

- *Compaction & dilatancy:* Loose soils will compact due to shearing whereas dense soils will dilate due to shearing. Compaction and dilatancy will come to an end as soon as the soil has reached a critical density. Clays are usually more compressible than sands and hardly show dilatancy, except when highly over-consolidated. Calcareous sands may also show compaction due to crushing or solution of material in water.
- *Memory of pre-consolidation stress:* When soils have been pre-loaded, they will ‘remember’ their pre-consolidation stress level. The behaviour due to stress changes below the pre-consolidation stress is stiff, whereas loading beyond the pre-consolidation stress is much softer. If pre-consolidated soils are reconstituted they lose the information about their pre-consolidation stress and will behave as normally consolidated soils.

### **Behaviour in engineering applications**

Before considering the aspects of soil that are relevant for changes of stress in geotechnical engineering applications, it is important to consider the initial soil conditions. The initial situation involves at least the effective vertical stress distribution (which is derived from the soil weight and the pore (water) pressure distribution), the horizontal effective stress distribution (or  $K_0$ -value), the pre-consolidation stress and preferably the initial void ratio.

Regarding changes of stress in geotechnical engineering applications due to loading, construction, excavation or any other cause, it should be noted that not all aspects mentioned in the beginning of this section play an equally important role in



each type of application. Therefore, a global overview is given here of the aspects that are most important for certain applications:

- *Embankment construction:* Involves primary loading (or partly reloading if the sub-soil is over-consolidated). The stress path is dominated by compression. Deviatoric loading may occur near the embankment sides. In general, the strain level can be quite high. If soft soils are involved also aspects as undrained loading, consolidation, creep and anisotropic behaviour may be important to consider (see for example Ladd et. al., 1993). In such cases care must be taken when assuming drained conditions, since this may lead to results that are too optimistic.
- *Slope stability:* Emphasis must be put here on soil strength and all its dependencies. Shearing is most important. Time-dependent behaviour may also play a role.
- *Excavation / retaining wall:* Involves mainly unloading (de-compression), partly combined with deviatoric loading (mobilisation of shear strength). Arching behind the wall plays an important role and may produce different load distributions on the wall than assumed in conventional analyses (see for example the results of the excavation test near Karlsruhe, as published by Von Wolffersdorff, 1994). The excavation test has also indicated that elastic perfectly-plastic models with a constant stiffness modulus produce unrealistically large pit bottom heave, whereas models that include stress(path)-dependent stiffness perform much more realistic. In order to accurately model the settlement trough behind a retaining wall, small strain stiffness is required. The strain level around the wall is low to medium. Note that when clay-type soils are considered, the assumption of undrained behaviour may be too favourable.
- *Tunnelling:* Tunnelling also involves unloading. The settlement trough above a (shield) tunnel is often observed as an inverted bell-shaped (Gaussian) curve (Peck, 1969), where the volume of the 'bell' is more or less equal to the volume loss due to the tunnelling process. In order to realistically represent such a form using finite elements, small strain stiffness is required. The strain level around the tunnel itself is low to medium. Another issue in tunnelling is tunnel heading stability, which involves a three-dimensional analysis. In that case soil strength is the major issue, in relation to the tunnel construction method.
- *Foundations:* Involves primarily loading and possibly shearing. Distinction should be made between deformation analysis and bearing capacity. For the former, the aspects of stiffness are important; for the latter the aspects of strength are dominant. Depending on the type of foundation, the strain level around the foundation is low (pile foundation) to medium (raft foundation), and can sometimes even be high. Some recommendations have been given by the ISSMGE Technical Committee on Piled Foundations (TC18), as reported by Poulos, 2001.
- *Dynamic analysis:* Dynamic analysis generally involves very small strains and thus small-strain stiffness. If cyclic loading effects need to be considered, strain-dependent stiffness and hysteresis are required. For earthquake analysis, the range of strain levels is larger than for vibrations only. Moreover, earthquakes may lead



to liquefaction of the soil, i.e. accumulation of excess pore pressures and reduction of shear strength.

For most of the above types of application the interaction between the soil and the structures in the soil also plays an important role. Although soil-structure interaction is considered to be a major subject for geotechnical engineering projects, it is beyond the scope of this contribution and will not be further discussed here.

## POSSIBILITIES AND LIMITATIONS OF SOME EXISTING MODELS FOR GEOTECHNICAL ENGINEERING APPLICATIONS

Considering the modelling of soil behaviour by means of constitutive relationships, quite a number of models have been proposed in the past. Constitutive models form the qualitative description of material behaviour, whereas the model parameters further quantify this behaviour. Since the eighties it is common for researchers to implement constitutive models in finite element programs with the purpose to validate their accuracy compared to soil testing data and to demonstrate their applicability in engineering applications. However, the number of models that appear in commercial finite element programs for geotechnical engineering applications on a larger scale is rather limited. In this contribution attention is focused on a limited number of frequently used models for which the possibilities and limitations with respect to different types of geotechnical engineering applications are discussed. The following models are considered:

- Hooke's law (LE)
- The Mohr-Coulomb model (MC)
- The Drucker-Prager model (DP)
- The Duncan-Chang model or Hyperbolic model (DC)
- The (Modified) Cam-Clay model (CC)
- The Plaxis Soft Soil (Creep) model (SS(C))
- The Plaxis Hardening Soil model (HS)

### Hooke's law

$$\begin{bmatrix} d\sigma_{xx} \\ d\sigma_{yy} \\ d\sigma_{zz} \\ d\sigma_{xy} \\ d\sigma_{yz} \\ d\sigma_{zx} \end{bmatrix} = \frac{E}{(1+\nu)(1-2\nu)} \begin{bmatrix} 1-\nu & \nu & \nu & 0 & 0 & 0 \\ \nu & 1-\nu & \nu & 0 & 0 & 0 \\ \nu & \nu & 1-\nu & 0 & 0 & 0 \\ 0 & 0 & 0 & \frac{1}{2}-\nu & 0 & 0 \\ 0 & 0 & 0 & 0 & \frac{1}{2}-\nu & 0 \\ 0 & 0 & 0 & 0 & 0 & \frac{1}{2}-\nu \end{bmatrix} \begin{bmatrix} d\varepsilon_{xx} \\ d\varepsilon_{yy} \\ d\varepsilon_{zz} \\ d\gamma_{xy} \\ d\gamma_{yz} \\ d\gamma_{zx} \end{bmatrix} \quad (1)$$

Eq. (1) represents Hooke's law of linear isotropic elasticity, here formulated as a relationship between increments of stress,  $d\sigma$ , and increments of strain,  $d\varepsilon$ . It has only two parameters: Young's modulus,  $E$ , and Poisson's ratio,  $\nu$ . Hooke's law may be thought of as the simplest available stress-strain relationship, but this is generally too crude to capture essential features of soil behaviour. Nevertheless, Hooke's law still

 @Seismicisolation

plays an important role in advanced constitutive modelling, since it often forms the elastic part of more advanced elastoplastic models. With a slight modification of Hooke's law as an isotropic model, it is possible to include anisotropy of stiffness, as formulated in Eq. (2) (e.g. Zienkiewicz & Taylor, 1987).

$$\begin{bmatrix} d\varepsilon_{xx} \\ d\varepsilon_{yy} \\ d\varepsilon_{zz} \\ d\gamma_{xy} \\ d\gamma_{yz} \\ d\gamma_{zx} \end{bmatrix} = \begin{bmatrix} 1/E_1 & -\nu_1/E_2 & -\nu_1/E_1 & 0 & 0 & 0 \\ -\nu_2/E_2 & 1/E_2 & -\nu_2/E_2 & 0 & 0 & 0 \\ -\nu_1/E_1 & -\nu_2/E_2 & 1/E_1 & 0 & 0 & 0 \\ 0 & 0 & 0 & 1/G_2 & 0 & 0 \\ 0 & 0 & 0 & 0 & 1/G_2 & 0 \\ 0 & 0 & 0 & 0 & 0 & 2(1+\nu_1)/E_1 \end{bmatrix} \begin{bmatrix} d\sigma_{xx} \\ d\sigma_{yy} \\ d\sigma_{zz} \\ d\sigma_{xy} \\ d\sigma_{yz} \\ d\sigma_{zx} \end{bmatrix} \quad (2)$$

Eq. (2) is based on the inverse relationship. In this case there are five parameters: Young's modulus in two directions, Poisson's ratio in two directions and an additional shear modulus,  $G$ . To some extend, Hooke's law or the anisotropic extension could be used to model stiff materials in soil, such thick concrete walls or plates, rock layers or far-field areas where plasticity does not play a role, but it is not suitable to model soil in general.

### Mohr-Coulomb

The Mohr-Coulomb model is an elastic perfectly-plastic model and forms, in fact, a combination of Hooke's law and the generalised form of Coulomb's failure criterion. The model involves five parameters, namely the two elastic parameters from Hooke's law (Young's modulus,  $E$ , and Poisson's ratio,  $\nu$ ), the two parameters from Coulomb's failure criterion (the friction angle,  $\phi$ , and cohesion,  $c$ ) and the dilatancy angle,  $\psi$ . The latter parameter comes from the use of a non-associated flow rule, which is used to model a realistic irreversible change in volume due to shearing. More information about the selection of these parameters is given in Section 4.

The elastic perfectly-plastic Mohr-Coulomb model is often used to model soil behaviour in general. It should be noted that this is only a first order model: Failure behaviour is generally quite well captured (at least for drained conditions), but the stiffness behaviour before reaching the local shear strength is poorly modelled. In fact, the stiffness behaviour below the failure contour is assumed to be linear elastic according to Hooke's law, given by a constant Young's modulus and Poisson's ratio. Hence, the model has limited capabilities to accurately model deformation behaviour before failure, especially in situations where the stress level is changing significantly or in the case that multiple different stress paths are followed. When using the MC model for excavations and retaining wall problems, it generally leads to a large pit bottom heave, which may cause an unrealistic uplift of the retaining wall. In tunnelling problems, the use of the Mohr-Coulomb model produces a settlement trough that is generally too wide. Nevertheless, the Mohr-Coulomb model could be used to get a first estimate of deformations (order of magnitude), but an accuracy of more than 50% should not be expected (deformations may be a factor 2 off).



Regarding its strength behaviour the Mohr-Coulomb model performs better. Researchers have indicated by means of true-triaxial tests that stress combinations causing failure in real soil samples agree quite well with the hexagonal shape of the Mohr-Coulomb failure contour (Goldscheider, 1984). Therefore, this model is well suitable to analyse the stability of dams, slopes, embankments and other geotechnical structures. However, the model does not include softening behaviour after a peak strength has been reached.

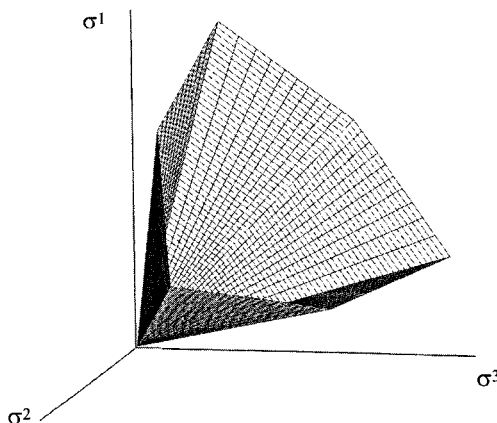


**FIG. 3. Failure contour of the Mohr-Coulomb model in principal stress space**

Therefore, to be on the safe side, it is advised to select the strength parameters such that they represent the residual strength rather than the peak strength, except if all stress points remain far from the critical state. Care must be taken if undrained materials (clays) are modelled using effective strength properties. This is, in principle, possible if the bulk stiffness of the water in the pores is explicitly taken into account and distinction is made between a change in effective stresses and the development of excess pore pressures. In the geotechnical finite element program Plaxis this is achieved by using the Undrained option in the corresponding material data set. In this case it must be noted that the effective stress path that is followed in undrained materials using the Mohr-Coulomb model may deviate significantly from what is observed in reality. In fact, soft soils, like normally consolidated clays, generally show a decreasing mean effective stress during shearing, whereas the Mohr-Coulomb model would predict a constant mean effective stress in this case. As a result, when using effective strength properties, the resulting shear strength is over-predicted. In that case it is preferred that the cohesion parameter is used to model the actual undrained shear strength, whilst the friction angle must be set equal to zero. Note that in this way the increase in shear strength as a result of consolidation is not automatically taken into account and must be changed manually.

### Drucker-Prager

The Drucker-Prager model (Drucker & Prager, 1952) is a simplification of the Mohr-Coulomb model in the sense that the hexagonal shape of the failure contour in principal stress space has been replaced by a simple cone (see Fig. 4).

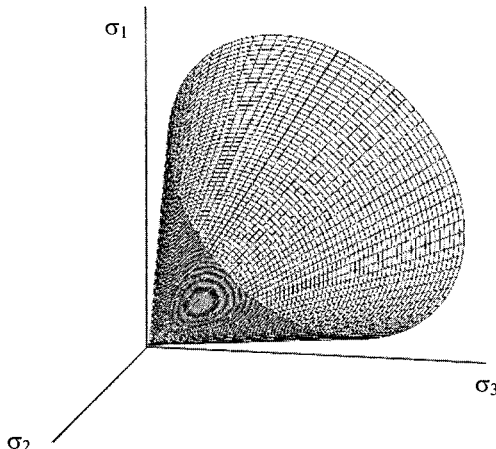


**FIG. 4. Failure contour of the Drucker-Prager model in principal stress space**

This may have major consequences for the modelling of failure. For problems where the dominant stress paths involve either triaxial compression or triaxial extension it is easy to select the friction parameter in the Drucker-Prager model such that the failure behaviour corresponds with failure in the Mohr-Coulomb model. This is also possible for plane strain problems, even when dilatancy is taken into account (Brinkgreve, 1994). However, if a problem involves multiple different stress paths it is impossible to select the friction parameter in the Drucker-Prager model such that the failure behaviour is well captured in all these paths. Hence, the Mohr-Coulomb model is preferred over the Drucker-Prager model. If no other model than Drucker-Prager is available, care must be taken with the selection of the strength parameters. Furthermore, the same limitations as described for the Mohr-Coulomb model are valid for the Drucker-Prager model.

### Duncan-Chang (Hyperbolic model)

The Duncan-Chang model (Duncan & Chang, 1970), which is also known as the Hyperbolic model (see Fig. 5), is a model that is particularly popular in the United States as a non-linear soil model. The model is on one hand based on Kondner's idea that the stress-strain curve in drained triaxial compression tests can be approximated by a hyperbola (Kondner, 1963), and on the other hand on Ohde's idea that soil stiffness can be formulated as a stress-dependent parameter using a power law formulation (Ohde, 1939). Moreover, at a given confining stress level, distinction is made between a (stress-dependent) primary loading stiffness,  $E_t = E_0 (1-q/q_{ult})^2$ , and a

**@Seismicisolation**

(constant) unloading and reloading stiffness,  $E_{ur}$ , where loading is defined by the condition  $d(\sigma_1/\sigma_3) > 0$ . Hence, the model involves a better description of the non-linear and stress(path)-dependent stiffness before failure. In this respect the Duncan-Chang model is preferred over the Mohr-Coulomb model. Failure itself is described in the model by means of the Mohr-Coulomb failure criterion, but this is not properly formulated in a plasticity framework. As a result, the model cannot describe dilatancy, since this would require a Poisson's ratio larger than 0.5, which is theoretically not admissible.

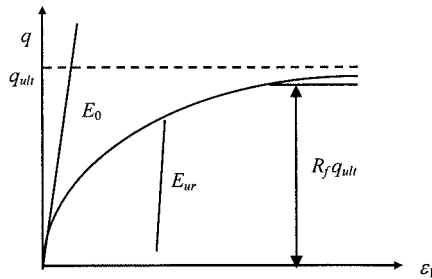


**FIG. 5. Duncan-Chang approximation of the stress-strain relationship in a standard drained triaxial test**

Another disadvantage is that the distinction between loading and unloading is not consistently formulated. Since loading is formulated as  $d(\sigma_1/\sigma_3) > 0$  and unloading as  $d(\sigma_1/\sigma_3) < 0$ , the model is inconsistent for neutral loading as, for instance, observed in oedometer testing where  $\sigma_1/\sigma_3 = 1/K_0$  and thus  $d(\sigma_1/\sigma_3) = 0$ . Although for such stress paths the lower  $E_t$ -value could be used, a slight deviation from this path could result in the use of the much stiffer  $E_{ur}$ -value, which would lead to a significantly different strain response.

Despite the inconsistencies, the model can be evaluated as an improved first order model for geotechnical engineering applications in general.

### (Modified) Cam-Clay

The Cam-Clay model was developed in the sixties at Cambridge University (Schofield & Wroth, 1968). This model is based on Critical State theory and was originally meant to simulate the behaviour of near-normally consolidated clays under triaxial compression test conditions. Shortly after the introduction of the original Cam-Clay model, a modified flow rule was proposed by Burland (1965). The latter model is known as the Modified Cam-Clay model, and is frequently used in geotechnical applications, especially in Anglo-Saxon countries.

The basic assumption of the Modified Cam-Clay model is that there is a logarithmic relationship between the mean effective stress,  $p'$ , and the void ratio,  $e$ . Hence, the model involves a linear stress-dependency of the stiffness, which is most realistic for near-normally consolidated clays. Distinction is made in the model between primary loading (i.e. loading beyond the isotropic pre-consolidation stress level,  $p_c$ ) and unloading or reloading (below and up to the pre-consolidation stress).

The non-linear behaviour is modelled by means of hardening plasticity. Starting from a normally consolidated stress state, any stress path involving ‘loading’ leads to plastic straining, but this should not be confused with failure. As a result, the pre-consolidation stress increases, which is associated with the development of plastic volumetric straining. The ratio between plastic volumetric strain and plastic deviatoric strain follows from an associated flow rule and depends on how much the material’s internal friction has been mobilised. The more the material friction is mobilised (i.e. shearing or deviatoric loading), the more plastic shear strain occurs. The situation that the material’s ‘true’ internal friction is mobilised is called Critical State. In this case the material has come in a state of critical void; there is no more volume change whilst the deviatoric strain goes to infinity. This state is associated with failure. In the Cam-Clay models the Critical State Line is comparable with the Drucker-Prager failure contour. Hence, the same remarks regarding the inaccuracy in describing failure as mentioned for the Drucker-Prager model also hold for the Modified Cam-Clay model. On the other hand, the Modified Cam-Clay model has many more features to describe the non-linear and stress(path)-dependent behaviour prior to failure than the Drucker-Prager model, especially for clay-type soils (see Fig. 6 for its non-linear behaviour in drained triaxial testing). In fact, the Modified Cam-Clay model is more accurate and suitable to describe deformation behaviour than failure.

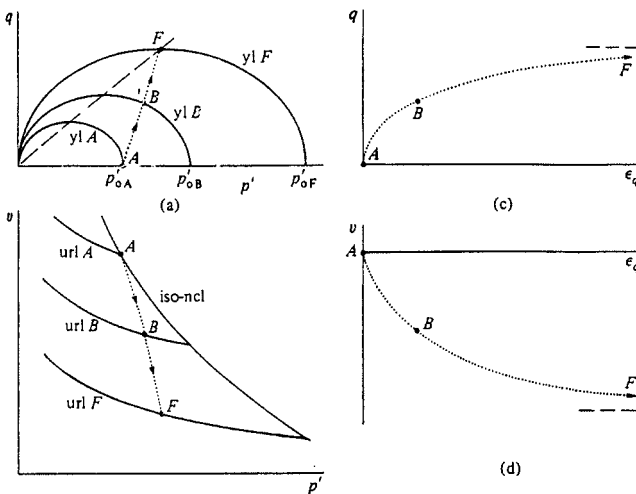


**FIG. 6. Behaviour of the Modified Cam-Clay model in drained triaxial compression (after Wood, 1990)**

For over-consolidated states of stress, the Modified Cam-Clay model involves Hooke’s law of isotropic elasticity. If deviatoric loading is applied to soils in a highly over-consolidated stress state, the Modified Cam-Clay model predicts an unrealistically long elastic range (which is only as good as Hooke’s law), followed to an unrealistically high peak strength (well above the Critical State Line), followed by softening behaviour until the Critical State is reached from the upper side. Care

@Seismicisolation

must be taken with such situations, since the predicted behaviour is much more favourable than real soils tend to show. Therefore it can be concluded that the Modified Cam-Clay model is not very suitable for highly over-consolidated soils. Moreover, softening behaviour may lead to mesh-dependency and numerical difficulties when implemented in a finite element program. Some finite element programs have taken additional measures to avoid softening or at least the high peak strengths. It is therefore recommended to review the corresponding program manuals and to evaluate how the Modified Cam-Clay model has been implementation before using it for geotechnical applications.

Since the advantages of the Modified Cam-Clay model are primarily contained in the hardening plasticity formulation, the model performs best in applications involving loading conditions, such as embankment construction or foundation problems. The model is most suitable for soft soils such as near-normally consolidated clays.

The Modified Cam-Clay model involves four model parameters, i.e. the isotropic logarithmic compression index,  $\lambda$ , the swelling index,  $\kappa$ , Poisson's ratio for unloading and reloading,  $\nu_{ur}$ , and the friction constant,  $M$ . The latter parameter is equivalent to the Drucker-Prager friction constant. However, this parameter does not only represent the material internal friction; it also implicitly determines the  $K_0$ -value in one-dimensional compression, although higher than in reality. Note that the Modified Cam-Clay model does not involve a cohesion parameter. Shear strength can only be modelled using an effective friction constant. In the case of primary undrained deviatoric loading of soft soils the model predicts a realistic reduction of mean effective stress and arrives at a lower and more realistic undrained shear strength than the Drucker-Prager model. In addition to the model parameters, the Modified Cam-Clay model involves two state parameters, i.e. the pre-consolidation stress,  $p_c$ , and the void ratio,  $e$ , for which initial values have to be specified. More details about the selection of parameters is given in Section 4.

### Plaxis Soft Soil model

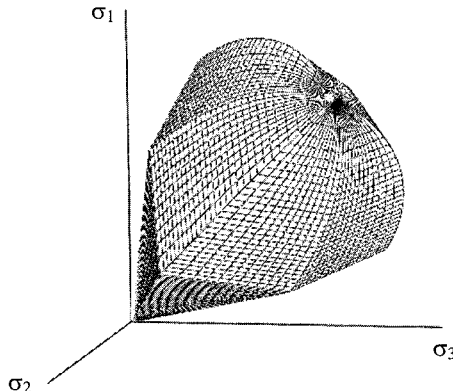


**FIG. 7. Yield contour of the Plaxis Soft Soil model**

@Seismicisolation

The Soft Soil model (Brinkgreve & Vermeer, 1997) is based on the Modified Cam-Clay model, but some of its drawbacks have been improved in this model. First of all, the model does not involve the over-prediction of the shear strength for over-consolidated states of stress. In fact, a Mohr-Coulomb failure criterion has been added to improve the capabilities of the model at failure. The “friction constant”  $M$ , which determines the steepness of the Critical State Line and therewith the  $K_0$ -value in one-dimensional compression, can be selected independent from the standard Mohr-Coulomb strength parameters  $\varphi$  and  $c$ , such that a more realistic  $K_0$ -value can be obtained.

The stiffness behaviour in the Soft Soil model is based on a logarithmic relationship between the mean effective stress,  $p'$ , and the volumetric strain,  $\varepsilon_v$  (rather than the void ratio). Therefore, this model has the slightly modified parameters  $\lambda^*$  and  $\kappa^*$  instead of the original Cam-Clay parameters and requires no input on the initial void ratio.

The Soft Soil model can best be applied in situations that involve primary loading conditions, such as embankment construction or foundation problems. The model has no advantages over the Mohr-Coulomb model in unloading problems, such as excavations or tunnel problems. In contrast to the Modified Cam-Clay model, the overall failure prediction of the Soft Soil model is quite good, also in undrained conditions. Therefore, this model can be considered a second order model, at least for near-normally consolidated clays for the ‘loading’ type of applications mentioned above. The Soft Soil model does not have capabilities to model anisotropic strength and stiffness, as generally observed for peat. Nevertheless, it could be used for peat as long as anisotropy does not play a major role in the application.

In addition to the Soft Soil model, a Soft Soil Creep model has been developed (Vermeer & Neher, 1999), which has capabilities to model secondary compression behaviour. This has been achieved by using visco-plasticity rather than hardening plasticity to formulate the model. This leads to an extra input parameter for creep, namely the modified creep index  $\mu^*$ . Other features of this creep model are similar to those of the Soft Soil model. Care must be taken with the selection of the initial over-consolidation ratio, since this ratio not only sets the initial pre-consolidation stress, but also the initial creep strain rate in situations where the stress state is dominated by the in-situ stresses. The Soft Soil Creep model is considered to be a more ‘academic’ model than the Soft Soil model.

### **Plaxis Hardening Soil model**

The Hardening Soil model (Brinkgreve & Vermeer, 1997; Schanz & Vermeer, 1998) is a true second order model for soils in general (soft soils as well as harder types of soil), for any type of application. The model involves friction hardening to model the plastic shear strain in deviatoric loading, and cap hardening to model the plastic volumetric strain in primary compression. Failure is defined by means of the Mohr-Coulomb failure criterion. Because of the two types of hardening, the model is also accurate for problems involving a reduction of mean effective stress and at the same time mobilisation of shear strength. Such situations occur in excavations (retaining wall problems) and tunnel construction projects.



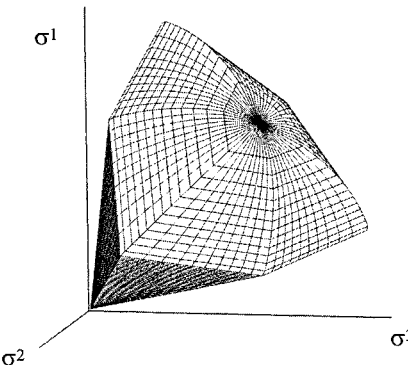


**FIG. 8. Yield contour of the Plaxis Hardening Soil model**

With respect to its stiffness behaviour the model involves a power law formulation for stress-dependent stiffness, similar as the one used in the Duncan-Chang model. In fact, the model shows correspondence with the Duncan-Chang model regarding its hyperbolic stress-strain response when simulating a standard drained triaxial test. Since the Hardening Soil model is based on hardening plasticity rather than non-linear elasticity, it overcomes the limitations and inconsistencies of the Duncan-Chang model with respect to dilatancy and neutral loading.

In undrained loading, the model nicely shows a reduction of mean effective stress, as observed for soft soils, whereas it may also show the increase in mean effective stress for harder type of soils (dilative soils).

The Hardening Soil model requires the input of 10 parameters, i.e. three reference stiffness parameters ( $E_{0c}^{ref}$  for triaxial compression,  $E_{ur}^{ref}$  for triaxial unloading and  $E_{oed}^{ref}$  for oedometer loading) at a reference stress level  $p^{ref}$ , a power,  $m$ , for the stress-dependent stiffness formulation, Poisson's ratio for unloading and reloading,  $\nu_{ur}$ , the Mohr-Coulomb strength parameters,  $\phi$  and  $c$ , the dilatancy angle,  $\psi$ , the  $K_0$ -value in primary one-dimensional compression ( $K_0^{nc}$ ), and a parameter called the failure ratio,  $R_f$ , which determines the strain level at failure. The latter parameter also appears in the Duncan-Chang model and can generally be taken 0.9.

The Plaxis Hardening Soil model can be used to accurately predict displacement and failure for general types of soils in various geotechnical applications. The model does not include anisotropic strength or stiffness, nor time-dependent behaviour (creep). Its capabilities for dynamic applications are limited, but this model is, in principle, without any doubt the most accurate general soil model of all models described in this contribution.

## SELECTION OF MODEL PARAMETERS

The parameters of the models described in Section 3 are used to quantify the mechanical behaviour of soils, and represent as such mainly the stiffness and strength properties, i.e. the properties that are of interest for deformation and stability. As mentioned in Section 2, stiffness and strength properties show a large dependence on

the stress level and the stress path that is followed in the application. Some models include this stress(path)-dependency to a certain extend in their formulation. Nevertheless, it is important to keep in mind how the model parameters have been obtained and in which stress range and stress paths they are valid.

Most parameters of the models as described in Section 3 have a clear physical meaning. That does not mean that they can be easily selected. In many situations parameters cannot directly be obtained, for example because only limited soil data are available or the available data are not directly usable for the application at hand. Hence, parameter selection must always include an evaluation of the selection procedure and an interpretation in view of the application.

In general, model parameters can be selected on the basis of:

- Laboratory soil test results (oedometer test, CRS test, triaxial tests (CD, CU, UU), direct or simple shear test (DSS), Torvane test)
- Field test results (standard penetration test (SPT), cone penetration test (CPT), pressuremeter test (Menard or CPM), dilatometer test (DMT), vane test)
- Correlations with general soil properties (from classification tests or other general soil tests, i.e.  $w_L$ ,  $w_P$ ,  $I_p$ ,  $I_L$ ,  $RD$ )
- Tables, norms, rules of thumb
- Experience

Laboratory tests have the advantage that these are usually done in well controlled conditions. However, the conditions, stress levels and stress paths at which the tests are done may deviate from the application. As a result, the parameters as determined from the tests have to be recalculated or re-interpreted in view of the application.

Field tests have the advantage that the conditions correspond with the application, but these tests cannot be used for a direct selection of parameters. Instead, parameters are selected based on correlations with field measurement quantities.

Correlations with general properties have the disadvantage that they are based on generalized data and not specifically based on the situation at hand; therefore their accuracy is lower by definition. This also applies to tables, norms and rules of thumb. Nevertheless, they can be quite useful to validate the order of magnitude, but it should be noted that the direct selection of parameters based on soil testing data from the application at hand is preferred. Although different methods always give different answers, the best parameter selection practice is in fact based on a combination of methods with cross-checking.

Before going into detail on the selection of parameters, first an overview is given of which parameter can be selected from which method. In Table 1 an indication is given whether the parameter can be selected directly (D) from the test, indirectly (I) (recalculation needed) or by correlation (C). Characters in brackets mean that selection depends on how the test is performed (for example whether it includes unloading or not).

**Table 1. Overview of model parameters and selection methods**

Parameters	Models	Oedometer	CRS	CD	CU	UU	DSS	Torvane	SPT	CPT	PM	DMT	Vane test	Classification	Tables, rules
$c'$	MC, DP, DC, SS(C), HS		D	D		D			C					C	
$\phi'$	MC, DC, SS(C), HS		D	D		D			C					C	
$M$ (friction)	DP, CC		I	I		I			I					I	
$s_u$	MC, DP, DC, HS				D		D	C	C			D	C	C	
$\psi$	MC, HS			D										C	
$E$	LE, MC, DP	I	I	I	I	I	I	C	C		C		C	C	
$E_{50}^{ref}$	DC, HS	I	C	D	I	D	I	I	I				C	C	
$E_{ur}^{ref}$	DC, HS	(D)		(D)	(I)	(D)				I				C	
$E_{oed}^{ref}$	HS	D	D				I	I	I	I	C		C	C	
$\lambda (*)$	CC, SS(C)	D	I						C	I	I		C	C	
$\kappa (*)$	CC, SS(C)	(D)	I						C				I	C	
$\mu^*$	SSC	(D)	D											C	
$v$	LE, MC, DP, DC	I		D										C	
$v_{ur}$	CC, SS(C), HS	(I)												C	
$m$ (power)	DC, HS	D	I	D	D								C	C	
$K_0^{nc}$	SS(C), HS	(D)										C	C		
$R_f$	DC, HS												C		

### Strength parameters

Most models involve an effective cohesion,  $c'$ , and an effective friction angle,  $\phi'$ , whereas in some models the shear strength can also be modelled by means of an undrained shear strength,  $s_u$ . The effective strength parameters can be directly obtained from consolidated triaxial tests at different confining pressures, when plotting principal stresses as Mohr stress circles in a  $(\sigma-\tau)$ -diagram (graphically) or plotting the principal stress difference as a function of the axial strain. In the latter case  $\phi'$  and  $c'$  can be obtained from the measured failure level,  $d$ , for two different confining pressures  $\sigma_3$  (solving two equations with two unknowns).

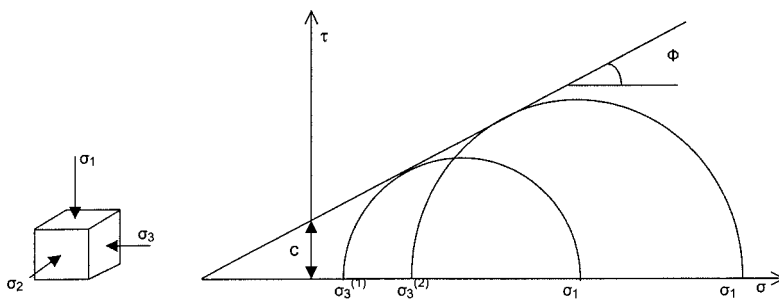


**FIG. 9. Selection of  $\phi'$  and  $c'$  based on two Mohr stress circles**  
**@Seismicisolation**

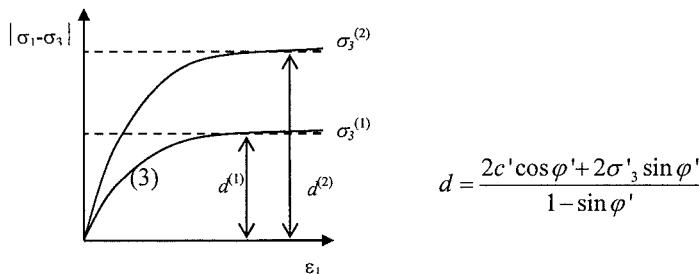


**FIG. 10. Calculation of  $\varphi'$  and  $c'$  from triaxial tests at different confining pressures  $\sigma_3$**

When no direct testing data is available, the friction angle of sands can be estimated from the soil density or void ratio (see Fig. 11).

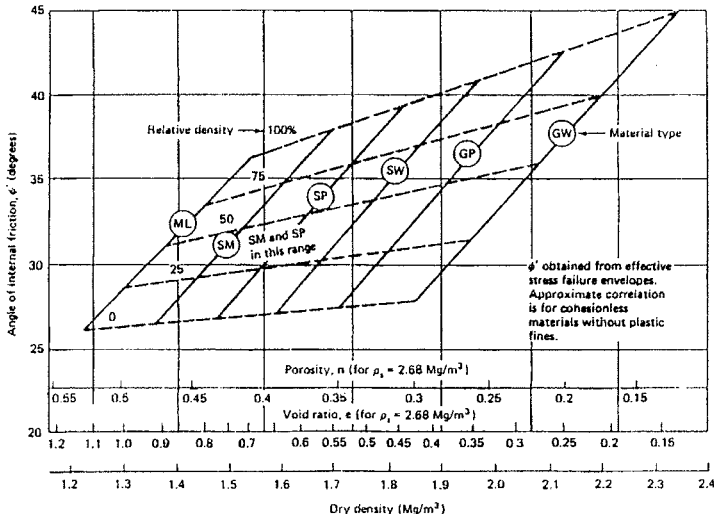


**FIG.11. Angle of internal friction depending on soil density or void ratio (sands) (from NAVFAC, 1982)**

Although the Mohr-Coulomb strength criterion is reasonably accurate, it should be noted that the two Mohr-Coulomb strength parameters  $\varphi'$  and  $c'$  do not perfectly describe failure in soils (see also Section 2 and Fig. 12). Therefore, it is important to realise for what stress levels they have been selected.

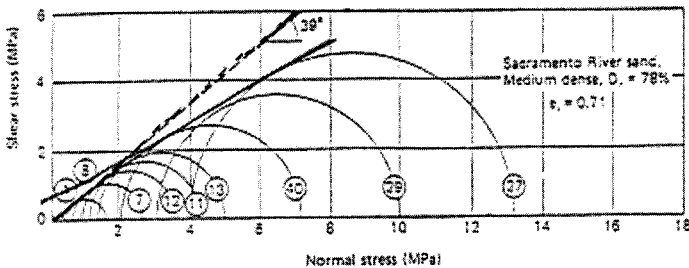


**FIG. 12. Example showing that a combination of  $\varphi'$  and  $c'$  is only valid in a certain stress range**

The friction constant  $M$  in the Drucker-Prager model and the Modified Cam-Clay model can be obtained from the friction angle in the following way:

$$M = \frac{6 \sin \varphi}{3 - \sin \varphi} \quad \text{for triaxial compression stress states} \quad (4a)$$

$$M = \frac{6 \sin \varphi}{3 + \sin \varphi} \quad \text{for triaxial extension stress states} \quad (4b)$$

$$M = \sqrt{3} \sin \varphi \quad \text{for plane strain stress states with zero dilatancy} \quad (4c)$$

Care must be taken with the first expression, since it over-estimates the shear strength for any other stress path than triaxial compression. The third equation is generally preferred.

Regarding the undrained shear strength,  $s_u$ , there are various correlations, in addition to a direct selection using unconsolidated tests like the UU triaxial test or vane tests. Some of the many proposed correlations are:

$$s_u = \left[ \frac{1}{10} \cdots \frac{1}{20} \right] (q_c - q_0) \quad \text{Correlation with cone resistance } q_c \text{ from CPT; } q_0 \text{ is the external load}$$

$$s_u \approx (0.11 + 0.0037 I_p) \sigma'_1 \quad \text{Skempton's correlation with vertical effective stress, involving the plasticity index } I_p \text{ (Skempton, 1957).}$$

$$s_u \approx 0.3 \sigma'_1 \quad \text{Approximation of the above correlation for medium plastic soils}$$

$$s_u \approx 0.2 \sigma'_1 (OCR)^{0.8} \quad \text{Ladd's correlation for over-consolidated clays (Ladd, 1991)}$$

For the Mohr-Coulomb model a theoretical relationship can be derived between the undrained shear strength and effective strength properties:

**@Seismicisolation**

$s_u = c' \cos \varphi' + (\sigma'_1 + \sigma'_3) \sin \varphi'$  Relationship between undrained shear strength and effective strength properties for plane strain applications using the Mohr-Coulomb model.

However, care must be taken with the latter relationship for parameter selection purposes, since the equation assumes a constant mean effective stress during undrained loading, whereas in reality the mean effective stress may reduce significantly, especially for soft soils. As a result, the undrained shear strength can be over-estimated when using effective strength parameters in the Mohr-Coulomb model for undrained loading.

### Stiffness parameters for clay

In general, strength parameters are considered to be less difficult to select than stiffness parameters. Hence, attention is now focused on the selection of stiffness parameters. For clays, the undrained shear strength,  $s_u$ , is often used in correlations on stiffness parameters. Vermeer et. al. (1985) have proposed an equation for the shear modulus of normally consolidated clays based on tests reported by Foott & Ladd, which also involves the plasticity index  $I_p$ :

$$G_{50} \approx \frac{5000}{I_p} c_u \quad \text{Correlation for shear modulus at 50% of strength for normally consolidated clays}$$

The undrained Young's modulus,  $E_u$ , is a factor three larger than the shear modulus. Please note the drained Young's modulus,  $E'$ , may be a factor 1.5 to 2.0 lower than the undrained Young's modulus, and thus 1.5 to 2.0 times higher than  $G_{50}$ .

For over-consolidated clays, Duncan & Buchignani (1976) have presented a graph that takes the over-consolidation ratio  $OCR$  into account:

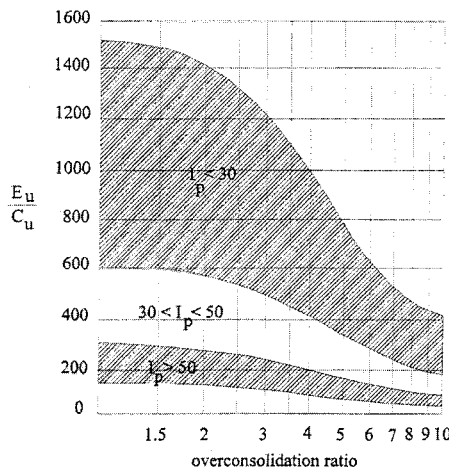


FIG.13. Undrained stiffness of over-consolidated clays, obtained from plate loading tests ( $C_u$  = undrained shear strength) (after Duncan & Buchignani, 1976)

@Seismicisolation

The primary loading stiffness of clays can be measured quite well from oedometer tests. When using a constant stiffness model (Mohr-Coulomb or Drucker-Prager), the oedometer stiffness is measured by taking the tangent to the  $(\sigma_1 - \epsilon_1)$ -curve at the desired stress level, or in case of a particular stress range by taking the secant stiffness from the starting stress level to the end stress level.



**FIG. 14. Selection of oedometer modulus from oedometer test results**

When using a model with a stress-dependent stiffness relationship (power law model, like the Duncan-Chang or Hardening-Soil model), the reference oedometer stiffness is taken as the tangent stiffness at the reference stress level.

For normally consolidated clays, the reference oedometer stiffness is about half the reference triaxial stiffness at 50% of strength:

$$E_{oed}^{ref} \approx \frac{1}{2} E_{50}^{ref} \quad \text{Approximate relation for normally consolidated clays}$$

Here it should be noted that the reference oedometer stiffness refers to a reference stress level that is based on the vertical effective stress, whereas the reference triaxial stiffness refers to the same reference stress level, but then based on the confining pressure, i.e. the lateral effective stress. Hence, one ‘finds’ these reference stiffnesses at different depths in the soil.

The actual oedometer stiffness can also be correlated to the cone resistance (CPT):

$$E_{oed} = \alpha q_c \quad \text{Correlation for oedometer stiffness of clays: } \alpha \text{ is around 3 for normally consolidated clays and around 5 for over-consolidated clays.}$$

Another correlation can be found in literature, based on the plasticity index  $I_p$ :

$$E_{oed} \approx \frac{500}{I_p} \sigma'_1 \quad \text{Correlation for oedometer stiffness of clays based on plasticity index and effective vertical stress}$$

In this case, a reference oedometer stiffness, for use in the Hardening-Soil model, can easily be obtained by entering the reference stress for  $\sigma'_1$  (usually 100 kPa):

$$E_{oed}^{ref} \approx \frac{50000 \text{ kPa}}{I_p} \quad \text{Oedometer stiffness for clays}$$

For clays, stiffness is often expressed as a logarithmic compression index, such as  $C_c$ . This implies a linear stress-dependency, which is equivalent to a power  $m = 1$  when using a power law formulation, like in the Hardening-Soil model. The logarithmic compression index  $C_c$  can be related to the Cam-Clay and Soft Soil model parameters  $\lambda$  and  $\lambda^*$ . Similarly, if unloading is considered in an oedometer test, the logarithmic swelling index can also be measured. For most clays the ratio of  $C_c/C_s$  is in the order 5 – 10. However, note that the ratio of  $\lambda/\kappa$  may be a factor 2 smaller (3 – 5). The difference is in the fact that  $C_c$  and  $C_s$  involve one-dimensional compression whereas  $\lambda$  and  $\kappa$  involve isotropic compression.

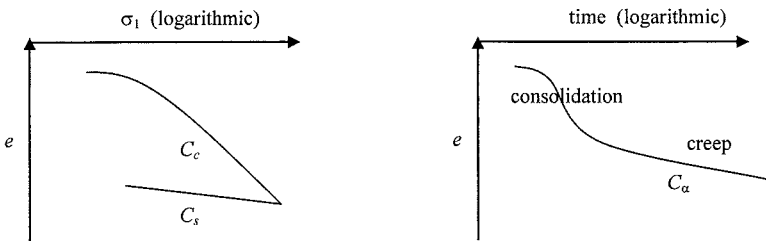


**FIG. 15. Indication of logarithmic compression index,  $C_c$ , swelling index,  $C_s$ , and creep index  $C_a$ .**

The following relationship can be used to calculate the Cam-Clay and Soft Soil (Creep) model parameters:

$$\lambda^* = \frac{\lambda}{1+e} = \frac{C_c}{2.3(1+e)} \quad \kappa^* = \frac{\kappa}{1+e} \approx \frac{C_s}{1+e} \quad \mu^* = \frac{C_a}{2.3(1+e)}$$

Where  $e$  is the void ratio; the initial void ratio,  $e_0$ , may be used as an approximation for the varying  $e$ . The factor 2.3 comes from the difference between the 10-log scale, as used for  $C_c$  and  $C_a$ , and the natural log scale, as used for  $\lambda$ ,  $\lambda^*$  and  $\mu^*$ . Please note that the relationship for  $\kappa$  and  $\kappa^*$  is only approximate.

Many correlations exist for the compression index of clay ( $C_c$ ). A well known correlation is the following one by Terzaghi & Peck (1948):

$$C_c \approx 0.9(w_L - 0.1) \quad \text{Correlation from Terzaghi \& Peck (1948)}$$

Another correlation for  $C_c$  as well as  $C_{ur}$  ( $= C_s$ ) based on the plasticity index, is obtained from a series of tests assembled by Kulhawy & Maine (1990), as indicated in Fig. 16.

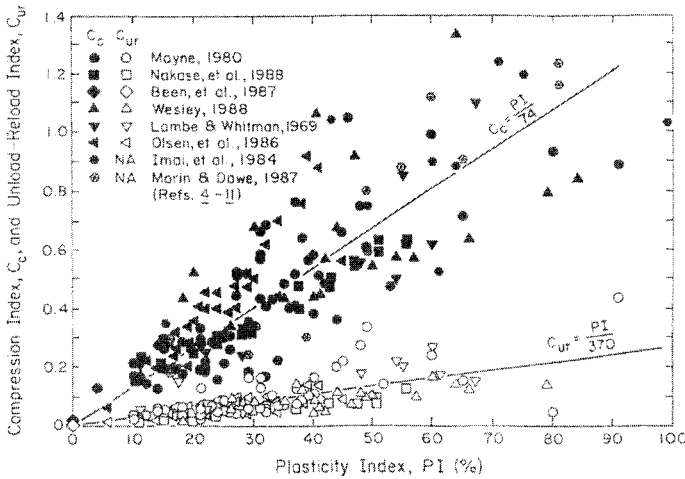


**FIG. 16. Correlation for  $C_c$  and  $C_{ur}$  ( $C_s$ ) based on plasticity index (Kulhawy & Maine, 1990)**

Based on the previous correlation, Vermeer proposed the following approximation for the reference oedometer stiffness in the Hardening-Soil model for normally consolidated clays and silts (for a reference pressure of 100 kPa and a power  $m = 1$ ):

$$E_{oed}^{\text{ref}} \approx \frac{500 \text{ kPa}}{w_L - 0.1} \quad \text{Correlation by Vermeer for HS model (NC clays and silts)}$$

To give an order of magnitude, the reference oedometer stiffness,  $E_{oed}^{\text{ref}}$ , is around 1 MPa for soft clays to around 3 MPa for stiff clays.

### Stiffness parameters for sand

The stiffness of sand is generally higher than the stiffness of clays. In addition, the stiffness of sands shows less stress-dependency than the stiffness of clays. For sandy soils the rate of stress-dependency in a power law formulation ( $m$ ) is generally in the range of 0.4 to 0.7; a power of 0.5 is a reasonable approximation, which means that the stiffness of sandy soils is proportional to the square root of the stress level.

The effective (drained) stiffness of sand can be measured from a standard drained triaxial test. The initial stiffness,  $E_0$ , is very difficult to measure. It is more common to determine the triaxial stiffness at 50% of strength ( $E_{50}$ ). This stiffness is also more representative for engineering problems, at least for situations involving primary loading.

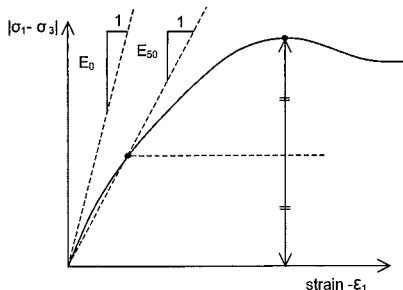


**FIG.17. Selection of sand stiffness from standard drained triaxial test**

Lengkeek has proposed the following correlation for the reference triaxial stiffness,  $E_{50}^{ref}$ , based on the relative density  $RD$ :

$$E_{50}^{ref} \approx RD \cdot 60 \text{ MPa} \quad \text{Correlation of triaxial stiffness by Lengkeek}$$

Approximations have also been proposed for the triaxial stiffness of sands in the following way:

$$E_{50} = E_{50}^{ref} \sqrt{\frac{\sigma'_3}{p^{ref}}} \quad \text{Stress-dependent triaxial stiffness of sands}$$

where the reference stiffness  $E_{50}^{ref}$  at a reference stress level of 100 kPa ranges from about 15 MPa for loose or silty sand to about 50 MPa for dense sand, at least for primary loading conditions.

In some countries it is more common to perform oedometer tests than triaxial tests to determine the stiffness of sands. The selection of the oedometer stiffness has been described before (see Fig. 14). Research by Schanz (1998) has indicated that for quartz sands the reference oedometer stiffness,  $E_{oed}^{ref}$ , is about equal to the reference triaxial stiffness,  $E_{50}^{ref}$ . Here, it should again be noted that the reference oedometer stiffness relates to a situation where the *vertical* effective stress is equal to the reference stress level (usually 100 kPa), whereas the reference triaxial stiffness relates a situation where the *lateral* effective stress is equal to the reference stress level.

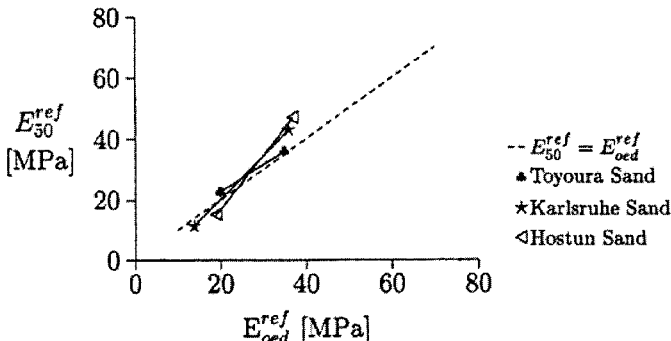


**FIG. 18. Experimental data on reference stiffnesses of quartz sands (Schanz, 1998)**

Approximations have also been proposed for the oedometer stiffness of sands in the following way (e.g. Janbu, 1963):

$$E_{oed} = E_{oed}^{ref} \sqrt{\frac{\sigma'_1}{p'^{ref}}} \quad \text{Stress-dependent oedometer stiffness of sands}$$

where the reference stiffness  $E_{oed}^{ref}$  at a reference stress level of 100 kPa ranges from about 15 MPa for loose or silty sand to about 50 MPa for dense sand, at least for primary loading conditions.

Correlations can also be found for the oedometer stiffness related to the cone resistance  $q_c$ :

$$E_{oed} = \alpha q_c \quad \text{Correlation for oedometer stiffness of sands, where } \alpha \text{ is generally in the range [1..3].}$$

However, this correlation is not very accurate and only gives an order of magnitude.

### Other parameters

A parameter that is generally given little attention is Poisson's ratio,  $\nu$ . Nevertheless, in some situations Poisson's ratio has a major influence on the stiffness behaviour and the stress path that is followed in an analysis. It should also be noted that the meaning and influence of Poisson's ratio can be different from one model to another. For example, in the Mohr-Coulomb model, Poisson's ratio plays a dominant role in one-dimensional compression in the sense that it fully determines the  $K_0$ -path. In fact, during one-dimensional compression it is only Hooke's law that plays a role here, which gives  $K_0 = \nu / (1-\nu)$ . The inverse relationship can be used to estimate the effective Poisson's ratio from a known or estimated  $K_0$ -value:

$$\nu = \frac{K_0}{1+K_0} \approx \frac{1-\sin\varphi}{2-\sin\varphi}$$

Estimation of Poisson's ratio based on  $K_0$  (for primary loading using Mohr-Coulomb or Drucker-Prager model). The approximation is based on Jaky's estimate of  $K_0 \approx 1 - \sin\varphi$  (Jaky, 1944).

Here, Poisson's ratio is typically in the order of 0.30–0.35, at least for primary loading situations. For unloading, Poisson's ratio is much lower and more in the range 0.10–0.25.

In situations of undrained behaviour Poisson's ratio can be used to model the incompressibility of undrained soils by selecting  $\nu$  close to 0.5. Care must be taken here, since computer programs can break down when  $\nu$  is taken very close or equal to 0.5. Some programs, like Plaxis, have a special option to model undrained behaviour by imposing a large bulk stiffness for the pore water, whilst Poisson's ratio always has to be entered as an effective parameter. The advantage is that distinction can be made between the change in effective stress and the change in (excess) pore pressure.

In hardening plasticity models, such as the Soft-Soil and Hardening-Soil model, Poisson's ratio is used as a parameter that only describes the elastic behaviour of the soil, which is explicitly used for unloading or reloading ( $\nu_{ur}$ ). In this case its value is typically in the range 0.10–0.25. The  $K_0$ -path in primary one-dimensional compression in such models is determined by plasticity parameters rather than by Poisson's ratio.

Another parameter that is often given little attention, but may have a significant influence is the dilatancy angle,  $\psi$ . Dilatancy is particularly relevant for dense sands or highly over-consolidated clays. For sand, the dilatancy angle can be measured from a standard drained triaxial test, when plotting the volume strain,  $\epsilon_v$ , as a function of the axial strain,  $\epsilon_1$ .

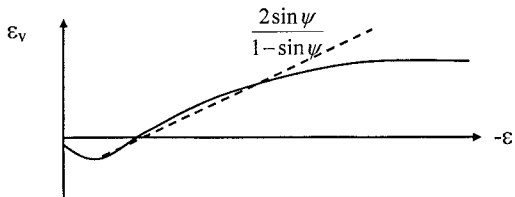


**FIG. 19. Selection of dilatancy angle from results of standard drained triaxial test**

The following correlation exists for the dilatancy angle of quartz sand:

$$\psi \approx \varphi - 30^\circ \quad \text{Correlation for quartz sand}$$

The correlation is also valid, to some extent, for very loose quartz sand with a friction angle below 30 degrees, resulting in a negative dilatancy angle (compaction). The correlation is not valid for calcareous sands or clays. For these types of soils it is recommended to use a zero dilatancy angle.

Please note that in reality the dilatancy effect comes to an end when the soil reaches its critical state. Most models where the dilatancy angle is a separate model

parameter do not automatically take the end of dilatancy into account. As a result, the expansion of the soil due to shearing will continue forever. If the situation is somehow constrained, this will lead to an unrealistic increase in confining pressure, and, as a result, to an over-prediction of the shear strength.

It should also be noted that soils that dilate under a low confining pressure may show compaction under high confining pressures (see Fig. 20). This effect should be taken into account when selecting a proper value for the dilatancy angle for a practical application.

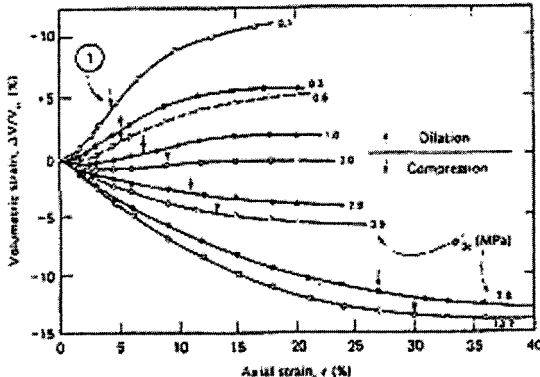


**FIG. 20. Influence of the confining pressure on the dilatancy behaviour of dense sand (results from standard drained triaxial tests)**

Care must be taken with the dilatancy angle in situations of undrained behaviour, where the soil behaviour is modelled using effective parameters and the undrained behaviour is modelled by imposing a high bulk stiffness for the pore water. The use of dilatancy can result in unrealistically high tensile excess pore stresses (suction) and unrealistically high effective stresses, which may raise the shear strength to unrealistically high values. In such a case it is recommended to use a zero dilatancy angle.

### Drained or undrained conditions

Sands are generally assumed to be draining materials, whereas clays are generally assumed to be undrained. However, it should be noted that there are other criteria that need to be taken into account to evaluate whether a soil layer is modelled drained or undrained. For example, if the stability of a clay embankment during construction is considered the situation should be modelled using undrained behaviour, whereas if the long term stability of the embankment is considered, the situation may be assumed drained. Another example: If an unsupported excavation in soft soil remains open for a long time, the assumption of undrained behaviour may be too favourable, so to be on the safe side it would be better to assume drained behaviour. Third example: If sand is quickly loaded, for example due to dynamic loading conditions, excess pore pressures may be generated, so that the situation is rather undrained instead of drained.

@Seismicisolation

A simple formula can help to determine if undrained behaviour applies:

$$T = \frac{k E_{oed}}{\gamma_w D^2} t$$

where

- $T$  = hydrodynamic period
- $k$  = soil permeability
- $E_{oed}$  = oedometer stiffness
- $\gamma_w$  = unit weight of water
- $D$  = drainage length
- $t$  = time (construction time or loading time)

Considering one-dimensional consolidation there is a relationship between the hydrodynamic period,  $T$ , and the well-known degree of consolidation,  $U$ . For relatively quick loading, resulting in  $T < 0.01$  ( $U < 0.1$ ), there is little consolidation, and the situation can be considered undrained. On the other hand, if the construction process takes a relatively long time, resulting in  $T > 0.4$  ( $U > 0.7$ ), sufficient consolidation can take place during construction, so that it is not necessary to consider undrained behaviour. In the intermediate interval it is advised to use the most unfavourable situation, i.e. undrained behaviour for loading conditions and drained behaviour for unloading conditions. Alternatively, one may consider a time-dependent coupled consolidation analysis (Biot, 1956).

## CONCLUSIONS

In this contribution an attempt has been made to assemble some information that may help geotechnical engineers with the selection of constitutive soil models for finite element applications. The possibilities and limitations of some frequently used models have been discussed. Moreover, some selection methods, correlations and other guidelines were given for the selection of the corresponding model parameters.

The author recognizes that the information presented here is far from complete in the sense that many more constitutive soil models exist that may be used for geotechnical engineering applications and that many more correlations and methods have been proposed in the literature for parameter selection. Nevertheless, the author expresses his wish that this contribution may help in making the right choices when using the finite element method for geotechnical engineering and design.

## REFERENCES

- Biot, M.A. (1956). "General solutions of the equations of elasticity and consolidation for porous material." *J. of Applied Mech.*, Vol. 23, No. 2.
- Brinkgreve, R.B.J. (1994). *Geomaterial models and numerical analysis of softening*. Dissertation. Delft University of Technology.



- Brinkgreve, R.B.J. and Vermeer, P.A. (1997). *Plaxis finite element code for soil and rock analysis – Version 7*. Balkema, Rotterdam.
- Burland, J.B. (1965). "The yielding and dilation of clay." (correspondence). *Géotechnique*, Vol. 15, 211-214.
- Coulomb, C. (1776). "Essai sur une application des règles de maximis et minimis à quelques problèmes de statique relatifs à l'architecteur." *Mémoires de Mathématique et de Physique Présentés à l'Academie Royale des Sciences*. Paris 7, 343-382.
- Drucker, D.C. and Prager, W. (1952). "Soil mechanics and plastic analysis or limit design." *Quart. Appl. Math.*, Vol. 10, No. 2, 157-165.
- Duncan, J.M. and Chang, C.-Y. (1970). "Nonlinear analysis of stress and strain in soils". *ASCE J. of the Soil Mech. And Found. Div.*, Vol. 96, 1629-1653.
- Duncan, J.M. and Buchignani, A.L. (1976). *An engineering manual for settlement studies*. Dept. of Civil Engineering, University of California at Berkeley.
- Goldscheider, M. (1984). "True triaxial tests on dense sands." In: *Constitutive relations for soils* (eds. G. Gudehus, F. Darve, I. Vardoulakis). Balkema, Rotterdam.
- Jaky (1944). "The coefficient of earth pressure at rest". *J. of the Union of Hungarian Engineers and Architects*, 355-358.
- Janbu, N. (1963). "Soil compressibility as determined by oedometer and triaxial tests." *Proc. Eur. Conf. On Soil Mech. and Found. Eng.*, DGEG.
- Kolymbas, D. (1985). "A generalized hypoplastic constitutive law." *Proc. 11<sup>th</sup> Int. Conf. on Soil Mech. and Found. Eng.* Balkema, Rotterdam.
- Kondner, R.L. (1963). "Hyperbolic stress-strain response: cohesive soils." *ASCE J. of the Soil Mech. and Found. Div.*, Vol. 89, 115-143.
- Kulhawy, F. and Mayne, J. (1990). *Manual on estimating soil properties for foundation design*.
- Ladd, C.C. (1991). "Stability evaluation during staged construction." *ASCE J. of Geotechnical Engineering*, Vol. 117, No. 4, 540-615.
- Ladd, C.C., Whittle, A.J. and Legaspi, D.E. (1994). "Stress-deformation behavior of an embankment on Boston Blue Clay." In: *Vertical and Horizontal Deformations of Foundations and Embankments, Proc. of Settlement '94, June 16-18, 1994, College Station, Texas*. ASCE Geotech. Eng. Div., 1730-1759.
- NAVFAC (1982). *Soil Mechanics (DM 7.1)*. Naval Facilities Engineering Command, Alexandria.
- Ohde, J. (1939). "Zur Theorie der Druckverteilung im Baugrund." *Der Bauingenieur*, Vol. 20, 451-459.
- Peck, R.B. (1969). "Deep excavations and tunnelling in soft ground." *Proc. 7<sup>th</sup> Int. Conf. on Soil Mech. and Found. Eng.*, Mexico.
- Poulos, H.G. (2001). "Methods of Analysis of Piled Raft Foundations." Report of ISSMGE committee TC18.
- Schanz, T. (1998). *Zur Modellierung des Mechanischen Verhaltens von Reibungsmaterialien*. Habilitation. Stuttgart University.
- Schofield, A. and Wroth, P. (1968). *Critical state soil mechanics*. McGraw-Hill, London.
- Skempton, A.W. (1957). Discussion on "the planning and design of the new Hong Kong airport" (Grace and Henry). *Proc. Inst. Civil Eng.* 7.
- Smith, I.M. and Griffith, D.V. (1982). *Programming the finite element method – Second edition*. J. Wiley & Sons.
- Termaat, R.J., Vermeer, P.A. and Vergeer, G.J.H. (1985). "Failure by large plastic deformations." *Proc. 11<sup>th</sup> Int. Conf. on Soil Mech. and Found. Eng.* Balkema, Rotterdam.
- Terzaghi, K. and Peck, R.B. (1948). *Soil mechanics in engineering practice*. J. Wiley & Sons.
- Vermeer, P.A. and Neher, H.P. (1999). "A soft soil model that accounts for creep." In: *Beyond 2000 in Computational Geotechnics – Ten Years of Plaxis International* (ed. R.B.J. Brinkgreve), Balkema, Rotterdam, 249-261.

- Vermeer, P.A., Neher, H.P., Vogler, U. and Bonnier, P.G. (2002). "3D Creep Analysis of the Leaning Tower of Pisa," Report in assignment of the International Committee for the Safeguard of the Leaning Tower of Pisa.
- Von Wolffersdorff, P.-A. (1994). "Feldversuch an einer Spundwand in Sandboden: Versuchsergebnisse und Prognosen." *Geotechnik* 17(2), 73-83.
- Wood, D.M. (1990). *Soil behaviour and critical state soil mechanics*. Cambridge University Press.
- Zienkiewicz, O.C. and Taylor, R.L. (1971). *The Finite Element Method – Fourth Edition*. Volume 1. McGraw-Hill, London.

## REVIEW OF THE STRUCTURED CAM CLAY MODEL

John P. Carter<sup>1</sup>, Member, ASCE, and Martin D. Liu<sup>2</sup>

**ABSTRACT:** The Cam Clay model and most models subsequently developed within the critical state framework are normally formulated to represent the behaviour of soils reconstituted in the laboratory, where the soil structure, if present, is standardised by the sample preparation method. However, as seen from both laboratory and in situ tests, soil behaviour may depend significantly on its structure. The structures of soils found in situ vary greatly, depending on their formation processes and their mechanical, electro-chemical and biological histories. The authors have proposed a relatively simple predictive model, known as the Structured Cam Clay (SCC) model, for solving practical geotechnical problems. In this paper a review of the performance of the Structured Cam Clay model is presented.

The paper contains the following four parts. (1) A summary is made of the generalisation of the critical state framework into a new four dimensional space, consisting of the current stress state, stress history, the current voids ratio, and the current soil structure. The key assumption of the theoretical derivation is that both the hardening and destructuring of natural clays are dependent on plastic volumetric deformation. (2) The main concepts and the formulation of the Structure Cam Clay model are introduced within the generalized framework and an explicit stress-strain matrix is obtained for SCC. (3) The capacity of the model for describing laboratory single element tests is evaluated and the main features of the model are summarised. (4) Techniques for refining the Structured Cam Clay model are also discussed.

### INTRODUCTION

The Cam Clay model and most models subsequently developed within the critical state framework are normally formulated to represent the behaviour of soils reconstituted in the laboratory, where the soil structure, if present, is standardised by

---

<sup>1</sup> Challis Professor of Civil Engineering, The University of Sydney, NSW 2006, AUSTRALIA,  
j.carter@civil.usyd.edu.au

<sup>2</sup> Research Fellow, Department of Civil Engineering, The University of Sydney, NSW 2006,  
AUSTRALIA

the sample preparation method. The mechanical properties of soil, at least of laboratory samples, have been unified theoretically into one simple and consistent framework. Within this framework the current stress state, stress history, and voids ratio (or specific volume) are the three dimensions in which the behaviour of a soil is defined (*e.g.*, see Muir-Wood, 1990).

The structures of soils found *in situ* vary greatly, depending on their formation processes and their mechanical, electro-chemical and biological histories. As seen from tests conducted *in situ* and laboratory tests on “undisturbed” samples recovered from the field, the behaviour of a natural soil may be highly dependent on its structure (*e.g.*, Burland, 1990; Carter *et al.*, 2000). Recently there have been significant developments in formulating constitutive models incorporating the influence of soil structure, such as those proposed by Gens and Nova (1993), Whittle (1993), Wheeler (1997), Kavvadas and Amorosi (2000) and Liu and Carter (2004a). In some of these recent studies (Liu and Carter, 2002, 2004b) the authors proposed a relative simple model, the Structured Cam Clay model (denoted as SCC), with the purpose of providing a relatively constitutive model suitable for the solution of boundary value problems encountered in geotechnical engineering practice. The SCC model has been implemented into the finite element program AFENA to solve practical geotechnical problems, such as simulating the performance of foundations on natural soils and the response of natural soils to cone penetration (*e.g.*, Liyanapathirana *et al.*, 2003a, 2003b, 2004). It was found that the SCC model captures well the main features of the behaviour of natural clays in both single element tests and boundary value problems, under both drained and undrained conditions. In this paper, a comprehensive review of the performance of this model is presented.

The paper contains the following four parts. (1) A general theoretical framework is introduced which describes the response of structured clays in a new four dimensional space, consisting of the current stress state, stress history, the current voids ratio and the current soil structure. (2) A summary of the concepts and formulation of the Structure Cam Clay model based on the above framework is provided. (3) The capacity of the model for describing laboratory single element tests is evaluated and the main features of the model are summarised. (4) Techniques for possible refinement of the Structured Cam Clay model are also discussed.

The stress and strain quantities used to describe soil behaviour are defined in the following section. In this treatment the properties of a reconstituted soil are called the intrinsic properties, and are denoted by the symbol \* attached to the relevant symbols.

## DEFINITIONS OF STRESS AND STRAIN PARAMETERS

The stress and strain quantities that are most useful for describing soil behaviour are defined as follows. The mean and the deviatoric stresses are given by:

$$p' = \frac{1}{3}(\sigma'_{11} + \sigma'_{22} + \sigma'_{33}) \quad (1)$$



$$q = \frac{1}{\sqrt{2}} \sqrt{[(\sigma'_{11} - \sigma'_{22})^2 + (\sigma'_{22} - \sigma'_{33})^2 + (\sigma'_{33} - \sigma'_{11})^2 + 6(\sigma'_{12}^2 + \sigma'_{23}^2 + \sigma'_{31}^2)]} \quad (2)$$

in which  $\sigma'_{ij}$  are the Cartesian components of effective stress.

The stress ratio  $\eta$  is given by:

$$\eta = \frac{q}{p'} \quad (3)$$

The corresponding incremental volumetric and deviatoric strains are defined as:

$$d\varepsilon_v = d\varepsilon_{11} + d\varepsilon_{22} + d\varepsilon_{33} \quad (4)$$

and

$$d\varepsilon_d = \frac{\sqrt{2}}{3} \sqrt{[(d\varepsilon_{11} - d\varepsilon_{22})^2 + (d\varepsilon_{22} - d\varepsilon_{33})^2 + (d\varepsilon_{33} - d\varepsilon_{11})^2 + 6(d\varepsilon_{12}^2 + d\varepsilon_{23}^2 + d\varepsilon_{31}^2)]} \quad (5)$$

## THEORETICAL FRAMEWORK FOR NATURAL CLAY BEHAVIOUR

A comprehensive study of the behaviour of reconstituted and naturally structured clays has been performed by the authors (for details see Liu and Carter, 2000a, 2003a). For convenience and completeness a summary of the proposed general theoretical framework used to describe natural clay behaviour is presented here. A key assumption of the proposed framework is that both the hardening and destructure of natural soils are dependent on plastic volumetric deformation. The proposed framework provides a useful basis for developing detailed constitutive models to serve various purposes and needs.

The formation and development of soil structure normally produces soil anisotropy. Destructuring usually leads to the reduction of anisotropy. In order to concentrate on introducing the physical concepts of the framework and to avoid the complexity of mathematical details, only the isotropic effect of soil structure is described in this theoretical framework. It is also assumed that the destructure resulting from stress variation is a monotonic and irrecoverable process, and is dependent only on the plastic volumetric deformation. For purely elastic deformation, there is no plastic deformation and consequently there can be no destructure.

### Surfaces in $p'$ - $q$ Space

The two-surface theory for modelling the elastoplastic deformation of materials (e.g., Dafalias and Popov, 1976; Hashiguchi, 1980) is adopted and extended in this

research. The two surfaces are the yield surface and the loading surface. However, an additional reference surface is also introduced, *i.e.*, the equivalent yield surface. Hence for a structured soil three significant surfaces may be defined in stress space, as illustrated in Fig. 1.

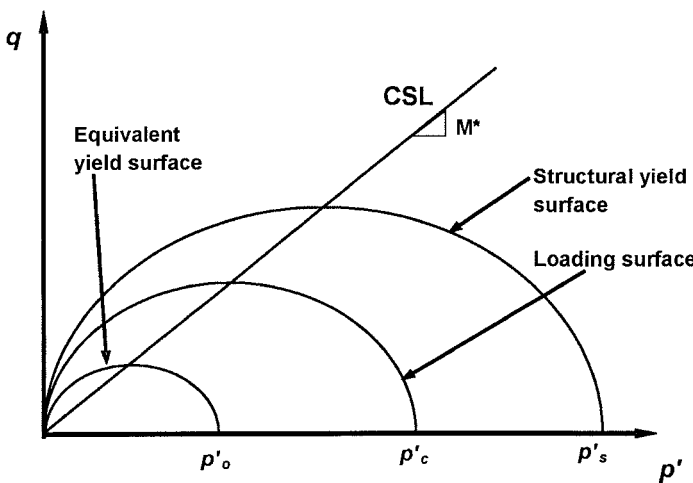


**FIG. 1. Three surfaces for a structured soil**

Similar to the proposal by Roscoe and Burland (1968), the yield surface in  $p'$ - $q$  space for a reconstituted clay is assumed to be elliptical (Fig. 1) and can be expressed as  $f = 0$ , where,

$$f = q^2 - M^{*2} p'(p'_o - p') , \quad (6)$$

and where  $M^*$  is the stress ratio at the critical state of deformation and  $p'_o$ , which represents the size of the yield surface, is the non-zero value of  $p'$  where the ellipse intersects the  $p'$  axis.

Because the effects of anisotropy are not studied in this paper, only variation in the size of the yield surface due to soil structure is modelled. Hence, the structural yield surface in the  $p'$ - $q$  space is also assumed to be elliptical in shape with the aspect ratio being equal to  $M^*$  (Fig. 1).  $p'_s$  is the size of the structural yield surface.

The loading surface is defined as the surface on which the current stress state always stays. The loading surface is also assumed to be elliptical and with the same aspect ratio  $M^*$  (Fig. 1). The size of the loading surface is denoted by  $p'_c$  and clearly  $p'_c$  is determined entirely by the current stress state.

The equivalent yield surface for a structured soil is defined as the yield surface for the same soil in a reconstituted state with the same voids ratio and the same stress state. The size of the equivalent yield surface is denoted by  $p'_e$ , which is given by

$$P'_e = \frac{e^{\left(\frac{e_{IC}^* - e}{\lambda^* - \kappa^*}\right)}}{p^{\left(\frac{\kappa^*}{\lambda^* - \kappa^*}\right)}}. \quad (7)$$

where  $e_{IC}^*$  and  $\lambda^*$  are the well known soil parameters defining the isotropic compression line of a reconstituted soil in the  $e - \ln p'$  space,  $\kappa^*$  is the swelling index, and  $e$  is the current voids ratio.

### Material Idealisation

In the general framework, soil is idealised as a sub-yielding and virgin yielding material. Plastic deformation can be induced by a stress change inside the structural yield surface, as well as by a stress change originating on the current yield surface causing it to expand. The former is referred to as sub-yielding, and the latter as virgin yielding. The structural yield surface varies isotropically with the change in plastic volumetric deformation. During virgin yielding, the structural yield surface expands and is coincident with the loading surface. During sub-yielding, the variation of the yield surface is dependent on destructuring as well as hardening, both of which are assumed to be determined by plastic volumetric deformation.

A sketch of the material idealisation is presented in Fig. 2. Suppose the initial state for a clay in situ is point A in Fig. 2, and its initial structural yield surface is defined by its size  $p'_{y,i}$ . For loading inside the structural yield surface, sub-yielding occurs. The structural yield surface varies as both hardening and destructuring of the yield surface are normally induced by the plastic deformation. As loading continues along stress path AB, the loading surface expands. Suppose that the loading surface and the structural yield surface coincide at point B, i.e.,  $p'_{c,B} = p'_{s,B}$ , then virgin yielding will commence at point B. Generally however,  $p'_{c,B} \neq p'_{y,i}$ . For virgin yielding along stress path BC, the structural yield surface coincides with the loading surface.

Suppose unloading occurs at point C and continues along the stress path CD, i.e.,  $dp'_c < 0$ . Consequently, sub-yielding occurs with unloading along path CD and the current loading surface turns inside the current structural yield surface and contracts. Suppose the stress path changes direction again at point D with  $dp'_c > 0$ . Reloading then commences and continues along stress path DE. The structural yield surface varies during both unloading and reloading. Suppose at point E the loading surface coincides with the structural yield surface, i.e.,  $p'_{c,E} = p'_{s,E}$ . In this case virgin yielding recommences at point E and continues for loading along stress path EF.

The variation of the structural yield surface is determined by two factors: the hardening mechanism and the destructuring mechanism. Both mechanisms are dependent on plastic volumetric deformation. It is assumed that the effects of the two mechanisms can be modelled independently and the change in the current yield surface can be expressed in terms of the hardening effect  $dH$  and the destructuring effect  $dD$  by the following equation,

$$dp'_s = dH - dD. \quad (8)$$



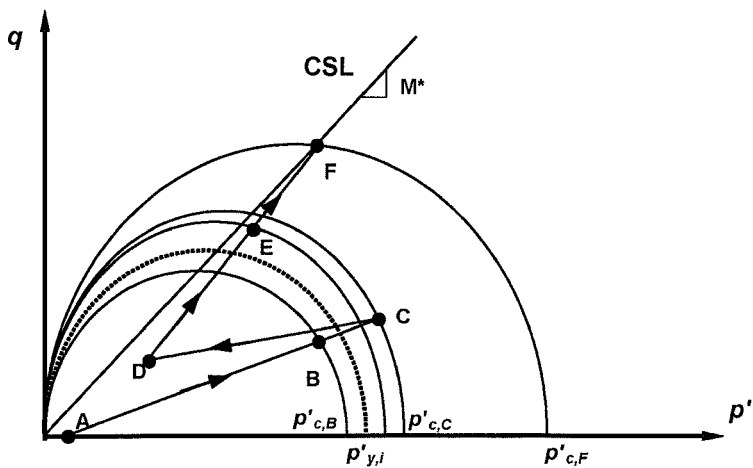
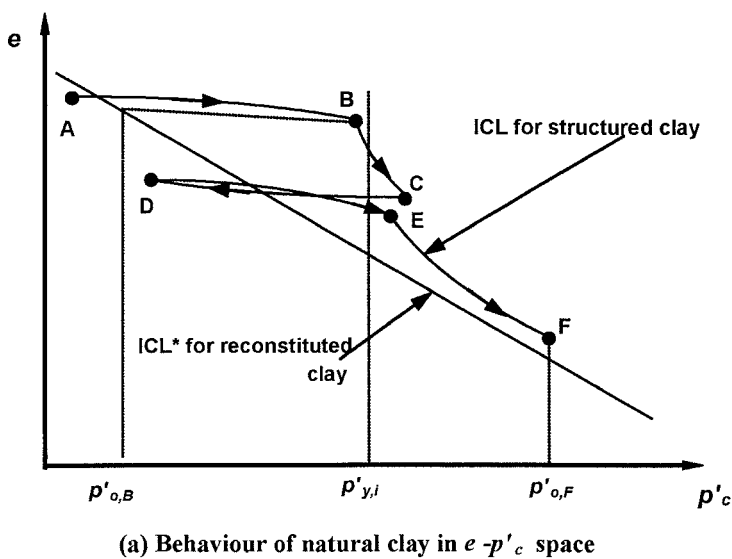


**FIG. 2. Material idealisation for the general framework**

Various hardening and destructuring functions can be formulated within the proposed framework of sub-yielding and virgin yielding, as described later.

## Volume-dependent Hardening and Destructuring

The proposed framework is derived by generalising the behaviour of structured clays during isotropic compression to loading along general stress paths. A fundamental assumption of the proposed theoretical framework for natural soils is that both the hardening and the destructuring of structured clay are dependent on plastic volumetric deformation only. The following consequences flow from this fundamental assumption. (1) The magnitude of plastic volumetric deformation of natural clay is dependent on the change in size of the yield surface, irrespective of the stress path. (2) The current yield surface evolves from the initial structural yield surface due to the effects of both hardening and destructuring, which are functions of the plastic volumetric deformation. Experimental evidence for the dependence of hardening and destructuring on volumetric deformation may be found in studies such as those by Calabresi and Scarpelli (1985), Graham and Li (1985), Clayton *et al.* (1992), Carter *et al.* (2000), and Cotecchia and Chandler (2000).

Consider first the isotropic compression behaviour of natural clays.

### *Isotropic Compression*

A general form of the equation describing the isotropic virgin compression of natural clays was proposed as (Liu and Carter, 1999a, 2000b),

$$e = e_{ic} + a \left( \frac{p'_{y,i}}{p'} \right)^b + c - \lambda * \ln p' , \quad (9)$$

where  $b$  is a parameter quantifying the rate of destructuring, termed the *destructuring index*, and  $c$  is that part of the additional voids ratio sustained by structure that cannot be eliminated by an increase in stress. Parameters  $a$  and  $b$  satisfy the following condition,

$$a + c = \Delta e_i , \quad (10)$$

where  $\Delta e_i$  is the initial value of the additional voids ratio ( $\Delta e$ ) sustained by the soil structure.

### *Virgin Yielding*

For general loading, virgin yielding occurs when  $p'_c = p'_s$  and  $dp'_c > 0$ . During virgin yielding, the current stress state stays on the yield surface, which is coincident with the loading surface.

It is assumed that elastic deformation of a soil is independent of soil structure. Following the Cam Clay tradition, virgin isotropic compression, described by equation (9), can be rewritten in terms of elastic and plastic parts as follows,

$$e = e^*_{IC} - \kappa^* \ln p' + a \left( \frac{p'_{y,i}}{p'} \right)^b - (\lambda^* - \kappa^*) \ln p' + c . \quad (11)$$

Based on the assumption that both the hardening and the destructuring of natural clay are dependent only on plastic volumetric deformation, the plastic part of the voids ratio change is dependent on the size of the current yield surface, not the mean effective stress. Hence  $p'$  in the third and fourth terms of equation (11) should be substituted by the size of the current structural yield surface,  $p'_s$ . For isotropic compression the size of the yield surface is equal to the value of the current mean effective stress, so that equation (11) can be rewritten as,

$$e = e^*_{IC} - \kappa^* \ln p' + a \left( \frac{p'_{y,i}}{p'_s} \right)^b - (\lambda^* - \kappa^*) \ln p'_s + c . \quad (12)$$

Equation (12) describes the change of voids ratio and there are three basic terms that vary with stress level in the equation. The first,  $\kappa^* \ln p'$ , describing the change associated with elastic deformation, is valid for loading along general stress paths. The third term,  $(\lambda^* - \kappa^*) \ln p'_s$ , describes the change associated with plastic deformation for clay in a reconstituted state. This term is the same as that appearing in the Cam Clay model to describe the voids ratio change associated with plastic deformation under general loading (Schofield and Wroth, 1968). The second term,

$a \left( \frac{p'_{y,i}}{p'_s} \right)^b$ , describes the change associated with the additional voids ratio sustained by soil structure, and is assumed to be a plastic deformation. It was suggested previously that the magnitude of plastic volumetric deformation of natural soil is dependent on the change in size of the yield surface, irrespective of the stress path. The second term therefore is also valid for loading along general stress paths. Consequently, equation (12) is valid for loading along general stress paths.

Taking the differential form of equation (12) and dividing both sides by  $(1+e)$ , the following equation for the total volumetric strain increment is obtained,

$$d\varepsilon_v = \frac{\kappa^*}{1+e} \left( \frac{dp'}{p'} \right) + [(\lambda^* - \kappa^*) + b(\Delta e - c)] \frac{dp'_s}{(1+e)p'_s} , \quad (13)$$

where

$$\langle a \rangle = \begin{cases} a & \text{if } a \geq 0 \\ 0 & \text{if } a < 0 \end{cases} . \quad (14)$$

$\Delta e$  is the current value of the additional voids ratio sustained by soil structure for loading along general stress paths. As shown in Fig. 3,  $\Delta e = e - e^*$ . It is necessary to add the sign function  $\langle \cdot \rangle$  to the term  $(\Delta e - c)$  in equation (13) because, as noted

 @Seismicisolation

previously, the voids ratio component  $c$  cannot be reduced by an increase in compressive stress.

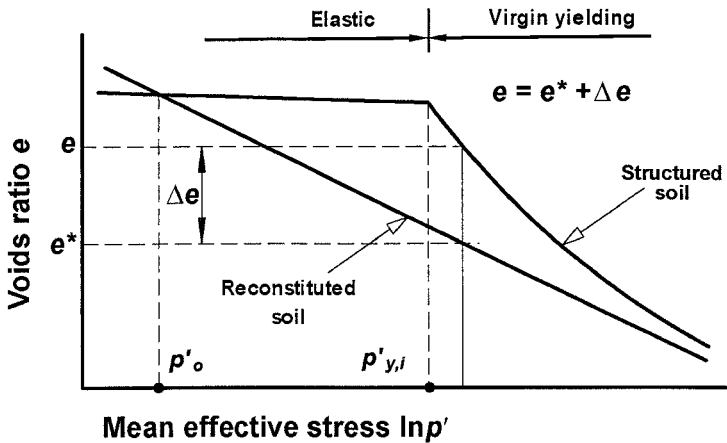


**FIG. 3. Idealisation of the compression behaviour of reconstituted and structured clays**

The first part of equation (13) represents elastic deformation. The plastic strain increment  $d\varepsilon_v^p$  can therefore be expressed as,

$$d\varepsilon_v^p = [(\lambda^* - \kappa^*) + b(\Delta e - c)] \frac{dp'_s}{(1+e)p'_s} . \quad (15)$$

The total volumetric deformation and the plastic volumetric deformation during virgin yielding are described by equations (13) and (15) separately. Alternatively equation (15) can be expressed as,

$$dp'_s = \frac{(1+e)p'_s d\varepsilon_v^p}{(\lambda^* - \kappa^*) + b(\Delta e - c)} . \quad (16)$$

Equation (16) is also applicable for a reconstituted clay, where  $\Delta e \equiv c \equiv 0$  and  $p'_s = p'_o$ . Hence, for reconstituted clay

$$dp'_o = \frac{(1+e)p'_o d\varepsilon_v^p}{(\lambda^* - \kappa^*)} . \quad (17)$$

### *Hardening and Destructuring*

For a reconstituted soil, a change in size of the yield surface is induced purely by plastic hardening (or softening). Hence, equation (17) is the hardening function for a reconstituted soil. If the hardening function for structured clay is assumed to be the same as that of the same soil in a reconstituted state, a general hardening function is obtained as follows,

$$dH = \frac{(1+e)p'_o d\varepsilon_v^p}{(\lambda^* - \kappa^*)} . \quad (18)$$

It may be seen from equation (9) that  $\Delta e \equiv \Delta e$ , if  $b = 0$ , in which special case the additional voids ratio sustained by soil structure remains the same during virgin yielding, *i.e.*, there is no destructuring if  $b = 0$ . The corresponding variation of the yield surface for a soil with  $b = 0$  during virgin yielding can be recovered from equation (16) as follows,

$$dp'_s = \frac{(1+e)p'_s d\varepsilon_v^p}{(\lambda^* - \kappa^*)} . \quad (19)$$

In more general cases where  $b \neq 0$ , the variation of the yield surface during virgin yielding with destructuring is given by equation (16), and therefore the effect of destructuring  $dD$  can be obtained as:

$$dD = dp'_s|_{no\;destructuring} - dp'_s|_{destructured} = \frac{(1+e)bp'_s d\varepsilon_v^p}{(\lambda^* - \kappa^*) \left[ 1 + b \left\langle \ln \left( \frac{p'_s}{p'_o} \right) - c \right\rangle \right]} \left\langle \ln \left( \frac{p'_s}{p'_o} \right) - c \right\rangle \quad (20)$$

It is assumed that equation (20) is also valid for general stress paths including both virgin yielding and sub-yielding. Assuming that expansive plastic volumetric strain also results in the removal of soil structure, the absolute value of plastic strain increment  $d\varepsilon_v^p$  should be employed in the destructuring function, so that equation (20) must be modified as,

$$dD = \frac{(1+e)bp'_s |d\varepsilon_v^p|}{(\lambda^* - \kappa^*) \left[ 1 + b \left\langle \ln \left( \frac{p'_s}{p'_o} \right) - c \right\rangle \right]} \left\langle \ln \left( \frac{p'_s}{p'_o} \right) - c \right\rangle . \quad (21)$$

Based on equation (8), an expression for  $dp'_s$  for sub-yielding is obtained as follows,

$$dp'_s = dH - dD = \frac{(1+e)p'_o d\varepsilon_v^p}{(\lambda^* - \kappa^*)} - \frac{(1+e)bp'_s |d\varepsilon_v^p|}{(\lambda^* - \kappa^*) \left[ 1 + b \left( \ln \left( \frac{p'_s}{p'_o} \right) - c \right) \right]} \left( \ln \left( \frac{p'_s}{p'_o} \right) - c \right). \quad (22)$$

### Sub-yielding

Sub-yielding may occur for a stress excursion inside the current yield surface inducing plastic volumetric deformation. The structural yield surface will vary according to the hardening and destructuring effects associated with such plastic deformation. The basic concept of this form of yielding is that the plastic volumetric deformation occurring during sub-yielding is linked to that which occurs during virgin yielding. The exact mathematical expression adopted for sub-yielding is based on examination of the available experimental data and the volumetric plastic strain increment during sub-yielding is defined as follows,

$$d\varepsilon_v^p = \left( 1 - \frac{\eta}{M^*} \right) \left[ \frac{\alpha(\lambda^* - \kappa^*) dp'_c + \alpha^3 b \Delta e |dp'_c|}{(1+e)p'_s} \right]. \quad (23)$$

where  $\alpha$  represents the kinematic hardening effect of stress history on the plastic deformation of the soil. A simple scalar expression for  $\alpha$  is suggested as,

$$\alpha = \begin{cases} \left( \frac{p'_c - p'_u}{p'_s - p'_u} \right) & \text{if } dp'_c \geq 0 \\ \left( 1 - \frac{p'_c}{p'_s} \right) & \text{if } dp'_c < 0 \end{cases}, \quad (24)$$

in which  $p'_u$  is the minimum size of the loading surface previously attained, i.e.,  $p'_u = \min \{p'_c\}$ . When the stress state returns to virgin yielding, the memory of the previous loading is lost, and  $p'_u = p'_c$ .

The current structural yield surface varies during sub-yielding. The change of the structural yield surface  $dp'_s$  can be computed directly from equation (22). The moment the current stress state reaches the yield surface and  $dp'_c > 0$ , virgin yielding commences.

The theoretical framework proposed thus far for natural clay behaviour has focused on the volumetric deformation of clays under general loading. The form of the corresponding deviatoric deformation has not yet been defined. However, it is noted that different flow rules may be adopted within the proposed framework, from which the deviatoric deformation can be computed.

## STRUCTURED CAM CLAY

It is possible to develop a particular and much simpler model within the general theoretical framework introduced in the previous section. This model has been named Structured Cam Clay (SCC). The aim of formulating SCC is to provide a relatively simple model suitable for geotechnical practitioners to use in solving boundary value problems. Consequently, necessary simplifications have been made. Some important details of the destructuring process, not included in the simplified volume-dependent destructuring described previously, are also incorporated in the treatment described here. Full details of the SCC model can be found in papers by Liu and Carter (2002, 2004b).

### Material Idealisation

As compared with the version adopted in the general framework illustrated in Fig. 2, a much simpler material idealisation is adopted in the SCC model, as shown in Fig. 3. In this case soil is idealised as an elastic and virgin yielding material. The yield surface varies isotropically with the change in plastic volumetric deformation. Soil behaviour is assumed to be elastic for any stress excursion inside the current structural yield surface, *i.e.*, there is no sub-yielding. Virgin yielding occurs for a stress change originating on the structural yield surface and causing it to expand. During virgin yielding, the current stress of a soil stays on the structural yield surface.

### Virgin Yielding

Provided that the isotropic compression line of a structured clay can be described by equation (9), the following volumetric deformation equation is derived based on the volumetric-dependent hardening and destructuring theory,

$$d\epsilon_v = \frac{\kappa^* dp'}{(1+e)p'} + (\lambda^* - \kappa^*) \frac{dp'_s}{(1+e)p'_s} + b(\Delta e - c) \frac{dp'_s}{(1+e)p'_s} . \quad (25)$$

If the effect of shearing on destructuring is also considered, a modification to the derived volumetric strain increment is required and the final equation proposed for the SCC model is as follows,

$$d\epsilon_v = \frac{\kappa^* dp'}{(1+e)p'} + (\lambda^* - \kappa^*) \frac{dp'_s}{(1+e)p'_s} + \left[ (\Delta e - c) + \frac{\gamma \eta \Delta e}{M^* - \eta} \right] \frac{bdp'_s}{(1+e)p'_s} , \quad (26)$$

where  $\gamma$  is a model parameter. The effect of shearing on destructuring is directly proportional to the value of  $\gamma$ .

Based on a trial and error method, the following new flow rule is proposed for naturally structured clays,



$$\frac{d\varepsilon_d^p}{d\varepsilon_v^p} = \frac{2\eta}{|M^*|^2 - \eta^2 + \varpi\eta^2 \left| 1 - \sqrt{\frac{P'_e}{P'_s}} \right|} . \quad (27)$$

where  $\varpi$  is a model parameter, and  $|x|$  represents the absolute value of the quantity  $x$ .

The deviatoric strain increment during virgin yielding is thus obtained as,

$$d\varepsilon_d = d\varepsilon_d^e + \frac{2\eta}{|M^*|^2 - \eta^2 + \varpi\eta^2 \left| 1 - \sqrt{\frac{P'_e}{P'_s}} \right|} \left\{ (\lambda^* - \kappa^*) + b \left[ (\Delta e - c) + \frac{\gamma\eta\Delta e}{M^* - \eta} \right] \right\} \frac{dp'_s}{(1+e)p'_s} \quad (28)$$

### Elastic Behaviour

For stress excursions within the current virgin yielding boundary, only elastic deformation occurs. The elastic deformation of a structured soil is assumed to follow Hook's law, and to be independent of soil structure. The elastic deformation can be written as,

$$d\varepsilon_v^e = \frac{3(1-2\nu^*)}{E^*} dp' , \quad (29)$$

$$d\varepsilon_d^e = \frac{2(1+\nu^*)}{3} \frac{dq}{E^*} , \quad (30)$$

where  $\nu^*$  is Poisson's ratio and  $E^*$  is the Young's modulus.  $E^*$ ,  $\nu^*$ ,  $p'$ , and the elastic swelling index  $\kappa^*$  are related by

$$E^* = \frac{3(1-2\nu^*)(1+e)}{\kappa^*} p' . \quad (31)$$

### Softening and Crushing

For stress states on the yield surface and with the stress ratio  $\eta > M^*$ , softening occurs. As is the situation for most models of the Cam Clay family, during a softening process soil behaves as a virgin yielding material and the stress state remains on the yield surface. Therefore, the volumetric deformation of a structured clay during softening is described by the same equation as for virgin yielding, *i.e.*, equation (26). However, the sign of the plastic deviatoric strain associated with destructuring has to be changed, so that the strain increment vector always points outside the yield surface, *i.e.*,

$$d\varepsilon_d^p = - \left\{ \left( \lambda^* - \kappa^* \right) + b \left[ \langle \Delta e - c \rangle - \frac{\gamma \eta \Delta e}{M^* - \eta} \right] \right\} \frac{2\eta}{|M^{*2} - \eta^2| + \varpi \eta^2} \frac{dp'_s}{1 - \sqrt{\frac{p'_e}{p'_s}}} \frac{dp'_s}{(1+e)p'_s} \quad (32)$$

It may be noticed that for both virgin yielding and softening behaviour the soil may reach a state with  $\eta = M^*$  but with  $\Delta e \neq 0$ . As is indicated in the flow rule, *i.e.*, equation (27), the resistance of the soil to continuous shear deformation is not zero under these conditions. Clearly, the critical state of deformation has not yet been achieved, even though the stress state in  $p'$  -  $q$  space has reached the critical state line (CSL). The concept of the crushing of soil structure is introduced for this situation.

It is assumed that during the crushing transition the effective stress state of the soil stays on the CSL but may travel along the line either upwards or downwards, *i.e.*, with hardening or softening. The stress and strain relationship for this transition process is described by the following set of equations

$$\begin{cases} dq = M^* dp' \\ dp' \geq 0 \text{ for } p'_s < p'_e, \text{ and } dp' \leq 0 \text{ for } p'_s > p'_e \\ d\varepsilon_v = \left( \frac{\kappa^*}{1+e} \right) \frac{dp'}{p'} + d\varepsilon_v^p \\ d\varepsilon_d = \frac{2(1+\nu^*)}{9(1-2\nu^*)} \left( \frac{\kappa^*}{1+e} \right) \frac{dq}{p'} + \frac{2|d\varepsilon_v^p|}{\varpi \eta \sqrt{1 - \sqrt{\frac{p'_e}{p'_s}}}} \end{cases} \quad (33)$$

There are now three equations for the three unknown quantities  $dp'$ ,  $dq$  and  $d\varepsilon_v^p$ . Consequently, the stress strain relationship is now fully defined. The additional voids ratio of the soil diminishes during the process of structural adjustment, and at end of the process the soil will reach a critical state of deformation, irrespective of its original structure.

### Modification of the Virgin Yield Locus

In order to model accurately the influence of the initial soil structure on the virgin yielding boundary, a simple modification is proposed, so that the initial structural yield surface is allowed to possess a shape different from the elliptical yield surface associated with stress history. The modification is relatively straightforward and involves extension of the concept of virgin yielding, which for some soils may lead to significant improvements in predicting the plastic deformation, particularly for some natural clays with anisotropic structural yield surfaces.

Suppose that the initial structural yield surface may be expressed as

$$f_{s,i}(p', q) = 0 \quad (34)$$

Suppose also that the initial state of a soil can be denoted as point A and the soil is loaded along the stress path AB in Fig. 4a. When the current stress state reaches the initial structural yield surface  $f_{s,i}$  at point C, virgin yielding occurs. For continuing loading, the virgin yielding boundary is made of the two areas defined by the initial structural yield surface  $f_{s,i}$  and  $p'_{c,max}$ .  $p'_{c,max}$  is the maximum size of the stress yield surface the soil has ever experienced, which is defined by equation (6). The value of  $p'_{c,max}$  at stress state B for stress path AB is shown in Fig. 4a. If the stress state of the soil turns inside the current yielding boundary, the soil behaves as a purely elastic material, and the yielding boundary remains unchanged.

The virgin yielding boundary is described by  $p'_{c,max}$  completely when the initial structural yield surface  $f_{s,i}$  is completely enclosed by the surface defined by  $p'_{c,max}$ . The initial structural yield surface subsequently has no further influence on the soil behaviour (Fig. 4b). It is obvious that the concept of yielding introduced above is valid regardless of whether or not the initial structural yield surface and the elliptical yield surface associated with loading are identical.

It is also assumed that the moment softening occurs the initial structural yield surface is destroyed and the current yield surface is identical to the virgin yielding boundary.

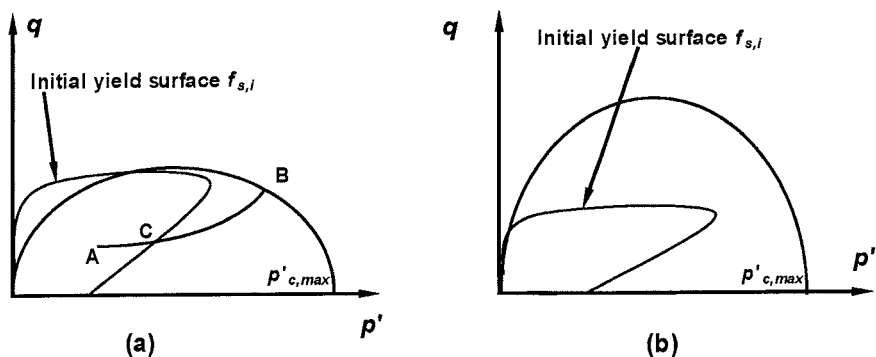


FIG. 4. Virgin yielding boundary

### Model Parameters

Ten parameters define the Structured Cam Clay model, and they are  $M^*$ ,  $e^*_{IC}$ ,  $\lambda^*$ ,  $\kappa^*$ ,  $v^*$ ,  $b$ ,  $c$ ,  $\gamma$ ,  $\varpi$  and  $p'_{y,i}$  (or initial structural yield surface  $f_{s,i}$ ). The first five parameters, denoted by the symbol  $*$ , are intrinsic soil properties and are independent of soil structure. These five intrinsic parameters are the same as those adopted in the Modified Cam Clay model (e.g., Muir Wood, 1990).

The new parameters, viz.,  $b$ ,  $c$ ,  $\gamma$ ,  $\varpi$  and  $p'_{y,i}$  ( $f_{s,i}$ ) are introduced to describe the influence of soil structure on its mechanical behaviour. A detailed study of the effects of parameters  $b$  and  $p'_{y,i}$  on the predicted compression behaviour of natural

**@Seismicisolation**

clays can be found from a paper by Liu and Carter (1999a, 2000b). Parameter  $c$  is the ultimate distance (at large mean stress) between the isotropic compression line for a structured soil and the same soil in a reconstituted state. It can be seen that these three parameters,  $b$ ,  $c$  and  $p'_{y,i}$ , have clear physical meaning, and can be determined conveniently from an isotropic compression test or an oedometer test on an intact soil sample.

Parameter  $\gamma$  describes the reduction of the additional voids with the current shear stress. The total plastic volumetric deformation associated with changes in the additional voids ratio is described completely in terms of four material parameters, *i.e.*,  $M^*$ ,  $b$ ,  $c$  and  $\gamma$ . The first three parameters can be determined independently from experimental data. Consequently, parameter  $\gamma$  can be identified independently by studying the variation of  $\Delta e$  with  $\eta$  during virgin shearing. Parameter  $\varpi$  describes the flow rule and can be determined from the measured plastic strain increment vector. Theoretically, all five new parameters can be identified directly from conventional laboratory tests on structured clays. The value  $\varpi = 1$  is normally adopted if there is insufficient data for its independent identification.

The adoption of an initial structural yield surface  $f_{s,i}$ , different from that described by the yield surface (6), is suggested if there is enough experimental evidence to identify it. A detailed study on the identification of the initial structural yield surface  $f_{s,i}$  for a number of natural soils can be found in a paper by Diaz-Rodriguez *et al.* (1992).

## PERFORMANCE OF SCC

The capacity of the Structured Cam Clay model for describing the behaviour of both naturally and artificially structured clays is demonstrated in this section. The performance of the model for clays subjected to compression and both drained and undrained shearing is demonstrated, and the predictions are compared with experimental data.

### Compression of Structured Clay

One set of compression tests on an artificially cemented clay was simulated and for these tests only the volumetric deformation has been computed. The soil was composed of a natural Avezzano clay, commercial bentonite, ordinary 425 Portland cement, and distilled water. As can be seen from equation (26), the volumetric deformation is not influenced by the values of parameters  $v^*$  and  $\varpi$ . Hence, for the present purpose there is no need to determine or specify values for these parameters.

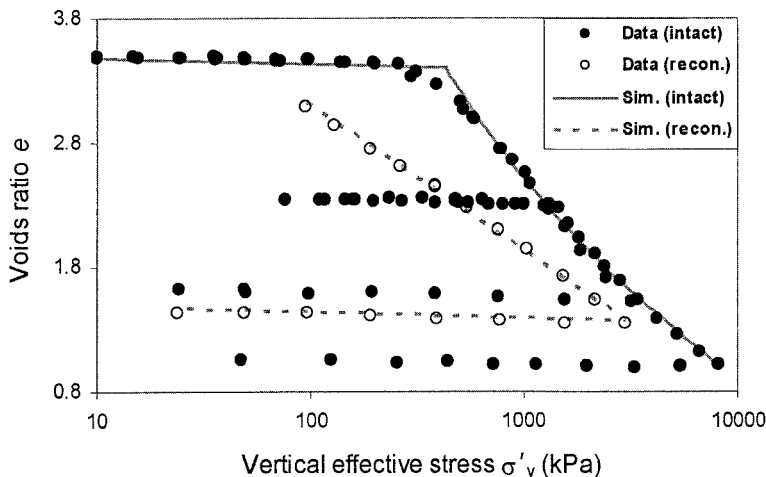
Five compression tests were performed on this artificial soil by Burghignoli *et al.* (1998). Based on two oedometer tests, the values of the model parameters were identified and listed in Table 1. The authors were not able to obtain data for the critical state strength and so a value of  $M^* = 1.5$  was assigned.  $e^*_{IC}$  was estimated from the oedometer test data, based on a method proposed by Liu and Carter (2002). The simulated behaviour of this clay in oedometer tests is shown in Fig. 5. It may be noticed that the cyclic compression behaviour of the clay is well simulated in this case.



**TABLE 1.** Model Parameters for an Artificially Cemented Clay

Parameter	$M^*$	$\lambda^*$	$\kappa^*$	$e^*_{IC}$	$v^*$	$b$	$c$	$w$	$\gamma$	$\sigma'_{yy,i}$ (kPa)
Value	1.5	0.505	0.02	5.383	--	0.7	0	--	0.5	430

Three more tests were also performed on identical specimens of this artificial soil. The stress paths for this set of tests are shown on the inset to Fig. 6. All specimens were initially loaded isotropically from stress state A ( $p' = 25$  kPa,  $e = 3.5$ ) to state B with  $p' = 300$  kPa. They were unloaded isotropically to state C with  $p' = 140$  kPa, and ultimately loaded along constant shear stress paths. Three values of shear stress ratios were chosen, and they were  $\eta = 0, 0.5$ , and 1.



cement. In the prediction, this development of soil structure was considered by choosing  $p'_{y,i} = 340$  kPa for the clay for reloading after point C.

The simulation for this set of tests is shown in Fig. 6. It is seen that the SCC model gives an approximate but reasonable description of the compression behaviour of this artificially structured clay.

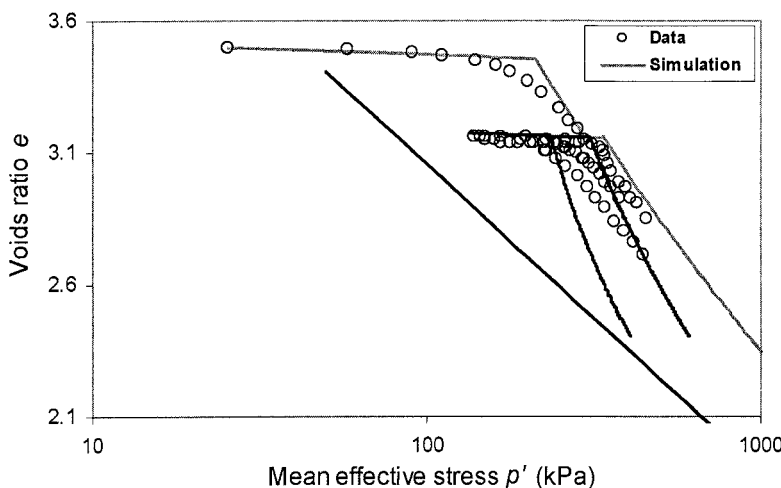


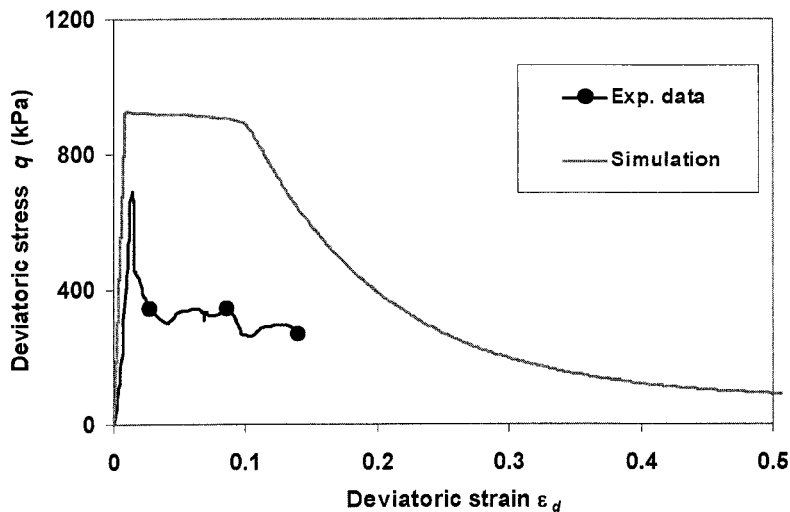
**FIG. 6. Compression behaviour of an artificially cemented clay (Test data after Burghignoli *et al.*, 1998)**

### Drained Shearing

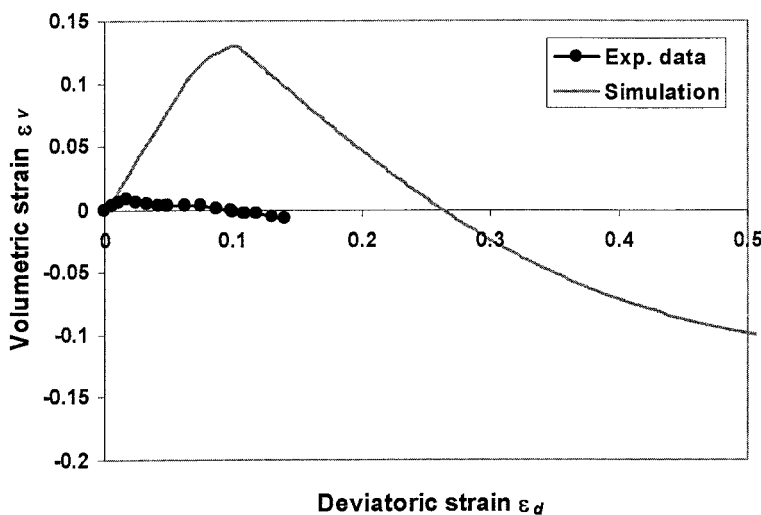
Results of experimental work carried out by Lagioia and Nova (1995) on a natural calcarenite have been compared with the model predictions. The natural calcarenite was formed by marine deposition. It is a coarse-grained material with a high degree of uniformity and calcareous inter-particle cement. An isotropic compression test on the cemented soil was used to identify soil parameters and their values are listed in Table 2. The value of Poisson's ratio and the critical state strength for the natural calcarenite were reported by Lagioia and Nova (1995). The initial state for the structured soil is defined by  $p' = 147$  kPa and  $e = 1.148$ , and so the initial value of the additional voids ratio due to soil structure is  $\Delta e_i = 0.15$ . The value of parameter  $\varpi$  was determined by curve fitting. Since  $E^*$  is assumed here to be a material constant,  $\kappa^*$  is calculated from equation (31). This value of  $\kappa^*$  is used in calculating the plastic deformation in equations (26), (28) and (32).

In all, eight drained shearing tests were considered with the confining pressure  $\sigma'_3$  ranging from 25 kPa to 3,500 kPa. A comparison between test results and the predictions for four tests are shown in Figs 7 to 10. For the test with  $\sigma'_3 = 3,500$  kPa,

**@Seismicisolation**



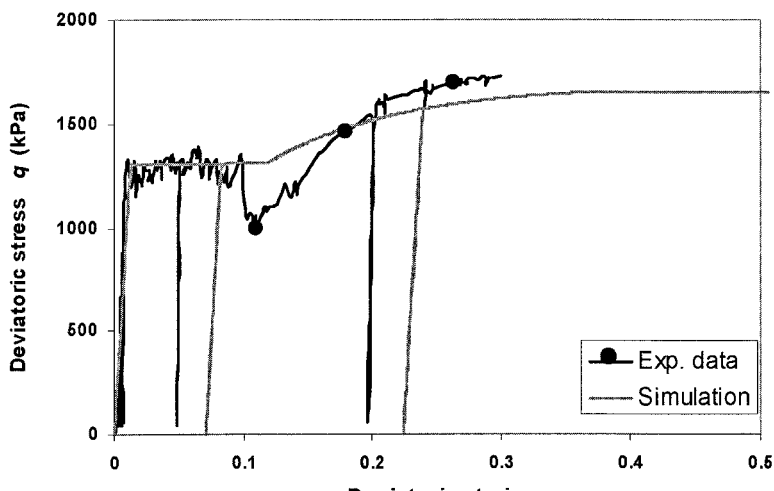
(a) Deviatoric stress and strain relationship



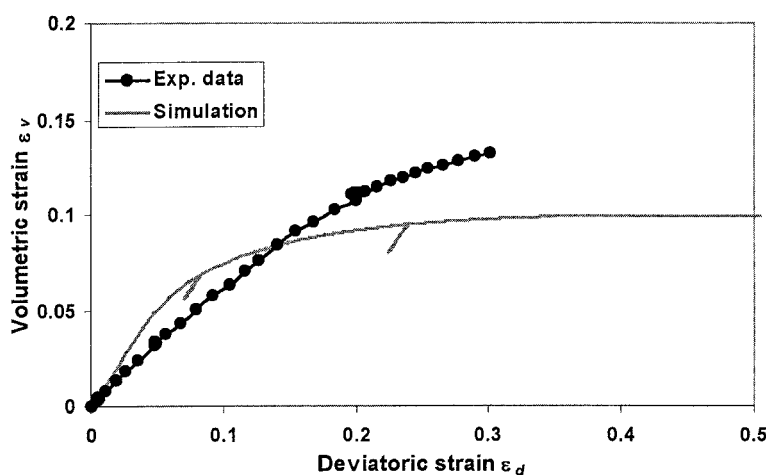
(b) Volumetric strain and deviatoric strain relationship

FIG. 7. Shearing behaviour of a calcarenite at  $\sigma'_3 = 25$  kPa (Test data after Lagioia and Nova, 1995)

@Seismicisolation



(a) Deviatoric stress and strain relationship



(b) Volumetric strain and deviatoric strain relationship

FIG. 8. Shearing behaviour of a calcarenite at  $\sigma'_3 = 600$  kPa (Test data after Lagioia and Nova, 1995)

@Seismicisolation

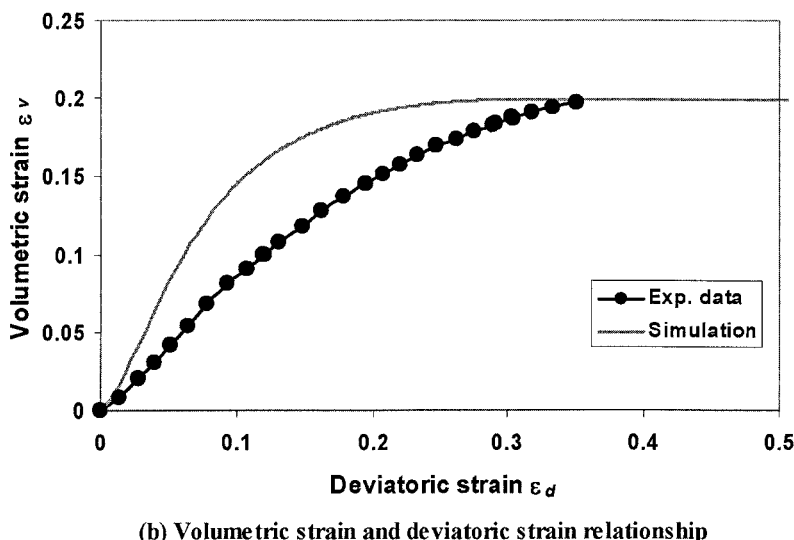
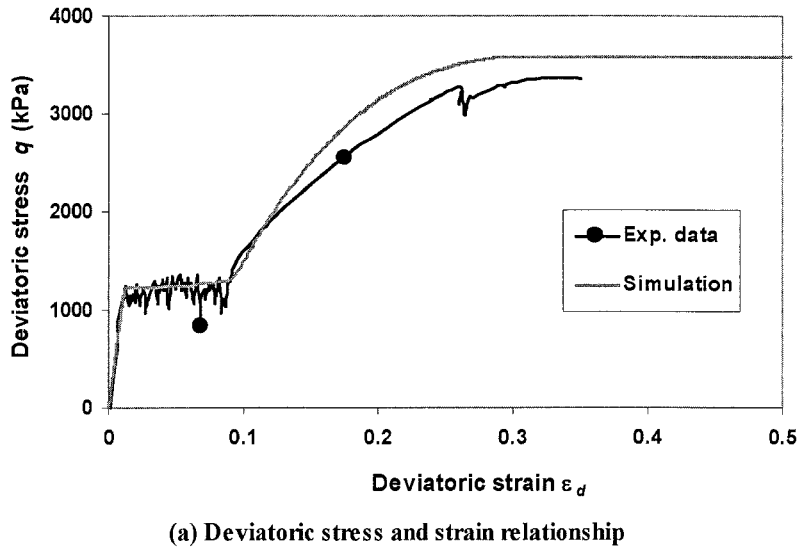
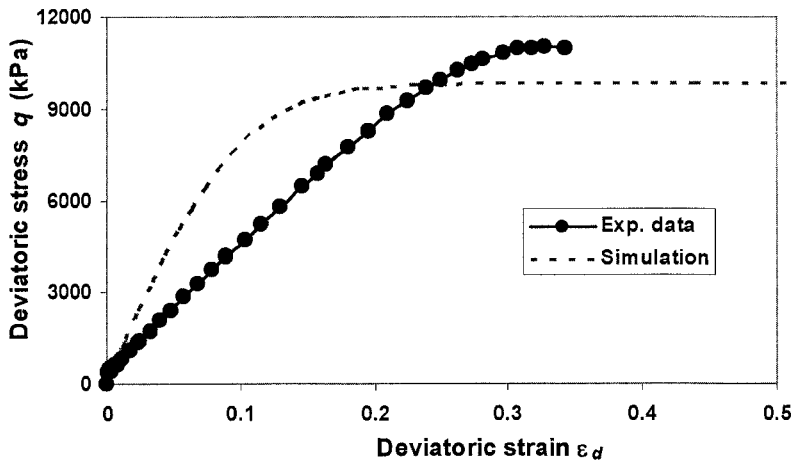
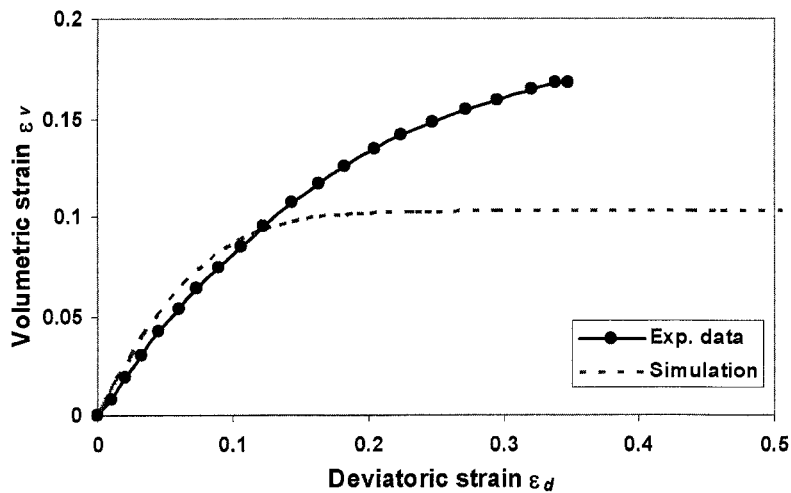


FIG. 9. Shearing behaviour of a calcarenite at  $\sigma'_3 = 1300$  kPa (Test data after Lagioia and Nova, 1995)

@Seismicisolation



(a) Deviatoric stress and strain relationship



(b) Volumetric strain and deviatoric strain relationship

FIG. 10. Shearing behaviour of a calcarenite at  $\sigma'_3 = 3500$  kPa (Test data after Lagioia and Nova, 1995)

@Seismicisolation

the initial stress state is much larger than the size of the initial structural yield surface. According to the proposed model, the structure of the soil at  $\sigma'_3 = 3,500$  kPa is effectively completely destroyed since the soil has a very high destructuring index, i.e.,  $b = 30$ . Thus the soil behaved essentially as a reconstituted material throughout this test. Destructuring of this sample was confirmed by Lagioia and Nova (1995).

TABLE 2. Model Parameters for a Natural Calcarenite

Parameter	$M^*$	$\lambda^*$	$E^*$ (kPa)	$e_{IC}^*$	$v^*$	$b$	$c$	$w$	$\gamma$	Initial structural yield surface
Value	1.45	0.208	76,923	2.383	0.13	30	0	4	2.1	Ellipse: $p'_{s,i} = 2,400$ kPa & aspect ratio of 1.12.

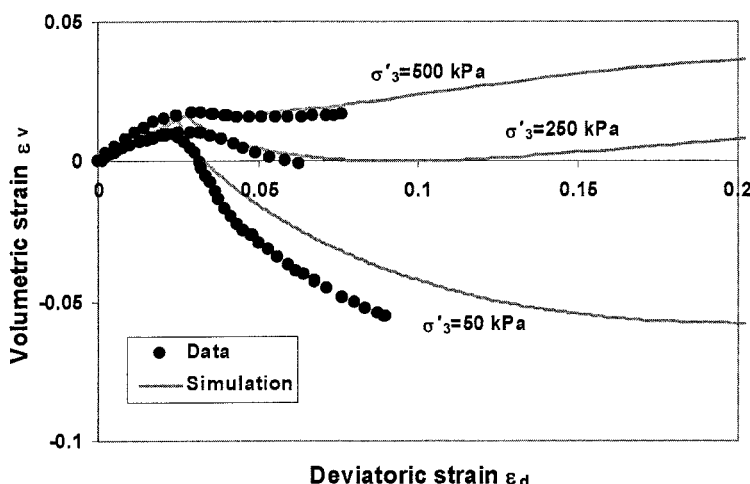
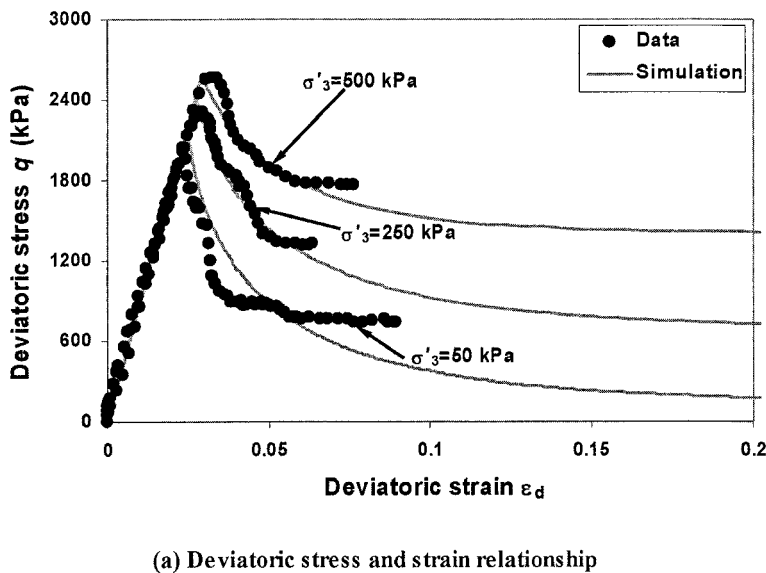
Considering the wide range of initial stresses, it is seen that the proposed model provides successful predictions of the behaviour of this natural and highly structured calcarenite. It is also observed in the simulations and in the experimental data (Figs 8 to 9) that both the deviatoric and the volumetric strains increase virtually at constant stress at the moment when virgin yielding commences, and that a large amount of plastic deformation is accumulated at the end of this process. These simulations are consistent with experimental observations of natural soil behaviour where the soils have a very sensitive structure (e.g., Westerberg, 1995, after Rouainia and Muir Wood, 2000; Arces *et al.*, 1998). It is also seen that for this particular soft clay, the proposed material idealisation, e.g., purely elastic behaviour for loading within the current structural yield surface, represents the soil accurately (see Fig. 8).

Results of the experimental work performed by Wong (1980) on a natural clayshale, the stiff Canadian La Biche shale, have also been compared with model simulations. Table 3 shows the values of model parameters used. The initial value of the additional voids ratio, which is calculated according to the in situ voids ratio of the soil, is 0.045. A comparison between the simulations and the experimental data is shown in Fig. 11. It is seen that the proposed model has the capability of modelling the drained shearing behaviour of this structured clayshale. For the clayshale in the test with  $\sigma'_3 = 500$  kPa, the volumetric deformation remains compressive even though the shear strength of the soil softens from a peak of 2,600 kPa to 1,800 kPa. This type of behaviour has been widely observed in structured clays and clayshales (e.g., Lo, 1972; Georgiannou *et al.*, 1993; Robinet *et al.*, 1999; Carter *et al.*, 2000). It may also be observed in Fig. 11a that the fact that the elastic deformation of the soil is independent of the initial stress level has been well represented by the SCC model.

TABLE 3. Model Parameters for a Natural Clayshale

Parameter	$M^*$	$\lambda^*$	$E^*$ (kPa)	$e_{IC}^*$	$v^*$	$b$	$c$	$w$	$\gamma$	$p'_{s,i}$ (kPa)
Value	1.45	0.06	73,000	0.668	0.25	0.2	0	1	1	3,700

@Seismicisolation



(b) Volumetric strain and deviatoric strain relationship

FIG. 11. Shearing behaviour of a clayshale (Test data after Wong, 1980)

@Seismicisolation

### Undrained Shearing of Natural Clays

The undrained behaviour of natural soft clays has also been simulated and compared qualitatively with experimental data reported by Adachi *et al.* (1995). Only qualitative comparison has been possible because substantial variation of the soil specimens, in terms of initial voids ratio and structure, was observed. The model parameters adopted for these simulations are listed in Table 4.

**TABLE 4. Model Parameters for Eastern Osaka Clay**

Parameter	M*	$\lambda^*$	$\kappa^*$	$e_{IC}^*$	v*	b	c	$\omega$	$\gamma$	$p'_{y,i}$ (kPa)
Value	1.28	0.355	0.0477	2.91	0.25	1	0	1	0.5	57.5

The behaviour of the intact clay and the clay in a reconstituted state in oedometer tests was simulated and the results are shown in Fig. 12. The corresponding experimental data are also shown in this figure. It is seen that the behaviour of the soft clay in one dimensional compression is well represented, although it is noted that the value of the intrinsic compression index  $\lambda^*$  adopted for this particular specimen is lower than that suggested by Adachi *et al.* (1995).

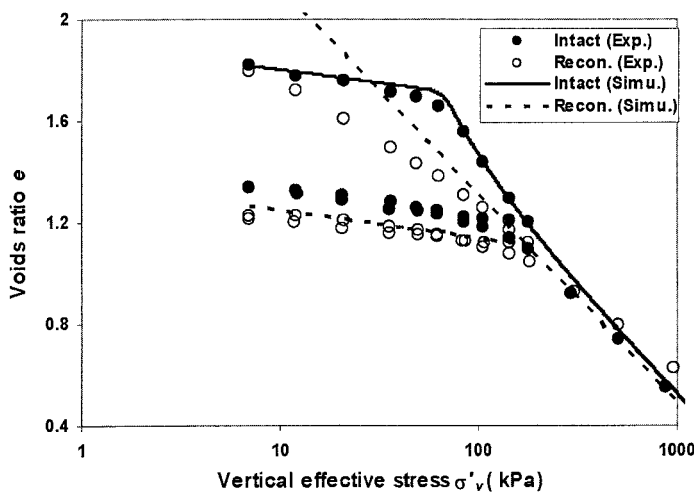


**FIG. 12. Comparison of soft clay behaviour in oedometer tests between experimental data and simulation**

Two sets of undrained triaxial compression tests were also simulated. The first set involves three tests on clay samples with different over-consolidation ratios. They

are one test on a reconstituted soil specimen in a virgin yielding state, and two tests on the intact clay in over-consolidated states. The size of the initial structural yield surface is 57.5 kPa. The initial states for the three tests are ( $p' = 57.5$  kPa,  $q = 0$  kPa,  $\Delta e_i = 0$ ), ( $p' = 46$  kPa,  $q = 0$  kPa,  $\Delta e_i = 0.22$ ) and ( $p' = 17.25$  kPa,  $q = 0$  kPa,  $\Delta e_i = 0.22$ ), respectively. The simulations are shown in Figs 13(a) and (b). Similar experimental data are shown in Figs 13(c) and (d). In this figure the stress terms are normalised by the size of the initial yield surface. It is seen that overall the simulations capture well important features of the behaviour of the naturally structured soft clays.

The following two features of the clay behaviour may be noted. Firstly, the model initially predicts the generation of negative pore pressures followed by very large positive pore water pressures during the softening of heavily over-consolidated Eastern Osaka clay. This feature of the behaviour of natural soft clay has been widely observed (e.g., Burland, 1990; Leroueil and Vaughan, 1990; Carter *et al.*, 2000). Secondly, unlike the model simulation, the undrained stress paths for the intact soil within the structural yield surface are obviously not vertical. Significant plastic volumetric deformation is induced during stress paths inside the assumed purely elastic deformation zone. Hence, some yielding of this soft clay must have occurred during shearing inside the structural yield surface. This aspect of soil behaviour cannot be captured by the SCC model.

The second set of tests involves four tests samples of the same intact clay with different degrees of destructuring. Destructuring was achieved by loading the intact specimens isotropically beyond the initial virgin yielding stress under fully drained conditions. The specimens were then subjected to undrained triaxial compression tests. The initial states for the four tests after isotropic loading are ( $p' = 57.5$  kPa,  $q = 0$  kPa,  $\Delta e_i = 0.22$ ,  $p'_e = 30.9$  kPa), ( $p' = 71.9$  kPa,  $q = 0$  kPa,  $\Delta e_i = 0.176$ ,  $p'_e = 43.8$  kPa), ( $p' = 115$  kPa,  $q = 0$  kPa,  $\Delta e_i = 0.11$ ,  $p'_e = 84.5$  kPa) and ( $p' = 172.5$  kPa,  $q = 0$  kPa,  $\Delta e_i = 0.0733$ ,  $p'_e = 140.2$  kPa), respectively. The sizes of the equivalent yield surfaces were calculated via equation (7). The simulations are shown in Fig. 14(a). Experimental data reported by Cotecchia and Chandler (1997) for a different natural clay are shown in Fig. 14(b) for comparison. The stresses plotted in Fig. 14 are normalised by the size of the equivalent yield surface. The behaviour of the soil in a reconstituted state is also presented for comparison. Theoretically, the soil reaches a reconstituted state when the structure of the soil is completely removed, *i.e.*,  $\Delta e = 0$ .

The patterns of the normalised stress paths affected by destructuring are consistent with experimental observations (Burland, 1990; Coop, 2000; Carter *et al.*, 2000). The behaviour of the soft clay has the following features. The boundary of the virgin yielding stress path normalised by  $p'_e$  for a naturally structured clay is larger than that of the soil in a reconstituted state. The larger the boundary, the more pronounced the soil structure. The difference between the two surfaces reduces with destructuring. It is also noted that the final state of soil at failure may be interpreted as being independent of soil structure. Consequently, the higher the shear strength of the structured clay, the larger the reduction in soil strength after the peak value is reached.



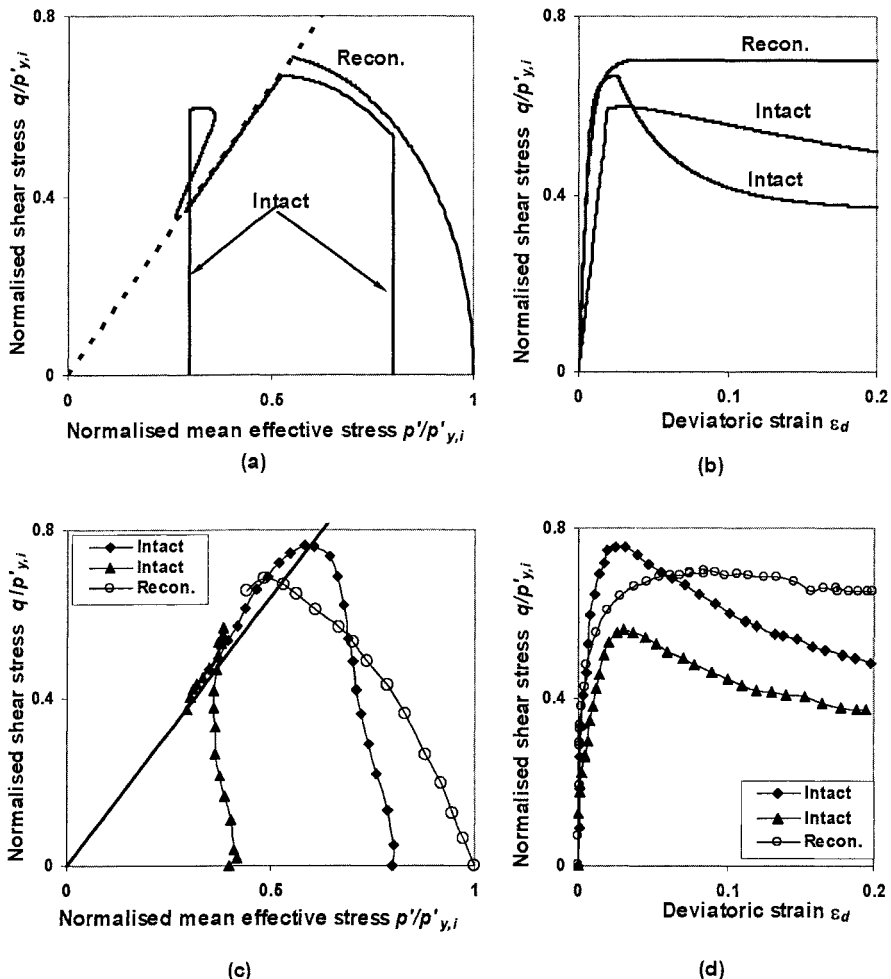


**FIG. 13. Comparison of soft clay behaviour between experimental data and simulation**

### SUGGESTIONS FOR IMPROVING SCC

The major aim of formulating the Structured Cam Clay model was to provide a constitutive model suitable for the solution of boundary value problems encountered in geotechnical engineering practice, *i.e.*, a practical tool. It was therefore necessary to keep the model relatively simple. It is perceived that a simple predictive model should possess the following features: an overall simple and consistent physical

@Seismicisolation

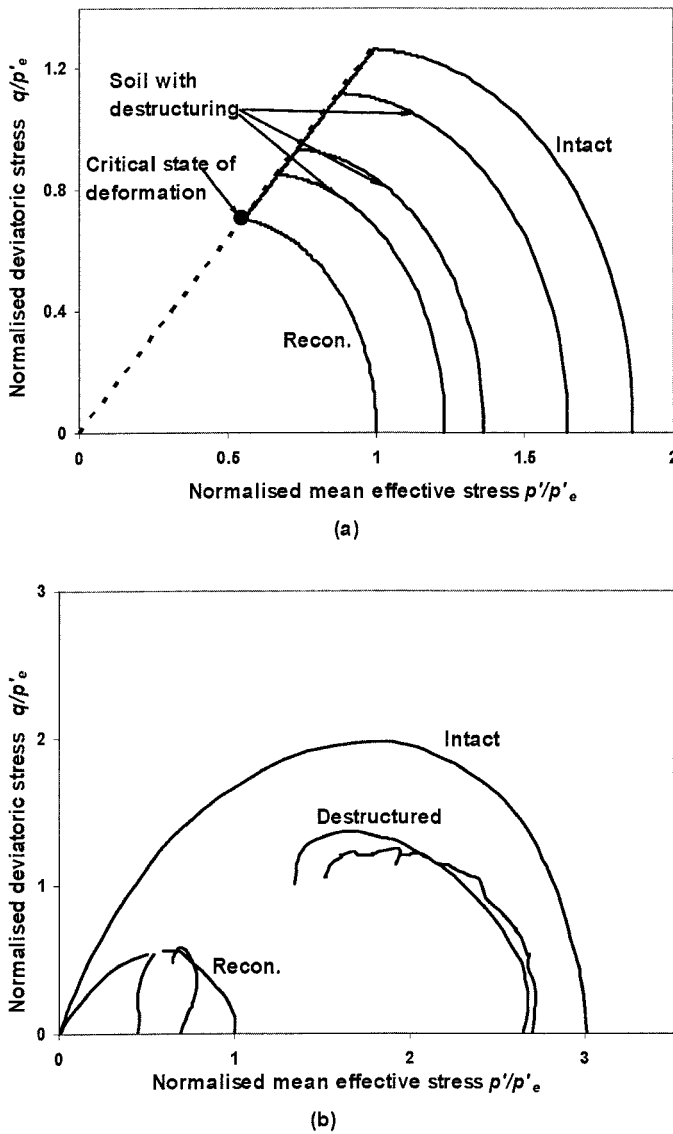


FIG. 14. Normalised stress paths for soft clay with different degrees of destructuring

model, explicitly expressed D matrix, and practically useful model parameters with clear physical meaning which are identifiable from conventional tests. In the

simulations reported in Section 4, it was seen that the SCC model captures well the main features of the behaviour of natural clays under both drained and undrained conditions. However, if more accurate descriptions of soil deformation or the description of more complicated material behaviour are required, further improvement of the model performance is possible by making some additional refinements.

There are three main areas where further refinement can be made. They are with respect to: (1) the behaviour of soil in general stress space; (2) the behaviour of soil for stress states inside the virgin yield surface, and (3) the anisotropic behaviour of natural soils including the effect of rotation of the principal stresses. Ideas for extending the model to describe the effects of loading in general stress space, including anisotropic strength and its influence on soil behaviour, are discussed here. In this generalisation, the Matsuoka-Nakai strength criterion and the concept of the Nakai stress tensor are introduced into the SCC model. Only a brief description is provided, but further details can be found in Matsuoka and Nakai (1982) and Nakai *et al.* (1984, 1986).

Matsuoka and Nakai (1982) proposed that the resistance of geo-materials to shearing is controlled by the ratio of the shear stress, denoted as  $t_s$ , over the normal stress, denoted as  $t_N$ , on a spatially mobilised plane, now referred to as the Matsuoka-Nakai failure plane. The stress parameters  $t_N$  and  $t_s$  can be expressed in term of a general stress state by the stress tensor proposed by Nakai *et al.* (1984, 1986). For simplicity, the situation in principal stress space is considered here. The Matsuoka-Nakai failure plane, denoted as SMP, is indicated in Fig. 15 for a cubic soil element. The cosines of the normal to the failure plane in principal stress space can be expressed as,

$$\cos(\text{SMP}, \sigma_i') = \sqrt{\frac{\sigma'_1 \sigma'_2 \sigma'_3}{\sigma'_i (\sigma'_1 \sigma'_2 + \sigma'_2 \sigma'_3 + \sigma'_3 \sigma'_1)}} \quad (35)$$

and the Matsuoka-Nakai strength criterion can be expressed as,

$$X = \frac{t_s}{t_N} = \sqrt{\frac{(\sigma'_1 + \sigma'_2 + \sigma'_3)(\sigma'_1 \sigma'_2 + \sigma'_2 \sigma'_3 + \sigma'_3 \sigma'_1)}{9\sigma'_1 \sigma'_2 \sigma'_3}} - 1 = X_f^*, \quad (36)$$

where  $X_f^*$  is a soil parameter which defines the strength of a soil.

Based on a study of the isotropic and anisotropic variation of the peak strength of geo-materials (Liu and Carter, 1999b; 2003b; 2004c) an extended form of the Matsuoka-Nakai criterion is proposed as follows,

$$\tilde{X} = \frac{\tilde{t}_s}{t_N} = X_f^*, \quad (37)$$

where

$$\tilde{t}_s = \{1 + r_1 \Delta e [1 - \sin(\text{SMP}, A)]\} \bar{t}_s , \quad (38)$$

where  $\bar{t}_s$  represents the isotropic translation, by a distance  $C$ , of the failure surface in the stress space along the isotropic compression line. Thus,  $\bar{t}_s$  and  $t_s$  are related by

$$\begin{aligned} \bar{t}_s &= \sqrt{\frac{(\sigma'_1 + C)(\sigma'_2 + C)(\sigma'_3 + C)}{9}} \times \\ &\sqrt{\left\{ (\sigma'_1 + \sigma'_2 + \sigma'_3 + 3C) - \frac{9(\sigma'_1 + C)(\sigma'_2 + C)(\sigma'_3 + C)}{[(\sigma'_1 + C)(\sigma'_2 + C) + (\sigma'_2 + C)(\sigma'_3 + C) + (\sigma'_3 + C)(\sigma'_1 + C)]} \right\}} \end{aligned} \quad (39)$$

$r_1$  is a parameter defining the soil strength anisotropy. If  $r_1 = 0$ , the proposed failure criterion is the same as equation (36) and the strength of material is isotropic. ( $\text{SMP}$ ,  $A$ ) represents the angle between the weakest plane of anisotropic soil strength and the Matsuoka-Nakai failure plane.  $\Delta e$  is the value of the additional voids ratio sustained by soil structure, *i.e.*, the difference in voids ratio between a structured soil and the same soil in a reconstituted state.

An outcome of this approach is that the conventional deviatoric shear stress  $q$  should be substituted by the new shear stress quantity,  $\tilde{X}p'$ . Therefore, the yield surface for the anisotropic soil is defined as,

$$\left( \frac{\tilde{X}p'}{0.5X_f^* p_s'} \right)^2 + \left( \frac{p' - 0.5p_s'}{0.5p_s'} \right)^2 - 1 = 0 . \quad (40)$$

The following flow rule is proposed for general stress states,

$$\frac{d\epsilon_d^p}{d\epsilon_v^p} = \frac{2\tilde{X}}{\left| X_f^{*2} - \tilde{X}^2 \right| + \varpi\tilde{X}^2 \left| 1 - \sqrt{\frac{p_e'}{p_s'}} \right|} . \quad (41)$$

It follows that the plastic deformation during virgin yielding is described by,

$$d\epsilon_v^p = (\lambda^* - \kappa^*) \frac{dp_s'}{(1+e)p_s'} + \left[ \langle \Delta e - c \rangle + \frac{\gamma\tilde{X}\Delta e}{X_f^{*2} - \tilde{X}^2} \right] \frac{bdp_s'}{(1+e)p_s'} , \quad (42)$$

and

$$d\varepsilon_d^p = \frac{2\tilde{X}}{\left|X_f^{*2} - \tilde{X}^2\right| + \varpi\tilde{X}^2} \left| 1 - \sqrt{\frac{p'_e}{p'_s}} \right| \left\{ (\lambda^* - \kappa^*) + b \left[ (\Delta e - c) + \frac{\gamma\tilde{X}\Delta e}{X_f^{*2} - \tilde{X}^2} \right] \right\} \frac{dp'_s}{(1+e)p'_s} \quad (43)$$

Compared with the constitutive equations for virgin yielding derived in the SCC model, the following differences may be observed. Parameters  $\tilde{X}$ ,  $X_f^*$ , and  $\tilde{X}p'$  are used instead of  $\eta$  and  $M^*$  and  $q$ . Details of the performance of this extended model will be presented in a future paper.

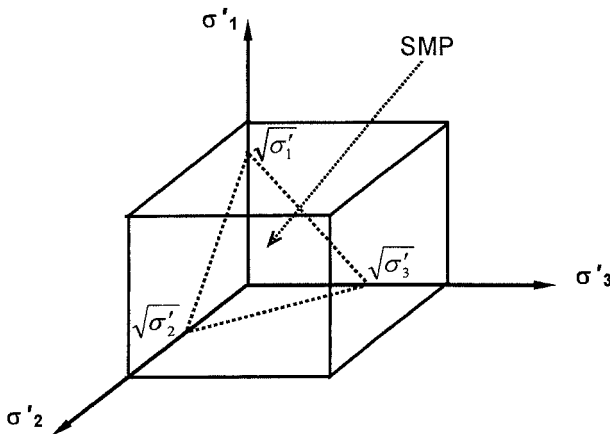


FIG. 15. A soil element and the Spatial Mobilized Plane

## CONCLUSIONS

In this paper, a review of modelling the behaviour of natural clays has been presented and a theoretical framework to describe natural soil behaviour was introduced. The fundamental hypothesis of the framework is that both the hardening and destructuring of natural soils are dependent on plastic volumetric deformation, which provides a premise for the derivation of the constitutive equations. A particular model, the Structured Cam Clay model was described in detail, and it was demonstrated that this simple predictive model has the capacity to capture many important features of the behaviour of naturally structured soils and can serve as a useful tool for the solution of boundary value problems encountered in geotechnical practice.

## ACKNOWLEDGEMENTS

Some of the work described here forms part of the research program of the Special Research Centre for Offshore Foundation Systems, established and supported under the Australian Research Council's Research Centres Program. In addition, a Discovery Grant from the Australian Research Council in partial support of this work is also gratefully acknowledged.

## REFERENCES

- Adachi, T., Oka F., Hirata, T., Hashimoto, T., Nagaya, J., Mimura, M., and Pradhan, T. B. S. (1995). "Stress-strain behaviour and yielding characteristics of Eastern Osaka clay." *Soils and Foundations*, Vol. 35(3), 1-13.
- Arces, M., Nocilla, N., Aversa, S. and Cicero, G. L. (1998). "Geological and geotechnical features of the Calcarenite di Marsala." *The Geotechnics of Hard Soils - Soft Rocks*, Evangelista and Picarelli (eds), 15-25.
- Burghignoli, A., Milizaano, S., and Soccodato, F. M. (1998). "The effect of bond degradation in cemented clayey soils." *The Geotechnics of Hard Soils - Soft Rocks*, Evangelista and Picarelli (eds), 465-472.
- Burland, J. B. (1990). "On the compressibility and shear strength of natural soils." *Géotechnique*, Vol. 40(3), 329-378.
- Calabresi, G. and Scarpelli, G. (1985). "Effects of swelling caused by unloading in over-consolidated clays." *Proc. 11<sup>th</sup> Int. Conference Soil Mechanics and Foundation Engineering*, Vol. 1, 411-414.
- Carter, J. P., Airey, D. W. and Fahey, M. (2000). "A review of laboratory testing of calcareous soils." *Engineering for Calcareous Sediments*, Al-Shafei (ed), Vol. 2, 401-431.
- Clayton, C. R., Hight, D. W., and Hopper, R. J., (1992). "Progressive destruction of Bothkennar clay, implications from sampling and reconsolidation procedures." *Géotechnique*, Vol. 42(2), 219-239.
- Coop, M. R. (2000). "The influence of in-situ state on the behaviour of carbonate sands." *Engineering for Calcareous Sediments*, Al-Shafei (ed), Vol. 2, 379-400.
- Cotecchia, F. and Chandler, R. J. (2000). "A general framework for the mechanical behaviour of clays." *Géotechnique*, Vol. 50(4), 431-447.
- Cotecchia, F. and Chandler, R. J. (1997). "The influence of structure on the pre-failure behaviour of a natural clay." *Géotechnique*, Vol. 47(3), 523-544.
- Dafalias, Y. F. and Popov, E. P. (1976). "Plastic internal variables formalism of cyclic plasticity." *J. Applied Mechanics*, ASME, Vol. 43, 645-651.
- Diaz-Rodriguez, J. A., Leroueil, S. and Aleman, J. D. (1992). "Yielding of Mexico City clay and other natural clays." *J. Geotechnical Engineering*, ASCE, Vol. 118(7), 981-995.
- Gens, A. and Nova, R. (1993). "Conceptual bases for a constitutive model for bonded soils and weak rocks." *Geotechnical Engineering of Hard Soils – Soft Rocks*, Anagnostopoulos *et al.* (ed), Vol. 1, 485-494.
- Georgiannou, V. N., Burland, J. B., and Hight, D. W. (1993). "The behaviour of two hard clays in direct shear." *Geotechnical Engineering of Hard Soils – Soft Rocks*, Anagnostopoulos *et al.* (ed), Vol. 1, 501-507.

- Graham, J. and Li, C. C. (1985). "Comparison of natural and remoulded plastic clay." *J. Geotechnical Engineering*, ASCE, Vol. 111(7), 865-881.
- Hashiguchi, K. (1980). "Constitutive equations of elastoplastic materials with elastic-plastic translation." *J. of Applied Mechanics*, ASME, Vol. 47, 266-272.
- Kavvadas, M. and Amorosi, A. (2000). "A constitutive model for structured soils." *Géotechnique*, Vol. 50(3), 263-273.
- Lagioia, R. and Nova, R. (1995). "An experimental and theoretical study of the behaviour of a calcarenite in triaxial compression." *Géotechnique*, Vol. 45(4), 633-648.
- Leroueil, S. and Vaughan, P. R. (1990). "The general and congruent effects of structure in natural soils and weak rocks." *Géotechnique*, Vol. 40(3), 467-488.
- Liu, M. D. and Carter, J. P. (1999a). "Virgin compression of structured soils", *Géotechnique*, Vol. 49(1), 43-57.
- Liu, M. D. and Carter, J. P. (1999b). "A failure criterion for intact and fissured clay." *Proc. 8<sup>th</sup> Australia-New Zealand Geomechanics Conference*, Hobart, Vol. 2, 861-867.
- Liu, M. D. and Carter, J. P. (2000a). "On the volumetric deformation of reconstituted soils." *Int. J. for Numerical and Analytical Methods in Geomechanics*, Vol. 24(2), 101-133.
- Liu, M. D. and Carter, J. P. (2000b). "Modelling the destructuring of soils during virgin compression." *Géotechnique*, Vol. 50(4), 479-483.
- Liu, M. D. and Carter, J. P. (2002). "Structured Cam Clay Model." *Canadian Geotechnical J.*, Vol. 39(6), 1313-1332.
- Liu, M. D. and Carter, J. P. (2003a). "The volumetric deformation of natural clays." *International J. of Geomechanics*, ASCE, Vol 3(3/4), 236-252.
- Liu, M. D. and Carter, J. P. (2003b). "A general strength criterion for geo-materials." *International J. of Geomechanics*, ASCE, Vol 3(3/4), 253-259.
- Liu, M. D. and Carter, J. P. (2004a). "Evaluation of the Sydney Soil Model." *Advances in Geotechnical Engineering: The Skempton Conference*, London, Vol 1, 498-509.
- Liu, M. D. and Carter, J. P. (2004b). "A Modification of the Structured Cam Clay model." in preparation.
- Liu, M. D. and Carter, J. P. (2004c). "An anisotropic strength criterion for geo-materials." in preparation.
- Liyanapathirana, D. S., Liu, M. D., Carter, J. P., and Airey, D. W. (2003a). "Predicting the behaviour of foundations on structured soils." *Proc. of 13<sup>th</sup> European Conference on Soil Mechanics and Geotechnical Engineering*, Prague, Vol. 2, 255-260.
- Liyanapathirana, D. S., Carter, J. P., Airey, D. W., and Liu, M. D. (2003b). "Bearing response of shallow foundations on structured soils." *Proc. of International Conference on Foundations: Innovations, Observations, Design and Practice*, Dundee, 521-530.
- Liyanapathirana, D.S., Carter, J. P. and Airey, D. W. (2004). "Analysis of cone penetration using the Structured Cam Clay model." *Proc. of 9<sup>th</sup> Australia New Zealand Conference in Geomechanics*, Auckland, Vol. 1, 295-301.

- Lo, K. Y. (1972). "An approach to the problem of progressive failure." *Canadian Geotechnical J.*, Vol. 9(4), 407-429.
- Matsuoka, H. and Nakai, T. (1982). "A new failure criterion for soils in three dimensional stress." *Proc. of conference on deformation and failure of granular materials, Delft*, Vermeer et al. (ed), 253-263.
- Muir-Wood, D. (1990). *Soil Behaviour and Critical State Soil Mechanics*, Cambridge University Press.
- Nakai, T. and Mihara, Y. (1984). "A new mechanical quantity for soils and its application to elastoplastic constitutive models." *Soils and Foundations*, Vol. 24(2), 82-94.
- Nakai, T. (1989). "An isotropic hardening elastoplastic model for sand considering stress path dependency in three dimensional stresses." *Soils and Foundations*, Vol. 29(2), 119-137.
- Robinet, J. C., Pakzad, M., Jullien, A., and Plas, F. (1999). "A general modelling of expansive and non-expansive clays." *Int. J. Numerical and Analytical Method in Geomechanics*, Vol. 23, 1319-1335.
- Roscoe, K. H. and Burland, J. B. (1968). "On the generalised stress-strain behaviour of 'wet clay'." *Engineering Plasticity*, Heyman and Leckie (ed), 535-609.
- Rouainia, M. and Muir Wood, D. (2000). "A kinematic hardening model for natural clays with loss of structure." *Géotechnique*, Vol. 50(2), 153-164.
- Schofield, A. N. and Wroth, C. P. (1968). *Critical State Soil Mechanics*, MacGraw-Hill, London.
- Wheeler, S. J. (1997). "A rotational hardening elasto-plastic model for clays." *Proc. 14<sup>th</sup> Int. Conference Soil Mechanics and Foundation Engineering*, Vol. 1, 431-434.
- Whittle, A. J. (1993). "Evaluation of a constitutive model for overconsolidated clays." *Géotechnique*, Vol. 43(2), 289-314.
- Wong, R. C. K. (1980). "Swelling and softening behaviour of La Biche shale." *Canadian Geotechnical J.*, Vol. 35, 206-221.

## INCREMENTALLY NON-LINEAR CONSTITUTIVE RELATIONS: NEW CHALLENGES

Félix A. Darve<sup>1</sup>, Cédric G. Lambert<sup>2</sup>

### ABSTRACT

Phenomenological constitutive relations have received great care during last years. Various visco-elasto-plastic relations have been proposed and the present situation is certainly not clear for end users.

We propose first to classify all the existing models in relation with the internal structure in order to emphasize a global view by ignoring the technical details. The notions of “tensorial zone” and of “incremental non-linearity” are recalled. Then two different criteria are considered in order to evaluate the models: the modelling of non proportional loading paths and the description of bifurcations, instabilities.

In a last section, a particular incrementally non-linear model with 5 parameters is presented and discussed.

In conclusion, it is emphasized that the phenomenological models are maybe reaching now their limits. The future of constitutive modelling might be based on multi-scale techniques.

### INTRODUCTION

For many years the study of the mechanical behaviour of geomaterials and its description by constitutive relations has been developed in the framework characterized by isotropic linear elasticity (Hooke's law) and by solid friction (Coulomb's law). However, since the end of the 1960's the development of more powerful numerical methods such as finite element method and the use of high-performance computers has brought to the fore of the scene the question that is becoming a crucial one: what constitutive relation for geomaterials must be introduced into a computer code? Thirty years later, the choice is large and the state of affairs confused; we will try to classify the various existing constitutive relations into some general classes with respect to the structure of the constitutive relationships.

<sup>1</sup>Professor, Institut National Polytechnique de Grenoble (INPG, UJF, CNRS), RNVO.

<sup>2</sup>PhD student, Institut National Polytechnique de Grenoble (INPG, UJF, CNRS), RNVO.



Any user of finite element codes must be able to characterize the capacities of any implemented constitutive model in order to interpret correctly the numerical results obtained and also in order to know if the physical phenomena, that the user considers to have an important influence on the behaviour of the engineering work being analyzed, can be effectively taken into account by the constitutive relation used.

The first part of this paper is devoted to a presentation of the incremental formulation of constitutive relations. Two main reasons make such an incremental presentation indispensable. The first one is physical and is the fact that, as soon as some plastic irreversibilities are mobilized inside the geomaterial, the global constitutive functional, which relates the stress state  $\sigma(t)$  at a given time  $t$  to the strain state  $\epsilon(t)$  history up to this time, is a priori very difficult to formulate explicitly since this functional is singular at all stress-strain states (or more precisely non-differentiable, as we shall show). An incremental formulation enables us to avoid this fundamental difficulty. The second reason is numerical and stems from the fact that geomaterial behaviour, and the modelling of engineering works generally, exhibit many non-linearity sources which imply that the associated boundary value problem must be solved by successive steps linked to increments of boundary loading. Such finite element codes need therefore, the constitutive relations to be expressed incrementally.

## PRINCIPLE OF DETERMINISM

### Principle of determinism in the large

The first expression of the principle of the determinism is obtained by stating that the stress state  $\sigma(t)$  at a given time  $t$  is a functional of the history of the tangent linear transformation up to this time  $t$ . It implies that it is necessary to know all the loading path in order to deduce the associated response path.

From a mathematical point of view, this is stated by the existence of a stress functional  $\mathcal{F}$ :

$$\sigma(t) = \mathcal{F}[\mathbf{F}(\tau)], \quad -\infty < \tau \leq t \quad (1)$$

where  $\mathbf{F}(\tau)$  is the tangent linear transformation at time  $\tau$ ; also called deformation gradient. The deformation gradient  $\mathbf{F}$  is the jacobian matrix of the position  $\phi(X, \tau)$  of the material point  $X$  at time  $\tau$ . The existence of such a functional, and not a function, is related to an essential physical characteristic: for irreversible behaviours the knowledge of the strain  $\epsilon(t)$  at time  $t$  does not enable us to determine the stress and vice versa. This stress-strain relationship, which must be studied in the framework of non-linear functionals, is moreover non-differentiable as soon as there exist some plastic irreversibilities. Owen and Williams (1969) showed in fact that the assumptions of non-viscosity and of differentiability of the stress functional  $\mathcal{F}$ , imply that there is no internal dissipation. In other words a non-viscous material whose constitutive functional is differentiable is necessarily elastic.

Basically, this is due to the fact that, in plasticity, the tangent loading modulus is not equal to the tangent unloading modulus.

Therefore, if one wants to describe the behaviour of inelastic materials (geomaterials are essentially of this kind) by using a stress-strain relationship, this relation must be formulated by a non-linear and non-differentiable functional.



There is clearly a need, therefore, to study constitutive relations using an incremental formulation and no longer a global one. Note that incremental form tends to rate form when the 'time' increment tends to zero. In the following, the terms increment or rate are employed in the same sense.

We are now going to introduce an incremental formulation using a second statement of the principle of determinism.

### Principle of determinism in the small

Let us consider a deformed solid, and let us assume that only quasi-static loading will be applied to it at a continuously varying rate.

The second principle of determinism, which can be called 'in the small' to distinguish it from the first one 'in the large', is obtained by stating that a small load applied during time increment  $dt$  induces a small uniquely determined response.

We denote by  $d\epsilon = \mathbf{D} dt$ , the incremental strain tensor equal to the product of strain rate tensor,  $\mathbf{D}$  (symmetric part of transformation rate  $\mathbf{L}$ :  $\mathbf{L} = \dot{\mathbf{F}} \mathbf{F}^{-1}$ ) and time increment  $dt$ , and by  $d\sigma = \hat{\sigma} dt$  the incremental stress tensor, equal to the product of an objective time derivative of Cauchy stress tensor  $\sigma$  and  $dt$ . Thus the second determinism principle implies, from a mathematical point of view, the existence of a tensorial function  $\mathbf{H}$  relating the three quantities:

$$\mathbf{H}_x(d\epsilon, d\sigma, dt) = 0 \quad (2)$$

What are the properties of this tensorial function  $\mathbf{H}$ ? The first remark concerns the fact that  $\mathbf{H}$  depends on the previous stress-strain history. This history is generally characterized by some scalar and tensorial variables which will appear as parameters  $\chi$  in relation (2). These parameters describe, as far as possible, the actual deformed state of the solid. Following the various constitutive theories, they are sometimes called 'memory variables', 'hardening parameters', 'internal variables', etc.

Secondly,  $\mathbf{H}$  must satisfy the objectivity principle; this means that  $\mathbf{H}$  must be independent of any movement of the observer relative to the solid. Thus  $\mathbf{H}$  is an isotropic function of all its arguments:  $d\epsilon$ ,  $d\sigma$  and also the state tensorial variables  $\chi$ , which characterize its present deformed state. But it is an anisotropic function of  $d\epsilon$  and  $d\sigma$ .

Finally,  $\mathbf{H}$  is essentially a non-linear function as soon as there are some plastic irreversibilities, since, if  $\mathbf{H}$  was linear, the functional  $\mathcal{F}$  would be differentiable, a property which excludes the existence of non-viscous irreversibilities.

We remark here also that this determinism principle, which has very wide applications in physics by connecting notions of cause and effect, is not always satisfied, particularly in cases such as bifurcation situations. In such conditions a continuous variation of state variables can induce, at the bifurcation point, a sudden change in the evolution of the system with loss of uniqueness as a result of local imperfections not taken into account by the analysis (see examples given by Darve (1984)). At such a bifurcation point an identical cause in terms of state variables can have different effects; such a situation is common in geomaterial behaviour when a shear band appears, by localisation of plastic strains, while the deformation, up to this state, is respecting mainly a diffuse mode Vardoulakis et al. (1978).



## APPLICATION TO NON-VISCOUS MATERIALS

In formulating constitutive relations it is often more convenient to replace the stress tensor  $\sigma$  and strain tensor  $\epsilon$ , of second order, by two vectors of  $\mathbb{R}^6$  defined in a six-dimensional related space:

$$\underline{\sigma} = \begin{pmatrix} \sigma_{11} \\ \sigma_{22} \\ \sigma_{33} \\ \sqrt{2}\sigma_{23} \\ \sqrt{2}\sigma_{31} \\ \sqrt{2}\sigma_{12} \end{pmatrix} \quad \text{and} \quad \underline{\epsilon} = \begin{pmatrix} \epsilon_{11} \\ \epsilon_{22} \\ \epsilon_{33} \\ \sqrt{2}\epsilon_{23} \\ \sqrt{2}\epsilon_{31} \\ \sqrt{2}\epsilon_{12} \end{pmatrix} \quad (3)$$

We will utilize greek indices, ranging from 1 to 6, in such a case and reserve latin indices, ranging from 1 to 3, to characterize tensorial components in the original three-dimensional space. The  $\sqrt{2}$  coefficients, which appear in the definition of these vectors, allow us to preserve the original metric unchanged (isometric mapping). For example,

$$\|\sigma\|^2 = \sigma_{ij}\sigma_{ij} = (\sigma_{11})^2 + (\sigma_{22})^2 + (\sigma_{33})^2 + 2(\sigma_{23})^2 + 2(\sigma_{31})^2 + 2(\sigma_{12})^2 = \sigma_\alpha\sigma_\alpha \quad (4)$$

The constitutive relation (2) will be written in the new notation as

$$H_x(d\epsilon_\alpha, d\sigma_\beta, dt) = 0 \quad (5)$$

where now  $H$  is a vectorial function (of  $\mathbb{R}^6$  space) of 13 variables.

Now let us particularize, in this section, the class of materials considered and restrict the study to the case of non-viscous materials or to cases of loading for which a given geomaterial exhibits negligible viscosity. This means that the loading rate (characterized by time gradation on loading path) has no influence on the material constitutive behaviour: at whatever rate the given loading path is followed, the response path remains unchanged. In other words the class of behaviour considered is rate independent.

This restriction of the constitutive law implies that the constitutive function  $H$ , which relates  $d\epsilon$  and  $d\sigma$ , is independent of the time increment  $dt$  during which the incremental loading has been applied. Therefore  $H$  is independent of  $dt$  and, in an equivalent manner if  $H$  is regular, one can now study the vectorial function  $G$ :

$$d\epsilon_\alpha = G_\alpha(d\sigma_\beta) \quad (6)$$

### Homogeneity of $G$

We have just seen that the behaviour of a non-viscous material is independent of the loading rate. This means that, in order to verify the one-to-one relation on a given loading path and its related unique response path, there is a dependency condition between the two rate vectors  $D$  and  $\dot{\sigma}$ .

From a mathematical point of view this independence of non-viscous behaviours on loading rates implies the following identity:

$$\forall \lambda \in \mathbb{R}^+ : G_\alpha(\lambda d\sigma_\beta) = \lambda G_\alpha(d\sigma_\beta) \quad (7)$$

**@Seismicisolation**

This is the first property of  $\mathbf{G}$ :  $\mathbf{G}$  is a homogeneous function of degree 1 in  $d\sigma$  with respect to the positive values of the multiplying parameter.

### Non-linearity of $\mathbf{G}$

Let us recall that we want to describe plastic irreversibilities, and consider the incremental strains, which are produced by a return incremental load  $-d\sigma$  applied after  $d\sigma$ . If the behaviour is purely elastic, this stress cycle would induce a strain cycle equally closed (with no permanent strain). Therefore for elastic behaviour:

$$\forall d\sigma \in \mathbb{R}^6 : \mathbf{G}(-d\sigma) = -\mathbf{G}(d\sigma) \quad (8)$$

In a more general manner,  $\mathbf{G}$  is linear for elasticity since a regular correspondence relationship between  $\sigma$  and  $\epsilon$  implies the existence of a linear relation between  $d\sigma$  and  $d\epsilon$ .

This incremental linearity, which is a characteristic property of elasticity if we consider non-viscous materials, must obviously not be confused with an eventual global linearity. The existence of such a global linear relationship between  $\sigma$  and  $\epsilon$  describes linear-elastic behaviour, while an incrementally linear relation is characteristic of all elastic constitutive relations.

Since we want to describe the behaviour of essentially inelastic media such as geomaterials, we need therefore to take into account non-linear function  $\mathbf{G}$ .

### Anisotropy of $\mathbf{G}$

The last property of  $\mathbf{G}$  that we will emphasize is its anisotropy. If we consider all the arguments of  $\mathbf{G}$ , which means the six components of  $d\sigma$  as well as the memory parameters  $\chi$  characterizing the previous strain history of the medium, the objectivity principle implies that  $\mathbf{G}$  is an isotropic function of the whole of its tensorial arguments.

However, let us now consider a deformed anisotropic sample of a geomaterial and carry out an experiment which consists of rotating the principal axes of incremental loading with respect to the sample. We do not obtain the same incremental response merely rotated in the same manner.

So nature requires us to consider functions  $\mathbf{G}$  anisotropic with respect to  $d\sigma$  and fixed parameters  $\chi$ . This anisotropy is directly linked to the geometrical meso-structure of the material, which is gradually modified by the strain (particularly irreversible) history. We have seen that this history can be characterized by scalar and tensorial state parameters  $\chi$ .

In simple cases this anisotropy is a priori directly imposed by the choice of these state parameters.

Having described the three main properties of  $\mathbf{G}$ , we will now focus on the first one (the homogeneity of degree 1) to see the mathematical consequences of such property. Let us recall for this purpose Euler's identity for homogeneous regular functions of degree 1 by writing it for a function of two variables, for example, as:

$$\forall x, y \in \mathbb{R} \times \mathbb{R} : f(x, y) = x \frac{\partial f}{\partial x} + y \frac{\partial f}{\partial y} \quad (9)$$

 @Seismicisolation

where partial derivatives  $\partial f/\partial x$  and  $\partial f/\partial y$  are homogeneous functions of degree 0. Therefore the six functions  $G_\alpha$ , which are homogeneous functions of degree 1 of the six variables  $d\sigma_\beta$ , satisfy the identity,

$$G_\alpha(d\sigma_\beta) = \frac{\partial G_\alpha}{\partial(d\sigma_\beta)} d\sigma_\beta, \quad \alpha, \beta \in \{1, 2, \dots, 6\}^2 \quad (10)$$

with summation on the repeated index  $\beta$ . If we note,

$$M_{\alpha\beta}(d\sigma_\beta) = \frac{\partial G_\alpha}{\partial(d\sigma_\beta)}, \quad \alpha, \beta \in \{1, 2, \dots, 6\}^2 \quad (11)$$

we obtain the following constitutive relation,

$$d\epsilon_\alpha = M_{\alpha\beta}(d\sigma_\gamma)d\sigma_\beta, \quad \alpha, \beta, \gamma \in \{1, 2, \dots, 6\}^3 \quad (12)$$

where the  $6 \times 6$  functions  $M_{\alpha\beta}$  are homogeneous of degree 0 of the six variables  $d\sigma_\gamma$ . Therefore they are in an equivalent manner functions only of the

$$u_\gamma = \frac{d\sigma_\gamma}{\|d\sigma\|}, \quad \gamma \in \{1, 2, \dots, 6\} \quad (13)$$

with

$$\|d\sigma\| = \sqrt{d\sigma_{ij}d\sigma_{ij}} = \sqrt{d\sigma_\alpha d\sigma_\alpha}, \quad i, j \in \{1, 2, 3\}^2, \quad \alpha \in \{1, 2, \dots, 6\} \quad (14)$$

finally we obtain ( $\alpha, \beta, \gamma \in \{1, 2, \dots, 6\}^3$ )

$$d\epsilon_\alpha = M_{\alpha\beta}(u_\gamma)d\sigma_\gamma \quad (15)$$

Equation (15) is the general expression for all rate independent constitutive relations. The existence of an elasto-plastic constitutive tensor  $\mathbf{M}$  has been proven, as well as its essential dependency of state variable  $\chi$  and the direction of  $d\sigma$

This constitutive matrix  $\mathbf{M}$ , which can be called “tangent constitutive matrix”, should be utilized to solve bifurcation problems by strain localization into shear bands Darve (1984) and also preferably used in finite element computations.

The relation (15) will now, allow us to propose a classification of all the existing rate independent constitutive relations with respect to their intrinsic structure.

## MAIN CLASSES OF RATE INDEPENDENT CONSTITUTIVE RELATIONS

The incremental non-linearity, which is also that of plastic irreversibilities, results, as we have just seen, from the constitutive tensor  $\mathbf{M}$  varying with the direction of the incremental loading. The mode of the chosen directional variation is very much influenced by the constitutive model used. It is precisely this mode of description of incremental non-linearity that we are going to take as a guide for this review of main classes of existing constitutive relations.

First of all we need to define the notion of “tensorial zone” Darve and Labanieh (1982). We will call a tensorial zone any domain in the incremental loading space on



which the restriction of  $\mathbf{G}$  is a linear function. In other words the relation between  $\mathbf{d}\epsilon$  and  $\mathbf{d}\sigma$  in a given tensorial zone is incrementally linear.

If we denote  $Z$  the tensorial zone being considered, the

$$\forall \mathbf{u} \in Z : \mathbf{M}(\mathbf{u}) \equiv \mathbf{M}^z \quad (16)$$

In zone  $Z$ , the constitutive relation is characterized by a unique tensor  $\mathbf{M}^z$ .

If  $\mathbf{u}$  belongs to  $Z$ ,  $\lambda \mathbf{u}$  belongs also to  $Z$  for all real positive values  $\lambda$ . Therefore a zone is defined by a set of half-infinite straight lines, whose apex is the same and is at the origin of the incremental loading space. Tensorial zones then comprise adjacent hypercones, whose common apex is this origin.

What does the constitutive relation become on the common boundary of two (or several) adjacent tensorial zones?

If  $\mathbf{M}^{z_1}$  and  $\mathbf{M}^{z_2}$  are constitutive tensors attached respectively to tensorial zones  $Z_1$  and  $Z_2$ , we must obviously satisfy the continuity requirement of the response to loading directions  $\mathbf{u}$  such that:

$$\forall \mathbf{u} \in Z_1 \cap Z_2 : \mathbf{M}^{z_1}\mathbf{u} \equiv \mathbf{M}^{z_2}\mathbf{u} \quad (17)$$

or equivalently

$$\forall \mathbf{u} \in Z_1 \cap Z_2 : (\mathbf{M}^{z_1} - \mathbf{M}^{z_2})\mathbf{u} \equiv 0 \quad (18)$$

Relation (18) can be called a ‘continuity condition’ for zone changes. This condition forbids, in particular, an arbitrary choice of constitutive tensors in two adjacent tensorial zones.

Gudehus (1979) studied in this way the continuity of several constitutive relations for axisymmetrical loading paths with fixed principal axes, as did Di Benedetto and Darve (1983) with rotating principal axes.

The “response-envelopes”, as proposed by Gudehus (1979), constitute geometrical diagrams which characterize completely a constitutive relation at a given stress strain state after a given strain history. At this state, all the incremental loading, having the same norm but oriented in all directions, are considered and all the incremental responses are plotted. ‘The extremities of the response vectors form a surface which is called “response-envelope”. Some examples will be given later.

This criterion of the number of tensorial zones has been chosen to classify the main classes of non-viscous constitutive relations, since this number characterizes the structure of the relation. In fact the directional dependency of the constitutive tensor  $\mathbf{M}$  with respect to the incremental loading can be described either in a discontinuous manner, by a finite number of different tensors related to the same number of tensorial zones (we will call such relations “incrementally piece wise linear”), or in a continuous manner by a continuous variation of the constitutive tensor with the direction of the incremental loading (relations called “incrementally non-linear”).

### Constitutive relations with one tensorial zone

The first class of relations that we are going to look at is related to the simplest assumption that only one tensorial zone

$$\forall \mathbf{u} : \mathbf{M}(\mathbf{u}) \equiv \mathbf{M} \quad (19)$$



We have here the class of elastic laws, since there is a unique linear relation between  $d\epsilon$  and  $d\sigma$  (incremental linearity):

$$d\epsilon_\alpha = M_{\alpha\beta} d\sigma_\beta \quad \alpha, \beta \in \{1, 2, \dots, 6\}^2 \quad (20)$$

These elastic laws may be isotropic or anisotropic, linear or non-linear (global non-linearity). The isotropic and linear case corresponds to the well known Hooke's law with its two constitutive constants: Young's modulus and Poisson's ratio.

### Constitutive relations with two tensorial zones

We now find laws with two tensorial zones, which can then be called "loading zones" and "unloading zones". These two tensorial zones are separated by a hyperplane in  $d\sigma$  space or in  $d\epsilon$  space.

These laws may be either of hypoelastic type with a unique loading-unloading criterion (for example, models proposed by Guélin (1980)) or of elastoplastic type with one regular plastic potential (for example, models proposed by Mroz (1967); Prevost (1978), or Dafalias and Hermann (1980)).

The model developed by Duncan and Chang (1970) is a non-linear isotropic hypoelastic model with a specific loading-unloading criterion. It is easy to verify that such a model cannot be continuous at the frontier between the two zones.

The classical elastoplastic relations utilize an elastic matrix  $\mathbf{M}^e$ , related to the unloading zone, and an elastoplastic matrix  $\mathbf{M}^{ep}$ , related to the loading zone.

### Constitutive relations with four tensorial zones

To this class belong the hypoelastic constitutive relations with two loading-unloading criteria proposed by Davis and Mullenger (1978) and elastoplastic models with a double plastic potential (Lade (1977), Loret (1981), Nova and Wood (1979) and Vermeer (1978), for example). This means that, after a given strain history, the direction of the plastic incremental strain vector is no longer defined in a unique way by the normal to a unique plastic potential (eventually a function of the history) but may coincide with two normals to two different potentials following the direction of the present incremental stress vector.

With respect to each of these two plastic mechanisms, the incremental stress may be considered to be a loading or an unloading. Therefore we obtain the following four possibilities:

1.  $(\partial f_1 / \partial \sigma) \cdot d\sigma > 0$ : loading for criterion 1;  $p_1$
2.  $(\partial f_1 / \partial \sigma) \cdot d\sigma < 0$ : unloading for criterion 1;  $e_1$
3.  $(\partial f_2 / \partial \sigma) \cdot d\sigma > 0$ : loading for criterion 2;  $p_2$
4.  $(\partial f_2 / \partial \sigma) \cdot d\sigma < 0$ : unloading for criterion 2;  $e_2$

Finally, four different constitutive tensors can be obtained:

$$\mathbf{M}^{e_1 e_2}, \mathbf{M}^{p_1 e_2}, \mathbf{M}^{e_1 p_2}, \mathbf{M}^{p_1 p_2}$$

Each of them is associated with a certain tensorial zone in  $d\sigma$  space.



### Constitutive relations with eight tensorial zones

By further increasing the number of tensorial zones we now find incrementally octolinear relations with eight tensorial zones.

The incremental octolinear relation developed by Darve and Labanieh (1982) belongs to this class. The basis of the laws with three plastic potentials is essentially the same as for the models with a double potential, which we have presented above. Concerning the incremental octolinear relation, the basis of this model derives from the assumption of eight tensorial zones in  $d\sigma$  space. It satisfies all the different continuity conditions for fixed principal stress and fixed principal strain axes Gudehus (1979) and has been generalized Darve (1980, 1990) to arrive at an "incrementally non-linear of second order" constitutive relation, which will be presented later.

### Constitutive relations with an infinite number of tensorial zones

We could say that they have an infinite number of tensorial zones, since each direction of  $d\sigma$  space is linked to a given tangent constitutive tensor which varies in a continuous manner with this direction. They may be of three different types. The endochronic models Valanis (1971); Bazant (1978) take into account non-linearity by introducing an intrinsic 'time' which is always increasing. The hypoplastic models by Kolymbas (1977) or Chambon et al. (1994) assume a priori a direct non-linear relation between  $de$  and  $d\sigma$  with also a scalar variable always positive. Thirdly we find models based on a non-linear interpolation between given constitutive responses, the non-linearity being linked to the kind of interpolation rule used (Darve, 1980). Another model has been proposed by Dafalias (1986) in the framework of his 'bounding surface' theory of plasticity.

The interest in incrementally non-linear constitutive relations is based mainly on the fact that it is not necessary to postulate the existence of either an elastic limit surface (since any purely elastic domain has disappeared) and the linked loading-unloading condition or a plastic potential. In fact the non-linearity of the incremental relation allows a direct description of the different behaviours in 'loading' and in 'unloading'. For this reason the incrementally non-linear relations may be closer to the physics that governs deformation of geomaterials.

## INCREMENTALLY NON-LINEAR CONSTITUTIVE RELATIONS OF SECOND ORDER

Let us recall relation (15):

$$d\epsilon_\alpha = M_{\alpha\beta}(u_\gamma)d\sigma_\gamma \quad (21)$$

with

$$u_\gamma = \frac{d\sigma_\gamma}{\|d\sigma\|} \quad \gamma \in \{1, 2, \dots, 6\}$$

We consider polynomial series expansions for 36 functions  $M_{\alpha\beta}$  of 6 variables  $u_\gamma$ :

$$M_{\alpha\beta}(u_\gamma) = M_{\alpha\beta}^1 + M_{\alpha\beta\gamma}^2 u_\gamma + M_{\alpha\beta\gamma\delta}^3 u_\gamma u_\delta + \dots \quad (22)$$



From equation (21) and equation (22) it follows that:

$$d\epsilon_\alpha = M_{\alpha\beta}^1 d\sigma_\beta + \frac{1}{\|d\sigma\|} M_{\alpha\beta\gamma}^2 d\sigma_\beta d\sigma_\gamma + \dots \quad (23)$$

The first term of equation (23) describes the elastic behaviors and both the first terms are incrementally non-linear constitutive relations of second order.

In this paper we will consider only loading paths which are defined in fixed stress-strain principal axes. In such a case the expression of the model is the following (for a more general presentation see Darve and Dendani (1989) or Darve (1990)) :

$$\begin{pmatrix} d\epsilon_1 \\ d\epsilon_2 \\ d\epsilon_3 \end{pmatrix} = \frac{1}{2} [\mathbf{N}^+ + \mathbf{N}^-] \cdot \begin{pmatrix} d\sigma_1 \\ d\sigma_2 \\ d\sigma_3 \end{pmatrix} + \frac{1}{2\|d\sigma\|} [\mathbf{N}^+ - \mathbf{N}^-] \cdot \begin{pmatrix} d\sigma_1^2 \\ d\sigma_2^2 \\ d\sigma_3^2 \end{pmatrix} \quad (24)$$

with

$$\|d\sigma\| = \sqrt{d\sigma_i d\sigma_i}, \quad i \in \{1, 2, 3\}$$

The two matrices  $\mathbf{N}^+$  and  $\mathbf{N}^-$  have the following form (for more details see Darve and Dendani (1989) or Darve (1990)):

$$\mathbf{N}^+ = \begin{bmatrix} \frac{1}{E_1^+} & -\frac{\nu_{12}^+}{E_2^+} & -\frac{\nu_{13}^+}{E_3^+} \\ -\frac{\nu_{21}^+}{E_1^+} & \frac{1}{E_2^+} & -\frac{\nu_{23}^+}{E_3^+} \\ -\frac{\nu_{31}^+}{E_1^+} & -\frac{\nu_{32}^+}{E_2^+} & \frac{1}{E_3^+} \end{bmatrix} \quad \mathbf{N}^- = \begin{bmatrix} \frac{1}{E_1^-} & -\frac{\nu_{12}^-}{E_2^-} & -\frac{\nu_{13}^-}{E_3^-} \\ -\frac{\nu_{21}^-}{E_1^-} & \frac{1}{E_2^-} & -\frac{\nu_{23}^-}{E_3^-} \\ -\frac{\nu_{31}^-}{E_1^-} & \frac{\nu_{32}^-}{E_2^-} & \frac{1}{E_3^-} \end{bmatrix} \quad (25)$$

Where  $E_i$  and  $\nu_{ij}$  are, respectively, tangent moduli and tangent Poisson's ratio on 'generalized triaxial paths'. These paths correspond to the conventional triaxial paths (the two constant lateral stresses are equal), but on 'generalized triaxial paths' the lateral stresses are fixed but independently. The superscript (+) means 'compression' in the axial direction for these paths and the superscript (-) means 'extension'.

The behavior of the studied material for these specific paths is assumed to be given by laboratory triaxial tests and described by analytical expressions. It is in these expressions that the constitutive constants appear as well as the state variables (stress tensor and void ratio) and the memory parameters (which are of two types of discontinuous and continuous nature). Thus  $\mathbf{N}^+$  and  $\mathbf{N}^-$  are depending on state variables and memory parameters.

It is clear from equation (24) that this relation is homogeneous of degree one with respect to  $d\sigma$ . Thus, it describes a rate independent behaviour. Equation (24) is also non linear in  $d\sigma$ , it means that it can describe plastic irreversible strains : for an elementary stress cycle ( $d\sigma, -d\sigma$ ) the irreversible strain is equal to:

$$\begin{pmatrix} d\epsilon_1 \\ d\epsilon_2 \\ d\epsilon_3 \end{pmatrix} = \frac{1}{\|d\sigma\|} [\mathbf{N}^+ - \mathbf{N}^-] \cdot \begin{pmatrix} d\sigma_1^2 \\ d\sigma_2^2 \\ d\sigma_3^2 \end{pmatrix} \quad (26)$$

**@Seismicisolation**

The recoverable strain has not an elastic nature since it is equal to:

$$\begin{pmatrix} d\epsilon_1 \\ d\epsilon_2 \\ d\epsilon_3 \end{pmatrix} = \frac{1}{2} [\mathbf{N}^+ + \mathbf{N}^-] \cdot \begin{pmatrix} d\sigma_1 \\ d\sigma_2 \\ d\sigma_3 \end{pmatrix} - \frac{1}{2\|\mathbf{d}\sigma\|} [\mathbf{N}^+ - \mathbf{N}^-] \cdot \begin{pmatrix} d\sigma_1^2 \\ d\sigma_2^2 \\ d\sigma_3^2 \end{pmatrix} \quad (27)$$

It means that it is not possible to decompose in an additive manner the strain into an elastic part and a plastic one. Elasticity and plasticity are intrinsically mixed into the constitutive relation.

Now we will see how equation (24) is degenerating in the one dimensional case and in the cases of an elastic material and a perfectly plastic one.

For the one dimensional case (24) degenerates into the following scalar expression:

$$d\epsilon = \frac{1}{2} \left( \frac{1}{E^+} + \frac{1}{E^-} \right) d\sigma + \frac{1}{2} \left( \frac{1}{E^+} - \frac{1}{E^-} \right) |d\sigma| \quad (28)$$

It is easy to verify that relation (28) is able to describe any rate independent one dimensional behaviour with one single expression (28). If one wants to interpret (24) with conventional elasto-plastic concepts, it is necessary to introduce a loading-unloading criterion and we obtain:

$$\begin{cases} d\sigma \geq 0 & : d\epsilon = \frac{1}{E^+} d\sigma & \text{(loading)} \\ d\sigma \leq 0 & : d\epsilon = \frac{1}{E^-} d\sigma & \text{(unloading)} \end{cases} \quad (29)$$

If the behaviour of the material is elastic, we obtain the same behaviour for ‘compressions’ and ‘extensions’ (as defined previously) which implies:

$$\mathbf{N}^+ = \mathbf{N}^-$$

Relation (24) degenerates into the following :

$$\begin{pmatrix} d\epsilon_1 \\ d\epsilon_2 \\ d\epsilon_3 \end{pmatrix} = [\mathbf{N}] \cdot \begin{pmatrix} d\sigma_1 \\ d\sigma_2 \\ d\sigma_3 \end{pmatrix} \quad (30)$$

Equation (30) is exactly the general expression of anisotropic non-linear elasticity in identical incremental stress-strain principal axes.

Finally, it is also possible to exhibit the equations of perfect plasticity as a degenerating case. Let us write relation (24) in the following form:

$$\begin{pmatrix} d\epsilon_1 \\ d\epsilon_2 \\ d\epsilon_3 \end{pmatrix} = [\mathbf{N}(u)] \cdot \begin{pmatrix} d\sigma_1 \\ d\sigma_2 \\ d\sigma_3 \end{pmatrix} \quad (31)$$

By inverting (31) we obtain:

$$d\sigma = \mathbf{N}^{-1}(u) d\epsilon \quad (32)$$

Conditions for perfect plasticity imply:

$$\begin{cases} \frac{d\sigma}{\|d\epsilon\|} = 0 \\ \|d\epsilon\| : \text{undetermined} \end{cases} \quad (33)$$

It follows therefore that:

$$\det \mathbf{N}^{-1}(u) = 0 \quad (34)$$

which represents the plastic condition.

$$\mathbf{N}^{-1}(u) d\epsilon = 0 \quad (35)$$

is a generalized flow rule, since the solution of equation (35) while equation (34) is verified gives the direction of  $d\epsilon$  but not its intensity. Condition (35) is directionally dependent with respect to  $d\sigma$  which reflects the fact that the flow rule is locally deformed into a vertex.

The incrementally 'octo-linear' model is given by the following relation:

$$\begin{pmatrix} d\epsilon_1 \\ d\epsilon_2 \\ d\epsilon_3 \end{pmatrix} = \frac{1}{2} [\mathbf{N}^+ + \mathbf{N}^-] \cdot \begin{pmatrix} d\sigma_1 \\ d\sigma_2 \\ d\sigma_3 \end{pmatrix} + \frac{1}{2} [\mathbf{N}^+ - \mathbf{N}^-] \cdot \begin{pmatrix} |d\sigma_1| \\ |d\sigma_2| \\ |d\sigma_3| \end{pmatrix} \quad (36)$$

The incremental structure of this model is the same as an elastoplastic relation with 3 plastic potentials. The constitutive constants for both the incremental non-linear model and octo-linear model are the same.

Both these constitutive relations (the non-linear one and the octo-linear model) can be viewed as interpolations between the generalized triaxial responses. The octo-linear model corresponds to a linear interpolation rule, while the incrementally non-linear model describes a quadratic non-linear interpolation. Indeed it is possible to define a family of incrementally non-linear relations depending on a positive scalar  $\rho$  as proposed by Darve F. & Laouafa F. (2000):

$$\begin{pmatrix} d\epsilon_1 \\ d\epsilon_2 \\ d\epsilon_3 \end{pmatrix} = \frac{1}{2} [\mathbf{N}^+ + \mathbf{N}^-] \cdot \begin{pmatrix} d\sigma_1 \\ d\sigma_2 \\ d\sigma_3 \end{pmatrix} + \frac{\sqrt{1+\rho}}{2} [\mathbf{N}^+ - \mathbf{N}^-] \cdot \begin{pmatrix} \frac{d\sigma_1^2}{\sqrt{d\sigma_1^2 + \rho \|d\sigma\|^2}} \\ \frac{d\sigma_2^2}{\sqrt{d\sigma_2^2 + \rho \|d\sigma\|^2}} \\ \frac{d\sigma_3^2}{\sqrt{d\sigma_3^2 + \rho \|d\sigma\|^2}} \end{pmatrix} \quad (37)$$

For  $\rho = 0$ , this relation coincides with the octo-linear model, while for  $\rho \rightarrow +\infty$  it converges toward the incrementally non-linear relation of second order.

According to the construction of "response-envelopes" as presented in section 4 (which characterize completely a constitutive relation at a given stress-strain state after a given strain history), octo-linear and non-linear models have been compared to

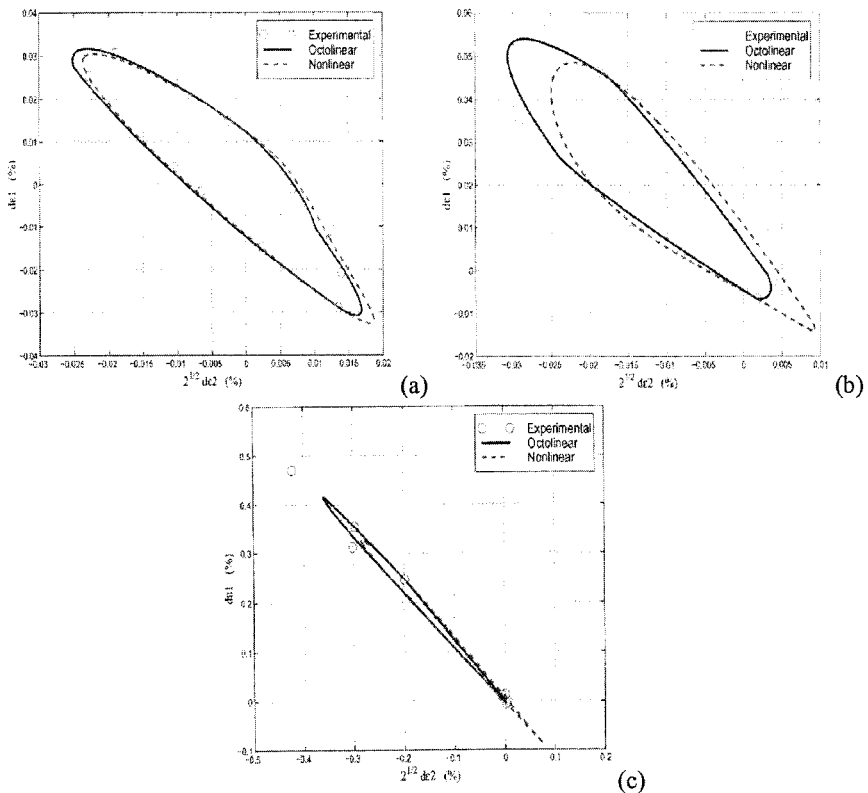


**FIG. 1. Strain response-envelopes. Experimental points compared to the octolinear model (continuous lines) and to the non-linear model (discontinuous lines) at 3 different stress states: an isotropic stress state of 100 kPa (a), and 2 deviatoric stress states ( $\sigma_1 = 200$  kPa,  $\sigma_2 = 100$  kPa (b);  $\sigma_1 = 400$  kPa,  $\sigma_2 = 100$  kPa (c))**

experimental results Royis and Doanh (1998), for axisymmetric conditions. Figure 1 shows such a comparison between experimental points and theoretical curves.

It is interesting to note the degeneration of the response-envelopes to a straight line close to the plastic limit condition. This straight line corresponds to a flow rule in axisymmetric conditions (i.e. same incremental strain direction for any incremental stress loading direction).

#### APPLICATION TO NON-PROPORTIONAL LOADING PATHS

Just to give one example to illustrate the capacity of the incremental non-linear model of second order to describe non-proportional loading paths, we recall here one of the benchmark tests which was considered during the international workshop in Cleveland Saada A. & Bianchini G. (1987).

@Seismicisolation

A circular stress path in the deviatoric stress plane was followed twice experimentally on a true triaxial apparatus and the strain response paths had to be predicted. Figures 2 and 3 give the predicted responses compared with the experimental results. What is obvious is the fact that large plastic strains were obtained during the tests, while for some elasto-plastic models only small elastic strains were predicted. The incremental non-linear model, because of its directional dependency, gives reasonable results (figure 2).

Another aspect is the fact that, due to the successive increase-decrease of the principal stresses, the principal strains are also varying in a complex manner. Here also predicted responses are satisfying (figure 3).

Other examples can be found in Darve et al. (1995) and Darve (1996).

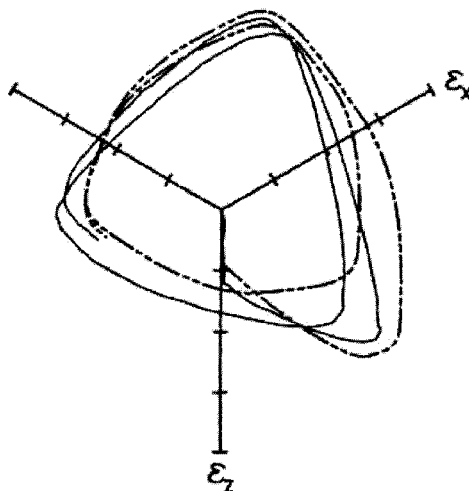


**FIG. 2. Predictions of the incremental non-linear model compared to experimental results for a circular stress loading path in the deviatoric stress plane (Saada A. & Bianchini G. (1987)). Diagrams plotted in the deviatoric strain plane**

#### DESCRIPTION OF BIFURCATIONS AND INSTABILITIES

Various kinds of failure modes have been noticed in practice due to geometric instabilities and material instabilities. In this last class it is possible to distinguish between localized and diffuse modes of failure. Localized failure has been extensively studied in the past, mainly by considering the vanishing values of the determinant of the acoustic tensor. The incrementally non-linear relation of second order has provided interesting results in this direction (Darve (1984)).

It seems that diffuse failure might be described properly by Hill's condition of stability. This condition corresponds to the vanishing values of second order work, and

**@Seismicisolation**

in the simplest cases, to the vanishing values of the determinant of the symmetric part of the constitutive matrix. Several papers have been published already on this question (for example, Darve F. & Laouafa F. (2000, 2001); Laouafa F. & Darve F. (2001)).

In this review paper it is proposed to consider just an example of such an analysis with the case of “q-constant” loading paths.

At a given stress-strain state,  $q$ -constant axisymmetric loading paths consist in maintaining  $q$  constant by an incrementally isotropic unloading defined by :  $d\sigma_1 = d\sigma_2 = d\sigma_3 = \text{negative constant}$ .

The proper conjugate variables to analyse this path are :  $\varepsilon_v - \sigma_3$  and  $q - \varepsilon_1$ , where :  $\varepsilon_v = \varepsilon_1 + 2\varepsilon_3$ , because we have :

$$W = \sigma_1\varepsilon_1 + 2\sigma_3\varepsilon_3 = \varepsilon_v\sigma_3 + q\varepsilon_1 \quad (38)$$

The second order work can thus be written as follows :  $d^2W = d\varepsilon_v d\sigma_3 + dq d\varepsilon_1$ , and with the constraint :  $dq = 0$ , it comes :

$$d^2W = d\varepsilon_v d\sigma_3 \quad (39)$$

If  $\varepsilon_v$  passes through a minimum value, this minimum will be an unstable state according to Hill's condition. On the contrary  $\sigma_3$  is monotonously decreasing.

As the relative volume variations  $\frac{\Delta V}{V_0}$  is equal to  $(-\varepsilon_v)$  :  $\frac{\Delta V}{V_0} = -\varepsilon_v$ , the minimum for  $\varepsilon_v$  is a maximum for  $\frac{\Delta V}{V_0}$ .

Thus a “small” additional positive volume variation (for a volume variation controlled loading) induces a sudden failure of the sample. It can be concluded that this maximum of volume variations is unstable following Lyapunov's definition of stability.

Now if the constitutive relation is written under the following form (for axisymmetric conditions) :

$$\begin{bmatrix} d\varepsilon_v \\ dq \end{bmatrix} \underset{\sim}{=} T \begin{bmatrix} d\sigma_3 \\ d\varepsilon_1 \end{bmatrix} \quad (40)$$

the analysis can be carried out as in other cases.

Along the path the constraint :  $dq = 0$  is fulfilled and, at  $\varepsilon_v$  minimum,  $d\varepsilon_v$  is zero. Thus, the bifurcation criterion is given by :

$$\det \underset{\sim}{T} = 0 \quad (41)$$

and the rupture rule by :

$$\underset{\sim}{T} \begin{bmatrix} d\sigma_3 \\ d\varepsilon_1 \end{bmatrix} = \begin{bmatrix} 0 \\ 0 \end{bmatrix} \quad (42)$$

With our octo-linear model, the bifurcation criterion is given by :

$$2 \frac{E_1^-}{E_3^-} (1 - V_3^{3-} - V_3^{1-}) + 1 - 2V_1^{3-} = 0 \quad (43)$$

The rupture rule corresponds to :

$$E_1^- d\varepsilon_1 + \left( 2 \frac{E_1^-}{E_3^-} V_3^{1-} - 1 \right) d\sigma_3 = 0 \quad (44)$$

**@Seismicisolation**

The unstable stress direction is obviously given by :  $d\sigma_1 = d\sigma_3$  and it is parallel to the hydrostatic line.

Finally one question is remaining open : are the volume variations possessing a maximum for a certain range of initial densities and a certain range of stress levels ? To answer to this question, we have simulated  $q$ -constant loading paths with our constitutive relations, the octo-linear model and the non-linear one.

Figure 4 presents the results for loose Hostun sand and for an initial isotropic pressure equal to 100 kPa. When the second order work is negative, the computed points are replaced by different symbols (triangles, squares, circles, depending on the value of  $q$ , see figure 4). The diagrams are composed of two parts. A first part is constituted by a triaxial compression until reaching various  $q$  values. Then  $q$  is maintained constant.

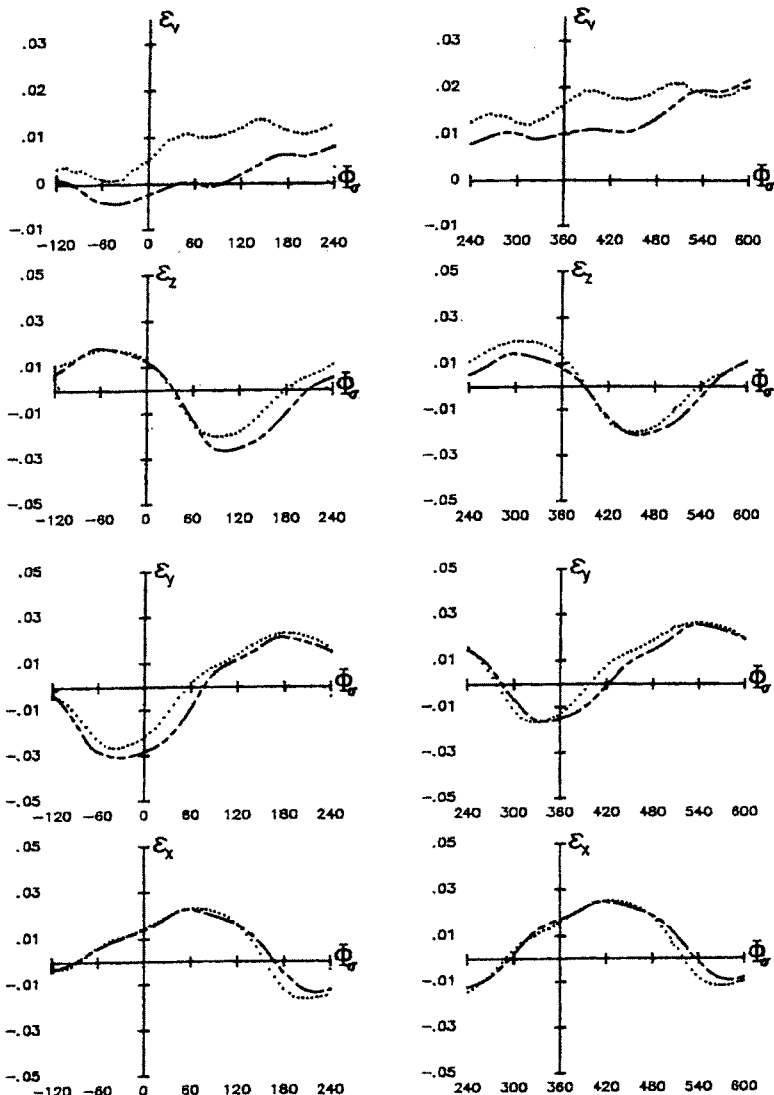
These results allow to validate our previous assumptions. For example, lateral pressure is decreasing monotonously. On the contrary the volume variations are indeed possessing a maximum. Of course it is verified that from this maximum, the second order work is negative.

Figure 5 shows the results obtained with dense Hostun sand. The same comments as previously are pertinent, except the fact that the volume variations do not reach any maximum. Note that the computations are stopped when Mohr-Coulomb plastic limit condition is reached. The second order work is always strictly positive.

Several conclusions can be drawn.

The most important one is certainly the fact that a diffuse mode of failure, which was repeatedly noted in experiments Chu J. & Leong W.K. (2003), can be properly analyzed by Hill's condition of stability Hill R. (1958).

It has been also shown (Darve F. & Lambert C. (2004)) that the bifurcation criterion and the failure rule are the same for undrained (i.e. isochoric) paths and  $q$ -constant paths. Finally a generalization of the notion of limit state has been brought out. For  $q$ -constant paths the stresses are monotonously decreasing ( $d\sigma_1 = d\sigma_2 = d\sigma_3 < 0$ ) while the dilatancy is reaching a maximum value. If one injects at this maximum a small amount of water inside the sample, a sudden failure is occurring without any localization pattern. Thus we can expect the existence of a limit surface in the strain space (dual of the classical limit surface in the stress space). Indeed the strains are limited on the hydrostatic axis or for one-dimensional compressions.



**FIG. 3.** Predictions of the incremental non-linear model compared to experimental results for a circular stress loading path in the deviatoric stress plane (Saada A. & Bianchini G. (1987)). Volume variations and principal strain variations versus the stress vector angle in the deviatoric stress plane

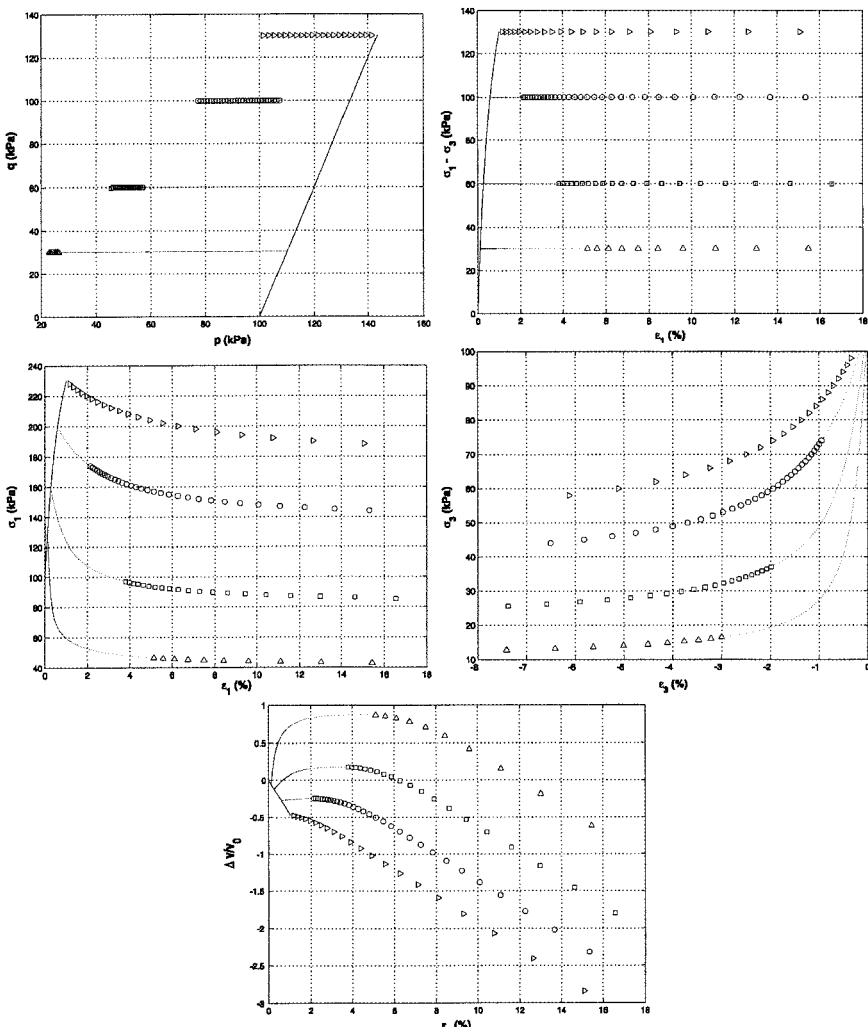


**FIG. 4.** Simulation of  $q$ -constant loading paths for loose Hostun sand by the octolinear constitutive model. Points are replaced by other symbols when the second order work takes negative values from the maximum of volume variations. The initial isotropic pressure is equal to 100 kPa

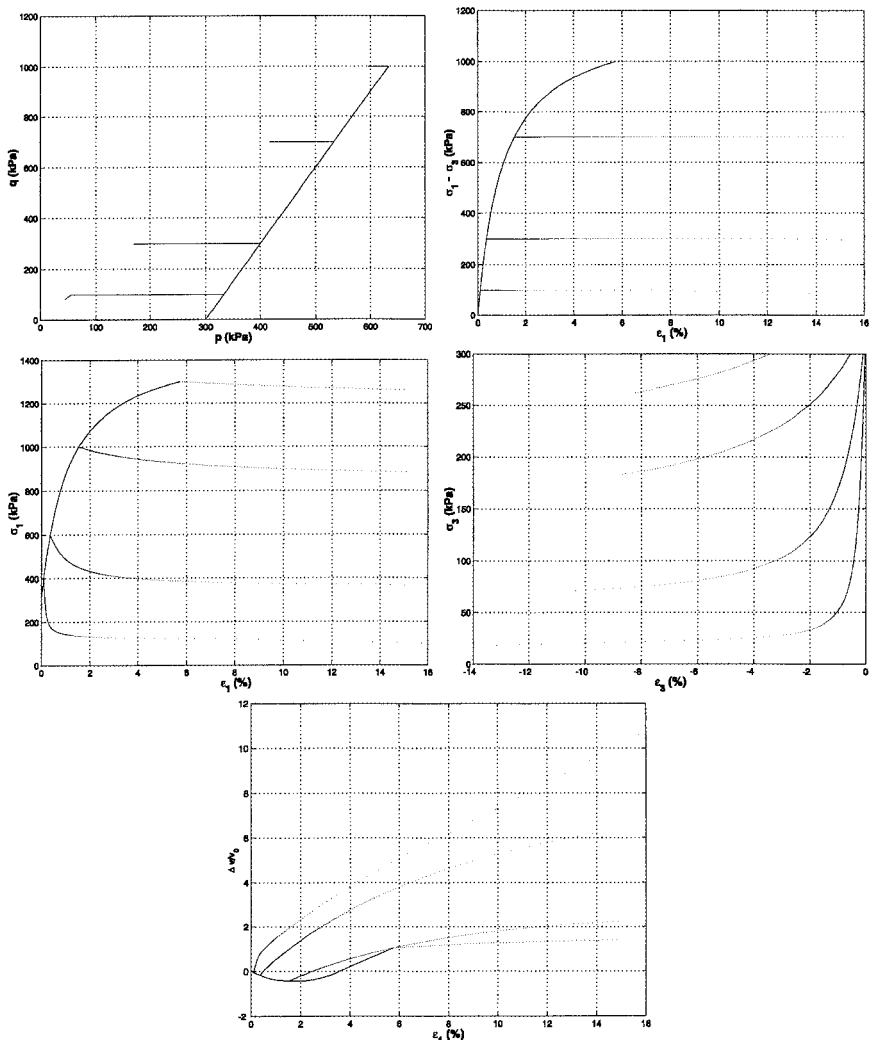


**FIG. 5. Simulation of  $q$ -constant loading paths for dense Hostun sand by the octo-linear constitutive model. The second order work is never vanishing**

## AN INCREMENTALLY NON-LINEAR MODEL WITH 5 PARAMETERS

To determine constitutive parameters from laboratory tests is long, costly and necessarily imprecise due to the samples remoulding. Inverse analysis from in-situ tests will certainly be more and more important in the future to calibrate constitutive relations. For that constitutive relations with few independent parameters have to be developed in order to assure as much as possible the uniqueness of the solution.

In this perspective two dual models have been built. The first one corresponds to equation 24 and 25, while the second one is given by :

$$\begin{pmatrix} d\sigma_1 \\ d\sigma_2 \\ d\sigma_3 \end{pmatrix} = \frac{1}{2} [\mathbf{P}^+ + \mathbf{P}^-] \cdot \begin{pmatrix} d\epsilon_1 \\ d\epsilon_2 \\ d\epsilon_3 \end{pmatrix} + \frac{1}{2 \|d\epsilon\|} [\mathbf{P}^+ - \mathbf{P}^-] \cdot \begin{pmatrix} d\epsilon_1^2 \\ d\epsilon_2^2 \\ d\epsilon_3^2 \end{pmatrix} \quad (45)$$

with

$$\|d\epsilon\| = \sqrt{d\epsilon_i d\epsilon_i}, \quad i \in \{1, 2, 3\}$$

and :

$$\mathbf{P}^+ = \begin{bmatrix} O_1^+ & K_2^{1+}O_2^+ & K_3^{1+}O_3^+ \\ K_1^{2+}O_1^+ & O_2^+ & K_3^{2+}O_3^+ \\ K_1^{3+}O_1^+ & K_2^{3+}O_2^+ & O_3^+ \end{bmatrix} \quad \mathbf{P}^- = \begin{bmatrix} O_1^- & K_2^{1-}O_2^- & K_3^{1-}O_3^- \\ K_1^{2-}O_1^- & O_2^- & K_3^{2-}O_3^- \\ K_1^{3-}O_1^- & K_2^{3-}O_2^- & O_3^- \end{bmatrix} \quad (46)$$

$O_i$  are generalized tangent oedometric moduli and  $K_i^j$  generalized tangent lateral pressure coefficients, defined by:

$$O_i = \left( \frac{\partial \sigma_i}{\partial \epsilon_i} \right)_{\epsilon_j, \epsilon_k}; \quad K_i^j = \left( \frac{\partial \sigma_j}{\partial \sigma_i} \right)_{\epsilon_j, \epsilon_k}$$

The generalized oedometric paths are characterized by constant lateral strains  $\epsilon_j$  and  $\epsilon_k$ .

The expressions of  $E_i$  and  $\nu_i^j$  (in the first "direct" model) and of  $O_i$  and  $K_i^j$  (in the second "dual" model) can be more or less complicated.

In the past (Darve and Dendani (1989)) we have proposed sophisticated expressions, while more recently (Darve F. & Roguiez X. (1999)) these four functions have been formulated in such a way that they depend on 5 parameters :  $E_i$  and  $\nu_i^j$  from  $(E, \nu, c, \phi, \psi)$  and  $O_i$  and  $K_i^j$  from  $(E_{oedom}, K_0, c, \phi, \alpha)$ , where only  $\alpha$  has not any classical meaning and allows to describe indirectly contractancy and or dilatancy (for more details, see Darve F. & Roguiez X. (1999)).

Fig. 6 and 7 just give examples in relation with the dual model. By recalling that the dual model is calibrated on oedometric paths, fig. 6 presents the predicted drained triaxial behaviour for a loose sand on the right and a dense sand on the left. Fig. 7 gives the predicted undrained behaviour for the same loose and dense sand in axial compression and axial extension.

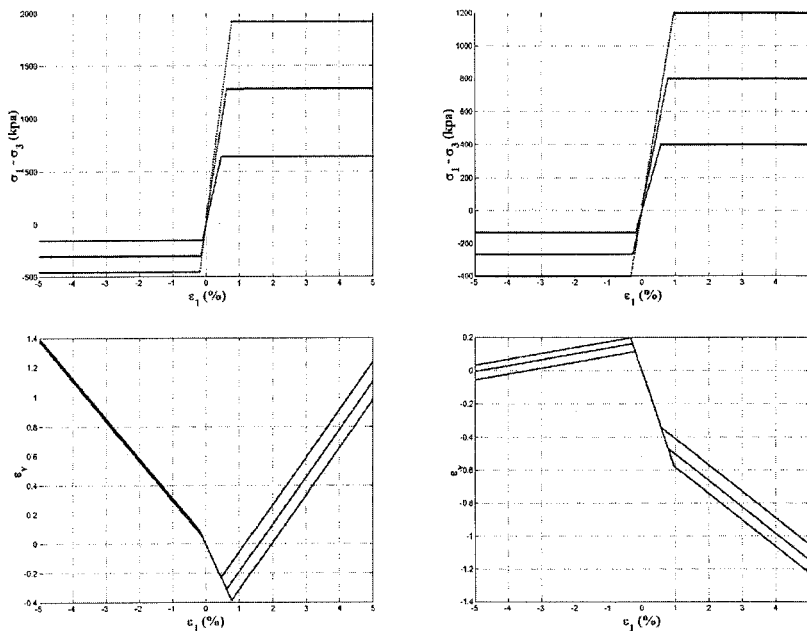


**FIG. 6.** Incrementally non-linear model with 5 parameters, calibrated on oedometric paths. Response paths to drained triaxial compression and extension for a dense sand on the left and a loose sand on the right

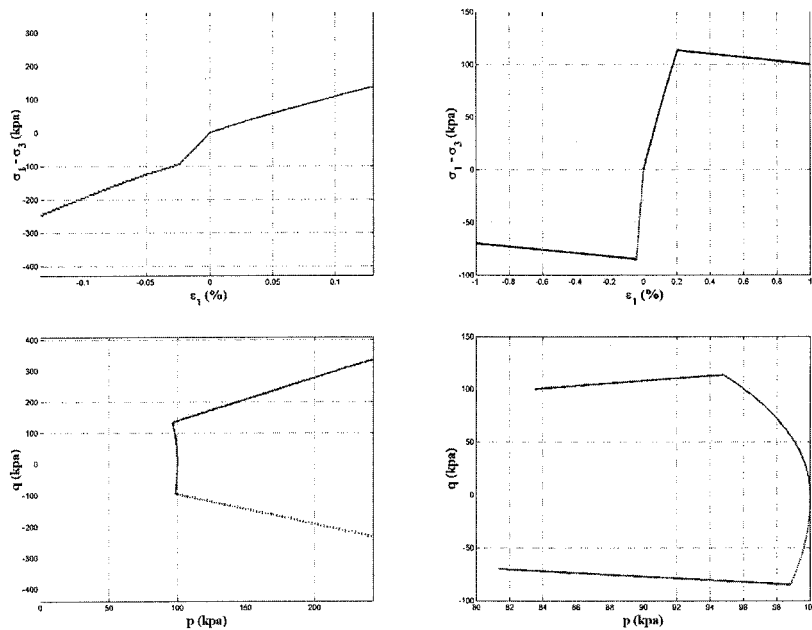


**FIG. 7. Incrementally non-linear model with 5 parameters, calibrated on oedometric paths. Response paths to undrained triaxial compression and extension for a dense sand on the left and a loose sand on the right**

## CONCLUSIONS

After a general introduction about the incremental constitutive formalism for rate-independent materials, the basic notions of “tensorial zone” and of “incremental non-linearity” have been presented and discussed. A classification of the existing models in relation with the number of their tensorial zones allowed to introduce the incrementally non-linear constitutive relations as generalizations of incrementally piece-wise linear models. According to the incrementally non-linear character of soil behaviour, the non-linear model of second order and the octo-linear model, which are obtained basically by a Taylor’s serie expansion, describe many non-linear features of soil behaviour.

Having in mind that, for classical monotonous loading paths, the predicted responses are not so different from a model to another (see for example, Saada A. & Bianchini G. (1987)), we have focused the illustrations of these constitutive models on the case of non-proportional loading paths and on the description of bifurcations and instabilities. For these last examples it has been emphasized that, besides the localized failure properly described by Rice’s criterion, the diffuse mode without localization pattern (the most known example is the liquefaction of loose sands) might be detected by Hill’s condition. Finally two very simple models with 5 parameters have been underlined.

As perspective it is now more and more obvious that the phenomenological constitutive relations will be replaced in the future by models based on multi-scale approaches. Such models, based on the micromechanics of granular media with elementary interaction laws between grains, allow to describe a complex macroscopic behaviour with very few physical constitutive parameters (see for example Nicot F. & Darve F. (2004)).

**Acknowledgements** The supports of European projects DIGA (5<sup>th</sup> PCRD HPRN-CT-2002-00220), LESSLOSS (6<sup>th</sup> PCRD) and french national projects PIR (RGCN) and ACI CatNat (2002) are gratefully acknowledged.

## REFERENCES

- Bazant Z. P. (1978), *Endochronic inelasticity and incremental plasticity*, Int. J. Solids Struct., 14 691-714.
- Chambon R., Desrues J. (1994), Hammad W. and Charlier R., *CLoE, a new rate-type constitutive model for geomaterials. Theoretical basis and implementation*, Int. J. Num. Anal. Meth. Geomech., 253-278.
- Chu J. and Leong W.K. (2003), *Recent progress in experimental studies on instability of granular soil*, Int. Workshop on Bifurcations and Instabilities in Geomechanics, Labuz et al. eds, Zwets and Zeitlinger publ., 175-192.
- Dafalias Y. F. (1986), *Bounding surface plasticity. i. mathematical foundation and hypoplasticity*, Int J. Eng. Mech., 112 (9) 966-987.

- Dafalias Y. F. and Hermann L. R (1980), *A bounding surface soil plasticity model*, In Proc. Symp. on Soils under Cyclic and Transient Loading, G. N. Pande & O. C. Zienkiewicz (eds), Balkema, 335-345.
- Darve F. (1980), *Une loi rhéologique incrémentale non-linéaire pour les solides*, Mech. Res. Comm., 7 (4) 295-212.
- Darve F. (1984), *An incrementally non-linear constitutive law of second order and its application to strain localization*, In Mechanics of Engineering Materials, C. S. Desai & R. H. Gallagher. John Wiley, 179-196.
- Darve F. (1990), *Incrementally non-linear constitutive relationships*, In Geomaterials Constitutive Equations and Modelling, F. Darve ed., Elsevier Applied Science, Taylor and Francis Books, 213-238.
- Darve F. (1996), *Liquefaction phenomenon of granular materials and constitutive instability*, Int. Journal of Engineering Computations, 7, 5-28.
- Darve F. and Dendani H. (1989), *An incrementally non-linear constitutive relation and its predictions*, In Constitutive Equations for granular non-cohesive soils, ed. A.S. Saada & Bianchini, Balkema, Rotterdam, 237-254.
- Darve F. and Labanieh S. (1982), *Incremental constitutive law for sands and clays, simulation of monotonic and cyclic test*, Int. J. Num. Anal. Meth. Geomech., 6, 243-273.
- Darve F. and Lambert C. (2004), *Continuous and discrete modelling of failure in geomechanics*, in Degradations and Instabilities in Geomaterials, Darve and Vardoulakis eds., Springer Verlag publ., chapter 7.
- Darve F. and Laouafa F. (2000), *Instabilities in Granular Materials and Application to Landslides*, Mech. Cohes. Frict. Mater., 5(8), 627-652.
- Darve F. and Laouafa F. (2001), *Modelling of granular avalanches as material instabilities*, in Bifurcation and Localization in Geomechanics, Muehlhaus et al. eds, Zwets and Zeitlinger publ., 29-36.
- Darve F. and Roguiez X. (1999), *Constitutive relations for soils, new challenges*, Rivista Italiana di Geotecnica, 4, 9-35.
- Darve F., Flavigny E. and Meghachou M. (1995), *Yield surfaces and principle of superposition revisited by incrementally non-linear constitutive relations*, In Int. Journal of Plasticity, 11(8) 927-948.
- Davis R. D. and Mullenger G. (1978), *A rate-type constitutive model for soils with critical state*, In Int. J. Num. Anal. Meth. Geomech., 2 255-282.
- Di Benedetto H. and Darve F. (1983), *Comparaison de lois rhéologique en cinématique rotationnelle*, In J. Mécan. Théor. Appl., 2(5) , 769-798.



- Duncan J. M. and Chang C. Y. (1970), *Non-linear analyses of stress and stress and strain in soils*, In J. Soil. Mech. and Found. Div., ASCE, 95(SM5), 1629-1653.
- Gudehus G. (1979), *A comparison of some constitutive laws for soils under radially loading symmetric loading and unloading*, In Proc. 3rd Int. Conf. Num. Meth. Geomech., W. Whittke (ed), Balkema, 4, 1309-1324.
- Guélin P. (1980), *Note sur l'hystérisis mécanique*, J. Mécan., 19(2), 217-247.
- Hill R. (1958), *A general theory of uniqueness and stability in elastic-plastic solids*, J. of the Mech. and Phys. of Solids, 6, 239-249.
- Kolymbas D. (1977), *A rate dependent constitutive equation for soils*, In Mech. Res. Comm., 4(6), 367-372.
- Lade P. V. (1977), *Elasto-plastic stress theory for cohesionless soils with curved yield surfaces*, In Int. J. Solids Struct., 13, 1019-1035.
- Laouafa F. and Darve F. (2001), *Modelling of slope failure by a material instability mechanism*, Computers and Geotechn., 29, 301-325.
- Loret B. (1981), *Formulation d'une loi de comportement élasto-plastique des milieux granulaires*, Thèse de D.I., Ecole Polytechnique.
- Mroz Z. (1967), *On the description of anisotropic work hardening*, In J. Mech. Phys. Sci., 15, 163-175.
- Nicot F. and Darve F. (2004), *Multiscale modelling of geomaterials*, in Numerical Models in Geomechanics, Pande and Pietruszczak eds., Balkema publ., 11-16.
- Nova R. and Wood D. M. (1979), *A constitutive model for sand in triaxial compression*, In Int. J. Num. Anal. Meth. Geomech., 3, 255-278.
- Owen D. R. and Williams W. O. (1969), *On the time derivatives of equilibrated response functions*, In ARMA, 33(4), 288-306.
- Prevost J. H. (1978), *Plasticity theory for soil stress-strain behaviour*, In J. Eng. Mech. Div., ASCE, 104(EM5), 1177-1194.
- Royis P. and Doanh T. (1998), *Theoretical analysis of strain response envelopes using incrementally non-linear constitutive equations*, In Int. J. Num. Anal. Meth. Geomechanics, 22, 97-132.
- Saada A., Bianchini G. (1987), *Constitutive Equations for Granular Soils*, A.A. Balkema publ.
- Valanis K. C. (1971), *A theory of viscoplasticity without a yield surface*, In Archives of Mechanics, 23, 517-551.

- Vardoulakis I., Goldscheider M. and Gudehus G. (1978), *Formation of shear bands in sand bodies as a bifurcation problem*, In Int. J. Num. Anal. Meth. Geomech., 2, 99-128.
- Vermeer P. (1978), *A double hardening model for sand*, In Geotechnique, 28(4), 413-433.

## **UNIFIED YET SIMPLIFIED DISTURBED STATE CONSTITUTIVE MODELS FOR SOILS AND INTERFACE/JOINTS**

Chandrakant S. Desai<sup>1</sup>

**ABSTRACT:** The disturbed state concept (DSC) provides a unified framework for characterization of the behavior of geologic materials and interfaces/joints. Important factors such as elastic, plastic and creep responses, stress paths, volume change (contraction and dilation), disturbance (softening and damage or stiffening), thermal effects, partial saturation and liquefaction can be included in the DSC. Because of its hierarchical nature, simplified models for specific applications can be derived from the DSC. It has been applied successfully for defining behavior of many geologic materials and interfaces/joints.

Procedures for determination of parameters based on laboratory tests have been developed. Various models from the DSC have been validated with respect to laboratory test data, and field or simulated practical problems by using computer (finite element) procedures in which DSC has been implemented. The DSC can provide unified and powerful models for a wide range of engineering materials.

### **INTRODUCTION**

In the continuing pursuits of realistic models for geologic materials and interfaces or joints, a great number of simple, simplified to complex constitutive models have been proposed. It is not the intention here to present a detailed review of such models, which includes elasticity, plasticity, creep, damage, micromechanics, microcracking leading to fracture and failure, and liquefaction. Such reviews are available in many publications, including Desai (2001b).

---

<sup>1</sup> Regents' Professor, Dept. of Civil Eng. and Eng. Mechanics, The Univ. of Arizona, Tucson, AZ 85721-0072, USA

## Scope

The modeling approach based on the disturbed state concept (DSC) is the main objective herein. It is believed that the DSC models provide a hierarchical and unified framework to include other models such as elasticity, conventional plasticity, continuous hardening plasticity, creep, microcracking leading to softening and liquefaction. At the same time, the number of parameters required in various versions of the DSC model are smaller or equal to the number in other available models for similar capabilities.

The description of the DSC model is divided in the following components:

1. Basic concept and hierarchical framework.
2. Parameter determination and calibration from laboratory and/or field tests.
3. Validations with respect to tests used for calibration and independent tests.
4. Implementation issues of DSC models in computer (finite element) procedures for validations with respect to and application to practical problems.

## BASIC CONCEPT AND HIERARCHICAL FRAMEWORK

Details of the DSC are given in various publications (Desai 1974, Desai 1987, Desai and Ma 1996, Desai and Toth 1992, Katti and Desai 1995, Park and Desai 2000), which are referenced in Desai (2001b). A brief description of the framework is given below with attention to the calibration for DSC parameters, typical examples of derived parameters, validations and numerical implementation.

## Equations

The DSC is based on the idea that the observed behavior of a material can be expressed through the behavior of the reference components in the deforming material. The reference components are usually called relative intact (RI) and fully adjusted (FA). The behavior of the RI part, which may not be affected by microstructural discontinuities, can be defined by using a continuum model: elasticity, plasticity or viscoplasticity. The RI part is transformed continuously to the FA part, distributed at random locations, Fig. 1. The RI and FA parts interact to yield the observed response, which is expressed in terms of the RI and FA behavior, connected through the disturbance function, which provides for the coupling. Based on the above concept, the incremental constitutive equations for DSC are derived as

$$\tilde{d}\sigma^a = (1 - D)\tilde{C}^i \tilde{d}\varepsilon^i + DC^c \tilde{d}\varepsilon^c + dD(\tilde{\sigma}^c - \tilde{\sigma}^i) \quad (1a)$$

or

$$\tilde{d}\sigma^a = \tilde{C}^{DSC} \tilde{d}\varepsilon^i \quad (1b)$$

where  $\tilde{\sigma}$  = stress vector,  $\tilde{\varepsilon}$  = strain vector, a, i and c denote observed, RI and FA behavior, respectively,  $\tilde{C}^i$  and  $\tilde{C}^c$  = constitutive matrices for the RI and FA parts, respectively, D = disturbance and d denotes increment.



The RI behavior can be expressed by using a suitable continuum model, e.g., linear elastic, nonlinear elastic, elasto-plastic or viscoplastic. Here, the hierarchical single surface (HSS) plasticity (associative) model ( $\delta_0$ ), derived on the general basis (Desai 1980), is used in which the yield function, F (Desai et al. 1986), is given by

$$F = J_{2D} - \left( -\alpha \bar{J}_1 + \gamma \bar{J}_1^2 \right) \left( 1 - \beta S_r \right)^{-0.50} = 0 \quad (2)$$

where  $J_{2D}$  = second invariant of the deviatoric stress tensor,  $\bar{J}_1 = J_1 + 3R$ ,  $J_1$  = first invariant of the stress tensor, R = bonding (tensile) strength, Fig. 2,  $\gamma$  = parameter related to the ultimate yield surface,  $\beta$  = parameter related to the shape of F in  $\sigma_1 - \sigma_2 - \sigma_3$  stress space,  $S_r$  = stress ratio =  $(\sqrt{27}/2) (J_{3D}/J_{2,3}^{3/2})$ ,  $J_{3D}$  = third invariant of the deviatoric stress tensor, and  $\alpha$  is the growth or hardening function. In Eq. (2), the stress invariants are nondimensionalized with respect to  $p_a$ , the atmospheric pressure constant.

In a simple form, the growth or hardening function is given by

$$\alpha = \frac{\alpha_1}{\xi^n} \quad (3a)$$

where  $\alpha_1$  and  $\eta_1$  = hardening parameters and  $\xi$  is the trajectory of or accumulated plastic strains:

$$\xi = \int (d\varepsilon_{ij}^p d\varepsilon_{ij}^p)^{1/2} \quad (3b)$$

in which  $\varepsilon_{ij}^p$  = plastic strain tensor, which is the sum of the deviatoric and volumetric plastic strains.

The FA part can be defined by assuming that it has no strength like in classical damage model (Kachanov 1986), or it has hydrostatic strength like in classical plasticity, or it has strength corresponding to the critical state models (Roscoe et al. 1958). It can be also defined by using the behavior of other states such as zero suction for partially saturated soils.

For soils, it is found appropriate to use the critical state equations to define the FA response (Roscoe, et al. 1958, Desai 2001b):

$$\sqrt{J_{2D}^c} = \bar{m} J_1^c \quad (4a)$$

$$e^c = e_o^c - \lambda \ln \left( \frac{J_1^c}{p_a} \right) \quad (4b)$$

where c denotes the critical state, e = void ratio,  $e_o^c$  = initial void ratio and  $\bar{m}$  and  $\lambda$  are the critical state parameters.

## Disturbance Function

The disturbance function, D, can be defined on the basis of observed stresses, volumetric strains, pore water pressures or nondestructive properties such as S- and P-wave velocities. In terms of stress, D is expressed as

$$D = \frac{\sigma^i - \sigma^a}{\sigma^i - \sigma^c} \quad (5a)$$

The disturbance, D, is also expressed as (Fig. 3)

$$D = D_u \left(1 - e^{-A\xi_D^Z}\right) \quad (5b)$$

where  $D_u$  = ultimate disturbance, A and Z are disturbance parameters, and  $\xi_D$  is the trajectory of deviatoric plastic strains.

## HIERARCHICAL APPROACH

Various continuum models can be derived from the DSC equations, Eq. (1). If  $D = 0$ , i.e., the material does not experience any microstructural changes leading to discontinuities, Eq. (1) reduces to that for standard continuum models:

$$\underset{\sim}{d\sigma^i} = C^i \underset{\sim}{d\varepsilon^i} \quad (6)$$

where  $C^i$  = constitutive matrix for continuum model, e.g., elasticity, plasticity, etc.

Various models such as von Mises, Drucker-Prager, critical state, Matsuoka and Nakai (1974), Lade and Kim (1988), etc. can be obtained as special cases of the HISS model, Eq. (2). Figure 4 shows various versions that can be derived from the DSC.

## Interface/Joints

The above approach has been formulated for interface/joint behavior with suitable yield function for RI behavior and critical state models for FA behavior (Desai and Ma 1992, Desai et al. 1995, Desai 2001b). This paper essentially addresses the soil behavior. One of the advantages of the DSC is that the same framework is used for soils and interface/joints. This is consistent with the fact that both deform in a coupled manner; hence, the same model framework is desirable.

## Advantages of DSC/HISS Models

The DSC allows for discontinuities experienced by a deforming material, that can often result in degradation or softening. It is essential to include the existence and effect of discontinuous material in the model; then only can it provide consistent and improved characterization compared to other models based on continuum plasticity proposed and used to account for such behavior (Mroz et al. 1978), Pestana and Whittle 1999, Elgamal et al 2002).

Because DSC allows for the coupling between the RI and FA responses, it can avoid such difficulties as spurious mesh dependence that occur in classical damage models (Kachanov 1986). Also, if such coupling is considered in the classical damage model by introducing additional enrichments (Bazant 1994, Mühlhaus 1995), the resulting models can be complex and may involve computational problems.

In the fracture mechanics approach, usually it is required to introduce cracks in *advance* of the loading. In contrast, the DSC does not need *a priori* introduction of cracks, and initiation and growth of microcracking, fracture and failure can be traced

at appropriate locations depending upon the geometry, loading and boundary conditions, on the basis of critical disturbance,  $D_c$ , obtained from test results (Desai 2001b, Park and Desai 2000, Pradhan and Desai 2004).

The DSC allows identification of and initiation and growth of microstructural instability or liquefaction by using the critical disturbance (Desai et al. 1998, Desai 2000b, Park and Desai 2000, Pradhan and Desai 2004).

The DSC/HISS models also possess the following advantages:

1. The yielding is assumed to be dependent on total plastic strain or plastic work. Hence, in contrast to other models such as critical state and cap, it includes the effect of plastic shear strains also.
2. The yield surface allows for different strengths along different stress paths.
3. Because of the continuous and special shape of the yield surface, it allows for deviatoric strains before the peak stress, which can be common in many geomaterials, Fig. 2.
4. The DSC allows for degradation and softening, with HISS model for the RI behavior. It can allow also for stiffening or healing.
5. Introduction of disturbance can lead to inclusion of nonassociative behavior, i.e., deviation of plastic strain increment from normality.
6. The DSC allows intrinsically the coupling between RI and FA parts and the nonlocal effects. Hence, it is not necessary to add extra or special enrichments, e.g., microcrack interaction, gradient and Cosserat schemes, etc. (Mühlhaus 1995).
7. The DSC is general and can be used for a wide range of materials: geologic, concrete, asphalt, ceramics, metal, alloys and silicon (Desai 2001), if appropriate test data is available.

### DSC and Damage Models

The damage approach (Kachanov 1986) is based on the actual cracks (damage) in a deforming material, and the resulting effect on the observed behavior. The DSC is different from the damage approach in that it considers a deforming material as a mixture of two or more reference components (e.g., RI and FA states); then the observed behavior is expressed in terms of the behavior of the components, which interact to yield the observed behavior. The disturbance represents the deviation of the observed behavior from the reference state(s). Damage model can be considered as a special case of DSC if the interaction is removed, e.g., the FA state is assumed to possess no strength. However, such a model, without interaction between RI and FA states, may not be realistic and possesses certain difficulties (Desai 2001b).



## PARAMETERS

Based on the RI (Eq. 2), FA (Eq. 4) and disturbance, D (Eq. 5), the parameters required are:

Elastic: E and  $\nu$  (or K and G)

RI: Plasticity  $\gamma$ ,  $\beta$ , n,  $a_1$ ,  $\eta$

FA: Critical state:  $e_o$ ,  $\bar{m}$ ,  $\lambda$

Disturbance:  $D_u$ , A and Z

where E = elastic modulus,  $\nu$  = Poisson's ratio, K = bulk modulus, and G = shear modulus. The above parameters are averaged from test data under different confining pressures, etc. If the variation is severe, then a parameter needs to be expressed as a function of the factor, which increases the number of parameters. The number of parameters can increase if additional factors such as temperature and rate dependence are considered.

## Physical Meanings and Curvefitting

A constitutive model for defining behavior of a material requires a certain level of curve fitting for calibration of parameters based on the test data. It is useful and desirable that such curve fitting is reduced as much as possible, particularly if the behavior is influenced by many factors. One of the ways is to develop parameters that have physical meanings, e.g., the parameters associated with physical states during the response, such as ultimate and initial stress, and change in volumetric strain. Most of the parameters in the DSC have such physical meanings; hence, the need for curve fitting is reduced and the procedures for the determination of parameters are simplified.

## Simple and Simplified Models

It is often said that a constitutive model should be simple, particularly for practical applications. A functional representation (e.g., parabola, hyperbola, spline, etc.) of a given (single) stress-strain response as a nonlinear elastic model, may be called a "simple" model. Such a function like the hyperbola extended to include the effect of the confining pressure may still be called "simple". However, since the soil behavior is affected by other practical factors such as irreversible (plastic) deformations, stress path, volumetric strains, creep and type of loading, the resulting model cannot be simple at all! It is apparent that such models by using only mathematical functions may not account for the practical factors.

Then, it is better to develop and use "simplified" models. A simplified model is intended to characterize the behavior affected by significant factors important for practical problems. Furthermore, it is obtained by deleting less significant factors from a general model developed by considering the physical nature of the problem, loading and other relevant conditions. In other words, the simplified model would include only the effect of the significant factors.

An important issue is how many parameters the model involves, and what type of tests are required to determine the parameters. The other important issue is how many significant factors are vital for practical problems and must be included in



the model? It is natural that the number of parameters would increase with the number of factors. Hence, for a practical application, one must adopt a model that contains the influence of the significant factors for a particular application. Then the issue of adopting a simple model that cannot include the significant factors is not relevant.

Indeed, for practical applications, it is desirable to develop as simplified model as possible with smaller number of parameters. The DSC/HISS model has been developed such that simplified models can be adopted depending upon the need of the practical application. Moreover, the DSC/HISS model is hierarchical in nature and allows selection of a model for required factors by introducing additional parameters in the same basic model.

The above approach can reduce the number of parameters and simplifies the procedure for their determination based on standard (e.g., triaxial and shear) tests.

The following Table 1 gives some of the specialized models. The number of parameters in the DSC model are less than or equal to those in any other available model of comparable capabilities.

**Table 1. Specialized Models from DSC/Hiss Model**

Specialization	Number of Parameters
Elastic	2
Classical Elastic-plastic:	
von Mises	3
MohrCoulomb	4
Drucker-Prager	4
Continuous Hardening:	
Critical State	5
HISS- $\delta_0$ Model	8*
HILL- $\delta_1$ Model	9
HILL- $\delta_0 + v_p$ Viscoplastic	11
HILL- $\delta_2$ : Anisotropic	12
HILL- $\delta_0$ : Disturbance	12

\*If the tensile strength R is not included, the number of parameters reduces by 1.

Note: The number of parameters increases by 2 if pore water pressure, and by about 2 for a parameter, if temperature is included.



### Parameter Determination

The laboratory tests used for the calibration include consolidation, triaxial and multiaxial tests. The field tests include nondestructive, e.g., S-wave measurements during earthquakes. Direct shear and simple shear (e.g., using the CYMDOF device) tests are used for DSC parameters for interfaces/joints.

The values of elastic moduli are found from the slopes of unloading responses. For instance, E is found from unloading slopes of  $\sigma_1 - \sigma_3$  vs  $\varepsilon_1$  plots from triaxial tests. Similarly, v can be found from plot of  $\varepsilon_v$  vs  $\varepsilon_1$  ( $\varepsilon_v$  = volumetric strain), G can be found from shear stress vs shear strain plot, and K can be found from mean pressure (p) vs  $\varepsilon_v$  plot. Determination of various elastic parameters are depicted in Fig. 5.

The parameters  $\gamma$  and  $\beta$  are related to the *ultimate response* and are found from the specialized expression for F (where  $\alpha = 0$ ) at the ultimate stress conditions, based on tests under different confining pressures:

$$F = J_{2D} - \gamma \bar{J}_1^2 (1 - \beta S_t)^{-0.50} = 0 \quad (7)$$

By substituting different values of ultimate stresses, Fig. 2,  $\gamma$  and  $\beta$  are found by using procedures such as the least-square method. Ultimate stress is adopted as the asymptotic value for a given curve, Fig. 6(a).

The phase change parameter is found from the point (b) in the stress-strain behavior, Fig. 6(b), where the response *transits from compressive to dilative*. One of the expressions for n is

$$n = \frac{2}{1 - \left( \frac{J_{2D}}{J_1} \cdot \frac{1}{F_s \gamma} \right)} \Bigg|_{d\varepsilon_v=0} \quad (8)$$

The *hardening parameters* are determined based on the following expression from Eq. (3).

$$\ln \alpha + \eta_i \ln \xi = \ln a_i \quad (9)$$

Here, the stress-strain curve, Fig. 7(a), is divided into increments and  $\xi$  is found as the accumulated plastic strain for a given increment. Then  $\alpha$  for a given  $\xi$  is found from Eq. (1), i.e., F = 0. The plot of (Fig. 7b)  $\ln \alpha$  vs  $\ln \xi$  yield the (average) values of  $a_i$  and  $\eta_i$ .

The *critical state parameters*, Eq. (4), are obtained from the plots of  $\sqrt{J_{2D}} - J_1$  for  $m$  and  $e^c$  vs  $\ln(J_1^c / p_a)$  for  $e_o^c$  and  $\lambda$ , Figs. 6d and 6e..

The disturbance parameter,  $D_u$ , is found from Eq. (5) by substituting the value of the residual (FA) stress, Fig. 6(a). Then the values of A and Z are obtained by plotting  $\ln(-\ln(D_u - D)/D_u)$  vs  $\ln \xi_D$ , Fig. 8, based on the following expression from Eq. (5):

**@Seismicisolation**

$$Z \ln(\xi_D) + \ln A = \ln \left[ -\ln \left( \frac{D_u - D}{D_u} \right) \right] \quad (10)$$

The values of D can be found from quasistatic or cyclic response, Fig. 1(c) or Fig. 9.

### Hierarchical Versions

Various plasticity models such as nonassociative ( $\delta_1$ ) and anisotropic hardening ( $\delta_2$ ) can be obtained by modifying or adding "corrections" for the factors that influence the specific behavior, to the basic associative ( $\delta_0$ ) model (Desai et al. 1986, Somasundaram and Desai 1988, Wathugala and Desai 1993).

### Creep Models

Various creep models, e.g., Maxwell, viscoelastic (ve), elastoviscoplastic (evp), and viscoelastic viscoplastic (vevp), can be obtained as specialization of the multicomponent DSC (Desai, 2001b). For example, the evp model can be defined based on the Perzyna's theory (1966), in which viscoplastic strain increment,  $\dot{\varepsilon}^{vp}$ , is expressed as

$$\dot{\varepsilon}^{vp} = \Gamma \langle \phi \rangle \frac{\partial F}{\partial \sigma} \quad (11)$$

where  $\Gamma$  = fluidity parameter, and  $\langle \cdot \rangle$  has the meaning of a switch-on-switch-off operator as

$$\left\langle \phi \left( \frac{F}{F_o} \right) \right\rangle = \begin{cases} \phi \left( \frac{F}{F_o} \right) & \text{if } \frac{F}{F_o} > 0 \\ 0 & \text{if } \frac{F}{F_o} \leq 0 \end{cases} \quad (12)$$

$F_o$  = reference value of F (e.g., yield stress or  $p_a$ ) and  $\phi$  = flow function. One of the expressions of  $\phi$  is

$$\phi = \left( \frac{F}{F_o} \right)^N \quad (13)$$

In the above equations,  $\Gamma$  and N are the viscous parameters. The values of  $\Gamma$  and N are found from a creep test, Fig. 10; details are given in (Desai et al. 1995, Desai 2001b).

### Liquefaction

Liquefaction in saturated soils (Fig. 9) subjected to dynamic (or static) loading can be identified in the DSC by locating the critical value of the disturbance,  $D_c$ , Eq. (5), Fig. 3, that represents the microstructural instability. There is no additional parameter needed for liquefaction. Details of the development and use of the DSC for liquefaction are given in various publications (Desai et al. 1998, Desai 2000b, Park and Desai 2000, Pradhan and Desai 2004).

### Partially Saturated Soils

The DSC model can be applied to model partially saturated soil by including factors such as suction and saturation (Geiser et al. 1997, Desai 2001b).

### Stiffening and Healing

The disturbance,  $D$ , can simulate softening or degradation. It can also define stiffening or healing in the microstructure; for example, chemical and thermal (causing particle fusing) effects can increase in the bonding in the microstructure (Desai, 2001b).

### Thermal Effects

The thermal effects can be introduced in the DSC model. Very often, the parameters are expressed as a function of temperature,  $T$ , as (Desai 2001b)

$$p = p_r \left( \frac{T}{T_r} \right)^c \quad (14)$$

where  $p$  = any parameter, and  $p_r$  is the value of the parameters at a reference temperature,  $T_r$  (e.g., the room temperature), and  $c$  = parameter.

### Parameters for Typical Materials and Interfaces/Joints

The DSC models have been used to model a wide range of materials, e.g., clays, sands (dry and saturated), glacial tills, partially saturated soils, rocks, concrete, asphalt concrete, metals, alloys (solder), silicon.

Application for interfaces include clay-steel, sand-steel, sand-concrete. Laboratory and/or field tests have been used to calibrate the DSC parameters by following the foregoing procedures. Details of the parameters have been presented in a number of publications, and also given in Desai (2001b).

Parameters only for typical geologic materials and interfaces are given in Tables 2 to 6.

**Table 2. Parameters for Saturated Marine Clay (Katti and Desai 1995)**

Parameter	Symbol	Value
Elastic	E	10 MPa (1500 psi)
	v	0.35
Plasticity – Ultimate	$\gamma$	0.047
	$\beta$	0.00
Phase Change	n	2.80
Growth/Hardening	$a_i$	0.0001
	$\eta_i$	0.78
Critical State	$\bar{m}$	0.0694
	$\lambda$	0.169
	$e_o^c$	0.903
Disturbance	D <sub>u</sub>	0.75
	A	1.73
	Z	0.309

**Table 3. Parameters for Ottawa Sand and Ottawa Sand-Concrete Interface  
(Park and Desai 2000)**

Sub Group	Parameter	Ottawa Sand	Ottawa Sand – Concrete Interface
Elastic	E	193000 kPa	3180.0 kPa
	v	0.380	0.42
Plasticity-Ultimate	$\gamma$	0.123	0.109
Phase Change	n	2.45	3.12
Growth/Hardening	$a_i$	0.8450	0.289
	$\eta_i$	0.0215	0.470
Critical State	$\bar{m}$	0.15	0.22
	$\lambda$	0.02	0.013
	$e_c^o$	0.601	0.598
Disturbance	Du	0.99	0.99
	Z	0.43	0.665
	A	4.22	0.595

**Table 4. Parameters for Nevada Sand and Sand-Aluminum Interface  
(Pradhan and Desai 2004)**

Sub Group	Parameter	Nevada Sand	Nevada Sand – Aluminum Interface
Elastic	E	40848.8 kPa	14.6 kPa
	v	0.316	0.384
Plasticity-Ultimate	$\gamma$	0.0675	0.246
	$\beta$	0.0	0.000
Phase Change	n	4.1	3.350
Growth/Hardening	$a_i$	0.1245	0.620
	$\eta_i$	0.0725	0.570
Critical State	$\bar{m}$	0.22	0.304
	$\lambda$	0.02	0.0278
	$e_c^o$	0.712	0.791
Disturbance	Du	0.99	0.990
	Z	0.411	1.195
	A	5.02	0.595

@Seismicisolation

**Table 5. Parameters for Sandstone (Desai and Salami 1987)  
(No disturbance or softening)**

Parameter	Symbol	Value – Sandstone
Elastic	E	25,500 MPa
	v	0.11
Plasticity – Ultimate	$\gamma$	0.0774
	$\beta$	0.750
Phase Change	n	7.20
Growth/Hardening	$a_i$	$0.467 \times 10^{-2}$
	$\eta_i$	0.345
Tensile Strength	R	2.90 MPa

**Table 6. Parameters for Quartz Mica Schist: Intact Rock and Rock Mass  
(Varadarajan et al. 2001)**

Parameter	Symbol	Value	
		Intact Rock	Rock Mass
Elastic	E	8591 MPa	6677 MPa
	v	0.2	0.2
Plasticity-Ultimate	$\gamma$	0.0202	0.0135
	$\beta$	0.4678	0.390
Phase Change	n	5.0	5.0
Growth/Hardening	$a_i$	$0.13 \times 10^{-12}$	$0.13 \times 10^{-12}$
	$\eta_i$	0.60	0.60
Bonding (Tensile) Stress	R	16.0	14.00
Disturbance	Du	0.97	0.97
	A	220.71	220.71
	Z	1.34	1.34

## VALIDATIONS

The DSC equations are integrated to predict the observed laboratory behavior for a wide range of materials (Desai, 2001b). For most of the materials, the DSC model provides very good correlations with the test data. Also, the DSC model has provided very good correlations for independent test data, which were *not* used for calibration of the parameters.

## IMPLEMENTATION

The DSC model has been implemented in numerical (finite element – FE) procedures. A number of schemes have been developed for solution of the FE equations involving both nonsymmetrical and symmetric stiffness matrices. One of the equations involving the symmetric matrix is given below:

$$\underline{k}_m^i \underline{dq}_{m+1}^i = d\underline{\underline{Q}}_{m+1}^i = \underline{\underline{Q}}_m^i - \underline{\underline{Q}}_m^{b(i)} \quad (15)$$

where  $\underline{k}_m^i$  = symmetric matrix based on the RI (plasticity) response,  $\underline{q}^i$  = displacement vector,  $\underline{\underline{Q}}^i$  = load vector,  $\underline{\underline{Q}}^b$  = balanced load, and  $m$  = step in incremental analysis, and  $d$  = increment. In the scheme based on Eq. (15) involves incremental solution with RI (HISS plasticity) response, which involves a positive definite matrix. Then at every step, the observed behavior is computed using Eq. (1) with an iterative procedure (Desai, 2001b).

The predictions from the FE procedures have been compared to laboratory and field data for practical problems, e.g., piles, footings, reinforced walls, dams, tunnels, shake table tests, centrifuge test, liquefaction, etc. (Desai, 2001b).

## COMPUTER CODES

Computer codes have been developed for

(a) Determination of DSC parameters based on laboratory data. Here, the user can input points on various stress-strain-volumetric responses, and the code yields the parameters.

This code also includes the integration of Eq. (1) by using the determined parameters so as to predict stress-strain-volumetric responses toward validations.

(b) Computer codes have been developed based on the finite element method for static and dynamic analysis including liquefaction of practical boundary value problems, e.g., (i) DSC-SST2D (Desai 1999), (ii) DSC-DYN2D (Desai 2001c), and (iii) DSC-DYN3D (Desai 2001a). These and other codes have been used to solve a wide range of problems in civil, mechanical and electronic engineering. The predictions compare very well with laboratory and/or field tests for practical problems.

## ACKNOWLEDGMENT

The results presented herein have been partly supported by a number of grants from the National Science Foundation, Washington, DC. Participation and

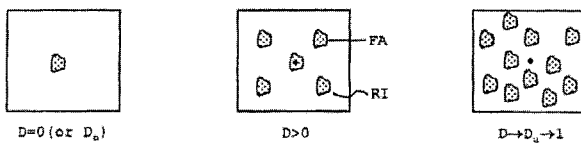


contributions of a number of students and colleagues are acknowledged; some are included in the references.

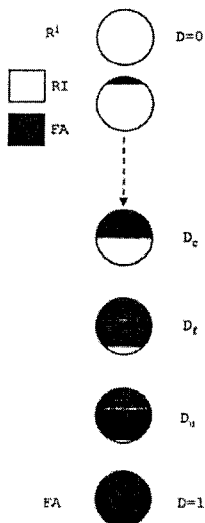
## REFERENCES

- Bazant, Z.P. (1994). "Nonlocal damage theory based on micromechanics of crack interactions," *J. Eng. Mech., ASCE*, 120, 593-617.
- Desai, C.S. (1999). "DSC-SST2D-computer code for static, dynamic, creep and thermal analysis: Solid, structure and soil-structure problems," *Reports and Manuals*, Tucson, AZ, USA.
- Desai, C.S. (2001a). "DSC-SST3D-computer code for static and coupled dynamic analysis: Solid, (porous) structure and soil-structure problems," *Report and Manuals*, Tucson, AZ, USA.
- Desai, C.S. (2001c). "DSC-DYN2D-dynamic and static analysis, dry and coupled porous saturated materials," *Report and Manuals*, Tucson, AZ, USA.
- Desai, C. S. (1974). "A consistent finite element technique for work-softening behavior," *Proc., Int. Conf. on Comp. Meth. in Nonlinear Mech.*, J.T. Oden (editor), Univ. of Texas, Austin, TX, USA.
- Desai, C.S. (1980). "A general basis for yield, failure and potential functions in plasticity," *Int. J. Numer. Analyt. Methods Geomech.*, 4, 361-375.
- Desai, C. S. (1987). "Further on unified hierarchical models based on alternative correction or disturbance approach," *Report*, Dept. of Civil Eng. & Eng. mechs., The Univ. of Arizona, Tucson, AZ, USA.
- Desai, C.S. (2000b). "Evaluation of liquefaction using disturbed state and energy approaches," *J. of Geotech. and Geoenv. Eng., ASCE*, 126, 7, 618-631.
- Desai, C.S. (2001b). *Mechanics of Materials and Interfaces: The Disturbed State Concept*, CRC Press, Boca Raton, FL, USA.
- Desai, C.S., and Ma. Y. (1992). "Modelling of joints and interfaces using the disturbed state concept," *Int. J. Num. and Analyt. Methods in Geomech.*, 16, 9, 623-653.
- Desai, C.S., Park, I.J., and Shao, C. (1998). "Fundamental yet simplified model for liquefaction instability," *Int. J. Num. Analyt. Meth. in Geomech.*, 22, 7, 721-748.
- Desai, C.S., and Salami, M.R. (1987). "A constitutive model for rocks," *J. Geotech. Eng., ASCE*, 113, 407-423.
- Desai, C.S., Samtani, N.C., and Vulliet, L. (1995). "Constitutive modeling and analysis of creeping slopes," *J. Geotech. Eng., ASCE*, 121, 43-56.
- Desai, C.S., Somasundaram, S., and Frantziskonis, G. (1986). "A hierarchical approach for constitutive modeling of geologic materials," *Int. J. Numer. Anal. Methods in Geomech.*, 10, 3, 225-257.
- Desai, C.S., and Toth, J. (1996). "Disturbed state constitutive modeling based on stress-strain and nondestructive behavior," *Int. J. Solids & Struct.*, 33, 11, 1619-1650.
- Elgamal, A., Yang, Z., and Parra, E. (2002). "Computational modeling of cyclic mobility and post-liquefaction site response," *Soil Dynamics and Earthquake Eng.*, 22, 259-271.

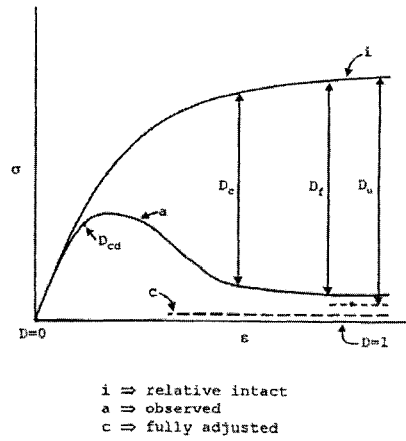
- Geiser, F., Laloui, L., Vulliet, L., and Desai, C.S. (1997). "Disturbed state concept for partially saturated soils," *Proc., 6<sup>th</sup> Intl. Symp. on Num. Models in Geomechanics*, Montreal, Pietruszka, S. and Pande, G.N. (Eds.), Canada, Balkema, Netherlands.
- Kachanov, L.M. (1986). *Introduction to Continuum Damage Mechanics*, Martinus Nijhoff Publishers, Dordrecht, The Netherlands.
- Katti, D.R., and Desai, C.S. (1995). "Modeling and testing of cohesive soil using the disturbed state concept," *J. of Eng. Mech., ASCE*, 121, 5, 648-658.
- Lade, P.V., and Kim, M.K. (1988). "Single hardening constitutive model for frictional materials. III. Comparisons with experimental data," *Computers and Geotechnics*, 6, 31-47.
- Matsuoka, H., and Nakai, T. (1974). "Stress-deformation and strength characteristics of soil under three different principal stresses," *Proc., Jap. Soc. Civil Engrs.*, 232, 59-70.
- Mroz, Z., Norris, V.A., and Zienkiewicz, O.C. (1978). "An anisotropic hardening model for soils and its application to cyclic loading," *Int. J. Num. & Analyt. Methods in Geomech.*, 2, 208-221.
- Mühlhaus, H.B. (Ed.) (1995). *Continuum Models for Materials with Microstructure*, John Wiley, UK.
- Park, I.J., and Desai, C.S. (2000). "Cyclic behavior and liquefaction of sand using disturbed state concept," *J. Geotech. Geoenv. Eng., ASCE*, 126, 9.
- Perzyna, P. (1966). "Fundamental problems in viscoplasticity," *Adv. in Appl. Mech.*, 9, 243-277.
- Pestana, J.M., and Whittle, A.J. (1999). "Formulation of a unified constitutive model for clays and sands," *Int. J. Num. & Analyt. Methods in Geomech.*, 23 (12), 1215-1243.
- Pradhan, S.K., and Desai, C.S. (2004). "DSC model for soil and interface including liquefaction and prediction of centrifuge tests," *J. of Geotech. and Geoenvir. Eng., ASCE*, tentatively approved.
- Roscoe, A.N., Schofield, A., and Wroth, P.C. (1958). "On yielding of soils," *Geotechnique*, 8, 22-53.
- Somasundaram, S., and Desai, C.S. (1988). "Modelling and testing for anisotropic behavior of soils," *J. Eng. Mech., ASCE*, 114, 1473-1496.
- Varadarajan, A., Sharma, K.G., Desai, C.S., and Hashemi, M. (2001). "Constitutive modeling of a schistose rock in the Himalaya," and "Analysis of a powerhouse cavern in the Himalaya," *Int. J. of Geomech.*, 1, 1, 83-107 and 109-127.
- Wathugala, G.W., and Desai, C.S. (1993). "Constitutive model for cyclic behavior of clays-theory, Part I," *J. of Geotech. Eng.*, 119, 4, 714-729.



(a) Clusters of RI and FA parts



(b) Symbolic representation of DSC



(c) Schematic of stress-strain response

**FIG. 1. Representations of DSC**

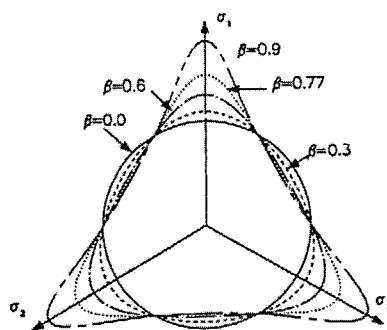
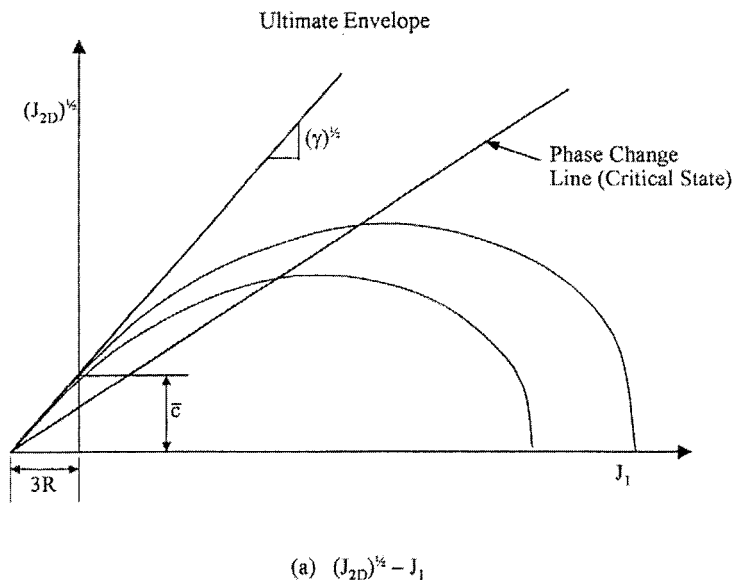


**FIG. 2. Plots of  $F$  in different stress spaces**

@Seismicisolation

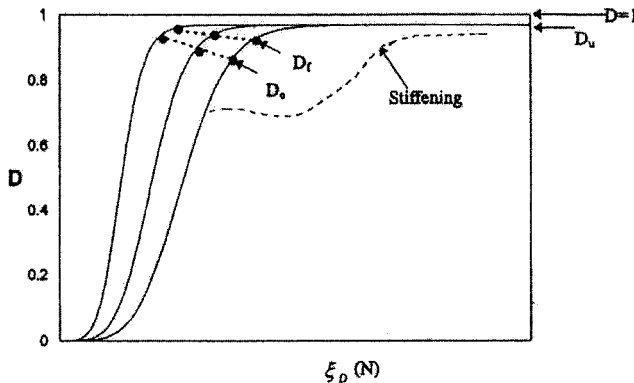


**FIG. 3. Disturbance for softening, stiffening behavior and critical disturbance**

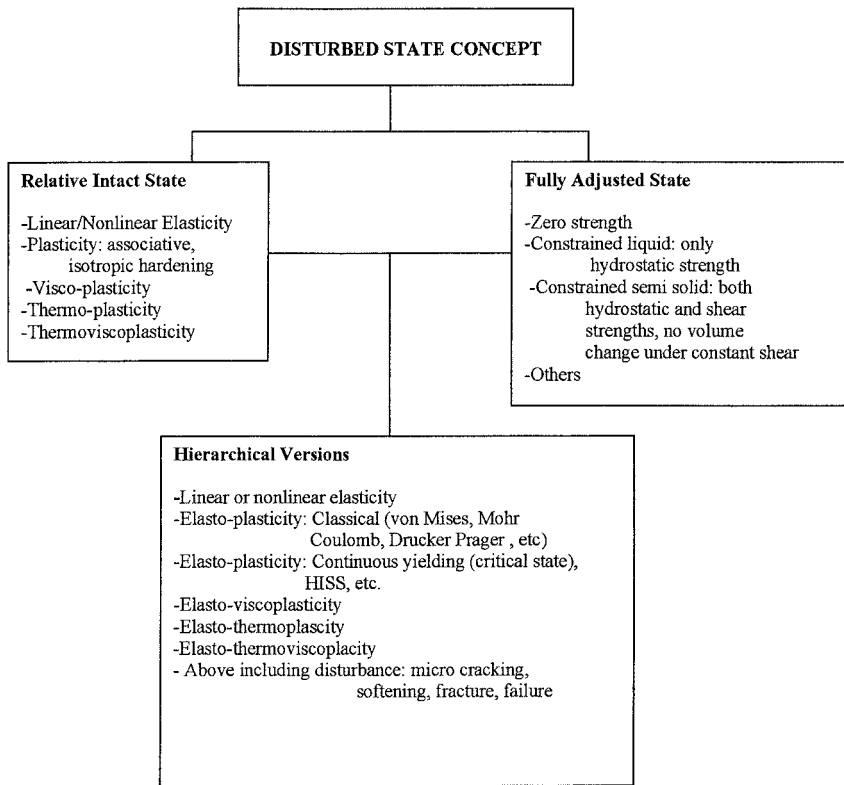


**FIG. 4. Hierarchical versions in DSC**  
**@Seismicisolation**

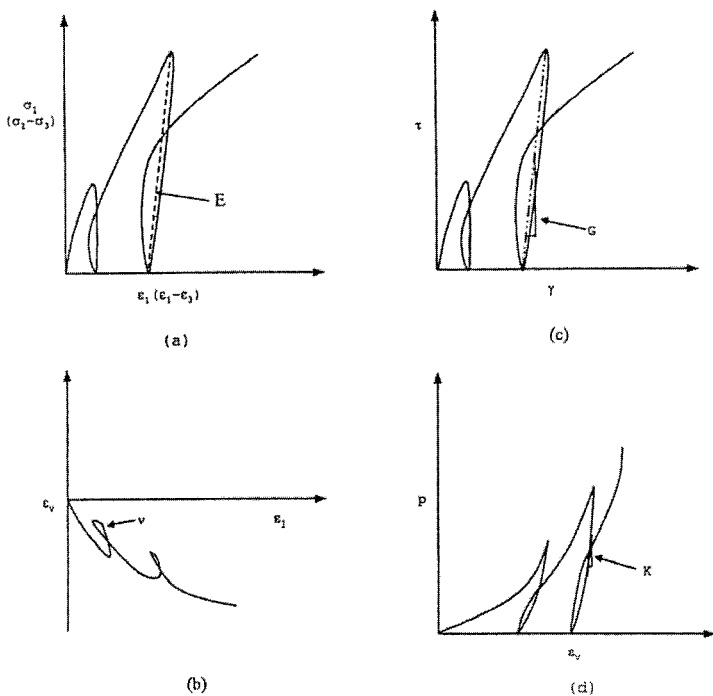


**FIG. 5. Elastic constants from test data**

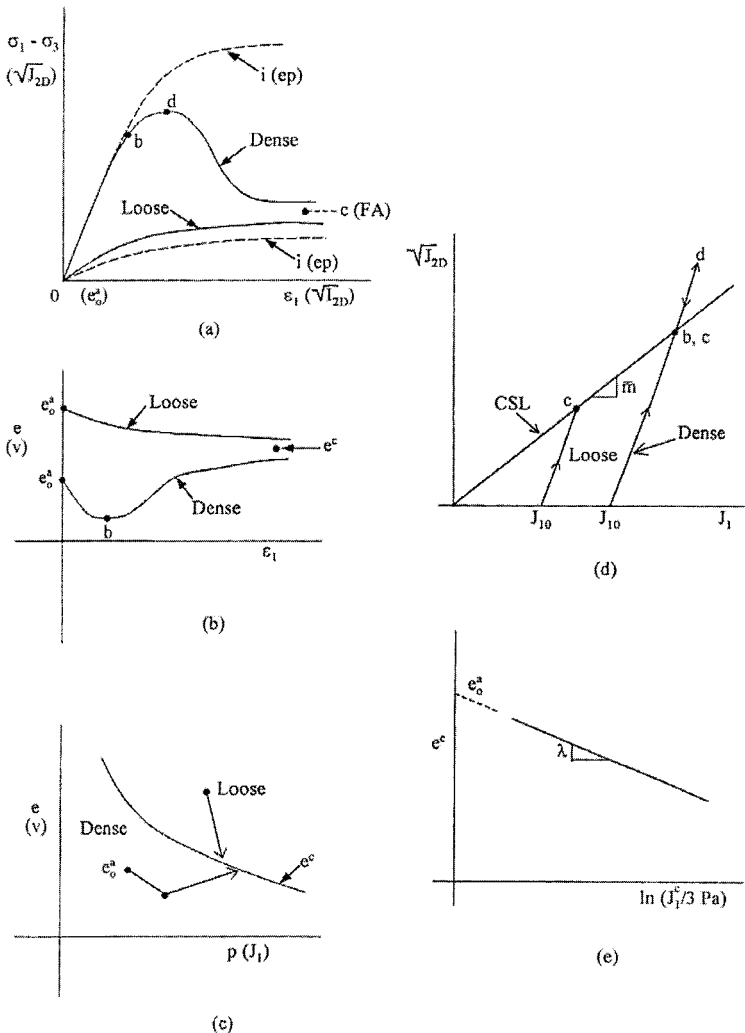
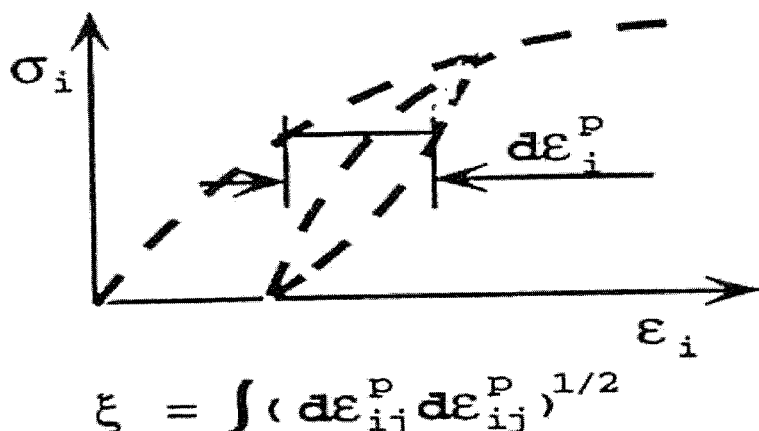
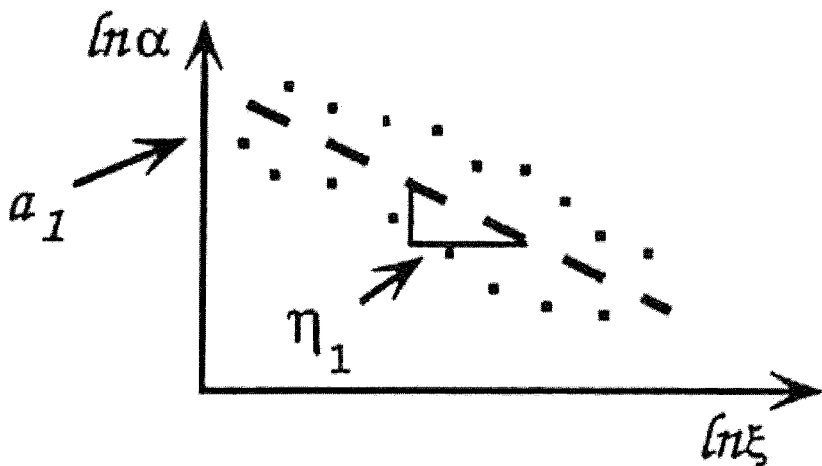


FIG. 6. Behavior of loose and dense geo-materials



(a)

FIG. 7. Hardening or growth parameters,  $a_1$  and  $n_1$ 

@Seismicisolation

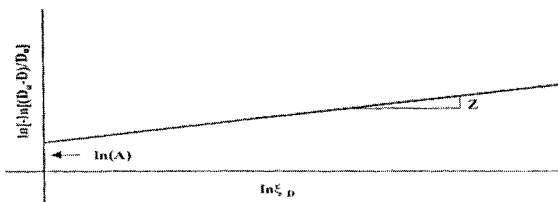


**FIG. 8. Determination of disturbance parameters, A and Z**

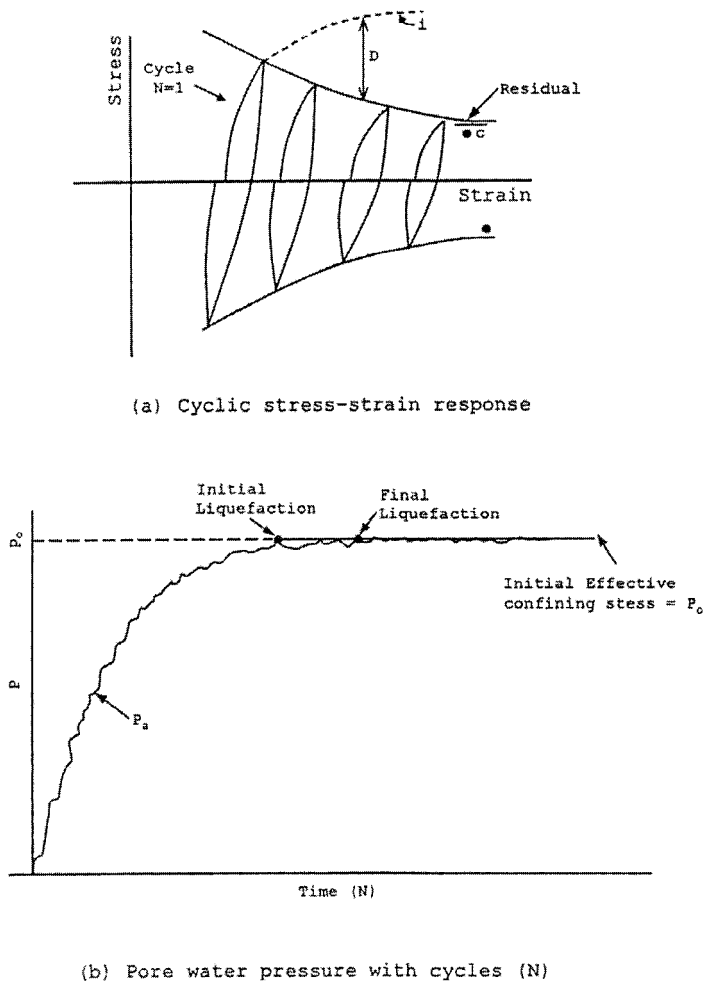


FIG. 9. Disturbance and liquefaction from cyclic test

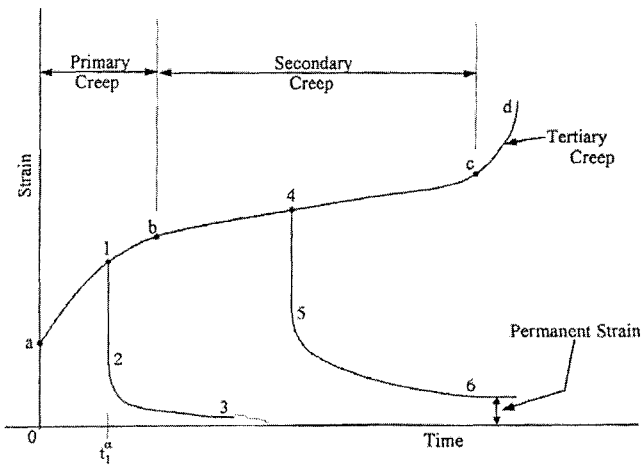


FIG. 10. Schematic of behavior for creep parameters,  $\Gamma$  and  $N$

## GEOTECHNICAL CONSTITUTIVE MODELS IN AN EXPLICIT, DYNAMIC SOLUTION SCHEME

Roger D. Hart<sup>1</sup>, Ph.D., P.E. Member, ASCE, and Christine Detournay<sup>2</sup>, Ph.D.

**ABSTRACT:** This paper describes a procedure for implementation and calibration of elastic-plastic constitutive models for soils and rocks in an explicit, dynamic-solution (EDS) numerical scheme. The EDS scheme offers several advantages for the development and testing of geotechnical models. For example, extremely nonlinear constitutive models can be implemented and tested with this scheme in a straightforward fashion. Also, physical instability and path-dependent processes are followed directly and do not introduce numerical instability problems. The elastic-plastic numerical formulation in the EDS scheme is described, and an example implementation is presented for the *Mohr-Coulomb* constitutive model.

Complex, nonlinear models can readily be implemented in an EDS scheme, such as hardening/softening models, and models accounting for both volumetric collapse and shear yield. It is also practical for modelers to incorporate variations of these models or develop their own constitutive models in an EDS scheme. This is important for model calibration purposes. Calibration of models implemented in this manner can be conducted by performing numerical tests that directly mimic laboratory tests (e.g., triaxial or direct shear tests) of a soil or rock specimen. An example is presented to illustrate this procedure.

---

<sup>1</sup>Director, Software Services, Itasca Consulting Group, Inc., 111 3<sup>rd</sup> Avenue South, Suite 450, Minneapolis, Minnesota, 55401, (612) 371-4711, rhart@itascacg.com

<sup>2</sup>Senior Engineer, Itasca Consulting Group, Inc., 111 3<sup>rd</sup> Avenue South, Suite 450, Minneapolis, Minnesota, 55401, (612) 371-4711, cdetournay@itascacg.com



## INTRODUCTION

Numerical solution schemes face several difficulties when implementing constitutive models to represent geomechanical material behavior. There are three characteristics of geo-materials that cause particular problems. One is physical instability. Physical instability can occur in a material if there is the potential for softening behavior when the material fails. When physical instability occurs, part of the material accelerates and stored energy is released as kinetic energy. Numerical solution schemes often have difficulties at this stage because the solution may fail to converge when a physical instability arises.

A second characteristic is the path dependency of nonlinear materials. In most geomechanical systems, there are an infinite number of solutions that satisfy the equilibrium, compatibility and constitutive relations that describe the system. A path must be specified for a "correct" solution to be found. For example, if an excavation is made suddenly, (e.g., by explosion) then the solution may be influenced by inertial effects that introduce additional failure of the material. This may not be seen if the excavation is made gradually. The numerical solution scheme should be able to accommodate different loading paths in order to apply the constitutive model properly.

A third characteristic is the nonlinearity of the stress-strain response. This includes the nonlinear dependence of both the elastic stiffness and the strength envelope on the confining stress. This can also include behavior after ultimate failure that changes character according to the stress level, e.g., different post-failure response in the tensile, unconfined and confined regimes. The numerical scheme needs to be able to accommodate these various forms of nonlinearity.

## EXPLICIT, DYNAMIC SOLUTION SCHEME

The difficulties faced in numerical simulations in geomechanics — physical instability, path dependence, and implementation of extremely nonlinear constitutive models — can all be addressed by using an *explicit, dynamic solution scheme*.

This scheme allows the numerical analysis to follow the evolution of a geologic system in a realistic manner, without concerns about numerical instability problems. In the explicit, dynamic solution (EDS) scheme, the full dynamic equations of motion are included in the formulation. By using this approach, the numerical solution is stable even when the physical system being modeled is unstable. With nonlinear materials, there is always the possibility of physical instability, e.g., the sudden collapse of a slope. In real life, some of the strain energy in the system is converted into kinetic energy, which then radiates away from the source and dissipates. The EDS approach models this process directly, because inertial terms are included — kinetic energy is generated and dissipated.

In contrast, schemes that do not include inertial terms must use some numerical procedure to treat physical instabilities. Even if the procedure is successful at preventing numerical instability, the *path* taken may not be a realistic one. The numerical scheme should not be viewed as a black box that will give "the solution. The way the system evolves physically can affect the solution. The EDS scheme can follow the physical path. By including the full law of motion, the EDS scheme can evaluate the effect of the loading path on the constitutive response.



The EDS scheme also allows the implementation of strongly nonlinear constitutive models because the general calculation sequence allows the field quantities (velocities/displacements and forces/stresses) at each element in the model to be physically isolated from one another during one calculation step. This implementation in the general calculation sequence is described as follows.

The calculation sequence for the EDS scheme is illustrated in Figure 1. The calculation solves two sets of equations every calculation step: motion and constitutive. The equations of motion are invoked to derive new velocities and displacements from stresses and forces. Then, strain rates are derived from velocities, and new stresses from strain rates. One calculation “timestep” is taken for every cycle around this loop. The key feature here is that each box in Figure 1 updates all model variables from known values that remain fixed while control is within that box. For example, the lower box takes the set of velocities already calculated and, for each element, computes new stresses. The velocities are assumed to be frozen for the operation of the box, i.e., the newly calculated stresses do not affect the velocities. This assumption is valid provided the timestep is sufficiently small that information cannot physically pass from one element to another. Of course, after several cycles of the loop, disturbances can propagate across several elements, just as they would propagate physically.

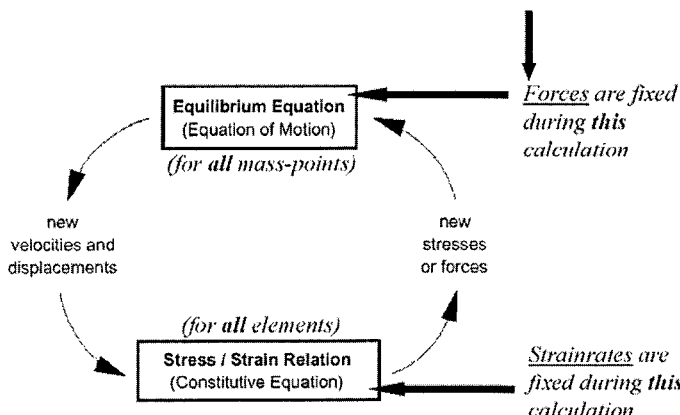


**FIG. 1. The Calculation Cycle**

The implementation of nonlinear constitutive models is straightforward with the EDS approach. The “input strain,” as indicated in the nonlinear stress-strain relation shown in Figure 2, is fixed, and there are no influences from other elements, *during one timestep*. The calculation simply moves from a previous stress state to a new stress state, obeying the governing equations (as described in the next section). There is no concept of “return path.” No iteration process is necessary when computing stresses from strains in an element, even if the constitutive law is very nonlinear. Therefore, this approach allows the user to focus on the implementation

@Seismicisolation

and calibration of a constitutive model without needing to be concerned about the appropriate iteration algorithm to use to satisfy compatibility and equilibrium.

Although the full dynamic equations of motion are solved, the method can also simulate quasi-static systems by including damping. Several forms of damping can be applied. One type, known as “local damping,” has been shown to provide efficient convergence for static solutions without introducing erroneous body forces (see Cundall, 1987 for details).

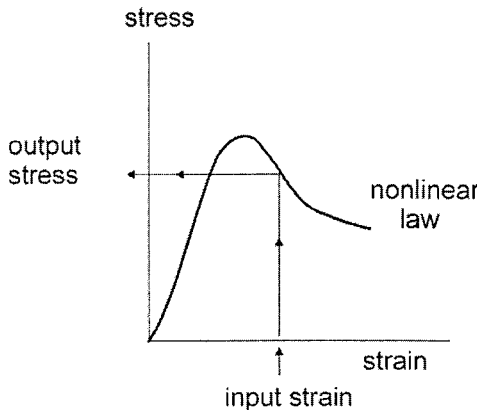


**FIG. 2. Constitutive Law Implementation**

The EDS scheme has been used over the past 30 years for numerical solutions of many nonlinear geological systems. See Cundall, 1971 and 1974 for early applications. Examples of commercial codes based on the EDS scheme are FLAC (Itasca, 2001) and FLAC3D (Itasca, 2002). The description given in the following section on the implementation of constitutive models in the EDS scheme is taken from the *Theory and Background* volume of the FLAC3D manual (Itasca, 2002).

### IMPLEMENTATION OF AN ELASTIC/PLASTIC LAW

This section focuses on the implementation of a constitutive model (Figure 2) in the lower box of Figure 1. Constitutive models in the EDS scheme are based on an incremental numerical algorithm. Given the stress state at time  $t$ , and the total strain increment for a timestep,  $\Delta t$ , the purpose is to determine the corresponding stress increment and the new stress state at time  $t + \Delta t$ . When plastic deformations are involved, only the elastic part of the strain increment will contribute to the stress increment. In this case, a correction must be made to the elastic stress increment as computed from the total strain increment in order to obtain the actual stress state for the new timestep.

#### Incremental Equations of the Theory of Plastic Flow

In order to describe the implementation of elastic/plastic constitutive laws in the EDS scheme, we consider below the implementation algorithm for the case when the

**@Seismicisolation**

incremental elastic stress-strain relations are linear functions of strain increment, and the yield relation is a linear function of the generalized stress components.

The components of the generalized stress- and strain-increment vectors may consist of the six components of the stress- and strain-increment tensors or other appropriately defined combinations of variables giving a measure of stress and strain-increments in specific constitutive model contexts. (As a notation convention in this section, we use the subscript  $n$  to refer to the range of generalized components from  $i = 1$  to  $i = n$ , e.g.,  $f(\underline{\sigma}_n)$  is used to represent  $f(\underline{\sigma}_1, \underline{\sigma}_2, \dots, \underline{\sigma}_n)$ ).

The description of plastic flow in the EDS scheme rests on the following five relations:

(1) the failure criterion:

$$f(\underline{\sigma}_n) = 0 \quad (1)$$

where  $\underline{\sigma}_n$  is a generalized stress vector of dimension  $n$  with components  $\underline{\sigma}_i$ ,  $i = 1, n$ , and  $f$ , the yield function, is a known function that specifies the limiting stress combination for which plastic flow takes place (This function is represented by a surface in the generalized stress space, and all stress points below the surface are characterized by elastic behavior.);

(2) the relation expressing the decomposition of strain increments,  $\Delta\varepsilon_i$ ,  $i = 1, n$ , of the generalized strain-increment vector into the sum of elastic and plastic parts:

$$\Delta\varepsilon_i = \Delta\varepsilon_i^e + \varepsilon_i^p \quad (2)$$

(3) the elastic relations between elastic strain increments and stress increments:

$$\Delta\underline{\sigma}_i = S_i(\Delta\underline{\varepsilon}_n^e) \quad i = 1, n \quad (3)$$

where  $S_i$  is considered, in this case, a linear function of the elastic strain increments  $\Delta\varepsilon_n^e$ ;

(4) the flow rule specifying the direction of the plastic-strain increment vector as that normal to the potential surface  $g(\underline{\sigma}_n) = constant$  — i.e.,

$$\Delta\varepsilon_i^p = \lambda \frac{\partial g}{\partial \underline{\sigma}_i} \quad (4)$$

where  $\lambda$  is a constant. (The flow rule is said to be associated if  $g = f$ , and non-associated otherwise.); and

(5) the requirement for the new stress-vector components to satisfy the yield function:

$$f(\underline{\sigma}_n + \Delta\underline{\sigma}_n) = 0 \quad (5)$$

This equation provides a relation for evaluation of the magnitude of the plastic-strain increment vector.

Substitution of the expression for the elastic-strain increment derived from Eq. 2 into the elastic relation Eq. 3 yields, taking into consideration the linear property of the function  $S_i$ :

$$\Delta\underline{\sigma}_i = S_i(\Delta\underline{\varepsilon}_n) - S_i(\Delta\underline{\varepsilon}_n^p) \quad (6)$$

In further expressing the plastic strain increment by means of the flow rule, Eq. 4, this equation becomes

$$\Delta\underline{\sigma}_i = S_i(\Delta\underline{\varepsilon}_n) - \lambda S_i\left(\frac{\partial g}{\partial \underline{\sigma}_n}\right) \quad (7)$$

where use has been made of the linear property of  $S_i$ .

In the special case where  $f(\underline{\sigma}_n)$  is a linear function of the components  $\underline{\sigma}_i$ ,  $i = 1, n$ , Eq. 5 may be expressed as

$$f(\underline{\sigma}_n) + f^*(\Delta\underline{\sigma}_n) = 0 \quad (8)$$

where, as a notation convention,  $f^*$  represents the function  $f$  minus its constant term,

$$f^*(.) = f(.) - f(0_n) \quad (9)$$

For a stress point  $\underline{\sigma}_n$  on the yield surface,  $f(\underline{\sigma}_n) = 0$ , and Eq. 8 becomes, after substitution of the expression Eq. 7 for the stress increment and further using the linear property of  $f^*$ :

$$f^*[S_n(\Delta\underline{\varepsilon}_n)] - \lambda f^*\left[S_n\left(\frac{\partial g}{\partial \underline{\sigma}_n}\right)\right] = 0 \quad (10)$$

We now define *new* stress components  $\underline{\sigma}_i^N$  and *elastic guesses*  $\underline{\sigma}_i^I$  as follows.

$$\underline{\sigma}_i^N = \underline{\sigma}_i + \Delta\underline{\sigma}_i \quad (11)$$

$$\underline{\sigma}_i^I = \underline{\sigma}_i + S_i(\Delta\underline{\varepsilon}_n) \quad (12)$$

Note that the term  $S_i(\Delta\varepsilon_n)$  in Eq. 12 is the component  $i$  of the stress increment induced by the total-strain increment  $\Delta\varepsilon_n$  in case no increment of plastic deformation takes place. This justifies the name of “elastic guess” for  $\underline{\sigma}_i^I$ .

From the definition Eq. 12, it follows, using the same arguments as above, that

$$f(\underline{\sigma}_n^I) = f^*[S_n(\Delta\varepsilon_n)] \quad (13)$$

Hence, an expression for  $\lambda$  may be derived from Eqs. 9, 10 and 13 that has the form

$$\lambda = \frac{f(\underline{\sigma}_n^I)}{f[S_n(\partial g / \partial \underline{\sigma}_n^I)] - f(0_n)} \quad (14)$$

Using the expression of the stress increment, Eq. 7, and the definition of the elastic guess, Eq. 12, the new stress may be explained from Eq. 11 as

$$\underline{\sigma}_i^N = \underline{\sigma}_i^I - \lambda S_i \left( \frac{\partial g}{\partial \underline{\sigma}_n} \right) \quad (15)$$

For clarity, recall that, in these last two expressions,  $S_i(\partial g / \partial \underline{\sigma}_n)$  is the stress increment obtained from the incremental elastic law, where  $\partial g / \partial \underline{\sigma}_i$  is substituted for  $\Delta\varepsilon_i$ ,  $i = 1, n$ .

### Implementation

An elastic guess  $\underline{\sigma}_i^I$ ,  $i = 1, n$  for the stress state at time  $t + \Delta t$  is first evaluated by adding to the stress components at time,  $t$ , increments computed from the total-strain increment for the step, using an incremental elastic stress-strain law (see Eq. 12). If the elastic guess violates the yield function, Eq. 15 is used to place the new stress exactly on the yield curve. Otherwise, the elastic guess gives the new stress state at time  $t + \Delta t$ .

If the stress point  $\underline{\sigma}_i^I$ ,  $i = 1, n$  is located above the yield surface in the generalized stress space, the coefficient  $\lambda$  in Eq. 15 is given by Eq. 14, provided the yield function is a linear function of the generalized stress vector components. Eq. 15 is still valid, but  $\lambda$  is set to zero in case  $\underline{\sigma}_i^I$ ,  $i = 1, n$  is located below the yield surface (elastic loading or unloading).

### Example Implementation – Mohr-Coulomb Model

The failure envelope for this model corresponds to a Mohr-Coulomb criterion (shear yield function) with tension cutoff (tension yield function). The position of a stress point on this envelope is controlled by a non-associated flow rule for shear failure and an associated rule for tension failure.



The Mohr-Coulomb criterion is expressed in terms of the principal stresses  $\sigma_1$ ,  $\sigma_2$  and  $\sigma_3$ , which are the three components of the generalized stress vector for this model ( $n = 3$ ). The components of the corresponding general stress vector are the principal strains  $\varepsilon_1$ ,  $\varepsilon_2$  and  $\varepsilon_3$ .

The incremental expression of Hooke's law in terms of the generalized stress and stress increments has the form

$$\begin{aligned}\Delta\sigma_1 &= \alpha_1\Delta\varepsilon_1^e + \alpha_2(\Delta\varepsilon_2^e + \Delta\varepsilon_3^e) \\ \Delta\sigma_2 &= \alpha_1\Delta\varepsilon_2^e + \alpha_2(\Delta\varepsilon_1^e + \Delta\varepsilon_3^e) \\ \Delta\sigma_3 &= \alpha_1\Delta\varepsilon_3^e + \alpha_2(\Delta\varepsilon_1^e + \Delta\varepsilon_2^e)\end{aligned}\quad (16)$$

where  $\alpha_1$  and  $\alpha_2$  are material constants defined in terms of the shear modulus,  $G$ , and bulk modulus,  $K$ , as

$$\begin{aligned}\alpha_1 &= K + \frac{4}{3}G \\ \alpha_2 &= K - \frac{2}{3}G\end{aligned}\quad (17)$$

For future reference, comparing those expressions with Eq. 3, we may write

$$\begin{aligned}S_1(\Delta\varepsilon_1^e, \Delta\varepsilon_2^e, \Delta\varepsilon_3^e) &= \alpha_1\Delta\varepsilon_1^e + \alpha_2(\Delta\varepsilon_2^e + \Delta\varepsilon_3^e) \\ S_2(\Delta\varepsilon_1^e, \Delta\varepsilon_2^e, \Delta\varepsilon_3^e) &= \alpha_1\Delta\varepsilon_2^e + \alpha_2(\Delta\varepsilon_1^e + \Delta\varepsilon_3^e) \\ S_3(\Delta\varepsilon_1^e, \Delta\varepsilon_2^e, \Delta\varepsilon_3^e) &= \alpha_1\Delta\varepsilon_3^e + \alpha_2(\Delta\varepsilon_1^e + \Delta\varepsilon_2^e)\end{aligned}\quad (18)$$

The failure criterion is a composite Mohr-Coulomb criterion with tension cutoff. In labeling the three principal stresses so that

$$\sigma_1 \leq \sigma_2 \leq \sigma_3 \quad (19)$$

this criterion may be represented in the plane  $(\sigma_1, \sigma_3)$  as illustrated in Figure 3. (Note that compressive stresses are negative.) The failure envelope  $f(\sigma_1, \sigma_3) = 0$  is defined from point  $A$  to  $B$  by the Mohr-Coulomb failure criterion  $f^s = 0$  with

$$f^s = \sigma_1 - \sigma_3 N_\phi + 2c\sqrt{N_\phi} \quad (20)$$

and from  $B$  to  $C$  by a tension failure criterion of the form  $f^t = 0$  with

$$f^t = \sigma_3 - \sigma' \quad (21)$$

where  $\phi$  is the friction angle,  $c$ , the cohesion,  $\sigma^t$ , the tensile strength and

$$N_\phi = \frac{1 + \sin(\phi)}{1 - \sin(\phi)} \quad (22)$$

Note that the tensile strength of the material cannot exceed the value of  $\sigma_3$  corresponding to the intersection point of the straight lines  $f^s = 0$  and  $\sigma_1 = \sigma_3$  in the  $f(\sigma_1, \sigma_3)$  plane. This maximum value is given by

$$\sigma_{\max}^t = \frac{c}{\tan \phi} \quad (23)$$

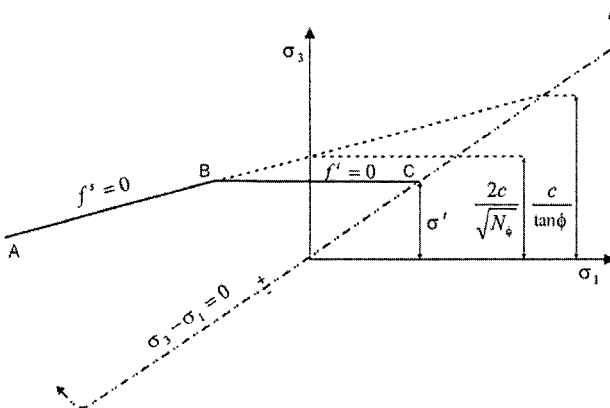


**FIG. 3. Mohr-Coulomb Failure Criterion**

The potential function is described by means of two functions,  $g^s$  and  $g^t$ , used to define shear plastic flow and tensile plastic flow, respectively. The function  $g^s$  corresponds to non-associated law and has the form

$$g^s = \sigma_1 - \sigma_3 N_\psi \quad (24)$$

where  $\psi$  is the dilation angle and

$$N_\psi = \frac{1 + \sin(\psi)}{1 - \sin(\psi)} \quad (25)$$

The function  $g^t$  corresponds to an associated flow rule and is written

$$g^t = -\sigma_3 \quad (26)$$

The flow rule is given a unique definition by application of the following technique. A function  $h(\sigma_1, \sigma_3) = 0$  is defined which is represented by the diagonal between the representation of  $f^s = 0$  and  $f^t = 0$  in the  $(\sigma_1, \sigma_3)$ -plane (see Figure 4). The function is selected with its positive and negative domains, as indicated on the figure, and has the form

$$h = \sigma_3 - \sigma^t + a^P(\sigma_1 - \sigma^P) \quad (27)$$

where  $a^P$  and  $\sigma^P$  are constants defined as

$$\begin{aligned} a^P &= \sqrt{1 + N_\phi^2} + N_\phi \\ \sigma^P &= \sigma^t N_\phi - 2c\sqrt{N_\phi} \end{aligned} \quad (28)$$

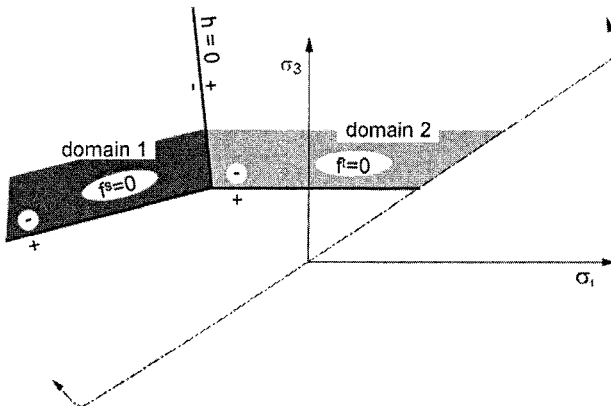


**FIG. 4. Mohr-Coulomb Model – Domains used in the Definition of Flow Rule**

An elastic guess violating the composite yield function is represented by a point in the  $(\sigma_1, \sigma_3)$ -plane located either in domain 1 or 2, corresponding to negative or positive domains of  $h = 0$ , respectively (see Figure 4). If the stress point falls within domain 1, shear failure is declared, and the stress point is placed on the curve  $f^s = 0$  using a flow rule derived using the potential function  $g^s$ . If the point falls within domain 2, tensile failure takes place, and the new stress point conforms to  $f^t = 0$  using a flow rule derived using  $g^t$ .

Note that, by ordering the stresses in Eq. 19, the case of a shear-shear edge is automatically handled by a variation on this technique. The technique, applicable for small-strain increments, is simple to implement: at each step, only one flow rule and corresponding stress correction is involved in case of plastic flow. In particular, when a stress point follows an edge, it receives stress corrections alternating between

two criteria. In this process, the two yield criteria are fulfilled to an accuracy that depends on the magnitude of the strain increment.

First, considering shear failure, partial differentiation of Eq. 24 yields

$$\begin{aligned}\frac{\partial g^s}{\partial \sigma_1} &= 1 \\ \frac{\partial g^s}{\partial \sigma_2} &= 0 \\ \frac{\partial g^s}{\partial \sigma_3} &= -N_\psi\end{aligned}\quad (29)$$

Substitution of  $\partial g^s / \partial \sigma_1$ ,  $\partial g^s / \partial \sigma_2$  and  $\partial g^s / \partial \sigma_3$  for  $\Delta \varepsilon_1^e$ ,  $\Delta \varepsilon_2^e$ , and  $\Delta \varepsilon_3^e$ , respectively, in Eq. (18) gives

$$\begin{aligned}S_1\left(\frac{\partial g^s}{\partial \sigma_1}, \frac{\partial g^s}{\partial \sigma_2}, \frac{\partial g^s}{\partial \sigma_3}\right) &= \alpha_1 - \alpha_2 N_\psi \\ S_2\left(\frac{\partial g^s}{\partial \sigma_1}, \frac{\partial g^s}{\partial \sigma_2}, \frac{\partial g^s}{\partial \sigma_3}\right) &= \alpha_2(1 - N_\psi) \\ S_3\left(\frac{\partial g^s}{\partial \sigma_1}, \frac{\partial g^s}{\partial \sigma_2}, \frac{\partial g^s}{\partial \sigma_3}\right) &= -\alpha_1 N_\psi + \alpha_2\end{aligned}\quad (30)$$

Eqs. (14) and (15) then yield, using  $f = f^s$  (see Eq. 20):

$$\begin{aligned}\sigma_1^N &= \sigma_1^I - \lambda^s(\alpha_1 - \alpha_2 N_\psi) \\ \sigma_2^N &= \sigma_2^I - \lambda^s \alpha_2(1 - N_\psi) \\ \sigma_3^N &= \sigma_3^I - \lambda^s(-\alpha_1 N_\psi + \alpha_2)\end{aligned}\quad (31)$$

and

$$\lambda^s = \frac{f^s(\sigma_1^I, \sigma_3^I)}{(\alpha_1 - \alpha_2 N_\psi) - (-\alpha_1 N_\psi + \alpha_2) N_\phi} \quad (32)$$

We now consider tensile failure. Partial differentiation of Eq. 26 gives

$$\begin{aligned}\frac{\partial g^t}{\partial \sigma_1} &= 0 \\ \frac{\partial g^t}{\partial \sigma_2} &= 0 \\ \frac{\partial g^t}{\partial \sigma_3} &= 1\end{aligned}\quad (33)$$

Using Eq. 18, we obtain:

$$\begin{aligned}S_1(\frac{\partial g^t}{\partial \sigma_1}, \frac{\partial g^t}{\partial \sigma_2}, \frac{\partial g^t}{\partial \sigma_3}) &= \alpha_2 \\ S_2(\frac{\partial g^t}{\partial \sigma_1}, \frac{\partial g^t}{\partial \sigma_2}, \frac{\partial g^t}{\partial \sigma_3}) &= \alpha_2 \\ S_3(\frac{\partial g^t}{\partial \sigma_1}, \frac{\partial g^t}{\partial \sigma_2}, \frac{\partial g^t}{\partial \sigma_3}) &= \alpha_1\end{aligned}\quad (34)$$

Eqs. 14 and 15, with  $f = f^t$ , as given by Eq. 21:

$$\begin{aligned}\sigma_1^N &= \sigma_1^I - \lambda^t \alpha_2 \\ \sigma_2^N &= \sigma_2^I - \lambda^t \alpha_2 \\ \sigma_3^N &= \sigma_3^I - \lambda^t \alpha_1\end{aligned}\quad (35)$$

and

$$\lambda^t = \frac{\sigma_3^I - \sigma^t}{\alpha_1} \quad (36)$$

Finally, substitution of Eq. 36 for  $\lambda^t$  in Eq. 35 gives

$$\begin{aligned}\sigma_1^N &= \sigma_1^I - (\sigma_3^I - \sigma^t) \frac{\alpha_2}{\alpha_1} \\ \sigma_2^N &= \sigma_2^I - (\sigma_3^I - \sigma^t) \frac{\alpha_2}{\alpha_1} \\ \sigma_3^N &= \sigma^t\end{aligned}\quad (37)$$

After evaluation of  $\sigma_1^N$ ,  $\sigma_2^N$  and  $\sigma_3^N$ , the stress-tensor components are evaluated in the system of reference axes, assuming that the principal directions have not been affected by the occurrence of a plastic correction.



In the implementation of the Mohr-Coulomb model in the EDS scheme, an elastic guess ( $\sigma'_i$ ) is first computed by adding, to the stress components, increments calculated by application of Hooke's law to the total strain increments  $\Delta\varepsilon_{ij}$ . Principal stresses  $\sigma'_1, \sigma'_2, \sigma'_3$  and corresponding directions are then calculated.

If the stresses  $\sigma'_1, \sigma'_2, \sigma'_3$  violate the composite yield criterion (see Eqs. 20 and 21), then either  $h(\sigma'_1, \sigma'_3) \leq 0$  or  $h(\sigma'_1, \sigma'_3) > 0$  (see Eq. 27). In the first case, shear failure takes place, and  $\sigma'_1, \sigma'_2$  and  $\sigma'_3$  are evaluated from Eq. 31, using Eq. 32. In the second case, tensile failure occurs, and new principal stress components are evaluated from Eq. 37.

If the point  $(\sigma'_1, \sigma'_3)$  is located below the representation of the composite failure envelope in the plane  $(\sigma_1, \sigma_3)$ , no plastic flow takes place for this step, and the new principal stresses are given by  $\sigma'_i, i = 1, 3$ .

The stress tensor components in the system of reference axes are then calculated from the principal values by assuming that the principal directions have not been affected by the occurrence of a plastic correction.

## INCORPORATION AND MODIFICATION OF COMPLEX MODELS

The approach described above can be extended to nonlinear and (and multiple) yield surfaces. For laws in which there is a direct relation between stain increments and stress increments, the procedure is direct. For example, for the modified Cam-clay model,  $\lambda$  is found from the solution of a quadratic. In all cases, current values of stress and strain increments are input to the constitutive model, and new stresses are calculated. The constitutive model acts within each element in isolation; there are no constraints or influences on the new stresses from other elements.

Hardening and softening rules are used to update the yield surface(s) after the direct solution for stress. In this case, the position of the yield surface lags one step behind the stress state.

Detailed descriptions for the implementation of several geotechnical constitutive models in the EDS scheme are provided in the *Theory and Background* volume for FLAC3D (Itasca, 2002), including

- *hardening/softening model*, in which the strength properties harden or soften after the onset of plastic yield,
- *ubiquitous-joint model*, in which yield can occur either in the solid or along a weakness plane,
- *double-yield model*, in which both volumetric collapse and shear yield are taken into account,
- *liquefaction model* for dynamic analysis, which accounts for volumetric changes and pore pressure generation as a function of cyclic shear strain,
- *modified Cam-clay model* in which both nonlinear elasticity and hardening/softening as a function of volumetric plastic strain are included.

The source files of these constitutive models are also provided, written in the C++ language. Models can be implemented and modified by the user of FLAC or FLAC3D by compiling the source file as a dynamic link library (DLL) that can be loaded into the code whenever it is needed. The emphasis of the object-oriented approach of C++ is to provide a base class that includes a framework for implementing constitutive models, which are classes derived from the base class. In this way, users may modify existing models or write their own models, following, as a guide, the procedure described in the previous section, and implement the model as a user-written model in the same way as existing models in FLAC and FLAC3D.

The procedure to create, load and run user-written models is described in the *Optional Features* volume of FLAC3D (Itasca, 2002). An example of a user-written DLL model is described by Konietzky et al, 2001, for the case of a thermo-mechanical constitutive model to represent hydration of concrete and backfill. Cundall et al, 2003 describe the DLL implementation of the nonlinear Hoek-Brown empirical model, including a plastic flow formulation that is dependent on the confining stress level.

A built-in programming language, named FISH, is also available to provide the capability to create user-written models in the EDS scheme in two-dimensional FLAC. See the *FISH in FLAC* volume of FLAC (Itasca, 2001) for a description of this facility. Several investigators have used FISH to program and insert constitutive models into FLAC to model specific types of geological material behavior, such as swelling soil due to wetting (Noorany et al, 1999), bounding surface hypoplasticity to simulate liquefaction (Wang and Makdisi, 1999), and anhydrite swelling (Rodriguez-Ortiz et al, 2003).

## CALIBRATION OF GEOTECHNICAL MODELS

Calibration of constitutive models developed in the EDS scheme is commonly conducted by performing numerical tests that mimic laboratory experiments on the specific soil or rock of interest. The selection of the types of laboratory experiments for model calibration is very important. The following example demonstrates the calibration procedure.

The double-yield constitutive model available in FLAC and FLAC3D (see the *Theory and Background* volume of FLAC3D (Itasca, 2002)) simulates volumetric hardening corresponding to irreversible compaction; increasing the isotropic pressure causes permanent volume decrease in this model. This behavior is common in materials such as lightly cemented sands, gravels and hydraulically placed backfill.

The model includes two components of failure: volumetric yield and shear yield. In order to calibrate the model to a specific material, it is best to evaluate the parameters of each component independently. This can be done by conducting two types of triaxial test:

1. a triaxial test in which axial stress and confining stress are kept equal, and
2. a triaxial test performed at constant mean stress.



The conditions for each test can be described in terms of the generalized stress components  $p$  and  $q$ , which are related to the directional stresses,  $\sigma_{xx}$ ,  $\sigma_{yy}$ ,  $\sigma_{zz}$ , by:

$$p = -\frac{\sigma_{xx} + \sigma_{yy} + \sigma_{zz}}{3}$$

$$q = -\frac{\sigma_{yy} - \sigma_{xx}}{2} \quad (38)$$

in which  $\sigma_{yy}$  is the axial stress, and  $\sigma_{xx}$  and  $\sigma_{zz}$  are the confining stresses in the x-direction and z-direction, respectively.

For the first type of triaxial test, an isotropic compression test, the axial stress and the confining stress are kept equal, i.e.,  $\sigma_{xx} = \sigma_{yy}$  or  $q = 0$ . This loading path produces volumetric yield but no shear yield.

For the second type of triaxial test, the mean stress is kept constant, i.e.,  $p$  is constant. This corresponds to a triaxial test with only increasing deviatoric stress. In the laboratory this requires that the confining stress be adjusted during the test to maintain constant mean stress. This loading path produces shear failure but no volumetric failure, and if material hardening occurs, the shear-yielding surface will change.

### Volumetric Yield Calibration

The volumetric yielding limit in the double-yield model is defined by two material properties and a table. These are:

$p_c$  — the “cap pressure” or the maximum mean stress that a material has experienced in the past;

$R$  — the ratio of current elastic bulk modulus to the current plastic bulk modulus; and

$p_c$  versus  $e_v^p$  — the “hardening curve” or table relating  $p_c$  to the plastic volumetric strain.

$p_c$  is the current location of the volumetric yield surface. If a material is overconsolidated,  $p_c$  may start at an initial preconsolidation stress,  $p_c^0$ . The parameter  $R$  controls the slope of the mean stress versus volumetric strain on volumetric unloading. (This is termed the “swelling” line in soil mechanics.)

As a material becomes more compact, its plastic stiffness ( $dp_c/de_v^p$ ) usually increases; it seems reasonable that the elastic stiffness will also increase, since the grains are being forced closer together. A simple rule is adopted whereby the incremental elastic stiffness,  $K_c$ , is a constant factor multiplied by the current incremental plastic stiffness: this factor is termed  $R$  and is greater than unity. The elastic constants are derived from  $R$  and the given table of  $p_c$  versus  $e_v^p$ , rather than using the given (input) bulk and shear moduli,  $K$  and  $G$ . The given moduli, however, serve two other purposes: first, they act as upper limits to the moduli computed

using  $R$ ; second, they determine a ratio of  $G/K$ . Only  $K_c$  is determined from the table and  $R$ ;  $G_c$  is then computed from it, by referring to the given  $K/G$  ratio.

Specifically:

$$K_c = R \frac{dp_c}{de_v^p} \quad K_c := \min(K_c, K) \quad G_c = G \frac{K_c}{K} \quad (39)$$

where  $K, G$  are input moduli;

$K_c, G_c$  are the current moduli used by the model; and

$dp_c / de_v^p$  is the current slope of the table  $p_c$  values versus  $e_v^p$  values.

The “hardening curve” and ratio,  $R$ , of elastic bulk modulus to plastic bulk modulus are volumetric parameters that may be derived from the isotropic compression test.

For example, consider the experimental graph of pressure versus volumetric strain, for an increasing stress level, with a small unloading excursion, as shown in Figure 5. The volumetric strain increment,  $de_v$ , at a point on the main loading path (assuming that we are above any preconsolidation stress level,  $p_c^0$ ) is composed of an elastic part,  $de_v^e$ , and a plastic part,  $de_v^p$ .

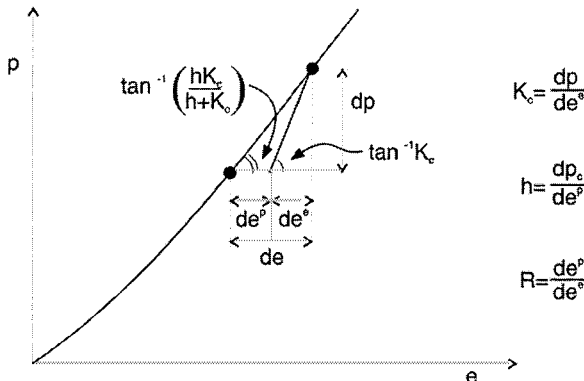


FIG. 5. Isotropic Consolidation Test ( $q=0$  and  $de=de_v$ )

Denoting the current plastic modulus by  $h$  and the current elastic modulus by  $K_c$ , the observed tangent modulus is of the form:

$$\frac{dp}{de_v} = \frac{hK_c}{h + K_c} \quad (40)$$

where  $e_v$  is the *total* volumetric strain. (Note that  $e = e_v$  in Figure 5.)

@Seismicisolation

We define  $R = K_c/h$ , thus:

$$\frac{dp}{de_v} = \frac{K_c}{1 + \frac{K_c}{h}} = \frac{K_c}{1+R} \quad (41)$$

Therefore:

$$1+R = \frac{K_c}{(dp/de_v)} \quad (42)$$

or

$$R = \frac{K_c}{(dp/de_v)} - 1 \quad (43)$$

From a loading/unloading cycle,  $K_c$  and  $(dp/de_v)$  can be determined and hence  $R$ . The loading table values  $(dp_c^P/de_v^P)$  can then be determined simply by multiplying the values from the loading/unloading curve by a constant factor – i.e.:

$$\frac{dp_c}{de_v^P} = h = \left\{ \frac{1+R}{R} \right\} \frac{dp}{de_v} \quad (44)$$

From this, it follows that values of  $p_c$  for a particular  $e_v^P$  can be obtained, to the first approximation, by multiplying the value  $p$  on the graph corresponding to  $e_v = e_v^P$  by the ratio  $(1+R)/R$ . For example, if  $R = 5$ , then the graph curve must be scaled by a factor of 1.2 to convert it to table values, assuming no over-consolidation.

Calibration of the double-yield model is typically done by conducting a single-element numerical test, exercising the model over stress paths similar to the physical tests and plotting similar graphs for comparison. An example illustrating the calibration of the volumetric yield parameters using this procedure is given in the *Theory and Background* volume of FLAC3D (Itasca, 2002).

### Shear Yield Calibration

Shear yield in the double-yield model is identical to the Mohr-Coulomb model with optional material hardening or softening. Shear yield properties (cohesion and friction) for a non-hardening material are conventionally obtained from the slope and intercept in a shear stress versus normal stress plot. Alternatively, shear yield can also be expressed in terms of  $p$  and  $q$ , i.e.:

$$\frac{q}{p} = M = \frac{\frac{1}{2}(\sigma_1 - \sigma_3)}{\frac{1}{3}(\sigma_1 + 2\sigma_3)} \quad (45)$$

in which  $\sigma_1$  and  $\sigma_3$  are the major and minor principal stresses.



Note that for cohesionless sand, at yield  $\sigma_1$  and  $\sigma_3$  can be related through the Mohr Coulomb criterion:

$$\sigma_1 = \sigma_3 N_\phi \quad (46)$$

Substituting Eq. 46 and 45 yields:

$$M = \frac{3 \sin \phi}{3 \sin \phi} \quad (47)$$

Therefore:

$$\phi = \sin^{-1} \left( \frac{3M}{3 + M} \right) \quad (48)$$

For a triaxial test at constant mean stress, an ultimate value of  $q$  can be determined directly from laboratory data. The ratio of  $q$  and  $p$  gives  $M$ , and hence  $\phi$ , by using Eq. 45 and 48.

If experimental data show signs of strength hardening (or softening), this procedure has to be modified. The hardening (or softening) of the shear yield surface can be controlled by hardening parameters that record some measure of accumulated plastic strain.

The hardening parameter is defined as:

$$\Delta e^{ps} = \left\{ \frac{1}{2} (\Delta e_1^{ps} - \Delta e_m^{ps})^2 + \frac{1}{2} (\Delta e_m^{ps})^2 + \frac{1}{2} (\Delta e_3^{ps} - \Delta e_m^{ps})^2 \right\}^{\frac{1}{2}} \quad (49)$$

in which  $\Delta e_m^{ps} = \frac{1}{3} (\Delta e_1^{ps} + \Delta e_3^{ps})$ , and  $\Delta e_1^{ps}$  and  $\Delta e_3^{ps}$  are the major and minor principal (plastic shear) strains.

The hardening parameters are used in look-up tables to determine new values of shear strength parameters. The new parameters are then used in the next step for the Mohr Coulomb yield criterion. Therefore, the look-up tables are part of the input parameters that need to be acquired from experimental data.

In a  $p$ - $q$  diagram a hardening situation is described as a change in the slope of the yield-surface line. Increasing slope means strength hardening and decreasing slope strength softening. As discussed above for non-hardening cases, the slope of the yield line can be related to the friction angle. If the plastic shear strain associated with a specific  $q/p$  ratio can be found, a hardening table for the friction angle can be obtained. The plastic shear strain can be calculated if the mean stress is kept constant and an unloading step is applied. By keeping mean stress constant, we are assured that no volumetric strain is generated, and the plastic strain is solely due to shearing. The unloading allows the elastic recoverable strain to be separated from the total strain in order to calculate the plastic strain component.

For example, consider a hardening cohesionless material subjected to several loading/unloading cycles during a constant-mean-stress test. The axial and radial

strains are monitored throughout the test. At an unloading point, the  $q/p$  ratio is found and the mobilized friction angle is calculated using Eq. 48. When the sample is totally unloaded, the axial and radial plastic strains are equal to the total strains because the elastic strains are completely recovered. The plastic strains are then used in Eq. 49 to calculate the hardening parameter.

Single-element numerical tests exercising the model over stress paths similar to the constant mean stress tests can be used to calibrate the shear yield component in a similar fashion to that for the volumetric yield component.

### Comments on Testing

It is important to note that conventional triaxial testing does not separate shear and volumetric failure modes. For example, the loading paths for uniaxial strain testing and for triaxial testing done at constant confining stress include both shear and volumetric loading components. For this reason, uniaxial strain tests and triaxial tests at constant confining stress are not recommended to calibrate shear and volumetric parameters; the dependency between shear and volumetric response will influence the parameter values.

Unfortunately, the triaxial tests described above to calibrate for volumetric yield and shear yield are not commonly performed. It is more usual to conduct uniaxial strain testing than testing at equal axial and confining stress, because uniaxial strain testing (i.e., the odometer test) is so simple to perform. Likewise, the triaxial test at constant confining stress is the most common test for studying strength. The triaxial test at constant mean stress requires more control and monitoring of radial strain, which can be difficult to accomplish. If only uniaxial strain testing data are available, it may be possible to derive volumetric yield parameters,  $R$  and  $p_c$ , that best fit these results. However, the procedure becomes more complicated and it is very difficult to assess the influence of shear strain on the volumetric parameters. Thus, the level of confidence that can be placed in properties derived from uniaxial strain testing is limited. The same can be said for the derivation of frictional properties from triaxial testing at constant confining stress. The influence of volumetric yielding on shear strength properties cannot be assessed. Data from at least one of the recommended triaxial test types are required in order to separate volumetric behavior from shear behavior.

### FINAL REMARKS

By using the EDS scheme it is practical for modelers to implement and modify a constitutive model to simulate specific behaviors of geological materials. It is recommended that the most appropriate model is the simplest one consistent with producing the mechanism(s) of interest. For example, the double-yield model described above is a simplified model for volumetric and shear yielding. In order to calibrate the model, numerical tests should be conducted that evaluate the mechanisms individually. The ability of the model to represent these mechanisms can then be readily assessed in the EDS scheme.

If the assumptions of the selected model are not sufficient to explain entirely the observed deformation and yield response of the material, these assumptions can be modified directly or a different model implemented and tested in the EDS scheme.



## REFERENCES

- Cundall, P., Carranza-Torres, C. and Hart, R. (2003). "A new constitutive model based on the Hoek-Brown criterion." *Proc. 3rd Int. FLAC Symposium*, R. Brummer, et al., eds., A. A. Balkema Publishing, 17-25.
- Cundall, P. A. (1987). "Distinct element models of rock and soil structure." *Analytical and Computational Methods in Engineering Rock Mechanics*, Chapter 4, E. T. Brown, ed., Allen & Unwin, London, 129-163.
- Cundall, P. A. (1974). "Rational design of tunnel supports: a computer model for rock mass behaviour using interactive computer graphics for the input and output of geometrical data." *Technical Report MRD-2-74*, U.S. Army Corps of Engineers, Missouri River Division.
- Cundall, P. A. (1971). "A computer model for simulating progressive large scale movements in blocky rock systems." *Proc. of the Symposium of the Int. Society for Rock Mechanics*, Vol. 1, Paper No. II-8.
- Itasca Consulting Group, Inc. (2001) *FLAC (Fast Lagrangian Analysis of Continua), Version 4.0*, Manual, ICG, Minneapolis.
- Itasca Consulting Group, Inc. (2002) *FLAC3D (Fast Lagrangian Analysis of Continua in 3 Dimensions), Version 2.1*, Manual, ICG, Minneapolis.
- Konietzky, H., et al. (2001). "A thermo-mechanical constitutive law for modeling the hydration of concrete and backfill and its practical application using the parallel version of FLAC3D." *Proc. 2nd Int. FLAC Conference*, D. Billaux, et al., eds., A. A. Balkema Publishing, 15-20.
- Noorany, I., Frydman, S. and Detournay, C. (1999). "Prediction of soil slope deformation due to wetting." *Proc. FLAC and Numerical Modeling in Geomechanics*. C. Detournay and R. Hart, eds., A. A. Balkema Publishing, 101-107.
- Rodriguez-Ortiz, J. M., Varona, P. and Velasco, P. (2003). "Modeling of anhydrite swelling with FLAC." *Proc. 3rd Int. FLAC Symposium*, R. Brummer, et al., eds., A. A. Balkema Publishing, 55-62.
- Wang, Z.-L., and Makdisi, F. I. (1999). "Implementing a bounding surface hypoplasticity model for sand into the FLAC program." *Proc. FLAC and Numerical Modeling in Geomechanics*, C. Detournay and R. Hart, eds., A. A. Balkema Publishing, 483-490.

## NORSAND: FEATURES, CALIBRATION AND USE

Michael G Jefferies<sup>1</sup>, C.Eng. & Dawn A Shuttle<sup>2</sup>, C.Eng., MASCE

**ABSTRACT:** NorSand is a generalized critical state model for soil based on the state parameter  $\phi$  and incorporating familiar ideas in geomechanics, some of which date back more than a century. NorSand has associated plasticity but dilates similarly to actual soil through the introduction of limited hardening. Limited hardening causes yield in unloading, replicating observed soil behavior with second order detail. Principal stress rotation always softens NorSand, realistically representing cyclic loading effects. NorSand is a sparse model with just eight soil properties required to capture these many aspects of soil behavior over a wide range of density and confining stress. It has been validated over a range of conditions, including the practically important case of plane strain. The paper provides an introduction to NorSand, describing the idealizations and illustrating model performance/ validation. Determining soil properties and  $\phi$  is discussed. Finally, implementing NorSand within finite element codes is reviewed. A spreadsheet with VBA open source code implementation of NorSand for common laboratory tests can be downloaded from the UBC website.

### INTRODUCTION

A striking feature of soil is that it exists over a spectrum of void ratio and that the actual void ratio (or the alternate identity, density) affects the soil's constitutive behavior. Obviously, a proper constitutive model for soil must explain the changes in soil behavior caused by changes in its void ratio. Recognition of the importance of void ratio to behavior of soil, or more generally any particulate media, goes back at least a century to Reynolds (1885). The seminal advance for constitutive modelling

---

<sup>1</sup> Golder Associates Ltd, Burnaby & Visiting Professor, UMIST  
geomek@hotmail.com

<sup>2</sup> Associate Professor, University of British Columbia, Vancouver  
dshuttle@civil.ubc.ca

was nearly fifty years ago in the widely recognized plasticity framework put forward by Drucker, Gibson & Henkel (1957). There have been several developments of the basic framework, with arguably the most influential being what has become known as *Critical State Soil Mechanics* (CSSM). Various workers have contributed to the critical state theory, and there is now a substantial literature. Cam Clay (Schofield & Wroth, 1968) is arguably the most widely taught model for soil.

Although critical state models explain the effect of void ratio on soil behavior, and they have had some notable successes as in, for example, explaining the effect of overconsolidation on clay strength, critical state models fell out of favor. The basic problem is neither Cam Clay, nor the various variants of Modified Cam Clay, dilate anything like actual dense soils. And dense soils, whether overconsolidated clays or sands, are materials of much practical interest for engineered construction. These original critical state models also poorly predict the behavior of loose sands, and liquefaction-related behaviors in particular.

The limitations of the original CSSM models are not a limitation of the framework itself. Been & Jefferies (1985, 1986) presented data showing that the peak dilation of various sands was uniquely related to the difference between the soils current void ratio and that of its critical state at the same mean stress, represented by the state parameter  $\lambda$ . Figure 1 shows an updated version of observed behaviors and which includes some twenty two different sands whose silt fraction ranges from none (in the case of laboratory standard reference sands) to as much as 25% (sands used in construction). There are more than two hundred triaxial tests on Figure 1. In effect Figure 1 steps back to a basic proposition of the CSSM, that soil behavior should scale with deviation from the critical state, and it is apparent from the figure that there are strong and simple trends. The critical state is substantially relevant to the behavior of dense soils.

Figure 1 has become key in the development of models that accurately capture the effect of void ratio on soil behavior. There are now several such models based on  $\lambda$ , either implicitly or explicitly (for example, Manzari & Dafalias 1997; Wan & Guo 1998; Li et al 1999; Gajo & Wood 1999). NorSand was the first of these models and is the subject of this Paper.

NorSand originated from observations about sand behavior, and especially large scale hydraulic fills. However, the model is particulate and is applicable to any soil in which particle to particle interactions are controlled by contact forces and slips rather than bonds. Current applications of NorSand range from well-graded tills through sands to clayey silts. These applications will be illustrated later.

In what follows a compression positive convention is adopted, with the bar superscript denoting effective stress. Most of the notation used is standard and a complete list of notation is given at the end of the paper.

## OVERVIEW OF NORSAND

### Idealizations

Critical state soil mechanics is based on two axioms, often unstated, but which define the framework: (1) a unique critical state locus (CSL) exists; (2) soils move to the CSL with shear strain. Axiom 1 is still regarded as controversial by some, but invariably this traces back to workers who confuse what is variously called the *phase*



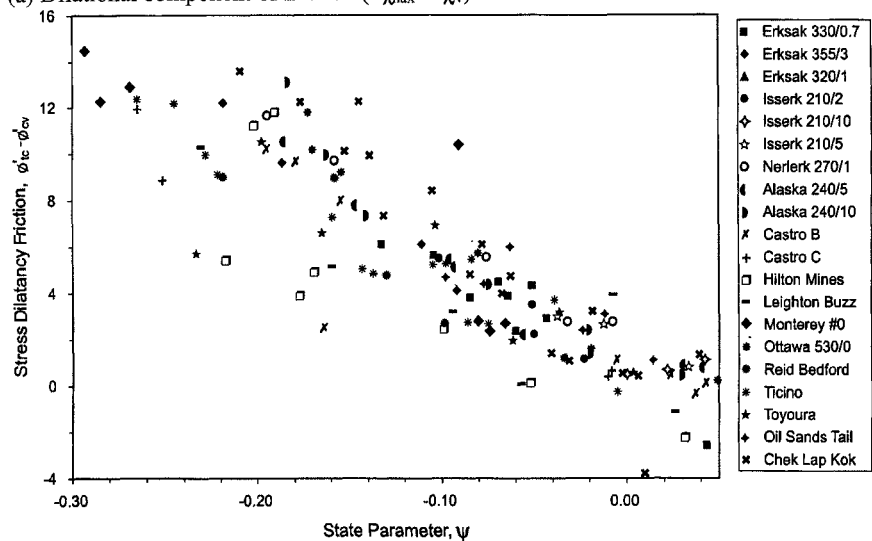
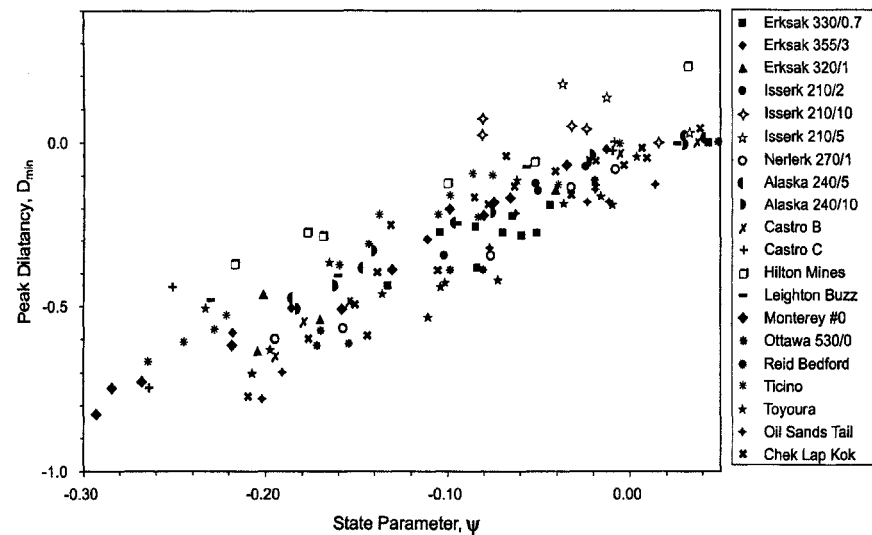
(a) Dilatational component of friction ( $I\gamma_{\max} - I\gamma_v$ )(b) Dilation at peak strength,  $D_{\min}$ 

FIG. 1. Sand strength and peak dilatancy in drained triaxial compression as a function of the state parameter

*transition condition* or the *pseudo steady state* with the critical state. A detailed experimental investigation of the critical state locus (CSL) was given in Been et al (1991, 1992), and which addresses issues of uniqueness in particular.

The several variants of the Cam Clay and Modified Cam Clay models of CSSM are based on the original insights about appropriate plasticity theory for soil put forward by Drucker et al (1957). These idealized CSSM models assume that the yield surface always intersects the CSL in the  $e - \bar{\varsigma}_m$  plane. Isotropic compression behavior then becomes the hardening law for all stress paths, and gives the models their predictive power for the effect of void ratio and pressure changes. But, the requirement for intersection of any yield surface with the CSL is also why these models cannot simulate most real soils.

NorSand is also an idealized critical state model and with four further ideas:

- ξ There are an infinity of possible yield surfaces in  $e - \bar{\varsigma}_m$  space such that any yield surface does not necessarily intersect the CSL, with the position of the current yield surface in the  $e - \bar{\varsigma}_m$  space being defined by  $\therefore$
- ξ The state parameter  $\therefore$  tends to zero (intersection of the yield surface with the CSL) as shear strain accumulates, ensuring compliance with Axiom 2 of critical state theory
- ξ The minimum possible dilation rate is linearly related to  $\therefore$
- ξ Principal stress rotation always softens (shrinks) the yield surface

The first of the ideas stems directly from the existence of an infinity of normal compression loci (NCL) in any soil. This is the opposite of what is found in most text books on soil behavior and in which the NCL is shown as a single surface that parallels the CSL in  $e - \bar{\varsigma}_m$  space. An infinity of NCL was first suggested by Ishihara et al. (1975) based on laboratory experiments. Field data from hydraulic filling of offshore landfill islands, which were patently normally consolidated because of underwater hydraulic fill placement, gave large-scale evidence for such an infinity of NCL (Stewart et al, 1983). Jefferies & Been (2000) presented detailed experimental evidence of this aspect of soil behavior.

An infinity of NCL forces two parameters to characterize the state of a soil:  $\therefore$  and  $R$ . The state parameter  $\therefore$  is a measure of the location of an individual NCL in  $e - \bar{\varsigma}_m$  state space, which is the second idea above. The overconsolidation ratio  $R$  represents the proximity of a state point to its yield surface when measured along the mean effective stress axis. The variable  $\bar{\varsigma}_{m,\max}$  is the equivalent maximum mean effective stress experienced by the soil, which might be thought of as a pre-consolidation pressure (although that term is commonly applied in the sense of vertical effective stress). Note in particular that  $R$  and  $\therefore$  are not alternate identities as is implied by Cam Clay or its variants;  $R$  and  $\therefore$  represent measures of different things and as illustrated on Figure 2.

The third idea implements the experimental observations presented on Figure 1, although it can be equally well argued as a first-order expectation from the axioms of CSSM theory (a soil denser than critical must dilate to reach the critical condition).



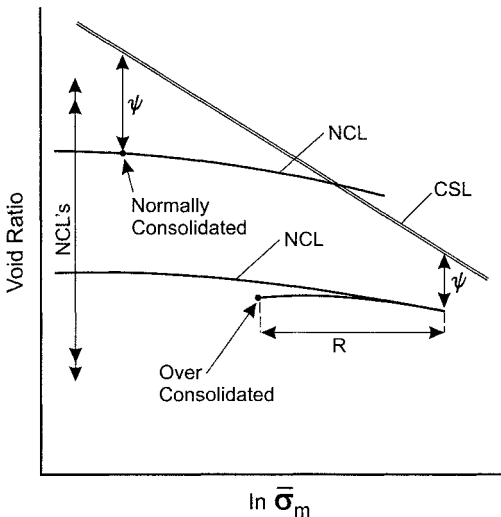


**FIG. 2. Definition of state parameter  $\psi$  and overconsolidation ratio  $R$**

The fourth idea is more subtle. Since plasticity is an abstraction of the underlying micromechanical behavior, and grain contacts align to carry the imposed principal stresses, it follows that any rotation of the major principal stress will result in load being applied at sub-optimal grain contact arrangements. This implies softening of the yield surface, as illustrated on Figure 3.

Because NorSand (like the Cam Clay variants) idealizes plastic work dissipation it is essential to use work conjugate stress and strain measures for self-consistency of the model. This requires a different deviatoric strain invariant from that commonly used in finite element analysis:

$$H_q = \frac{1}{3} (\sin T - \sqrt{3} \cos T) H_1 + 2 \sin T H_2 + (\sin T + \sqrt{3} \cos T) H_3 \quad (1)$$

Notice that (1) is defined in terms of incremental strain and uses the current Lode angle. It is also linear, allowing decomposition of strain into elastic and plastic components within the invariant. Although uncommon, this strain invariant is some twenty years old having been first suggested by Resende & Martin (1985).

### Model Description

The critical state, which is the condition at which the soils deforms continuously and indefinitely at constant volume, is used as the reference framework. The void ratio of the critical state  $e_c$  depends on the mean effective stress  $\bar{\sigma}_m$ , and various relationships have been proposed for this. These different relationships are details, and preference for one relationship over another to fit the behavior of a particular soil is only an issue for calibration as the basic framework of NorSand is unchanged. For many purposes the familiar  $e_c = C \ln(\bar{\sigma}_m)$  idealization is both simple and sufficiently accurate.

@Seismicisolation

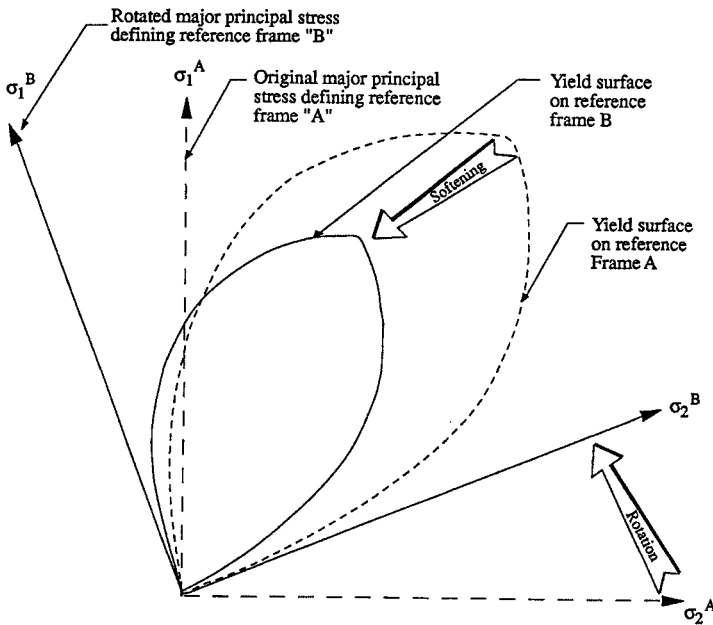


**FIG. 3. Yield surface softening induced by principal stress rotation**

The critical state is also a relationship between mean and shear stress, and this has been extensively investigated. To a high precision and high stress levels, the critical state is fitted by  $\bar{\zeta}_{q,c} M \bar{\zeta}_{m,c}$  (where the subscript 'c' denotes critical conditions and  $M$  is a soil property). More precisely,  $M$  varies with the proportion of intermediate principal stress (usually given as the Lode angle) and the soil property is conventionally defined under triaxial compression conditions as  $M_{tc}$  with the subscript 'tc' being used to indicate this. Although the variation in peak strength with Lode angle has been investigated for several soils, there has been far less investigation of  $M$  itself. Jefferies & Shuttle (2002) suggested that  $M$  be taken as an average of the Mohr-Coulomb and Matsuoka & Nakai (1974) criteria, but this is only a first estimate and there is evidence that  $M$  in triaxial extension is less than either of these criteria indicate. Further experimental data in this area would be helpful.

NorSand is a plasticity model for soil. As such, and in common with other plasticity models, it comprises three items: (1) a yield surface; (2) a flow rule; and, (3) a hardening law. These three aspects of the NorSand model are described below, with the equations of the model equations summarized on Table 1. The version of the NorSand presented here corresponds to the modified version given in Jefferies & Shuttle (2002), with the extension for plastic yield in unloading based on Jefferies (1997) and the implementation of principal stress rotation after Been et al (1993).

The NorSand yield surface has the familiar bullet-like shape of the classical Cam Clay model but with one important difference – there is an internal cap so that the soil cannot unload to very low mean stress without yielding. This internal cap is taken as a flat plane, and its location depends on the soil's current state parameter. Figure 4 illustrates the NorSand yield surface for two cases, a very loose soil and a very dense soil. As is also illustrated on Figure 4, the location of the internal cap controls the limiting stress ratio  $K_L$  that the soil can sustain; what is sometimes called the *Hvorslev Surface* is seen to be merely a hardening limit for the true yield surface. This internal cap is no more than a strict implementation of the ideas of Drucker et al (1957), and gives realistic dilatancy with normality.

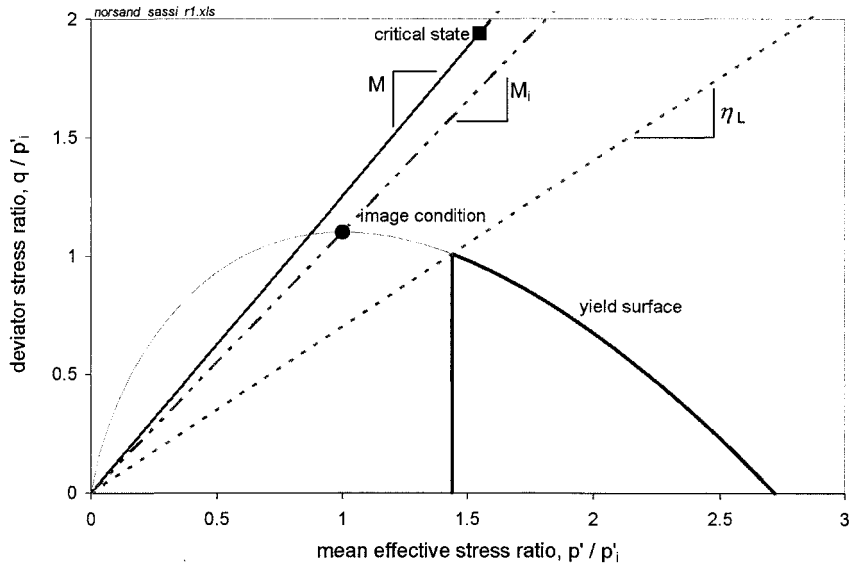
The plastic dilatancy  $D^p$  is determined from the idealized stress-dilatancy relationship that underlies the model, but as there are three strain rates this is insufficient to determine each of them. The intermediate principal strain rate is therefore interpolated depending on the Lode angle. This interpolation approach is somewhat unusual for plasticity models, but is taken to ensure consistency with the work dissipation postulate that is the basis of the model.

The third aspect of the model is the hardening law, which describes how the yield surface increases or decreases in size with plastic straining. The size of the yield surface is controlled by what is termed the image stress  $\bar{\sigma}_{m,i}$  and which forms the object of the hardening law. It is called the image stress because it represents a situation in which one of the two conditions for the critical state is met, and the meaning is readily apparent from Figure 4. The image condition is what others refer to as the pseudo steady state, although there is nothing pseudo about it.

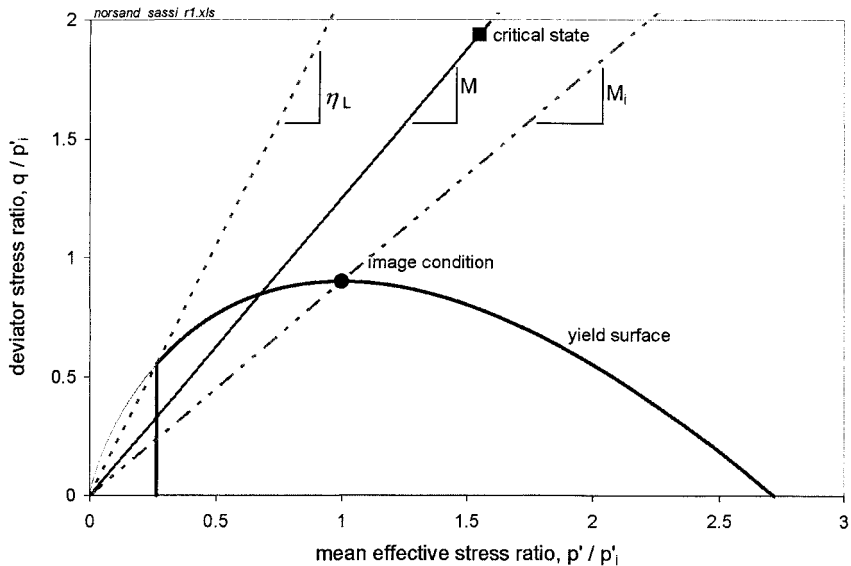
NorSand is an isotropic model hardening which expands or contracts the yield surface, as required by the hardening law, while retaining its shape. The position of the internal cap evolves with the changing state parameter. Whether the yield surface hardens or softens depends on two things: the current state parameter; and, the direction of loading. Loading past the internal cap always softens the yield surface, as does principal stress rotation. However, the key determinant in the general hardening is the state parameter. As illustrated on Figure 4, the critical state does not usually intersect the yield surface (this is the largest single difference between NorSand and Cam Clay). This divergence of yield surface from critical state is used as the basis of the hardening law, and the hardening law acts to move the yield surface towards the critical state under the action of plastic shear strain – which directly captures the essence of critical state principles.

Elasticity in soils is arguably a more complicated aspect than plasticity. Various elastic models can be used depending on the tradeoff between complexity and accuracy. Pestana & Whittle (1995) looked at elastic models that accounted for the effect of void ratio in some detail with Jefferies & Been (2000) suggesting a further refinement. However, for most situations involving soil modelling this sophistication is unwarranted. On one hand the soil fabric (grain arrangement) substantially affects modulus and thus elastic modulus should be measured insitu. On the other hand, plastic strains often dominate. For most purposes a simple constant shear rigidity  $I_r$  and constant Poisson's ratio is a sufficient representation of elasticity and this approach is used here. This is equivalent to the constant N idealization of the classic CSSM models.





(a) Very loose sand



(b) Very dense sand

**FIG. 4. Illustration of NorSand yield surfaces and limiting stress ratios**

**@Seismicisolation**

**TABLE 1. Summary of NorSand**

Internal Model Variables	$\psi_i = \psi + \lambda \ln(\bar{\sigma}_{m,i}/\bar{\sigma}_m)$ where $\psi = e - e_c$ $M_i = M -  \psi_i $
Critical State	$e_c = \Gamma - \lambda \ln(\bar{\sigma}_m)$ AND $\eta_c = M = (M_{MC} + M_{MN})/2$ where $M_{MC} = (3\sqrt{3})/(\cos\theta(1+6/M_{tc}) - \sqrt{3}\sin\theta)$ and $\frac{27 - 3M_{MN}^2}{3 - M_{MN}^2 + 8/9M_{MN}^3 \sin(\theta)(3/4 - \sin^2(\theta))} = \frac{27 - 3M_{tc}^2}{3 - M_{tc}^2 + 2/9M_{tc}^3}$
Yield Surface & Internal Cap	$\frac{\eta}{M_i} = 1 - \ln\left(\frac{\bar{\sigma}_m}{\bar{\sigma}_{m,i}}\right)$ with $\left(\frac{\bar{\sigma}_{m,i}}{\bar{\sigma}_m}\right)_{\max} = \exp(-\chi_{tc}\psi_i/M_{i,tc})$
Hardening Rule	<i>On outer yield surface:</i> $\frac{\dot{\bar{\sigma}}_{m,i}}{\bar{\sigma}_{m,i}} = H \frac{M_i}{M_{i,tc}} \left( \frac{\bar{\sigma}_m}{\bar{\sigma}_{m,i}} \right)^2 \left[ \left( \frac{\bar{\sigma}_{m,i}}{\bar{\sigma}_m} \right)_{\max} - \frac{\bar{\sigma}_{m,i}}{\bar{\sigma}_m} \right] \dot{\varepsilon}_q^p$ <i>On internal cap:</i> $\frac{\dot{\bar{\sigma}}_{m,i}}{\bar{\sigma}_{m,i}} = - \frac{H}{2} \frac{M_i}{M_{i,tc}} \left  \dot{\varepsilon}_q^p \right $ <i>During principal stress rotation:</i> $\frac{\dot{\bar{\sigma}}_{m,i}}{\bar{\sigma}_{m,i}} = -H_r \frac{\dot{\alpha}}{\pi}$
Stress Dilatancy & Plastic Strain Rate Ratios	$D^p = \dot{\varepsilon}_q^p / \dot{\varepsilon}_q^p  M_i - \eta  \Rightarrow D_{tc}^p = D^p M_{i,tc} / M_i$ and $D_{te}^p = D^p M_{i,te} / M_i$ define $z_{3,tc} = \frac{2D_{tc}^p - 3}{6 + 2D_{tc}^p}$ and $z_{3,te} = \frac{2D_{te}^p - 6}{3 + 2D_{te}^p}$ $\Rightarrow \frac{\dot{\varepsilon}_3}{\dot{\varepsilon}_1} = z_{3,tc} - (z_{3,tc} - z_{3,te}) \cos(\frac{3\theta + 90}{2})$ define $a = (\sin\theta + \sqrt{3}\cos\theta)/3$ , $b = -2\sin\theta/3$ , $c = (\sin\theta - \sqrt{3}\cos\theta)/3$ $\Rightarrow \frac{\dot{\varepsilon}_2}{\dot{\varepsilon}_1} = (aD^p - 1 + \frac{\dot{\varepsilon}_3}{\dot{\varepsilon}_1}(cD^p - 1))/(1 - bD^p)$
Elasticity	$I_r = \frac{G}{\bar{\sigma}_m}$ with $K = \frac{2(1+\nu)}{3(1-2\nu)} G$

## Parameters and Soil Properties

NorSand is a sparse model. For the variant presented here, in which the CSL has been taken as the approximate semi-log form and with the simplest representation of elasticity, there are eight model properties. These are summarized on Table 2 with typical ranges in values for sands indicated. How to determine these soil properties is presented later in the paper after the model performance has been illustrated, and examples of calibrated parameter sets are given then. All the properties are dimensionless, although  $\Gamma$  has a reference stress level associated with it. Several of the parameters are familiar including  $\Gamma$ ,  $\lambda$ ,  $M_{tc}$ ,  $I_r$ , and  $\nu$  and as such require no further comment. Only three parameters may be unfamiliar.

The parameter  $\chi_{tc}$  is the slope of the trend line for minimum dilatancy in Figure 1(b). In the original version of NorSand this trend was thought to be a model constant. But, further data has shown that  $\chi_{tc}$  varies somewhat from soil to soil and could also be a function of soil fabric. The reference condition is taken as triaxial compression because dilatancy is itself a function of Lode angle.

The plastic hardening modulus  $H$  can in principle be a function of soil fabric, and data to date suggests that it is also a function of  $\psi$ . Figure 5 shows some data illustrating these aspects. There is some evidence that  $H$  is proportional to  $1/(\lambda - \kappa)$  and which is what might be anticipated from analogy to Cam Clay. On the other hand, such a linkage should also be anticipated to be affected by soil fabric.

The plastic softening modulus for principal stress rotation,  $H_r$ , like  $H$ , might also be expected to vary with  $\psi$ .  $H_r$  may also be related to  $H$ . At the present there have been insufficient experiments simulated with NorSand to establish convincing trends, and no relationships have been discovered using self-consistency criteria. For the moment, therefore,  $H_r$  is treated as a soil property in its own right, representing the amount of damage to the hardened yield surface that is caused by rotation of principal stress.

**TABLE 2. NorSand Soil Properties with Typical Range for Sands**

<i>Property</i>	<i>Typical Range</i>	<i>Remark</i>
<i>CSL</i>		
$\Gamma$	0.9 – 1.4	‘Altitude’ of CSL, defined at 1 kPa
$\lambda$	0.01 – 0.07	Slope of CSL, defined on base e
<i>Plasticity</i>		
$M_{tc}$	1.2 – 1.5	Critical friction ratio, triaxial compression as reference condition
$H$	50 – 500	Plastic hardening modulus for loading, often $f(\psi)$
$H_r$	15 – 30	Plastic softening modulus for principal stress rotation
$\chi_{tc}$	2.5 – 4.5	Relates minimum dilatancy to $\psi$ . Often taken as 3.5. Triaxial compression as reference condition
<i>Elasticity</i>		
$I_r$	100-800	Dimensionless shear rigidity
$\nu$	0.1 – 0.3	Poisson’s ratio, commonly 0.2 adopted

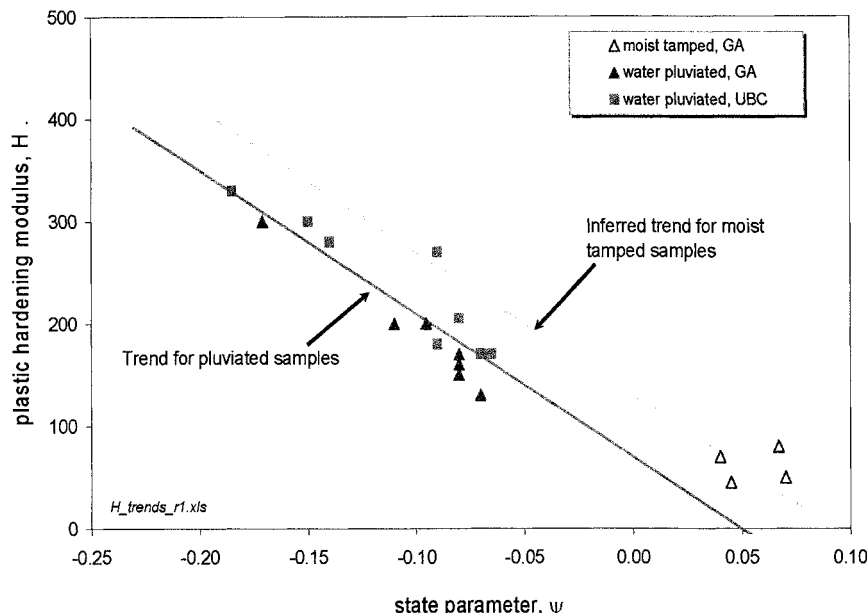


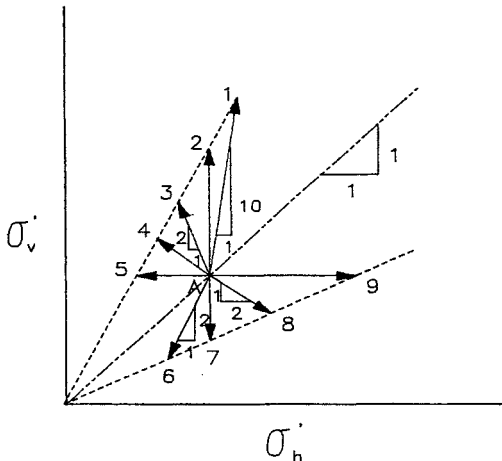
**FIG. 5. Trend in plastic hardening modulus with  $\psi$  for Erksak sand**

There is less experience at applying NorSand to silts and clays, with work in this area being recent. Some calibrated parameter sets are presented later. What can be noted is that with well-graded sandy silts the dilatancy parameter  $\chi_{tc}$  takes much greater values, presumed to be a consequence of less void ratio space between  $e_c$  and  $e_{min}$  with such soils.  $H$  seemingly scales with  $1/(\lambda - \kappa)$  as noted earlier.

### NORSAND PERFORMANCE (VALIDATION)

NorSand has been used to simulate the behavior of many soils. A particularly interesting set of data, from the viewpoint of model validation, are tests on Erksak sand at UBC (Sasitharan, 1989; Vaid & Sasitharan, 1992). These tests explored the effect of stress path on dilatancy, and were carried out using triaxial equipment that could impose various chosen stress paths as illustrated on Figure 6. NorSand was calibrated to a dense test under standard drained compression, as shown on Figure 7, giving the parameter set  $M_{tc}=1.26$ ,  $\chi_{tc}=4.1$ ,  $I_1=500$  and  $H=205$ .

With the calibration established, the soil properties were left constant and other tests for different densities and paths predicted. The prediction for the effect of changing density is shown on Figure 7, as is the results for two samples in the different Paths 3 and 5. Excellent similarity between model and data is evident.

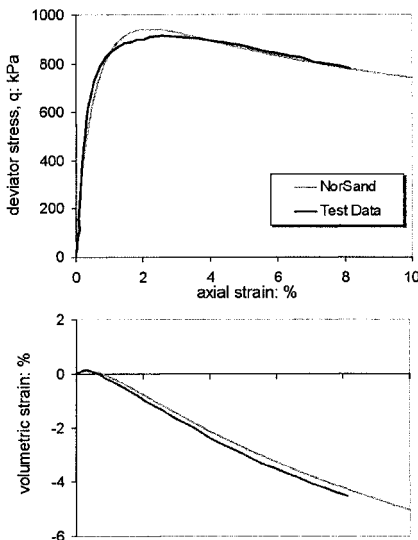
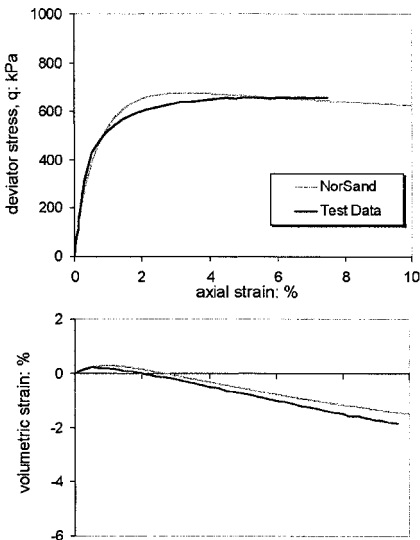
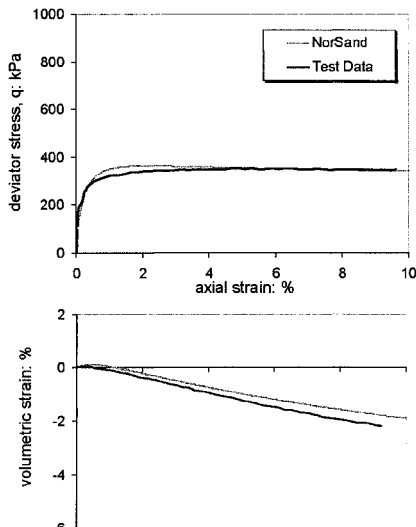
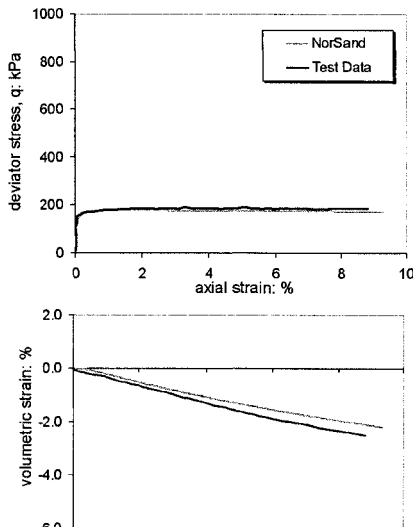


**FIG. 6. Stress paths used in UBC tests on Erksak sand (after Sasitharan, 1989)**

Extension tests, which are the load paths 6-8 inclusive, impose two changes on the sand. First, the intermediate principal stress and strain now equal the major rather than minor principal values. The change in stress conditions affects  $M$ , as discussed earlier. Second, this change in strain conditions makes the axial strain now the minor, not major, principal value. The standard stress-strain plots found in the literature for extension tests compare deviator stress with minor principal strain.

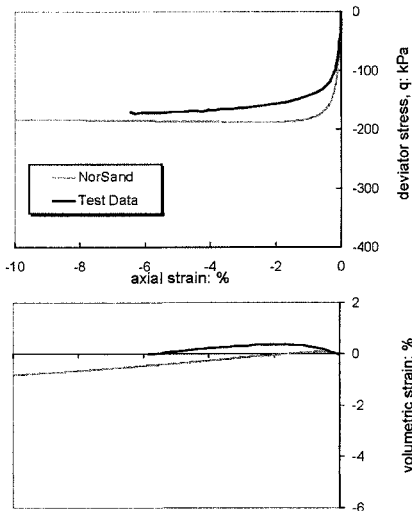
The predictions of the NorSand model for Paths 7 and 8 are shown on Figure 8, again using the triaxial compression calibration. Both tests are weaker, softer, and less dilatant than predicted by NorSand. That NorSand is too strong in triaxial extension is unsurprising given that it presently uses the same friction angle in triaxial extension as compression. If this conventional wisdom is neglected and instead a value of  $M$  used in keeping with the test data, then the fit of model to the tests is improved as also shown on Figure 8 using  $M_{te}=0.82$ . The hardening modulus was also reduced to get the best fit in triaxial extension. As the UBC pluviated samples are known to be markedly anisotropic, it is not entirely surprising that  $H$  might need to change from compression to extension loading because of the  $90^\circ$  change in principal stress. A good fit is obtained by reducing hardening to  $H=85$ .

Test Path 6 is unusual compared to the other paths as, for NorSand, it represents initial unloading. The simulation using the best-fit parameter set for the other extension tests is shown on Figure 9. An equivalent fit is obtained to the other extension test. However, a feature of this test was the initial dilatancy, and in particular the sharp change in the volumetric strain behaviour seen in the initial stages of the test – this is illustrated in the expanded view shown on the right hand side of Figure 9. NorSand shows exactly the same behavior as seen in the test data, although the elastic volumetric strain only extends for about half as far as in the test. This could be readily modelled by introducing a slight over-consolidation (to simulate initial fabric) and so expand the yield surface to get a larger elastic zone.

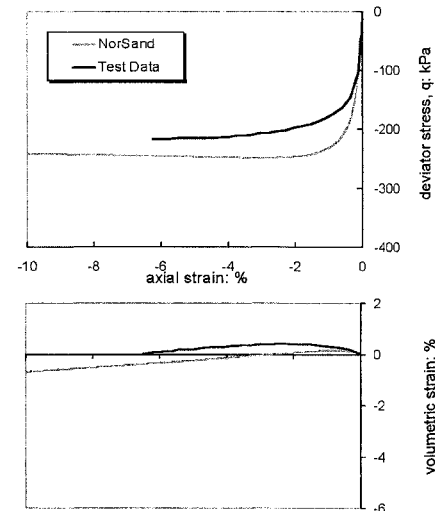
**Calibration: UBC 250dr70-2****Path 2: UBC 250dr26-2 [prediction]****Path 3: UBC 250dr26-3 [prediction]****Path 5: UBC 250dr26-5 [prediction]**

**FIG. 7.** NorSand predictions for several stress paths in UBC triaxial compression tests on Erksak Sand (data from Sasitharan, 1989)

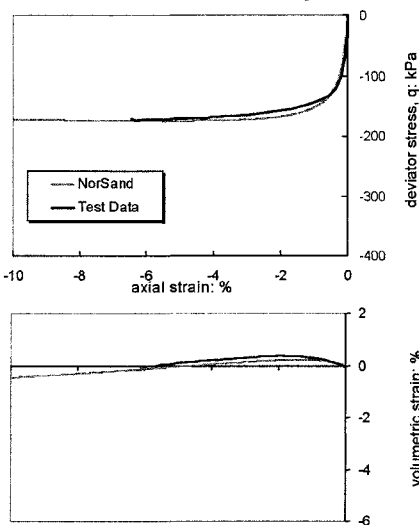
**Path 7: UBC 250dr26-7**  
(compression calibration)



**Path 8: UBC 250dr26-8**  
(compression calibration)



**Path 7: UBC 250dr26-7-best fit**



UBC 250dr26-8 (same best fit parameters)

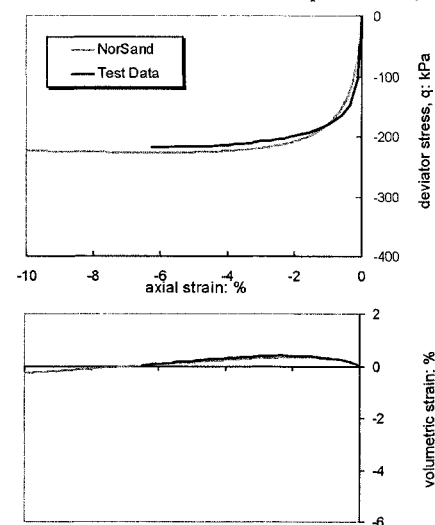


**FIG. 8. NorSand simulations of UBC triaxial extension tests on Erksak Sand using triaxial compression and best-fit calibrations (data from Sasitharan, 1989)**

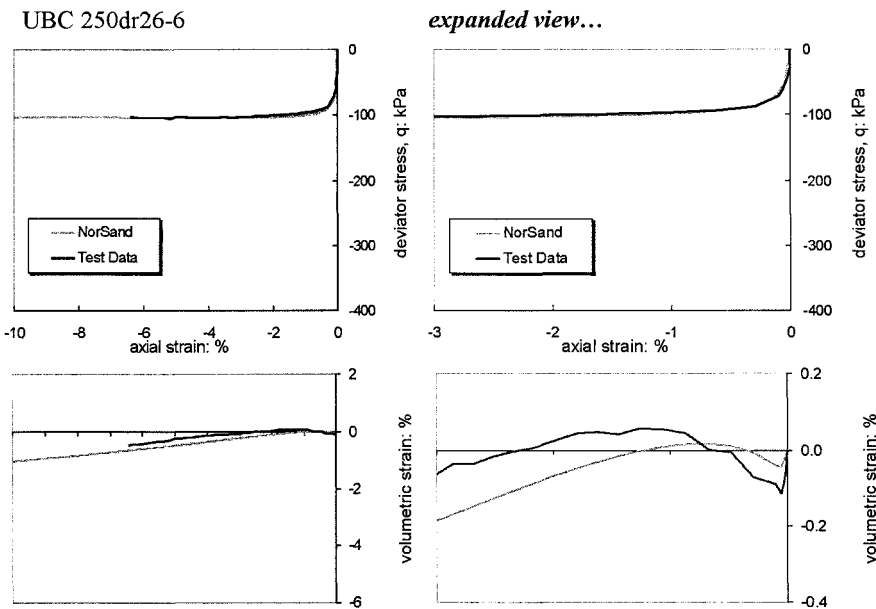
Continuing with the theme of stress paths involving unloading, the NorSand yield surfaces shown on Figure 4 indicate that any unloading from peak strength in conventional triaxial compression will involve yield in unloading. Figure 10 compares such an unloading on an Erksak sand sample. As can be seen, NorSand matches the measured behavior to the extent of even second order detail – and this with no additional parameters from the basic eight discussed earlier. An aspect of this detailed modeling of yield in unloading is the representation of inelastic energy storage and which affects the stress-dilatancy rule, see Drucker & Seereeram (1987), Jefferies (1997), and Collins & Muhunthan (2003).

Static liquefaction of loose sand is a subject of some interest. Figure 11 shows two simulations of liquefaction compared to test data. These are also on Erksak sand, and the two tests shown cover the range from contractive behavior followed by slight dilation to contractive behavior leading to extreme strength loss. The parameters used to simulate these undrained tests were established from dense drained triaxial compression tests – there is no curve fitting and these tests are true predictions of loose sand behavior from a dense drained calibration. There is a good match between the model and the sand behavior.

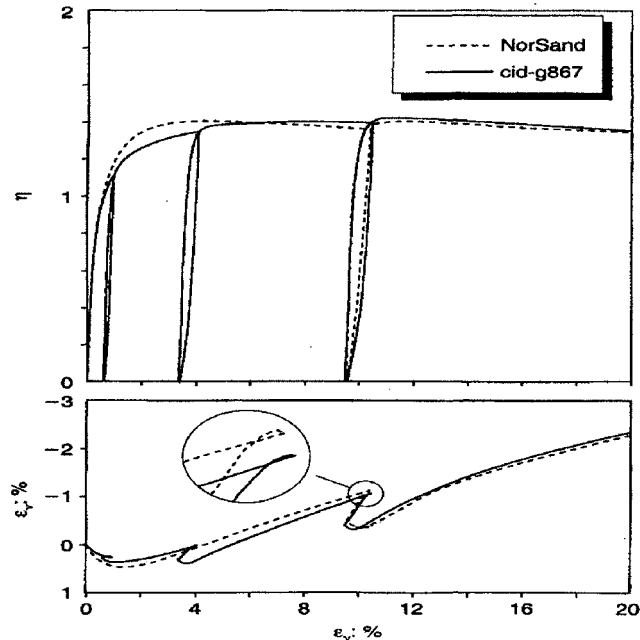
Cyclic liquefaction, or cyclic mobility as it is often called, is arguably a less important issue than outright static liquefaction but nevertheless attracts attention. Depending on the imposed cyclic stress changes, there are a range of possible behaviors from elastic through to yield in unloading and on to cyclic accumulation of excess pore pressure. The response of NorSand under cyclic loadings is largely controlled by the softening from principal stress rotation, principal stress rotation being the basic feature of such loading in the field. Figure 12 illustrates the response in cyclic simple shear and compares the NorSand simulation with test data on Nevada sand. Like the static liquefaction case, most of the properties were determined from calibration to dense drained tests. The exception is the plastic modulus  $H_r$  and which was determined by iterating to best fit the test data.

A happy result of using principal stress rotation in NorSand is that the effect of “static bias” on cyclic mobility is predicted naturally. Static bias is an issue which continues to confuse standard practice in liquefaction assessments and design of remediation, as a glance at the recent results of the NCEER workshop (Youd et al, 2001) will illustrate. Figure 12 presents two tests on Nevada sand, one with static bias and one without, the data coming from the VELACS project. Reasonable predictions of soil behavior are obtained in both cases and using constant soil properties. These simulations actually used an earlier version of NorSand in which the variable nature of  $M_i$  was not recognized.

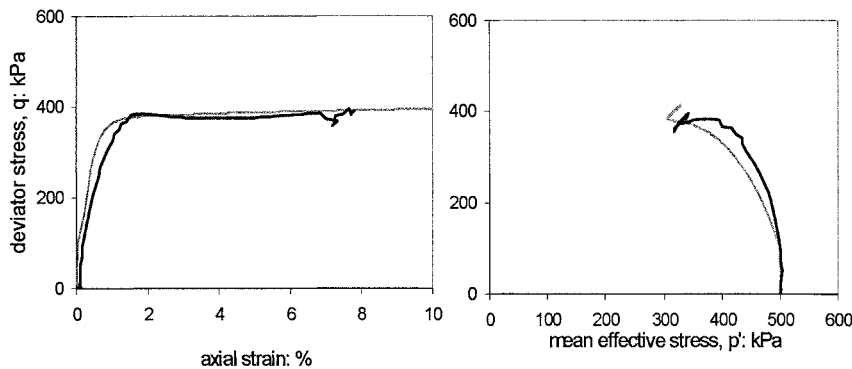
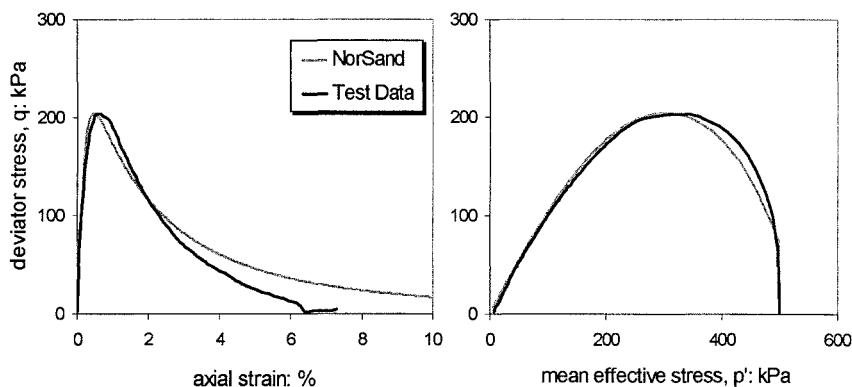
The above examples are presented to illustrate the range of NorSand and its versatility. However, it is plane strain that is one of the most important situations for practical engineering, and NorSand was subject to detailed validation for this condition. Interested readers are referred to Jefferies & Shuttle (2002).



**FIG. 9.** Norsand simulations for Path 6 of UBC Erksak Sand tests



**FIG. 10.** Yield of NorSand in unloading and reloading  
@Seismicisolation

**Test L602****Test C609**

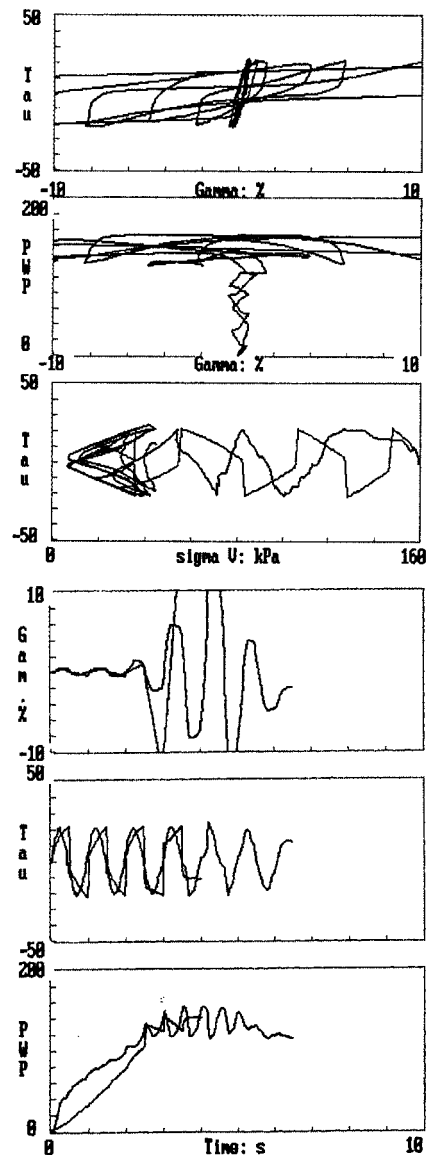
**FIG. 11. NorSand predictions for liquefaction in undrained triaxial compression of Erksak Sand using calibration from dense drained tests.**

### PROCEDURES FOR CALIBRATION OF NORSAND

The critical state parameters  $M_{tc}$ ,  $\Gamma$ ,  $\lambda$  are determined using triaxial compression tests on reconstituted samples of loose soil. Reconstituted samples are sufficient as the critical state properties are independent of soil structure. Loose soil is used to ensure completely contractive behavior, and which then provides a clear indication of the critical state without localization issues. Commonly samples are prepared by moist tamping. In all cases testing should use modern triaxial equipment with internal load transducers and digital data acquisitions systems. Bender elements are very helpful.

Testing should aim to have two samples tested undrained and two tested drained.

(a) Without static bias – Test CSS4006



(b) with static bias – Test CSS4011

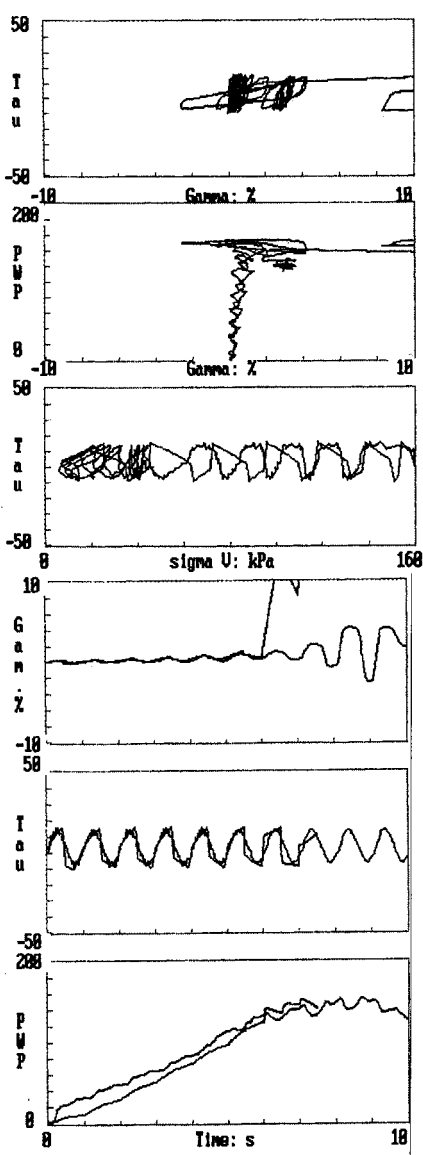
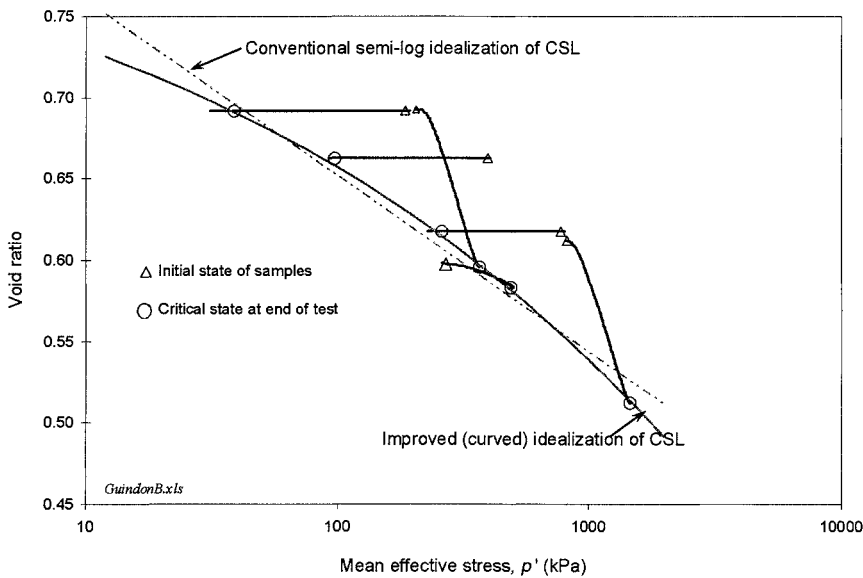


FIG. 12. NorSand simulations of undrained cyclic simple shear of Nevada Sand (after Been et al, 1992)

@Seismicisolation

A fifth sample is in reserve depending on what is found with the first four. It is essential to use sample freezing on completion of shear so that accurate void ratios are measured for the end of test condition (Sladen & Handford, 1987), and this is readily achieved by placing the triaxial sample on its pedestal in a domestic freezer.

The two loose undrained tests are typically consolidated isotropically to 50 kPa and 500 kPa effective confining stress. Undrained shear will then produce substantially contractive behavior and lead to a clear determination of the critical state mean effective stress for that sample's void ratio at the start of shear and comfortably within the strain limits of the test equipment. It is very inconvenient to ascertain the critical void ratio of denser samples using undrained tests, as the initial cell pressures have to be very large. A simpler approach is to use drained triaxial tests on very loose samples, typically from initial effective confining stresses of 200 kPa and 800 kPa. Such samples will be contractive and reach the critical state within the limits of the triaxial test. Figure 13 illustrates some state paths for these procedures on an example soil (a silty sand with 35% silt sized or smaller). The best-fit straight line on the semi-log plot through the end of test conditions gives the  $\Gamma$  and  $\lambda$  parameters for the soil. Generally this simple representation of the CSL is satisfactory for practical engineering, although a curved line is usually a slightly more accurate representation of the CSL as also indicated on Figure 13 (eg Verdugo, 1992). The end of test condition for the drained samples gives  $M_{tc}$ , the drained tests being preferred as the undrained tests often lead to low stresses and where transducer resolution and pore pressure lags can lead to uncertainties.



**FIG. 13. Example of CSL Determination**

@Seismicisolation

With the CSL established, in principle one further test on a drained sample prepared as dense as possible, and typically tested at 100 kPa initial effective confining stress, will give an estimate of the maximum dilatancy of the soil. The measured data is processed into stress dilatancy form (ie  $\eta$  vs  $D$ ) and as at peak strength the incremental elastic strains are zero the parameter  $D^p$  can be read directly from this plot. Since the CSL is known, as is the sample's void ratio, then so is  $\psi$ . Hence  $\chi$  follows immediately. In practice it is preferable to test at least two dense samples to get some redundancy in the parameter estimate.

The elastic shear modulus is ideally and simply measured using bender elements. In the absence of bender equipment, in principle a sample can be unloaded/reloaded during triaxial shear, but then issues arise on the ability of the triaxial equipment to resolve small strains as well as the effects of yield in unloading (and which thus requires the unload/reload cycle to be markedly before peak strength and of small amplitude). Poisson's ratio is usually not measured but assumed to be 0.15 to 0.2.

The final parameters of interest are the hardening moduli  $H$  and  $H_r$ . Both are determined by formal modelling of experiments. Formal modelling is used because this provides the opportunity to optimize all the parameter estimates to test data.

$H$  is determined under conditions of fixed principal stress direction, a requirement met by the conventional triaxial test equipment. Drained tests are used, ideally with concurrent bender element measurements so that the elastic modulus is known. The calibration procedure used is to guess  $H$ , compute the entire stress strain behavior, and compare the computed behaviour to that measured.  $H$  is then revised and the process repeated until a best-fit is obtained. This is exactly the procedure used to produce the calibration plot shown on Figure 6. The NorSand equations of Table 1 are very easy to implement using a Euler scheme within the VBA environment of Excel, numerical integration being required because there are no closed form solutions to the equations. The spreadsheet used to produce the figures of this paper can be downloaded from the UBC Civil Engineering website at <http://www.civil.ubc.ca/research/geotech/DownloadSoftware.htm>, and all code is open source.

In evaluating  $H$  it is important to model tests over at least loose and dense states, since the available experience to date is that  $H$  depends on  $\psi$  (Figure 4 above). Thus the two drained tests used for the CSL determination are modelled as well as the dense tests used to estimate  $\chi$ .

A weak point is the reliance on reconstituted samples, since there is no assurance at all that such reconstitution in any way replicates insitu fabric. To date, this issue has been approached by reconstituting samples using pluviated as well as moist tamped techniques, allowing the effect of fabric on  $H$  to be estimated. Of course this weakness is not specific to NorSand, all models using laboratory calibrations have to face the same issue of the relevance of laboratory samples to actual insitu conditions. It may prove possible to determine  $H$  insitu using the self-bored pressuremeter (Shuttle, 2004) but further work is needed in this area.

$H_r$ , the modulus for the effect of principal stress rotation, is evaluated using tests with smooth rotation of principal stress. Cyclic triaxial tests are excluded as the principal stress flips in that test have proven too coarse to estimate  $H_r$  so far. Both hollow cylinder tests and simple shear tests are applicable, and cyclic simple shear



has proven convenient. The procedure used is to model the soil behavior, iterating on estimated  $H_r$ , to get the best fit of model to data. This is how Figure 10 was produced. A spreadsheet environment is adequate.

Although it is common for laboratory testing to focus on preparing samples with conditions as close as possible to those found insitu, such an approach is misguided for models like NorSand. Testing for models that predict the effect of density and stress level on soil behavior should be targeted to cover the extremes of possible void ratios to the extent that it can be practically done. It is somewhat less important to target a wide range of stresses, but a range of initial confining stress of 50 kPa to 500 kPa should be sought. The goal is to get the end-member behavior as that provides the greatest opportunity to discern any limitations of the model in representing the soil of interest, and also operates the model in an interpolation rather than an extrapolation mode.

Table 3 presents some example parameters sets for NorSand properties of various soils, as well as the reference where the details of the calibration can be found. Three of the soils shown in the table are standard laboratory quartz sands, one (Erksak) is a construction sand that is a hard quartz material but which contains about 1% silt. The Bennett silty sand is almost the exact opposite of these laboratory sands, being well graded material used to construct the core of a large dam. Bonnie Silt is the silt used in the VELACS tests. Bothekennar Clay is the soil from the UK's soft-soil research site. In all cases NorSand provided an excellent representation of the test data.

## DETERMINING THE STATE PARAMETER $\psi$ INSITU

A central question in NorSand, or any other state parameter based model, is determining the soil's  $\psi$  insitu. In virtually all cases this will require insitu testing rather than trying to recover undisturbed samples, although sometimes with more silty to clay samples careful logging of water content can be a substantial help.

The methodology to determine  $\psi$ insitu is primarily based on the cone penetration test (CPT), a test that provides both excellent repeatability, accuracy, and a continuous profile. Initially, work concentrated on calibration chamber data. The calibration chamber is essentially a large triaxial cell, typically about 1.2 m in diameter. Sand is carefully placed at constant and known density, and the desired stress regime applied with vertical and radial stresses independently controlled. The CPT is pushed into the sand in the calibration chamber, just as in the field, with CPT data recorded in the usual way. Testing over a range of densities and applying a range of confining stress levels develops a map between CPT penetration resistance  $q_c$ , initial confining stress, geostatic stress ratio, and state (or relative density). However, because setting up a sample of sand in adequately sized calibration chambers is not a trivial undertaking (over 2 tons of sand is involved) the number of such programs is small.

Fifteen years ago, Golder Associates undertook a systematic evaluation of the then available data from calibration chamber tests on the CPT. A sample of sand was obtained from each of the reported chamber programs, and was tested to determine the respective CSLs. This then allowed the CPT data to be expressed in terms of  $\psi$ .



**TABLE 3. Some Examples of Calibrated Soil Property Sets for NorSand**

Soil	$\Gamma$	$\lambda_e$	$M_{lc}$	$\chi$	H	$H_r$	$I_r$	$\nu$	Reference
Erksak Sand	0.817	0.014	1.26	4.1	<i>Pluviated: 70 – 1400 <math>\psi</math> moist tamped: 130–1400 <math>\psi</math></i>	n/a	150 to 1000	0.2	This paper
Ticino Sand	0.962	0.0248	1.23	3.5	115 – 420 $\psi$	n/a	300 – 500	0.2	Shuttle & Jefferies (1998)
Hilton Mines Sand	1.315	0.0738	1.39	3.5	65	n/a	300 – 500	0.2	Shuttle & Jefferies (1998)
Brasted Sand	0.902	0.02	1.27	2.8	50 – 1125 $\psi$	n/a	500	0.2	Jefferies & Shuttle (2002)
Nevada Sand	0.910	0.020	1.20	3.5	100 – 300 $\psi$	15 to 30	175	0.2	Been et al (1993)
Bennett silty sand	0.450	0.018	1.40	3.5	100 to 150	n/a	300 – 500	0.2	Shuttle & Jefferies (2000)
Bonnie Silt	1.10	0.07	1.32	3.8	20 to 45	n/a	40 to 80	0.2	Vyazmensky (2004)
Bothkennar Clay	2.76	0.181	1.83	3.5	300	n/a	36.6	0.2	Shuttle (2003)

The results were reported in two papers (Been et al., 1986, 1987) and showed that the CPT responded to soil state according to the simple equation:

$$Q = \frac{3}{1+2K_0} k \exp(-m\psi) \quad (2)$$

where  $k$ ,  $m$  are two soil specific coefficients,  $K_0$  is the geostatic stress ratio, and the dimensionless CPT resistance is  $Q = q_c / \bar{\sigma}_v$ . Since the two Been et al. papers were published, additional chamber testing has produced data on five more sands: Erskak (Been et al., 1987), Syncrude Tailings (Golder Associates, 1987), Yatesville silty sand (Brandon et al., 1990) and Chep Lap Kok and West Kowloon (Golder Associates 1996). The data from these five sands continue to show the same trends. The equation for the CPT behavior is readily inverted to give  $\psi$  from measured CPT resistance.

Although the equation relating CPT resistance and  $\psi$  is simple and consistent with a proper dimensionless approach, it has been criticized on the grounds that careful examination of the reference chamber test data indicates significant bias with stress level. At least  $k$ , and possibly  $m$ , were functions of stress level (Sladen, 1988, 1989). In terms of the uncertainty introduced by neglecting stress level, Sladen suggested that a potential bias of "as much as 0.2 could not be ruled out." Sladen overstates the situation, as a bias of  $\Delta\psi=0.2$  requires taking the most extreme misfit across the entire database. Whereas, in reality, interest is in the divergence between the trend lines as a function of mean stress. Nevertheless, there is a bias with stress level, leading to an uncertainty of  $|\Delta\psi| < 0.05$  across the stress range considered.

The existence of a stress level bias in (2) is curious given the dimensionless formulation. Shuttle & Jefferies (1998) used NorSand in a finite element analysis of cavity expansion to directly address the stress level effect postulated by Sladen. The detailed numerical simulations showed that (2) was an accurate representation of the relationship between penetration resistance and state, as shown on Figure 13 for Ticino sand. The stress level bias was caused by treating  $k$ ,  $m$  as constants. These parameters should be functions of  $G/\bar{\sigma}_m$  but which was neglected in the work of Been et al. Extensive numerical simulations produced relationships for  $k$ ,  $m$  in terms of the soil's properties, and the approximate inversion was obtained by fitting trend lines to the numerical results to give a closed form method. The approximate inverse form is:

$$k = (f_1(I_r) f_2(M) f_3(N) f_4(H) f_5(\lambda) f_6(v))^{1/4.5} \quad (3)$$

$$m = 1.45 f_7(I_r) f_8(M) f_9(N) f_{10}(H) f_{11}(\lambda) f_{12}(v) \quad (4)$$

where the fitted functions  $f_1$  -  $f_{12}$  are simple algebraic expressions and are given in Shuttle & Jefferies (1998). The performance of the approximate inversion was verified by taking 10 sets of randomly generated soil properties/states and computing the  $Q$  value using the full numerical procedure. This computed  $Q$  was then input to the inversion to recover the estimated value of  $\psi$ . The inversion recovers  $\psi$  with an accuracy of  $\pm 0.02$ . These numerical simulations were made using an earlier version



of NorSand which used Nova's flow-rule (Nova, 1982) – to use (3) and (4), simply set  $f_3$  and  $f_9$  to unity and determine the remaining properties as described in this paper. The approximate inversion to determine  $\psi$  from CPT data is readily used in practical situations by adopting a seismic CPT for at least some of the soundings. The seismic CPT allows  $G$  to be determined from shear wave velocity measurements using the straightforward polarity reversal method. It is not onerous to do, and has small cost impact on a site investigation.

A difficulty arises at the moment when dealing with silts. These soils are very prone to disturbance, like sands. And even if sampled are often too soft to be set-up in a triaxial test without collapsing under their self-weight. However, CPT soundings in such soils are usually not drained and the excess pore pressures prevent the application of (2) – (4) to determine  $\psi$  insitu. Further work is required to establish a proper methodology to estimate  $\psi$  in silts, although a first order empirical approach has been suggested by Plewes et al (1992).

## FINITE ELEMENT IMPLEMENTATION OF NORSAND

NorSand has been implemented in finite element codes using an incremental viscoplastic formulation (Zienkiewicz & Cormeau, 1974), both within the downloadable public domain finite element codes from the Smith and Griffiths (1998) book as well as large strain codes developed for research. The viscoplastic algorithm was originally developed to model time dependent material behavior, and was then adapted to represent plasticity. In this context viscoplasticity refers to a numerical technique and does not involve any time-dependence in the strength properties of the soils.

The viscoplastic solution technique involves a conventional elastic analysis with material non-linearity (i.e. plasticity) introduced by iteratively modifying the loading vector. The loads vector at each load step comprises the externally applied loads and a set of self-equilibrating body-loads. Body-loads are used to redistribute stresses within the system, without altering the external loading. This is achieved as follows. Within any load increment, the material is allowed to sustain stresses outside the yield surface for a finite time, where time is an internal fiction used only within the load step. Instead of plastic strains we now treat the strain as viscoplastic. When applied to time independent materials the viscoplastic equation becomes:

$$\dot{\varepsilon}^{vp} = F \frac{\partial Q}{\partial \sigma} \quad (5)$$

where positive  $F$ , the amount by which the yield surface has been violated, drives the strain rate.  $F=0$  defines yield.  $Q$  is the plastic potential, which for NorSand is the same as the yield surface. Time is allowed to advance within the load step to accumulate the viscoplastic strain within the iterations. The plastic strains work harden or soften the soil, as appropriate, at each integration point (so modifying  $F$  for the next iteration). At the same time the loads outside of the current yield surface are redistributed to adjacent parts of the soil mass through the body-loads until the applied and internal loads are balanced.



The numerics are taken as converged when the stresses generated by the loads satisfy the yield criterion within the specified tolerance. The next load increment is then applied, and the procedure repeated.

Despite the simplicity of this approach, viscoplasticity is not commonly used with critical state models (Potts, 2003). However, implementation of NorSand is straightforward. It is only necessary to calculate the magnitude of the plastic strain increments (see Equation 5) and update the location of the current yield surface as a function of the incremental plastic shear strain invariant. The flow chart for a subroutine to do this is given in Table 4. Details of the finite element implementation of NorSand can be found in Shuttle (2004).

The viscoplastic implementation of NorSand in finite elements has been verified under a variety of stress paths and initial states. Figure 15 shows an example for triaxial compression of a very dense sand with state parameter,  $\psi$ , equal to -0.3. Three step sizes of 0.1%, 0.5% and 1.0% were considered and for all of the step sizes the fit between the finite element and direct integration solutions is excellent.

## APPLICATION OF NORSAND

The finite element implementation of NorSand has allowed it to be used on problems relevant to geotechnical engineers. However, outside of academia, finite element models are typically only used for “non-routine” projects. Even in such non-routine applications the constitutive model is rarely more advanced than Non-Associated Mohr-Coulomb (as even a casual survey of the user manuals for the various commercial codes will indicate). The additional effort in the parameter determination for any advanced constitutive model is only justified for situations where accurate representation of volume changes is important to the overall behavior of the structure. These situations include problems involving large strain, confinement, or excess pore pressure generation. NorSand has been used for a variety of such applications.

NorSand was used for the analysis of compaction grouting at Bennett Dam (Shuttle & Jefferies, 2000). Bennett Dam provides about one quarter of the electric power for British Columbia, Canada. The dam, located on the Peace River in the north-east of the province, has a crest length of 1.6 km, a maximum height of 183 m, and the reservoir, known as Williston Lake, is 404 km long. Compaction grouting was used for the repair of sinkholes in the dam core, and due to the importance of this dam a high level of control during grouting was required.

Because compaction grouting deliberately aims to change the void ratio of soil, analysis of compaction grouting is a natural use for models like NorSand since the model intrinsically account for the effect of void ratio and stress changes on the soil behaviour. In the case of the repairs to Bennett dam, NorSand was implemented within a finite element program to develop a prognosis of what could be achieved by compaction grouting and under what circumstances. This prognosis was used to set the initial grouting parameters. The ground response to grout was electronically monitored and this measured response was then back-analyzed in near-real time to understand how grouting was improving the ground, with appropriate changes to the grouting protocol then being implemented as needed.



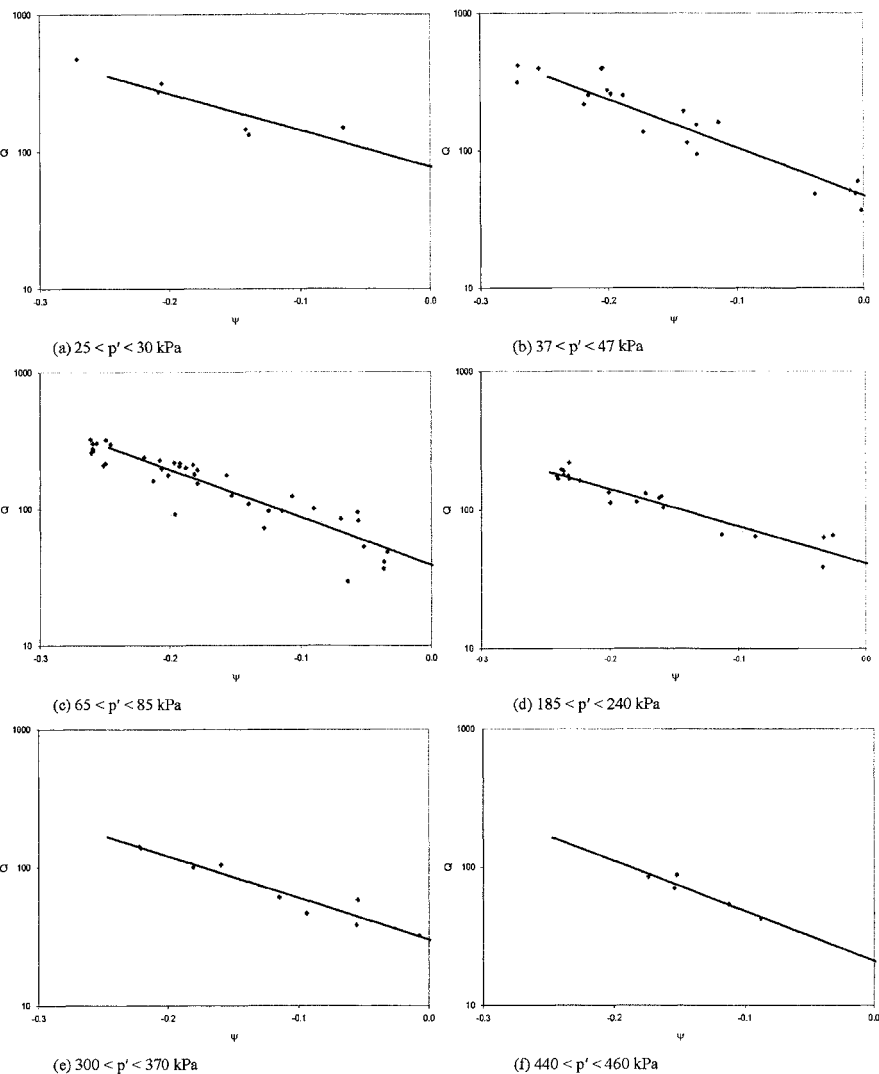


**FIG. 14. Comparison of CPT resistance in Ticino Sand with trendlines from numerical simulations using finite element implementation of NorSand**

**Table 4: Implementation of NorSand subroutine within viscoplastic algorithm**

*In the main finite element code:*

For iteration  $j$

Apply load increment elastically to get new stresses  $\bar{\sigma}_{new}$

Loop over all integration points

*Call NorSand subroutine*

compute  $M_i$

calculate  $\bar{\sigma}_{m,i\_visco}$  using the new stresses  $\bar{\sigma}_{m,i\_visco} = \frac{\bar{\sigma}_{m,i,new}}{(1 - \eta_{new})/M_i}$

calculate F from  $F = 0.5M_i(\bar{\sigma}_{m,i\_visco} - \bar{\sigma}_{m,i})$

Is  $F > 0$  (ie yield exceeded) at current location of yield surface?

NO – exit subroutine with no additional plastic strains

YES – accumulate “viscous” strain for iteration  $j$

Calculate  $\dot{\varepsilon}_1^{vp}/\dot{\varepsilon}_3^{vp}, \dot{\varepsilon}_2^{vp}, \dot{\varepsilon}_3^{vp}$

$$\dot{\varepsilon}^{vp} = F \frac{\partial Q}{\partial \sigma}$$

$$(\delta\varepsilon^{vp})^j = \Delta t (\dot{\varepsilon}^{vp})^j$$

– update yield surface

$$\bar{\sigma}_{m,i,max} = \bar{\sigma}_{m,old} \exp\left(-\frac{\chi \psi_{i,old}}{M_{i,tc}}\right)$$

$$\dot{\bar{\sigma}}_{m,i} = H \frac{M_i}{M_{i,tc}} \left( \frac{\bar{\sigma}_m}{\bar{\sigma}_{m,i}} \right)_{old} \left[ \bar{\sigma}_{m,i,max} - \bar{\sigma}_{m,i} \right] \dot{\varepsilon}_q^{vp}$$

$$\bar{\sigma}_{m,i} = \bar{\sigma}_{m,i} + \dot{\bar{\sigma}}_{m,i}$$

$$F = 0.5M_i(\bar{\sigma}_{m,i\_visco} - \bar{\sigma}_{m,i})$$

End viscous flow loop

End Subroutine

End loop integration points

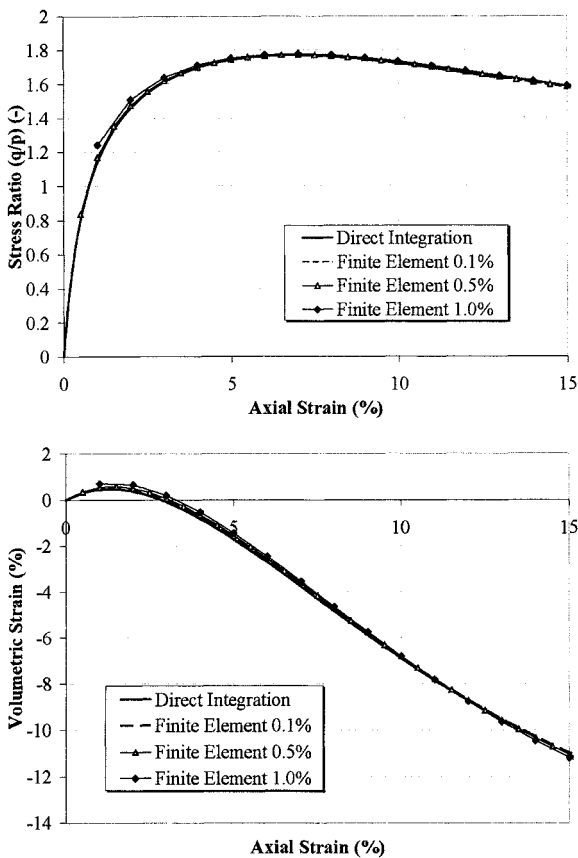


**FIG. 15. Verification of finite element implementation of Norsand with  $\psi_0 = -0.3$**

Pile installation is also a situation where large strains develop near the pile wall. The pile's capacity is related to the stresses developed in the soil close to the pile wall, which changes over time as the installation induced pore pressures' dissipate. NorSand has been used to model a soft, sensitive, marine silt and clay soil at the Colebrook research site in Surrey, British Columbia within a Biot coupled finite element code. The finite element pore pressures were compared with those measured during a field study of helical pile performance carried out by Weech (2002). Results are given in Vyazmensky et al. (2004) and Vyazmensky (2004).

As noted above, it is rather rare to find anything more sophisticated than a mixture of non-linear elasticity and Non-Associated Mohr-Coulomb in engineering practice. Part of the reason is the variability and uncertainty of in place soil properties and the expense of capturing these factors within a normal consulting environment. However, NorSand can be readily used in engineering practice requiring finite element analysis, as the parameters are few and most are well understood. The key

issue to use NorSand is: how dense is the ground ? This is a well understood question in engineering practice, although of course it is  $\psi$  that is required rather than density itself. And the answer leads to the whole range of detailed behaviors that NorSand computes. In effect, NorSand has no more data demand than Modified Cam Clay but realistically simulates a vastly larger range of soil behaviors. As to how to answer "How dense?", a self-consistent methodology has been developed for inversion of the CPT data to give  $\psi$ . And the CPT is reliable, accurate, and inexpensive. CPT soundings ought to be the backbone of any site investigation, and reliance of any  $\psi$ -based model (including NorSand) on the CPT can hardly be viewed as onerous.

## CONCLUSION

The NorSand constitutive model generalizes the ideas of critical state soil mechanics, and is based on idealized postulates of soil behavior. Depending on the detail sought in terms of representing the CSL and elasticity, as few as eight soil properties are required, most of which are in common use today. The model is fully 3-D, computable in finite element simulations, and captures many aspects of soil behavior (and with second order detail). This simplicity and performance follows from recognizing that soil has an infinity of NCL, and which are characterized by the state parameter,  $\psi$ .

The sparse parameter set of NorSand imposes a demand for input data that is well within what can be achieved in good engineering practice. Broadly, NorSand requires a few triaxial tests on reconstituted samples to determine the soil properties used (which are density and stress level independent), and insitu testing to determine the elasticity and  $\psi$  of the strata of interest. This insitu testing is readily accomplished using a seismic CPT. The methodology to asses  $\psi$  from CPT data was summarized, and further details can be found in the cited references.

NorSand is readily implemented in finite element codes, and is fully compatible with standard numerical methods as found in, for example, the public domain codes published by the University of Manchester group. There are no difficulties with convergence, as illustrated by the verification presented.

Constitutive models are only useful if they are used. Realistically, this requires implementing NorSand within commercial software since research codes are usually devoid of the input/output interfaces that are essential for finite element modeling in engineering practice. A current University of British Columbia (UBC) project aimed at improving understanding of geosynthetic pull-out tests uses the FLAC finite difference software. NorSand is currently being coded as a FLAC "FISH" function, and this routine should be downloadable in the near future from the UBC web site (<http://www.civil.ubc.ca/research/geotech/DownloadSoftware.htm>).

## REFERENCES

- Been, K. & Jefferies, M.G. (1985). "A state parameter for sands", *Geotechnique* 35, 99-112.
- (1986). Reply to Discussion *Geotechnique* 36, 123-132.
- Been K., Crooks J.H.A., Becker D.E. and Jefferies M.G. (1986). "The cone penetration test in sands: Part I, state parameter interpretation", *Geotechnique* 36, 239-249.
- Been K., Jefferies M.G., Crooks J.H.A. and Rothenberg L. (1987). "The cone penetration test in sands: Part II, general inference of state", *Geotechnique*, 37, 285-299.
- Been K., Lingnau, B.E., Crooks J.H.A. and Leach, B.. (1987b) "Cone penetration test calibration of Erksak (Beaufort Sea) sand", *Can. Geot. J.* 24, 601-610.
- Been, K., Jefferies, M.G. and Hachey, J. (1991). "The critical state of sand", *Geotechnique* 41, 365-381.
- (1992); Reply to Discussion *Geotechnique* 42, 660-663.
- Been, K., Jefferies, M.G., Hachey, J.E. & Rothenburg, L. (1993); Numerical prediction for Model No 2. In *Verification of Numerical Procedures for Analysis of Soil Liquefaction Problems* (Arulanandan & Scott, eds), 331-341. Balkema.
- Brandon, T.L., Clough, G.W. and Rajardjo, R.P. (1990). "Evaluation of liquefaction potential of silty sands based on cone penetration resistance", *Research Report* to National Science Foundation, Grant ECE-8614516, Virginia Polytechnic Institute.
- Collins, I.F. & Muhunthan, B. (2003). "On the relationship between stress-dilatancy, anisotropy, and plastic dissipation of granular materials", *Geotechnique* 53, 611-618.
- Drucker D.C., Gibson R.E. and Henkel D.J. (1957). "Soil mechanics and work-hardening theories of plasticity", *J. Soil Mechanics and Foundation Engineering*, American Society of Civil Engineers 122, 338-346.
- Drucker, D.C. & Seereeram, D. (1987). "Remaining at yield during unloading and other unconventional elastic-plastic response", *Trans. ASME, J Appl Mech.* 109, 22-26.
- Gajo & Wood, D.M. (1999).; Severn-Trent sand, a kinematic hardening constitutive model: the q-p formulation. *Geotechnique* 49, 595-614.
- Golder Associates (1987). "Cone penetrometer calibration chamber tests on Syncrude Tailings", *Project report* 872-2402 to Syncrude Canada Limited.
- Golder Associates (1996). "Review of Sand Fill Characterization Study", *Project Report* 9452-1095 to Hong Kong University of Science and Technology.
- Ishihara, K., Tatsuoka, F. & Yasuda, S. (1975). "Undrained deformation and liquefaction of sand under cyclic stresses", *Soil & Foundations* 15, 29-44.
- Jefferies, M.G. (1993). "NorSand: a simple critical state model for sand", *Geotechnique* 43, 91-103.
- Jefferies, M.G. (1997). "Plastic work and isotropic softening in unloading", *Geotechnique*, 47, 1037-1042.
- Jefferies, M.G. & Been, K. (2000). "Implications for critical state theory from isotropic compression of sand", *Geotechnique* 50, 419-429.

@Seismicisolation

- Jefferies, M.G. and Shuttle,D.A. (2002). "Dilatancy In General Cambridge-Type Models", *Geotechnique* 52, 625-638.
- Li, X-S., Dafalias, Y.F., & Wang, Z-L. (1999). "State dependent dilatancy in critical state constitutive modelling of sand", *Can Geot. J.* 36, 599-611.
- Manzari, M.T. & Dafalias, Y.F. (1997). "A critical state two-surface plasticity model for sands", *Geotechnique* 47, 255-272.
- Matsuoka, H. & Nakai, T. (1974). "Stress-deformation and strength characteristics of soil under three different principal stresses", *Trans. JSCE* 6, 108-109.
- Nova, R. (1982). "A constitutive model under monotonic and cyclic loading", in *Soil Mechanics – Transient and Cyclic Loads* (eds Pande & Zienkiewicz), 343-373. Wiley.
- Pestana, J.M. & Whittle, A.J. (1995). "Compression model for cohesionless soils", *Geotechnique* 45, 611-631.
- Plewes, H.D., Davies, M.P., and Jefferies, M.G. (1992); CPT based screening procedure for evaluating liquefaction susceptibility. *Proc 45th Can. Geot. Conf.*, Toronto
- Potts, D.M. (2003); "Numerical analysis: a virtual dream or practical reality?", the 42<sup>nd</sup> Rankine Lecture, *Geotechnique* 53, 535-573.
- Resende, L. & Martin, J.B. (1985). "Formulation of Drucker-Prager Cap Model", *ASCE J. Eng Mech* 111, 855-881.
- Reynolds O. (1885). "On the dilatancy of media composed of rigid particles in contact, with experimental illustrations", *Philosophical Magazine*, 20, 469-481.
- Sasitharan, S. (1989); "Stress path dependency of dilatancy and stress-strain response of sand". M.Sc. Thesis, University of British Columbia.
- Schofield, A. & Wroth, C.P. (1968). *Critical State Soil Mechanics*. McGraw-Hill.
- Sladen, J.A. (1988); Discussion: Cone penetration test calibration for Erksak sand. *Can. Geotech. J* 26, 173-177.
- Sladen J.A. (1989); Problems with interpretation of sand state from cone penetration test. *Geotechnique* 39, 323-332.
- Sladen, J.A. & Handford, G. (1987). "A potential systematic error in the laboratory testing of very loose sands", *Can. Geotech. J.* 24, 462-466.
- Shuttle, D.A. & Jefferies, M.G. (1998); "Dimensionless and unbiased CPT interpretation in sand". *IJNAMG* 22, 351-391.
- Shuttle, D.A. and M.G. Jefferies (2000) "Prediction and Validation of Compaction Grout Effectiveness", *ASCE Geotechnical Special Publication 104*, Advances in Grouting and Ground Modification, (eds Krizek & Sharp).
- Shuttle, D.A. (2003); "Effect Of Pore Pressure Dissipation On SBP Tests In Clay" *Proc. 56<sup>th</sup> Can. Geotech. Conf.*, Winnipeg..
- Shuttle, D.A. (2004); "Can sand fabric be determined using a self-bored pressuremeter?". Submitted to the *Can. Geot. J.*.
- Smith I.M. & Griffiths D.V. 1998. *Programming the Finite Element Method*. Third Edition, John Wiley and Sons.
- Stewart,H.R., Jefferies,M.G., and Goldby,H.M. (1983). "Berm construction for the Gulf mobile Arctic caisson", Proc 15th Offshore Tech Conf, Houston. OTC 4552.

- Vaid, Y.P. & Sasitharan, S. (1992). "The strength and dilatancy of sand". *Can. Geotech. J.* 29, p522-526.
- Verdugo, R. (1992). Discussion on 'The critical state of sand'. *Geotechnique* 42, p655-658.
- Vyazmensky, A. (2004). "Numerical modelling of time dependent pore pressure response induced by helical pile installation", M.A.Sc. Thesis, University of British Columbia.
- Vyazmensky, A.M., Shuttle, D.A. and Howie, J.A. (2004). "Coupled Modelling Of Observed Pore Pressure Dissipation After Helical Pile Installation", *Proc. GeoQuebec 2004* (in press).
- Wan, R.G. & Guo, P.J. (1998). "A simple constitutive model for granular soils: modified stress-dilatancy approach", *Computers and Geotechnics*, 22, p109-133.
- Weech, C.N. (2002). "Installation and Load Testing of Helical Piles in a Sensitive Fine-Grained Soil", M.A.Sc. Thesis, University of British Columbia.
- Youd et al (2001). "Summary report from the 1996 NCEER and 1998 NCEER/NSF workshops on evaluation of liquefaction resistance of soils", *ASCE J. Geot. & Geoenviron. Eng* 127, 817-833.
- Zienkiewicz O.C. & Cormeau I.C. (1974). "Viscoplasticity, plasticity and creep in elastic solids. A unified numerical approach". *Int. J. Num. Meth. Eng.* 8, 821-845.

## APPENDIX: NOTATION

### Stress Variables

$\sigma_{1, 2, 3}$	[FL <sup>-2</sup> ]	Principal stresses, bar superscript denoting effective
$\bar{\sigma}_m$	[FL <sup>-2</sup> ]	Mean effective stress (= $p'$ under triaxial conditions)
		$\bar{\sigma}_m = (\bar{\sigma}_1 + \bar{\sigma}_2 + \bar{\sigma}_3)/3$
$\bar{\sigma}_q$	[FL <sup>-2</sup> ]	Deviatoric stress invariant (= $q$ under triaxial conditions)
		$\bar{\sigma}_q = (\frac{1}{2}(\sigma_1 - \sigma_2)^2 + \frac{1}{2}(\sigma_2 - \sigma_3)^2 + \frac{1}{2}(\sigma_3 - \sigma_1)^2)^{1/2}$
$\eta$	[-]	Dimensionless shear measure as ratio of stress invariants $\eta = \bar{\sigma}_q / \bar{\sigma}_m$
$\theta$	[Rad]	Lode angle, $\sin(3\theta) = -13.5\bar{\sigma}_1\bar{\sigma}_2\bar{\sigma}_3/\bar{\sigma}_q^3$

### Strain Variables (dot superscript denotes rate)

$e$	[-]	Void ratio
$\varepsilon_{1, 2, 3}$	[-]	Principal strains (assumed coaxial with principal stresses)
$\dot{\varepsilon}_v$	[-]	Volumetric strain $\dot{\varepsilon}_v = \dot{\varepsilon}_1 + \dot{\varepsilon}_2 + \dot{\varepsilon}_3$
$\dot{\varepsilon}_q$	[-]	Shear strain measure work conjugate with $\bar{\sigma}_q$
		$\dot{\varepsilon}_q = \frac{1}{3}((\sin\theta + \sqrt{3}\cos\theta)\dot{\varepsilon}_1 - 2\sin\theta\dot{\varepsilon}_2 + (\sin\theta - \sqrt{3}\cos\theta)\dot{\varepsilon}_3)$
$D^p$	[-]	Plastic dilatancy, $\dot{\varepsilon}_v^p / \dot{\varepsilon}_q^p$

### Variables & Parameters

$G$	[FL <sup>-2</sup> ]	Shear modulus, a model parameter
$H$	[-]	Plastic hardening modulus, a model parameter
$Hr$	[-]	Plastic softening modulus under principal stress rotation
$I_r$	[-]	Soil rigidity, $G / \bar{\sigma}_m$
$M$	[-]	Critical friction ratio, a model parameter
$Q$	[-]	Dimensionless CPT tip resistance
$q_c$	[FL <sup>-2</sup> ]	CPT tip resistance
$\nu$	[-]	Elastic Poisson's ratio, a model parameter and usually constant
$\alpha$	[Rad]	Included angle between direction of major principal stress and coordinate frame of reference
$\chi$	[-]	Dilatancy constant, a model parameter
$\phi$	[Rad]	Mohr Coulomb friction angle
$\Gamma$	[-]	Reference void ratio on CSL, a model parameter
$\lambda$	[-]	Slope of CSL in $e$ - $\ln(\sigma_m)$ space, a model parameter
$\kappa$	[-]	Slope of elastic line in $e$ - $\ln(\sigma_m)$ space
$\psi$	[-]	State parameter, $\psi = e - e_c$

### Subscripts

$cv$	Constant volume = critical state
$L$	Limit value
$I$	Image condition on yield surface
$tc$	Triaxial compression condition ( $\theta = \pi/6$ )
$te$	Triaxial extension condition ( $\theta = -\pi/6$ )

## PARAMETER ESTIMATION FOR TIME-DEPENDENT BOUNDING SURFACE MODELS FOR COHESIVE SOILS

Victor N. Kaliakin, Member ASCE<sup>1</sup>

**ABSTRACT:** The elastoplastic-viscoplastic bounding surface constitutive model, a generalized three-invariant formulation, has been shown to accurately simulate the time related behavior of cohesive soils. In the present paper a brief overview of the model is given, the parameters associated with this model are identified and the process for determining their values is discussed. The availability of parameter databases is also discussed.

### INTRODUCTION

Over the past thirty years several constitutive models, possessing varying degrees of sophistication, have been developed to simulate the mechanical behavior of soils. A very promising class of plasticity-based constitutive models for such materials is that founded on the bounding surface concept (Dafalias 1975). The prominent feature of this concept is the fact that inelastic deformations can occur for stress points within or on a bounding surface in general three-dimensional stress space at a pace depending on the proximity of the actual stress point to a properly defined "image" point on the surface itself. Thus, unlike classical elastoplasticity formulations, inelastic states are not restricted only to those lying on a surface, thus avoiding the abrupt transition between elastic and inelastic response and, consequently, better simulating the inelastic behavior of soils.

Beginning in the late 1970's, the bounding surface concept has been successfully used to simulate the response of cohesive soils. A form of a bounding surface/yield surface model was briefly mentioned (Mroz et al. 1978) and subsequently fully developed within the framework of critical state soil mechanics by Mroz and his co-workers (Mroz et al. 1979). Anisotropic response has also been considered by Pietruszczak and Mroz (1979).

A direct bounding surface formulation for isotropic soil plasticity was qualitatively presented by Dafalias for the case of zero elastic range (Dafalias 1979a) and in conjunction with implied loading surfaces and a quasi-elastic range (Dafalias 1979b). The latter version of the model was subsequently developed fully within the

<sup>1</sup> Associate Professor, Department of Civil and Environmental Engineering, University of Delaware, Newark, DE 19716, kaliakin@ce.udel.edu.

framework of two stress invariants (Dafalias and Herrmann 1980; 1982a). It was next extended to a three-invariant formulation (Dafalias and Herrmann 1982b, Dafalias et al. 1982), generalized (Dafalias and Herrmann 1986), and then subsequently simplified (Kaliakin and Dafalias 1989).

The theoretical basis for a time-dependent version of the model for isotropic cohesive soils was proposed by Dafalias (1982a, 1982b, 1986). This model was refined and implemented by Kaliakin (1985) and presented and verified by Kaliakin and Dafalias (1990a,b). In the literature this model has been referred to as the Dafalias-Kaliakin model (Leidwanger-Rabis et al. 1995). It has been extensively verified using numerous experimental results (Dafalias and Herrmann 1980, 1982, 1986) and actual field measurements (Poran et al. 1986; Shen et al. 1986; Kaliakin et al. 1990, Leidwanger-Rabis et al. 1995).

The issue of anisotropy, in conjunction with bounding surface models, was discussed by Dafalias (1982b). This led to the progressive development of the anisotropic, rate-independent bounding surface model for cohesive soils (Anandarajah et al. 1984, Anandarajah and Dafalias 1985, 1986).

The development of an anisotropic, time-dependent bounding surface model was initiated by Al-Shamrani and Sture (1994, 1998). This model combined the rate-independent anisotropic model proposed by Anandarajah and Dafalias (1986) with the isotropic time-dependent model developed by Kaliakin and Dafalias (1990a). Unfortunately, the resulting model was quite complex and involved a rather large number of model parameters. Essentially the same model, though extended to finite deformations, was presented by Voyiadjis and Kim (2003). Not only did this model require a large number of model parameters, it also lacked a complete set of experimental data (at large strains) from which to determine the model parameter values.

Realizing that previous anisotropic time-dependent bounding surface formulations were overly complex, Ling et al. (2002) proposed a somewhat more rational model that reduced the total number of parameters without compromising predictive capabilities. To date, only time-independent simulations and predictions generated using this model have been presented in the literature (Ling et al. 2002, 2003). In more recent work (Pan 2004), the model of Ling et al. (2002) was extended and refined and fundamental simulative and predictive capabilities of the model are next investigated.

Throughout the development of the bounding surface model care was taken to avoid introducing an excessive number of parameters. Furthermore, a concerted effort was made to relate these parameters to constants familiar to the geotechnical engineering community. The focus of this paper is the identification and calibration of these model parameters. Since the anisotropic version of the elastoplastic-viscoplastic model is not yet deemed mature, the present emphasis will be on the isotropic version of the model. It is, however, important to point out that many of the parameters associated with the isotropic version of the model are likewise associated with its anisotropic counterpart. Furthermore, the values of these common parameters are determined in an *identical* fashion for both versions of the model.

## OVERVIEW OF THE MODEL

Although quite general in nature (Kaliakin and Dafalias 1990a), the elastoplastic-viscoplastic bounding surface model is specialized herein for the case of isotropic cohesive soils. In the subsequent development tensors are presented in indicial form with the indices obeying the summation convention over repeated indices.

The material state is defined in terms of the effective stress  $\sigma'_{ij}$  and  $n$  scalar or tensor internal variables  $q_n$  that account for the non-conservative nature of soils. The effective stress is related to the total (phenomenological) stress  $\sigma_{ij}$  and to the pore fluid pressure  $u$  by

$$\sigma_{ij} = \sigma'_{ij} + \delta_{ij}u \quad (1)$$

where  $\delta_{ij}$  represents the Kronecker delta, and compressive stresses are taken as positive.

The dependence of the bounding surface on the effective stress is expressed in terms of three stress invariants, namely,

$$I_1 = \sigma'_{kk} \quad (2)$$

$$J = \sqrt{\frac{1}{2} s_{ij} s_{ij}} \quad (3)$$

$$\theta = \frac{1}{3} \sin^{-1} \left[ \frac{\sqrt{3}}{2} \frac{s_{ij} s_{jk} s_{ki}}{(J)^3} \right] ; \quad -\frac{\pi}{6} \leq \theta \leq \frac{\pi}{6} \quad (4)$$

where  $s_{ij}$  denotes the deviatoric part of  $\sigma'_{ij}$ . The values of  $\theta = \pm \pi/6$  correspond to conditions of axisymmetric compression and extension, respectively. A section of the elliptical bounding surface, for a given value of  $a$ , is shown in Figure 1. Analytically, the bounding surface is defined by

$$F(\bar{I}_1, \bar{J}, \bar{\theta}, q_n) = 0 \quad (5)$$

where a bar indicates an “image” point on the bounding surface.

The prominent feature of the bounding surface concept is the prediction of inelastic deformations for stress points  $(I_1, J, \theta)$  within or on the surface at a pace depending on the proximity  $\delta$  of  $(I_1, J, \theta)$  to a unique “image” point on the surface, assigned by the “radial” mapping rule (Dafalias and Herrmann 1986); viz.,

$$\bar{I}_1 = b(I_1 - CI_o) + CI_o \quad (6)$$

$$\bar{J} = bJ \quad (7)$$

 @Seismicisolation

$$\bar{\theta} = \theta \quad (8)$$

where  $b$  ( $b \geq 1$ ) is determined in terms of the material state,  $I_o$  represents a measure of the preconsolidation history, and  $C$  ( $0 \leq C < 1$ ) is a dimensionless model parameter (Figure 1). The direction of inelastic loading-unloading is defined as the gradient of  $F$  at  $(\bar{I}_1, \bar{J}, \bar{\theta})$ . To complete the formulation, a relation between the plastic modulus  $K_p$  (associated with the actual stress point) and a “bounding” plastic modulus  $\bar{K}_p$  (associated with the “image” point) is established as a function of the Euclidean distance  $\delta$  between  $(I_1, J, \theta)$  and  $(\bar{I}_1, \bar{J}, \bar{\theta})$ ; viz.,

$$K_p = \bar{K}_p + H \frac{\delta}{\langle r - s_p \delta \rangle} \quad (9)$$

where  $H$  denotes a proper scalar hardening function of the state,  $s_p$  ( $s_p \geq 1$ ) is a dimensionless model parameter,  $r$  represents the Euclidean distance between the points  $CI_o$  and  $(\bar{I}_1, \bar{J}, \bar{\theta})$ , and the symbols  $\langle \rangle$  denote Macaulay brackets. An explicit expression for  $H$  shall be given in a subsequent section.

The bounding surface hardens isotropically. The hardening is controlled by a single internal variable that measures the change in volumetric strain. More precisely, this internal variable is the inelastic part  $e^i$  of the incremental change in void ratio  $e$ . For convenience, the evolution of the surface is related to  $I_o$  through the following expression (Kaliakin and Dafalias 1990a):

$$\frac{dI_o}{de^i} = -\frac{I_o}{\lambda - \kappa} \quad (10)$$

where the parameters  $\lambda$  and  $\kappa$  denote the slopes of the consolidation and swell/recompression lines, respectively, on a plot of void ratio versus the natural logarithm of  $I_1$ .

The strain rate is additively decomposed into elastic and an inelastic part. The latter consisting of a delayed (viscoplastic) and an instantaneous (plastic) part; viz.,

$$\dot{\varepsilon}_{ij} = \dot{\varepsilon}_{ij}^e + \dot{\varepsilon}_{ij}^v + \dot{\varepsilon}_{ij}^p \quad (11)$$

where  $\varepsilon_{ij}$  denotes the infinitesimal strain tensor, the superscripts  $e$ ,  $v$  and  $p$  denote its elastic, viscoplastic and plastic components, respectively, and a superposed dot indicates a material time derivative or rate.

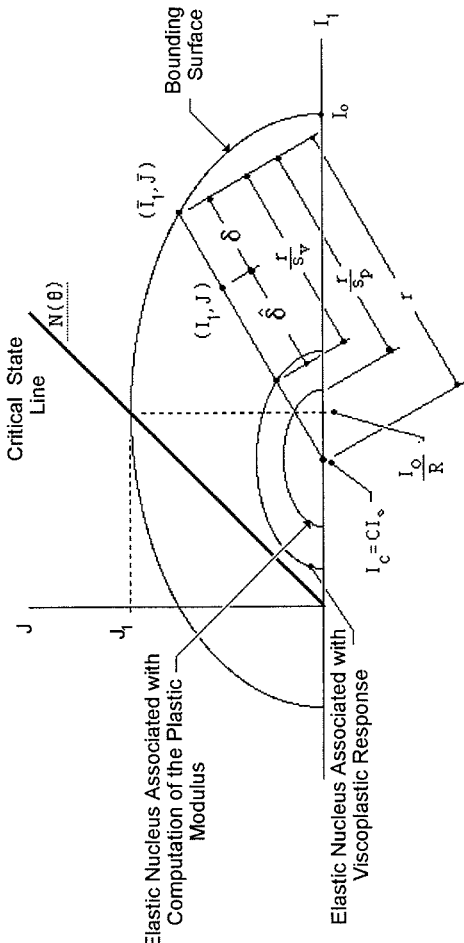


**FIG. 1. Schematic Illustration of the Radial Mapping Rule and of the Bounding Surface in Stress Invariants Space**

Assuming elastic isotropy to be independent of the rate of loading and to be unaltered by inelastic deformation, the response associated with the elastic strain rate

is expressed in terms of the elastic bulk and shear moduli,  $K$  and  $G$ , respectively. The former modulus is related to  $I_1$  through

$$K = \frac{(1 + e_{in})I_1}{3\kappa} \quad (12)$$

where  $e_{in}$  represents the void ratio at initiation of loading. The elastic shear modulus is computed from  $K$  and a specified value of Poisson's ratio  $\nu$ .

The equation for the viscoplastic strain rate is based upon a generalization of the theory of Perzyna (1966). According to this theory, this rate is a function of the "distance" between the current stress and that on the boundary of a "quasi-static" elastic domain. For the present development the normalized overstress

$$\Delta\hat{\sigma} = \frac{\hat{\delta}}{r - \frac{r}{s_v}} = \frac{s_v}{b(s_v - 1)} - 1 \quad (13)$$

constitutes this "distance." The elastic domain is represented by the implicitly defined "elastic nucleus" (Figure 1). Although the boundary of the nucleus is equivalent to the concept of a yield surface, it is not identical since the point  $(I_1, J, \theta)$  can cross this boundary and move outside with a smooth inelastic transition at  $\delta = r/s_v$ . Assuming an associative flow rule, it follows that

$$\dot{\varepsilon}_{ij}^p = \langle \phi \rangle \frac{\partial F}{\partial \bar{\sigma}'_{ij}} = \left\langle \frac{1}{V} (\Delta\hat{\sigma})^n \right\rangle \frac{\partial F}{\partial \bar{\sigma}'_{ij}} \quad (14)$$

where  $V$  and  $n$  represent model parameters whose values can be determined from a single creep or stress relaxation experiment. The creep process terminates as the stress point  $(I_1, J, \theta)$  approaches (in the limit) the elastic nucleus. It is well known that after the primary phase of creep, the creep rate either decreases (tending, in the limit, to zero) or, at high stress levels, increases to the tertiary phase followed by creep rupture. By controlling the size of the elastic nucleus (via  $s_v$ ) and the specific functional form of the scalar overstress function (via  $V$  and  $n$ ), the former case can realistically be simulated using the present model. The model does not purport to simulate creep rupture well.

The plastic strain rate is given by

$$\dot{\varepsilon}_{ij}^p = \langle L \rangle \frac{\partial F}{\partial \bar{\sigma}'_{ij}} \quad (15)$$

where an associative flow rule has again been assumed. The scalar loading index  $L$  is given by



$$L = \frac{1}{K_p} \left\{ F_{,i_1} \dot{I}_1 + F_{,j} \dot{J} + \frac{1}{b} F_{,\theta} \dot{\theta} - \langle \phi \rangle \bar{K}_p \left[ \frac{1}{b} - C \left( 1 - \frac{1}{b} \right) \frac{F_{,i_1}}{F_{,i_o}} \right] \right\} \quad (16)$$

In equation (16), and in the subsequent equations, the partial derivative with respect to an invariant is denoted with a comma followed by the symbol of the invariant as a subscript. The loading index  $L$  accounts for the coupling of plastic-viscoplastic hardening for states on and within the bounding surface (Kaliakin and Dafalias 1990a). Loading, unloading and neutral loading is denoted by  $L > 0$ ,  $L < 0$ , and  $L = 0$ , respectively.

Based on equations (11), (14) and (15), the constitutive relations, in inverse form, are given by the following general expression

$$\dot{\sigma}'_{ij} = C_{ijkl} (\dot{\varepsilon}_{kl} - \dot{\varepsilon}_{kl}^v - \dot{\varepsilon}_{kl}^p) \quad (17)$$

where  $C_{ijkl}$  represents a tensor of elastic moduli given by

$$C_{ijkl} = \left( K - \frac{2}{3} G \right) \delta_{ij} \delta_{kl} + G (\delta_{ik} \delta_{jl} + \delta_{il} \delta_{jk}) \quad (18)$$

## DISCUSSION OF MODEL PARAMETERS

To better understand the apportionment of parameters associated with the present bounding surface model, consider the following overview of microscopic phenomena that underlie the macroscopic behavior of cohesive soils. Within a loaded cohesive soil, sufficiently large changes in effective stress cause an instantaneous plastic rearrangement of soil particles and/or particle clusters. The word "instantaneous" requires further explanation. It is a well-known fact that the testing of cohesive soils under drained conditions requires a finite waiting period between the application of load and the measurement of deformations. This is to allow for the dissipation of excess pore pressure within the sample, a process that is slowed by the low permeability of the soil and by the fact that drainage occurs only at the boundaries of the soil mass. Were it possible to establish drainage at all points within the sample, the above deformations would indeed appear to occur instantaneously in real time. Thus, if no further deformation of the particles occurs, the constitutive relations for cohesive soils in relation to effective stress could be formulated solely within the framework of rate independent elastoplasticity. However, the deformation continues past the instantaneous phase, and is attributed primarily to various diffusion processes that slowly change the partial equilibrium achieved during the instantaneous phase. Macroscopically these processes produce a delayed deformation of the soil that can be modeled in a unified manner within the framework of viscoplasticity. The instantaneous (elastoplastic) and delayed (viscoplastic) deformations are, however, known to occur simultaneously, with the development rate of the latter being slow enough to exhibit measurable effects only after considerable time has elapsed. Conversely, in the case of very rapid loading, the



delayed phenomena do not have a chance to become active to a significant degree. Instead it is the instantaneous elastoplastic response that almost fully accounts for the very rapid deformations that result.

Based on the above discussion it is possible to segregate the model parameters into elastoplastic and viscoplastic ones. In particular, associated with the model are twelve parameters that define the elastoplastic response and three parameters that define the viscoplastic response (Table 1). The parameter values are determined in accordance with the calibration procedure shown in Fig. 2. It is important to point out that the reason for having a large number of parameters is the desire to account for even relatively minute details of the stress-strain-time response; such details cannot be accounted for by simpler models that employ a lesser number of parameters. If such perfection is not desired, the actual number of model parameters can be reduced significantly. Further details pertaining to such simplifications are given in the fourth section of this paper.

In its most general form, the present bounding surface formulation becomes a fully three-dimensional time dependent constitutive model. With a single set of parameter values, the model predicts the behavior of cohesive soils at all overconsolidation ratios, subjected to either monotonic or cyclic compression and/or extension loading, under either drained or undrained conditions. The overconsolidation ratio (OCR) is defined as the ratio of the maximum preconsolidation stress to the current value of  $I_1$ .

To establish all the parameter values, a minimum of eight laboratory tests are required, namely: (1) A single isotropic or anisotropic (zero lateral strain) consolidation test with both loading and unloading phases; (2) Standard undrained (preferable) or drained axisymmetric compression and extension tests (with pore pressure measurements) on specimens in the normally, lightly, and heavily overconsolidated regions (a total of six tests); and, (3) At least one long term test (such as undrained or drained creep or stress relaxation) in order to calibrate time dependent response. The parameters entering the most general form of the elastoplastic-viscoplastic bounding surface formulation are now discussed.

### Elastoplastic Model Parameters

The parameters in this category are determined from results of standard laboratory tests of short enough duration to ensure that viscoplastic effects are negligible. For purposes of identification, these parameters are divided into three groups: the *traditional material constants*, the *surface configuration parameters*, and the *hardening parameters* (Table 1).

#### *Traditional Material Constants*

The traditional material constants are distinguished from the remaining elastoplastic model parameters by the fact that each member may be directly and independently determined from the results of simple, well-established laboratory experiments.

The slopes  $\lambda$  and  $\kappa$  are established by fitting straight lines to the virgin compression and swell/re-compression portions, respectively, of isotropic or one-dimensional consolidation test results (represented as plots of  $e$  vs.  $\ln I_1$ ).



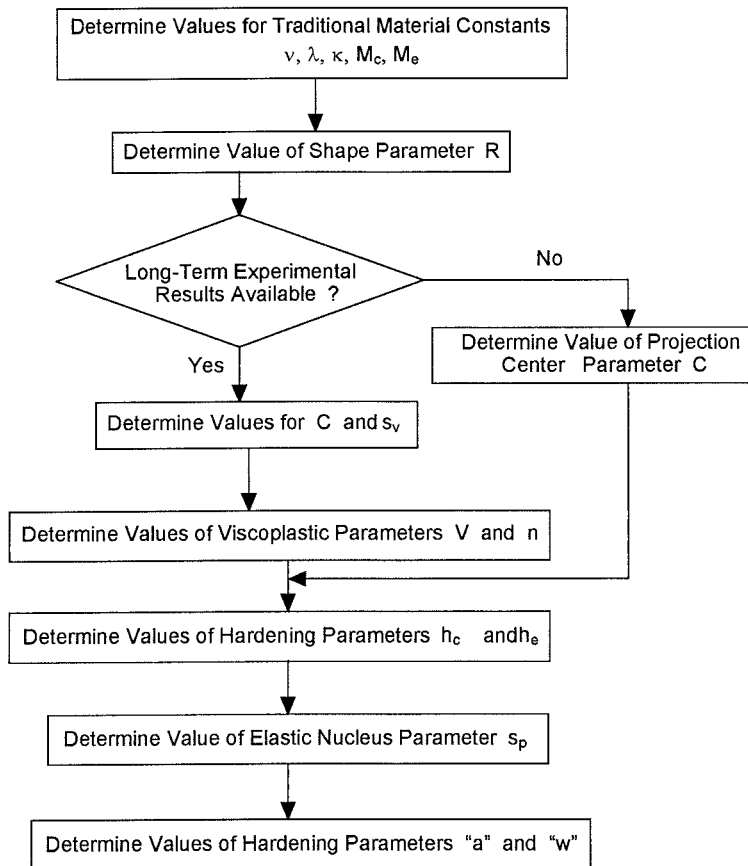


**FIG. 2. Recommended Calibration Procedure for Parameters Associated with the Elastoplastic-Viscoplastic Bounding Surface Model for Cohesive Soils**

The values of  $\lambda$  and  $\kappa$  are related to the more commonly known compression index ( $C_c$ ) and swelling index ( $C_s$ ) in the following manner:

$$\lambda = \frac{C_c}{2.303} , \quad \kappa = \frac{C_s}{2.303} \quad (19)$$

For a specific value of the Lode angle  $\theta$ , the failure surface is assumed to be straight and to coincide with the critical state line. In  $I_1 - J$  space, the slope of the critical state line is denoted by  $N$  (Figure 1). This parameter may take on different values in compression and extension; these are denoted by  $N_c$  and  $N_e$ , respectively. Plotting, for a fixed value of  $\theta$ , the values of  $I_1$  and  $J$  at ultimate conditions for each test under consideration and then fitting a straight line through these ultimate values and the origin typically determine this parameter. The slope of this line represents the desired value of  $N$ . This process is carried out for both compression and extension loading with the particular value of  $N$  determined in each case denoted by  $N_c$  and  $N_e$  respectively. These parameters are related to their counterparts  $M_c$  and  $M_e$  in triaxial stress space in the following manner:

$$N_c = \frac{M_c}{3\sqrt{3}} , \quad N_e = \frac{M_e}{3\sqrt{3}} \quad (20)$$

The parameters  $N_c$  and  $N_e$  are related to the friction angle from the Mohr-Coulomb failure criterion in the following manner:

$$N_c = \frac{6 \sin \phi'_c}{3\sqrt{3}(3 - \sin \phi'_c)} , \quad N_e = \frac{6 \sin \phi'_e}{3\sqrt{3}(3 + \sin \phi'_e)} \quad (21)$$

In equations (21), which are derived on the basis of the assumption of a purely frictional material,  $\phi'_c$  and  $\phi'_e$  represent the effective angle of internal friction in compression and extension respectively. These quantities are easily determined from most any standard laboratory strength test (e.g. from direct shear, simple shear, and/or axisymmetric triaxial tests).

A relation having the following form has traditionally described the variation of  $N$  with  $\theta$ .

$$N(\theta) = g(\theta, k)N_c \quad (22)$$

where  $k = N_e/N_c$ , with  $N_e = N(-\pi/6)$  and  $N_c = N(\pi/6)$  being the values of  $N$  associated with triaxial extension and compression, respectively. The dimensionless function  $g(\theta, k)$  must take on the values  $g(-\pi/6, k) = k$  and  $g(\pi/6, k) = 1$ . A simple form of this function, attributed to Gudehus (1973) and Argyris (Zienkiewicz and Pande 1977), and used by Dafalias and Herrmann (1982a, 1982b, 1986) in conjunction with bounding surface models for clays is

$$g(\theta, k) = \frac{2k}{1 + k - (1 - k)\sin 3\theta} \quad (23)$$

The relationship between the elastic bulk modulus  $K$  and  $\kappa$  is given by equation (12). The elastic shear modulus  $G$  is computed from  $K$  and a constant

Poisson's ratio  $\nu$ . In this case  $G$  is an increasing function of  $I_1$  and consequently invalidates the existence of an elastic potential (Houlsby 1985). Variations in  $G$  have no effect on the undrained stress path ( $I_1$  vs.  $J$ ), on the ultimate values of  $J$ , or on the pore pressure.

The determination of the remainder of the elastoplastic model parameters is complicated by the fact that their direct measurement in laboratory tests is not possible. Instead, these parameters must be established by a trial-and-error curve-fitting procedure that, in the most general case, utilizes the results of the laboratory tests described above.

#### *Surface Configuration Parameters*

The dimensionless parameter  $R$  defines the point  $(I_1 = I_o/R, J_1)$  that constitutes the intersection of the bounding surface with the critical state line (Figure 1). It defines the ratio of the major to minor axes for the entire surface, and is independent of Lode angle  $\theta$ . Experience has shown that a very close initial estimate of the "optimal" value of  $R$  may be obtained by considering only the undrained stress path of a normally consolidated (OCR = 1.0) soil subjected to an axisymmetric state of stress (DeNatale 1983). If experimental results for both compression and extension loading are available, this fitting procedure will, in general, yield slightly different values of  $R$ . An average value must be chosen keeping in mind that, in order to assure that the origin in stress space is not outside the bounding surface,  $R$  must be greater than or equal to 2.0.

The dimensionless parameter  $C$  ( $0 \leq C < 1$ ) defines the point along the  $I_1$ -axis that serves as the projection center in the "radial mapping rule" (Figure 1). Consequently, this parameter partly determines to which portion of the bounding surface the actual stress point is mapped. The value of  $C$  has no affect on the material response for states lying on the bounding surface. Since the associative flow rule has been assumed, variations in  $C$  (for stress states within the surface) thus alter the degree to which the material tends to dilate or compact. In the current formulation, different elastic nuclei are assumed for purposes of computing the plastic modulus (eq. 9) and the normalized overstress (eq. 13). Since both nuclei have the projection center as their center of homology, it follows that the selection of suitable values for  $C$  influences the magnitude of both quantities. If results for long term experiments are available and time dependent predictions are desired, a value for the projection center parameter  $C$  should be determined along with the value of  $s_v$  (see Figure 2). If, on the other hand, time dependent predictions are not desired, a suitable value for  $C$  is determined from a best fit of a family of undrained stress paths for lightly overconsolidated specimens subjected to standard short-term test conditions.

The dimensionless elastic zone parameter  $s_p$ , which enters equation (9), defines the extent of the elastic nucleus in the manner shown in Figure 1. A domain of purely elastic behavior is defined by the locus of states for which  $\delta > r/s_p$ . A value of  $s_p = 1$  causes the elastic nucleus to shrink to a point (the projection center), and thereby permits inelastic behavior to occur at any point within or on the bounding surface. A value of  $s_p = \infty$  implies purely elastic behavior at all points within the surface; as a result, the bounding surface behaves like a yield surface in the classical sense. Typical values for  $s_p$  are listed in Table 1.



**TABLE 1.** Typical Values of Parameters Associates with the Elastoplastic-Viscoplastic Bounding Surface Model for Cohesive Soils.

Traditional Material Constant (1)	Typical Value (2)	Range of Values (3)
$\lambda$	0.20	0.10 – 0.20
$\kappa$	0.05	0.02 – 0.08
$N_c$	0.19	0.15 – 0.27
$N_e$	0.15	0.12 – 0.19
$\nu$	0.22	0.15 – 0.30
<hr/>		
Surface Configuration Parameter		
$R$	2.30	2.00 – 2.80
$C$	0.30	0.00 – 0.50
$s_p$	1.10	1.00 – 1.50
<hr/>		
Hardening Parameter		
$h_c$	18.0	5.00 – 50.0
$h_e$	18.0	4.00 – 60.0
$a$	1.20	1.10 – 1.20
$c$	5.00	5.00 – 5.10
<hr/>		
Viscoplastic Parameter		
$s_v$	3.5	2.00 – 6.00
$V$	$3.0 \times 10^7$ kPa-min	$10^6 – 10^8$ kPa-min
$n$	2.80	2.00 – 4.00

### Hardening Parameters

The final group of elastoplastic parameters consists of the dimensionless hardening parameters  $h_c$ ,  $h_e$ ,  $a$  and  $w$  that control the degree of plastic hardening (or softening) occurring at stress points *within* the bounding surface through the hardening function  $H$ . This function relates the plastic moduli  $K_p$  and  $\bar{K}_p$  in the manner given in eq. (9). The following functional form of  $H$ , which represents a modification of earlier forms (Kaliakin and Dafalias 1989), is used:

$$H = \frac{1+e_{in}}{\lambda - \kappa} p_a [h(\theta)z^{0.02} + h_o(1-z^{0.02})] \frac{1}{2} \left[ a + \text{sgn}(n_p) \left( n_p \right)^{\frac{1}{w}} \right] \quad (24)$$

where  $\alpha$  and  $w$  are model parameters and  $h_o = (h_c + h_e)/2$ . In eq. (24)  $e_{in}$ ,  $\lambda$ , and  $\kappa$  are as previously defined. The quantity  $p_a$  denotes the atmospheric pressure, which is used to give  $H$  the proper units of stress cubed. The variable  $z$  is defined by  $z = J/J_1 = JR/NI_o$  (see Figure 1), and may be thought of as a weighting factor with respect to  $h(\theta)$  and  $h_o$ .

The dimensionless quantity  $h(\theta)$  defines the degree of hardening for points within the bounding surface, except those within the immediate vicinity of the  $I_1$ -axis where  $z$  approaches zero. Of all the hardening quantities,  $h(\theta)$  has the most fundamental and significant role. It is a function of the Lode angle  $\theta$  and varies in magnitude from a value of  $h_c = h(\pi/6)$  (corresponding to a state of triaxial compression) to a value of  $h_e = h(-\pi/6)$  (corresponding to a state triaxial extension). More precisely, this interpolation is given by (recall eq. 23)

$$h(\theta) = g(\theta, k)h_c = \frac{2\mu}{1 + \mu - (1 - \mu)\sin 3\theta} h_c \quad (25)$$

where  $\mu = h_e/h_c$ . The quantity  $h_o$  represents the hardening parameter for states in the immediate vicinity of the  $I_1$ -axis (i.e., for  $z \approx 0$ ). It is included in the formulation to assure continuity when the stress point crosses the  $I_1$ -axis, thereby improving numerical behavior in this region. Since it is typically set equal to the *average* of  $h_c$  and  $h_e$ ,  $h_o$  does not enter into the calibration process for the model parameters.

Finally, the quantity  $n_p$  represents the component in the  $I_1$ -direction of the unit outward normal to the bounding surface in invariant stress space. It ranges in value from +1 (corresponding to  $J = 0$  and  $I_1 > 0$ ) to -1 (for  $J = 0$  and  $I_1 < 0$ ). In conjunction with  $n_p$ , the model parameters  $\alpha$  and  $w$  control the decrease of  $H$  for heavily overconsolidated specimens (Kaliakin and Dafalias 1989).

By definition, variations in the hardening parameters do not affect the predicted material response of normally consolidated samples, or of any stress state lying on the bounding surface. The parameters  $h_c$  and  $h_e$  are thus determined by matching the results of lightly- and moderately overconsolidated specimens; the parameters  $\alpha$  and  $w$  are then determined from results of heavily overconsolidated specimens. The degree of inelastic hardening increases with  $h_c$  and/or  $h_e$ . The higher the value of these parameters, the greater is the magnitude of the plastic modulus  $K_p$ , and the "stiffer" is the response within the bounding surface. If  $h_c = h_e \approx \infty$ , the bounding surface assumes the role of a classical yield surface.

Before leaving the hardening parameters, it is interesting to note that both the exponent on  $z$  and the quantity  $h_o$  appearing in equation (24) were originally model parameters. However, subsequent experience indicated that in typical simulations these parameters were practically invariant. As such these values were *fixed* within the formulation, thus removing them from consideration by the analyst. In addition, experience with the model is showing that, with very minor exceptions, the dimensionless parameters  $\alpha$  and  $w$  are equal to 1.20 and 5.00, respectively.

### Viscoplastic Model Parameters

The viscoplastic contribution enters the constitutive relations through the values of  $s_v$ ,  $V$  and  $n$  appearing in eq. (14). As previously mentioned, these parameters do not affect the elastoplastic response; as such, during the calibration of the elastoplastic parameters, the values selected for the viscoplastic parameters are immaterial. Furthermore, in the course of calibrating the viscoplastic parameters, the values of the elastoplastic ones require no changes.

The values for these parameters are determined by matching the results of at least one long-term laboratory experiment. In particular, under conditions of undrained creep, the constitutive equations considerably simplify (Kaliakin and Dafalias 1990a) and allow the dimensionless parameter  $s_v$  to be determined in closed form. In theory  $s_v$  may assume any value in the range  $1 < s_v \leq \infty$ , though it typically falls within the more limited range listed in Table 1. A value of  $s_v = \infty$  implies purely elastic behavior (with respect to the viscoplastic response) at all points within the surface. As a result, the bounding surface behaves like a yield surface in a classical elastoviscoplasticity model.

The parameters  $V$  and  $n$  are then determined in a trial-and-error manner. The "viscosity parameter"  $V$  has units of viscosity; i.e., force-time/(length)<sup>2</sup>. The units used need not be explicitly defined, for they are the reciprocal of whatever time and stress units are assumed for the loading history. The parameter  $n$  is dimensionless. Typical values for  $V$  and  $n$  are given in Table 1.

### SIMPLIFIED FORMS OF THE MODEL

The current bounding surface formulation, in its most general form, requires the determination of parameters that define the initial state of the material (i.e., the initial effective stress state and the value of  $e_{in}$ ), as well as (depending upon which form of the bounding surface is used) sixteen or eighteen separate model parameters (Fig. 2). The latter include twelve parameters associated with the elastoplastic response and three parameters defining the viscoplastic response. Since in many applications a less general form of the model is sufficient, a brief discussion regarding the associated simplifications of the calibration procedure is presented in this section.

### Time -Independent Analysis of Overconsolidated Specimens

In light of the inaccuracies associated with the in situ-, as well as laboratory determination of soil properties, simplicity in constitutive modeling (at the expense of accuracy of predictions) is often justified. In such instances the difference between the values of certain bounding surface model parameters corresponding to triaxial compression and extension is neglected. This reduces the number of required parameter values and laboratory tests.

Simplified rate independent analyses of overconsolidated samples require knowledge of the quantities defining the initial state of the material, as well as the following model parameters:  $\lambda$ ,  $\kappa$ ,  $N_c$ ,  $N_e$ ,  $v$ ,  $R$ ,  $C$ ,  $s_p$ ,  $h_c$  ( $= h_e = h_o$ ),  $a$  and  $w$ . The values for  $\lambda$  and  $\kappa$  are obtained by matching the results of a single consolidation test (with loading and unloading phases). Using the procedure detailed in the previous section, values for the parameters  $N_c$ ,  $R$ ,  $C$ ,  $s_p$ ,  $h_c$ ,  $a$  and  $w$  are obtained by matching predicted results to those obtained from three isotropically consolidated-undrained



triaxial compression tests with pore pressure measurements. If the effective friction angle is determined, values for  $N_c$  and  $N_e$  can be computed using eqs. (20). If, on the other hand, the effective friction angle is not determined, a value for  $N_c$  must then be determined from the ultimate values of  $I_1$  and  $J$ . In this case  $N_e$  can, with little loss in accuracy, be assumed to equal 0.8 times  $N_c$ . If the results of any of the four laboratory tests mentioned above are unavailable, acceptable model predictions can still be obtained by setting a given parameter equal to the "typical" value given in Table 1.

### Time -Independent Analysis of Normally Consolidated Specimens

As mentioned in the discussion of the Surface Configuration Parameters, the projection center parameter  $C$ , the elastic nucleus parameter  $s_p$  as well as the hardening parameters  $h_c$ ,  $h_e$ ,  $a$ , and  $w$  do not affect the model predictions for stress points on the bounding surface. In the course of analyzing normally consolidated soils in either triaxial compression or triaxial extension, the stress point always lies on the surface (Fig. 1). Analyses under such conditions thus only require knowledge of the quantities defining the initial state of the material, as well as the following model parameters:  $\lambda$ ,  $\kappa$ ,  $N_c$  or  $N_e$ ,  $v$  and  $R$ . The determination of these parameters requires data from a single consolidation test (with loading and unloading phases) as well as a single consolidated-drained or undrained triaxial test (the latter with pore pressure measurements) on a normally consolidated sample in compression or extension.

In the simplified analyses discussed above, the consideration of viscoplastic effects requires knowledge of the values of four additional parameters ( $s_v$ ,  $V$  and  $n$ ). These are determined in the manner described in the section on Viscoplastic Model Parameters.

From the summary presented above, it is apparent that the number of required model parameters varies considerably with the degree of chosen simplification. In any case, with a single set of parameter values, the model predicts the behavior of soils at all degrees of overconsolidation, subjected to either monotonic or cyclic compression and/or extension loading, under either drained or undrained conditions.

### PARAMETER DATABASE

Ideally a sufficient amount of laboratory data is available from which the model parameter values can be determined following the procedure shown in Figure 2. Practically, however, this data will often be *incomplete*. As such, the analyst must assign "representative" values to some of the parameters. To facilitate such an undertaking, a rather extensive database of parameter values associated with the simulation of various cohesive soils has been compiled over time (Kaliakin and Dafalias 1991). The availability of such a database particularly aids analysts with little or no experience with the bounding surface constitutive model.

In order to enhance the understanding of the present model and to make the parameter values available in a more "user-friendly" manner, the database has been enhanced using the concept of hypermedia (Kaliakin 1991, 1993). With the demise of hypermedia and the growth of the Internet, this effort evolved into the development of the present web-based database that is available at the following URL: [http://www.ce.udel.edu/faculty/kaliakin/model\\_parameters.html](http://www.ce.udel.edu/faculty/kaliakin/model_parameters.html). The parameter values listed at this site are updated as new information becomes available, thus



maintaining a current list for users of the model. Since the database contains a large number of traditional model parameter values, it will likewise be useful to users of other constitutive models for soils.

## CONCLUSION

The elastoplastic-viscoplastic bounding surface model represents a novel approach to mathematically simulating the time related behavior of isotropic cohesive soils. Throughout the development of this constitutive model care was taken to avoid introducing an excessive number of parameters. Furthermore, a concerted effort was made to relate these parameters to constants familiar to the geotechnical engineering community. As a result of these special considerations, the following benefits were realized: (1) For a given material the parameter values are determined by following a well-defined calibration procedure that involves standard laboratory experiments; (2) The values of all parameters fall within fairly narrow ranges; (3) Due in part to their relation to standard geotechnical engineering constants and in part to the rather wide application of the model, a rather extensive database of parameter values has been developed for various cohesive soils; and, (4) The values of a few parameters were found to vary little with material type; as such they were fixed internally within the model and thus removed from consideration by the analyst.

## NOTATION

The following symbols are used in this paper:

$a$	=	hardening parameter
$b$	=	variable used in relating the actual and image stress points
$C$	=	projection center parameter
$C_c$	=	compression index
$C_s$	=	swell index
$C_{ijkl}$	=	tensor of elastic moduli
$e$	=	void ratio (ratio of volume of voids to volume of solids)
$e_{in}$	=	initial void ratio
$F$	=	analytical representation of the bounding surface
$G$	=	elastic shear modulus
$H$	=	scalar hardening function
$h_c, h_e$	=	hardening parameters
$h_o$	=	hardening parameter associated with states in vicinity of the I-axis
$I_1$	=	first invariant of the effective stress tensor
$I_o$	=	intersection of the bounding surface with the positive I-axis
$J$	=	square root of the second deviatoric stress invariant
$K$	=	elastic bulk modulus
$k$	=	the ratio $M_e / M_c = N_e / N_c$
$K_p$	=	plastic modulus
$L$	=	scalar loading index
$M$	=	slope of critical state line in triaxial (two-invariant) stress space
$N$	=	slope of critical state line in stress invariants space
$n$	=	parameter associated with viscoplastic response



$n_p$	=	component in the I-direction of the unit outward normal
$\bar{OCR}$	=	overconsolidation ratio
$p'$	=	mean normal effective stress
$p_a$	=	atmospheric pressure
$q$	=	deviatoric stress (principal stress difference)
$q_n$	=	internal variables
$r$	=	radial distance
$R$	=	parameter defining the shape of the bounding surface
$s_p, s_v$	=	parameters controlling the size of elastic nuclei
$s_{ij}$	=	deviatoric part of the effective stress tensor
$u$	=	pore fluid pressure
$V$	=	parameter associated with viscoplastic response
$w$	=	hardening parameter
$z$	=	$JR / NI_o$
$\delta$	=	Euclidean distance in stress space
$\delta_{ij}$	=	Kronecker delta
$\varepsilon_{ij}$	=	infinitesimal strain tensor
$\phi$	=	scalar overstress function
$\phi'$	=	effective angle of internal friction
$\kappa$	=	slope of the swell/re-compression line in a plot of $e$ vs. $\ln p'$
$\lambda$	=	slope of the consolidation line in a plot of $e$ vs. $\ln p'$
$\mu$	=	the ratio $h_e / h_c$
$\nu$	=	Poisson's ratio
$\theta$	=	"Lode" angle
$\Delta\hat{\sigma}$	=	normalized overstress
$\sigma'_{ij}$	=	effective stress tensor
$\sigma_{ij}$	=	total stress tensor

subscripts:

$c$	=	denotes compression
$e$	=	denotes extension

superscripts:

$e$	=	denotes an elastic quantity
$v$	=	denotes a viscoplastic quantity
$p$	=	denotes a plastic quantity

## REFERENCES

- Al-Shamrani, M. A. and S. Sture (1994). "Characterization of Time-Dependent Behavior of Anisotropic Cohesive Soils." *Computer Methods and Advances in Geomechanics*, H. J. Siriwardane and M. M. Zaman, eds., 1: 505-511.
- Al-Shamrani, M. A. and S. Sture (1998). "Time-dependent Bounding Surface Model for Anisotropic Cohesive Soils." *Soils and Foundations*, 38(1): 61-76.
- Anandarajah, A., Y. F. Dafalias, and L. R. Herrmann (1984). "A Bounding Surface Plasticity Model for Anisotropic Clays." *Proceedings of the 5<sup>th</sup> Engineering Mechanics Division Specialty Conference*, Wyoming: Laramie, II: 937-940.
- Anandarajah, A. and Y. F. Dafalias (1985). "An Anisotropic Hardening Bounding Surface Constitutive Model for Clays." *Proceedings of the Fifth International Conference on Numerical Methods in Geomechanics*, T. Kawamoto and Y. Ichikawa, eds., Rotterdam: Balkema, 1: 267-275.
- Anandarajah, A. and Y. F. Dafalias (1986). "Bounding Surface Plasticity III: Application to Anisotropic Cohesive Soils," *Journal of Engineering Mechanics, ASCE*, 112(12): 1292-1318.
- Dafalias, Y. F. (1975). "On Cyclic and Anisotropic Plasticity: i). A General Model Including Material Behavior Under Stress Reversals, ii). Anisotropic Hardening for Initially Orthotropic Materials," Ph.D. Dissertation, University of California, Berkeley.
- Dafalias, Y. F. (1979a). "A Bounding Surface Plasticity Model," Proceedings of the Seventh Canadian Congress of Applied Mechanics, Sherbrooke, Canada: 89-90.
- Dafalias, Y. F. (1979b). "A Model for Soil Behavior under Monotonic and Cyclic Loading Conditions," *Transactions of the Fifth International Conference on SMIRT*, Berlin, Germany, K (1/8).
- Dafalias, Y. F. (1982a). "Bounding Surface Elastoplasticity - Viscoplasticity for Particulate Cohesive Media," *Deformation and Failure of Granular Materials*, IUTAM Symposium on Deformation and Failure of Granular Materials, Delft, the Netherlands, P. A. Vermeer and H. J. Luger, eds., Rotterdam: A. A. Balkema, 97-107.
- Dafalias, Y. F. (1982b). "On Rate Dependence and Anisotropy in Soil Constitutive Modeling," *Results of the International Workshop on Constitutive Relations for Soils*, G. Gudehus, et al., eds., France: Grenoble, A. A. Balkema: 457-462.
- Dafalias, Y. F. (1986). "On Elastoplasticity-Viscoplasticity Constitutive Modelling of Cohesive Soils," Chapter 13 in *Geomechanical Modelling in Engineering Practice*, R. Dungar and J. A. Studer, eds., Amsterdam: Balkema, 313-330.
- Dafalias, Y. F. and Herrmann, L. R. (1980). "A Bounding Surface Soil Plasticity Model," Proceedings of the International Symposium on Soils Under Cyclic and Transient Loading, G. N. Pande and O. C. Zienkiewicz, ed., Balkema, pub., Rotterdam, 335-345.
- Dafalias, Y. F. and Herrmann, L. R. (1982a). "Bounding Surface Formulation of Soil Plasticity," Ch. 10 in: *Soil Mechanics – Transient and Cyclic Loads*, G. N. Pande and O. C. Zienkiewicz, ed., J. Wiley and Sons, Inc., Chichester, U. K., 253-282.

- Dafalias, Y. F. and Herrmann, L. R. (1982b). "A Generalized Bounding Surface Constitutive Model for Clays," *Application of Plasticity and Generalized Stress-Strain in Geotechnical Engineering*, R. N. Yong and E. T. Selig, eds., New York: ASCE, 78-95.
- Dafalias, Y. F. and Herrmann, L. R. (1986). "Bounding Surface Plasticity II: Application to Isotropic Cohesive Soils," *Journal of Engineering Mechanics, ASCE*, 112(12): 1263-1291.
- Dafalias, Y. F., Herrmann, L. R., and De Natale, J. S. (1982). "The Bounding Surface Plasticity Model for Isotropic Cohesive Soils and its Application at the Grenoble Workshop," *Results of the International Workshop on Constitutive Relations for Soils*, G. Gudehus, F. Darve, and I. Vardoulakis, eds. France: Grenoble, 273-287.
- DeNatale, J. S. (1983). "On the Calibration of Constitutive Models by Multivariate Optimization. A Case Study: The Bounding Surface Plasticity Model," Ph.D. Dissertation, University of California, Davis.
- Gudehus, G. (1973). "Elastoplastische Stofffleichungen fur trockenen Sand," *Ingenieur – Archiv*, Vol. 42.
- Herrmann, L. R., Kaliakin, V. N., Shen, C. K., Mish, K. D. and Zhu, Z-Y, 1987, "Numerical Implementation of a Plasticity Model for Cohesive Soils," *Journal of the Engineering Mechanics, ASCE*, 113(4): 500-519.
- Houlsby, G. T. (1985). "The Use of a Variable Shear Modulus in Elastic-Plastic Models for Clays," *Computers and Geotechnics*, 1: 3-13.
- Kaliakin, V. N. (1985). "Bounding Surface Elastoplasticity-Viscoplasticity for Clays." Dissertation presented to the University of California, Davis, in partial fulfillment of the requirements for the degree of Doctor of Philosophy.
- Kaliakin, V. N. (1991). "Hypermedia and its Application to Geotechnical Databases," *ASCE Geotechnical Congress*, ASCE, 88-98.
- Kaliakin, V. N. (1993). "Parameter Estimation for Elastoplastic-Viscoplastic Bounding Surface Model for Cohesive Soils," appearing in *Material Parameter Estimation for Modern Constitutive Equations* (AMD-Vol. 168), L. A. Bertram, S. B. Brown and A. D. Freed, eds., ASME Press: 171-182.
- Kaliakin, V. N. and Dafalias, Y. F. (1989). "Simplifications to the Bounding Surface Model for Cohesive Soils," *International Journal for Numerical and Analytical Methods in Geomechanics*, 13(1): 91-100.
- Kaliakin, V. N. and Dafalias, Y. F. (1990a). "Theoretical Aspects of the Elastoplastic-Viscoplastic Bounding Surface Model for Cohesive Soils," *Soils and Foundations*, 30(3): 11-24.
- Kaliakin, V. N. and Dafalias, Y. F. (1990b). "Verification of the Elastoplastic-Viscoplastic Bounding Surface Model for Cohesive Soils," *Soils and Foundations*, 30(3): 25-36.
- Kaliakin, V. N., Muraleetharan, K. K., Dafalias, Y. F., Herrmann, L. R. and Shinde, S. B. (1990). "Foundation-Response Predictions Below Caisson-Retained Island," *Journal of Geotechnical Engineering, ASCE*, 116(9): 1291-1308.
- Kaliakin, V. N., and Dafalias, Y. F. (1991). "Details Regarding the Elastoplastic-Viscoplastic Bounding Surface Model for Isotropic Cohesive Soils," Civil Engineering Report 91-1, University of Delaware, Newark, DE.



- Leidwanger-Rabis, C., Chambon, R. Catel, P. Charlier, R. and Li, X. L. (1995). "A Parametric Analysis for the Dafalias-Kaliakin Bounding Surface Viscoplastic Model Based on the Dilupress L. D. Test." *Computers and Geotechnics*, 17, 473-505.
- Ling, H. I., Yue, D., Kaliakin, V. N. and Themelis, N. J. (2002). "An Anisotropic Elasto-Plastic Bounding Surface Model for Cohesive Soils," *Journal of Engineering Mechanics, ASCE*, 128(7): 748-758.
- Ling, H. I., Yue, D. and Kaliakin, V. N. (2003). "Geosynthetic-Reinforced Containment Dike Constructed over Soft Foundation: Numerical Analysis," *Reinforced Soil Engineering: Advances in Research and Practice*, edited by H. I. Ling, D. Leshchinsky, and Tatsuoka, F., New York: Marcel Dekker, Inc., 283-295.
- Mroz, Z., Norris, V. A. and Zienkiewicz, O. C. (1978). "An Anisotropic Hardening Model for Soils and its Application to Cyclic Loading," *International Journal for Numerical and Analytical Methods in Geomechanics*, 2: 203-221.
- Mroz, Z., Norris, V. A. and Zienkiewicz, O. C. (1979). "Application of an Anisotropic Hardening Model in the Analysis of Elastoplastic Deformation of Soils," *Géotechnique*, 29: 1-34.
- Pan, Z. (2004). "Further Assessment of Predictive Capabilities of Bounding Surface Models for Cohesive Soils," MCE thesis, Department of Civil and Environmental Engineering, University of Delaware.
- Perzyna, P. (1966). "Fundamental Problems in Viscoplasticity", *Adv. Applied Mech.*, 9, 243-377.
- Pietruszczak, S. and Mroz, Z. (1979). "Description of Anisotropy of Naturally  $K_0$ -Consolidated Clays," *Proceedings of the Euromechanics Colloquium*, France: Villa-de-Lans, 115.
- Poran, C. J., Kaliakin, V. N., Herrmann, L. R., Romstad, K. M., Lee, D.-F. and Shen, C. K. (1986). "Prediction of Trial Embankment Behavior Hertfordshire County Councils – Stansford Abbotts", Proceedings of the Reinforced Embankment on Soft Ground, King's College, London.
- Shen, C. K., Sohn, J., Mish, K., Kaliakin, V. N. and Herrmann, L. R. (1986). "Centrifuge Consolidation Study for Purposes of Plasticity Theory Validation," *Consolidation of Soils: Testing and Evaluation*, ASTM STP 892, R. N. Yong and F. C. Townsend, Eds., American Society for Testing and Materials, pp. 593-609.
- Voyiadjis, G. Z. and D. Kim (2003). "Finite Element Analysis of the Piezocone Test in Cohesive Soils Using an Elastoplastic-Viscoplastic Model and Updated Lagrangian Formulation," *International Journal of Plasticity*, 19: 253-280.
- Zienkiewicz, O. C. and Pande, G. N. (1977). "Some Useful Forms of Isotropic Yield Surfaces for Soil and Rock Mechanics." Chapter 5 in *Finite Elements in Geomechanics*, G. Gudehus, ed.. London: Wiley-Interscience: 179-190.

## HYPOPLASTICITY AS A CONSTITUTIVE FRAMEWORK FOR GRANULAR SOILS

D. Kolymbas<sup>1</sup> and I. Herle<sup>2</sup>

**ABSTRACT:** A family of hypoplastic constitutive models enables to model the mechanical behaviour of soils and other granular materials. The model framework can be represented with a single tensorial evolution equation for the effective stress. Starting from several general requirements, a particular form of the constitutive equation can be defined. Adding void ratio as an additional state variable, the critical state concept is incorporated. A further refinement of the model can be achieved by adopting intergranular strains which take into account the recent deformation history. A straightforward calibration of the model contributes to convincing predictions of element tests and boundary value problems.

### INTRODUCTION

Soils belong to the family of particulate materials, which are the most interesting (from the point of view of mechanics) solids. They result from other solids which have been broken down into small grains. Some researchers consider the individual grains and their interaction. The main stream of research, however, disregards the individual grains and considers soil as a lumped body, a continuum. Although soil results from multiple fracture processes, it still possesses stiffness and can be considered as solid, provided that an externally (or internally) applied pressure holds the grains together. We obtain thus a very important property of soil: Its stiffness depends on stress, it increases with increasing stress level  $|\text{tr } \mathbf{T}|$ . This should be contrasted with elastic materials, which exhibit constant stiffness.  $\mathbf{T}$  denotes the CAUCHY stress,  $\text{tr } \mathbf{T}$  is the first invariant, i.e. the sum of principal stresses. The modulus  $|.|$  is used, because compressive stresses are here negative. In general we follow the tensor notation of NLFT (Truesdell C., and W. Noll 1965).

<sup>1</sup>Institute of Geotechnical and Tunnel Engineering, University of Innsbruck, Austria, e-mail: geotechnik@uibk.ac.at

<sup>2</sup>Institute of Geotechnical Engineering, TU Dresden, Germany, e-mail: ivo.herle@mailbox.tu-dresden.de



Another property of soil results from the obvious fact that grains, and in particular their mutual contacts, are arranged according to the deformation applied. If the deformation changes, then the scheme of grain contacts is also re-arranged, which implies a change of stiffness. Thus, stiffness also depends on deformation. In terms of continuum mechanics, the actual deformation can be expressed by the stretching tensor  $\mathbf{D}$ , which is the symmetric part of the velocity gradient  $\partial\mathbf{v}/\partial\mathbf{x}$ . Now, a change of  $\mathbf{D}$  can be a change of the direction of  $\mathbf{D}$  or a mere change of the time scale, i.e.  $\mathbf{D} \rightarrow \lambda\mathbf{D}$ . In a first approximation we consider soil as rate-independent, i.e. its stiffness does not depend on the time scale. We can model the mechanical behaviour of soil by a tensor-valued function that expresses the rate of stress  $\dot{\mathbf{T}}$  as a function of stress  $\mathbf{T}$  and stretching  $\mathbf{D}$ ,

$$\dot{\mathbf{T}} = h(\mathbf{T}, \mathbf{D}) , \quad (1)$$

and the aforementioned rate-independence implies a mathematical restriction to the function  $h(., .)$ , see sect. Rate Independence. Hypoplasticity emanated from the attempt to find appropriate mathematical expression for this function. The search procedure was guided by the material behaviour, as it is revealed by means of element tests, and by general restrictions, as the one referring to rate-independence.

To turn back to the mechanical behaviour of soil, we observe that a particulate body cannot sustain tensile principal stress (unless the grains are somehow glued together). It turns out that also compressive principal stresses are not sustainable, if one is much smaller than the other ones. Thus, not all stress states are feasible, the range of accessible stress states is limited by a surface in the stress space, that is called the limit surface. In physical terms, the inaccessibility of stress states beyond this surface is expressed by the fact that the stress remains unchanged upon continuation of the deformation. This behaviour is often called 'plastic flow'.

The mathematical expression of the limit surface is the starting point of the elasto-plastic theories. Based on this and aided by a series of accompanying notions such as 'flow rule', 'normality rule', 'consistency' and 'decomposition of strain into elastic and plastic parts', a frame is built that allows the mathematical simulation of the mechanical behaviour of soils. Due to the many accompanying notions, elasto-plastic theories are pretty complicated and they do not usually allow a direct insight into the mathematical relation that connects stresses with stains (or the corresponding rates). In the view of the authors, hypoplasticity is much simpler and — which counts more — easier in calibration and implementation.

An often posed question in relation to hypoplasticity refers to the material constants appearing in the equation. Some users are confused by the fact that these constants are not directly measured quantities such as the friction angle  $\varphi$ . In elastoplastic theories, quantities such as  $\varphi$  are basic ingredients and appear explicitly in the mathematical relations. However, it should be taken into account that quantities such as  $\varphi$  are not material constants. Sand can exhibit

a wide range of  $\varphi$ -values depending on void ratio and on stress level. Thus,  $\varphi$  is inappropriate as material constant. One has to search for appropriate material constants that appear in the mathematical relation and have the same value for a given soil, no matter what the actual void ratio and the stress level is. Only such quantities deserve being called 'material constants' (or 'material parameters'). Elastoplastic theories using  $\varphi$  as a material parameter insinuate that  $\varphi$  does not depend on void ratio and stress level.

At present, there are two versions of hypoplasticity, the one being developed in Karlsruhe, therefore termed K-hypoplasticity, and the other one in Grenoble, termed G-hypoplasticity (Desrues J. and R. Chambon 1993). Both approaches have many similarities (though being developed independently from each other) but also some differences, as pointed out in (Tamagnini C., G. Viggiani and R. Chambon 2000).

### Incremental Nonlinearity

$d\sigma/d\epsilon = \dot{\sigma}/\dot{\epsilon}$  represents the incremental stiffness of the materials considered (see Fig. 1). Since with anelastic (plastic) materials  $|d\sigma|$  (as well as the stiffness)

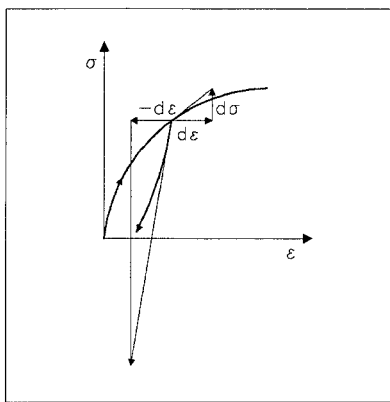


FIG. 1. Different stiffness at loading and unloading

is much larger at unloading than at loading, we infer that for such a material the function  $d\sigma = f(d\epsilon)$  or  $\dot{\sigma} = f(\dot{\epsilon})$  must be nonlinear in  $\dot{\epsilon}$  (or  $d\epsilon$ ). This non-linearity remains, no matter how small  $d\epsilon$  is. Therefore it is called 'non-linearity in the small' or 'incremental non-linearity'. Note that incremental non-linearity has nothing to do with the curved form of the stress-strain curve for loading. This curve can be, of course, linearized for small  $|d\epsilon|$ , a fact which led many people to believe that in physics every relation can be linearized 'in the small'. Thus, all elastoplastic and hypoplastic relations are incrementally non-linear.

## Objective Stress Rate

The time derivative of the stress tensor,  $\dot{\mathbf{T}}$ , is a quantity which depends on rotations of either the considered body or the observer. This means that it does not necessarily express stress changes due to deformation. Since a constitutive equation aims to express only stress changes due to deformation, it must use so-called objective stress rates, i.e. stress rates registered by a co-rotated observer. This can be achieved by the so-called co-rotated (ZAREMBA or JAUMANN) stress rate

$$\ddot{\mathbf{T}} = \dot{\mathbf{T}} - \mathbf{W}\mathbf{T} + \mathbf{T}\mathbf{W}, \quad (2)$$

where the spin-tensor  $\mathbf{W}$  is the antimetric part of the velocity gradient. It should be noted that there are many other objective stress rates (D. Kolymbas and I. Herle 2003), and a large part of the literature is devoted to the question of which of the objective stress rates is the proper one to be used in constitutive modelling.

## Rate Independence

Rate-independent materials are defined as materials without an internal time scale. I.e., the rate of deformation is immaterial for the final stress. In other words, rate-independent materials are invariant with respect to changes of time scale. If we deform a rate-independent material twice as fast, then the stress rate will also be doubled. Considering constitutive equations of the rate-type, this means that the stress rate  $\dot{\mathbf{T}}$  is positively homogeneous of the first degree with respect to  $\mathbf{D}$ :

$$h(\mathbf{T}, \lambda\mathbf{D}) = \lambda h(\mathbf{T}, \mathbf{D}) \text{ for } \lambda > 0 . \quad (3)$$

Note that this homogeneity does by no means imply linearity (cf. the relation  $y = |x|$ , which is homogeneous in the above sense, but not linear). Soils are not exactly rate-independent. Clays are more pronouncedly rate-dependent than sands. However, for a first approximation we can consider soils as rate-independent materials.

## Homogeneity in Stress

Assume that the relation  $\dot{\mathbf{T}} = h(\mathbf{T}, \mathbf{D})$  is homogeneous in  $\mathbf{T}$ , i.e.  $h(\lambda\mathbf{T}, \mathbf{D}) = \lambda^n h(\mathbf{T}, \mathbf{D})$ . Let us investigate the consequences of this assumption. Consider a stress state  $\mathbf{T}_1$ . We now determine the stretching in such a way that  $\dot{\mathbf{T}} = h(\mathbf{T}_1, \mathbf{D}_1) = \lambda\mathbf{T}_1$ . If we then continuously apply  $\mathbf{D}_1$ , then we shall obtain a stress path which is a straight line passing through the origin of stress space (see Fig. 2). This follows from our assumption, because

$$\ddot{\mathbf{T}}(t+dt) = h(\mathbf{T}_1 + \lambda\mathbf{T}_1 dt, \mathbf{D}_1) = (1 + \lambda dt)^n h(\mathbf{T}_1, \mathbf{D}_1) = (1 + \lambda dt)^n \dot{\mathbf{T}}(t) . \quad (4)$$

In other words, our assumption implies that proportional strain paths (i.e. paths with  $\mathbf{D} = \text{const}$ ) are connected by homothetic stress paths (i.e. straight stress

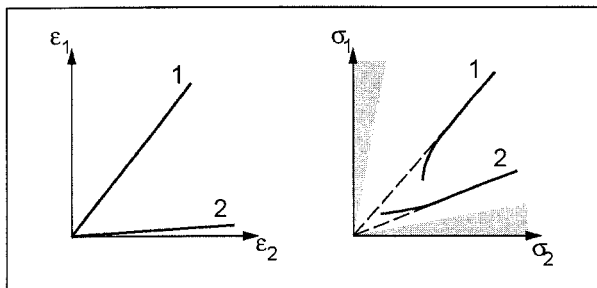


FIG. 2. Proportional stress paths corresponding to proportional strain paths

paths passing through the origin of the stress space) which are asymptotically reached independently on the initial stress. Note that proportional stress paths must be limited within a fan, because we know that there are inaccessible (unfeasible) stress states.

Let us now consider the degree of homogeneity. Knowing that  $d\sigma/d\epsilon = \dot{\sigma}/\dot{\epsilon}$  or  $\dot{\mathbf{T}}/\mathbf{D}$  is the stiffness, we infer that  $\dot{\mathbf{T}}/\mathbf{D}|_{\lambda\mathbf{T}} = \lambda^n\dot{\mathbf{T}}/\mathbf{D}|\mathbf{T}$ . In other words, if we increase the stress by a factor  $\lambda$ , the stiffness is increased by the factor  $\lambda^n$ . Experimentalists in soil mechanics often remark that *normalized* stress-strain curves coincide (this is in particular the case with normally consolidated clays). The consequence is  $n = 1$ . Setting  $n = 1$  would imply that the friction angle is invariant with respect to the stress level. This is an acceptable approximation to start with. However, if the changes of stress level at a given void ratio are considerable, then the variation of friction (and dilatancy) angles may not be neglected.

## GENERAL FRAMEWORK

Hypoplasticity is developed starting from the ansatz  $\dot{\mathbf{T}} = h(\mathbf{T}, \mathbf{D})$ . In the course of its history several mathematical expressions have been introduced. They were found by a trial-and-error procedure that was guided by general mathematical restrictions and the existing knowledge on material behaviour. Referring to the latter, it should be noted that the experimental outcomes are sometimes ambiguous and biased by unregistered departures from the assumed homogeneity of deformation. These departures are inevitable and have deep-seating explanation and mathematical implications. Experimental results referring to large monotonous deformations are considered as the most reliable ones, since the influence of initial inhomogeneities can be expected to asymptotically fade out.

Regarding the eq.  $\dot{\mathbf{T}} = h(\mathbf{T}, \mathbf{D})$  we observe that the only variables are the stress  $\mathbf{T}$  and the stretching  $\mathbf{D}$ . This means that the history of past deformation can only be stored in the actual stress  $\mathbf{T}$ . This is a very restrictive assumption

which, however, covers many aspects of soil behaviour. It also implies, however, that repeated stress load cycles will produce the same (additional) strains. This so-called ratchetting behaviour is not realistic. Almost to the same amount unrealistic is what classical elasto-plastic theories predict for stress cycles: additional stress cycles would not produce additional strain. Hypoplasticity with intergranular strain (see sect. 2.5) is an attempt to overcome the aforementioned shortcoming.

If we include in the list of variables of  $\mathbf{h}(\cdot)$  the void ratio  $e$ , we can cover pycnotropy, i.e. the dependence of material behaviour on density. Pertinent modifications of hypoplasticity are introduced by WU, GUDEHUS and other (see sect. Hypoplasticity).

### Hypoelasticity

TRUESELL (Truesdell C. 1965) has introduced constitutive relations of the form  $\dot{\mathbf{T}} = \mathbf{h}(\mathbf{T}, \mathbf{D})$ . He required that the function  $\mathbf{h}(\cdot)$  be linear in  $\mathbf{T}$  and in  $\mathbf{D}$ . He introduced the name hypoelasticity for such relations. Hypoelastic constitutive equations may produce curved stress-strain curves, and in some cases these stress-strain curves reach a horizontal plateau and can thus model plastic yield. However, the imposed incremental linearity implies equal stiffness for loading and unloading and thus renders hypoelastic relations inappropriate to describe anelastic (plastic) materials. Despite this, some hypoelastic relations have been launched in soil mechanics (e.g. by DAVIS and MULLENGER 1978). To overcome the equal stiffness at loading and unloading, they are (in most cases tacitly) endowed with additional stress-strain relations holding for unloading. Strictly speaking, these relations (regarded as a whole) are not hypoelastic any more.

### Elastoplasticity

We have seen that the problem of producing different stiffness at loading and unloading can be treated by introducing at least two different linear relations between  $\dot{\sigma}$  and  $\dot{\epsilon}$ , of which one holds for loading and one for unloading. This is the approach of the theory of elastoplasticity. It requires a series of precautions. First, what should be considered as loading and what as unloading has to be defined. This is accomplished by the introduction of the so-called yield surface, a surface in the stress space. Only such stress increments which start from this surface and point outwards are considered as loading, the remaining being unloading stress increments. Another precaution refers to the expectation that in the transition between loading and unloading the response must be continuous. This is accomplished by the so-called consistency condition. It is typical for the theory of elastoplasticity to consider a decomposition of strain into elastic and plastic parts, which cannot be distinguished in experiments. The most common theories of elastoplasticity require that the behaviour is elastic inside the yield surface, an assumption which is not realistic for soils. Another point of concern in elastoplasticity is how the yield surface changes its shape and position with loading. The stress-strain relation for loading is determined by the so-called

flow rule, which states that the increment (or rate) of the plastic strain is always normal to a so-called plastic potential surface. A special case arises if the plastic potential surface is set equal to the yield surface. This special case is called the normality condition. A set of very useful theorems has been formulated for such materials. However, normality is not realistic for frictional soils as it would imply that the dilatancy angle is equal to the friction angle, which is not the case. After all, we can summarize: Elastoplastic constitutive laws consist of two or more linear relations between  $d\varepsilon$  and  $d\sigma$ . As a whole, they are incrementally non-linear.

### Hypoplasticity

Elastoplastic and hypoelastic equations are both of the general form

$$\dot{\mathbf{T}} = \mathbf{h}(\mathbf{T}, \mathbf{D}) \quad . \quad (5)$$

Starting from the fact that every function  $\mathbf{h}(\mathbf{T}, \mathbf{D})$  can be represented according to the general representation theorem,

$$\begin{aligned} \mathbf{h}(\mathbf{T}, \mathbf{D}) = & \psi_1 \mathbf{1} + \psi_2 \mathbf{T} + \psi_3 \mathbf{D} + \psi_4 \mathbf{T}^2 + \psi_5 \mathbf{D}^2 + \psi_6 (\mathbf{T}\mathbf{D} + \mathbf{D}\mathbf{T}) \\ & + \psi_7 (\mathbf{T}\mathbf{D}^2 + \mathbf{D}^2\mathbf{T}) + \psi_8 (\mathbf{T}^2\mathbf{D} + \mathbf{D}\mathbf{T}^2) + \psi_9 (\mathbf{T}^2\mathbf{D}^2 + \mathbf{D}^2\mathbf{T}^2) \end{aligned} \quad (6)$$

( $\psi_i$  are scalar functions of invariants and joint invariants of  $\mathbf{T}$  and  $\mathbf{D}$ ), the experiment was undertaken to find such a function which appropriately describes the mechanical properties of soils (Kolymbas D. 1991). In order to avoid the shortcomings of hypoelasticity, this function has to be non-linear in  $\mathbf{D}$ . On the other hand, it should be homogeneous of the first degree in  $\mathbf{D}$  in order to describe rate independent materials and homogeneous in  $\mathbf{T}$  in order to describe proportional stress paths in case of proportional strain paths. Therefore, the design of such a function had to proceed along the above stated representation theorem and some general mathematical restrictions:

- non-linearity in  $\mathbf{D}$
- homogeneity in  $\mathbf{D}$  and  $\mathbf{T}$

with avoidance of any recourse to notions from the theory of elastoplasticity such as yield functions, decomposition of strain etc.

This experiment (every theory is, virtually, a Gedanken experiment) was more or less successful, as a function was found by trial and error which was able to describe many aspects of soil behaviour. Thus, a new approach to constitutive modelling was created. The name 'hypoplastic equations' fits very well, as the relation between hypoplasticity and elastoplasticity is the same as the one between hypoelasticity and elasticity: The theories with "hypo" do not use any potential. It should be mentioned that DAFALIAS (Dafalias Y.F. 1986) coined the term hypoplasticity earlier for something else, which can be considered as a general case of what we call hypoplasticity.

Let us now have a look at some hypoplastic equations. Most of them consist of 4 tensorial terms combined together with 4 material parameters, e.g. (Wu W.

and D. Kolymbas 1990):

$$\dot{\mathbf{T}} = C_1(\text{tr } \mathbf{T})\mathbf{D} + C_2 \frac{\text{tr}(\mathbf{T}\mathbf{D})}{\text{tr } \mathbf{T}} \mathbf{T} + C_3 \frac{\mathbf{T}^2}{\text{tr } \mathbf{T}} \sqrt{\text{tr } \mathbf{D}^2} + C_4 \frac{\mathbf{T}^{*2}}{\text{tr } \mathbf{T}} \sqrt{\text{tr } \mathbf{D}^2} \quad . \quad (7)$$

with the deviatoric stress  $\mathbf{T}^*$  defined as

$$\mathbf{T}^* = \mathbf{T} - \frac{1}{3}(\text{tr } \mathbf{T})\mathbf{1} \quad . \quad (8)$$

An alternative representation of hypoplastic constitutive equations is to summarize the linear terms by  $\mathbf{L}[\mathbf{D}]$  and the non-linear terms by  $\mathbf{N}[\|\mathbf{D}\|]$  with  $\|\mathbf{D}\| = \sqrt{\text{tr } \mathbf{D}^2}$ . Then, a hypoplastic equation assumes the general form

$$\dot{\mathbf{T}} = \mathbf{L}[\mathbf{D}] + \mathbf{N}[\|\mathbf{D}\|]. \quad (9)$$

As already stated, the experiment to describe soil behaviour with a sort of hypoelastic equation, extended to comprise terms which are non-linear though homogeneous of the first degree in  $\mathbf{D}$ , was successful. Several equations could be found with only 4 material parameters (Kolymbas D. 1987; Wu W. 1992; Wu W. and E. Bauer 1994; Wu W. and D. Kolymbas 1990) which were capable to describe

- the triaxial test as characterized by a stiffness decreasing down to zero at the limit state and a corresponding volumetric strain curve exhibiting first contractancy and then dilatancy
- incrementally non-linear behaviour, i.e. unloading stiffness much larger than at loading
- realistic asymptotic properties (referring to proportional paths).

However, void ratio was not taken into account, and, therefore, such simple hypoplastic constitutive models were not capable of describing the difference of friction angle and stiffness between dense and loose samples, or the decrease of the peak friction angle to the residual one with increasing volumetric strain (softening). But this was not expected from such a simple constitutive model. To achieve this, in more recent versions elaborated in Karlsruhe (Bauer E. 1996; Gudehus G. 1996; Kolymbas D. I. Herle, and P.-A. v. Wolffersdorff 1995; Wu W. and E. Bauer 1993; Wu W., E. Bauer, and D. Kolymbas 1996) several tensorial terms are multiplied with scalar factors which aim to model the influence of density and stress level as well as the transition to the so-called critical state. Of course, such factors increase the intricacy of the model. The general representation of a hypoplastic model reads then:

$$\dot{\mathbf{T}} = \mathcal{L}(\mathbf{T}, e) : \mathbf{D} + \mathbf{N}(\mathbf{T}, e)\|\mathbf{D}\| \quad (10)$$

The reader has hopefully noticed, that hypoplastic constitutive relations are directly presented without any reference to any sort of surfaces in stress space. However, various surfaces can be derived from a hypoplastic equation, as will be explained in Section 11.11.



## Development of Hypoplastic Models

The constitutive equation by Kolymbas (D. Kolymbas 1978) (called at that time *a nonlinear viscoplastic constitutive law*) can be considered as the first hypoplastic model. It is a rate-type equation, incrementally nonlinear and it can describe dilatancy, contractancy, limit states and also the asymptotic behaviour of soil (G. Gudehus et al. 1977). An advanced version of this model (D. Kolymbas 1985; Kolymbas, D. 1988) can be written as

$$\dot{\mathbf{T}} = C_1 \frac{1}{2} (\mathbf{T} \cdot \mathbf{D} + \mathbf{D} \cdot \mathbf{T}) + C_2 \text{tr}(\mathbf{T} \cdot \mathbf{D}) \mathbf{1} + \left[ C_3 \mathbf{T} + C_4 \frac{\mathbf{T} \cdot \mathbf{T}}{\text{tr} \mathbf{T}} \right] \|\mathbf{D}\| . \quad (11)$$

Eq. (11) is a special case of Eq. (10):  $\mathcal{L}$  und  $\mathbf{N}$  are tensorial functions homogeneous of the first degree with respect to  $\mathbf{T}$ . The void ratio is not included and different densities have to be modelled with different parameters  $C_1$  to  $C_4$ .

A detailed investigation of Eq. (11) has shown that one can find deformation paths resulting in tensile stresses which are not meaningful in case of dry granular materials. Subsequently WU (Wu W. 1992) succeeded in modifying  $\mathcal{L}$  and  $\mathbf{N}$  so that the calculated stress states remain always in the compressive range. His formulation was:

$$\dot{\mathbf{T}} = C_1 (\text{tr} \mathbf{T}) \mathbf{D} + C_2 \frac{\text{tr}(\mathbf{T} \cdot \mathbf{D})}{\text{tr} \mathbf{T}} \mathbf{T} + \left[ C_3 \frac{\mathbf{T} \cdot \mathbf{T}}{\text{tr} \mathbf{T}} + C_4 \frac{\mathbf{T}^* \cdot \mathbf{T}^*}{\text{tr} \mathbf{T}} \right] \|\mathbf{D}\| , \quad (12)$$

with the stress deviator  $\mathbf{T}^* = \mathbf{T} - (\text{tr} \mathbf{T}/3) \mathbf{1}$ . It was possible to determine the model parameters  $C_1$  to  $C_4$  from a calibration procedure (fitting the measured data in selected states) (D. Kolymbas 1994). An interpretation of these constants is however meaningless as they are not outcomes of experiments.

The characterization of soil states solely by the stress tensor represents a strong limitation for numerical modelling. One sand at various densities has to be described by different model parameters in spite of the same granulometric properties. Moreover, the simulated void ratio does not remain constant at large shear deformations. Loose skeletons become denser (contractant behaviour) and dense skeletons increase their volume (dilatant behaviour) if there is not a deformation constraint. To overcome this shortcoming, the relative density should be taken into account in the constitutive equation.

The common definition of relative density index

$$D_r = \frac{e_{max} - e}{e_{max} - e_{min}} \quad (13)$$

is pressure-independent because the maximum and minimum void ratios  $e_{max}$  and  $e_{min}$  are determined as single values from standard tests. On the other hand, it is often stated that dense granular materials at high pressures (e.g. at 1 MPa) behave like loose ones at low pressures (e.g. at 0.1 MPa).

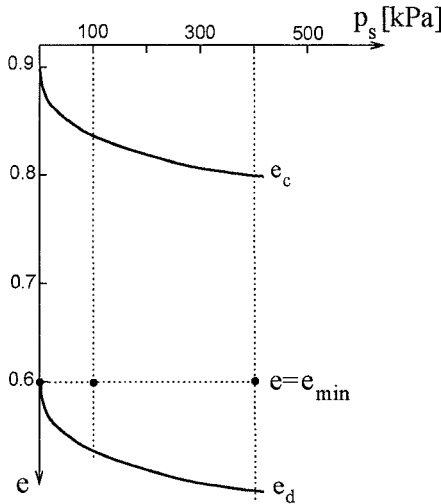


**FIG. 3.** Decrease of the pressure-dependent relative density with increase of the mean pressure in case of a constant void ratio.

This contradiction can be overcome if one considers a pressure-dependent relative density

$$D_p = \frac{e_c - e}{e_c - e_d} . \quad (14)$$

$e_c$  and  $e_d$  are the pressure-dependent critical and lowest void ratios, and they both decrease with increasing mean pressure  $p_s$ . In case of a constant void ratio, this results in decreasing  $D_p$  with increasing  $p_s$ . As shown in the example of Fig. 3 for  $e = e_{min}$  and thus  $D_r = 1$ : the pressure-dependent relative density changes from  $D_p = 1.0$  at  $p_s \approx 0$  to  $D_p = 0.65$  at  $p_s = 400$  kPa, i.e. the grain skeleton changes from dense one to medium dense one. Therefore, the behaviour at higher pressures even for  $D_r = 1$  corresponds to the behaviour of medium dense skeletons at lower pressures.

Following the outlined concept, WU (Wu W. 1992; Wu W. and E. Bauer 1993) proposed an extended version of his model

$$\dot{\mathbf{T}} = h(\mathbf{T}, \mathbf{D}, e) = \mathcal{L}(\mathbf{T}) : \mathbf{D} + I_e(e, \text{tr}\mathbf{T}) \mathbf{N}(\mathbf{T}) \|\mathbf{D}\| \quad (15)$$

using the scalar pressure- and density-dependent factor

$$I_e = (1 - a) \frac{e - e_{min}}{e_{crit} - e_{min}} + a \quad (16)$$

which already resembles Eq. (14). Nevertheless,  $e_{min}$  is a constant and the functions for  $e_{crit}$  and  $a$  include six additional constants which are difficult to

determine.

A further modification was accomplished by BAUER (E. Bauer and W. Wu. 1994) who introduced the factor

$$I_s = \left( \frac{e_{i0}}{e} \right)^\beta \quad (17)$$

as an additional scalar multiplier:

$$\dot{\mathbf{T}} = I_s [\mathcal{L}(\mathbf{T}) : \mathbf{D} + I_e(e, \text{tr}\mathbf{T}) \mathbf{N}(\mathbf{T}) \|\mathbf{D}\|] \quad (18)$$

$e_{i0}$  and  $\beta$  are further material constants.

KOLYMBAS *et al.* (Kolymbas D. I. Herle, and P.-A. v. Wolffersdorff 1995) chose another way and extended Eq. (12) by using 6 terms together with a back stress tensor which evolves with mean pressure and void ratio. In spite of having a lower number of constants than Eq. (18), they were able to reproduce many basic features of material behaviour, including critical states. However, the determination of the constants was still based on a calibration procedure which was sensitive to the interpretation of experimental results.

Requirements on physically sound material parameters which could be determined from simple experiments stimulated GUDEHUS (Gudehus G. 1996) to the modification of Eq. (18). He considered the relative void ratio

$$r_e = \frac{e - e_d}{e_c - e_d} = 1 - D_p \quad (19)$$

using the two pressure-dependent limit void ratios  $e_c$  und  $e_d$ . The minimum void ratio  $e_d$  is reached by densification with shear cycles of a small amplitude. Another limit void ratio,  $e_i$ , corresponds to the maximum void ratio during an isotropic compression starting from the suspension of grains. Thus,  $e_i$  is the upper bound of possible void ratios whereas  $e_d$  is the lower bound. All three limit void ratios decrease with the mean effective pressure  $p_s = -\text{tr}\mathbf{T}/3$ . Such a decrease of  $e_i$  and  $e_c$  with  $p_s$  has been confirmed experimentally (e.g. (R. Verdugo and K. Ishihara 1996) for sand or (K. Roscoe, A. Schofield and C. Wroth 1958) for clay and steel balls). The variation of  $e_d$  with  $p_s$  is usually neglected (R. Verdugo and K. Ishihara 1996). Using  $r_e$ , the factor  $I_e$  in Eq. (18) was replaced by the factor

$$f_d = r_e^\alpha \quad (20)$$

with  $\alpha$  being a material parameter.

In order to get realistic void ratios at low as well as at high mean pressures, BAUER (E. Bauer and W. Wu. 1994; Bauer E. 1996) proposed the following equation:

$$\frac{e_i}{e_{i0}} = \frac{e_c}{e_{c0}} = \frac{e_d}{e_{d0}} = \exp \left[ - \left( \frac{3p_s}{h_s} \right)^n \right]. \quad (21)$$

At zero pressure the values of  $e_i$ ,  $e_c$  and  $e_d$  correspond to  $e_{i0}$ ,  $e_{c0}$  and  $e_{d0}$  and for high pressures they tend to zero (Fig. 10). The ultimate hardness  $h_s$ , which

is different than the hardness of single grains, scales the mean pressure  $p_s$ . The exponent  $n$  takes the pressure sensitivity of the grain skeleton into account.

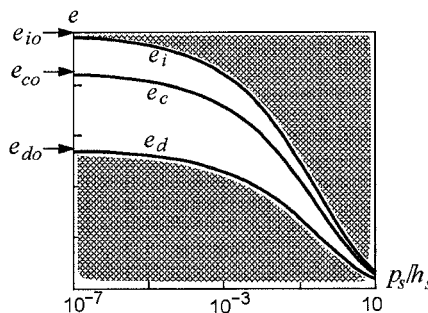


FIG. 4. Decrease of  $e_i$ ,  $e_c$  and  $e_d$  with increase of the mean effective pressure  $p_s$ ; grey areas lie outside of the applicability range of the hypoplastic model.

A similar concept of pressure-dependent limit void ratios can be also found in the CAM-CLAY constitutive model (A. Schofield and C. Wroth 1968). Nevertheless, in this model the decrease of  $e_i$  and  $e_c$  with increasing  $p_s$  is characterized with a logarithmic relation, which is valid only in a limited pressure range and  $e_d$  is not considered.

In range of low pressures Eq. (21) corresponds to the compression law

$$E_s = v \left( \frac{T_1}{T_0} \right)^w \quad (22)$$

proposed already by OHDE (J. Ohde 1939).  $T_1$  denotes the vertical stress in oedometer and the parameter  $v$  equals to the oedometric modulus  $E_s = T_1/D_1$  at the vertical stress  $T_1 = T_0$ . The exponent  $w$  is a material constant. The comparison of Eq. (22), which has found many applications in soil mechanics (K. Hrubař 1958; N. Janbu 1963; P. Vermeer 1982; J. Pestana and A. Whittle 1995), with Eq. (21) can be done for  $p_s \ll h_s$ :

$$\exp \left[ - \left( \frac{3p_s}{h_s} \right)^n \right] \approx 1 - \left( \frac{3p_s}{h_s} \right)^n \quad (23)$$

In order to link Eq. (21) with Eq. (18), the following consistency condition was postulated (Gudehus G. 1996): the calculated stress rates in case of isotropic compression starting from  $e_{i0}$  must be identical with both equations. This condition yields another scalar factor,  $f_b$ , which does not need any additional material parameters and is involved in the factor  $I_s$  in Eq. (18).

The use of the material parameters  $C_1$  to  $C_4$  was circumvented by prescribing the shape of the limit stress surface in the critical state (E. Bauer. 1995; P.-A. von Wolffersdorff 1990; E. Bauer 1997). The experimentally confirmed

MATSUOKA-NAKAI criterion (H. Matsuoka and T. Nakai 1977) was chosen as an appropriate one to describe the critical state in stress space. Assuming the same ratio of the maximum and minimum principal stress in triaxial compression and extension, a single parameter  $\varphi_c$  (critical friction angle) is sufficient for the characterization of the critical stress surface.

### Recent Deformation History

In the hypoplastic models described up to this point, stress tensor and void ratio are the only state variables. They are sufficient for the material characterization during monotonous deformation processes. However, in case of cyclic deformation, an additional state variable is needed. This may be demonstrated in Fig. 5 where idealized experimental isotropic compression curves are plotted. In the point  $b$ , different soil behaviour can be observed: there is difference in stiffness between reloading (full line) and primary loading (dashed line) in spite of the same stress, void ratio and deformation direction.

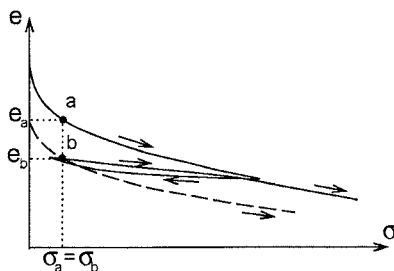


FIG. 5. Isotropic compression curve. In the point  $b$ , stress and void ratio does not fully characterize the state of soil.

NIEMUNIS and HERLE (A. Niemunis and I. Herle 1997) proposed the so-called *intergranular strain*, which is a tensorial state variable storing the recent deformation history. Simplifying the representation of the intergranular strain into one dimension, one can write

$$\begin{aligned}\dot{\delta} &= \left(1 - \frac{|\delta|}{R}\right) D && \text{for } D\delta > 0 \\ \dot{\delta} &= D && \text{for } D\delta \leq 0\end{aligned}\quad (24)$$

with  $\delta$  being the intergranular strain, and  $R$  a material parameter. If  $\delta < R$ , the incremental stiffness is increased, viz

$$\begin{aligned}\dot{T} &= \frac{1}{R} [m(R - |\delta|) + |\delta|] MD && \text{for } D\delta > 0 \\ \dot{T} &= mMD && \text{for } D\delta \leq 0,\end{aligned}\quad (25)$$

with  $M$  being the incremental hypoplastic stiffness  $M = f(T, e, D/|D|)$  and  $m$  a material parameter.

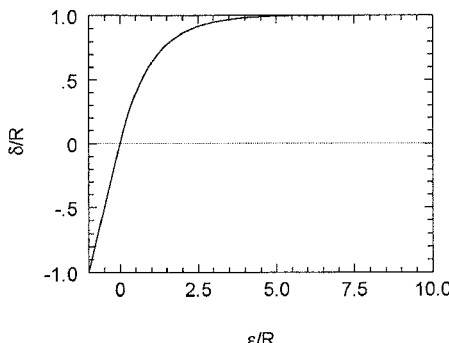


FIG. 6. Evolution of intergranular strain  $\delta$  during monotonic deformation.

The outlined evolution equation for  $\delta$  possesses asymptotic properties as  $\delta \rightarrow R$  for monotonic deformation (Fig. 6). In case of cyclic deformation, an asymptotic stabilization of  $\delta$  is obtained too (Fig. 7).

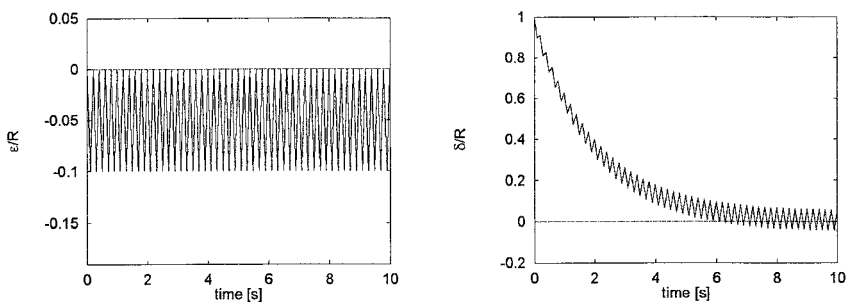


FIG. 7. Evolution of intergranular strain  $\delta$  during cyclic deformation.

Several successful applications in calculations of boundary value problems (summarized e.g. in (G. Gudehus. 1997)) support this concept.

### Limit States

A very important property of granular materials is their ability to flow (or yield), i.e. to undergo large deformations without stress change, as soon as the stresses and the void ratio obtain their critical values. This sort of flow should be attributed as ‘plastic’ flow and distinguished from the flow of fluids. The latter has a pronounced viscous (rate-dependent) character.

**@Seismicisolation**

Plastic flow occurs as soon as the stress state  $\mathbf{T}$  and the strain rate  $\mathbf{D}$  fulfil the condition  $h(\mathbf{T}, \mathbf{D}) = 0$ . In the theory of elastoplasticity the first condition is called the yield (limit) surface, and the second condition is called the flow rule. 'Flow' means that stiffness vanishes for particular  $\mathbf{T}$  and  $\mathbf{D}$  values.

In elastoplasticity the yield function is the starting point. The mathematical relation  $h(\mathbf{T}, \mathbf{D})$  is based upon the yield function. In contrast, it can be shown that a yield function is contained in a hypoplastic formulation  $\dot{\mathbf{T}} = h(\mathbf{T}, \mathbf{D})$ , i.e. the yield function  $f(\mathbf{T})$  can be derived from the constitutive relation. To this purpose we rewrite (following a proposition of CHAMBON ()) the equation (9) in the form

$$\dot{\mathbf{T}} = \mathbf{L}(\mathbf{T}, \mathbf{D}) + \mathbf{N}(\mathbf{T})||\mathbf{D}|| = \mathbf{A}(\mathbf{T}) [\mathbf{D} + \mathbf{B}||\mathbf{D}||] \quad , \quad (26)$$

with  $\mathbf{A}(\mathbf{T})$  being a matrix operator applied to its tensorial argument written in brackets. It is obvious that  $h(\mathbf{T}, \mathbf{D}) = 0$  occurs for

$$\mathbf{D}^0 := \mathbf{D}/||\mathbf{D}|| = -\mathbf{B} \quad . \quad (27)$$

Consequently, the function  $f(\mathbf{T})$  reads

$$f(\mathbf{T}) = \mathbf{B}^2 - 1 \quad , \quad (28)$$

with  $\mathbf{B}$  being a function of  $\mathbf{T}$ . in other words, the yield surface reads:

$$f(\mathbf{T}) = \mathbf{B}^2 - 1 = 0 \quad . \quad (29)$$

Due to the homogeneity of  $h(\mathbf{T}, \mathbf{D})$  (and consequently also of  $\mathbf{B}$ ) in  $\mathbf{T}$ , the surface  $f(\mathbf{T}) = 0$  is a cone with apex at the origin  $\mathbf{T} = \mathbf{0}$ . The cross section of this cone with the deviatoric plane reveals the influence of the intermediate principal stress, i.e. the yield surface differs from the MOHR-COULOMB criterion.

In classical soil mechanics the yield surface is considered as a limit, i.e. it is expected that no stress path can transcend this surface. According to our understanding, this is an unnecessary and also unrealistic restriction. There is in fact no reason (either conceptual or experimental) why this surface should be conceived as a limit which encloses all feasible stress states. Experiments show that the yield surface can be transcended (Wu W. 1992; Wu W. and A. Niemunis 1997). This fact can easily be modelled by constitutive equations of the type (9). Moreover, such equations make possible to analytically determine a surface in the stress space which encloses all feasible stress states. This surface is called bound surface, its derivation is stated in (Wu W. and A. Niemunis 1996). Of course, the bound surface lies outside the yield surface.

### Dilatancy and Pore Pressure

The tendency of soils to contract or dilate at shearing is known as a peculiar feature of granular materials. Some people believe that dilatancy can be modelled even with a linear elastic model if the POISSON's ratio is properly

chosen. However, this is not true, as in linear elastic materials the hydrostatic and the deviatoric stresses and strains are completely uncoupled. It is in this coupling that dilatancy resides, since it means that the volumetric strain is affected by deviatoric stress and vice versa. In the course of conventional triaxial tests with dense sand, an initial contractancy (or negative dilatancy) is followed by dilatancy. The initial contractancy is often attributed to compressibility since the volumetric decrease is accompanied with an increase of the hydrostatic stress. However, the initial volume decrease occurs also in tests with constant hydrostatic stress, so that "contractancy" appears to be a suitable name.

A reference is often made to the angle of dilatancy. However, this angle is by no means a material constant. Much more it depends on the deformation mode and stage, on the density and on the stress level. We should get rid of the preoccupation that the dilatancy angle (as well as the friction angle) are material constants.

Let us now consider suppressed dilatancy (or contractancy) in case of undrained deformations of water saturated soil. An often cited expression is "the soil wants to decrease its volume but it cannot; consequently the hydrostatic effective stress is decreased". Of course, such an explanation is not very satisfactory. A much better approach is to consider pore water as imposing the internal constraint of incompressibility. Then, the porewater pressure  $p$  is constitutively indeterminate and can only be determined from static boundary conditions. The constitutive equation is now changed to

$$\mathring{\mathbf{T}} = \mathbf{h}(\mathbf{T}, \mathbf{D}) - p\mathbf{1} . \quad (30)$$

Here,  $\mathbf{T}$  should be understood as the effective stress. Thus, the pore pressure build up in the course of undrained tests can be easily and realistically modelled by means of hypoplasticity.

### Barotropy and Pyknontropy

These words of greek origin were introduced in order to express the fact that the soil behaviour depends on stress level (i.e. on  $\text{tr } \mathbf{T}$ ) and on density (Kolymbas D. 1991). Contrary to an initial assumption valid mainly in the mechanics of normal consolidated clays, normalized stress strain curves referring to tests on sands do *not* coincide. The experimental observation, that the friction and dilatancy angles are gradually decreased by increased stress level, points to the fact that the function  $\mathbf{h}(\mathbf{T}, \mathbf{D})$  is not homogeneous with respect to  $\mathbf{T}$ . Thus, sand is not a self-similar material, i.e. it cannot model itself at geometrically reduced scale model tests.

Pyknontropy stems from the obvious fact that the behaviour of granular materials depends on density (void ratio). It is a very astonishing fact that granulates (contrary to other atomistic materials like e.g. gases) do not have a unique relation between density and stress level. Even more, at one and the same stress level the void ratio may range between two limits. As GUDEHUS (Gudehus G. 1996) pointed out, these limits must be stress level dependent.

## Softening

It is one of the open questions in soil mechanics, whether softening (see Fig. 8) exists or not. Traditionally, softening was considered as a principal part of soil behaviour. Later on it became "fashionable" to deny softening as being only an apparent effect due to the inhomogeneous deformation of the samples. The view in hypoplasticity is that a large amount of the registered softening is due to the inhomogeneous sample deformation. However, the 'material' softening, i.e. the softening which would be exhibited by a fictitious sample undergoing homogeneous deformation, is also there. We have to admit that the onset of inhomogeneous deformation makes the experimental approach unfeasible. We can, however, proceed by reasoning. It is a matter of fact that dense samples have a higher strength (i.e. peak stress deviator) than loose ones. In the course of deformation, dilatancy transforms a sample from dense to loose. Consequently, its strength must decrease and this is material softening.

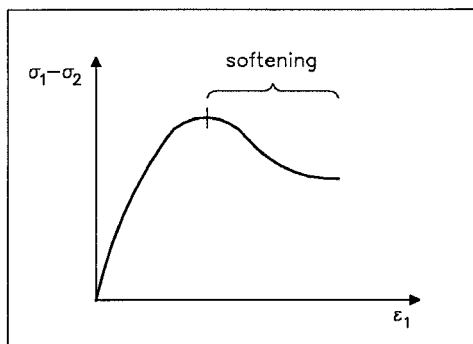


FIG. 8. Softening in triaxial test deformation

## Rate Dependence of Soils

Referring to rate dependence, we should distinguish related notions such as viscosity, relaxation, time dependence. All these notions have in common that they imply one or more material parameters bearing the dimension of time. An explicit appearance of time  $t$  in the constitutive equation implies that there is no invariance with respect to the time coordinate. In other words, the material exhibits ageing. This can only be defined within the framework of particular constitutive relations.

In soil mechanics, rate dependence is more pronounced for clays and is mainly manifested as creep (secondary consolidation) or increase of shear stresses by increasing the deformation rate, respectively. Such rate dependence resides in the grain skeleton and not in the free pore fluid (cf. consolidation according to TERZAGHI's theory). Also sands are rate dependent (di Prisco C. and S. Imposimato 1996) but to a much lesser degree than clays.

Another phenomenon is relaxation, i.e. the decrease of stress with time when the deformation remains constant. The measurement of relaxation is very difficult as the measurement of forces by means of load cells requires a minute deformation of the load cell and, consequently, also of the sample such that the condition  $\epsilon = \text{const}$  is not perfectly fulfilled. The often assumed correspondence between relaxation and creep is directly applicable to viscoelastic materials only. For the general case, it is a very difficult task to incorporate relaxation in a constitutive relation. Perhaps this task is also of minor importance since the stress drop due to relaxation is quickly recovered as soon as the deformation is resumed.

There have been several attempts to model rate dependence in hypoplasticity using a constitutive relation  $\mathbf{h}(\mathbf{T}, \mathbf{D})$  which is no more homogeneous with respect to  $\mathbf{D}$  (Kolymbas D. 1977; Wu W. et al. 1993; Gudehus G. 1996). A review of these relations together with a promising proposal was given by NIEMUNIS (Niemanis A. 1996).

## CALIBRATION

A constitutive relation is of no use if the parameters involved cannot be adapted to a particular material. The values of these parameters constitute the identity card of this material with respect to a particular constitutive model. Moreover, a particular parameter is useless unless it is embedded within a constitutive model. The process of the determination of the values of the parameters of a constitutive model is called "calibration" or "parameter identification". In the overwhelming number of publications on constitutive models the calibration is often simply omitted as being not worth mentioning. In fact it is — with the majority of models — a task which can take up to several months of work! Considering hypoplastic constitutive equations, the calibration is straightforward by fitting the equation to the outcomes of one or several (say triaxial) tests (Kolymbas, D. 1988). Knowing the strain increment and the stress increment at a particular stress state from experiments, the only unknowns in the equation are the material constants. To solve a system of four linear equations is no problem nowadays.

For the determination of the parameters of the hypoplastic model it is sufficient to consider fixed directions of principal stresses  $T_1 \leq T_2 \leq T_3$  which coincide with principal stretchings  $D_1, D_2, D_3$ . Denoting  $\hat{T}_j = T_j/(T_1 + T_2 + T_3)$  we can write:

$$\begin{aligned}\dot{T}_j &= \frac{f_s}{\hat{T}_1^2 + 2\hat{T}_2^2} \left[ D_j + a^2 (\hat{T}_1 D_1 + 2\hat{T}_2 D_2) \hat{T}_j + \right. \\ &\quad \left. + f_d \frac{a}{3} (6\hat{T}_j - 1) \sqrt{D_1^2 + 2D_2^2} \right] \quad (31)\end{aligned}$$

Consider Eq. (31) in case of a large monotonic shear deformation. Due to the asymptotic properties of simple grain skeletons a critical state with

$$\dot{T}_j = 0, \quad D_1 = 2D_2 = 0, \quad \text{and } e = e_c \quad (32)$$

will be approached. For a standard triaxial compression test, in which a cylindrical sample is compressed axially at a constant lateral stress  $T_2 = T_3$ , and using  $\dot{T}_1 + \dot{T}_2 + \dot{T}_3 = 0$ , Eq. (31) reduces to

$$a(T_1 - T_2) - \sqrt{\frac{3}{2}}(T_1 + 2T_2) = 0 . \quad (33)$$

Inserting the definition of the critical friction angle

$$\sin \varphi_c = \left( \frac{T_1 - T_2}{T_1 + T_2} \right)_c \quad (34)$$

one obtains a relation between  $a$  and  $\varphi_c$ :

$$a = \frac{\sqrt{3}(3 - \sin \varphi_c)}{2\sqrt{2} \sin \varphi_c} \quad (35)$$

There is enough experimental evidence (D. Cornforth 1973) that  $\varphi_c$  can be estimated from the angle of repose if cohesive forces are negligible.  $\varphi_c$  depends mainly on the grain size and angularity, being only little affected by nonuniformity of the grain size distribution (I. Herle and G. Gudehus 1999).

The second parameter related to the critical state is  $e_{c0}$ . It is defined at pressure zero, hence no direct measurement is possible. Nevertheless, a change of  $e_c$  with  $p_s$  has been the topic of many experimental studies enabling an extrapolation of  $e_c-p_s$  curves to  $p_s = 0$ . It can be observed that  $e_{c0} \approx e_{max}$  (M. F. Riemer et al. 1990; I. Herle and G. Gudehus 1999). This can be explained by reaching rather a critical state in  $e_{max}$ -tests, in which granular materials undergo large shear deformations at very low pressures.  $e_{max}$  shows a good correlation with granulometric properties (J. Kolbuszewski and M. Frederick 1963; T. Youd 1973): it decreases with increasing  $C_u$  and decreasing angularity.

The maximum void ratio,  $e_i$ , during isotropic compression is higher than  $e_{max}$ . In case of a skeleton composed from identical spheres, the value of  $e_{i0}$  corresponds to the theoretical maximum void ratio of a regular array of spheres, i.e.  $e_{i0} = 0.91$ . Comparing this value with the experimentally measured  $e_{max} \approx 0.75$  for glass spheres, the ratio  $e_{i0}/e_{max} \approx 1.20$  is obtained. One can get a similar value assuming an array of identical cubes (I. Herle and G. Gudehus 1999).

The decrease of  $e_i$  with increase of  $p_s$  is modelled by Eq. (21) using the constants  $h_s$  and  $n$ . This relation describes a stress-strain curve for any proportional compression (a compression with constant components  $D_i \leq 0$ ) which starts from a void ratio  $e_{p0}$  at pressure zero, with  $e_{p0}$  corresponding uniquely to the particular direction of stretching,  $e_{i0} \geq e_{p0} \geq e_{c0}$  (Bauer E. 1996). Consequently, for the experimental determination of  $h_s$  and  $n$ , a simple oedometer test is sufficient. Small variations of an initial void ratio do not influence the course of the measured curve (I. Herle and G. Gudehus 1999), thus it is possible to prepare the specimen at  $e$  close to  $e_{max}$ .

It is not appropriate to determine  $h_s$  and  $n$  from a numerical fitting of the measured data. Due to the strong nonlinearity of Eq. (21), more combinations

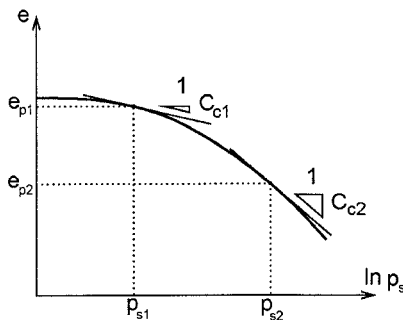


FIG. 9. Determination of the exponent  $n$  for the pressure range between  $p_{s1}$  and  $p_{s2}$  from  $C_c$  and  $e$  at the pressure range boundaries.

of  $h_s$  and  $n$  can give a satisfactory solution. It is better to consider compression indices  $C_c = de/d \ln(T_1/T_0)$  at the boundaries of the experimental pressure range (Fig. 9). Making use of

$$K = -\frac{\dot{p}_s}{\dot{e}/(1+e)} = \frac{p_s(1+e)}{C_c} \quad (36)$$

and of a rate form of Eq. (21), one obtains

$$h_s = 3 p_s \left( \frac{n e}{C_c} \right)^{1/n} \quad (37)$$

and

$$n = \frac{\ln \left( \frac{e_1 C_{c2}}{e_2 C_{c1}} \right)}{\ln \left( \frac{p_{s2}}{p_{s1}} \right)}. \quad (38)$$

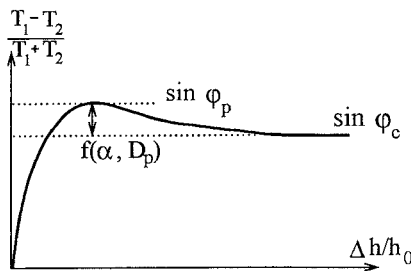


FIG. 10. The exponent  $\alpha$  controls the relation between  $\varphi_p$ ,  $\varphi_c$  and  $D_p$ .

**@Seismicisolation**

During shearing of an initially dense grain skeleton at constant mean (or lateral) pressure, a peak value of the friction angle  $\varphi_p > \varphi_c$  can be observed. The difference between  $\varphi_c$  and  $\varphi_p$  increases with increase of the pressure-dependent relative density and its value is controlled by the exponent  $\alpha$ , see Eq. (20) and Fig. 10. Measuring  $T_1$  and  $e$  at peak (i.e. when  $\dot{T}_1 = 0$ ) in a standard triaxial test with  $\dot{T}_2 = \dot{T}_3 = 0$ , the value of  $\alpha$  can be calculated using Eq. (31), see also Fig. 11.

There are numerous publications on relations between  $\varphi_p$  and grain properties (e.g. (T. Lambe and R. Whitman 1969)). From the dependence of  $\alpha$  on  $\varphi_p$ , a growth of  $\alpha$  with increasing angularity and decreasing  $C_u$  can be concluded.

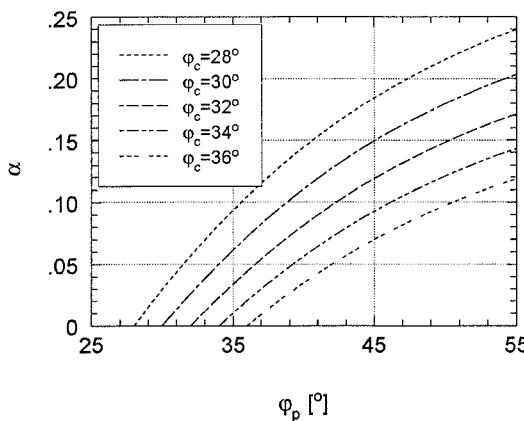


FIG. 11. Relation between  $\alpha$ ,  $\varphi_p$  and  $\varphi_c$  for  $D_p = 0.8$ .

The exponent  $\beta$  is the last parameter of the hypoplastic model to be determined. After Eq. (31)

$$\dot{T}_j \sim \left(\frac{e_i}{e}\right)^{\beta} D_j , \quad (39)$$

i.e. the exponent  $\beta$  controls an increase of the incremental stiffness  $E = \dot{T}_j/D_j$  during a decrease of  $e$ .  $\beta$  can be determined from the ratio of E-values of a dense and a loose sample, e.g. in oedometer compression tests. Usually, at the same pressure,  $E$  increases proportionally with decrease of  $e$ , thus  $\beta \approx 1$  is valid in most cases (I. Herle and G. Gudehus 1999).

## PERFORMANCE

Measured and calculated results of oedometer compression tests are plotted together in Fig. 12. The dense specimen (open points) was prepared with an initial void ratio  $e_0 = 0.65$ . The loose one (filled points) with  $e_0 = 0.77$ . The

**TABLE No. 1.** Parameters of the hypoplastic model for various granular soils.

material	$\varphi_c$ [°]	$h_s$ [MPa]	$n$	$e_{d0}$	$e_{c0}$	$e_{i0}$	$\alpha$	$\beta$
Hochstetten gravel	36	32000	0.18	0.26	0.45	0.50	0.10	1.9
Hochstetten sand	33	1500	0.28	0.55	0.95	1.05	0.25	1.0
Hostun sand	31	1000	0.29	0.61	0.96	1.09	0.13	2.0
Karlsruhe sand	30	5800	0.28	0.53	0.84	1.00	0.13	1.0
Lausitz sand	33	1600	0.19	0.44	0.85	1.00	0.25	1.0
Toyoura sand	30	2600	0.27	0.61	0.98	1.10	0.18	1.1
Zbraslav sand	31	5700	0.25	0.52	0.82	0.95	0.13	1.0

experiments were performed in a so-called soft-oedometer (D. Kolymbas and E. Bauer 1993) which enables the measurement of horizontal stresses. The stress paths show an increase of  $K_0$  with decreasing density which is correctly predicted by the model. The calculated stress-strain curves are very close to the measured ones, including the unloading branch.

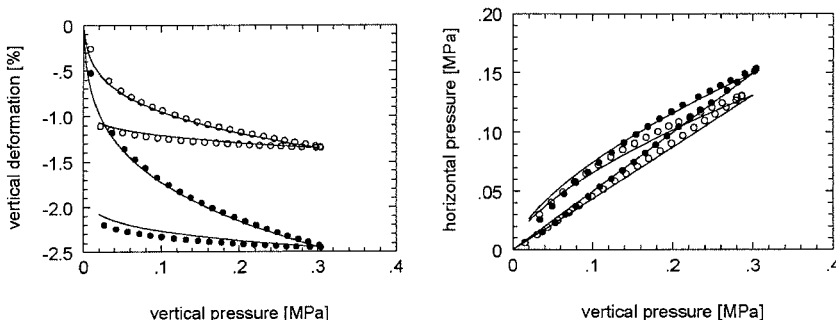


**FIG. 12.** Measured (points) and calculated (lines) results of oedometer compression tests with Karlsruhe sand (test results from (Bauer E. 1996)). A loose sand is denoted by filled points, a dense one by empty points.

Outputs of standard triaxial compression tests (D. Kolymbas and W. Wu 1990) with a dense Karlsruhe sand at different cell pressures are plotted in Fig. 13. Calculation results depicted in Fig. 14 reproduce the experimental behaviour reliably: the stress deviator increases with the cell pressure whereas the dilatancy decreases. The calculated values fit the measured ones also very well. This can be seen in Fig. 15 where a comparison of the calculated and measured peak friction angles is shown not only for changes in the cell pressure (a) but also for changes in density (b).

Experimental results of undrained triaxial tests with Lausitz sand at different

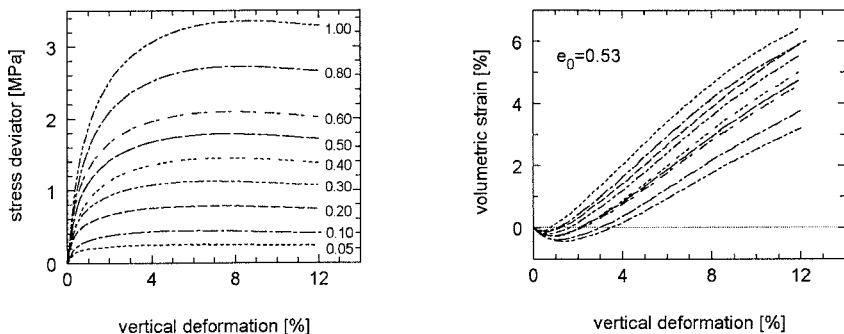


FIG. 13. Measured results of triaxial compression tests with Karlsruhe sand (D. Kolymbas and W. Wu 1990). Numbers denote the cell pressure in MPa.

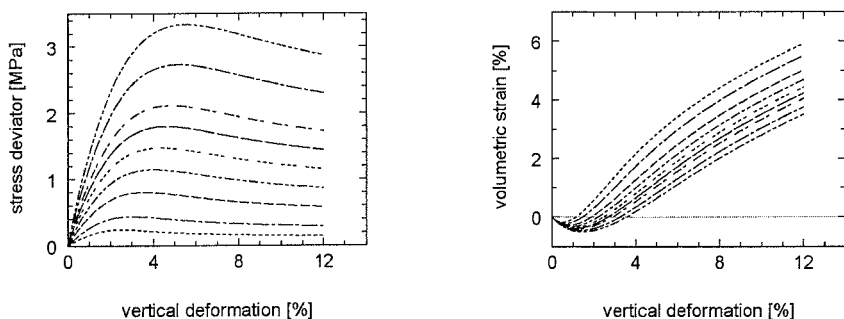


FIG. 14. Calculated results of triaxial compression tests with parameters for Karlsruhe sand from Tab. 1.

densities and at different cell pressures are summarized in Fig. 16, and their recalculation in Fig. 17. Values of the void ratio in Figs. 16 and 17 are after the isotropic consolidation of the specimens. The pattern of the complex observed behaviour is realistically captured. The stress deviator increases rapidly and unlimited (in the displayed scale) in case of the dense specimens which is contrasted by reaching a maximum followed by a decrease (softening) in case of the loose specimens. Pore pressures of the loose specimens increase only and reach a plateau for large deformations. In case of the dense specimens, initially positive pore pressures change to negative values. The stress paths do not surpass a line of limiting stress ratio.

One can also notice some discrepancies between observed and calculated behaviour (initial slope of the stress paths, rate of softening for loose samples and rate of increase of the stress deviator for dense samples). They are presumably due to the violation of some assumed properties of simple grain skeletons in case

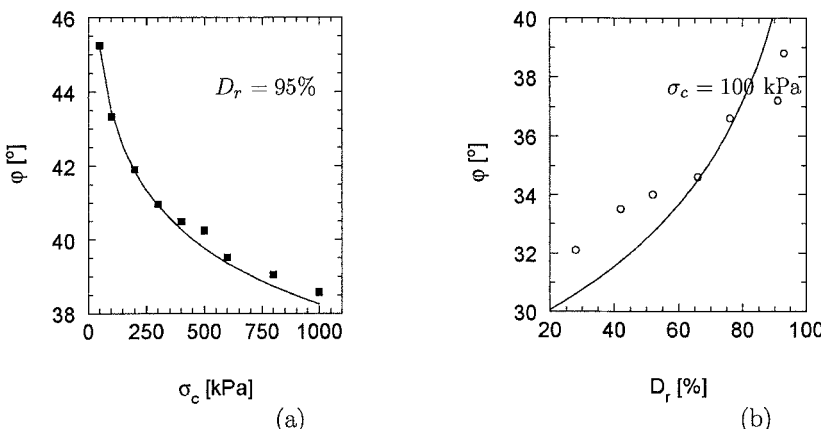


FIG. 15. Measured (points) and calculated (lines) relation between the maximum friction angle  $\varphi$  from standard triaxial tests with Karlruhe sand and cell pressure (a) and relative density (b).

of real soils. E.g., for sudden changes of the direction of a deformation path, like a beginning of undrained shearing after an isotropic compression, there is a memory effect in a granular material, viz. the stress tensor and the void ratio do not sufficiently represent the actual state. The introduction of an *intergranular strain* tensor (A. Niemunis and I. Herle 1997) can overcome this deficiency.

## NUMERICAL SIMULATION OF ELEMENT TESTS

How can we obtain simulations of laboratory element tests by using an equation of the rate type? First, we have to start from a known stress state. If the test to be simulated has kinematical boundary conditions, then the stretching  $\mathbf{D}$  is known, e.g. in case of the oedometer test all but one components of  $\mathbf{D}$  are equal to zero and the only non-vanishing component corresponds to the rate of compression (cf. exercise 4 in chapter 6). With knowledge of  $\mathbf{T}$  and  $\mathbf{D}$  the constitutive equation  $\dot{\mathbf{T}} = \mathbf{h}(\mathbf{T}, \mathbf{D})$  makes possible to evaluate  $\dot{\mathbf{T}}$ . Multiplying  $\dot{\mathbf{T}}$  with a sufficiently small time step  $\Delta t$  gives  $\Delta\mathbf{T} \approx \dot{\mathbf{T}}\Delta t$ . The new stress state is then obtained to  $\mathbf{T} + \Delta\mathbf{T}$ . This process can be continued and corresponds to a numerical integration of the evolution equation  $\dot{\mathbf{T}} = \mathbf{h}(\mathbf{T}, \mathbf{D})$  (so-called EULER-forward integration). The procedure is a little more difficult if not all of the boundary conditions are of the kinematic type.

If we have to simulate a stress-controlled element test (i.e.  $\dot{\mathbf{T}}$  is prescribed,  $\mathbf{D}$  is searched), then the constitutive equation  $\dot{\mathbf{T}} = \mathbf{h}(\mathbf{T}, \mathbf{D})$  has to be inverted. It can be shown (see e.g. sect. 5) that unique invertibility is possible for all stress states inside the limit surface. So-called mixed boundary conditions are given if some components of  $\dot{\mathbf{T}}$  and some components of  $\mathbf{D}$  are described, the remaining ones being searched. The uniqueness of solutions of the constitutive equation for

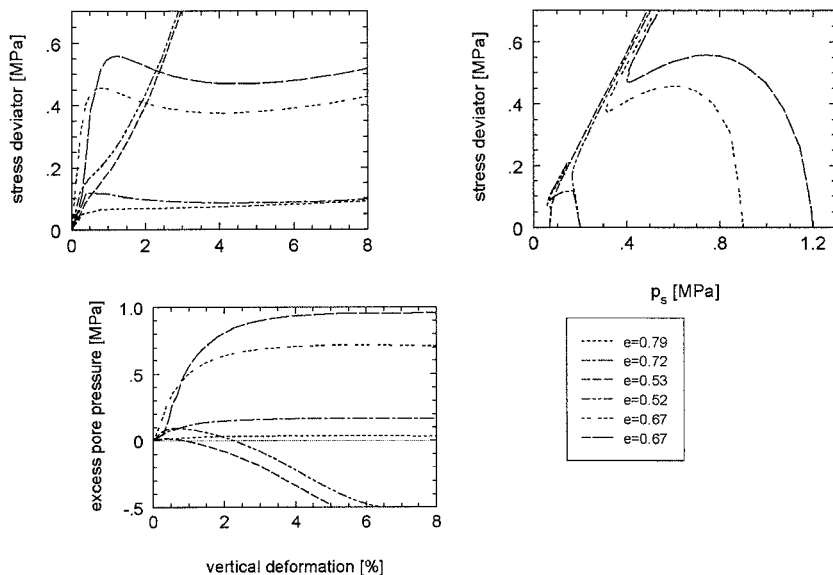


FIG. 16. Measured results of triaxial undrained tests with Lausitz sand (I. Herle 1997).

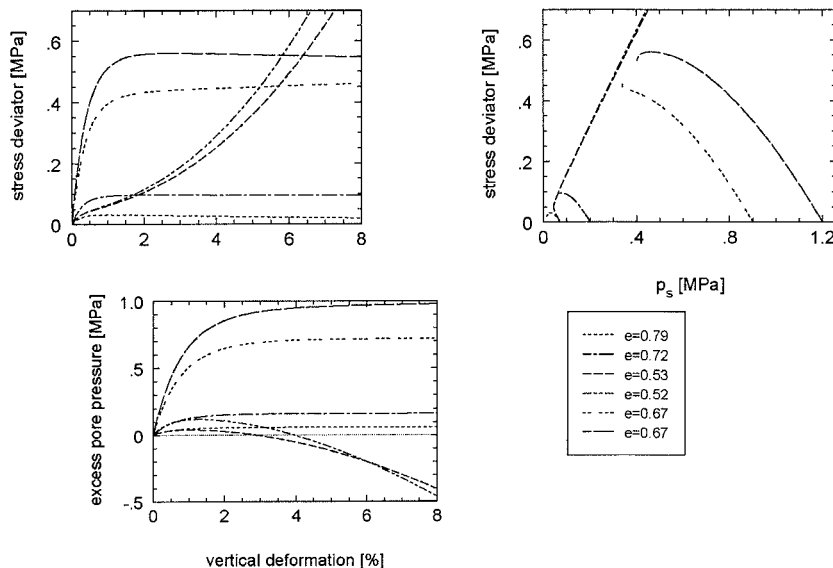


FIG. 17. Calculated results of triaxial undrained tests with parameters for Lausitz sand from Tab. 1.

**@Seismicisolation**

element tests with mixed boundary conditions has very interesting implications sect. 5. It turns out that uniqueness is given if the second order work  $\text{tr}(\dot{\mathbf{T}}\mathbf{D})$  is positive for all possible  $\mathbf{D}$ -tensors. This condition is fulfilled for stresses lying within a surface called the 'bifurcation surface'. This surface lies in the interior of the region bounded by the limit surface. When a stress path trespasses the bifurcation surface, the element test is no more controllable. The deformation loses homogeneity and peculiar patterns of deformation (mostly localization of deformation into thin shear bands) may occur. In terms of elastoplasticity, negativeness of second order work is also termed 'loss of ellipticity'. Also in FEM calculations, loss of ellipticity may imply severe numerical problems. It is interesting to note that this mathematical property correlates perfectly with the loss of homogeneity, as observed in laboratory tests.

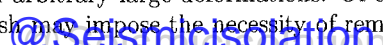
## FEM-IMPLEMENTATIONS OF HYPOPLASTICITY

One of the main fields of application (but by no means the only one) of constitutive models is the implementation into finite element (FEM) codes. This was also the case with a series of dissertation theses (Ziegler M. 1986; Weidner, J. 1990; Sikora Z. 1992; Rombach G.A. 1991; Ruckenbrod C. 1995; Tejchman J. and E. Bauer 1996; Lyle, C. 1993; Hügel H.M. 1995).

Despite the fact that hypoplasticity is rather new and cannot resort to the instruments already developed for elastoplasticity (e.g. radial return algorithms), the performance of hypoplastic laws in FEM-calculations and the comparison with measured results is satisfactory (Hügel H.M. 1995; von Wolffersdorff, P.-A. 1997; Herle I. and J. Tejchman 1997; W. Wehr et al. 1997).

As known, the approximative solutions obtained with FEM are presented as linear combinations of a priori defined shape functions. Thus, the solution is given by a finite number of, usually, nodal displacements and the corresponding stresses. The method itself consists in establishing equilibrium not at every point of a continuous body but only at some selected points, the so-called nodes. This approach can be derived from the field equations of equilibrium,  $\partial\sigma_{ij}/\partial x_j + \rho g_i = 0$ , by multiplying them with  $u_i$ , the field of virtual displacements, and setting the integral over the body equal to zero. The resulting equation is known as the weak form of the equilibrium conditions. Applying the theorem of GAUSS and using appropriate virtual displacements leads to the aforementioned equilibrium conditions for the nodes.

If the material behaviour is path-dependent, then we may not apply the entire load or boundary displacement at once. Instead, we have to decompose the loading action (be it a boundary traction or displacement) into sufficiently small steps and seek to fulfil nodal equilibrium at each step. Moreover, the imposed non-linearity requires to solve a system of non-linear algebraic equations, a task which can be achieved by application of, say, NEWTON's method. The decomposition of the loading process into small steps allows in principle, to solve problems with arbitrary large deformations. Of course, an overly large deformation of the mesh may impose the necessity of remeshing.



The FEM programme ABAQUS allows to implement particular constitutive equations within the subroutine UMAT. This subroutine has to be programmed in such a way that for given stress  $\sigma_{ij}(t)$  and strain  $\varepsilon_{ij}(t)$  at time  $t$  and for given strain and time increments,  $\Delta\varepsilon_{ij}$  and  $\Delta t$ , respectively, it returns the stress  $\sigma_{ij}(t+\Delta t)$  and the Jacobian  $\partial\dot{\sigma}_{ij}/\partial\dot{\varepsilon}_{kl}$  at time  $t+\Delta t$ . Depending on whether the given strain increment is small enough or not, it may be necessary to subdivide it into smaller steps (so called sub-stepping).

### Initial Stress

Equation (7) is of the rate type, i.e. it is an evolution equation which makes possible to calculate the stress changes due to a given increment of deformation. The initial stress has to be known or assumed. Thus, the problem of determining the stress can only be back-stepped but not entirely solved by means of equations of the rate type. This fact is, of course, not very pleasant, but there is no means how to circumvent it. We also can rely upon the fact that the influence of the initial state fades with increasing length of the history. Besides this fact there are some cases (e.g. one-dimensional consolidation corresponding to sedimentation) where we can determine the initial stress by reasoning.

The problem of determination of the initial stress is traditionally hidden by elastoplasticity, where it is usually tacitly assumed that the initial stress results from the theory of elasticity. The latter has to be applied for a deformation starting from a stress free state: The gravity is 'switched on' and the transition to the deformed state is considered to be elastic. This simplification is reflected in almost all existing finite element codes. It is not realistic for soils.

### Shear Banding

A typical pattern of inhomogeneous deformation is the localization of deformation within a narrow zone called a shear band (see Fig. 18). Such shear bands

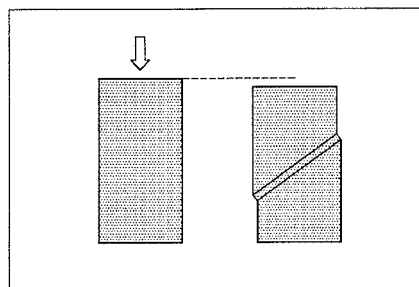


FIG. 18. Soil sample before and after shear-banding

constitute one of the most fascinating phenomena in geotechnics. Since to the work of DESRUES (J. Desrues et al. 1996) based on tomography, we know that

**@Seismicisolation**

also apparently non-localized inhomogeneous deformation modes are actually localized.

The transition to localized deformation may occur either gradually or suddenly. In the latter case it consists in a drastic change of the deformation direction, as experiments by VARDOLAKIS show. If a constitutive model is capable of realistically describing also this new direction, then it will be possible to predict when and under which inclination a shear band can occur.

This ability is not self-evident since many constitutive models (e.g. the elasto-plastic ones) are suggested or tested only for some particular fans of deformation directions. It is therefore a good check of constitutive relations to try to predict the formation of shear bands. This test has been passed by several versions of the hypoplastic relations (Kolymbas D. 1981; Kolymbas, D. 1988; Kolymbas D. and G. Rombach 1989; Sikora Z. and W. Wu 1991; Tejchman J. and E. Bauer 1996; Tejchman J. and W. Wu 1996; Wu W. and Z. Sikora 1991; Wu W. and Z. Sikora 1992).

### Applications

The hypoplastic model with material parameters determined using the presented procedure was also successfully applied in a variety of real boundary value problems. A cavity expansion analysis has allowed a realistic evaluation of CPT and pressuremeter tests (R. Cudmani 1996; V. Osinov and R. Cudmani 2001). A successful FEM calculation of the behaviour of an eccentrically loaded footing and of a sheet-pile wall during excavation was performed by HÜGEL (Hügel H.M. 1995) und VON WOLFFERDORFF (von Wolffersdorff, P.-A. 1997). A class A prediction was published by HERLE and TEJCHMAN (Herle I. and J. Tejchman 1997) for model tests offfootings on sand (F. Tatsuoka et al. 1997). A realistic FE-analysis of the pull-out behaviour of sand anchors was shown by WEHR *et al* (W. Wehr et al. 1997). Numerous realistic FE-calculations of granular flow in silos within a polar continuum were made by TEJCHMAN (J. Tejchman 1996) and ZAIMI (S.-A. Zaimi 1998). These results confirm the ability of the hypoplastic equation to model the behaviour of real granular materials not only qualitatively but also quantitatively, provided that realistic material parameters and initial state variables are at disposal. RACKWITZ has obtained realistic simulations of anchor pull-out tests in sand (Rackwitz, F. 2003).

### References

- Bauer, E. (1996). "Calibration of a comprehensive hypoplastic model for granular materials." *Soils and Foundations*, 36(1):13–26.
- Bauer, E. (1995). "Modelling of critical stress in hypoplasticity." In *NUMOG V*, pages 15–20, Davos, Balkema.
- Bauer, E. (1997). "An objective description of critical states in hypoplasticity." In A. Asaoka, T. Adachi, and F. Oka, editors, *IS-Nagoya'97: Deformation and Progressive Failure in Geomechanics*, pages 347–352. Pergamon.



- Bauer, E., and Wu, W. (1994). "Extension of hypoplastic constitutive model with respect to cohesive powders." In Siriwardane and Zaman, editors, *Computer Methods and Advances in Geomechanics*, pages 531–536. Balkema.
- Cornforth, D. (1973). "Prediction of drained strength of sands from relative density measurements." In *Evaluation of relative density and its role in geotechnical projects involving cohesionless soils*, STP 523, pages 281–303, ASTM.
- Cudmani R. (1996). "Anwendung der Hypoplastizität zur Interpretation von Drucksondierwiderständen in nichtbindigen Böden." *Geotechnik*, 19(4):266–273.
- Dafalias, Y.F. (1986). "Bounding surface plasticity." I: Mathematical foundation and hypoplasticity. *J. Eng. Mech. ASCE*, Vol. 112, 966–987.
- Davis, R.O., and Mullenger, G. (1978). "A rate-type constitutive model for soil with a critical state." *International Journal of Numerical and Analytical Methods in Geomechanics*, Vol. 2, 255–282.
- Desrues, J., and Chambon, R. (1993). "A new rate type Constitutive Model for Geomaterials: CloE." In: D. Kolymbas (editor) *Modern Approaches to Plasticity*, Elsevier.
- Desrues, J., Chambon, R., Mokni, M., and Mazerolle, F. (1996) "Void ratio evolution inside shear bands in triaxial sand specimens studied by computed tomography." *Géotechnique*, 46(3):529–546.
- di Prisco, C., and Imposimato, S. (1996). "Time dependent mechanical behaviour of loose sand." *Mech. of Cohesive-Frictional Materials and Structures*, Vol. 1, 45–73.
- Gudehus G. (1997). "Attractors, percolation thresholds and phase limits of granular soils." In Behringer and Jenkins, editors, *Powders and Grains*, pages 169–183. Balkema.
- Gudehus, G., Goldscheider, M., and Winter, H. (1977) "Mechanical properties of sand and clay and numerical intergration methods: some sources of errors and bounds of accuracy." In G. Gudehus, editor, *Finite Elements in Geomechanics*, pages 121–150. Wiley.
- Gudehus, G. (1996). "A comprehensive constitutive equation for granular materials." *Soils and Foundations*, 36(1):1–12.
- Herle, I. (1997). "Hypoplastizität und Granulometrie einfacher Korngerüste." Veröffentlichungen des Institutes für Bodenmechanik und Felsmechanik der Universität Fridericiana in Karlsruhe. Heft 142.
- Herle, I., and Gudehus, G. (1999). "Determination of parameters of a hypoplastic constitutive model from properties of grain assemblies." *Mechanics of Cohesive-Frictional Materials*, 4(5):461–486.
- Herle, I., and Tejchman, J. (1997). "Effect of grain size and pressure level on bearing capacity of footings on sand." *Int. Symp. on Deformation and Progressive Failure in Geomechanics*, Nagoya.
- Hruban, K. (1958). "Přetvoření a napětí fyzikálně nelineárního poloprostoru." Rozpravy ČSAV, 68(1).
- Hügel, H.M. (1995). "Prognose von Bodenverformungen." *Publ. Series of In-*

- stitut für Bodenmechanik und Felsmechanik der Universität Fridericiana in Karlsruhe*, No. 136.
- Janbu, N. (1963). "Soil compressibility as determined by oedometer and triaxial tests." In *Proc. ECSMFE, Wiesbaden*, pages 19–25.
- Kolbuszewski, J., and Frederick, M. (1963). "The significance of particle shape and size on the mechanical behaviour of granular materials." In *Proc. EC-SMFE, Wiesbaden*, pages 253–263, 1963.
- Kolymbas, D. (1977). "A rate-dependent constitutive equation for soils." *Mech. Res. Comm.*, 4:367–372.
- Kolymbas, D. (1981). "Bifurcation analysis for sand samples with a non-linear constitutive equation." *Ingenieur-Archiv*, 50, 131–140.
- Kolymbas, D. (1987). "A novel constitutive law for soils." *Second Int. Conf. on Constitutive Laws For Engineering Materials: Theory and Applications, Tucson, Arizona, January 1987*, Elsevier.
- Kolymbas, D. (1988). "Eine konstitutive Theorie für Böden und andere körnige Stoffe." *Publ. Series of Institut für Bodenmechanik und Felsmechanik der Universität Fridericiana in Karlsruhe*, Vol. 109.
- Kolymbas, D. (1988). "Generalized hypoelastic constitutive equation." In Saada and Bianchini, editors, *Constitutive Equations for Granular Non-Cohesive Soils*, pages 349–366. Balkema.
- Kolymbas, D. (1991). "Computer-aided design of constitutive laws." *International Journal for Numerical and Analytical Methods in Geomechanics*, 15, 593–604.
- Kolymbas, D. (1991). "An outline of hypoplasticity." *Archive of Applied Mechanics*, 61:143–151.
- Kolymbas, D., I. Herle, and P.-A. v. Wolffersdorff (1995). "Hypoplastic constitutive equation with back stress." *International Journal of Numerical and Analytical Methods in Geomechanics*, 19(6):415–446.
- Kolymbas, D., and Rombach, G. (1989). "Shear band formation in generalized hypoelasticity." *Ingenieur-Archiv*, 59, 177–186.
- Kolymbas, D. (ed.) (2000). "Constitutive Modelling of Granular Materials." Springer.
- Kolymbas, D. (1978). "Ein nichtlineares viskoplastisches Stoffgesetz für Böden." Veröffentlichungen des Institutes für Bodenmechanik und Felsmechanik der Universität Fridericiana in Karlsruhe. Heft 77.
- Kolymbas, D. (1985). "A generalized hypoelastic constitutive law." In *Proc. XI Int. Conf. Soil Mechanics and Foundation Engineering*, volume 5, page 2626, San Francisco. Balkema.
- Kolymbas, D. (1994). "Hypoplasticity as a constitutive framework for granular materials." In Siriwardane and Zaman, editors, *Computer Methods and Advances in Geomechanics*, pages 197–208. Balkema.
- Kolymbas, D., and Bauer, E. (1993). "Soft oedometer – a new testing device and its application for the calibration of hypoplastic constitutive laws." *Geotechnical Testing Journal*, 16(2):263–270.

- Kolymbas, D., and Herle, I. (2003). "Shear and objective stress rates in hypoplasticity." *International Journal for Numerical and Analytical Methods in Geomechanics*, 27(9):733–744.
- Kolymbas, D., and Wu, W. (1990) "Recent results of triaxial tests with granular materials." *Powder Technology*, 60:99–119.
- Lambe, T., and Whitman, R. (1969). *Soil mechanics*. Wiley.
- Lyle, C. (1993). "Spannungsfelder in Silos mit starren, koaxialen Einbauten." Diss., Fakultät für Maschinenbau und Elektrotechnik der TU Carol-Wilhelmina zu Braunschweig.
- Matsuoka, H., and Nakai, T. (1977). "Stress-strain relationship of soil based on the 'SMP'." In *Constitutive equations of soils. Proc. of specialty session 9, IX ICSMFE, Tokyo*, pages 153–162.
- Niemunis, A., and Herle, I. (1997). "Hypoplastic model for cohesionless soils with elastic strain range." *Mechanics of Cohesive-Frictional Materials*, 2(4):279–299.
- Niemunis, A. (1996). "A visco-plastic model for clay and its FE-implementation." In: *XI Colloque Franco-Polonais en Mécanique des Sols et des Roches Appliquée*, E. Dembicki, W. Cichy, L. Balachowski (Eds.), University of Gdańsk.
- Ohde, J. (1939). "Zur Theorie der Druckverteilung im Baugrund." *Bauingenieur*, 20:451–459, 1939.
- Osinov, V., and Cudmani, R. (2001). "Theoretical investigation of the cavity expansion problem based on a hypoplasticity model." *International Journal for Numerical and Analytical Methods in Geomechanics*, 25:473–495.
- Pestana, J., and Whittle, A. (1995). "Compression model for cohesionless soils." *Géotechnique*, 45(4):611–631, 1995.
- Rackwitz, F. (2003). "Numerical Analyses of Single Tension Piles and Groups of Tension Piles in Sand Based on Loading Tests." Veröffentlichungen des Grundbauinstituts der Technischen Universität Berlin. Heft 32.
- Riemer, M. F., Seed, R. B., Nicholson, P. G., and Jong, H.-L (1990). "Steady state testing of loose sands: limiting minimum density." *Journal of Geotechnical Engineering ASCE*, 116(2):332–337.
- Rombach, G. A. (1991). "Schüttguteinwirkungen auf Silozellen, Exzentrische Entleerung." Veröffentlichungen Heft 14, Dissertation, Institut für Massivbau und Baustofftechnologie der Universität Fridericiana in Karlsruhe.
- Roscoe, K., Schofield, A., and Wroth, C. (1958). "On the yielding of soils." *Géotechnique*, 8(1):22–53.
- Ruckenbrod, C. (1995). "Statistische und dynamische Phänomene bei der Entleerung von Silozellen." Schriftenreihe des Institutes für Massivbau und Baustofftechnologie der Universität Fridericiana in Karlsruhe, Heft 26.
- Schofield, A., and Wroth, C. (1968) *Critical state soil mechanics*. McGraw-Hill, London.
- Schultze, E., and Moussa, A. (1961). "Factors affecting the compressibility of sand." In *Proc. 5th ICSMFE, Paris*, volume 1, pages 335–340.

- Sikora, Z. (1992). "Hypoplastic flow of granular materials. A numerical approach." *Publ. Series of Institut für Bodenmechanik und Felsmechanik der Universität Fridericiana in Karlsruhe*, Vol. 123.
- Sikora, Z., and Wu, W. (1991). "Shear band formation in biaxial tests." *Proc. Int. Conf. on Constitutive Laws for Engineering Materials*, Tucson, Arisona, USA.
- Tamagnini, C., Viggiani, G., and Chambon, R. (2000). "A review of two different approaches to hypoplasticity." In D. Kolymbas, editor, *Constitutive Modelling of Granular Materials*, pp. 107-145. Springer.
- Tatsuoka, F., Goto, S., Tanaka, T., Tani, K., and Kimura, Y. (1997). "Particle size effects on bearing capacity of footings on granular material." In A. Asaoka, T. Adachi, and F. Oka, editors, *IS-Nagoya'97: Deformation and Progressive Failure in Geomechanics*, pages 133-138. Pergamon.
- Tejchman, J. (1996). "Shear banding and autogeneous dynamics in granular bodies." *Veröffentlichungen des Institutes für Bodenmechanik und Felsmechanik der Universität Fridericiana in Karlsruhe*, Heft 140.
- Tejchman, J., and Bauer, E. (1996). "Numerical simulation of shear band formation with a polar hypoplastic constitutive model." *Computers and Geotechnics*, Vol. 19, No. 3, 221-244.
- Tejchman, J., and Wu, W. (1996). "Numerical simulation of shear band formation with a hypoplastic constitutive model." *Computers and Geotechnics*, 18(1):71-84.
- Truesdell, C. (1965). Hypo-elasticity. *J. Rational Mech. Anal.*, Vol. 4, 83-133, 1955. Springer-Verlag.
- Truesdell, C., and Noll, W. (1965). "The non-linear field theories of mechanics." *Handbuch der Physik III/c*. Springer-Verlag.
- Valanis, K. C. (1982). "An endochronic geomechanical model for soils." *IUTAM Conference on Deformation and Failure of Granular Materials*. Balkema, 159-165.
- Verdugo, R., and Ishihara, K. (1996). "The steady state of sandy soils." *Soils and Foundations*, 36(2):81-91.
- Vermeer, P. (1982). "A five-constant model unifying well-established concepts." In *Results of the International Workshop on Constitutive Relations for Soils, Grenoble*, pages 477-483. Balkema.
- von Wolffersdorff, P.-A. (1997). "Verformungsprognosen für Stützkonstruktionen." *Publ. Series of Institut für Bodenmechanik und Felsmechanik der Universität Fridericiana in Karlsruhe*, Vol. 141.
- von Wolffersdorff, P.-A. (1996). "A hypoplastic relation for granular materials with a predefined limit state surface." *Mechanics of Cohesive-Frictional Materials*, 1:251-271.
- Wehr, W., Tejchman, J., Herle, I., and Gudehus, G. (1997). "Sand anchors - a shear zone problem." In A. Asaoka, T. Adachi, and F. Oka, editors, *IS-Nagoya'97: Deformation and Progressive Failure in Geomechanics*, pages 787-792. Pergamon.

- Wehr, W., Tejchman, J., Herle, I., and Gudehus, G. (1997). "Sand anchors – a shear zone problem." *Int. Symp. on Deformation and Progressive Failure in Geomechanics*, Nagoya.
- Weidner, J. (1990). "Vergleich von Stoffgesetzen granularer Schüttgüter zur Silodruckermittlung." Veröffentlichungen Heft 10, Dissertation, Institut für Massivbau und Baustofftechnologie der Universität Fridericiana in Karlsruhe.
- Wu, W. (1992). "Hypoplasticity als mathematisches Modell zum mechanischen Verhalten granularer Stoffe." *Publ. Series of Institut für Bodenmechanik und Felsmechanik der Universität Fridericiana in Karlsruhe*, Vol. 129.
- Wu, W., and Bauer, E. (1993). "A hypoplastic model for barotropy and pyknotropy of granular soils." In: D. Kolymbas, editor, *Modern Approaches to Plasticity*, 225-245. Elsevier.
- Wu, W., and Bauer, E. (1994). "A simple hypoplastic constitutive model for sand." *International Journal of Numerical and Analytical Methods in Geomechanics*, 18:833-862.
- Wu, W., Bauer, E., and Kolymbas, E. (1996). "Hypoplastic constitutive model with critical state for granular materials." *Mechanics of Materials*, 23:45-69.
- Wu, W., Bauer, E., Niemunis, A., and Herle, I. (1993). "Visco-hypoplastic models for cohesive soils." In: D. Kolymbas, editor, *Modern Approaches to Plasticity*, 365-383. Elsevier.
- Wu, W., and Kolymbas, D. (1990). "Numerical testing of the stability criterion for hypoplastic constitutive equations." *Mechanics of Materials*, 9:245-253.
- Wu, W., and Niemunis, A. (1996). "Failure criterion, flow rule and dissipation function derived from hypoplasticity." *Mechanics of Cohesive-Frictional Materials*, 1:145-163.
- Wu, W., and Niemunis, A. (1997). "Beyond Failure in Granular Materials." *Int. J. for Numerical and Analytical Methods in Geomechanics*, Vol. 21, No. 2, 153-174.
- Wu, W., and Sikora, Z. (1991). "Localized bifurcation in hypoplasticity." *International Journal of Engineering Science*, 29(2):195-201.
- Wu, W., and Sikora, Z. (1992). "Localized Bifurcation of Pressure Sensitive Dilatant Granular Materials." *Mechanics Research Communications*, Vol. 29, 289-299.
- Youd, T. (1973). "Factors controlling maximum and minimum densities of sands." In *Evaluation of relative density and its role in geotechnical projects involving cohesionless soils*, STP 523, pages 98-112. ASTM.
- Zaimi, S.-A., Guillot, J.-B., Petit, C., and Steiler, J.-M. (1998). "Modelling the flow of solids in the blast furnace." In *Iron and Steel Making*. Toronto.
- Ziegler, M. (1986). "Berechnung des verschiebungsabhängigen Erddrucks in Sand." Veröffentlichungen Heft 101, Institut für Bodenmechanik und Felsmechanik der Universität Fridericiana in Karlsruhe.

## SINGLE HARDENING MODEL FOR SOILS: PARAMETER DETERMINATION AND TYPICAL VALUES

Poul V. Lade<sup>1</sup>, Member, Geo-Institute

**ABSTRACT:** An elasto-plastic constitutive model with a single yield surface has been developed for the behavior of frictional materials such as sand, clay, concrete, and rock. Hooke's law is employed to model the elastic strains, and the framework for the plastic behavior consists of a failure criterion, a nonassociated flow rule, a yield criterion that describes contours of equal plastic work, and a work-hardening/softening law. For soils the model incorporate eleven parameters that can all be determined from simple experiments. The components of the model are reviewed, determination of all material parameters is demonstrated, typical values of material parameters are given for selected sands, and the capabilities of the model are described.

### INTRODUCTION

An important feature of the constitutive model presented here is the application of a single isotropic yield surface shaped as an asymmetric tear-drop with the pointed apex at the origin of the principal stress space. This yield surface, expressed in terms of stress invariants, describes the locus at which the total work is constant. The total plastic work (due to shear strains as well as volumetric strains) serves as the hardening parameter, and it is used to define the location and shape of the yield surface. This concept results in mathematical consistency in the model, and application of a single yield surface produces computational efficiency when used in large computer programs. The nonassociated flow rule is derived from a potential function that describes a three-dimensional surface shaped as a cigar with an asymmetric cross-section. The model is devised such that the transition from hardening to softening occurs abruptly at the peak failure point, but the pointed peak is hardly noticeable in actual comparisons with experimental data.

<sup>1</sup> Professor, Department of Civil Engineering, The Catholic University of America, Washington, D.C. 20064, Lade@cua.edu

Each component of the model has already been developed, presented, and discussed in the literature (Lade 1977; Lade and Nelson 1987; Kim and Lade 1988; Lade and Kim 1988a, b), and the model has been implemented in a subroutine for use in finite element and finite difference programs (Lade and Jakobsen 2002; Jakobsen and Lade 2002). The main principles and the governing equations for each component will be given here. While the model has been developed for frictional materials such as sand, clay, concrete, and rock, the specific procedures employed for determination of material parameters for sands are presented in connection with derivation of parameters for Sand No. D. Values of material parameters are given for several sands, and the ability of the model to account for various aspects of observed three-dimensional sand behavior is briefly described.

While parameter derivation and typical values are given for sands in this presentation, similar procedures and typical values are given for clays in a separate publication (Lade 2005).

## REQUIRED EXPERIMENTAL DATA

The material parameters required for a constitutive model should, in principle, be derivable from any set of experiments that are sufficiently varied to contain the material behavior during different modes of loading. Information is required regarding the behavior during hydrostatic (isotropic) compression and during shearing. Thus, experimental data must be available with the behavior during these two modes. Typically, the results of one isotropic compression test and three triaxial compression tests, including unloading-reloading cycles, contain this behavior and are required for material parameter determination. The results of these experiments must be complete, with measurements of all stresses and all strains, including the volumetric strain in drained tests and the pore water pressures in undrained tests. Other types of experiments such as  $K_0$ -compression, plane strain tests, and triaxial extension tests may also be used, but these experiments are more complex and they require other specialized expressions for each component of the model than those given below for the Single Hardening Model.

The expressions given below for the Single Hardening Model are those required assuming the availability of results of one isotropic compression test and three triaxial compression tests. For sands, the tests should be consolidated-drained (CD) tests, while for clays, the tests should be consolidated-undrained (CU) tests. These tests are the simplest to perform for each of the two types of soil, while they still contain the necessary information required to characterize the three-dimensional behavior of the soils.

## COMPONENTS OF CONSTITUTIVE MODEL

The total strain increments observed in a material when loaded are divided into elastic and plastic components such that:

$$d\varepsilon_{ij} = d\varepsilon_{ij}^e + d\varepsilon_{ij}^p \quad (1)$$



These strains are then calculated separately, the elastic strains by Hooke's law, and the plastic strains by a plastic stress-strain law. Both are expressed in terms of effective stresses.

Below are a brief review of the framework and the components of the constitutive model. In order that the presentation follows a logic developmental sequence, the components are presented in the following order: Elastic behavior, failure criterion, flow rule, yield criterion, and work-hardening/softening law.

### Elastic Behavior

The elastic strain increments, which are recoverable upon unloading, are calculated from Hooke's law, using a model for the nonlinear variation of Young's modulus with stress state (Lade and Nelson, 1987). The value of Poisson's ratio,  $\nu$ , being limited between zero and one half for most materials, is assumed to be constant. The expression for Young's modulus was derived from theoretical considerations based on the principle of conservation of energy. According to this derivation, Young's modulus  $E$  can be expressed in terms of a power law involving non-dimensional material constants and stress functions as follows:

$$E = Mp_a \left[ \left( \frac{I_1}{p_a} \right)^2 + 6 \frac{1+\nu}{1-2\nu} \left( \frac{J'_2}{p_a^2} \right) \right]^\lambda \quad (2)$$

in which  $I_1$  is the first invariant of the stress tensor, and  $J'_2$  is the second invariant of the deviatoric stress tensor, given as follows:

$$I_1 = \sigma_x + \sigma_y + \sigma_z \quad (3)$$

$$J'_2 = \frac{1}{6} \left[ (\sigma_x - \sigma_y)^2 + (\sigma_y - \sigma_z)^2 + (\sigma_z - \sigma_x)^2 \right] + \tau_{xy}^2 + \tau_{yz}^2 + \tau_{zx}^2 \quad (4)$$

The parameter  $p_a$  is atmospheric pressure expressed in the same units as  $E$ ,  $I_1$  and  $\sqrt{J'_2}$ , and the modulus number  $M$  and the exponent  $\lambda$  are constant, dimensionless numbers. The three material parameter  $\nu$ ,  $M$ , and  $\lambda$  may be obtained from the unloading-reloading cycles of simple tests such as triaxial compression tests. The model can be used for materials with effective cohesion, as explained below.

### Failure Criterion

A general, three-dimensional failure criterion has been developed for soils, concrete, and rock (Lade, 1977, 1982, 1984, 1993c; Kim and Lade, 1984). The criterion is expressed in terms of the first and third stress invariants of the stress tensor:

$$f_n = \left( \frac{I_1^3}{I_3} - 27 \right) \left( \frac{I_1}{P_a} \right)^m \quad (5a)$$

$$f_n = \eta_1 \text{ at failure} \quad (5b)$$

in which  $I_1$  is given in Eq. 3 and

$$I_3 = \sigma_x \sigma_y \sigma_z + \tau_{xy} \tau_{yz} \tau_{zx} + \tau_{yx} \tau_{zy} \tau_{xz} - (\sigma_x \tau_{yz} \tau_{zy} + \sigma_y \tau_{zx} \tau_{xz} + \sigma_z \tau_{xy} \tau_{yx}) \quad (6)$$

The parameters  $\eta_1$  and  $m$  are constant dimensionless numbers.

Figure 1 shows that in principal stress space, the failure criterion is shaped like an asymmetric bullet with the pointed apex at the origin of the stress axes, and the cross-sectional shape in the octahedral plane is triangular with smoothly rounded edges in a fashion that conforms to experimental evidence. The apex angle increases with the value of  $\eta_1$ . The failure surface is always concave towards the hydrostatic axis, and its curvature increases with the value of  $m$ . For  $m = 0$  the failure surface is straight, and the shape of the cross-sections does not change with the value of  $I_1$ . For  $m > 0$ , the cross-sectional shape of the failure surface changes from triangular to become more circular with increasing value of  $I_1$ . Similar changes in cross-sectional shape are observed from experimental studies on soil, concrete, and rock. If  $m > 1.979$  the failure surface becomes convex towards the hydrostatic axis (Kim and Lade, 1984). Analysis of numerous sets of data for concrete and rock indicates that  $m$ -values rarely exceed 1.5 (Lade, 1984).

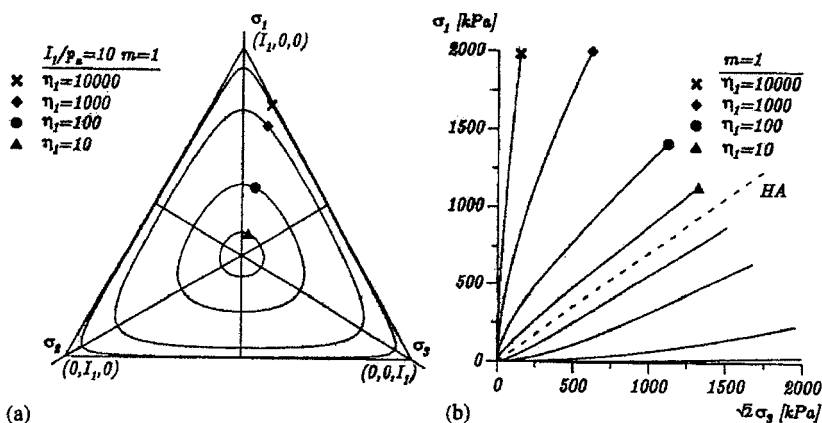


**FIG. 1. Characteristics of failure criterion in principal stress space: Traces shown in (a) octahedral plane, and (b) triaxial plane.**

In order to include the effective cohesion and the tension which can be sustained by cemented soils, concrete, and rock, a translation of the principal stress space along the hydrostatic axis is performed (Lade, 1982, 1984, 1993c; Kim and Lade, 1984). Thus, a constant stress,  $a p_a$ , is added to the normal stresses before substitution in Eq. 5:

$$\bar{\sigma}_i = \sigma_i + a \cdot p_a \quad (i = 1, 2, 3) \quad (7)$$

in which 'a' is a dimensionless parameter. The value of  $a \cdot p_a$  reflects the effect of the tensile strength of the material. The three material parameters,  $\eta_1$ ,  $m$ , and  $a$ , may be determined from results of simple tests such as triaxial compression tests.

### Plastic Potential and Flow Rule

The plastic strain increments are calculated from the flow rule:

$$d\varepsilon_{ij}^p = d\lambda_p \frac{\partial g_p}{\partial \sigma_{ij}} \quad (8)$$

in which  $g_p$  is a plastic potential function and  $d\lambda_p$  is a scalar factor of proportionality. A suitable plastic potential function for frictional materials was developed and presented by Kim and Lade (1988). This function is different from the yield function and nonassociated flow is consequently obtained. The plastic potential function is written in terms of the three invariants of the stress tensor:

$$g_p = \left( \psi_1 \frac{I_1^3}{I_3} - \frac{I_1^2}{I_2} + \psi_2 \right) \left( \frac{I_1}{p_a} \right)^\mu \quad (9)$$

in which  $I_1$  and  $I_3$  are given in Eqs. 3 and 6, and the second stress invariant is defined as:

$$I_2 = \tau_{xy}\tau_{yx} + \tau_{yz}\tau_{zy} + \tau_{zx}\tau_{xz} - (\sigma_x\sigma_y + \sigma_y\sigma_z + \sigma_z\sigma_x) \quad (10)$$

The material parameters  $\psi_2$  and  $\mu$  are dimensionless constants that may be determined from triaxial compression tests. The parameter  $\psi_1$  is related to the curvature parameter  $m$  of the failure criterion as follows (Kim and Lade 1988):

$$\psi_1 = 0.00155 \cdot m^{-1.27} \quad (11)$$

The parameter  $\psi_1$  acts as a weighting factor between the triangular shape (from the  $I_3$  term) and the circular shape (from the  $I_2$  term). The parameter  $\psi_2$  controls the intersection with the hydrostatic axis, and the exponent  $\mu$  determines the curvature of meridians. The corresponding plastic potential surfaces are shown in Fig. 2. They are



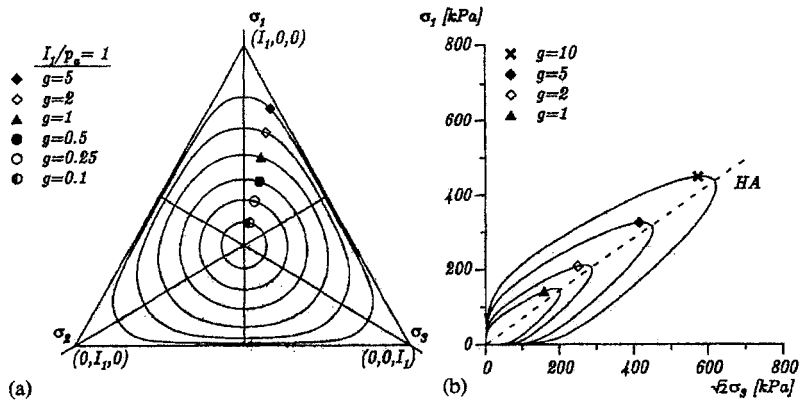


**FIG. 2. Characteristics of the plastic potential function in principal stress space:** Traces shown in (a) octahedral plane, and in (b) triaxial plane.

shaped as asymmetric cigars with smoothly rounded triangular cross-sections similar but not identical to those for the failure surfaces.

The derivatives of  $g_p$  with regard to the stresses are

$$\frac{\partial g_p}{\partial \sigma_{ij}} = \left[ \frac{I_1}{p_a} \right]^{\mu} \left\{ \begin{array}{l} G - (\sigma_y + \sigma_z) \frac{I_1^2}{I_2^2} - \psi_1 (\sigma_y \sigma_z - \tau_{yz}^2) \frac{I_1^3}{I_3^2} \\ G - (\sigma_z + \sigma_x) \frac{I_1^2}{I_2^2} - \psi_1 (\sigma_z \sigma_x - \tau_{zx}^2) \frac{I_1^3}{I_3^2} \\ G - (\sigma_x + \sigma_y) \frac{I_1^2}{I_2^2} - \psi_1 (\sigma_x \sigma_y - \tau_{xy}^2) \frac{I_1^3}{I_3^2} \\ 2 \frac{I_1^2}{I_2^2} \tau_{yz} - 2\psi_1 (\tau_{xy} \tau_{zx} - \sigma_x \tau_{yz}) \frac{I_1^3}{I_3^2} \\ 2 \frac{I_1^2}{I_2^2} \tau_{zx} - 2\psi_1 (\tau_{xy} \tau_{yz} - \sigma_y \tau_{zx}) \frac{I_1^3}{I_3^2} \\ 2 \frac{I_1^2}{I_2^2} \tau_{xy} - 2\psi_1 (\tau_{yz} \tau_{zx} - \sigma_z \tau_{xy}) \frac{I_1^3}{I_3^2} \end{array} \right\} \quad (12a-f)$$

where

$$G = \psi_1 (\mu + 3) \frac{I_1^2}{I_3} - (\mu + 2) \frac{I_1}{I_2} + \frac{\mu}{I_1} \psi_2 \quad (13)$$

### **Yield Criterion and Work Hardening/Softening Relation**

The yield surfaces are intimately associated with and derived from surfaces of constant plastic work, as explained by Lade and Kim (1988a). The isotropic yield function is expressed as follows:

$$f_p = f_p'(\sigma_{ij}) - f_p''(W_p) = 0 \quad (14)$$

in which

$$f_p' = \left( \psi_1 \frac{I_1^3}{I_3} - \frac{I_1^2}{I_2} \right) \left( \frac{I_1}{p_a} \right)^h \cdot e^q \quad (15)$$

where  $h$  is constant and  $q$  varies from zero at the hydrostatic axis to unity at the failure surface. The expressions for  $I_1$ ,  $I_2$ , and  $I_3$  in Eq. 15 are given in Eqs. 3, 10, and 6, respectively. The parameter  $\psi_1$  acts as a weighting factor between the triangular shape (from the  $I_3$  term) and the circular shape (from the  $I_2$  term), as in the expression for the plastic potential, Eq. 9. The constant parameter  $h$  is determined on the basis that the plastic work is constant along a yield surface.

The value of  $q$  varies with stress level  $S$  defined as:

$$S = \frac{f_n}{\eta_1} = \frac{1}{\eta_1} \left( \frac{I_1^3}{I_3} - 27 \right) \left( \frac{I_1}{p_a} \right)^m \quad (16)$$

in which  $f_n$  is the expression for the failure criterion in Eq. 5a, and  $\eta_1$  is the value of  $f_n$  at failure, given in Eq. 5b. The stress level  $S$  varies from zero at the hydrostatic axis to unity at the failure surface, and the variation of  $q$  with  $S$  is expressed as

$$q = \frac{\alpha S}{1 - (1 - \alpha)S} \quad (17)$$

in which  $\alpha$  is constant.

For *hardening* the yield surface inflates isotropically with plastic work according to:

$$f_p'' = \left( \frac{1}{D} \right)^{\rho} \left( \frac{W_p}{p_a} \right)^{\rho} \quad (18)$$

In Eq. 16 the values of  $\rho$  and  $D$  are constants for a given material. Thus,  $f_p''$  varies with the plastic work only. The values of  $D$  and  $\rho$  are given by:

$$D = \frac{C}{(27\psi_1 + 3)^{\rho}} \quad (19)$$

@Seismicisolation

and

$$\rho = \frac{p}{h} \quad (20)$$

The parameters  $C$  and  $p$  in Eq. 19 are used to model the plastic work during isotropic compression:

$$W_p = Cp_a \left( \frac{I_1}{p_a} \right)^p \quad (21)$$

The yield surfaces are shaped as asymmetric tear-drops with smoothly rounded triangular cross-sections and traces in the triaxial plane as shown in Fig. 3. As the plastic work increases, the isotropic yield surface inflates until the current stress point reaches the failure surface. The relation between  $f_p''$  and  $W_p$  is described by a monotonically increasing function whose slope decreases with increasing plastic work, as shown in Fig. 4.

For *softening* the yield surface deflates isotropically according to an exponential decay function:

$$f_p'' = Ae^{-B\frac{W_p}{p_a}} \quad (22)$$

in which  $A$  and  $B$  are positive constants to be determined on the basis of the slope of the hardening curve at the point of peak failure,  $S = 1$ , as indicated in Fig. 4. Thus,

$$A = \left[ f_p'' e^{B \frac{W_p}{p_a}} \right]_{S=1} \quad (23)$$

and

$$B = \left[ b - \frac{df_p''}{d\left(\frac{W_p}{p_a}\right)} \frac{1}{f_p''} \right]_{S=1} \quad (24)$$

in which both the size of the yield surface  $f_p''$  and the derivative  $df_p''/d(W_p/p_a)$  are obtained from the hardening curve at peak failure, indicated by  $S = 1$ . The value of  $df_p''/d(W_p/p_a)$  is negative during softening. The parameter  $b$  is greater than or equal to zero, where the lower limit corresponds to that of a perfect plastic material. A default value of  $b = 1$  is built into the model, so  $b$  occurs as an optional material parameter.

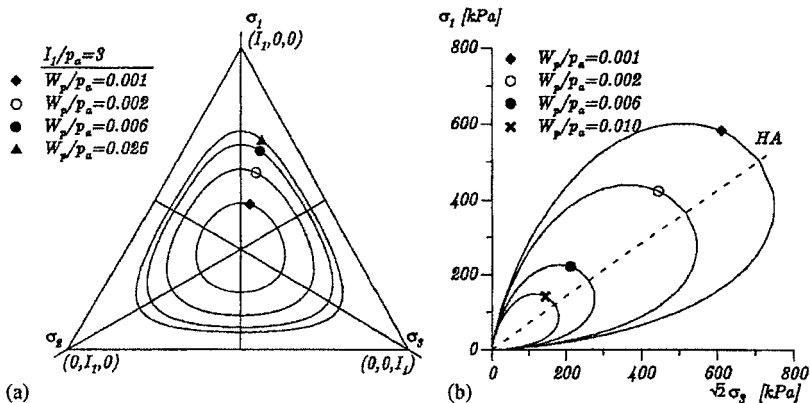


FIG. 3. Characteristics of the yield function in principal stress space: Traces shown in (a) octahedral plane, and in (b) triaxial plane.

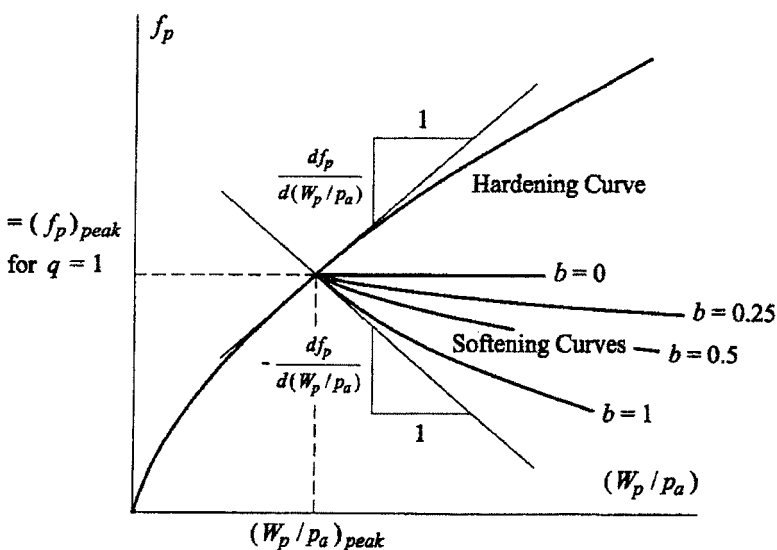


FIG. 4. Modeling of work hardening and softening.

@Seismicisolation

Using the expression for the plastic potential in Eq. 9, the relation between plastic work increment and the scalar factor of proportionality  $d\lambda_p$  in Eq. 8 may be expressed as:

$$d\lambda_p = \frac{dW_p}{\mu g_p} \quad (25)$$

in which the increment of plastic work can be determined by differentiation of the hardening and softening equations.

Combining Eqs. 23 and 24 with 25 and substituting this into Eq. 8 produces the expression for the incremental plastic strain increments.

## MATERIALS WITH EFFECTIVE COHESION

As explained in connection with the failure criterion, it is possible to include the effective cohesion and the tension that can be sustained by cemented soils, concrete, and rock. This is done by translating the principal stress space along the hydrostatic axis, i.e., by adding a constant stress to the normal stress, as in Eq. 7, before substitution into the failure criterion in Eq. 5.

A similar technique has been shown to work for the elastic modulus variation (Lade and Nelson, 1987), the plastic potential (Kim and Lade, 1988), the yield criterion and the work-hardening/softening law (Lade and Kim, 1988a). Inconsistencies in the plastic behavior of materials with effective cohesion are overcome by assuming that there exists an initial yield surface which goes through the origin of the real stress space, as shown in Fig. 5. This implies that only elastic strains occur during major portions of tension type tests in which the main parts of the stress paths are located inside the yield surface. Thus, the stresses applied along the stress paths indicated in Fig. 5 do not produce plastic strains until they are close to failure. The existence of an initial yield surface appears to simulate experimental observations with good accuracy.

The technique of performing all calculations in the translated stress space provides a convenient tool for mathematical treatment of materials with effective cohesion. Following all the necessary calculations, the stresses are again modified to hold conventional physical meaning. For cohesionless materials for which ' $a$ ' is zero, the calculations are performed in the original stress space.

## EFFECTS OF PRESHEARING AND OVERCONSOLIDATION

An experimental investigation of the behavior of sand near failure was undertaken by Lade and Prabucki (1995) to study the shape, location and movement of the plastic yield surface in the hardening regime and the softening regime near peak failure. This investigation confirmed that the yield surface, defined as a contour of constant plastic work as measured from the origin of stress, captures the behavior of soil with good accuracy in both the hardening and in the softening regime. It was found that preshearing to peak failure produced effects similar to overconsolidation observed in clays in the region of lower confining pressures, as shown in Fig. 6. In this region, the yield surface was found to move out beyond the failure surface for normally



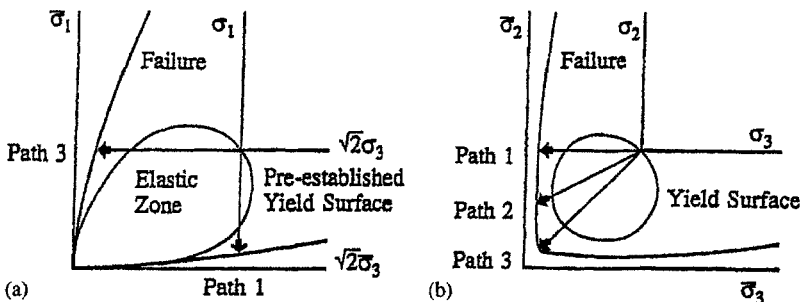


**FIG. 5.** Biaxial stress paths for concrete employed by Kupfer et al. (1969) and assumed as initial yield surface in (a) triaxial plane, and (b) biaxial plane.

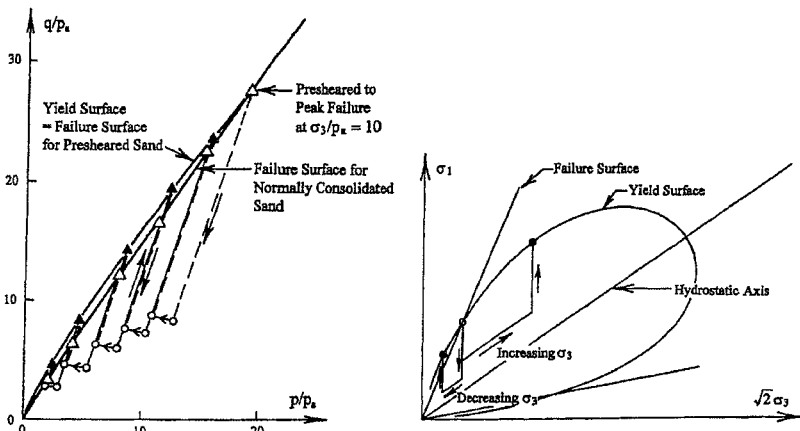


**FIG. 6.** Effects of preshearing and overconsolidation on failure surface for soils.

consolidated sand, i.e. the sand became stronger. The observed pattern of yielding is captured with good accuracy by the yield criterion employed in the single hardening constitutive model.

#### DETERMINATION OF MATERIAL PARAMETERS

The governing functions of the Single Hardening Model have been presented and the material parameters identified. The material parameters depend on the specific material and may be calibrated to results of isotropic and triaxial compression tests as

outlined by Lade (1977), Kim and Lade (1988), Lade and Kim (1988a, b). The calibration procedure is also demonstrated below for Sand No. D, a fine sand, dredged from the ocean bottom and tested in isotropic compression and drained triaxial compression tests..

### Elastic Behavior

The constant value of Poisson's ratio,  $\nu$ , may be determined easiest from the initial slope of the reloading branch of the volume change curve,  $\Delta\epsilon_v/\Delta\epsilon_l$ , as seen in Fig. 7. The strains in this portion of the curve are considered to be entirely elastic and Poisson's ratio is determined as:

$$\nu = -\frac{\Delta\epsilon_3}{\Delta\epsilon_1} = \frac{1}{2} \left( 1 - \frac{\Delta\epsilon_v}{\Delta\epsilon_l} \right) \quad (26)$$

The average value obtained from the unloading-reloading curves from tests with different confining pressures is representative of the elastic Poisson's ratio for the material.

The dimensionless, constant values of the modulus number  $M$  and the exponent  $\lambda$  may be determined from the initial slopes of the unloading-reloading cycles in the triaxial compression tests, as also illustrated in Fig. 7. These initial slopes are

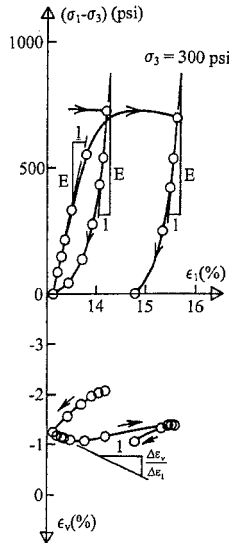


**FIG. 7. Determination of Young's moduli and Poisson's ratio from stress-strain and volumetric strain relations from unloading-reloading cycles in triaxial compression tests on Sand No. D (1 psi = 6.895 kPa).**

@Seismicisolation

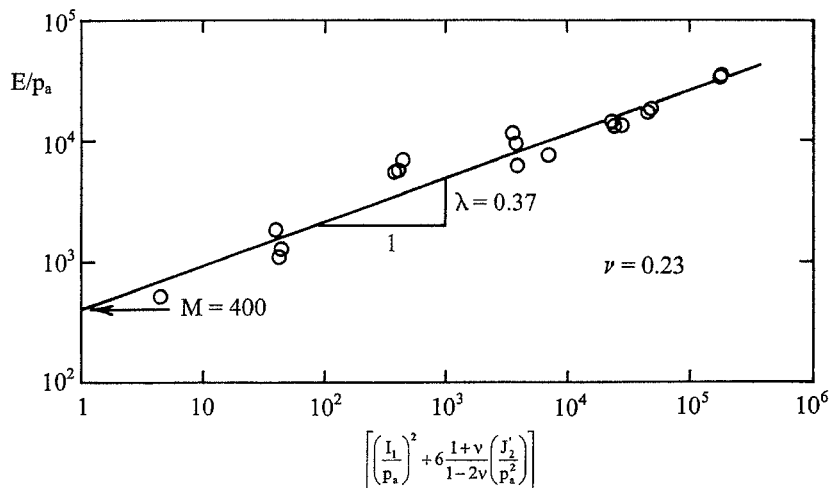


**FIG. 8. Determination of  $M$  and  $\lambda$  for Young's modulus variation for Sand No. D.**

considered to represent the elastic Young's moduli of the material. The corresponding values of the stress invariants in Eq. 2 are calculated from the stresses at the points of reversal. In order to determine the values of  $M$  and  $\lambda$ , Eq. 2 is rearranged and logs are taken on both sides of the equation:

$$\log\left(\frac{E}{p_a}\right) = \log M + \lambda \log\left[\left(\frac{I_1}{p_a}\right)^2 + 6 \frac{1+\nu}{1-2\nu} \left(\frac{J'_2}{p_a^2}\right)\right] \quad (27)$$

Thus, by plotting  $E/p_a$  versus the stress function on the right hand side of Eq. 27 on log-log scales, as shown in Fig. 8, the value of  $M$  is determined as the intercept between the best fitting straight line and the vertical line corresponding to unity of the stress function. The slope of the straight line corresponds to the exponent  $\lambda$ .

#### Failure Criterion

The expression for the failure criterion in Eq. 5 is rearranged and logs are taken on both sides of the equation:

$$\log\left(\frac{I_1^3}{I_3} - 27\right) = \log \eta_1 + m \log\left(\frac{p_a}{I_1}\right) \quad (28)$$

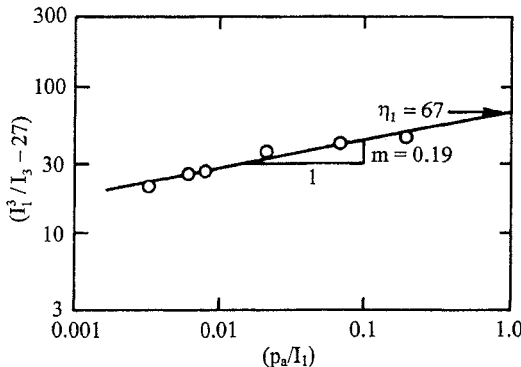


**FIG. 9. Determination of  $\eta_I$  and  $m$  for failure criterion for Sand No. D.**

By plotting  $(I_1^3/I_3 - 27)$  versus  $(p_a/I_1)$  on log-log scales, as shown in Fig. 9, the value of  $\eta_I$  is determined as the intercept between the best fitting straight line and the vertical line corresponding to  $(p_a/I_1) = 1$ . The slope of the straight line is the exponent  $m$ .

#### Plastic Potential Parameters

In the plastic potential, the parameter  $\psi_I$  is determined from Eq. 11, and the other parameters,  $\psi_2$  and  $\mu$ , can be determined using triaxial compression test data. This is done by expressing the incremental plastic strain ratio defined as:

$$\nu_p = -\frac{d\varepsilon_3^p}{d\varepsilon_1^p} \quad (29)$$

The plastic strain increments in Eq. 29 are calculated from the results of the triaxial compression tests by subtracting the elastic strain increments from the measured strain increments. Substitution of Eqs. 12 for the plastic strain increments under triaxial compression conditions ( $\sigma_2 = \sigma_3$ ) produces the following equation:

$$\xi_y = \frac{1}{\mu} \xi_x - \psi_2 \quad (30)$$

where

$$\xi_x = \frac{1}{1 + \nu_p} \left[ \frac{I_1^3}{I_2^2} (\sigma_1 + \sigma_3 + 2\nu_p \sigma_3) + \psi_1 \cdot \frac{I_1^4}{I_3^2} (\sigma_1 \sigma_3 + \nu_p \sigma_3^2) \right] - 3\psi_1 \cdot \frac{I_1^3}{I_3} + 2 \frac{I_1^2}{I_2} \quad (31)$$

and

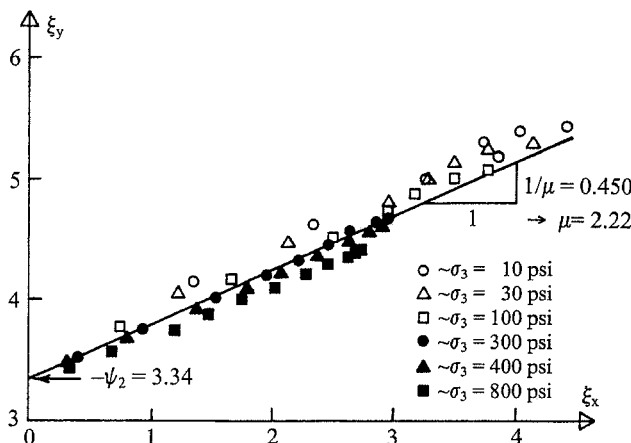


**FIG. 10.** Determination of  $\psi_2$  and  $\mu$  for the plastic potential function for Sand No. D (1 psi = 6.895 kPa).

$$\xi_y = \psi_1 \cdot \frac{I_1^3}{I_3} - \frac{I_1^2}{I_2} \quad (32)$$

Thus,  $1/\mu$  and  $-\psi_2$  can be determined by linear regression between  $\xi_x$  and  $\xi_y$  determined from several data points. Fig. 10 is a plot of  $\xi_x$  and  $\xi_y$  for the triaxial compression tests on Sand No. D. All data points are consistent with Eq. 32. The value of  $-\psi_2$  is the intercept value of  $\xi_y$  at  $\xi_x = 0$ , and the value of  $1/\mu$  is the slope of the best fitting straight line.

#### **Yield Criterion and Work-Hardening/Softening Relation**

The work-hardening relation along the hydrostatic axis, expressed in Eq. 21, is determined first, because the parameter values of  $C$  and  $p$  are required in determination of  $q$  in the yield criterion.

The plastic work along the hydrostatic axis is calculated from

$$W_p = \int \{\sigma_{ij}\}^T \{d\varepsilon_{ij}^p\} \quad (33)$$

which for an isotropic compression test reduces to:

$$W_p = \int \sigma_3 \cdot d\varepsilon_v^p \quad (34)$$

compression tests by subtracting the elastic strains from the measured strains.  $W_p/p_a$  is then plotted as a function of  $I_1/p_a$ , which for isotropic compression is equal to  $3\sigma_3/p_a$ .

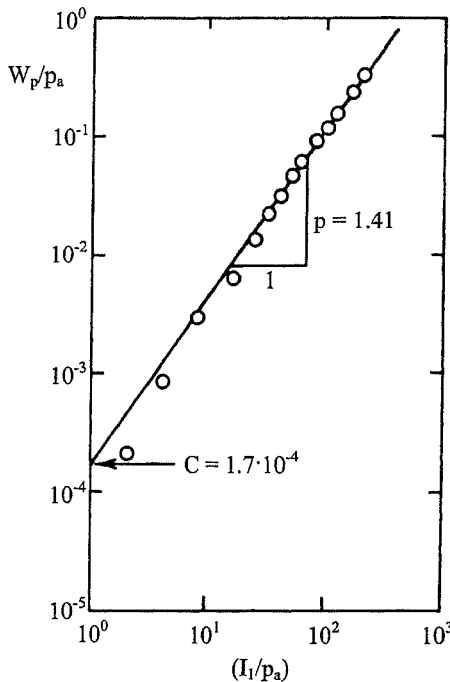


**FIG. 11. Determination of  $C$  and  $p$  for work-hardening relation for Sand No. D.**

The diagram in Fig. 11 shows the relationship between  $W_p/p_a$  and  $I_l/p_a$ , plotted on log-log scales for Sand No. D. This relationship is modeled by Eq. 21 in which  $C$  and  $p$  are determined as shown in Fig. 11. On this diagram  $C$  is the intercept with  $I_l/p_a = 1$  and  $p$  is the slope of the straight line.

The yield criterion in Eq. 15 requires two parameter values. The value of  $h$  is determined on the basis that the plastic work is constant along a yield surface. Thus, for two stress points,  $A$  on the hydrostatic axis and  $B$  on the failure surface, the following expression is obtained for  $h$ :

$$h = \frac{\ln\left(\psi_1 \cdot \frac{I_{1B}^3}{I_{3B}} - \frac{I_{1B}}{I_{2B}}\right) \cdot e}{\frac{27\psi_1 + 3}{\ln \frac{I_{1A}}{I_{1B}}}} \quad (35)$$

in which  $e$  = the base of natural logarithms.

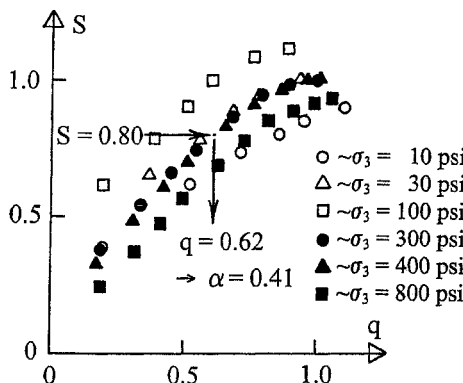


**Fig. 12. Determination of  $\alpha$  for yield criterion for Sand No. D (1 psi = 6.895 kPa).**

Substituting Eqs. 15 and 18 into Eq. 14 and solving for  $q$  produces:

$$q = \ln \frac{\left( \frac{W_p}{D \cdot p_a} \right)^{1/\rho}}{\left( \psi_1 \cdot \frac{I_1^3 - I_1^2}{I_3 - I_2} \right) \left( \frac{I_1}{p_a} \right)^h} \quad (36)$$

The variation of  $q$  from Eq. 36 with  $S$  from Eq. 16 is shown in Fig. 12 for Sand No. D. This variation may be expressed by Eq. 17 in which  $\alpha$  is constant. The best fitting value of  $\alpha$  is determined from Eq. 17 using simultaneous values of  $q$  and  $S$  at  $S = 0.80$ .

### TYPICAL PARAMETER VALUES

The components of the constitutive model and the corresponding 11 parameter values have been determined from isotropic compression tests and drained triaxial compression tests for many different sands without effective cohesion. Thus,  $a = 0$  and this parameter is not listed. The characteristics of these sands (void ratios, relative densities) and their model parameter values are listed in Table 1. None of the parameters have dimensions. All dimensions are controlled, where appropriate, by the dimension of the atmospheric pressure,  $p_a$ , as in Eq. 2.

From Table 1 it may be seen that several parameter values vary in a systematic manner with relative density. Thus, the  $M$ -values increase with increasing relative density, while the values of Poisson's ratio for sands are typically around 0.2. The values of  $\eta_1$  and  $m$  increase with relative density, but it is more difficult to discern a consistent pattern in the remaining parameters. It should be noted that the parameters appear in the mathematical expressions as pairs ( $\lambda$  and  $M$ ,  $m$  and  $\eta_1$ ,  $C$  and  $p$ ,  $\psi_2$  and

Table 1. Parameter values for select sands for the Single Hardening Model.

Sand Type	Void Ratio, $e$	Rel. Density, $D_r$ (%)	$\nu$	$M$	$\lambda$	$\eta_l$	$m$	$C \cdot 10^4$	$P$	$\psi_2$	$\mu$	$h$	$\alpha$
Sand No. D	0.534	89	0.23	400	0.37	67	0.19	1.7	1.41	-3.34	2.22	0.60	0.41
Fine Silica sand	0.76	30	0.27	440	0.22	24.7	0.10	3.24	1.25	-3.69	2.26	0.355	0.515
Sacramento River sand <sup>1</sup>	0.61	100	0.20	900	0.28	80	0.23	0.396	1.82	-3.09	2.01	0.765	0.229
Sacramento River sand <sup>1</sup>	0.87	38	0.20	510	0.28	28	0.093	1.27	1.65	-3.72	2.36	0.534	0.794
Painted Rock material <sup>2</sup>	0.40	100	0.20	920	0.24	101	0.21	3.51	1.25	-3.26	2.82	0.501	0.313
Painted Rock material <sup>2</sup>	0.48	70	0.20	350	0.33	67	0.16	0.46	1.78	-3.39	2.72	0.698	0.386
Crushed Napa basalt <sup>3</sup>	0.53	100	0.20	1050	0.17	280	0.423	0.814	1.61	-2.97	2.80	0.546	0.727
Crushed Napa basalt <sup>3</sup>	0.66	70	0.20	590	0.19	130	0.30	4.57	1.39	-2.90	2.55	0.542	0.851
Monterey No. 0 sand	0.57	98	0.17	1,120	0.33	104	0.16	0.269	1.44	-3.38	2.30	0.49	0.896
Monterey No. 0 sand	0.78	27	0.17	800	0.26	36	0.12	2.14	1.26	-3.60	2.50	0.43	0.577
Santa Monica Beach sand	0.613	88.5	0.15	1,270	0.23	107	0.25	1.44	1.39	-3.16	2.07	0.56	0.49
Santa Monica Beach sand	0.681	64.9	0.19	1,050	0.24	59.1	0.165	2.12	1.37	-3.34	2.20	0.57	0.58
Santa Monica Beach sand	0.755	39.2	0.22	820	0.26	37.7	0.105	2.26	1.42	-3.62	2.27	0.58	0.68
Santa Monica Beach sand	0.815	18.4	0.26	600	0.27	31.2	0.095	2.36	1.55	-3.74	2.36	0.67	0.46
Eastern Scheldt sand <sup>4</sup>	0.67	73	0.20	460	0.41	70.2	0.283	1.27	1.61	-3.15	2.06	0.553	0.617

All sand data are from the author's files, except as follows: <sup>1</sup>Lee and Seed (1967); <sup>2</sup>Al-Hussaini (1971); <sup>3</sup>Al-Hussaini (1972); <sup>4</sup>Jakobsen and Praastrup (1998).

$\mu$ ,  $h$  and  $\alpha$ ), and they combine to produce moduli or strengths through the magnitudes of the stresses. Scatter in the experimental data therefore plays a role in the derived parameter values. Although there are ranges of values in which each parameter tends to fall, there does not appear to be a general pattern of variation for sands that may be helpful in indicating approximate values of parameters in the absence of actual test data.

## MODEL CAPABILITIES

The Single Hardening Model has been developed for all types of frictional materials such as sands, clays, cemented soils, concrete, and rocks. The parameters for sands listed in Table 1 may be used to calculate strains for any three-dimensional combination of effective stresses during primary loading, neutral loading, unloading, and reloading. The model has been exercised for many different stress paths, and it has been employed in prediction of overconsolidation and preshearing effects (Lade and Prabucki 1995). It has been used to predict strains and volume changes under drained conditions (Lade and Kim 1988b, 1995) as well as strains and pore water pressures under undrained conditions (Lade 1990; Lade and Kim 1995). It has also been employed to predict instability and liquefaction in silty sands (Yamamoto and Lade 1999) as well as shear banding in sands under three-dimensional stress conditions (Lade 2003). The model forms the basis for development of a rotational kinematic hardening model for large three-dimensional stress reversals in soils (Lade and Inel 1997, Inel and Lade 1997). Incorporation of time effects such as creep in the model has also been achieved (Lade and Liu 2001).

## MODEL IMPLEMENTATION

The Single Hardening Model has been incrementalized (Lade and Jakobsen, 2002) and an implementation algorithm has been produced and formulated as a user-defined material module, a so-called UMAT for the ABAQUS finite element program (Jakobsen and Lade, 2002).

## REFERENCES

- Al-Hussaini, M.M. (1971). "Drained plane strain and triaxial compression tests on crushed Napa basalt." *USAEE WES, Miss., Report S-71-2*, No. 2.
- Al-Hussaini, M.M. (1972). "Plane strain and triaxial; compression tests on Painted Rock Dam material." *USAEE WES, Miss., Report S-71-2*, No. 3.
- Inel, S., and Lade, P.V. (1997) "Rotational Kinematic Hardening Model for Sand, Part II. Characteristic Work Hardening Law and Predictions," *Computers and Geotechnics*, Elsevier, 21(3), 217-234.
- Jakobsen, K.P., and Lade, P.V. (2002). "Implementation algorithm for a single hardening constitutive model for frictional materials," *Int J. Num. Analyt. Meth. Geomech.*, Wiley, 26, 661-681.
- Jakobsen, K.P., and Praastrup, U. (1998). "Drained triaxial tests on Eastern Scheldt sand." *Aalborg University Geotech. Engr. Papers*, ISSN 1398-6465 R9822.
- Kim, M.K., and Lade, P.V. (1984). "Modelling rock strength in three dimensions." *Int. J. Rock Mech. Min. Sci. & Geomech. Abstr.*, 21, 21-33.



- Kim, M.K., and Lade, P.V. (1988). "Single Hardening Constitutive Model for Frictional Materials, I. Plastic Potential Function." *Computers and Geotechnics*, Elsevier, 5(4), 307-324.
- Kupfer, H., Hilsdorf, H.K., and Rusch, H. (1969). "Behavior of concrete under biaxial stresses." *J. Am. Conc. Inst.*, 66, 656-666.
- Lade, P.V. (1977). "Elasto-plastic stress-strain theory for cohesionless soil with curved yield surfaces." *Int J Solids Struct*, Pergamon Press, 13, 1019-1035.
- Lade, P.V. (1982). "Three-parameter failure criterion for concrete." *J. Engr. Mech.*, ASCE, 108, 850-863.
- Lade, P.V. (1984). "Failure Criterion for frictional materials." *Mech Engr. Materials*, C.S. Desai and R.H. Gallagher (eds.), Chapter 20, Wiley, New York, 385-402.
- Lade, P.V. (1990). "Single hardening model with application to NC clay." *J Geotech Engr.*, ASCE, 116(3), 394-414.
- Lade, P.V. (1993). "Rock strength criteria: The theories and the evidence." In *Comprehensive Rock Engineering Principles, Practice & Projects*, edited by J.A. Hudson. Vol. 1: *Fundamentals*, edited by E.T. Brown, Chapter 11, Oxford: Pergamon Press, 255-284.
- Lade, P.V. (2003) "Analysis and Prediction of Shear Banding Under 3D Conditions in Granular Materials," *Soils and Foundations*, JGS, 43(4), 161-172.
- Lade, P.V. (2005). "Calibration of the Single Hardening Model for Clays." *Proc. 11<sup>th</sup> Int. Conf. IACMAG*, Turin, Italy.
- Lade, P.V., and Inel, S. (1997) "Rotational Kinematic Hardening Model for Sand, Part I. Concept of Rotating Yield and Plastic Potential Surfaces," *Computers and Geotechnics*, Elsevier, 21(3), 183-216.
- Lade, P.V., and Jakobsen, K.P. (2002). "Incrementalization of a single hardening constitutive model for frictional materials," *Int. J. Num. Analyt. Meth. Geomech.*, Wiley, 26, 647-659.
- Lade, P.V., and Kim, M.K. (1988a). "Single Hardening Constitutive Model for Frictional Materials, II. Yield Criterion and Plastic Work Contours." *Computers and Geotechnics*, Elsevier, 6(1), 13-29.
- Lade, P.V., and Kim, M.K. (1988b). "Single Hardening Constitutive Model for Frictional Materials, III. Comparisons with Experimental Data." *Computers and Geotechnics*, Elsevier, 6(1), 31-47.
- Lade, P.V., and Kim, M.K. (1995). "Single hardening constitutive model for soil, rock and concrete." *Int J Solids Struct* Pergamon Press, 32, 1963-1978.
- Lade, P.V., and Nelson, R.B. (1987). "Modelling the elastic behavior of granular materials." *Int J Num Analyt Meth Geomech.*, 11, 521-542.
- Lade, P.V., and Liu, C.-T. (2001). "Modeling creep behavior of granular materials," *Proc. 10th Int. Conf. Computer Methods and Advances in Geomechanics*, Tucson, Arizona, Balkema, C.S. Desai et al. (eds.), 277-284.
- Lade, P.V., and Prabucki, M.-J. (1995). "Softening and preshearing effects in sand." *Soils and Foundations*, JGS, 35(4), 93-104.
- Yamamoto, J.A., and Lade, P.V. (1999). "Experiments and modelling of silty sands susceptible to static liquefaction," *Mech. Cohesive-Frictional Materials*, Wiley, 4(6), 545-564.

@Seismicisolation

## SELECTION AND CALIBRATION OF SOIL CONSTITUTIVE MODEL PARAMETERS USING GENETIC ALGORITHMS

Emir José Macari<sup>1</sup>, M. ASCE, Prasad Samarajiva<sup>2</sup>, P.E., M. ASCE,  
and Wije Wathugala<sup>3</sup>, P.E., M. ASCE

**ABSTRACT:** This paper presents the results of a study that uses an innovative numerical method called the “genetic algorithm” for material parameter optimization in constitutive modeling. A genetic algorithm based hybrid method of obtaining material parameters is used to optimize material parameters of a disturbed state concept based constitutive model. The “genetic algorithm” and the new fitness function were found to be capable of optimizing material parameters of complex constitutive models.

### INTRODUCTION

Engineers use a variety of methods to optimize material parameters of constitutive models, depending on the degree of complexity of a constitutive model. For example, the best values of two linear elastic parameters may be found by plotting the isotropic compression/tension behavior and the shear behavior. However, adding sophistication and accuracy to constitutive models results in the introduction of complexities along with more model parameters. As a result, the procedure of optimizing material parameters becomes complex as well. In such cases, engineers use mathematical methods such as regression and the least square methods to optimize material parameters (Macari, et al., 1991). In recent years, various engineering disciplines have used a method called the genetic algorithm (GA) to solve optimization problems. The genetic algorithm, in essence, is a solution-optimizing scheme loosely based on Darwin’s theory of evolution (Goldberg, 1989). The GA promotes the best sets of solutions from a solution pool, to survive and produce offsprings that populate the next generation pool of solutions. In theory, applying such a solution filtration scheme for a substantial number of generations may result in a more fit set of solutions. The model presented by Samarajiva (2000) utilizes the GA to fine tune material parameters obtained using approximate experimental methods. Prior to Samarajiva (2000), Koumousis and Georgio (1994), used the GA to optimize steel roof trusses; Adeli and Cheng (1993) used the GA to

<sup>1</sup> Dean and Professor, College of Science, Mathematics and Technology, University of Texas at Brownsville, Brownsville, TX 78520

<sup>2</sup> Geotechnical Engineer, FUGRO Consultants LP, Houston, TX 77081

<sup>3</sup> Project Manager, ACTA Inc., Torrance CA 90505



optimize space structures; and Wu and Chow (1995) introduced a GA based method for discreet optimization of structures. Additional studies have been done on structure-optimization using the GA by Hajela and Lee (1995). Tresar and Dresik (1995) used the GA for dynamic analysis of structures. Chan et al. (1994); Fwa et al. (1994); and Chakroborty et al. (1995) used the genetic algorithm for optimization problems in transportation engineering. Simpson and Priest (1993) used the GA to identify the maximum discontinuity frequency in rock structures. Pal et al. (1996) used the genetic algorithm to optimize material parameters of a constitutive model.

In the model proposed by Samarajiva (2000), it was difficult to directly determine the “intact” parameters for this model because available laboratory experiments are not sufficient to quantify partially disturbed state of the hypothesized material behavior. In other words, without knowing the degree of disturbance at a “partially disturbed state” (this being a micro-mechanical value, not easily quantified), it is difficult to determine the stress and strain conditions of the “intact state.” Hence, it is difficult to determine the “intact” material model parameters. One possible solution to this problem is to make a “best estimate” of a material parameter set and correct them iteratively based on the success of that material parameter set. In such a scenario, the GA may be used to perform an efficient search for a suitable set of material parameters.

In this paper, a hybrid method of searching material parameters for the constitutive model proposed by Samarajiva (2000) is presented. For the sake of clarity, a very brief discussion of the constitutive model used in this study (Samarajiva, 2000) is presented in the ensuing section. Afterwards, details of the implementation of the GA, parameter calibration procedure, and calibrated material parameters for Sacramento River sands are presented.

## CONSTITUTIVE MODEL

The constitutive model for sands used here is developed by modifying the constitutive model proposed by Wathugala and Desai (1987) and the disturbed state concept developed by Desai and co-workers (Desai 1974, Desai 1992; and Desai 2001). For a more comprehensive overview of DSC, readers are referred to the textbook by Desai (2001) and the book chapter by Wathugala (2000).

In DSC, conceptually, when a sand element is subjected to an external action, micro-structural changes take place inside the material. Initially, the material is considered intact (FIG 1 (a)). It is hypothesized that the increase of external action transforms sands into a disturbed state. The well-known critical state of soils may be considered as the disturbed state of sands. In the process of deformation, a random distribution of critical state and intact state clusters exist in the material (FIG 1 (b)). Eventually, the material fails by reaching the fully disturbed “critical” state (FIG 1 (c)). However, an experimental study will only reveal the superficial behavior of sands which can also be considered as the statistical average of intact and critical states without quantification of degree of disturbance. The behavior of the “critical state,” the behavior of the “intact state,” and the quantification of disturbance of the constitutive model is discussed in ensuing sub-sections.



## Critical State Behavior of Sands

Wathugala and Desai (1987) expressed a relationship for the critical state stress behavior in terms of stress invariants based on work by Roscoe et al. (1963). There, the square root of the second invariant of the deviatoric stress ( $\sqrt{J_{2D}}$ ) is related to the confinement pressure ( $J_1$ ) irrespective of initial density and initial confinement by the relationship,

$$\sqrt{J_{2D}} = mJ_1 \quad (1)$$

where  $m$  is a material parameter.

A relationship for the critical void ratio ( $e^c$ ) and the confining pressure ( $J_1$ ) was expressed by Wathugala and Desai (1989), based on work by Roscoe et al. (1963), as,

$$e^c = e_0^c - \lambda \ln\left(\frac{J_1}{3P_a}\right) \quad (2)$$

where  $\lambda$  and  $e_0^c$  are material parameters.

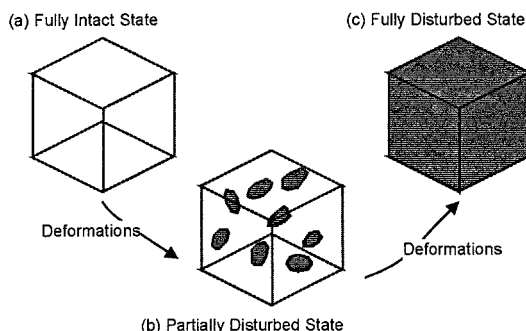


**FIG 1 Illustration of Growth of the Critical State in a Sand Element**

## Intact Behavior of Sands

To emulate the intact behavior, a modified version of HiSS family  $\delta_0^*$  model by Wathugala (1990) was used. The hierarchical single surface (HiSS) modeling approach (Desai 1980, Desai et al. 1986) allows for progressive development of models of higher grades corresponding to different levels of complexities. The  $\delta^*$  series of the HiSS models is developed to capture the behavior of cohesive soils in addition to all the previous capabilities of HiSS models (Wathugala, 1990, Wathugala and Desai 1993).

HiSS  $\delta_0^*$  model family identifies the virgin loading (VL), unloading (UL) and reloading (RL) using a convex reference surface passing through the current stress point. The reference surface is defined in terms of stress invariants as

$$R = \left( \frac{J_{2D}}{P_a^2} \right) - F_{br} F_s \quad (3)$$

where  $P_a$  is the atmospheric pressure and,

$$F_{br} = -\alpha_r \left( \frac{J_1}{P_a} \right)^{n_1} + \gamma \left( \frac{J_1}{P_a} \right)^{n_2} \quad (4)$$

The symbols  $\gamma$ ,  $n_1$  and  $n_2$  are material parameters. The current value for  $\alpha_r$  is obtained by the condition  $R=0$ . The function  $F_{br}$  defines the shape of  $R$  in the  $J_1, \sqrt{J_{2D}}$  space and the function,

$$F_s = (1 - \beta S_r)^l \quad (5)$$

describes the shape of  $R$  in the octahedral plane, where

$$S_r = \frac{\sqrt{27}}{2} J_{3D} J_{2D}^{-\frac{3}{2}} \quad (6)$$

The symbols  $\beta$  and  $l$  are material parameters ( $l$  defaults to -0.5).

The  $\delta_0^*$  plasticity model, as defined by Wathugala (1990), uses the associative flow rule. On yielding, when loading becomes virgin loading, the reference surface coincides with the yield surface  $F$ . The yield surface is defined as,

$$F = \left( \frac{J_{2D}}{P_a^2} \right) - F_b F_s \quad (7)$$

where

$$F_b = -\alpha_{ps} \left( \frac{J_1}{P_a} \right)^{n_1} + \gamma \left( \frac{J_1}{P_a} \right)^{n_2} \quad (8)$$

and the hardening function  $\alpha_{ps}$  is given by,

$$\alpha_{ps} = \frac{h_1}{\xi^{h_2}_V} \quad (9)$$

$$\xi = \int (d\varepsilon_{ij}^P d\varepsilon_{ij}^P)^{1/2} \quad (10)$$

$$\xi_V = \int \frac{1}{\sqrt{3}} |d\varepsilon_{ii}^P| \quad (11)$$

where  $h_1$  and  $h_2$  are material parameters and the state variables  $\xi$  and  $\xi_V$  are the trajectories of total and volumetric plastic strains.

Shear experiments show that the stress state of dense sands crosses above the critical state line before reaching the critical state. The shearing stress state of loose sands, on the other hand, monotonically reaches the critical state line at failure. Therefore, for the model to work properly, the slope of the phase change line of the intact behavior should not be lower than the slope of critical state line. In order to achieve such a control parameter  $\gamma$  was redefined by Samarajiva (2000) as a function of the initial void ratio ( $e_0$ ) and the initial confinement pressure ( $J_{1(0)}$ ) given by,

$$\gamma = \gamma_{\min} + \left[ \frac{e_{\max} - e_0}{e_{\max} - e_{\min}} \right]^{k_2} \left( \bar{\gamma} - \gamma_{\min} \right) \exp(-\chi J_{1(0)} / 3P_a) \quad (12)$$

where,

$$\gamma_{\min} = m^2 \sqrt{1 + \beta S_r} \left( \frac{n_1}{n_1 - 2} \right) \quad (13)$$

and,  $k_2$ ,  $\bar{\gamma}$ , and  $\chi$  are material parameters.

## Mechanics of Disturbance

Disturbance ratio,  $D$ , is defined as,

$$D = \frac{M^c}{M} \quad (14)$$

where  $M$  is the mass of solids in the material and  $M^c$  is the mass of solids in the disturbed phase. The scalar  $D$  represents the extent of disturbance phase in the material. Initially,  $D=0$  and its final value is equal to unity. Value  $D=1$  represents a fully disturbed material at the critical state. The proposed model uses Frantziskonis and Desai's (1987) damage function,  $D$ , for sands which, expresses the mass fraction of sands at critical state in terms of the trajectory of deviatoric plastic strains ( $\xi_D$ ), given by the relationship,

$$D = D_u [1 - \exp(-A \xi_D^{k_1})] \quad (15)$$

where  $A$  and  $k_1$  are material parameters and  $D_u = 1$ . State variable  $\xi_D$  is given by,

$$\xi_D = \int \sqrt{d \in_i^P d \in_j^P} \quad (16)$$

where  $\in_i^P$  is the deviatoric plastic strain.



## Constitutive Relationships

The new incremental stress-strain relationship between average stresses and intact strains is given by,

$$d\sigma_{ij}^A = E_{ijkl}^{DSC} d\varepsilon_{kl}^I \quad (17)$$

where

$$E_{ijkl}^{DSC} = \left\{ [D(k-1)+1]C_{ijkl}^I - D(k-1)\frac{C_{ijkl}^I \delta_{ij}}{3} + S_{ij}^I [R_{kl}^I (k-1) + T_{kl}^I D] \right\}, \quad (18)$$

$$T_{kl}^I = m \left\{ \frac{2J_{2D}^I \delta_{ij} - J_1^I S_{ij}^I}{2(J_{2D}^I)^{3/2}} \right\} C_{ijkl}^I, \quad (19)$$

$$R_{kl}^I = \frac{dD}{d\xi_D} \frac{n_{ij}^F C_{ijkl}^{e(I)} \sqrt{n_{Dmn}^Q n_{Dmn}^Q}}{\{n_{ij}^F C_{ijuv}^{e(I)} n_{uv}^Q + H^V\}}, \quad (20)$$

and

$$k = \frac{\sqrt{J_{2D}^C}}{\sqrt{J_{2D}^I}} \quad (21)$$

where  $C_{ijkl}^I$  is the elasto-plastic stiffness of the intact state,  $C_{ijkl}^e$  is the elastic stiffness of the intact state,  $H^V$  is the virgin plasticity modulus of the intact model,  $n_{ij}$  is the unit normal to the intact state reference surface, and  $S_{ij}$  is the deviatoric component of the stress tensor. It should be noted that superscripts A, I, and C denote the Average behavior, Intact behavior, and Critical behavior respectively. Prior to the critical state globules reaching the critical stress levels ( $\sqrt{J_{2D}^A} < mJ_1^A$ ), stresses of the critical and the intact state are assumed to be the same ( $k=1$ ).

Using the above formulations, the relationship between average stresses and average strains is established as,

$$d\sigma_{ij}^A = C_{ijkl}^{DSC} d\varepsilon_{kl}^A \quad (22)$$

where

$$C_{ijkl}^{DSC} = \left\{ [D(k-1)+1]C_{ijkl}^I - D(k-1)\frac{C_{ijkl}^I \delta_{ij}}{3} + S_{ij}^I [R_{kl}^I (k-1) + T_{kl}^I D] \right\} \times \\ \left\{ \delta_{ik} \delta_{jl} + \frac{\delta_{ij}}{3(1+e_0)} (e^I - e^C) R_{kl}^I + D(\lambda C_{mnkl}^I - \delta_{kl})(1+e_0) \right\}^{-1} \quad (23)$$

It is possible to calculate the average stress increment corresponding to the average strain increment and vice-versa by numerically integrating equations 22 and 23 if the current state is fully defined. A modified Euler algorithm is used for the integration of the formulations.

## DETERMINATION OF MATERIAL PARAMETERS

In this model, elastic parameters and critical state parameters can be obtained directly from test results since sands in the initial parts of the triaxial tests can be considered "fully intact" and sands in the final part of the triaxial tests can be considered "fully critical." However, the intact state parameters defined in HiSS  $\delta_0^*$  plasticity model and parameters associated with the degree of disturbance (Eqn 15) cannot be found directly. Here, the genetic algorithm is used to refine the intact parameters using already determined elastic parameters, critical state parameters, and approximately determined intact state parameter ranges. The method of determination of elastic parameters and critical state parameters are not discussed here since those methods are very straightforward (Samarajiva, 2000). However, details of determination of approximate intact state and disturbance parameters are discussed in ensuing section.

## APPROXIMATE INTACT STATE PARAMETERS

### Ultimate Parameters $n_i$ , $\gamma$ , and $\beta$

At ultimate conditions the intact stresses reach the phase change line of the intact model (FIG 2). At the failure (residual) point  $\sqrt{J_{2D}}$  is a maximum; therefore  $F_b$  (Eqn. 8) is also a maximum. Then,

$$\frac{\partial F_b}{\partial J_1} = 0 \quad (24)$$

or

$$\left[ \left( \frac{J_{2D}}{J_1^2} \right)_{PC}^{-2} \left( \frac{n_i}{n_i - 2} \right) \right] \gamma^2 - S_r \beta = 1 \quad (25)$$

where subscript PC stands for phase change.

In order to solve Eqn. (25) for  $\gamma$ , and  $\beta$ , it is necessary to assume a value for  $n_i$  (usually 2.1~2.6). Using Eqn. (25) and a minimum of two triaxial tests (with different  $S_r$ ) conducted at the same density and the same initial confinement pressure with loose sand stress-strain behavior (sufficiently high confinement pressure), parameters  $\gamma$  and  $\beta$  can be obtained. Now, having found  $\beta$ , which is not dependent on confinement pressure, parameter  $\gamma$  for two additional stress or relative density

states should be obtained to determine  $k_2$ ,  $\gamma$  and  $\chi$  at a later stage (after the genetic algorithm optimization procedure).

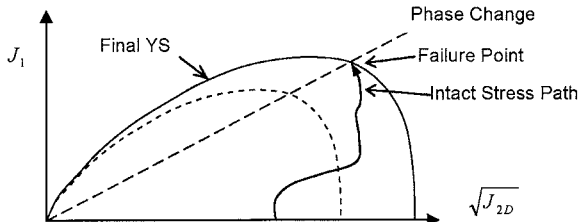


**FIG 2 Illustration of Failure Point of Intact Phase**

### Hardening Parameters $h_1$ and $h_2$

Having approximately evaluated  $n_1$ ,  $\gamma$ , and  $\beta$ , it is possible to evaluate  $h_1$  and  $h_2$  for GA optimization. On yielding,  $F = 0$ , therefore

$$\alpha_{ps} = \left[ \gamma - \left( \frac{J_{2D}}{J_1} \right) \frac{1}{F_s} \right] \left( \frac{P_a}{J_1} \right)^{n_1-1} \quad (26)$$

Taking the natural logarithm of Eqn. (9) yields,

$$\ln(\alpha_{ps}) = -h_2 \ln(\xi_v) + \ln(h_1) \quad (27)$$

By using the hydrostatic compression portions of one or several triaxial tests, and Eqns. (26) and (27), it is possible to estimate values of  $h_1$  and  $h_2$  approximately by solving two simultaneous equations or by least square methods.

### Damage Parameters $A$ and $k_1$

The available set of approximate intact parameters can be used to obtain approximate damage parameters. All of the estimated parameters will be further refined using the genetic algorithm for predictions. Based on the assumption that, stresses of average, intact and critical phases are the same until the failure in the loose sands, it is possible to obtain an approximate stress-strain response of the intact phase for a given stress path. Therefore, it is possible to estimate the approximate intact void ratios for the given stress path. The critical void ratios can be directly calculated for a given confinement using Eqn (2). The average void ratios can be calculated from the experiments. Now it is possible to plot the approximate evolution of the void ratios of the three phases (FIG 3).

By taking the natural logarithm twice on Eqn. (15), the following linear relationship can be obtained.

$$k_1 \ln(\xi_D) - \ln\left(-\ln\left(1 - \frac{D}{D_u}\right)\right) = -\ln(A) \quad (28)$$

Now it is possible to solve for approximate values of  $A$  and  $k_1$  using the approximated intact values and the corresponding values from the graph of  $e$  vs.  $\sqrt{I_{2D}}$ . With the availability of a set of approximate material parameters, it is possible to obtain a refined set of material parameters using the genetic algorithm.

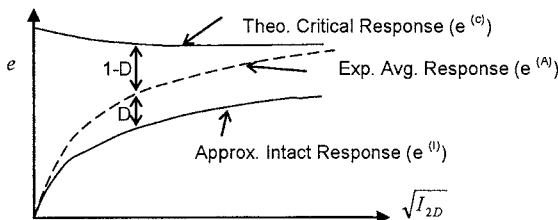


**FIG 3 Illustration of Void Ratio Behavior of a Loose Sand**

### Intact Parameters $k_2$ , $\bar{\gamma}$ , and $\chi$

Here, it is assumed that the appropriate values for  $n_1$ ,  $\gamma$ , and  $\beta$  from three tests (two initial densities and two initial confinement pressures) are available from the GA search. By taking the natural logarithm of rearranged Eqn. (12),

$$\ln(\gamma - \gamma_{\min}) = \ln(\bar{\gamma} - \gamma_{\min}) + k_2 \ln\left(\frac{e_{\max} - e}{e_{\max} - e_{\min}}\right) - \chi\left(\frac{J_1}{3P_a}\right) \quad (29)$$

Using Eqn. (29), it is possible to calculate  $k_2$ ,  $\bar{\gamma}$ , and  $\chi$  by solving three simultaneous equations or by using least square method for more than three simultaneous equations.

### GENETIC ALGORITHM

As in the biological evolution process, there are three basic steps in creating a new generation from an existing generation (FIG 4). Reproduction, in which a decision based on the fitness of a material parameter set is made on how many copies of a gene will go to the mating pool, is the first step. Crossover or mating, in which offsprings are produced for the next generation, is the second step. Mutations, in which random changes of genes occur is the third step. The current research uses a simple form of the GA for material parameter tuning (Goldberg, 1989a) in which binary strings, called chromosomes, are used to represent material parameter sets. However, it is possible to use real numbers directly without binary coding for genetic algorithm computations (Eshelman & Schaffer (1993) and Wright (1991)). Details of the implementation of the GA and the new fitness function are discussed in the ensuing sections.

**@Seismicisolation**

## Binary Representation of Material Parameters

The proposed approach uses binary strings to represent material parameters (genes) in the GA. A binary string  $S$  of length  $L$  can be used to discretize a real material parameter  $X$  ( $a \leq X \leq b$ ) using equation,

$$X = a + \frac{B(b-a)}{2^L - 1} \quad (30)$$

where  $B$  is the decimal value of the binary string  $S$ . For a three bits long gene, the string 000 corresponds to the lower bound  $a$  and the string 111 corresponds to the upper bound  $b$ . If  $S = 101$ ,  $L = 3$ ,  $a = 3.2$ ,  $b = 10.5$  then,  $B = 1 \times 2^0 + 0 \times 2^1 + 1 \times 2^2 = 5$  and  $X = 3.2 + (5/(2^3 - 1)) \times (10.5 - 3.2) = 8.414$ . As result of the discretization, the search space of  $X$  is limited to (e.g. 8) discrete points within the range. If necessary, a non-linear discretization scheme may be used for decoding and encoding. Such methods are useful when different points of the range  $a \leq X \leq b$  need to be searched or examined at a different resolution.

In the case of a multi-parameter problem, such as for many sophisticated constitutive models, binary strings representing material parameters are concatenated into a single string to represent a set of parameters. For example, if there are six binary coded three bit parameters  $S_1 = 101$ ,  $S_2 = 100$ ,  $S_3 = 111$ ,  $S_4 = 001$ ,  $S_5 = 010$ , and  $S_6 = 000$  then the final string (chromosome) of 18 bits is given by 101|100|111|001|010|000. For optimization purposes, it is theoretically possible to search a space of  $2^{18}$  combinations for parameter sets within given limits. Practically, actual search space in computations will be controlled by the size of a population and the maximum number of generations. For example, a 50-member population, evolving over 100 generations, will have a maximum search space of 5000 out of  $2^{18}$  possibilities. Later, the effects of increased search space, i.e. size of a gene pool and number of generations, on efficiency of the genetic algorithm will be discussed.

## Reproduction

Based on the fitness of the chromosomes (concatenated binary string), decisions are made on how many copies of each string will go into the mating pool. Strings with higher fitness values have higher survival probabilities. As a result, a proportionately higher number of copies of such strings are made available to the mating pool to create the next generation. The probability of survival of the  $i^{th}$  chromosome out of a population of  $n$  chromosomes is given by,

$$p_i = \frac{f_i}{\sum f_i} \quad (31)$$

where  $f_i$  is the fitness of the  $i^{th}$  string. Therefore, the number of copies made by the  $i^{th}$  string is given by,

 @Seismicisolation

$$n_i = n \times p_i \quad (32)$$

where  $n$  is the size of the population (FIG 5). Usually, the fitness values get scaled by a MAXMIN factor so that, the best chromosome will have a survival probability of MAXMIN times the worst chromosome. Some advanced algorithms copy a percentage of the best genes directly into the next generation without crossover.

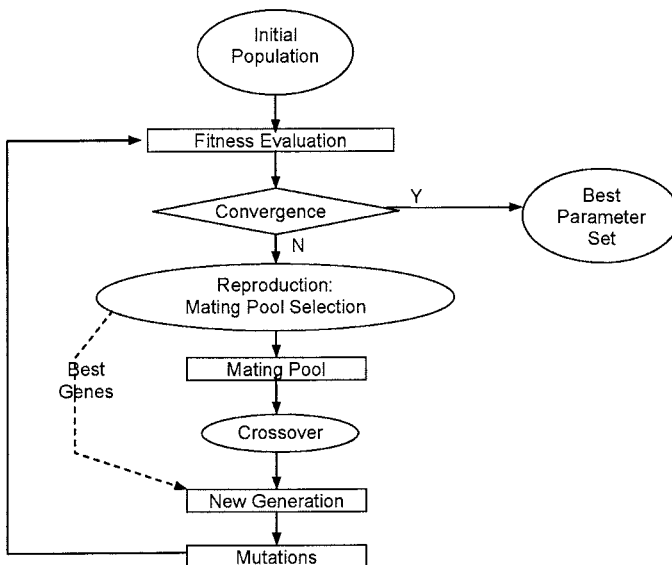


**FIG 4 Flow Chart of the Genetic Algorithm**

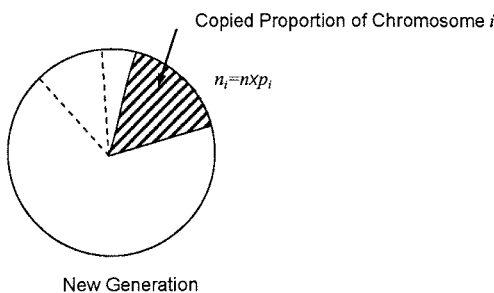


**FIG 5 Proportional Copying of Chromosomes for Crossover**

### Crossover and Mutation

Crossover is the mating process in which an exchange of bits of each mating pair is performed to produce offsprings. Selection of bits can either be random or specific (FIG 6). Current research mainly uses a random bit mating procedure

**@Seismicisolation**

involving all the chromosomes. The mutation operation flips bits of randomly selected chromosomes to prevent homogenization of a population (FIG 7). However, mutations take place only occasionally, similar to the biological evolution (De Jong, 1975). The effects of crossover schemes and mutations will be discussed later for efficiency of the genetic algorithm.

### Fitness Function

For successful optimization, it is necessary to evaluate the accuracy of the material parameter sets' prediction as accounted for in terms of a fitness function. The material parameter sets with higher fitness should survive to produce offsprings. Therefore, it is necessary to devise a fitness function such that the parameter sets with better predictions result in higher fitness values. Samarajiva (2000) introduced an unfitness function using the differential area between predicted and observed curves (FIG 8). For this purpose, the differential areas of the  $\sqrt{J_{2D}}$  vs.  $\sqrt{I_{2D}}$  graph, the  $\sqrt{J_{2D}}$  vs.  $J_1$  graph, and the  $I_1$  vs.  $\sqrt{I_{2D}}$  graph were used. Symbols  $J_1$ ,  $I_1$ ,  $J_{2D}$ , and  $I_{2D}$  denote first invariant of stress tensor, first invariant of strain tensor, second invariant of deviatoric stress tensor, and second invariant of deviatoric strain tensor respectively. An unfitness function is the opposite of a fitness function in which higher values indicate lower fitness to survive. Therefore, the fitness may be measured by reassigning the  $f_i$  value as given by,

$$f_i = f_{\max} - f_i \quad (33)$$

where  $f_{\max}$  is the fitness of the most unfit parameter set.

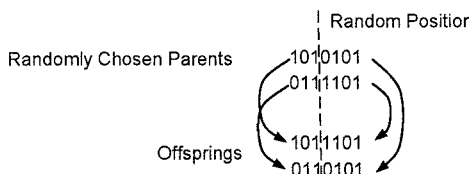


**FIG 6 Illustration of Crossover Procedure for 6 Bit Genes**

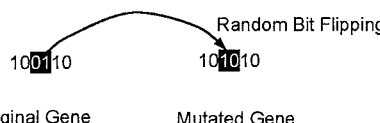


**FIG 7 Illustration of Mutation of a 6 bit Gene**

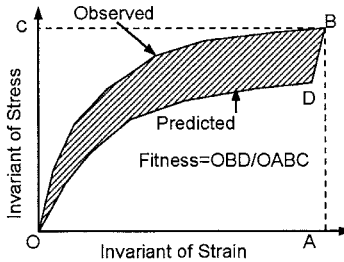


**FIG 8 Unfitness Function Computation (Pal et al., 1996)**

The proposed unfitness function is given by,

$$f_i = \frac{A_{(\sqrt{J_{2D}}, \sqrt{I_{2D}})}}{(\sqrt{J_{2D,max}} - \sqrt{J_{2D,min}})(\sqrt{I_{2D,max}} - \sqrt{I_{2D,min}})} \times \\ \left\langle A_{(I_1, \sqrt{I_{2D}})} / (I_{1,max} - I_{1,min})(\sqrt{I_{2D,max}} - \sqrt{I_{2D,min}}) | 1.0 \right\rangle \times \\ \left\langle A_{(\sqrt{J_{2D}}, J_1)} / (\sqrt{J_{2D,max}} - \sqrt{J_{2D,min}})(J_{1,max} - J_{1,min}) | 1.0 \right\rangle \times \\ (1.0 + \sum w_j \Delta Error_j) \quad (34)$$

where  $A_{(\sqrt{J_{2D}}, \sqrt{I_{2D}})}$  is the differential area of the  $\sqrt{J_{2D}}$  vs.  $\sqrt{I_{2D}}$  graph,  $A_{(I_1, \sqrt{I_{2D}})}$  is the differential area of the  $I_1$  vs.  $\sqrt{I_{2D}}$  graph and  $A_{(\sqrt{J_{2D}}, J_1)}$  is the differential area of the  $\sqrt{J_{2D}}$  vs.  $J_1$  graph. Brackets  $\langle x | 1.0 \rangle$  implies that,

$$\begin{aligned} \langle x | 1.0 \rangle &= x \quad \text{if } x \neq 0 \\ \langle x | 1.0 \rangle &= 1 \quad \text{if } x = 0 \end{aligned} \quad (35)$$

Such a notation is introduced to present a single formula for both stress and strain controlled predictions. Discrepancy of predictions and observations of all three invariant graphs at  $j^{\text{th}}$  point (FIG 9) is given by,

$$\Delta Error_j = \langle \Delta Error(\sigma)_j | \Delta Error(\varepsilon)_j \rangle \quad (36)$$

$$\Delta Error(\sigma)_j = \frac{\sqrt{(\sqrt{J_{2D,P}} - \sqrt{J_{2D,O}})^2 + (J_{1,P} - J_{1,O})^2}}{\max(\sqrt{(\sqrt{J_{2D,P}} - \sqrt{J_{2D,O}})^2 + (J_{1,P} - J_{1,O})^2})} \quad (37)$$

$$\Delta Error(\varepsilon)_j = \frac{\sqrt{(\sqrt{I_{2D,P}} - \sqrt{I_{2D,O}})^2 + (I_{1,P} - I_{1,O})^2}}{\max(\sqrt{(\sqrt{I_{2D,P}} - \sqrt{I_{2D,O}})^2 + (I_{1,P} - I_{1,O})^2})} \quad (38)$$

Normalization of the errors by the maximum error is introduced to prevent over-representation of error in a final unfitness value. It should be noted that certain parts of the proposed unfitness function get nullified in strain to stress predictions or stress to strain predictions. The weight applied to each point is symbolized by  $w_j$ . In the proposed function, the weight may vary between 0.0 and 1.0. Assigning unit weights to several points near a special trend may be considered as restraining that trend in the genetic algorithm. For example, it is possible to emphasize the importance of initial slope of a graph by assigning unit weights to several points along the line. In the numerical implementation, the error, ( $\Delta Error_j$ ) becomes the weight ( $w_j$ ) for each unpredicted point, i.e. the maximum possible penalty for that point. As a result, unfitness of such parameter sets will be substantially higher than other sets.

## VERIFICATION OF ALGORITHM AND FITNESS FUNCTION

It is necessary to verify the validity of a genetic algorithm. For the purpose of verification, a simulated stress-strain curve was used since the exact values of the parameters were known. The parameters used for the curve generation, search range for the parameters, and the parameters obtained using the GA are given in Table 1. In this study, elastic parameters ( $E$  and  $\nu$ ) are not searched using GA since such parameters were directly obtained from the experimental data (Samarajiva, 2000). For the sake of simplicity, parameter  $\gamma$  is searched instead of its associated parameters  $k_2$ ,  $\bar{\gamma}$  and  $\chi$ . These parameters may be found using three or more values for  $\gamma$  at different initial densities and confinement stresses (Samarajiva, 2000). The strain path used in the simulations, in the form of invariants, are shown in FIG 10. A crossover rate of 100%, a mutation rate of 2%, a MAXMIN factor of 5, a population size of 10 and equal weights for all points were used in this simulation. FIG 11 presents the best fitness value of the generations and the best overall fitness values, plotted against the generation number. The stress-strain behavior of the simulated test and the predictions from the GA optimized material parameters are presented in FIG 12 and FIG 13. Even though the obtained material parameters are not identical, this simulation shows the capability of the GA in searching material parameters. It is evident that the GA is capable of optimizing material parameters with a very modest population size, using the proposed unfitness function, compared to previous studies found in the literature (De Jong (1975) and Pal et al. (1996)).

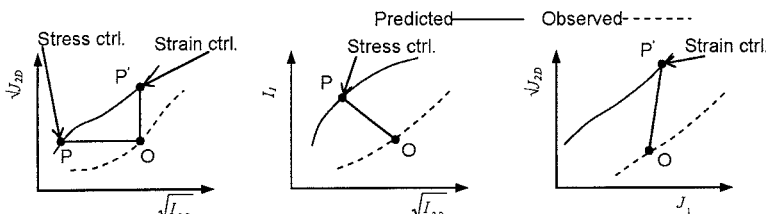
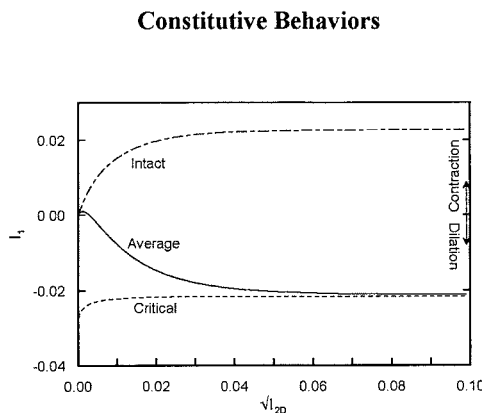


FIG 9 Illustration of Difference Between Observed and Predicted

@Seismicisolation



**FIG 10      Simulated Strain Behavior GA Comparisons**

#### SACRAMENTO RIVER SANDS PARAMETERS AND SIMULATIONS

A series of triaxial compression tests conducted by Lee (1965) on Sacramento River sand shows the effects of density and confinement pressure on stress-strain behavior of sands very well. In Lee's tests (1965), sands at two relative densities (100% and 38%) subjected to varying degrees of initial confinement pressures were tested. Here, the loose sands show mostly compaction behavior except at very low confinement pressures. The dense sands on the other hand show compaction behavior at very high confinement pressures. However, triaxial tests, in general, show non-uniform deformations and stress distributions. Loose sand samples bulge with multiple internal shear bands as they approach failure causing non-uniform stresses and strains (Macari et al., 1997). Dense sand samples commonly fail along a distinct band. In triaxial tests of dense sands, near the critical state, changes of strain take place predominantly within shear bands. As a result, triaxial tests of dense sands show global dilations smaller than the critical state. Elastic and critical state parameters were found using the methods explained by Samarajiva (2000) in Table 2. Initial estimates for intact state parameters are presented in Table 3. GA refined parameters for two loose sands with different initial confinement pressures and a dense sand are presented in Table 4 (Samarajiva, 2000). Final parameters  $\gamma$  function are presented in Table 5.

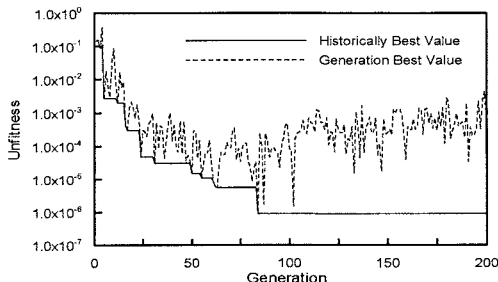


FIG 11 Unfitness of Generations in Verification Study

Table 1 Parameters for GA Verifications

Parameter	Value	Search Range	Parameter from GA
$h_1$	0.027	0.02-0.03	0.024915
$h_2$	0.340	0.30-0.40	0.300684
$n_1$	2.600	2.5-2.7	2.598925
$\gamma$	0.400	0.35-0.45	0.367302
$\beta$	0.000	0.0-0.1	0.071163
$A$	30.000	20.0-40.0	35.210166
$k_1$	0.750	0.70-0.80	0.7989250

Table 2 Elastic and Critical State Parameters for Sacramento River Sands

Parameter	Value
$E$	62500 kPa
$\nu$	0.29
$m$	0.2450
$e_0^c$	0.9602
$\lambda$	0.1096

Table 3 Ranges for Intact State Parameters for Sacramento River Sands

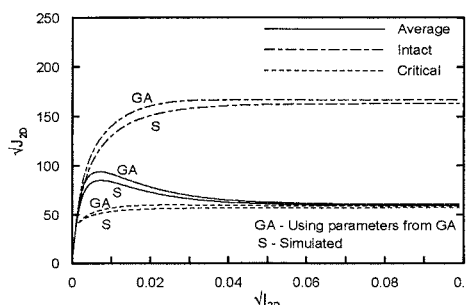
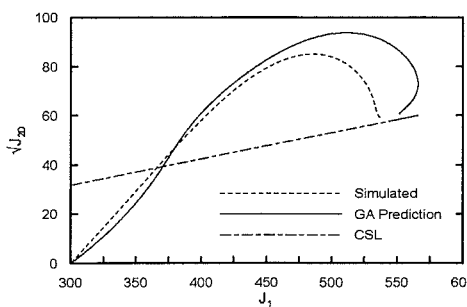
Parameter	Range
$h_1$	0.30-0.50
$h_2$	0.30-0.90
$n_1$	2.05-2.30
$\gamma$	1.26-1.50
$\beta$	0.00-0.05
$A$	10.0-30.0
$k_1$	0.70-0.90

**Table 4 GA optimized Parameters for Sacramento River Sands**

Parameter	Test		
	Loose Sand-1	Loose Sand-2	Dense Sand
$h_1$	0.3938		
$h_2$	0.7396		
$n_1$	2.1243		
$\gamma$	1.3000	2.3101	2.9310
$\beta$	0.0308		
$A$	19.9600		
$k_1$	0.7422		

**Table 5  $\gamma$  Function Parameter For Sacramento River Sands**

Parameter	Value
$k_2$	2.1700
$\gamma$	11.2500
$\chi$	0.1780

**FIG 12 Stress-Strain Behavior from Simulated Tests and GA Parameters****FIG 13 Stress Behavior from Simulated Tests and GA Parameters**

@Seismicisolation

## CONCLUSIONS

In order to find material parameters for the constitutive model (Samarajiva, 2000) using the GA, a new fitness function was introduced that evaluates fitness of material parameters based on stress and strain invariants. The fitness function equally emphasizes stress and strain behavior. In addition, the proposed fitness function eliminates material parameters that cause premature termination of predictions by introducing a new penalty scheme. The proposed fitness function for constitutive modeling was found to rapidly improve (within 100 generations) the fitness of the material parameter pool, when reasonable ranges of the parameters are given. The random crossover method, a mutation rate of about 1%, and a MAXMIN factor of 10 is recommended for the proposed GA. However, the readership is cautioned to not to interpret these numbers as a general trend.

Based on the predictions of real material behavior (Samarajiva, 2000), the proposed search methodology was found to be highly practical and efficient. In this optimization, three (3) triaxial compression tests (Sacramento River Sand-Lee (1965)) conducted on loose sand (2) and dense sand (1) were used to obtain a general set of material parameters. In the GA optimization and predictions, stress was considered the controlling parameter. FIG 14 and FIG 15 show the prediction of a test on Sacramento River Sand that was not used in the parameter optimization. Based on the predictions of real material behavior (Samarajiva, 2000), the estimation of material parameters using the genetic algorithm and the proposed fitness function was found to be highly practical and successful. The use of a genetic algorithm may successfully overcome the limitations of having a large number of material parameters for a given constitutive model.

The fitness evaluation of a material parameter set in the genetic algorithm becomes numerically difficult when none of the experimental readings are predicted. The present fitness evaluation scheme assigns very high unfitness values that may undermine the relative importance of the remaining sets of parameters. The improvement of the genetic algorithm, capable of considering an arbitrary number of laboratory tests and arbitrary number of parameters for optimization is desirable in future developments.

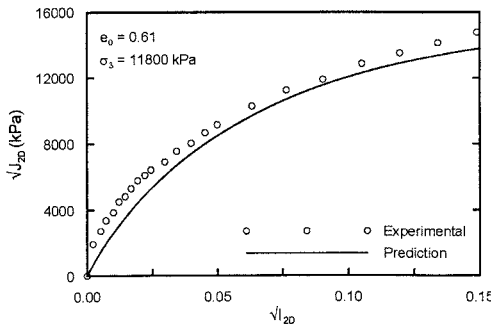


**FIG 14 Prediction of Drained Triaxial Stress Behavior of Sacramento River Sands (Lee 1965) Using GA Tuned Constitutive Model**

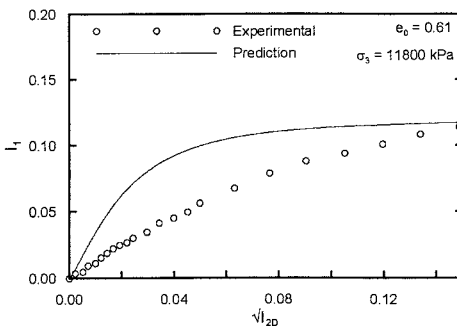


**FIG 15 Prediction of Drained Triaxial Volumetric Behavior of Sacramento River Sands Using GA Tuned Constitutive Model**

## APPENDIX I. NOTATION

The following symbols are used in this paper:

$J_1$ =	first invariant of stress tensor
$I_{2D}$ =	second invariant of deviatoric stress tensor
$I_1$ =	first invariant of strain tensor
$J_{2D}$ =	second invariant of deviatoric strain tensor
$e, e_{\max}, e_{\min}, e_0$ =	void ratio, max. void ratio, min. void ratio, initial void ratio
$e_0^C, \lambda$ =	critical state material parameter
$P_a$ =	atmospheric pressure
$R$ =	intact state reference surface
$n_1, n_2, \beta, l, h_1, h_2, \gamma$ =	intact state material parameter
$\alpha_{ps}$ =	intact state hardening function
$\xi, \xi_V, \xi_D$ =	trajectories of total, volumetric, and deviatoric plastic strains
$n_{ij}^R$ =	unit normal to the intact state reference surface
$\bar{\gamma}, k_2, \chi$ =	sub parameter of $\gamma$
$D$ =	disturbance function
$D_u, A$ =	disturbance function parameters
$C_{ijkl}^I, C_{ijkl}^e$ =	elasto-plastic stiffness and elastic stiffness of the intact state
$H^{v\pi}$ =	virgin plastic modulus of intact state
$C_{ijkl}^{DSC}$ =	disturbed state stiffness matrix
$a, b$ =	lower and upper bounds of a GA parameter
$L$ =	length of GA parameter in binary form
$B$ =	decimal value of GA parameter
$f_i$ =	fitness of the $i^{\text{th}}$ string in a GA mating pool
$n$ =	size of the GA population

$p_i$  = probability of survival of  $i^{\text{th}}$  string in GA

$n_i$  = number of copies made by  $i^{\text{th}}$  string in GA

$\Delta Error(\sigma)_j$  = error of predicted stress at  $j^{\text{th}}$  point

$\Delta Error(\varepsilon)_j$  = error of predicted strain at  $j^{\text{th}}$  point

$\Delta Error_j$  = error of the prediction at  $j^{\text{th}}$  point

$w_j$  = weight of error

## REFERENCES

- Adeli, H. and Cheng, N. T. (1993). "Integrated Genetic Algorithm for Optimization of structures." *Journal of Aerospace Engineering*, ASCE, 6(4). pp. 276-296.
- Chakraborty, P., Deb, K., and Subrahmanyam, P. S. (1995). "Optimal scheduling of urban transit system using genetic algorithm." *Journal of Transportation Engineering*, 121, pp. 544-553.
- Chan, W. T., Fwa, T. F. and Tan, C. Y. (1994). "Road-maintenance planning using genetic algorithms: 1." *Journal of Transportation Engineering*, 120, pp.693-709.
- De Jong, K.A. (1975). "An Analysis of the Behavior of a Class of Genetic Adaptive System." Ph.D. Thesis, University of Michigan, Ann Arbor, Michigan, USA .
- Desai, C. S. (1974). "A Consistent Finite Element Technique for Work-Softening Behavior." *Proc. Int. Conf. on Comp. Meth. in Nonlinear Mech.*, J. T. Oden et al (eds). University of Texas at Austin.
- Desai, C. S. (1980). "A General Basis for Yield, Failure and Potential Functions in Plasticity." *Int. J. Num. and Anal. Meth. in Geomech.* 4, 361-375.
- Desai, C.S. (1987). "Further on Unified Hierarchical Models Based on Alternative Correction or 'Damage' Approach." *Internal Research Report*, Dept. of Civil Engineering and Engineering Mechanics, Univ. of Arizona, Tucson.
- Desai, C.S. (1992) "The Disturbed State as a Phase Transformation Through Self-Adjustment Concept for Modeling of Mechanical Response of Materials and Interfaces." *Report*, Dept, of Civil Engineering and Engineering Mechanics, The University of Arizona.
- Desai, C.S. (2001). "Mechanics of Materials and Interfaces: The Disturbed State Concept." CRC Press, Boca Raton, FL, 2000, 712 pp., ISBN 084930248X
- Desai, C.S., Somasundaram, S., and Frantziskonis, G. (1986). "A Hierarchical Approach for Constitutive Modeling of Geologic Materials.", *Int. J. Num. and Anal.Meth. in Geomechanics*, 10, 225-257.
- Eshelman, L.J. and Schaffer, J.D. (1993). "Real-coded Genetic Algorithms and Interval-schemata." *Foundations of Genetic Algorithms II*, D. Whitley ed., Morgan Kaufman, San Mateo, California, pp. 187-202.
- Frantziskonis, G.N. and Desai, C.S. (1987). "Constitutive Model With Strain Softening." *Int. J. of Solids and Struct.*, Vol. 23, No. 6, 1987, pp. 751-767.
- Fwa, T. F., Tan, C. Y., and Chan, W. T. (1994). "Road-maintenance planning using genetic algorithms: 11." *Journal of Transportation Engineering*, 120, pp. 710-722.
- Goldberg, D.E. (1989). "Genetic Algorithms in Search, Optimization and Machine Learning." Addison-Wesley Publishing Company.
- Goldberg, D.E. (1989a). "Sizing Population for serial and Parallel Genetic Algorithms." *Proceedings of Third International Conference on Genetic Algorithms*, Ed. J.D. Schaffer, Morgan Kaufman (1989a)..
- Hajela, P. and Lee, E. (1995). "Genetic algorithm in truss topological optimization." *International Journal of Solids and Structures*, 32, pp. 3341-3357.
- Koumousis, V. K. and Georgio, P. G. (1994). "Genetic algorithms in discrete optimization of steel truss roofs." *Journal of Computing in Civil Engineering*, 8 (1994). pp. 309-325.



- Lee, K.L. (1965). "Triaxial Compressive Strength of Saturated Sands Under Seismic Loading Conditions." Ph.D. Dissertation, University of California at Berkeley, 521 pp.
- Macari-Pasqualino, E.J., Runesson, K., and Sture, S. (1991). "Analysis of Low Effective Stress Characteristics of Granular Materials in Reduced Gravity." *ASCE Geotechnical Engineering Congress; Boulder, Colorado*; June 13-15, 1991, Vol. II, pp. 1222- 1233.
- Pal, S., Wathugala, G.W., and Kundu, S. (1996). "Calibration of a Constitutive Model Using Genetic Algorithm." *Computers and Geotechnics*, Vol. 19, No 4(1996). pp. 325-348.
- Roscoe, K.H., Schofield, A., and Thurairajah, A. (1963) "Yielding of Clays in State Wetter Than Critical." *Geotechnique*, Vol 13, No 3, 1963, pp. 211-240
- Samarajiva, P. M. (2000). "Constitutive Modeling of Cohesionless Granular Materials Using Disturbed State Concept." Ph.D. Dissertation, Dept. of Civil and Environmental Engineering, Louisiana State University, Baton Rouge, Louisiana.
- Simpson A. R. and Priest, S. D. (1993), "The application of genetic algorithms to optimization problems in Geotechnics," *Computers and Geotechnics*, 15 pp. 1-19.
- Tesar, A. and Dresik, M. (1995), "Genetic algorithm for dynamic tuning of structures," *Computers and Structures*, 57, pp. 287-295.
- Wathugala, G.W. (1990), "Finite Element Dynamic Analysis of Nonlinear Porous Media with Applications to Piles in Saturated Clay." Ph.D. Dissertation, Dept. of Civil Engineering and Engineering Mechanics, Univ. of Arizona, Tucson.
- Wathugala, G.W. (2000), "Chapter 10: Unified Disturbed State Concept and HiSS Plasticity Models," invited Chapter for *Modelling in Geomechanics*, Eds. Zaman, Booker and Gioda, John Wiley & Sons, Ltd., in press. pp. 217-246.
- Wathugala, G.W. and Desai, C.S. (1987), "Constitutive Model for Soils with Strain Softening and Shear Dilation," *Internal Research Report*, Dept. of Civil Engineering and Engineering Mechanics, Univ. of Arizona, Tucson.
- Wathugala, G.W. and Desai, C.S. (1989), "Damage Based Constitutive Model for Soils," *Proc. of the 12th Canadian Congress of Applied Mechanics (CANCAM'89)*, Ottawa, May 28-June 1, pp. 530-531.
- Wathugala, W. and Desai, C. S. (1993), "Constitutive Model for Cyclic Behavior of Clays. I: Theory," *J. Geotech. Engng.*, 119, 4, 714-729.
- Wright, A.H. (1991), "Genetic Algorithm for Real Parameter Optimization," *Foundations of Genetic Algorithms*, G.J.E. Rawlins ed., Morgan Kaufman, San Mateo, California, pp.205-218.
- Wu, S. and Chow, P. (1995), "Steady-state genetic algorithms for discrete optimization of trusses," *Computers and Structures*, 56 979-991.

## SMP CRITERION-BASED UNIFIED CONSTITUTIVE MODEL FOR GEOMATERIALS

Hajime Matsuoka<sup>1</sup>, Yang-Ping Yao<sup>2</sup> and De'An Sun<sup>3</sup>

**ABSTRACT:** A unified and simple constitutive model for both clay and sand under three-dimensional stress conditions is presented. The model was developed from the modified Cam-clay model, and the following two points are considered. First, a so-called transformed stress tensor based on the SMP criterion is applied to the modified Cam-clay model to improve the model capability in describing the behavior of soils in general stresses including triaxial compression. The transformed stress tensor is deduced from what we transform the SMP criterion to a circle in the transformed  $\pi$ -plane. The model realizes the consistency from the shear yield to the shear failure and the combination of the critical state theory with the SMP criterion. Secondly, a new hardening parameter is introduced in order to develop a unified constitutive model for both clay and sand. It can not only describe the dilatancy from lightly to heavily dilative sand, but also be reduced to the plastic volumetric strain for normally consolidated clay. The results predicted by the presented model are compared in detail with the test results of sand and clay in triaxial compression, true triaxial, plane strain and triaxial extension. It is shown that the presented model can describe well the drained and undrained behavior of clay and sand along various stress paths including triaxial compression, triaxial extension, plane strain, and true triaxial conditions. Only five conventional soil parameters are needed in the model.

### INTRODUCTION

The Cam-clay models are the most popular and fundamental constitutive models for normally consolidated clay. The original Cam-clay model was proposed by Roscoe et al. (1963). The modified Cam-clay model whose yield curve is elliptical in the  $p$ - $q$  plane was introduced by Roscoe and Burland (1968). The stress parameters

---

<sup>1</sup>Department of Civil Engineering, Nagoya Institute of Technology, Nagoya 466-8555, Japan; Tel/Fax 81(52)7355483; email: matsuoka@doboku2.ace.nitech.ac.jp

<sup>2</sup>Department of Civil Engineering, Beihang University, Beijing 100083, China; Tel 86 (10) 82316111; email: ypyao@263.net

<sup>3</sup>Department of Civil Engineering, Nagoya Institute of Technology, Nagoya 466-8555, Japan; Tel/Fax 81 (52) 7357162; email: sun@doboku2.ace.nitech.ac.jp

used in the Cam-clay models are  $p$  and  $q$ , which are expressed as follows using the principal stress  $\sigma_i$  and the stress tensor  $\sigma_{ij}$ :

$$\left. \begin{aligned} p &= \frac{1}{3}(\sigma_1 + \sigma_2 + \sigma_3) = \frac{1}{3}\sigma_{ii} \\ q &= \frac{1}{\sqrt{2}}\sqrt{(\sigma_1 - \sigma_2)^2 + (\sigma_2 - \sigma_3)^2 + (\sigma_3 - \sigma_1)^2} = \sqrt{\frac{3}{2}(\sigma_{ij} - p\delta_{ij})(\sigma_{ij} - p\delta_{ij})} \end{aligned} \right\} \quad (1)$$

where  $\delta_{ij}$  is Kronecker's delta. It is seen from Equation (1) that  $p = \sigma_{oct}$  ( $\sigma_{oct}$ : normal stress on the octahedral plane) and  $q = (3/\sqrt{2})\tau_{oct}$  ( $\tau_{oct}$ : shear stress on the octahedral plane). Therefore, the Extended Mises criterion ( $q/p=\text{const.}$  or  $\tau_{oct}/\sigma_{oct}=\text{const.}$ ) was adopted for the shear yield and the shear failure of clay in the Cam-clay model. The shear yield is caused by the increase in stress ratio  $\eta$  ( $=q/p$ ), while the compressive yield is caused by the increase in mean stress  $p$ .

However, it is well known that the failure of soil is not explained by the Extended Mises criterion but by the Mohr-Coulomb criterion or the SMP criterion (Matsuoka and Nakai, 1974) and others (e.g. Lade and Duncan 1975). Taking the consistency in the shear deformation and the shear failure into consideration, the Mohr-Coulomb criterion or the SMP criterion for the shear yield as well as the shear failure of soil should be introduced. On this basis, some researchers attempted to extend the Cam-clay models to three-dimensional models for soils (e.g. Zienkiewicz and Pande, 1977; Nakai and Mihara 1984). However, Wroth and Houlsby(1985) commented that further study is necessary to improve the Cam-clay models by combining the critical state theory with the failure criteria proposed by Matsuoka and Nakai(1974) and Lade and Duncan(1975). Here we present a transformed stress method to solve this problem (Matsuoka et al. 1999).

On the other hand, the plastic volumetric strain  $\varepsilon_v^p$  is taken as a hardening parameter in the Cam-clay models, which is not appropriate for dilative sand. So far, a lot of hardening parameters to describe the dilatancy of soils, have been developed (e.g., Lade 1977, Nova and Wood 1979, Nakai 1989). Several plasticity models have been proposed for dilative sand (e.g., Hashiguchi and Ueno 1977, Pastor et al. 1985, Prevost 1985, Dafalias 1986). However, many models are very complicated in the description of the dilatancy. Here we present a simple three-dimensional elastoplastic model for both clay and sand (Yao et al. 1999a).

In this paper, firstly, a method for the transformation of the curved surface of the SMP criterion to a cone in the transformed principal stress space is introduced using a transformed stress  $\tilde{\sigma}_{ij}$ . The transformed stress  $\tilde{\sigma}_{ij}$  is applied to the modified Cam-clay model so that the model becomes a reasonable three-dimensional model by the SMP criterion. Secondly, a new hardening parameter is introduced on the basis of the consideration that the unified yield and plastic potential functions, which are the same as those of the Cam-clay model, are adopted for both clay and sand. Finally, the model prediction will be compared with the measured drained and undrained behavior of clay and sand not only under triaxial compression, but also under triaxial extension, plane strain, and true triaxial conditions.

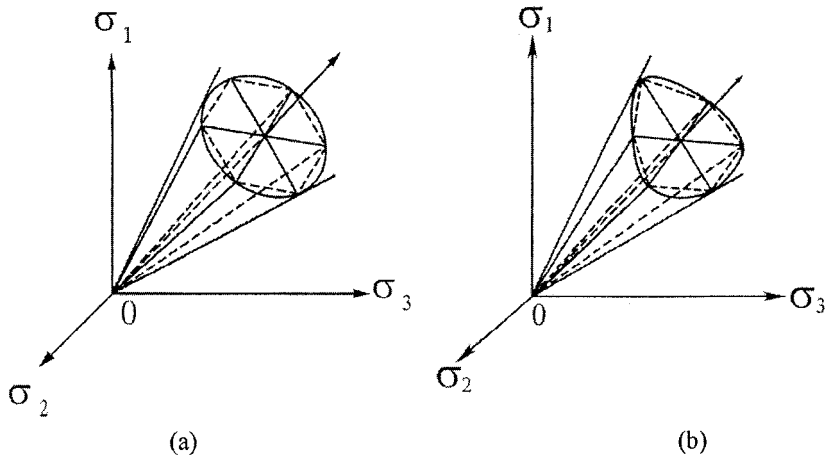


**FIG. 1. Shapes of (a) Extended Tresca and Extended Mises failure criteria and (b) Mohr-Coulomb and SMP failure criteria in principal stress space**

Throughout this paper, the term stress is to be interpreted as effective stress, the term Cam-clay model as the modified Cam-clay model.

### THE SMP CRITERION AND TRANSFORMED STRESS

In contrast with the Extended Mises failure criterion used in the early stage of soil mechanics, one of the criteria describing well the recent test results of soil is the SMP failure criterion (Matsuoka and Nakai 1974), which can be written as

$$\frac{\tau_{\text{SMP}}}{\sigma_{\text{SMP}}} = \sqrt{\frac{I_1 I_2 - 9I_3}{9I_3}} = \text{const.} \quad \text{or} \quad \frac{I_1 I_2}{I_3} = \text{const.} \quad (2)$$

where  $\tau_{\text{SMP}}$  and  $\sigma_{\text{SMP}}$  are the shear and normal stresses on the SMP, and  $I_1$ ,  $I_2$ , and  $I_3$  are the first, second, and third effective stress invariants.

Figures 1 and 2 show the shapes of the Extended Tresca, Extended Mises, Mohr-Coulomb, and SMP failure criteria in principal stress space and in the  $\pi$ -plane, respectively. We can see from Figure 1 that just as the cone of the Extended Mises criterion circumscribes the regularly hexagonal pyramid of the Extended Tresca criterion, the SMP criterion is a smoothly convex curved surface circumscribing the irregularly hexagonal pyramid of the Mohr-Coulomb criterion in principal stress space. We can also see from Figure 2 that just as the circle of the Extended Mises criterion circumscribes the regular hexagon of the Extended Tresca criterion, the SMP criterion is a smoothly convex curve circumscribing the irregular hexagon of the Mohr-Coulomb criterion in the  $\pi$ -plane.

Figure 3 shows the Extended Mises, Mohr-Coulomb, and SMP criteria with the stress states at failure in the  $\pi$ -plane obtained by the triaxial compression, triaxial

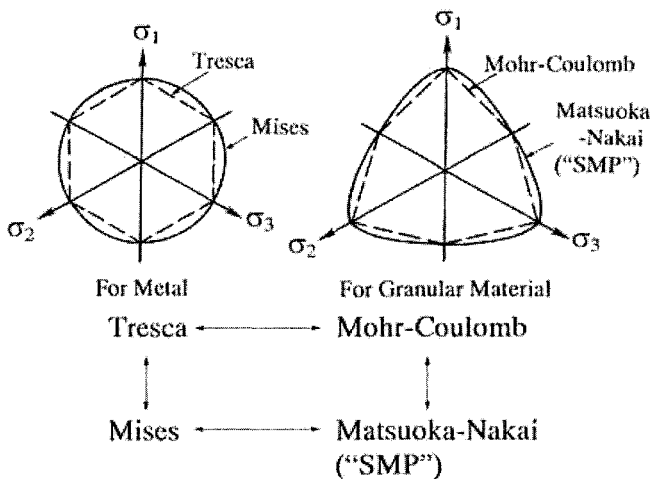


FIG. 2. Mutual relationship among Extended Tresca, Extended Mises, Mohr-Coulomb and SMP failure criteria in  $\pi$ -plane

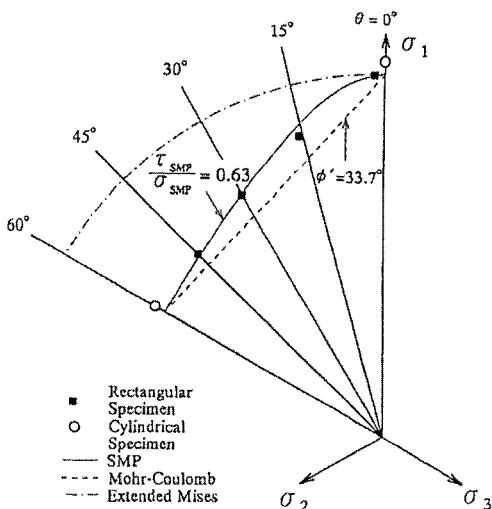
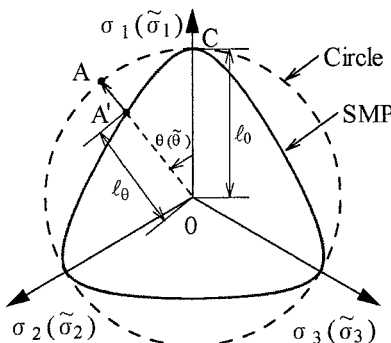


FIG. 3. Comparison of Extended Mises, Mohr-Coulomb and SMP criteria with stress states at failure in  $\pi$ -plane obtained by triaxial compression and extension and true triaxial tests on Fujinomori clay (after Nakai and Matsuoka 1986)

extension, and true triaxial tests on Fujinomori clay (Nakai and Matsuoka 1986). It is seen from Figure 3 that the measured points (marks  $\circ$  and  $\blacksquare$ ) are closest to the solid curve drawn by the SMP failure criterion and are far from the dash-dotted curve drawn by the Extended Mises failure criterion which is adopted in the Cam-clay models.

@Seismicisolation



**FIG. 4. The SMP criterion in  $\pi$ -plane(solid line) and transformed  $\pi$ -plane(broken circle)**

The Extended Mises failure criterion is not so appropriate for clay that some researchers have adopted the Mohr-Coulomb failure criterion as the failure criterion in their models. However, they continue using  $p$  and  $q$  as the stress parameters, which means that the shear yield of soil obeys the Extended Mises criterion. From the view of the consistency and continuation in the shear deformation and the shear failure, it is suitable to adopt the Mohr-Coulomb or the SMP failure criterion not only as the shear failure criterion, but also as the shear yield criterion of soil. As it can be seen that the prediction of the SMP failure criterion is better than that of the Mohr-Coulomb failure criterion, we select the SMP criterion rather than the Mohr-Coulomb criterion as the shear failure and the shear yield criteria.

In order to combine the SMP criterion with the Cam-clay model, a transformed stress  $\tilde{\sigma}_{ij}$  has been introduced (Matsuoka et al. 1999). The curved surface of the SMP criterion in principal stress space, as shown in Figure 1(b), can be transformed into a cone in the transformed principal stress space. So, we can use the Cam-clay model in the transformed stress space instead of the ordinary stress space. How to obtain the transformed stress tensor  $\tilde{\sigma}_{ij}$  is described as follows.

When the value of  $\tau_{SMP}/\sigma_{SMP}$  is given, the shape and size of the SMP criterion in principal stress space (Figure 1(b)) is definite. The length of OC shown in Figure 4 for a given  $p$  can be expressed in the following function.

$$\ell_0 = f(\tau_{SMP}/\sigma_{SMP}, p) \quad (3)$$

The concrete expression of  $\ell_0$  is given as follows (see Matsuoka et al. 1999 for the derivation):

$$\ell_0 = \sqrt{\frac{2}{3}} \frac{6p}{3\sqrt{1+8(\tau_{SMP}/\sigma_{SMP})^2/9-1}} = \sqrt{\frac{2}{3}} \frac{2I_1}{3\sqrt{(I_1I_2-I_3)/(I_1I_2-9I_3)-1}} \quad (4)$$

In order to transform the curve of the SMP criterion with  $OC=\ell_0$  in the  $\pi$ -plane of

**@Seismicisolation**

$\sigma_i$  space (Figure 4) into a circle with the radius of  $\ell_0$  in the  $\pi$ -plane of  $\tilde{\sigma}_i$  (the principal value of  $\tilde{\sigma}_{ij}$ ) space (Figure 4) under the same angle ( $\tilde{\theta} = \theta$ ) between the  $\tilde{\sigma}_i$  or  $\sigma_i$  axis and the directions of the transformed stress vector and the ordinary stress vector projected on the  $\pi$ -plane (Figure 4), and under the same mean value ( $\tilde{p} = p$ ) of  $\tilde{\sigma}_i$  and  $\sigma_i$ , the following equations can be made:

$$\tilde{p} = p \quad (5)$$

$$\tilde{\theta} = \theta \quad (6)$$

$$\sqrt{\tilde{s}_j \tilde{s}_{ij}} = \ell_0 \quad (7)$$

where  $\theta$  and  $\tilde{\theta}$  are Lode's angles of ordinary and transformed stresses (Figure 4), i.e.,

$$\theta = \frac{1}{3} \arccos\left(\sqrt{6} \frac{s_{ik} s_{kl} s_{li}}{(s_{mn} s_{mn})^{3/2}}\right) \quad (8)$$

$$\tilde{\theta} = \frac{1}{3} \arccos\left(\sqrt{6} \frac{\tilde{s}_{ik} \tilde{s}_{kl} \tilde{s}_{li}}{(\tilde{s}_{mn} \tilde{s}_{mn})^{3/2}}\right) \quad (9)$$

and  $\tilde{s}_{ij}$  is the deviatoric transformed stress tensor ( $= \tilde{\sigma}_{ij} - \tilde{p}\delta_{ij}$ ).  $\tilde{p}$  is mean transformed stress, i.e.,

$$\tilde{p} = \frac{1}{3}(\tilde{\sigma}_1 + \tilde{\sigma}_2 + \tilde{\sigma}_3) = \frac{1}{3}\tilde{\sigma}_{ii} \quad (10)$$

Taking Eqs. (8) and (9) into consideration, Eqs. (6), (7) can be rewritten as

$$\frac{\tilde{s}_{ik} \tilde{s}_{kl} \tilde{s}_{li}}{(\tilde{s}_{mn} \tilde{s}_{mn})^{3/2}} = \frac{s_{ik} s_{kl} s_{li}}{(s_{mn} s_{mn})^{3/2}} \quad (11)$$

$$\sqrt{\tilde{s}_j \tilde{s}_{ij}} = \frac{\ell_0}{\ell_0} \sqrt{s_j s_{ij}} \quad (12)$$

where  $\ell_0$  is the length of OA', as shown in Figure 4

In the condition that the principal directions of  $\tilde{\sigma}_{ij}$  and  $\sigma_{ij}$  are the same, as shown in Figure 4,  $\tilde{\sigma}_{ij}$  of point A, which corresponds to  $\sigma_{ij}$  of point A', can be obtained from Eqs.(5), (11) and (12) as follows:

$$\tilde{\sigma}_{ij} = \tilde{p}\delta_{ij} + \tilde{s}_{ij} = \tilde{p}\delta_{ij} + \frac{\ell_0}{\ell_0} s_{ij} = p\delta_{ij} + \frac{\ell_0}{\sqrt{s_{kl} s_{kl}}} s_{ij} \quad (13)$$

When the stress  $\sigma_{ij}$  is given,  $\ell_0$  can be calculated from Eq. (4), and then the

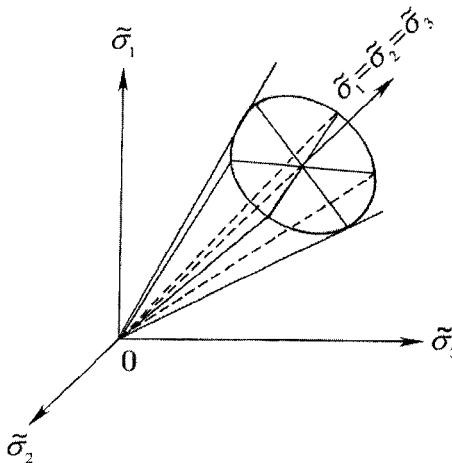


**FIG. 5. Shape of the SMP criterion in transformed principal stress**

transformed stress  $\tilde{\sigma}_{ij}$  can be calculated from Eq. (13).

From the above derivation, it can be known that the shape of the SMP criterion becomes a cone with the axis being the space diagonal  $\tilde{\sigma}_1 = \tilde{\sigma}_2 = \tilde{\sigma}_3$  in the transformed principal stress space (see Figure 5), and becomes a circle with the center being the origin O in the  $\tilde{\sigma}$ -plane (see Figure 4). Taking the similarity in the shapes of the Extended Mises criterion in the principal stress space and the SMP criterion in the transformed principal stress space, i.e., both are cones with the axis being the space diagonal, into consideration, we can revise any model such as the Cam-clay models using the transformed stress tensor  $\tilde{\sigma}_{ij}$  instead of the ordinary stress  $\sigma_{ij}$ .

#### A UNIFIED HARDENING PARAMETER FOR BOTH CLAY AND SAND

In the modified Cam-clay model, the yield and plastic potential functions are adopted to be in the same form as follows:

$$f = g = c_p \left[ \ln \frac{p}{p_0} + \ln \left( 1 + \frac{q^2}{M^2 p^2} \right) \right] - \varepsilon_v^p = 0 \quad (14)$$

where  $p_0$  is the initial mean stress,  $M$  is the value of  $q/p$  at the critical state,  $d\varepsilon_v^p (= d\varepsilon_{ii}^p)$  is the plastic volumetric strain increment and

$$c_p = \frac{\lambda - \kappa}{1 + e_0} \quad (15)$$

where  $\lambda$  is the compression index,  $\kappa$  is the swelling index and  $e_0$  is the initial void ratio at  $p=p_0$ . It is reasonable that Eq. (14) is also chosen as the plastic potential

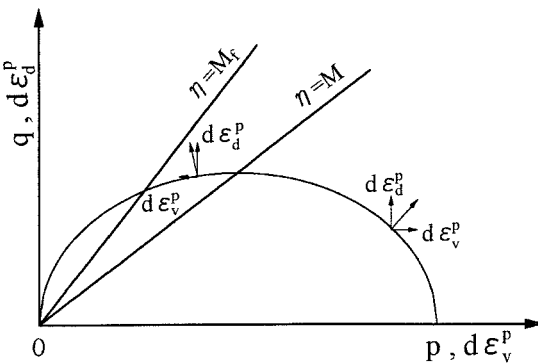


FIG. 6. Direction of plastic strain increment

function for dilative sand, because this equation can describe that the plastic volumetric strain increment is negative before the phase transformation ( $\eta=M$ ) (Ishihara et al., 1975) and positive after the phase transformation (see Figure 6). In order to adopt the associated flow rule, the yield function similar to Eq. (14) is also used for sand. However, the plastic volumetric strain cannot be used as the hardening parameter because it does not increase monotonously with loading (see the test results of the next section in detail). In this part, a new hardening parameter  $H$  is derived to describe the hardening behavior of clay and sand (Yao et al. 1999a). The yield and plastic potential functions for sand are written as

$$f = g = c_p \left[ \ln \frac{p}{p_0} + \ln \left( 1 + \frac{q^2}{M^2 p^2} \right) \right] - H = 0 \quad (16)$$

The hardening parameter is usually considered to be a combination of the stress tensor  $\sigma_{ij}$  and plastic strain increment tensor  $d\epsilon_{ij}^p$ , e.g., the plastic work type hardening parameter. Thus, the following hardening parameter is assumed:

$$H = \int dH = \int [c_1(\sigma_{ij})d\epsilon_v^p + c_2(\sigma_{ij})d\epsilon_d^p] \quad (17)$$

where  $c_1(\sigma_{ij})$  and  $c_2(\sigma_{ij})$  are the functions of the stress tensor respectively,  $d\epsilon_d^p (= \sqrt{2(d\epsilon_{ij}^p - d\epsilon_v^p \delta_{ij}/3)(d\epsilon_{ij}^p - d\epsilon_v^p \delta_{ij}/3)/3})$  is the plastic deviator strain increment. In the modified Cam-clay model, the following stress-dilatancy equation is adopted:

$$\frac{d\epsilon_v^p}{d\epsilon_d^p} = \frac{M^2 - \eta^2}{2\eta} \quad (18)$$

where  $\eta$  is the stress ratio ( $=q/p$ ).

Substituting Eq. (18) into Eq. (17) gives

$$H = \int \left[ c_1(\sigma_{ij}) d\varepsilon_v^p + c_2(\sigma_{ij}) \frac{2\eta}{M^2 - \eta^2} d\varepsilon_v^p \right] = \int c(\sigma_{ij}) d\varepsilon_v^p \quad (19)$$

where  $c(\sigma_{ij})$  is the function of the stress tensor. By substituting Eq. (19) to Eq. (16), the total differential form of the yield function is expressed as

$$\begin{aligned} df &= \frac{\partial f}{\partial p} dp + \frac{\partial f}{\partial q} dq + \frac{\partial f}{\partial H} dH \\ &= \frac{\partial f}{\partial p} dp + \frac{\partial f}{\partial q} dq - c(\sigma_{ij}) d\varepsilon_v^p \\ &= \frac{\partial f}{\partial p} dp + \frac{\partial f}{\partial q} dq - c(\sigma_{ij}) \Lambda \frac{\partial f}{\partial p} = 0 \end{aligned} \quad (20)$$

So the proportionality constant  $\Lambda$  can be written as

$$\Lambda = \frac{1}{c(\sigma_{ij})} \frac{\frac{\partial f}{\partial p} dp + \frac{\partial f}{\partial q} dq}{\frac{\partial f}{\partial p}} \quad (21)$$

From Eq. (16), the following two differential equations can be obtained:

$$\frac{\partial f}{\partial p} = \frac{c_p M^2 - \eta^2}{p M^2 + \eta^2} \quad (22)$$

$$\frac{\partial f}{\partial q} = \frac{c_p}{p} \frac{2\eta}{M^2 + \eta^2} \quad (23)$$

By substituting Eqs. (22) and (23) into Eq.(21), the plastic deviator strain increment can be expressed as follows along the constant mean stress path ( $dp=0$ ).

$$d\varepsilon_d^p = \Lambda \frac{\partial f}{\partial q} = \frac{1}{c(\sigma_{ij})} \frac{c_p}{p} \frac{4\eta^2}{M^4 - \eta^4} dq \quad (24)$$

Figure 7 shows the results of triaxial compression test on normally consolidated clay called Fujinomori clay and Toyoura sand arranged in (a)  $\eta \sim \varepsilon_d$  and (b)  $(M_f^4 - \eta^4)/4\eta^2 \sim d\eta/d\varepsilon_d$  (data from Nakai and Matsuoka 1986). It can be seen from Figure 7(a) that the shapes of the curves  $\eta \sim \varepsilon_d$  for clay and sand are alike. The stress ratios ( $q/p$ ) at failure for clay and sand are  $M$  and  $M_f$  respectively. In fact,  $M_f$  is not constant during shearing. If the change in  $M_f$  is considered during shearing, more complex behavior (e. g., the softening) of soils can be described (Yao et al. 1999b). In this part,  $M_f$  is simply assumed to be a constant to focus attention on explaining the sand dilatancy behavior. Therefore, compared with the equation of

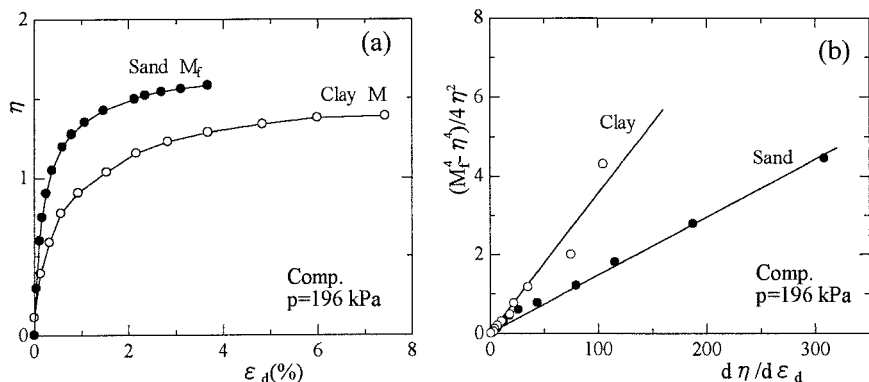


FIG. 7. Triaxial compression test results for clay and sand

the plastic deviator strain increment for clay in the Cam-clay model when the mean stress is constant (Eq. (25)), the equation of the plastic deviator strain increment for sand is assumed to be Eq. (26) when the mean stress is constant.

$$\frac{d\epsilon_d^p}{d\eta} = c_p \frac{1}{p} \frac{4\eta^2}{M^4 - \eta^4} dq \quad (\text{Clay}) \quad (25)$$

$$\frac{d\epsilon_d^p}{d\eta} = \rho \frac{1}{p} \frac{4\eta^2}{M_f^4 - \eta^4} dq \quad (\text{Sand}) \quad (26)$$

where  $\rho$  is a constant. On the other hand, Eqs. (25) and (26) can be also rewritten into the following linear forms respectively.

$$\frac{M^4 - \eta^4}{4\eta^2} = c_p \frac{d\eta}{d\epsilon_d^p} \quad (\text{Clay}) \quad (27)$$

$$\frac{M_f^4 - \eta^4}{4\eta^2} = \rho \frac{d\eta}{d\epsilon_d^p} \quad (\text{Sand}) \quad (28)$$

The validity of Eqs. (27) and (28) is confirmed by the test results of triaxial compression from Figure 7(b). So, Eq. (26) is rational. It is worth noting that  $M_f = M$  for clay and the elastic deviator strain is very small under a constant mean stress in Figure 7(b). Combining Eqs. (24) and (26) gives

$$c(\sigma_{ij}) = \frac{c_p}{\rho} \frac{M_f^4 - \eta^4}{M^4 - \eta^4} \quad (29)$$

Substituting Eq.(29) into Eq.(19) gives

$$H = \int dH = \int \frac{c_p}{\rho} \frac{M_f^4 - \eta^4}{M^4 - \eta^4} d\varepsilon_v^p \quad (30)$$

When  $\eta = 0$  (isotropic compression stress path), Eq.(30) becomes

$$H = \int dH = \int \frac{c_p}{\rho} \frac{M_f^4}{M^4} d\varepsilon_v^p \quad (31)$$

Moreover, under the isotropic compression condition ( $\eta = q/p = 0$ ),  $\varepsilon_v^p = c_p \ln(p/p_0)$ . In addition, Eq.(16) becomes  $H = c_p \ln(p/p_0)$  when  $\eta = 0$ . So, the following equation can be obtained from the above two equations.

$$H = \int dH = \int d\varepsilon_v^p \quad (32)$$

Letting Eq.(31) be equal to Eq.(32) gives

$$\rho = \frac{c_p M_f^4}{M^4} \quad (33)$$

Finally, we can obtain the following equation of the new hardening parameter for sand by substituting Eq.(33) into Eq.(30).

$$H = \int dH = \int \frac{M^4}{M_f^4} \frac{M_f^4 - \eta^4}{M^4 - \eta^4} d\varepsilon_v^p \quad (34)$$

If  $M = M_f$ , Eq.(34) becomes  $H = \int dH = \int d\varepsilon_v^p$ , which is the same as the hardening parameter for clay in the Cam-clay model. Therefore, the new hardening parameter (Eq. (34)) is a unified one for both clay and sand.

In order to make the new hardening parameter be applicable not only to triaxial compression but also to triaxial extension, plane strain and general stress state,  $H$  is revised by the transformed stress  $\tilde{\sigma}_{ij}$  as

$$\tilde{H} = \int d\tilde{H} = \int \frac{M^4}{M_f^4} \frac{M_f^4 - \tilde{\eta}^4}{M^4 - \tilde{\eta}^4} d\varepsilon_v^p \quad (35)$$

In order to check the validity of  $H$  along various stress paths, the values of  $\tilde{H}$  were calculated along the stress paths shown in Figure 8 in triaxial tests on Toyoura sand (data from Nakai 1989). The values of the mean stress and stress ratios are the same ( $p=588\text{kPa}$ ,  $\sigma_1/\sigma_3 = 4$ ) at points F and F'. The stress path dependency of the hardening parameter  $\tilde{H}$  is to be verified through four kinds of triaxial compression tests (paths: ADEF, ABCF, AF and ABEF) and three kinds of triaxial extension tests (paths: AD'F', ACF' and AF'). Figure 9 shows the variations of  $\tilde{H}$  along the seven kinds of stress paths under triaxial compression and extension conditions. It is obvious from Figure 9 that the values of the hardening parameter  $\tilde{H}$  are uniquely determined at the same stress state, regardless of the stress path in triaxial



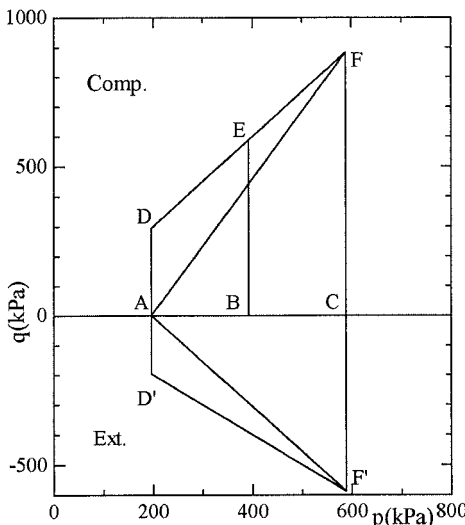
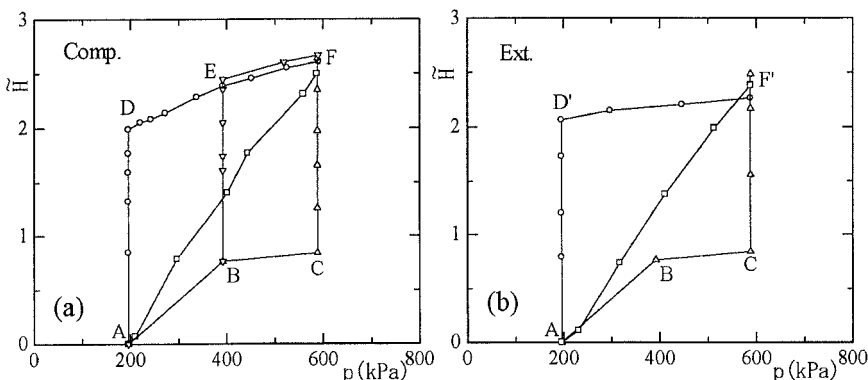
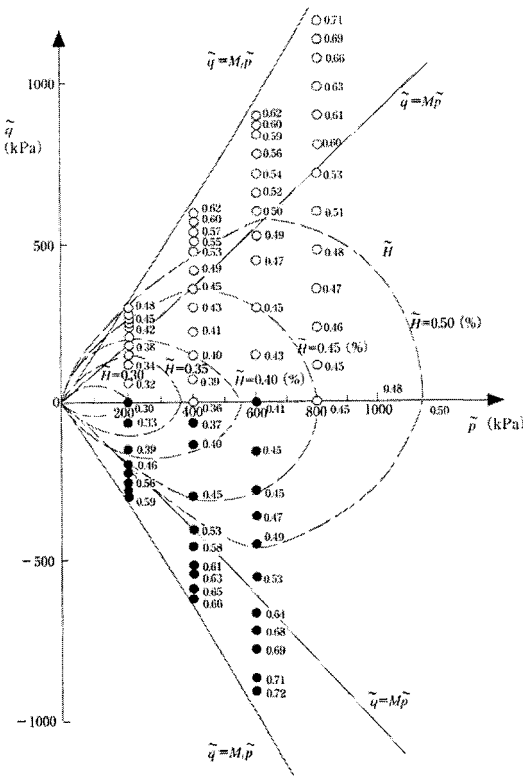


FIG. 8. Stress paths of triaxial tests for examining the new hardening parameter

FIG. 9. Relation between the hardening parameter and mean stress  $p$ 

compression and extension and the previous stress history. So,  $\tilde{H}$  is a state quantity. Figure 10 shows the values of  $\tilde{H}$  arranged from results of triaxial compression and extension tests on Toyoura sand under constant mean stress  $p$  and the contour lines of  $\tilde{H}$ . It can be seen that the contour lines are close to the yield curves of the Cam-clay model. Therefore, we can employ  $\tilde{H}$  as a new hardening parameter for sand with the yield functions similar to that of the Cam-clay model. How the hardening parameter  $\tilde{H}$  describes the dilatancy of soil is explained as follows. From Eq. (35),

$$d\epsilon_v^p = \frac{M_f^4 M^4 - \tilde{\eta}^4}{M^4 M_f^4 - \tilde{\eta}^4} d\tilde{H} \quad (36)$$



**FIG. 10.** Values of hardening parameter along various stress paths and its contour lines

Since  $\tilde{H}$  is a hardening parameter,  $d\tilde{H}$  is always larger than or equal to zero. Taking this into account, the following dilatancy characteristics are obtained from Eq. (36):

- (1)  $0 \leq \tilde{\eta} < M$  (negative dilatancy condition):  $d\varepsilon_v^p > 0$
- (2)  $\tilde{\eta} = M$  (phase transformation condition):  $d\varepsilon_v^p = 0$
- (3)  $M < \tilde{\eta} \leq M_f$  (positive dilatancy condition):  $d\varepsilon_v^p < 0$

#### A UNIFIED ELASTOPLASTIC MODEL FOR BOTH CLAY AND SAND

In the presented model, the equations of the yield surface and plastic potential remain the same as those of the Cam-clay model, but the transformed stress tensor  $\tilde{\sigma}_{ij}$  based on the SMP criterion and the new hardening parameter are adopted to model the mechanical behavior of clay and sand in three-dimensional stresses. The total strain increment is given by the summation of the elastic component and the plastic component as usual:

@Seismicisolation

$$d\epsilon_{ij} = d\epsilon_{ij}^e + d\epsilon_{ij}^p \quad (37)$$

here, the elastic component is given by Hooke's law.

$$d\epsilon_{ij}^e = \frac{1+\nu}{E} d\sigma_{ij} - \frac{\nu}{E} d\sigma_{mm} \delta_{ij} \quad (38)$$

where  $\nu$  is Poisson's ratio, and the elastic modulus E is expressed as

$$E = \frac{3(1-2\nu)(1+e_0)}{\kappa} p \quad (39)$$

And, the plastic component is given by assuming the flow rule not in the  $\sigma_{ij}$ -space but in the  $\tilde{\sigma}_{ij}$ -space.

$$d\epsilon_{ij}^p = \Lambda \frac{\partial g}{\partial \tilde{\sigma}_{ij}} \quad (40)$$

where the plastic potential function g (or the yield function f), the hardening parameter  $\tilde{H}$ , the proportionality constant  $\Lambda$  and the stress gradient  $\partial g / \partial \tilde{\sigma}_{ij}$  are given respectively as follows:

$$f = g = c_p \left[ \ln \frac{\tilde{p}}{\tilde{p}_0} + \ln \left( 1 + \frac{\tilde{q}^2}{M^2 \tilde{p}^2} \right) \right] - \tilde{H} = 0 \quad (41)$$

$$\tilde{H} = \int d\tilde{H} = \int \frac{M_f^4}{M_f^4 - \tilde{\eta}^4} \frac{M_f^4 - \tilde{\eta}^4}{M^4 - \tilde{\eta}^4} d\epsilon_v^p \quad (42)$$

$$\Lambda = \frac{M_f^4}{M^4} \frac{M^4 - \tilde{\eta}^4}{M_f^4 - \tilde{\eta}^4} \left( d\tilde{p} + \frac{2\tilde{p}\tilde{q}}{M^2 \tilde{p}^2 - \tilde{q}^2} d\tilde{q} \right) \quad (43)$$

$$\frac{\partial g}{\partial \tilde{\sigma}_{ij}} = \frac{c_p}{M^2 \tilde{p}^2 + \tilde{q}^2} \left[ \frac{M^2 \tilde{p}^2 - \tilde{q}^2}{3\tilde{p}} \delta_{ij} + 3(\tilde{\sigma}_{ij} - \tilde{p}\delta_{ij}) \right] \quad (44)$$

In the above equations, the deviator stress  $\tilde{q}$  and the transformed stress ratio  $\tilde{\eta}$ ,  $M(\tilde{\eta}$  at critical state) and  $M_f(\tilde{\eta}$  at peak) are written respectively as follows:

$$\tilde{\eta} = \tilde{q} / \tilde{p} \quad (45)$$

$$\tilde{q} = \sqrt{3\tilde{s}_{ij}\tilde{s}_{ij}} / 2 \quad (46)$$

$$M = \frac{6 \sin \phi_{pt}}{3 - \sin \phi_{pt}} \quad (47)$$

$$M_f = \frac{6 \sin \phi}{3 - \sin \phi} \quad (48)$$

**Table 1 Model parameters**

	M	$M_f$	$\lambda/(1+e_0)$	$\kappa/(1+e_0)$	v
Toyoura sand	0.95	1.66	0.00403	0.00251	0.3
Fujinomori clay	1.42		0.0508	0.0112	0.3

where  $\phi_{pt}$  is the angle of internal friction at the phase transformation, and  $\phi$  is the angle of internal friction at the shear failure.

## PREDICTIONS VERSUS EXPERIMENTAL RESULTS

The model capability in predicting drained and undrained behavior of normally consolidated clay and sand is examined not only under triaxial compression, but also under triaxial extension, and true triaxial conditions on normally consolidated Fujinomori clay and Toyoura sand (experimental data from Nakai and Matsuoka 1986; Nakai et al. 1986, 1989). The values of soil parameters used in model predictions for Fujinomori clay and Toyoura sand are listed in Table 1, which are the same as those used in the original papers. These soil parameters are determined by results of the isotropic consolidation test and the drained conventional triaxial compression test. In following figures, the mark  $\circ$  represents the measured result, and the solid line represents the predicted results by the presented model. For normally consolidated clay Fujinomori clay, the predicted results by the modified Cam-clay model are together shown by the dashed lines. For normally consolidated clay, the presented model becomes the modified Cam-clay model revised by the SMP criterion (Matsuoka et al. 1999), and the model parameters are the same as those in the Cam-clay model.

Figure 11 shows the predicted and experimental results of Fujinomori clay in triaxial compression and triaxial extension under  $p=196\text{kPa}$ , in terms of the relations of (a)  $\tilde{q}/\tilde{p} \sim \varepsilon_d \sim \varepsilon_v$  and (b)  $q/p \sim \varepsilon_d \sim \varepsilon_v$ . The curves in Figure 11 are the predicted results by the presented model. The data of triaxial compression and triaxial extension tests are uniquely arranged in the  $\tilde{q}/\tilde{p} \sim \varepsilon_d$  relationship and are arranged to two curves in the  $q/p \sim \varepsilon_d$  relationship. The difference in the stress-strain relation can be described by the presented model.

Figure 12 shows the predicted and experimental results on the drained behavior of Fujinomori clay in triaxial compression and triaxial extension at  $\sigma_3=196\text{kPa}$ , in terms of the relations among major and minor principal stress ratio  $\sigma_1/\sigma_3$ , the major principal strain  $\varepsilon_1$  and the volumetric strain  $\varepsilon_v$ . It can be seen from Figure 12(a) that the results predicted by the modified Cam-clay model and the presented model are the same in triaxial compression. This is because we have supposed that the transformed stress  $\tilde{\sigma}_{ij}$  is equal to the stress  $\sigma_{ij}$  in triaxial compression. It can be seen from Figure 12(b) that the results predicted by the presented model are better than those predicted by the Cam-clay model, compared with the experimental results. This is because the presented model can account for the difference in the shear



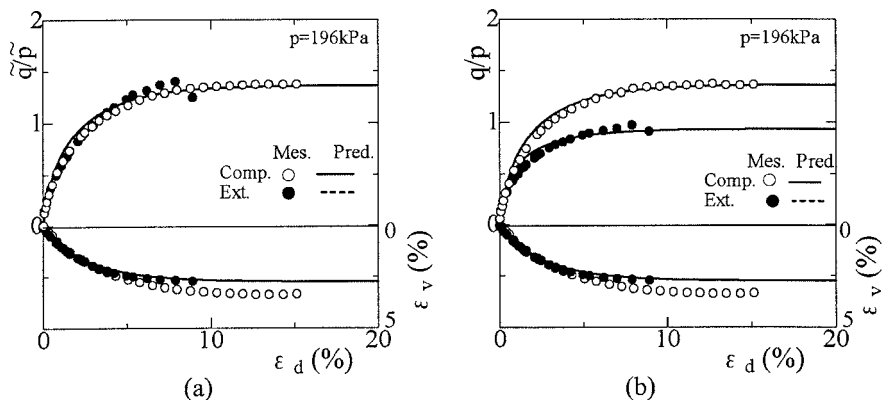


FIG. 11. Predicted and measured results of triaxial compression and extension tests on Fujinomori clay

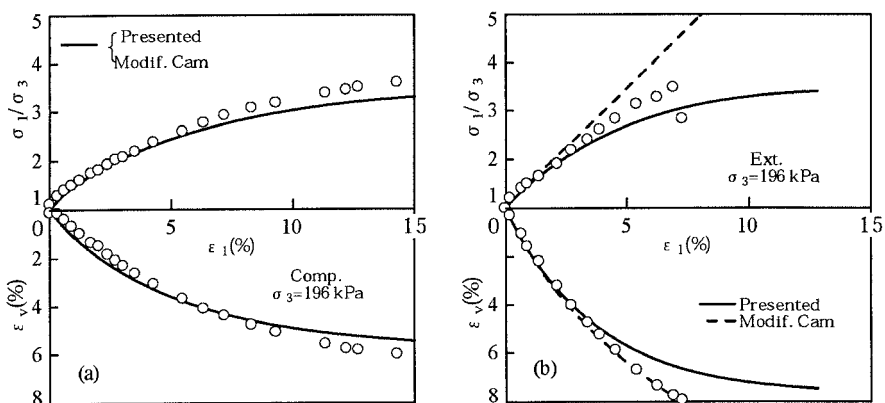


FIG. 12. Comparison between predicted and measured stress-strain behaviour ( $\sigma_3=196\text{kPa}$ )

strength and the shear yield of clay between the triaxial compression and triaxial extension stresses.

Figure 13 shows that the predicted results and the true triaxial test results ( $\theta=0^\circ$ ,  $\theta=15^\circ$ ,  $\theta=30^\circ$ ,  $\theta=45^\circ$ , and  $\theta=60^\circ$ ) on drained behavior of Fujinomori clay at  $p=196\text{kPa}$ , in terms of the relations among the principal stress ratio  $\sigma_1/\sigma_3$ , principal strains ( $\epsilon_1, \epsilon_2$  and  $\epsilon_3$ ) and volumetric strain  $\epsilon_v$ . It is seen from Figure 13(a) that the predicted results by the modified Cam-clay model and the presented model are the same in triaxial compression. As the stress condition changes from the triaxial compression ( $\theta=0^\circ$ ) to the general stress conditions ( $\theta>0^\circ$ ), the modified Cam-clay model overpredicts the shear strength due to adoption of the Extended Mises criterion and cannot predict the experimental stress-strain behavior precisely, but the presented model can predict the stress-strain behavior of clay accurately, as

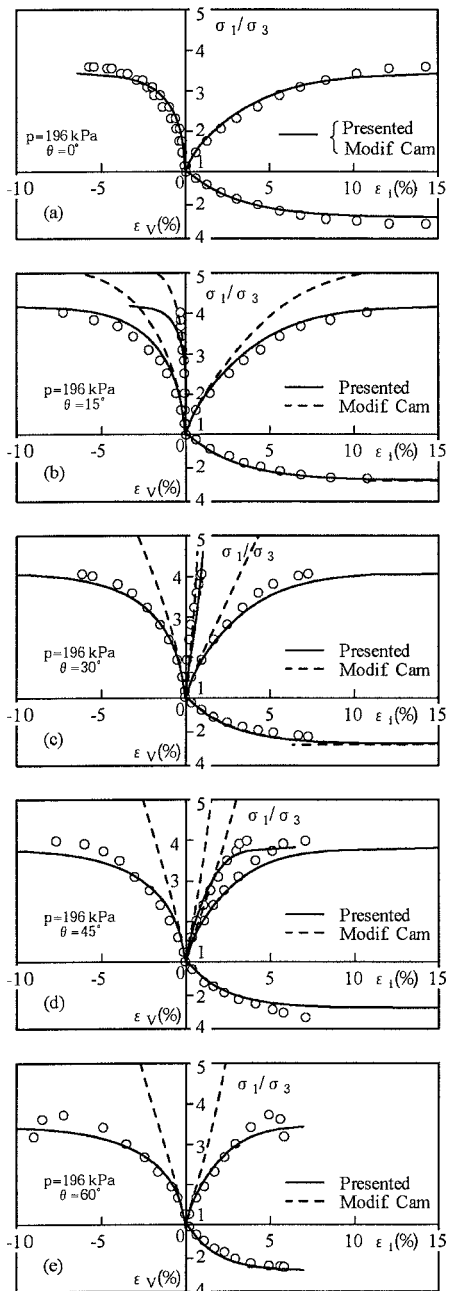
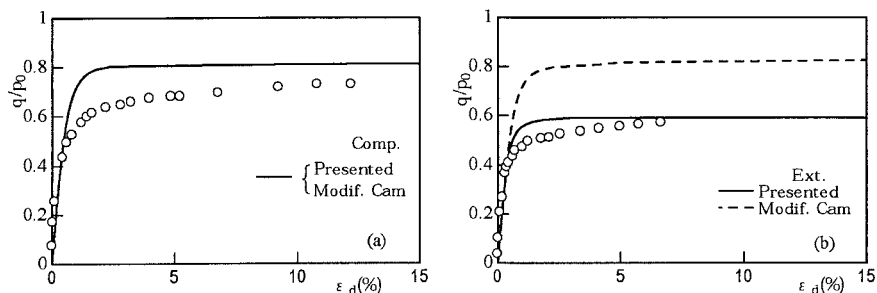
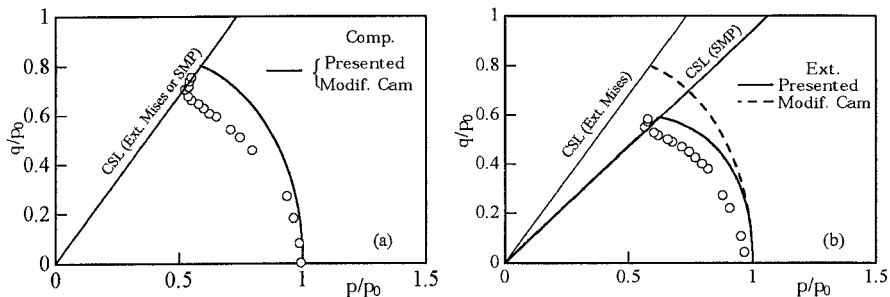


FIG. 13. Comparison between predicted and measured stress-strain behavior under three different principal stresses (Data after Nakai et al. 1986)

@SeismicIsolation



**FIG. 14. Comparison between predicted and measured stress-strain behavior under undrained (a) triaxial compression and (b) triaxial extension (Data after Nakai and Matsuoka 1986)**



**FIG. 15. Comparison between predicted and measured undrained stress paths under (a) triaxial compression and (b) triaxial extension (Data after Nakai and Matsuoka 1986)**

shown in Figure 13(b)-(e).

Therefore, if there is an elastoplastic model for soils, which uses  $p$  and  $q$  or  $p$  and  $\eta$  ( $=q/p$ ) as stress parameters and can predict the test results of soils only under triaxial compression condition, the model can predict the stress-strain behavior of soils under the general stress conditions including triaxial compression, as long as  $p$  and  $q$  or  $p$  and  $\eta$  ( $=q/p$ ) are replaced with  $\tilde{p}$  and  $\tilde{q}$  or  $\tilde{p}$  and  $\tilde{\eta}$  ( $=\tilde{q}/\tilde{p}$ ).

Figures 14 and 15 show the predicted and experimental results of undrained triaxial compression and triaxial extension tests on Fujinomori clay. Figure 14 shows the stress-strain behavior under undrained triaxial compression and triaxial extension, respectively, in terms of the relation between the normalized deviator stress  $q/p_0$  ( $p_0$ : initial confining pressure equal to 196kPa) and the deviator strain  $\epsilon_d$ . The presented model can explain the difference in the  $q/p_0 \sim \epsilon_d$  relations under triaxial extension condition, but the Cam-clay model cannot. Figure 15 shows the stress paths during undrained triaxial compression and triaxial extension tests, respectively, in terms of the relation between the normalized stresses  $q/p_0$  and  $p/p_0$ . It can be seen from Figure 15(b) that the stress path predicted by the Cam-clay model is higher than that predicted by the presented model, in triaxial extension test, while the stress

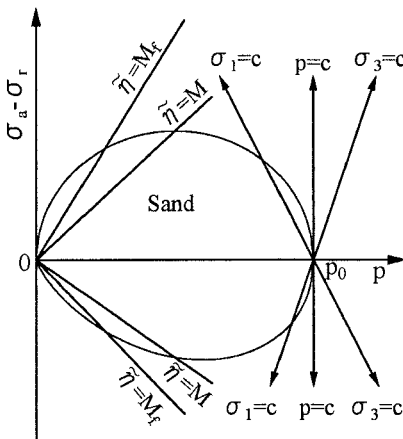


**FIG. 16. Stress paths in triaxial compression and extension for sand**

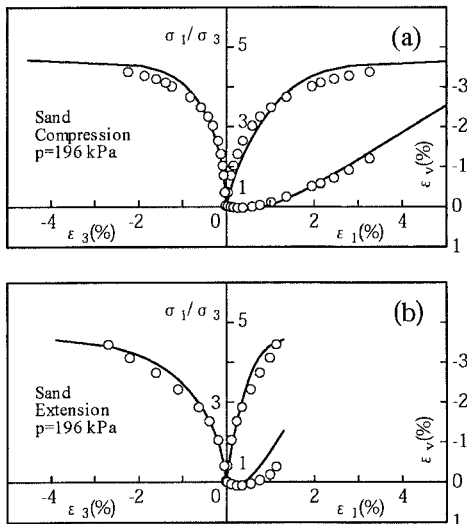


**FIG. 17. Comparison between predicted and test results under triaxial compression and extension conditions when  $p=\text{const.}$  for sand**

paths predicted by the presented model and the Cam-clay model are the same in triaxial compression test.

It is obvious from Figures 11-15 that the results predicted by the presented model are better than the results predicted by the modified Cam-clay model. From the preceding comparison between the model predictions and the observed results of element tests on normally consolidated clay, the presented model is good for

**@Seismicisolation**

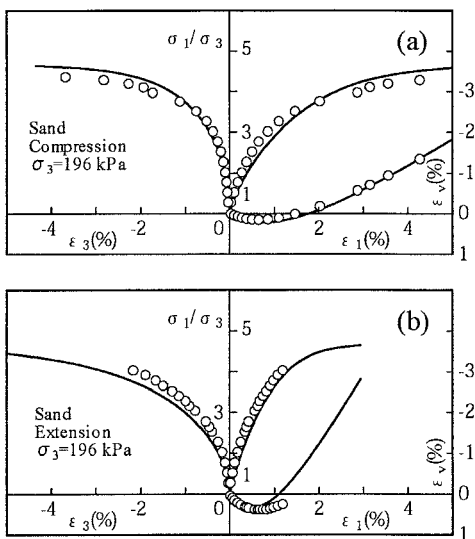


**FIG. 18. Comparison between predicted and test results under triaxial compression and extension conditions when  $\sigma_3 = \text{const.}$  for sand**

predicting deformation and strength of normally consolidated clay in three-dimensional stresses. In order to validate the model capability in predicting the mechanical behavior of sand, a comparison of the prediction and test results of Toyoura sand was conducted along various stress paths as shown in Figure 16.

Figure 17 shows the predicted and test results on the drained behavior of Toyoura sand under triaxial compression and extension conditions when  $p=196\text{kPa}$ . It can be seen from Figure 17 that the results (solid lines) predicted by the presented model agree well with the test results (mark ○) for sand under triaxial compression and extension conditions.

Figure 18 shows the predicted and test results on the drained behavior of Toyoura sand under triaxial compression and extension conditions when  $\sigma_3=196\text{kPa}$ . It can be seen from Figure 18 that the results (solid lines) predicted by the presented model agree well with the test results (mark ○) for sand under triaxial compression and extension conditions.

Figure 19 shows the predicted and test results on the drained behavior of Toyoura sand under the triaxial compression and extension conditions when  $\sigma_1=196\text{kPa}$ .

Therefore, the presented model can reasonably describe the stress-strain response of sand in three-dimensional stresses, and the dilatancy of sand along various stress paths.

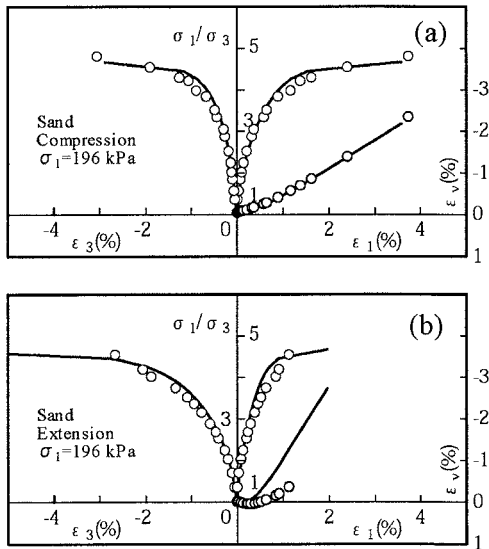


FIG. 19. Comparison between predicted and test results under triaxial compression and extension conditions when  $\sigma_1 = \text{const.}$  for sand

## DERIVATION OF ELASTOPLASTIC CONSTITUTIVE TENSOR

In order to apply the presented model to engineering practice, the elastoplastic constitutive tensor of the presented model used in solving elastoplastic boundary value problem by means of the finite element method is given here. The elastic part of the stress-strain relation can be written in the incremental form as

$$d\sigma_{ij} = D_{ijkl}^e d\epsilon_{kl}^e = D_{ijkl}^e (d\epsilon_{kl} - d\epsilon_{kl}^p) \quad (49)$$

Where  $\epsilon_{kl}$  and  $\epsilon_{kl}^p$  are the total strain tensor and its plastic component, respectively.

$D_{ijkl}^e$  is the elastic constitutive tensor, and from generalized Hooke's law for isotropic materials,

$$D_{ijkl}^e = L\delta_{ij}\delta_{kl} + G(\delta_{ik}\delta_{jl} + \delta_{il}\delta_{jk}) \quad (50)$$

where L and G are Lame's constants, which can be written from  $e = e_0 - \kappa \ln p / p_0$  in the elastic region by

$$G = \frac{E}{2(1+\nu)} = \frac{3(1-2\nu)(1+e_0)}{2(1+\nu)\kappa} p \quad (51)$$

$$L = \frac{E}{3(1-2\nu)} - \frac{2}{3}G = \frac{(1+e_0)}{\kappa} p - \frac{2}{3}G \quad (52)$$

where  $E$  and  $\nu$  are the elastic modulus and Poisson's ratio respectively.

As shown in Eq. (41), the yield function  $f$  is the function of the transformed stress tensor and the hardening parameter  $\tilde{H}$ , i.e.,

$$f = f_1(\tilde{\sigma}_{ij}) - \tilde{H} = 0 \quad (53)$$

Substituting Eq. (13) into Eq. (53) gives

$$f = f_2(\sigma_{ij}) - \tilde{H} = 0 \quad (54)$$

The consistency condition can be written as

$$df = \frac{\partial f}{\partial \sigma_{ij}} d\sigma_{ij} + \frac{\partial f}{\partial \tilde{H}} d\tilde{H} = 0 \quad (55)$$

Substituting Eqs. (49), (35) and (40) into Eq. (55) gives

$$\frac{\partial f}{\partial \sigma_{ij}} D_{ijkl}^e \left( d\varepsilon_{kl} - \Lambda \frac{\partial f}{\partial \tilde{\sigma}_{kl}} \right) + \frac{\partial f}{\partial \tilde{H}} \frac{M^4 M_f^4 - \tilde{\eta}^4}{M_f^4 M^4 - \tilde{\eta}^4} \Lambda \frac{\partial f}{\partial \tilde{\sigma}_{ij}} \delta_{ij} = 0 \quad (56)$$

From Eq. (54) we get  $\partial f / \partial \tilde{H} = -1$ , and arranging (56) gives

$$\Lambda = \frac{\frac{\partial f}{\partial \sigma_{ij}} D_{ijkl}^e d\varepsilon_{kl}}{X} \quad (57)$$

where

$$X = \frac{M^4}{M_f^4} \frac{M_f^4 - \tilde{\eta}^4}{M^4 - \tilde{\eta}^4} \frac{\partial f}{\partial \tilde{\sigma}_{ij}} \delta_{ij} + \frac{\partial f}{\partial \sigma_{ij}} D_{ijkl}^e \frac{\partial f}{\partial \tilde{\sigma}_{kl}} \quad (58)$$

Substituting Eqs. (40) and (57) into Eq. (49), we can get a general form of the presented model.

$$d\sigma_{ij} = D_{ijkl} d\varepsilon_{kl} \quad (59)$$

where the elastoplastic constitutive tensor is

$$D_{ijkl} = D_{ijkl}^e - D_{ijmn}^e \frac{\partial f}{\partial \tilde{\sigma}_{mn}} \frac{\partial f}{\partial \tilde{\sigma}_{st}} D_{stkl}^e / X \quad (60)$$

Introducing the elastic constitutive tensor of Hooke's law for isotropic elasticity into Eq. (58) and (60), we can obtain

$$X = \frac{M^4}{M_f^4} \frac{M_f^4 - \tilde{\eta}^4}{M^4 - \tilde{\eta}^4} \frac{\partial f}{\partial \tilde{\sigma}_{ii}} + L \frac{\partial f}{\partial \sigma_{ii}} \frac{\partial f}{\partial \tilde{\sigma}_{jj}} + 2G \frac{\partial f}{\partial \sigma_{ij}} \frac{\partial f}{\partial \tilde{\sigma}_{ij}} \quad (61)$$

$$D_{ijkl} = L\delta_{ij}\delta_{kl} + G(\delta_{ik}\delta_{jl} + \delta_{il}\delta_{jk}) - \left( L \frac{\partial f}{\partial \tilde{\sigma}_{mn}} \delta_{ij} + 2G \frac{\partial f}{\partial \tilde{\sigma}_{ij}} \right) \left( L \frac{\partial f}{\partial \tilde{\sigma}_{mn}} \delta_{kl} + 2G \frac{\partial f}{\partial \tilde{\sigma}_{kl}} \right) / X \quad (62)$$

Eqs. (60) and (62) are the generalized expressions of the presented constitutive model in the incremental form.

In coding finite element program using Eqs. (60) and (62), it is necessary to calculate  $\partial f / \partial \tilde{\sigma}_{ij}$  and  $\partial f / \partial \sigma_{ij}$ . About  $\partial f / \partial \tilde{\sigma}_{ij}$ , see Eq. (41). The calculation of  $\partial f / \partial \sigma_{ij}$  is as follows. From the compound differential law,

$$\frac{\partial f}{\partial \sigma_{ij}} = \frac{\partial f}{\partial \tilde{\sigma}_{kl}} \frac{\partial \tilde{\sigma}_{kl}}{\partial \sigma_{ij}} \quad (63)$$

From Eq. (13),

$$\frac{\partial \tilde{\sigma}_{kl}}{\partial \sigma_{ij}} = \frac{\partial(p\delta_{kl})}{\partial \sigma_{ij}} + \frac{\partial}{\partial \sigma_{ij}} \left( \frac{s_{kl}}{\ell_0} \right) \ell_0 + \frac{s_{kl}}{\ell_0} \frac{\partial \ell_0}{\partial \sigma_{ij}} \quad (64)$$

By considering Eq. (4) and  $\ell_0 = \sqrt{s_{ij}s_{ij}}$ , Eq. (64) can be written as

$$\frac{\partial \tilde{\sigma}_{kl}}{\partial \sigma_{ij}} = \frac{1}{3} \delta_{ij} \delta_{kl} + \left( \delta_{ik} \delta_{jl} - \frac{1}{3} \delta_{ij} \delta_{kl} - \frac{s_{kl} s_{ij}}{\ell_0^2} \right) \frac{\ell_0}{\ell_0} + \frac{s_{kl}}{\ell_0} \frac{\partial \ell_0}{\partial I_m} \frac{\partial I_m}{\partial \sigma_{ij}} \quad (65)$$

where  $I_m$  ( $m=1, 2$  and  $3$ ) is the stress invariable, so  $\partial \ell_0 / \partial I_m$  can be easily calculated using Eq. (4).

Sun et al. (2004) has shown an example to demonstrate usefulness of the model in the finite element analysis for predicting deformation of normally consolidated clay and sand layers under embankment loading.

## CONCLUSION REMARKS

The main results are summarized as follows:

- (1) A transformed stress tensor  $\tilde{\sigma}_{ij}$  has been proposed by comparing the shapes of the Extended Mises criterion and the SMP criterion in principal stress space. The SMP surface becomes a cone with the axis being the space diagonal in the transformed principal stress space, and a circle with center being the origin in the transformed  $\pi$ -plane.
- (2) As an example, the transformed stress tensor  $\tilde{\sigma}_{ij}$  is applied to the modified Cam-clay model to combine the critical state theory with the SMP criterion. The consistency from the shear yield to the shear failure for soils is satisfied in the revised model, which means that the behavior of both yield and failure obey the SMP criterion. The revised model, with the same soil parameters as the Cam-clay model, is capable of predicting the drained and undrained behavior of clay in general stress

conditions. The comparison of the revised model predictions with the experimental results indicates good performance in predicting the behavior of clay, not only under triaxial compression, but also under triaxial extension, and true triaxial conditions.

(3) The SMP criterion is considered to be one of the yield and failure criteria for frictional materials such as sand and clay with the stress-induced anisotropy. This SMP criterion becomes a cone in the transformed principal stress space and a circle in the transformed  $\pi$ -plane, which are similar to those of the Extended Mises criterion for isotropic materials. Therefore, the frictional materials can be regarded as isotropic materials in the transformed stress space. This is why we have introduced the transformed stress tensor  $\tilde{\sigma}_{ij}$  for the frictional materials like soils.

(4) A new hardening parameter was presented on the basis of the consideration that the unified yield and plastic potential functions are adopted for both clay and sand. It can not only describe the dilatancy from lightly to heavily dilative sand, but also be reduced to the plastic volumetric strain for clay. The physical meaning of this hardening parameter is clear. The validity of the hardening parameter  $\tilde{H}$  is confirmed by the test results of triaxial compression and extension tests on sand along the various stress paths.

(5) An elastoplastic model was presented by applying the transformed stress tensor  $\tilde{\sigma}_{ij}$  based on the SMP criterion and the new hardening parameter  $\tilde{H}$  to the modified Cam-clay model. The model can reasonably describe the stress-strain behavior of clay and sand in three-dimensional stresses.

(6) Five soil parameters ( $\lambda$ ,  $\kappa$ ,  $M$ ,  $M_f$  and  $v$ ) used in the model can be determined through a loading and unloading isotropic consolidation test and a conventional triaxial compression test.

## REFERENCES

- Dafalias, Y. F.(1986). "Bounding surface plasticity I Theory." *Journal of Engineering Mechanics ASCE*, 112(12), 1242-1291.
- Hashiguchi, K., and Ueno, M. (1977). "Elasto-plastic constitutive laws of glandular materials." In *Proceedings of Special Session 9 of 9th International Conference on Soil Mechanics and Foundations Engineering*, Tokyo, 73-82.
- Ishihara, K., Tatsuoka, F., and Yasuda, S. (1975). "Undrained deformation and liquefaction of sand under cyclic stresses." *Soils and Foundations*, 15(1), 29-44.
- Lade, P. V. (1977). "Elasto-plastic stress-strain theory for cohesionless soils with curved yield surface." *International Journal of Solids and Structures*, 13, 1019-1035.
- Lade, P. V., and Duncan, J. M. (1975). "Elasto-plastic stress-strain theory for cohesionless soil." *Journal of Geotechnical Engineering ASCE*, 101(10), 1037-1053.
- Matsuoka, H., and Nakai, T. (1974). "Stress-deformation and strength characteristics of soil under three different principal stresses." *Proc. of JSCE*, 232, 59-74.
- Matsuoka, H., Yao, Y. P., and Sun, D. A.(1999). "The Cam-clay models revised by the SMP criterion." *Soils and Foundations*, 39(1), 81-95.



- Nakai, T. (1989). "An isotropic hardening elastoplastic model for sand considering the stress path dependency in three-dimensional stresses." *Soils and Foundations*, 29(1), 119-137.
- Nakai, T., and Matsuoka, H.(1986). "A generalized elastoplastic constitutive model for clay in three-dimensional stresses," *Soils and Foundations*, 26(3), 81-98.
- Nakai, T., Tsuzuki, K., Yamamoto, M., and Hishida, T. (1986). "Analysis of plane strain tests on normally consolidated clay by an elastoplastic constitutive models." *Proc. of the 21st Japan National Conference on Soil Mechanics and Foundation Engineering*, 2, 453-456 (in Japanese).
- Nova, R., and Wood, D. M. (1979). "A constitutive model for sand in triaxial compression." *International Journal for Numerical and Analytical methods in Geomechanics*, 3(3), 255-278.
- Pastor, M., Zienkiewicz, O. C., and Leung, K. H. (1985). "A simple model for transient loading in earthquake analysis part II." *International Journal for Numerical and Analytical Methods in Geomechanics*, 9, 477-498.
- Prevost, J. H. (1985). "A simple plasticity theory for frictional cohesionless soils." *Soil Dynamics and Earthquake Engineering*, 4(1), 9-17.
- Roscoe, K. H., and Burland, J. B.(1968). "On the generalised stress-strain behaviour of 'wet' clay." *Engineering Plasticity*, Cambridge University Press, 535-609.
- Roscoe, K. H., Schofield, A. N., and Thurairajoh, A.(1963). "Yielding of clay in state wetter than critical." *Geotechnique*, 13(3), 211-240.
- Sun, D. A., Matsuoka, H., Yao, Y. P., and Ishii, H. (2004). "Anisotropic hardening elastoplastic model for clays and sands and its application to FE analysis." *Computers and Geotechnics*, 31(1), 37-46.
- Wroth, C. P., and Houlsby, G. T. (1985). "Soil mechanics-property characterization and analysis procedures." In *Proceedings of 11th International Conference on Soil Mechanics and Foundations Engineering*, San Francisco, 1, 1-55.
- Yao, Y. P., Matsuoka, H., and Sun, D. A.(1999a). "A unified elastoplastic model for clay and sand with the SMP criterion." In *Proceedings of 8th Australia-New Zealand Conference on Geomechanics*, Hobart, 2, 997-1002.
- Yao, Y. P., Matsuoka, H., and Sun, D. A.(1999b). "A unified elastoplastic model of sand dependent on stress level and void ratio." In *Proceedings of 2nd Inter. Symposium on Pre-failure Deformation characteristics of Geomaterials*, Torino, 589-596.

## A SIMPLE ELASTOPLASTIC MODEL FOR GEOMATERIALS BASED ON TIJ-CONCEPT AND ITS CALIBRATION BY VARIOUS TEST DATA

Teruo, Nakai<sup>1</sup>, Member, Japanese Geotechnical Society and Masaya Hinokio<sup>2</sup>,  
Member, Japanese Geotechnical Society

**ABSTRACT:** An isotropic hardening elastoplastic model for soils is presented, which can describe typical deformation and strength behavior of normally and over consolidated soil under general stress conditions. This model can take into consideration the influence of intermediate principal stress on the deformation and strength of soil upon using the concept of modified stress  $t_{ij}$ . The influence of stress path on the direction of plastic flow is considered by dividing the plastic strain increment into two components. After inclusion of the parameter ‘ $\rho$ ’ and subloading surface concept, this model can express the influence of density and confining pressure on the soil behavior. Only one material parameter  $\alpha$  for representing the influence of density is added to the parameters of the previous model, which are fundamentally the same as those of Cam-clay model. The validity of the model is checked by monotonic and cyclic loading tests on normally and over consolidated clays.

### INTRODUCTION

For the appropriate prediction of the deformation and failure of the soil, we have to carry out numerical analysis using a simple and generalized constitutive model for soils. The well-known Cam clay model is certainly the first elastoplastic model applicable to the practical deformation analysis of ground. This model is certainly very simple, - i.e., the number of material parameters is few, and the meaning of each parameter is clear. However, the basic Cam clay model (e.g., Schofield and Wroth, 1968) has problems to describe the soil behavior in the following points:

- (i) Influence of intermediate principal stress on the deformation and strength of soil
- (ii) Stress path dependency on the direction of plastic flow

<sup>1</sup> Professor, Department of Civil Engineering, Nagoya Institute of Technology, Gokiso-cho, Showa-ku, Nagoya 466-8555, Japan, nakai@tut1.ac.nitech.ac.jp

<sup>2</sup> Research Associate, Department of Civil Engineering, Nagoya Institute of Technology, Gokiso-cho, Showa-ku, Nagoya 466-8555, Japan, hino@tut1.ac.nitech.ac.

- (iii) Positive dilatancy during strain hardening
- (iv) Soil anisotropy and non-coaxiality
- (v) Behavior of soil under cyclic loading
- (vi) Influence of density and/or confining pressure on the deformation and strength
- (vii) Behavior of structured soil
- (viii) Time effect and age effect

We also have developed simple constitutive models for clay and sand – named the  $t_{ij}$ -clay model (Nakai and Matsuoka, 1986) and  $t_{ij}$ -sand model (Nakai, 1989). In these models, the influence of intermediate principal stress on the deformation and strength of soil and the stress path dependency of plastic flow are particularly taken into consideration. However, the  $t_{ij}$ -clay model is applicable to normally consolidated clays but cannot describe the elastoplastic behavior of over consolidated clays with positive dilatancy, and some material parameters of the  $t_{ij}$ -sand model depend on the density and/or confining pressure even for the same sand.

In the present study, the above models for clay and sand are extended to a simple model that can take into account the influence of the density and/or confining pressure on the deformation and strength of soil, as well as the influence of intermediate principal stress on the deformation and strength and the influence of stress path on the plastic flow (Nakai and Hinokio, 2004).

### CONCEPT OF $T_{IJ}$

In most of isotropic hardening models such as the Cam clay model, their yield functions are formulated using stress parameters (mean stress  $p$  and deviator stress  $q$ ) and assuming flow rule in ordinary stress space  $\sigma_{ij}$ . However, such models cannot describe the stress-strain behaviour and the strength in three-dimensional stresses in a uniform manner. Nakai and Mihara (1984) proposed a method, which has been

**Table 1 Comparison of tensors and scalars related to stress and strain increment between ordinary concept and  $t_{ij}$ -concept**

	ordinary concept	$t_{ij}$ concept
tensor normal to reference plane	$\delta_{ij}$ (unit tensor)	$a_{ij}$ (tensor normal to SMP)
stress tensor	$\sigma_{ij}$	$t_{ij} = a_{ik}\sigma_{kj}$
mean stress	$p = \sigma_{ij}\delta_{ij}/3$	$t_N = t_{ij}a_{ij}$
deviatoric stress tensor	$s_{ij} = \sigma_{ij} - p\delta_{ij}$	$t'_ij = t_{ij} - t_Na_{ij}$
deviatoric stress	$q = \sqrt{(3/2)s_{ij}s_{ij}}$	$t_S = \sqrt{t'_ijt'_ij}$
stress ratio tensor	$\eta_{ij} = s_{ij}/p$	$x_{ij} = t'ij/t_N$
stress ratio	$\eta = q/p = \sqrt{(3/2)\eta_{ij}\eta_{ij}}$	$X = t_S/t_N = \sqrt{x_{ij}x_{ij}}$
strain increment normal to reference plane	$d\varepsilon_{ij} = d\varepsilon_{ij}\delta_{ij}$	$d\varepsilon_{SMP}^* = d\varepsilon_{ij}a_{ij}$
deviatoric strain increment tensor	$d\varepsilon_{ij}' = d\varepsilon_{ij} - d\varepsilon_{ij}\delta_{ij}/3$	$d\varepsilon_{ij}' = d\varepsilon_{ij} - d\varepsilon_{SMP}^*a_{ij}$
strain increment parallel to reference plane	$d\varepsilon_{ij}'' = \sqrt{(2/3)d\varepsilon_{ij}d\varepsilon_{ij}}$	$d\gamma_{SMP}^* = \sqrt{d\varepsilon_{ij}'d\varepsilon_{ij}'}$

called  $t_{ij}$ -concept, to take into account uniquely the influence of intermediate principal stress on soil behavior, by introducing the modified stress tensor  $t_{ij}$  and

**@Seismicisolation**

assuming the flow rule in the modified stress space. The stress and strain increment tensors and their parameters using the ordinary concept and the  $t_{ij}$ -concept are compared in Table 1. The stress tensors and parameters in the ordinary models are defined as the quantities related to normal and parallel components of  $\sigma_{ij}$  to the octahedral plane. On the other hand, the stress tensors and stress parameters of the  $t_{ij}$ -concept are those normal and parallel components of the modified stress  $t_{ij}$  to the spatially mobilized plane (briefly SMP; Matsuoka and Nakai, 1974). Here,  $a_{ij}$  is the symmetric tensor whose principal values are determined by the direction cosines ( $a_1$ ,  $a_2$  and  $a_3$ ) of the normal to the SMP. The principal values are expressed as

$$a_i = \sqrt{\frac{I_3}{I_2 \sigma_i}} \quad (i = 1, 2, 3) \quad (1)$$

where  $I_1$ ,  $I_2$ , and  $I_3$  are the first, second and third invariants of  $\sigma_{ij}$ . The modified stress tensor is then defined by the product of  $a_{ik}$  and  $\sigma_{kj}$  as follows

$$t_{ij} = a_{ik} \sigma_{kj} \quad (2)$$

The principal axes of  $t_{ij}$  coincide with those of  $\sigma_{ij}$ , because the principal axes of  $a_{ij}$  and  $\sigma_{ij}$  are identical. In the isotropic hardening model based on  $t_{ij}$ -concept, we formulated the yield function using the stress parameters ( $t_N$  and  $t_S$ ) instead of ( $p$  and  $q$ ) and assuming the flow rule not in  $\sigma_{ij}$  space but in  $t_{ij}$  space such as

$$d\epsilon_{ij}^p = \Lambda \frac{\partial f}{\partial t_{ij}} \quad (\text{where } f = f(t_N, X, H) = 0, H : \text{strain hardening parameter}) \quad (3)$$

## FORMULATION OF MODEL

### Model satisfying associated flow rule in $t_{ij}$ space

Usually the yield function of soil is presented as a logarithmic function of the mean stress plus an increasing function of stress ratio. Using the stress parameters of the  $t_{ij}$ -concept in Table 1, we give the yield function in the following form:

$$f = \ln \frac{t_N}{t_{N0}} + \zeta(X) - \ln \frac{t_{N1}}{t_{N0}} = \ln \frac{t_N}{t_{N0}} + \zeta(X) - \left( \ln \frac{t_{N1e}}{t_{N0}} - \ln \frac{t_{N1e}}{t_{N1}} \right) = 0 \quad (4)$$

$$\zeta(X) = \frac{1}{\beta} \left( \frac{X}{M^*} \right)^\beta \quad (5)$$

Here,  $t_N$  and  $X \equiv t_S/t_N$  are the mean stress and the stress ratio based on the  $t_{ij}$ -concept, and  $t_{N1}$  determines the size of the yield surface (the value of  $t_N$  at  $X=0$ ). The value of  $M^*$  in Eq. (5) is expressed as follows using principal stress ratio  $X_{CS} \equiv (t_S/t_N)_{CS}$  and plastic strain increment ratio  $Y_{CS} \equiv (d\epsilon_{SMP}^{pp}/d\gamma_{SMP}^{pp})_{CS}$  at critical state:

$$M^* = \left( X_{CS}^\beta + X_{CS}^{\beta-1} Y_{CS} \right)^{1/\beta} \quad (6)$$

and these ratios  $X_{CS}$  and  $Y_{CS}$  are represented by the principal stress ratio at critical state in triaxial compression  $R_{CS} = (\sigma_1/\sigma_3)_{CS(comp.)}$ .

$$X_{CS} = \frac{\sqrt{2}}{3} \left( \sqrt{R_{CS}} - \frac{1}{\sqrt{R_{CS}}} \right) \quad (7)$$

$$Y_{CS} = \frac{1 - \sqrt{R_{CS}}}{\sqrt{2} \left( \sqrt{R_{CS}} + 0.5 \right)} \quad (8)$$

Now,  $t_{N1e}$  is the mean stress  $t_N$  equivalent to the present plastic volumetric strain (or void ratio), which is defined as

$$\varepsilon_v^p = C_p \ln \frac{t_{N1e}}{t_{N0}} \quad \left( C_p = \frac{\lambda - \kappa}{1 + e_0} \right) \quad (9)$$

Although  $t_{N1e}$  coincides with  $t_{N1}$  in normally consolidated states,  $t_{N1e}$  is larger than  $t_{N1}$  in over consolidated states. The ratio  $t_{N1e}/t_{N1}$  corresponds to the over consolidation ratio in a broad sense. Figure 1(a) shows the yield surface (solid curve) passing through the present stress state P and its similar curve passing through  $t_{N1e}$  on  $t_N$  axis, which is the yield surface for a normally consolidated soil with same void ratio (broken curve). In the subloading concept by Hashiguchi (1980), the solid curve and broken curve are called subloading surface and normal yield surface, respectively.

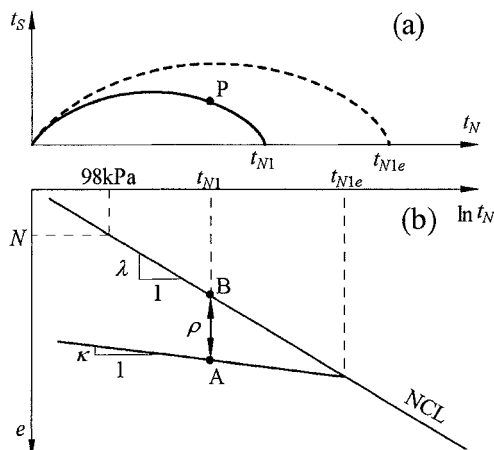


FIG. 1. Shape of yield surface and normally yield surface, and definition of  $\rho$

@Seismicisolation

Assuming a rational evolution rule for the size of both curves with plastic strain developments, Hashiguchi (1980) proposed a method to describe unconventional plasticity behavior as seen in over consolidated clay. Introducing this concept directly, Asaoka et al. (1997) extended Cam clay model to one valid for over consolidated clay as well. In the present study, we intend to revise the concept, keeping the basic idea of Hashiguchi, to make it more suitable for the observed soil behavior and to handle it more easily. Now, points A and B on  $e$ - $\ln t_N$  diagram in Fig. 1(b) indicate the void ratios of over consolidated soil and normally consolidated soil at the same stress state  $P$ . The difference of the void ratios  $\rho$  between A and B can be regarded as an index of soil density. In a mechanical sense, void ratio itself is, therefore, not suitable for representing the soil density. We can see from Fig. 1 that there is the following relation between  $\rho$  and the ratio  $t_{N1e}/t_{N1}$ .

$$\rho = (\lambda - \kappa) \ln \frac{t_{N1e}}{t_{N1}} = (1 + e_0) C_p \ln \frac{t_{N1e}}{t_{N1}} \quad (10)$$

From Eqs. (4) to (10), we can obtain

$$f = \ln \frac{t_N}{t_{N0}} + \zeta(X) - \frac{1}{C_p} \left( \varepsilon_v^p - \frac{\rho}{1 + e_0} \right) = 0 \quad (11)$$

The consistency condition ( $df=0$ ) gives

$$df = \frac{\partial f}{\partial \sigma_{ij}} d\sigma_{ij} - \frac{1}{C_p} \left( d\varepsilon_v^p - d\left(\frac{\rho}{1 + e_0}\right) \right) = \frac{\partial f}{\partial \sigma_{ij}} d\sigma_{ij} - \frac{1}{C_p} \left( \Lambda \frac{\partial f}{\partial t_{ii}} - d\left(\frac{\rho}{1 + e_0}\right) \right) = 0 \quad (12)$$

Here, we assume that the increment of  $\rho/(1+e_0)$ , which represents the change of density during plastic deformation, is influenced by the present density  $\rho$  and mean stress  $t_N$ . Then, it can be given by the following equation using a function  $L(\rho, t_N)$ :

$$d\left(\frac{\rho}{1 + e_0}\right) = \Lambda \cdot L(\rho, t_N) \quad (13)$$

Therefore, from Eqs. (12) and (13), the proportionality constant  $\Lambda$  for an over consolidated soil is expressed as

$$\Lambda = \frac{\frac{\partial f}{\partial \sigma_{ij}} d\sigma_{ij}}{h^p} = \frac{\frac{\partial f}{\partial \sigma_{ij}} d\sigma_{ij}}{\frac{1}{C_p} \left( \frac{\partial f}{\partial t_{ii}} - L(\rho, t_N) \right)} \quad (14)$$

Here,  $L(\rho, t_N)$  has to be formulated to explain the behaviour from a normally consolidated condition to an over consolidation state; i.e., (i) Whenever plastic deformation occurs,  $\Lambda$  is positive, (ii) The over consolidated state moves toward

normally consolidated state with development of plastic deformation, so that the increment  $d(\rho/(1+e_0))$  should be negative. (iii)  $L(\rho, t_N)$  becomes 0 at normally consolidated state ( $\rho=0$ ). To satisfy these conditions, the function  $L(\rho, t_N)$  should be negative at  $\rho>0$  and  $L(\rho, t_N)=0$  at  $\rho=0$ . Now, we will pay attention to the experimental results that there are unique relations between stress ratio and strains regardless of mean principal stresses. In order to describe the unique relations in over consolidated states as well, the dimensions of  $L(\rho, t_N)$  in Eq. (14) have to be the same as  $\partial f/\partial t_{ii}$ . Furthermore, the stiffness and strength of over-consolidated soils become large with increase of density  $\rho$ . Here, the denominator of  $h^p$  in Eq. (14) represents the stiffness, and the relation between density and peak strength is obtained from the condition of  $h^p=0$ . Satisfying the above conditions, we define  $L(\rho, t_N)$  as

$$L(\rho, t_N) = -\frac{G(\rho)}{t_N} \quad (15)$$

and Eq. (14) is rewritten as

$$\Lambda = \frac{\frac{\partial f}{\partial \sigma_{ij}} d\sigma_{ij}}{h^p} = \frac{\frac{\partial f}{\partial \sigma_{ij}} d\sigma_{ij}}{\frac{1}{C_p} \left( \frac{\partial f}{\partial t_{mm}} + \frac{G(\rho)}{t_N} \right)} \quad (16)$$

Here,  $G(\rho)$  is a monotonically increasing function which satisfies the condition of  $G(0)=0$ . We will give it by the following equation using one material parameter  $a$ .

$$G(\rho) = a \cdot \rho^2 \quad (17)$$

The loading condition of soil through its hardening process to softening process is presented as follows, in the same way as Hashiguchi (1980), Asaoka et al. (1997) and others:

$$\begin{cases} d\varepsilon_{ij}^p \neq 0 & \text{if } \Lambda = \frac{df}{h^p} \geq 0 \\ d\varepsilon_{ij}^p = 0 & \text{if } \Lambda = \frac{df}{h^p} < 0 \end{cases} \quad (18)$$

The elastic strain increment  $d\varepsilon_{ij}^p$  is given by generalized Hooke's law.

$$d\varepsilon_{ij}^e = \frac{1+\nu_e}{E_e} d\sigma_{ij} - \frac{\nu_e}{E_e} d\sigma_{kk} \delta_{ij} \quad (19)$$

Young's modulus  $E_e$  is expressed in terms of the swelling index  $\kappa$  and Poisson's ratio  $\nu_e$  as

$$E_e = \frac{3(1-2\nu_e)(1+e_0)p}{\kappa} \quad (20)$$

### Extension to model considering stress path dependency on the direction of plastic flow

According to usual plasticity, the direction of plastic flow (direction of plastic strain increments) is independent of the direction of stress increments. It is, however, experimentally known that the direction of plastic flow is influenced by the direction of stress increments except at and after peak strength. In the previous models for clay and sand ( $t_{ij}$ -clay model and  $t_{ij}$ -sand model), such stress path dependency was considered by dividing the plastic strain increment into two components – the plastic strain increment  $d\varepsilon_{ij}^{p(AP)}$  satisfying the associated flow rule in  $t_{ij}$ -space as mentioned above and the isotropic plastic strain increment  $d\varepsilon_{ij}^{p(IC)}$  under increasing mean stress – in spite of using just one yield function and one strain hardening parameter. The same method is employed in the present modeling to consider the stress path dependency on the direction of plastic flow. Referring to the previous model for clay (Nakai and Matsuoka, 1986), we can give the isotropic plastic strain increment  $d\varepsilon_{ij}^{p(IC)}$  and the plastic strain increment  $d\varepsilon_{ij}^{p(AP)}$  satisfying the associated flow rule in  $t_{ij}$ -space by

$$d\varepsilon_{ij}^{p(IC)} = d\varepsilon_v^{p(IC)} \frac{\delta_y}{3} = \frac{\frac{1}{t_{N1}} \langle dt_N \rangle}{\frac{1}{C_p} \left( 1 + \frac{G(\rho)}{a_{kk}} \right)} \cdot \frac{\delta_y}{3} \quad (21)$$

$$d\varepsilon_{ij}^{p(AP)} = \Lambda^{(AP)} \frac{\partial f}{\partial t_{ij}} = \frac{\frac{\partial f}{\partial \sigma_{kl}} d\sigma_{kl} - \frac{1}{t_{N1}} \langle dt_N \rangle}{\frac{1}{C_p} \left( \frac{\partial f}{\partial t_{mm}} + \frac{G(\rho)}{t_N} \right)} \cdot \frac{\partial f}{\partial t_{ij}} = \frac{df - \frac{1}{t_{N1}} \langle dt_N \rangle}{h^p} \cdot \frac{\partial f}{\partial t_{ij}} \quad (22)$$

Here, the symbol  $\langle \rangle$  denotes the Macaulay bracket, i.e.,  $\langle A \rangle = A$  if  $A \geq 0$ ; otherwise  $\langle A \rangle = 0$ .

Hence, the strain increments, of which the stress path dependency on plastic flow is considered, are summarized as follows:

(i) elastic region ( $\Lambda = df/h^p < 0$ ):

$$d\varepsilon_{ij} = d\varepsilon_{ij}^e \quad (23)$$

(ii) elastoplastic region with strain hardening ( $\Lambda = df/h^p \geq 0$  and  $h^p \geq 0$ ):

 @Seismicisolation

$$d\epsilon_{ij} = d\epsilon_{ij}^e + d\epsilon_{ij}^p = d\epsilon_{ij}^e + d\epsilon_{ij}^{p(AF)} + d\epsilon_{ij}^{p(IC)} \quad (24)$$

(iii) elastoplastic region with strain softening ( $\Lambda = df/h^p \geq 0$  and  $h^p < 0$ ):

$$d\epsilon_{ij} = d\epsilon_{ij}^e + d\epsilon_{ij}^p \quad (25)$$

The derivative of yield function  $f$ , mean stress  $t_N$  and stress variables with respect to  $t_{ij}$  and  $\sigma_{ij}$  are shown in APPENDIX.

## VALIDATION OF PRESENT MODEL BY TEST DATA ON CLAY

### Fundamental feature of present model

Every shear test was carried out in the laboratory to check the validation of the model. Details of these laboratory tests were described in the paper by Nakai and Hinokio (2004). Table 2 shows the values of material parameters for saturated Fujinomori clay (F-clay). As indicated in the table, one parameter is added to the parameters which are fundamentally the same as those of Cam clay model. The parameters except parameter ' $a$ ' can be obtained from consolidation and shear tests on normally consolidated soils. Parameter ' $\beta$ ', which represents the shape of yield surface, can be determined from the observed stress-strain-dilatancy curve of a shear tests, and the other parameter ' $a$ ' can be determined from the strength of over-consolidated soil. Figure 2 shows the yield surface of the Cam clay model for Fujinomori clay in  $p$ - $q$  plane. Figure 3 shows the yield surface of the proposed model in (a)  $t_N$ - $t_S$  plane and (b)  $p$ - $q$  plane. In these figures, the upper half indicates the triaxial compression condition, and the lower half indicates the triaxial extension condition. We can see that the yield surface of  $t_{ij}$  model is symmetric with respect to  $t_N$ -axis but not symmetric with respect to  $p$ -axis. It is also noted that the direction of plastic flow of  $t_{ij}$  model is not normal to the yield surface represented in  $p$ - $q$  plane, because the flow rule is assumed in modified stress  $t_{ij}$  space. Also, though the yield

**Table 2 Values of material parameters for Fujinomori clay**

$C_f = \lambda(1+\epsilon_0)$	$5.08 \times 10^{-2}$	Same parameters as Cam-clay model
$C_e = \kappa(1+\epsilon_0)$	$1.12 \times 10^{-2}$	
$N = e_{NC}$ at $p=98\text{ kPa}$ & $q=0\text{ kPa}$	0.83	
$R_{CS} = (\sigma_i/\sigma_3)_{CS(\text{comp.})}$	3.5	
$\nu_e$	0.2	
$\beta$	1.5	Shape of yield surface (same as original Cam-clay at $\beta=1$ )
$a$	500	Influence of density and confining pressure

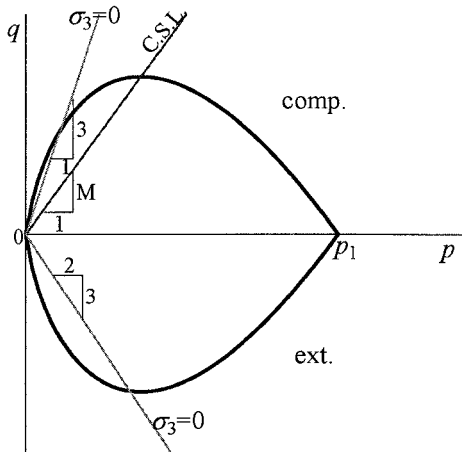
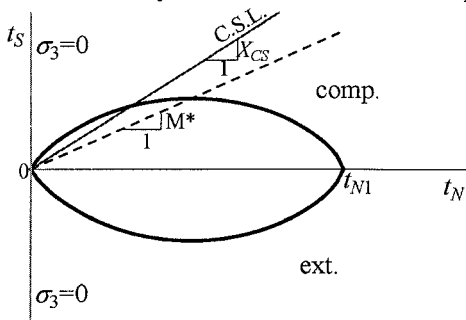
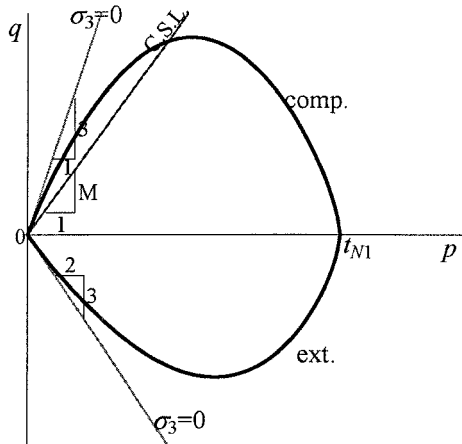


**FIG. 2. Yield surface of Cam clay model and tension zone on  $p - q$  plane**



**(a) Yield surface of proposed model and tension zone on  $t_N - t_S$  plane**



**(b) Yield surface of proposed model and tension zone on  $p - q$  plane**  
**FIG. 3. Yield surface of proposed model and tension zone**

@Seismicisolation

surface of the original Cam clay model is not smooth at the tip on  $p$ -axis, that of the proposed model is smooth over the whole surface. The previous  $t_{ij}$  models for clay and sand also have the singular points at the origin and the tip on isotropic axis. Such smoothness of the present yield surface is one of the advantages in numerical computations in the same way as the modified Cam clay model (Roscoe and Burland, 1968). Now, the lines in which the minor principal stress  $\sigma_3$  is zero are indicated in every figure. It can be seen that though models formulated using  $p$  and  $q$  such as Cam clay model have tension zones on and inside the yield surface, there is no tension zone in the yield surface formulated using  $t_N$  and  $t_S$ . Models based on the  $t_{ij}$ -concept not only are capable of describing properly the influence of the intermediate principal stress but also have the above-mentioned benefit for numerical computations.

### Conventional triaxial tests under monotonic and cyclic loadings

Figure 4 shows the results of triaxial compression and extension tests on clays with different over consolidation ratios (OCR=1, 2, 4 and 8). Here, tests of OCR=8 are carried out under  $p=98\text{kPa}$ , and the other tests are under  $p=196\text{kPa}$ . The model predicts well not only the influence of over consolidation ratio on the deformation, dilatancy and strength of clay but also the influence of intermediate principal stress on them. Figures 5 to 7 are the results and stress paths of drained cyclic triaxial tests on normally consolidated clay. As shown in stress path of diagram (c) in each figure, Fig. 5 is the cyclic constant mean principal test under constant amplitude of stress ratio, Fig. 6 is the results of the cyclic constant mean principal test under increasing stress ratio with number of cycles, and Fig. 7 is the results of cyclic constant radial stress test. We can see that in spite of using an isotropic hardening law, the proposed model can describe cyclic behavior of clay under triaxial conditions. This is because

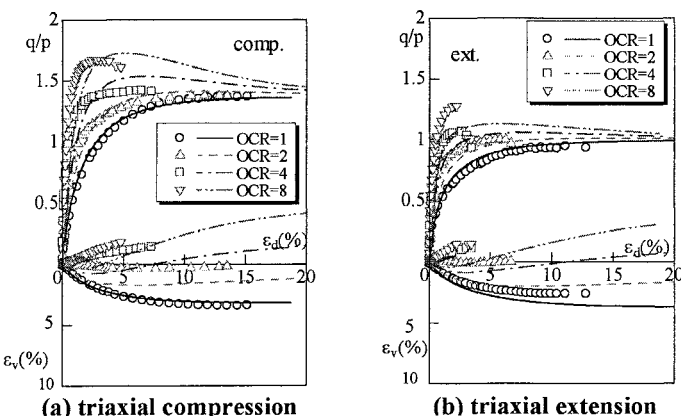
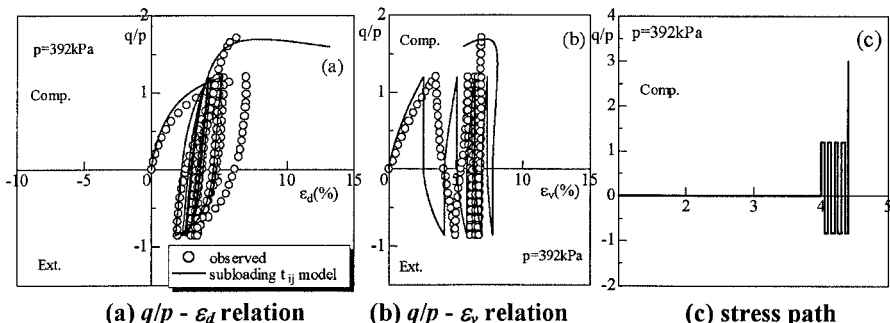


FIG. 4. Observed and calculated results of triaxial compression and extension tests with different over consolidation ratio under monotonic loading

@Seismicisolation

of the subloading surface concept and the loading condition in Eq. (18). The reason why the present model can describe the behavior of clays as they become stiffer with increasing number of cycles is because the state variable  $\rho$  increases under cyclic loadings, even if the clay is initially normally consolidated ( $\rho_0=0$ ).



**FIG. 5. Observed and calculated results of cyclic constant mean principal stress tests with constant amplitude of stress ratio**

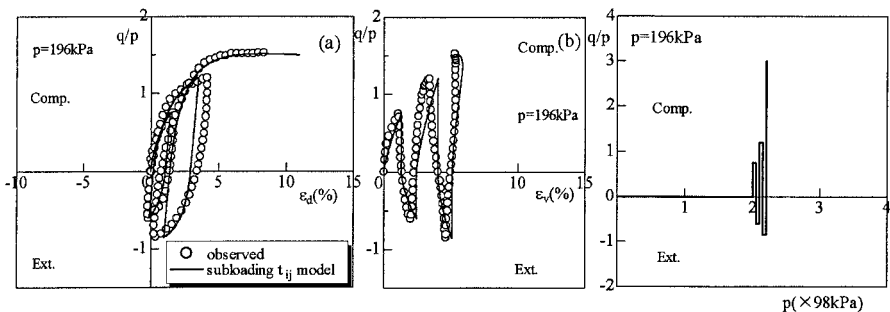


**FIG. 6. Observed and calculated results of cyclic constant mean principal stress tests with increasing amplitude of stress ratio**

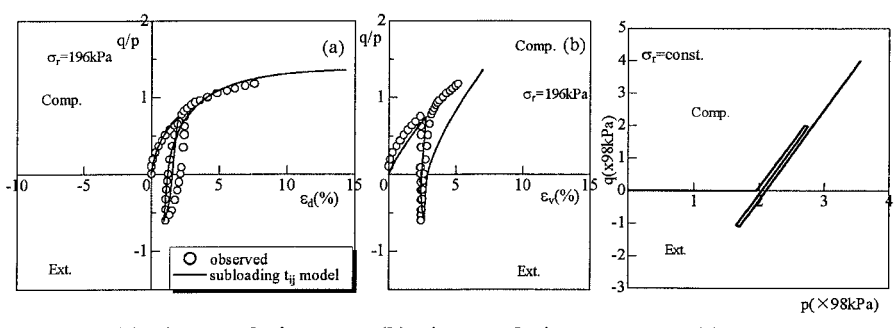


**FIG. 7. Observed and calculated results of cyclic constant radial stress tests**

### True triaxial tests under monotonic and cyclic loadings

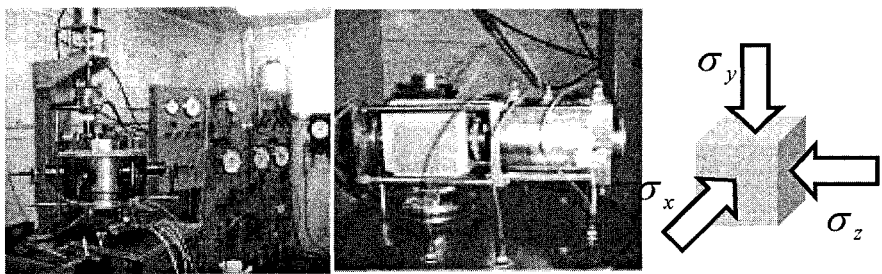
Real ground conditions are under three different principal stresses and may undergo cyclic loadings in three-dimensional stresses – e.g., under earthquake. To investigate the behavior of clay in general three-dimensional stress conditions, not only monotonic true triaxial tests but also cyclic true triaxial tests on normally consolidated clay were carried out. In particular, the directions of shear stress and/or mean principal stress are changed in cyclic loading tests. Photo 1 shows two views of the chamber type apparatus used (left view shows the complete apparatus and the controlling devices and right view shows the inside of the chamber), together with the schematic diagram of the specimen on which three principal stresses are applied. As seen from these photos,  $\sigma_x$  is applied by chamber water pressure and the other two principal stresses ( $\sigma_y$  and  $\sigma_z$ ) are applied by rigid plates. Details of the apparatus are described by Nakai et al. (1986).

Figure 8 shows the observed (symbols) and calculated (curves) variations of the three principal strains ( $\varepsilon_1$ ,  $\varepsilon_2$  and  $\varepsilon_3$ ) and the volumetric strain  $\varepsilon_v$  against stress ratio  $q/p$  in true triaxial tests ( $\theta=0^\circ$ ,  $15^\circ$ ,  $30^\circ$ ,  $45^\circ$  and  $60^\circ$ ) on normally consolidated clay under constant mean principal stress ( $p=196\text{ kPa}$ ). Figure 9 shows the stress paths on the octahedral plane for these tests. Here,  $\theta$  denotes the angle between  $\sigma_1$ -axis and the corresponding radial stress path on the octahedral plane, where  $\theta=0^\circ$  and  $60^\circ$  represent the stress path under triaxial compression and triaxial extension conditions, respectively. There is the following relation between the angle  $\theta$  and the intermediate principal stress parameter  $b$ .

$$b = \frac{2 \tan \theta}{\sqrt{3} + \tan \theta} \quad (26)$$

where  $b$  is represented using three principal stresses as

$$b = \frac{\sigma_2 - \sigma_3}{\sigma_1 - \sigma_3} \quad (27)$$



**Photo 1 True triaxial test apparatus and specimen under three different principal stresses.**

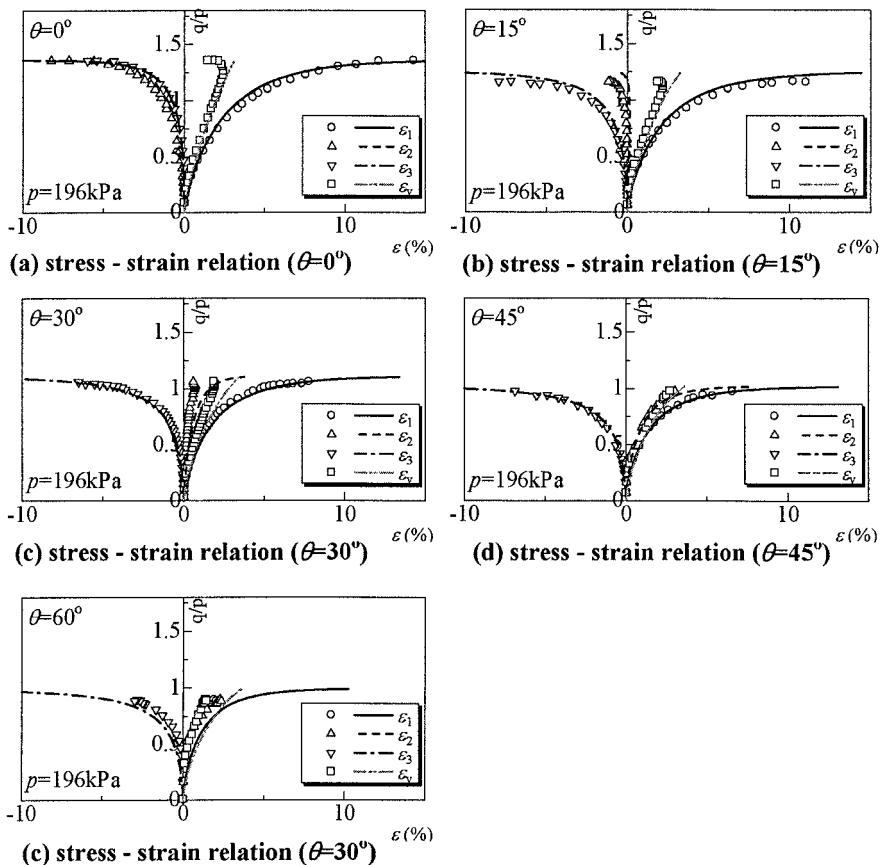


FIG. 8. Observed and calculated results of cyclic true triaxial tests under constant mean principal stress

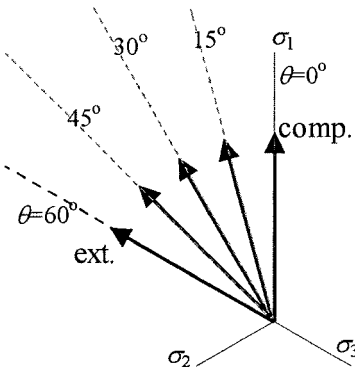


FIG. 9. Stress path on octahedral plane in true triaxial test

@Seismicisolation

Two minor principal strains in triaxial compression condition ( $\theta=0^\circ$ ) and two major principal strains in triaxial extension condition ( $\theta=60^\circ$ ) are almost same. We can see that though the loading systems in horizontal principal stresses ( $\sigma_x$  and  $\sigma_y$ ) are different – one is applied by chamber pressure and the other is applied by rigid plate, the apparatus has an adequate accuracy. As can be seen from Fig. 8, the present model predicts well the three-dimensional stress-strain behavior of clay, in the same way as the previous model. From Figs. 8(b) and (c), i.e.,  $\varepsilon_2$  is negative in diagram (b) but is positive in diagram (c), we can presume that the stress condition  $\theta$  in plane strain condition ( $\varepsilon_2=0$ ) lies within  $15^\circ < \theta < 30^\circ$ , that is the same as the results reported by many researchers.

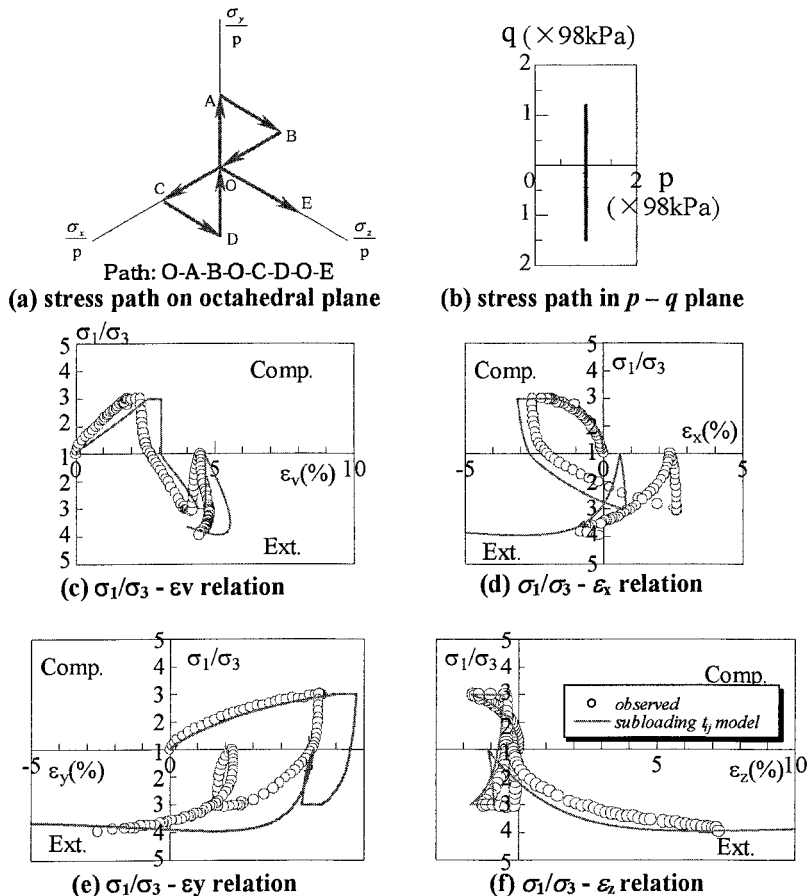
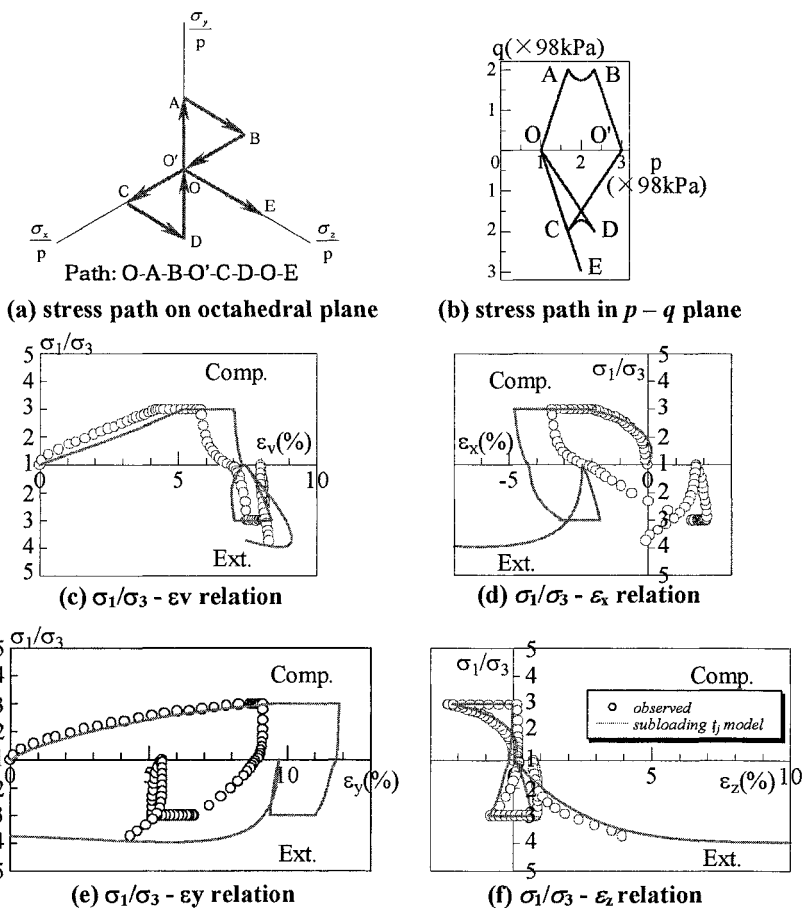


FIG. 10. Observed and calculated results of cyclic true triaxial tests under constant mean principal stress

@Seismicisolation



**FIG. 11. Observed and calculated results of cyclic true triaxial tests under varying mean principal stress**

Figure 10 shows the stress path of the cyclic true triaxial test (diagrams (a) and (b)) and the variations of principal strains and volumetric strain against major-minor principal stress ratio. As can be seen, the stress path describes shape of a bow tie on the octahedral plane under constant mean principal stress. Figure 11 shows those of the cyclic test with change of mean principal stress. It can be seen from these figures that as a whole the present model describes the cyclic behavior of clay under three different principal stresses as well.

### Plane strain tests on Ko consolidated clay

Plane strain tests were carried out using the chamber type true triaxial apparatus mentioned before. Figure 12 shows schematically the specimen under plane strain condition and stress paths of the tests carried out. To produce the plane strain condition, the plate in z-direction is fixed ( $\epsilon_z=0$ ). Each test was started from normally K0 consolidated condition ( $\sigma_y=196\text{ kPa}$ ,  $\sigma_x=\sigma_z=196\text{ kPa}$ ). Although seven tests were

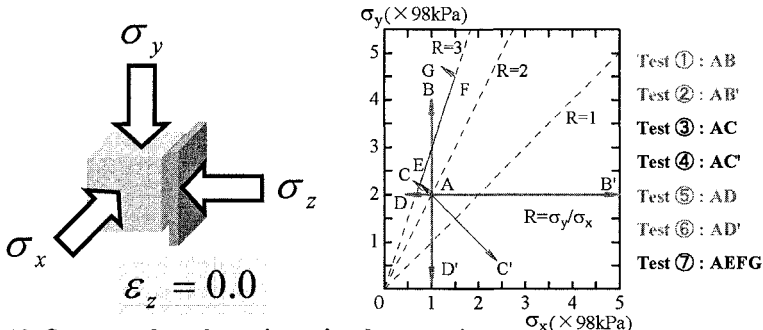
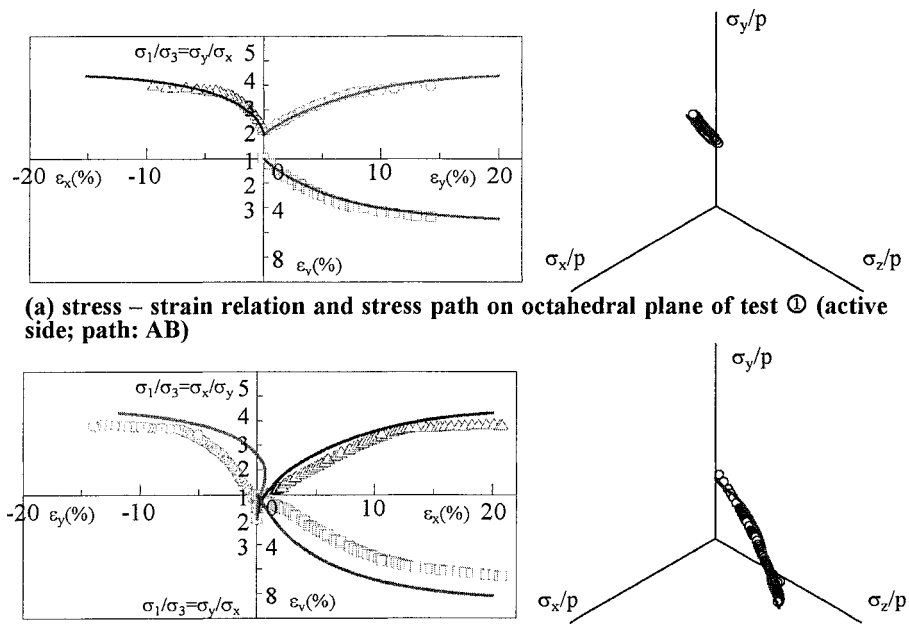
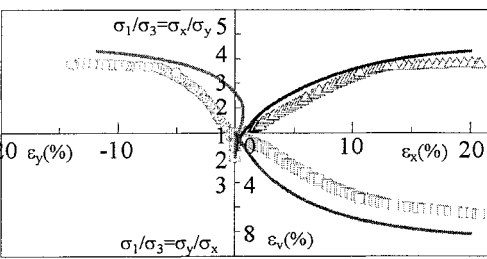


FIG. 12. Stress path and specimen in plane strain tests



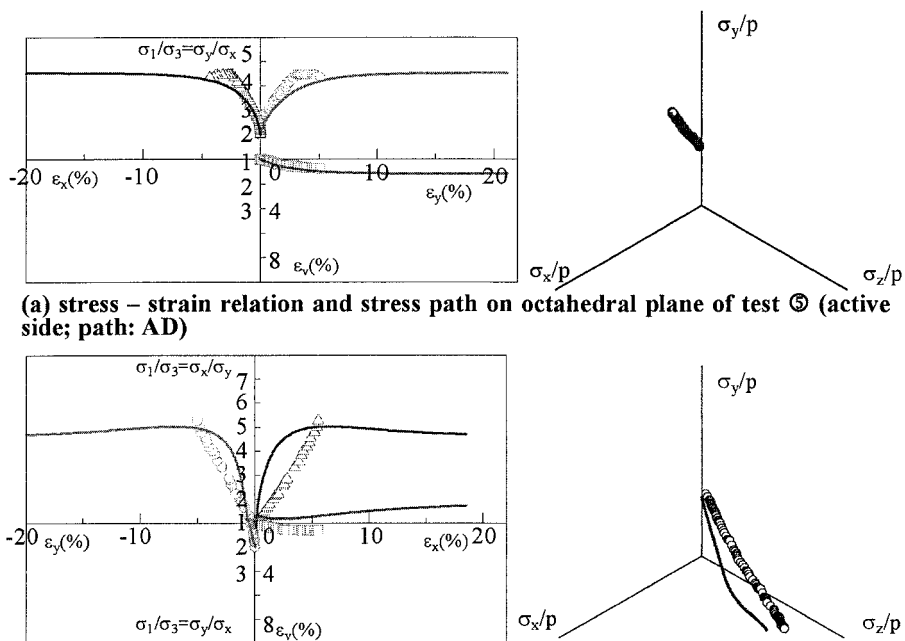
(a) stress – strain relation and stress path on octahedral plane of test ① (active side; path: AB)



(b) stress – strain relation and stress path on octahedral plane of test ② (passive side; path: AB')

FIG. 13. Observed and calculated results of plane strain tests under constant minor principal stress

@Seismicisolation



(a) stress – strain relation and stress path on octahedral plane of test ⑤ (active side; path: AD)

(b) stress – strain relation and stress path on octahedral plane of test ⑥ (passive side; path: AD)

**FIG. 14. Observed and calculated results of plane strain tests under constant major principal stress**

carried out, the results of 4 tests (tests ①, ②, ③ and ④) are presented here. Figure 13 shows the results of plane strain tests under constant minor principal stress ( $\sigma_3=196\text{kPa}$ ), together with the diagram of stress paths. These tests roughly correspond to the conditions of the inserted schematic picture. Figure 14 shows the results of the tests under constant major principal stress ( $\sigma_1=196\text{kPa}$ ). In each figure, diagram (a) is the principal stress ratio– principal strains– volumetric strain relation and the stress path on the octahedral plane normalized by mean stress  $p$  at active side, and diagram (b) is those at passive side. We can see that the proposed model describes well the plane strain behavior of clay under active and passive states as a whole, though there is some disagreements between tests result and the calculated curves in test ④ in which the direction of the major principal stress changes and the mean stress decreases

#### Torsional shear tests on isotropically and anisotropically consolidated clay

To investigate the influence of the continuous rotation of principal stress axes on the behavior of clay including soil dilatancy during shear, cyclic torsional shear tests were carried out. The chamber type hollow cylinder apparatus in Photo 2 is used.

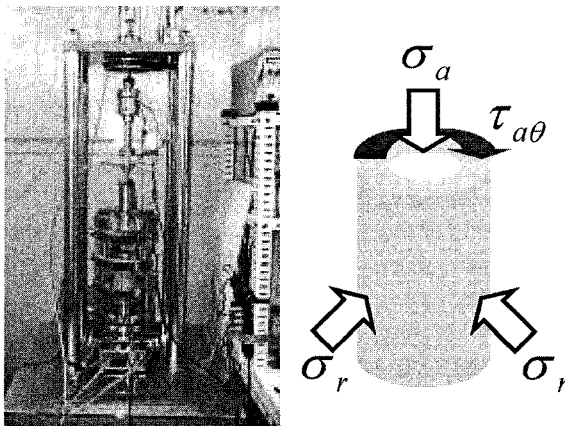


**Photo 2** Chamber type hollow cylinder apparatus and stress condition of specimen under torsional shear loading

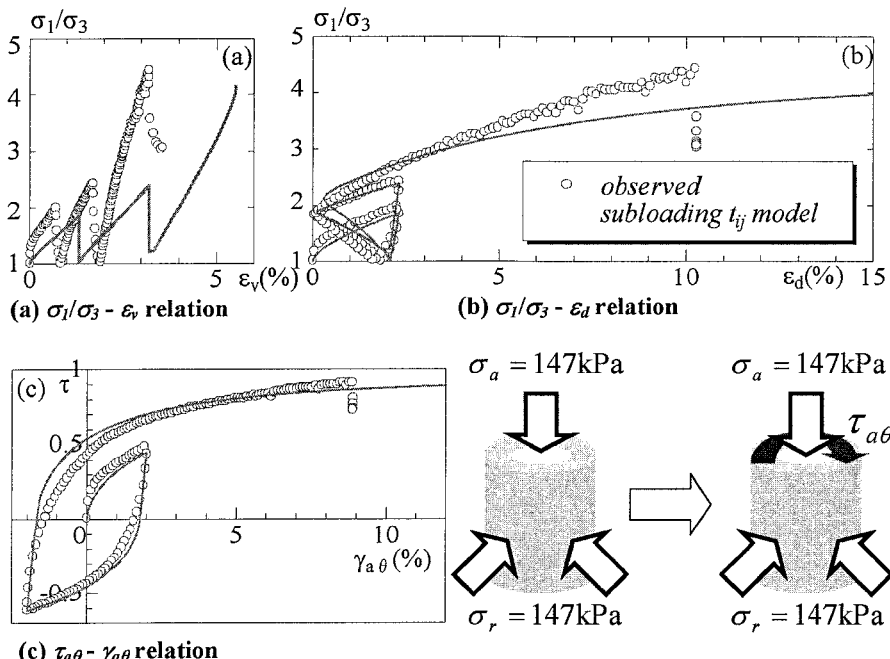


**FIG. 15.** Observed and calculated results of cyclic torsional shear tests from isotropic stress condition

@Seismicisolation

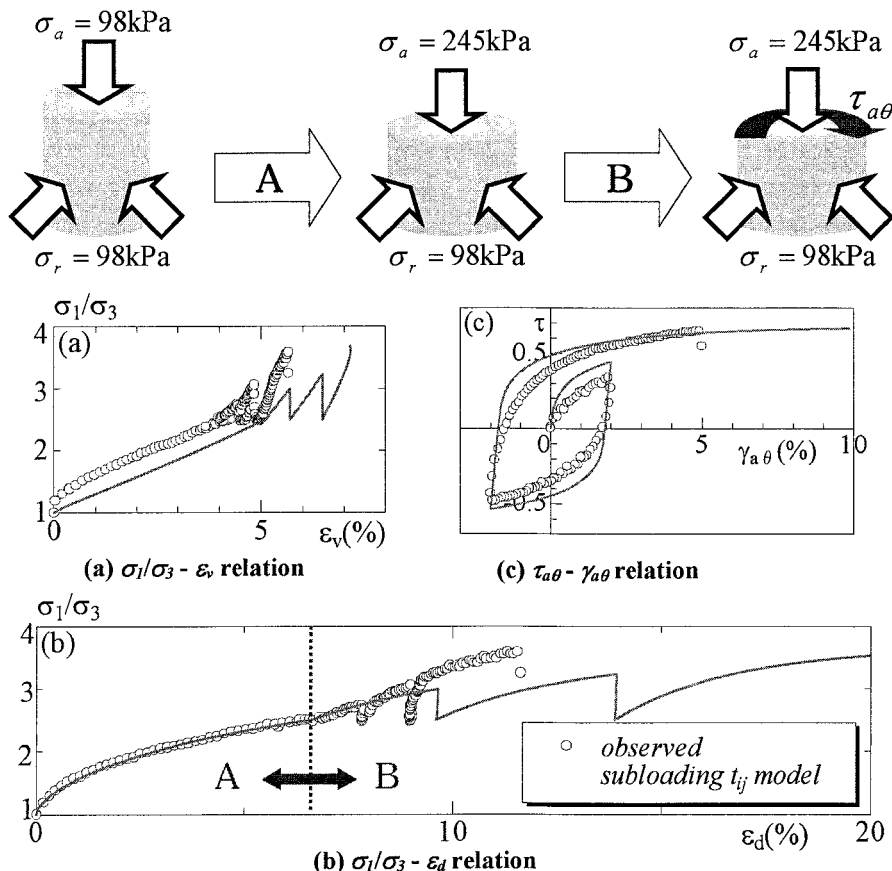


**FIG. 16. Observed and calculated results of cyclic torsional shear tests from anisotropic stress condition**

Figure 15 shows the results of cyclic torsional shear tests on normally and isotropically consolidated clay. The test procedure is indicated at the upper part of the figure. In this test, the principal axes does not rotate continuously during cyclic loading, and its stress state is the same as that of true triaxial test of  $b=(\sigma_2-\sigma_3)/(\sigma_1-\sigma_3)=0.5$ . Diagrams (a) and (b) show the variations of volumetric strain  $\varepsilon_v$  and deviatoric strain  $\varepsilon_d$  against principal stress ratio  $\sigma_1/\sigma_3$ , respectively, and (c) is the relation between torsional shear  $\tau_{a\theta}$  and shear strain  $\gamma_{a\theta}$ . Figure 16 shows the results of the torsional test in which axial stress is load till  $\sigma_1/\sigma_3=3$  (process A) and then cyclic torsional stress is applied to the specimen (process B). The continuous rotation of principal stress axes occurs during torsional shear loading. It can be seen that though there is a good agreement of  $\tau_{a\theta} - \gamma_{a\theta}$  relation in diagram (c), the model over-predict the deviatoric strain  $\varepsilon_d$  in the process B in which the principal axes

rotate continuously from anisotropic stress condition. This is because isotropic hardening model cannot take into account the anisotropy (this is one of the major topics under research in our laboratory). However, the proposed model describes the behavior of clay under such complex stress conditions, though it is an isotropic hardening model.

## CONCLUSIONS

(1) A simple isotropic hardening elastoplastic model for soils (named subloading  $t_{ij}$  model) is formulated by extending the previous models. This model particularly considers the following mechanical characteristics of soils, which Cam clay model cannot describe:

- Influence of intermediate principal stress on the deformation and strength of soil
- Stress path dependency of the direction of plastic flow
- Positive dilatancy during strain hardening
- Influence of density and/or confining pressure on the deformation and strength
- Behavior of soil under cyclic loading (not full-considered)

Only one material parameter which represents the influence of density (OCR) is added to the parameters which are fundamentally the same as the Cam clay model.

(2) The validity of the model is confirmed by conventional triaxial tests on normally consolidated clays and over-consolidated clays with different OCR under monotonic and cyclic loadings. Furthermore, through the comparison of analytical results of the true triaxial tests, plane strain tests and torsional shear tests with the test results under monotonic and cyclic loadings, it is shown that the present model is capable to describe the behavior of clays in general three-dimensional stress conditions with unified material parameters.

## ACKNOWLEDGEMENT

The authors are indebted to Messrs. M.H. Shahin, T. Kido, and T. Nishimura and Miss M. Miyata, graduate students of Nagoya Institute of Technology, for their experimental and computational assistance and useful discussions.

## REFERENCES

- Asaoka, A., Nakano, M. and Noda, T. (1997). "Soil-water coupled behavior of heavily over-consolidated clay near/at critical state." *Soils and Foundations*, Vol. 37, No. 1, 13-28.
- Hashiguchi, K. (1980). "Constitutive equation of elastoplastic materials with elastoplastic transition." *Jour. of Appli. Mech.*, ASME, Vol. 102, No. 2, 266-272.
- Matsuoka, H. and Nakai, T. (1974). "stress-deformation and strength characteristics of soil under three different principal stresses." *Proc. of JSCE*, Vol. 232, 59-70.
- Nakai, T. and Hinokio, T. (2004). "A simple elastoplastic model for normally and over consolidated soils with unified material parameters." *Soils and foundations*, Vol. 44, No. 2, 53-70.



- Nakai, T. and Mihara, Y. (1984). "A new mechanical quantity for soils and its application to elastoplastic constitutive models." *Soils and Foundations*, Vol. 24, No. 2, 82-94.
- Nakai, T. (1985). "Finite element computations for active and passive earth pressure problems of retaining wall." *Soils and Foundations*, Vol. 25, No. 3, 98-112.
- Nakai, T. and Matsuoka, H. (1986). "A generalized elastoplastic constitutive model for clay in three-dimensional stresses." *Soils and Foundations*, Vol. 26, No. 3, 81-98.
- Nakai, T., Matsuoka, H., Okuno, N. and Tsuzuki, K. (1986). "True triaxial tests on normally consolidated clay and analysis of the observed shear behavior using elastoplastic constitutive models." *Soils and Foundations*, Vol. 26, No. 4, 67-78.
- Nakai, T. (1989). "An isotropic hardening elastoplastic model for sand considering the stress path dependency in three-dimensional stresses." *Soils and Foundations*, Vol. 29, No. 1, 119-137.
- Roscoe, K. H. & Burland, J. B. (1968). "On the generalized stress-strain behavior of wet clay." Heyman and F. A. Leckie (eds.), *Engineering Plasticity*, Cambridge University Press: 535-609.
- Schofield, A. N. and Wroth, C. P. (1968). *Critical State Soil Mechanics*, McGraw-Hill, London.

## APPENDIX

### Partial derivatives of yield function and stress variables

Generally yield function of isotropic hardening model based on  $t_{ij}$ -concept is given by the following form as a function of mean stress  $t_N$  and stress ratio  $X$

$$f = f(t_N, X) = \ln t_N + \zeta(X) - \ln t_{N1} = 0 \quad (A1)$$

and definitions of tensors and scalars related to in  $t_{ij}$ -concept are shown in Table 1.

We will firstly show the derivatives of  $f$  with respect to modified stress  $t_{ij}$ .

$$\frac{\partial f}{\partial t_{ij}} = \frac{\partial f}{\partial t_N} \frac{\partial t_N}{\partial t_{ij}} + \frac{\partial f}{\partial X} \frac{\partial X}{\partial t_{ij}} \quad (A2)$$

$$\frac{\partial f}{\partial t_N} = \frac{1}{t_N} \quad (A3)$$

$$\frac{\partial t_N}{\partial t_{ij}} = \frac{\partial(t_{kl}a_{kl})}{\partial t_{ij}} = a_{ij} \quad (A4)$$

$$\frac{\partial f}{\partial X} = \zeta'(X) \quad (A5)$$

$$\frac{\partial X}{\partial t_{ij}} = \frac{\partial(\sqrt{x_{kl}x_{kl}})}{\partial x_{mn}} \frac{\partial x_{mn}}{\partial t_{ij}} = \frac{1}{X \cdot t_N} (x_{ij} - X^2 a_{ij}) \quad (A6)$$

Next, the derivative of  $f$  with respect to the ordinary stress  $\sigma_{ij}$  is expressed as follows:

$$\frac{\partial f}{\partial \sigma_{ij}} = \frac{\partial f}{\partial t_N} \frac{\partial t_N}{\partial \sigma_{ij}} + \frac{\partial f}{\partial X} \frac{\partial X}{\partial \sigma_{ij}} \quad (A7)$$

$$\frac{\partial t_N}{\partial \sigma_{ij}} = \frac{\partial}{\partial \sigma_{ij}} \left( 3 \frac{I_3}{I_2} \right) \quad (A8)$$

$$\frac{\partial X}{\partial \sigma_{ij}} = \frac{\partial}{\partial \sigma_{ij}} \left( \sqrt{\frac{I_1 I_2 - 1}{9 I_3}} \right) \quad (A9)$$

where,  $I_1$ ,  $I_2$  and  $I_3$  are the first , second and third invariants of  $\sigma_{ij}$ . Therefore, the terms  $d\sigma$  and  $dt_N$  can be given using general stress increment  $d\sigma_{ij}$

## A SIMPLE ELASTOPLASTIC MODEL FOR SOILS AND SOFT ROCKS

Roberto Nova<sup>1</sup>

**ABSTRACT:** A simple elastoplastic strainhardening model of soil and soft rock behaviour is presented. The physical meaning of the few constitutive parameters characterising the constitutive law is discussed and the procedure for their determination is outlined. Typical values of the parameters for various types of geomaterials are given. Examples of model performance in drained and undrained tests is illustrated, both for axisymmetric and fully three dimensional loading conditions.

### INTRODUCTION

In the early stages of constitutive modelling of soils, the reference materials were selected in such a way that their behaviour was relatively simple and repetitive (i.e., such that similar specimens subject to the same loading conditions behave similarly). Kaolinitic clay reconstituted in the laboratory starting from slurry was chosen as the representative material for clays. Quartz sand with rounded particles and more or less uniform particle size, such as Hostun R.F. sand at Grenoble, was instead the representative material for sands and coarse geomaterials in general. Models based on the theory of elastoplasticity with hardening such as Cam Clay (Schofield and Wroth (1968)) or Lade (1977), Vermeer (1978), Nova and Wood (1979) were capable of reproducing the observed behaviour of normally consolidated clay and virgin sand with an acceptable degree of accuracy.

Natural soil behaviour is more complex, however. Diagenetic bonds are developed between grains affecting their behaviour in various ways. For instance soils acquire tensile strength and, since bonds are often fragile in nature, they often develop a collapsible structure, giving rise to unexpected instabilities. Despite such differences, the mathematical structure of the constitutive models describing bonded

---

<sup>1</sup>Professor, Milan University of Technology (Politecnico)  
Piazza Leonardo da Vinci, 32  
20133 Milano - ITALY

geomaterials can be obtained by modifying the original models for unbonded soils slightly. This fact conjectured by Nova (1986) and qualitatively demonstrated by Leroueil and Vaughan (1990), was exploited by a number of authors to model various kind of soft rocks such as shale, tuff, calcarenite, marl or chalk (see e.g. Shao & Henry (1991), Nova (1992), Kavvadas et al. (1993), Gens & Nova (1993)).

Natural soil behaviour is more complex, however. Diagenetic bonds are developed between grains affecting their behaviour in various ways. For instance soils acquire tensile strength and, since bonds are often fragile in nature, they often develop a collapsible structure, giving rise to unexpected instabilities. Despite such differences, the mathematical structure of the constitutive models describing bonded geomaterials can be obtained by modifying the original models for unbonded soils slightly. This fact conjectured by Nova (1986) and qualitatively demonstrated by Leroueil and Vaughan (1990), was exploited by a number of authors to model various kind of soft rocks such as shale, tuff, calcarenite, marl or chalk (see e.g. Shao & Henry (1991), Nova (1992), Kavvadas et al. (1993), Gens & Nova (1993)).

Soil bonding evolves with time. Uncohesive sediments are gradually transformed into sedimentary rocks (diagenesis). On the other hand, given enough time, even the hardest rock such as granite can be transformed into a residual soil by the action of weathering. Nova and Lagioia (1996) postulated that both diagenesis and weathering effects could be described in the same framework, by taking the parameters characterising bond strength as time dependent. In particular weathering effects were thoroughly investigated by Nova and co-workers (Nova (2000), Nova et al. (2003)).

In order to achieve good accuracy in reproducing the observed behaviour, the number of constitutive parameters has been steadily increasing from 4 (for the original Cam Clay model) to the order of 20 for the most up to date constitutive laws. For instance the model by Nova et al. (2003), that allows for non-linear elasticity, non-associated plastic flow rule, hardening depending on plastic volumetric as well as deviatoric strains, variable degree of cementation, needs as many as 17 parameters to be fully characterised.

The model that is presented here is a simpler version of it, trying to limit the number of parameters to what is believed to be the minimum necessary to cope with the complex phenomena discussed above. In this way the presentation of the mathematical structure is simpler, the physical meaning of the parameters easy to grasp and the procedure of their determination straightforward. Notwithstanding its simplicity, it will be shown in the following that the model can describe the behaviour of a wide class of soils and soft rocks well enough, for engineering purposes at least. Nevertheless, to show the potentialities of the full model, some recent results obtained with it will be eventually presented.

## MODEL FOR UNCEMENTED SOILS

Consider remoulded clay or freshly deposited ('virgin') sand specimens. When one of these is subjected to a cycle of loading-unloading and reloading, some common features of the experimental results can be observed:

- soil behaviour is non-linear and irreversible, i.e. only part of the strains occurring in the loading phase can be recovered upon unloading;



- b) in a cycle of unloading-reloading, instead, the observed behaviour is more or less reversible and characterised by a larger stiffness than upon virgin loading;
- c) when the stress state reaches the level at which unloading started, a marked stiffness change is observed and the soil behaves as it would be virgin, i.e. as if the unloading-reloading cycle would have not been performed;
- d) furthermore, soil behaviour is very much sensitive to the value of the isotropic effective pressure at which it is tested, i.e. stiffness and strength depend very much on it.

The simplest way to cope with such observations is to assume that soil behaviour can be considered as elastic-plastic with hardening, as initially conjectured by Drucker et al. (1957).

It is assumed that strain rates  $\dot{\varepsilon}_{hk}$  can be decomposed into a reversible (elastic) part and a permanent (plastic) component:

$$\dot{\varepsilon}_{hk} = \dot{\varepsilon}_{hk}^e + \dot{\varepsilon}_{hk}^p \quad (1)$$

In order to establish whether plastic strains occur under a given stress increment  $\sigma'_{ij}$ , it is defined a loading function  $f(\sigma'_{ij}, p_k)$  that depends on the state of effective stress and on a set of variables  $p_k$ . These are known as hidden variables or hardening parameters and depend on the ‘history’ of the soil volume element via the experienced plastic strains.

If

$$f(\sigma'_{ij}, p_k) < 0 \quad (2)$$

only elastic strain increments can take place, whatever is the stress rate. If

$$f(\sigma'_{ij}, p_k) = 0 \quad (3)$$

two possibilities exist. If the stress increment is such that the loading function takes a negative value after this is applied to the soil volume element ( $df < 0$ ), only elastic strains occur. If on the contrary the value of the loading function does not change after the stress increment ( $df = 0$ ), then plastic strains as well as elastic take place.

Plastic strain rates are assumed to be derivable from a plastic potential (flow rule)

$$\dot{\varepsilon}_{ij}^p = \Lambda \frac{\partial g}{\partial \sigma'_{ij}} \quad (4)$$

where  $\Lambda$  is a plastic multiplier that can be determined from the hardening rules, i.e. from the evolution rules of the hardening parameters:

$$\dot{p}_s = \frac{\partial p_s}{\partial \varepsilon_{hk}^p} \dot{\varepsilon}_{hk}^p = \frac{\partial p_s}{\partial \varepsilon_{hk}^p} \Lambda \frac{\partial g}{\partial \sigma'_{hk}} \quad (5)$$

By imposing the condition  $df = 0$  (Prager’s consistency rule)

$$df = 0 = \frac{\partial f}{\partial \sigma'_{ij}} \dot{\sigma}'_{ij} + \frac{\partial f}{\partial p_s} \frac{\partial p_s}{\partial \varepsilon_{hk}^p} \Lambda \frac{\partial g}{\partial \sigma'_{hk}} \quad (6)$$

$$\Lambda = - \frac{\frac{\partial f}{\partial \sigma'_{ij}} \dot{\sigma}'_{ij}}{\frac{\partial f}{\partial p_s} \frac{\partial p_s}{\partial \varepsilon_{hk}^p} \frac{\partial g}{\partial \sigma'_{hk}}} \quad (7)$$

Plastic strain rates are eventually determined via Equation (4).

In the model that is presented here, named Sinfonietta Classica (Nova (1988)), the following expressions are taken for the constitutive functions:

$$g = 9(\gamma - 3) \ln \frac{p'}{p_g} - \gamma J_{3\eta} + \frac{9}{4}(\gamma - 1)J_{2\eta} = 0 \quad (8)$$

$$f = 3\beta(\gamma - 3) \ln \frac{p'}{p_c} - \gamma J_{3\eta} + \frac{9}{4}(\gamma - 1)J_{2\eta} \leq 0 \quad (9)$$

where

$$p' \equiv \frac{1}{3}\sigma'_{ij}\delta_{ij} \quad (10)$$

$$J_{2\eta} \equiv \eta_{ij}\eta_{ij} \quad (11)$$

$$J_{3\eta} \equiv \eta_{ij}\eta_{jk}\eta_{ki} \quad (12)$$

and the stress ratio tensor is defined as

$$\eta_{ij} \equiv \frac{s_{ij}}{p'}; \quad (13)$$

For unbonded soils, the hidden variables reduce to one,  $p_c$ . This controls the size of the elastic domain and its evolution rule is given by:

$$\dot{p}_c = \frac{p_c}{B_p} \left( \dot{\epsilon}_v^p + \xi \left( \dot{\epsilon}_{hk}^p \dot{\epsilon}_{hk}^p \right)^{\frac{1}{2}} + \psi \left( \dot{\epsilon}_{ij}^p \dot{\epsilon}_{jk}^p \dot{\epsilon}_{ki}^p \right)^{\frac{1}{3}} \right) \quad (14)$$

where

$$\dot{\epsilon}_v^p \equiv \dot{\epsilon}_{ij}^p \delta_{ij} \quad (15)$$

$$\dot{\epsilon}_{hk}^p \equiv \dot{\epsilon}_{hk}^p - \frac{1}{3}\dot{\epsilon}_v^p \delta_{hk} \quad (16)$$

The elastic behaviour is assumed to be governed by a hypoelastic relationship:

$$\dot{\epsilon}_{ij}^e = \frac{1}{3}B_e \frac{p'}{p'} \delta_{ij} + L\dot{\eta}_{ij} \quad (17)$$

It is readily apparent that the tangent elastic bulk modulus of the soil increases linearly with the isotropic pressure. The shear modulus follows the same trend. It can be shown in fact that:

$$G = \frac{p'}{2L} \quad (18)$$

It is further assumed that stresses cannot be negative (tension cut-off) and that there exists a small elastic nucleus delimited by a surface given by Equation (8) with  $p_c = p_{c0}$ . Furthermore, the behaviour within the nucleus is considered to be linear elastic. The volumetric compliance is assumed to be equal to  $B^e / p_{c0}$ , while the shear modulus is equal to  $p_{c0} / 2L$ .

A picture of the elastic domain (and of the elastic nucleus) is shown in Figure 1 in the axisymmetric (so-called 'triaxial') and deviatoric planes.

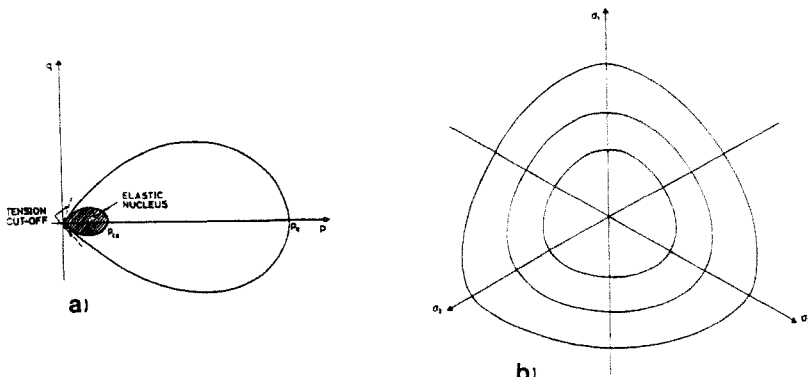


**FIG. 1. Picture of elastic domain: a) 'triaxial' plane; b) deviatoric plane**

## PARAMETER MEANING AND DETERMINATION

The constitutive law is characterised by 7 non-dimensional parameters and a reference pressure  $p_{eo}$ . The plastic potential is characterised by the single parameter  $\gamma$ . The actual value of  $p_g$  is unessential, in fact, since only the derivatives of  $g$  matter. It can be proven that the value of  $\gamma$  is directly linked to that of the inclination of the so-called characteristic state line,  $M$ , in axisymmetric compression (Luong (1980)). This in turn is linked to the mobilised friction angle at constant volume, i.e. associated to zero plastic volumetric strains,  $\phi'_{cv}$ :

$$\gamma = \frac{9 - M^2}{\frac{2}{9}M^3 + 3 - M^2} \quad (19)$$

$$M = \frac{6\sin\phi'_{cv}}{3 - \sin\phi'_{cv}} \quad (20)$$

Since  $\phi'_{cv}$  typically ranges from  $22^\circ$  for clays to  $36^\circ$  for sands and gravels  $\gamma$  can vary between 3.44 and 4.41.

The loading function is characterised by  $\gamma$  and  $\beta$ . The latter controls the deviation from normality, due to the spherical part only. If  $\beta = 3$  normality holds. In general  $\beta$  is smaller than 3, however. Typical values are  $\beta = 2$  for clays and  $\beta = 1.2$  for sands.

The assumption that the flow rule is non-associated, so that plastic potential and loading function do not coincide, has far reaching consequences. Non-normality implies non-symmetry of the constitutive tensor, what implies in turn that a series of instabilities can occur in the hardening regime, i.e. at stress ratio levels lower than that corresponding to drained failure for homogeneous strain states (see e.g. Nova (1989) or Imposimato and Nova (1998a)). In particular it can be proven that non-normality is a necessary condition to model the existence of a peak of the deviator stress in undrained tests and *a fortiori* for the occurrence of static liquefaction. Loss

of control (instability) occurs in this case if the undrained test is partially load controlled. Bifurcations in the form of strain localisation in bands (shear bands) can be also predicted in the hardening regime when the constitutive tensor is non-symmetric. Either drained or undrained shear banding is possible (Imposimato and Nova (1998b)).

It can be shown that the plastic deformability of soil linearly depends on  $\beta$ . This parameter can be then determined by fitting the calculated curve to the data of the drained test. Because of such proportionality, the value of  $\beta$  can be calibrated also on the value of the coefficient of earth pressure at rest  $K_0$  or the inclination of the 'instability line', i.e. the locus of the peaks in undrained tests (Lade (1992)).

Hardening depends in general on three parameters:  $B_p$ ,  $\xi$  and  $\psi$ . The first one indicates the logarithmic volumetric plastic compliance under isotropic loading. In this case in fact from Equation (14):

$$\dot{\varepsilon}_v^p = B_p \frac{\dot{P}_e}{P_c} \quad (21)$$

This Equation can be derived from the log-log expression (Butterfield (1979)) between specific volume (i.e.  $v = 1 + e$ , where  $e$  is the void ratio) and the isotropic pressure.

The value of  $B_p$  depends on the type and density of the material tested. For dense silica sand, the order of magnitude of  $B_p$  is 0.01, while for loose sand the order of magnitude can be two or four times larger. For virgin clay it ranges from 0.02 to 0.1, depending on clay plasticity.

For normally consolidated kaolin and loose sand, hardening depends on plastic volumetric strains only ( $\xi = \psi = 0$ ). For medium dense and dense sand, for gravel, silt and silty clay, hardening depends also on plastic deviatoric strains (Nova (1977)). The parameters  $\xi$  and  $\psi$  control in fact the value of dilatancy at failure,  $d_f$ . In axisymmetric conditions:

$$d_f = \frac{\dot{\varepsilon}_v^p}{\dot{\varepsilon}_d^p} = -3 \left( \frac{\xi}{\sqrt{6}} \frac{\dot{\varepsilon}_d^p}{|\dot{\varepsilon}_d^p|} + \frac{\psi}{\sqrt[3]{36}} \right) \quad (22)$$

where the deviator strain,  $\dot{\varepsilon}_d$ , is defined as:

$$\dot{\varepsilon}_d \equiv \frac{2}{3} (\dot{\varepsilon}_1 - \dot{\varepsilon}_3) \quad (23)$$

The value of  $\xi$  and  $\psi$  can be then derived from the results of drained compression and extension tests, by measuring the slope of the tangent to the volumetric strain, deviatoric strain relationship at failure. In this case the stress state does not change and elastic strain rates are zero.

The parameter  $\xi$  depends on the type and density of the soil. The denser the sand the higher the  $\xi$  value. A typical value for dense sand is 0.3, while a silty clay can have  $\xi = 0.1$ . When  $\xi$  is positive, dilatancy at failure is negative (expansion) in drained tests, while in undrained tests the stress path has a characteristic hook across the phase transformation line (Ishihara et al. (1975)). Indeed the model predicts that phase transformation line and characteristic state coincide. An alternative way to

determine M is then to perform an undrained test and find what is the stress ratio for which the tangent to the effective stress ratio is vertical.

In carbonate sands, grain crushing provokes a continuous compaction even when the limit stress state is achieved. This can be modelled by taking negative values of  $\xi$ . In general such values are small (e.g.  $\xi = -0.05$ ).

The last hardening parameter  $\psi$  is generally ten times smaller than  $\xi$  and can be put equal to zero for most practical purposes. In this case the absolute value of the dilatancy at failure is the same in compression and extension. Experimental data show however that there is actually a small difference that can be accounted for by taking  $\psi$  positive (see e.g. Lanier and Zitouni (1988)).

It is worth noting that the stress ratio at failure in drained tests,  $\eta_f$ , depends on  $d_f$  and on  $\gamma$ . Once  $d_f$  has been determined,  $\gamma$  can be back-calculated from the measured value of  $\eta_f$  which is directly linked to the friction angle  $\phi'$  via a relationship formally identical to Equation (20).

The hypoelastic parameters are  $B_e$  and  $L$ . The first is similar to  $B_p$ , but relative to the volumetric compressibility in isotropic unloading-reloading, and therefore smaller than that. The ratio  $B_e/B_p$  is typically of the order of 0.1/0.2 for clays. However, the lower is  $B_p$ , the higher tends to be the ratio between the two parameters. For dense sands it can reach 1.0.

The other elastic parameter  $L$  is linked to the shear modulus  $G$ , as in Equation (18). It can be determined from the slope of the deviatoric stress, deviatoric strain unloading-reloading curve. The value of  $G$  ranges from 30 to 600 times the value of the confining pressure when passing from normally consolidated clays to dense sands. The value of  $L$  can be determined accordingly.

The value of  $p_{eo}$  is actually the most difficult parameter to be determined for virgin soils. It is in fact a fictitious dimensional parameter introduced only to avoid the singularities at the origin of axes, both for elastic and plastic moduli. Its precise value is important only for small stress levels, however. In particular it is irrelevant for the simulation of triaxial tests with confining pressures larger than 50 kPa. In fact, the value of  $p_{eo}$  can be assumed of the order of few dozens of kPa, so that, when the soil is consolidated under a stress of that order of magnitude, the frontier of the elastic nucleus is bypassed and  $p_{eo}$  plays no role. In a boundary value problem, e.g. a shallow foundation, however, the value of  $p_{eo}$  determines the size of the elastic nucleus and influences the behaviour of the soil elements close to the free surface. These behave elastically, in fact, since their stress state falls within the elastic nucleus. It should be borne in mind, however, that the superficial layers of the soil are often partially saturated. Pore water suction gives the soil an apparent cohesion. Therefore, under small stress increments, soil behaviour is actually elastic in the upper crust.

## MODEL PREDICTION FOR SAND AND REMOULDED CLAY

The model presented was initially developed to predict the behaviour of samples of two types of sand tested with two apparatus on occasion of the Cleveland Workshop



on Constitutive Equations for Granular non-cohesive soils (Saada and Bianchini (1988)).

Both types of materials tested are fine uniform silica sands. The former comes from a quarry at Hostun near Grenoble, while the latter was obtained from Reid Bedford Bend, South of Vicksburg.

Several predictors were given the experimental results of some triaxial compression and extension tests together with the results of an isotropic consolidation test. Such experiments can be considered as routine tests, which can be easily performed in almost any geotechnical laboratory. The constitutive parameters of the models were calibrated on the basis of such results.

The predictors were then asked to provide the calculated results in more complex tests performed with a hollow cylinder apparatus and a cubic triaxial cell.

In the former case the test was conducted at constant cell pressure and constant angle  $\hat{\beta}$  defined as:

$$\tan 2\hat{\beta} = \frac{2\tau_{\theta z}}{\Delta\sigma_z} \quad (24)$$

The axial stress  $\sigma_z$  and torsional stress  $\tau_{\theta z}$  were increased or decreased starting from a spherical state of stress.

In the latter test the intermediate stress was kept constant as well as  $b$  defined as

$$b = \frac{\sigma_y - \sigma_x}{\sigma_z - \sigma_x} \quad (25)$$

where x, y, z are the axes of the cube. Tests started after an isotropic compression to a given cell pressure. Experimental results were disclosed to authors only after predictions were given.

A comparison between the results predicted by means of the model presented (dotted curves) and the experimental data is shown in figures 2 and 3. The overall agreement is generally satisfactory and in some cases is really good. An equally good agreement was obtained with different types of sand in various monotonic triaxial tests.

The model was also applied to describe the behaviour of remoulded clays. In figures 4 and 5 it is shown a comparison between the calculated and the experimental data of a drained and an undrained test on a normally consolidated silty clay, known as Pontida clay, a site near Bergamo. The constitutive parameters were determined on the basis of the results of the drained test. The calculated curve in the undrained test is therefore an actual prediction. It is interesting to note that the characteristic hook of the effective stress path in the undrained test, which is typical of silty clays and dense sands, is correctly modelled.

It is also noteworthy that the constitutive law adopted is able to reproduce the observed peak in the undrained test. As already mentioned, the fact that the flow rule is non-associated is a necessary condition. It is not sufficient however. Figure 6 shows a qualitative comparison between calculated results and the experimental data of three undrained test on Banding Sand reported by Castro (1975). The only differences in the three simulated experiments are in the dilatancy parameter  $\xi$  and the compressibility  $B_p$ . The behaviour of a very loose sand is modelled by

taking  $\xi = 0$ . In this case, for large strains, it is achieved a state of full liquefaction, i.e. very small ultimate shear strength. The behaviour of a denser sand can be reproduced by taking  $\xi$  positive. The denser the sand the higher  $\xi$ . If this is high enough, no peak occurs in the deviatoric stress-strain law, as experimentally observed for dense sands.

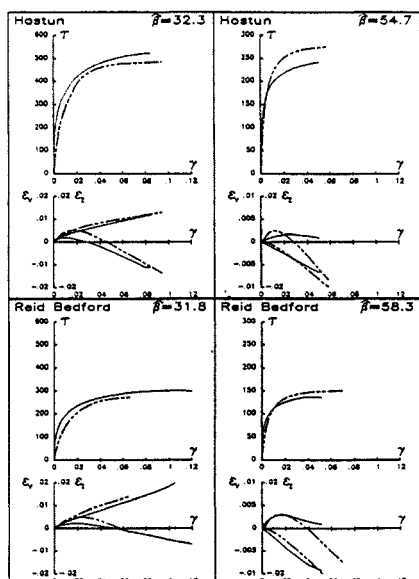


**FIG. 2. Silica sand. Comparison between predictions and actual test results - hollow cylinder apparatus- after Nova (1988)**

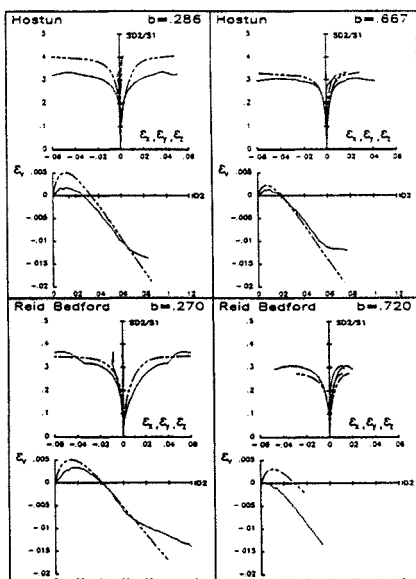


**FIG. 3. Silica sand. Comparison between predictions and actual test results -cubic triaxial cell- after Nova (1988)**

## MODEL FOR BONDED SOILS AND SOFT ROCKS

Most natural soils are characterized by diagenetic bonds which are destroyed by sampling and/or remoulding. In order to model such materials it is then necessary to modify the presented constitutive law in such a way that the effects of the bonds could be accounted for.

From a macroscopic viewpoint, the existence of such bonds is essentially reflected by the occurrence of a non-zero tensile strength. Moreover the size of the "initial" elastic domain is not only controlled by the maximum past pressure but also by the degree of cementation.

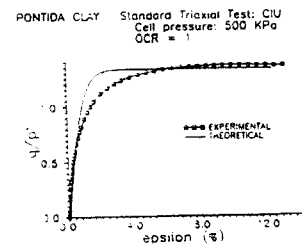
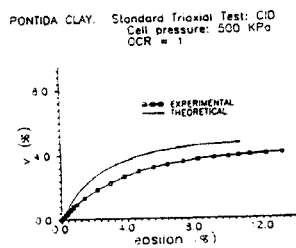
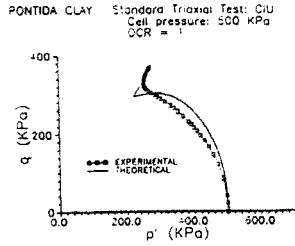
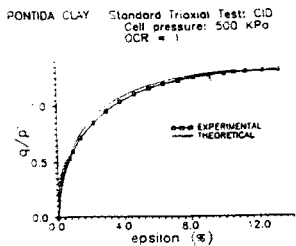
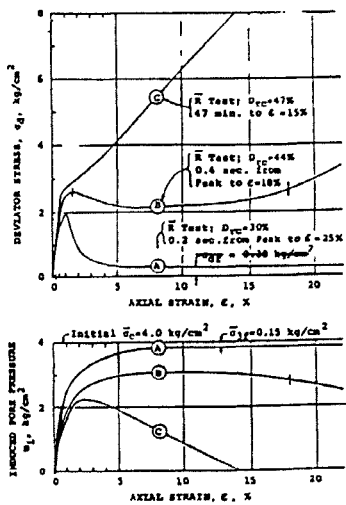
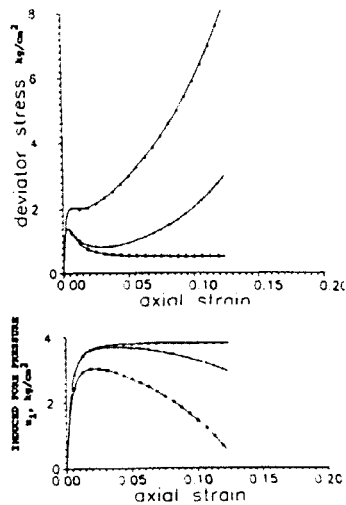


**FIG. 5.** Normally consolidated silty clay-comparison between back-predictions and experimental results in an undrained triaxial test - after Nova (1988)



a)



b)

**FIG. 6.** Undrained test on Banding sand a) experimental results-after Castro (1975); b) back-calculated results - after Nova (1988)

It was then decided to modify the constitutive law by introducing two new parameters,  $p_t$  and  $p_m$ , whose meaning is illustrated in figure 7. The former is linked to the tensile strength of the natural soil, while the latter controls the growth in size of the initial elastic domain. In fact those parameters should be intimately connected, since both effects are linked to the same physical reason. It is assumed in the following that those are proportional to each other:

$$p_m = \alpha p_t \quad (26)$$

The evolution law of  $p_t$ , and then of  $p_m$  via Equation (26), is assumed as:

$$\dot{p}_t = -\rho p_t |\dot{\epsilon}_v^p| \quad (27)$$

The role played by  $p_c$  for uncemented soils is now played by  $p_s$ . Its evolution law is then given by Equation (14).

As proposed by Kim and Lade (1984) and Desai et al. (1986) in similar contexts, it will be assumed that the expressions of the constitutive functions are formally the same as those employed for uncemented soils. The arguments of the functions will be however  $p^*$  and  $\eta_{ij}^*$  defined as follows:

$$p^* = p' + p_t \quad (28)$$

$$\eta_{ij}^* = \frac{s_{ij}}{p^*} \quad (29)$$

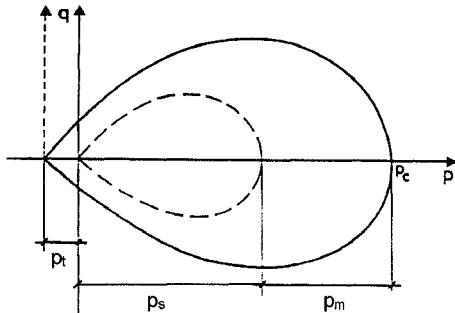


**FIG. 7. Modification of elastic domain due to cementation**

A dummy variable can be introduced for mathematical convenience:

$$p_c = p_t + p_s + p_m \quad (30)$$

In total three additional constitutive parameters are introduced: the initial value of  $p_t$ ,  $p_{t0}$ , the proportionality constant  $\alpha$  and a decay parameter of the bond strength,  $\rho$ . The value of  $p_{t0}$  can be determined from the results of tensile tests. Typical values of  $p_{t0}$  for soft rocks are between 100 and 200 kPa. The value of the initial value of  $p_s$ ,  $p_{s0}$  can be taken equal to that of  $p_{c0}$ , characterising the elastic nucleus for the uncemented soil. An isotropic compression test allows the yield value  $p_{c0}$  for the soft rock to be determined. Since  $p_{s0}$  is small,  $\alpha$  can be evaluated as a first approximation as the ratio between  $p_{c0}$  and  $p_{t0}$ . Such a value is usually between 10 and 20.

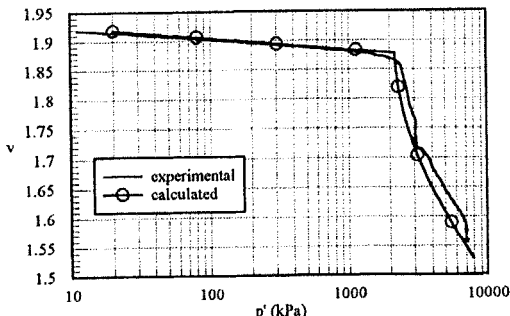


**FIG. 8.** Natural Calcarene: isotropic compression test (after Lagioia and Nova (1993); experimental data from Coop and Atkinson (1993))

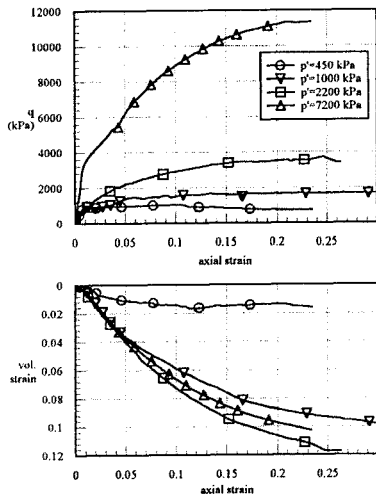


**FIG. 9.** Natural Calcarene: constant isotropic pressure tests : experimental data from Coop and Atkinson (1993)

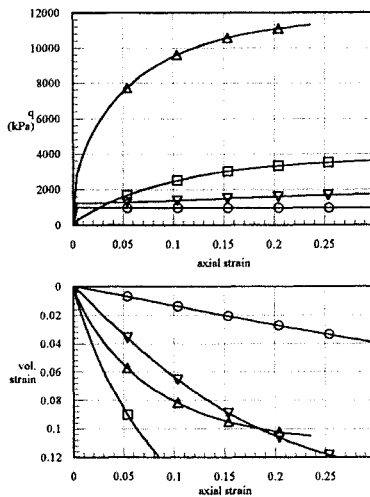
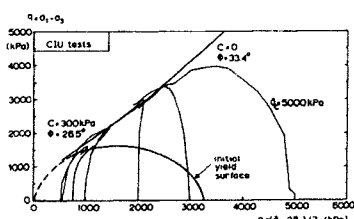


**FIG. 10.** Natural Calcarene: constant isotropic pressure tests : calculated results (after Lagioia and Nova (1993))

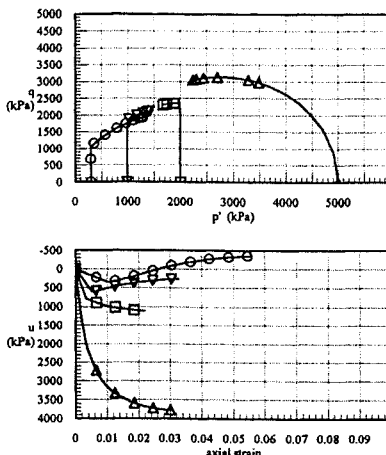
Finally, the parameter  $\rho$  depends on the bond fragility, since it measures the rate at which the bonds are broken and the soft rock is transformed into a soil. It can be determined only by fitting theoretical results to experimental data in an isotropic compression test. The higher the  $\rho$  value, the faster the compression curve will join the corresponding curve for an uncemented material. Such a parameter can usually vary between 0.5 and 5.

Figure 8 shows a comparison between experimental data and calculated results (after Lagioia and Nova (1993)) for a specimen of a natural calcarenite tested in isotropic compression (data after Coop and Atkinson (1993)).

@Seismicisolation



**FIG.11.** Corinth marl: undrained tests : experimental data from Anagnostopoulos et al. (1991)



**FIG.12.** Corinth marl: undrained tests: calculated results (after Lagioia and Nova (1993))

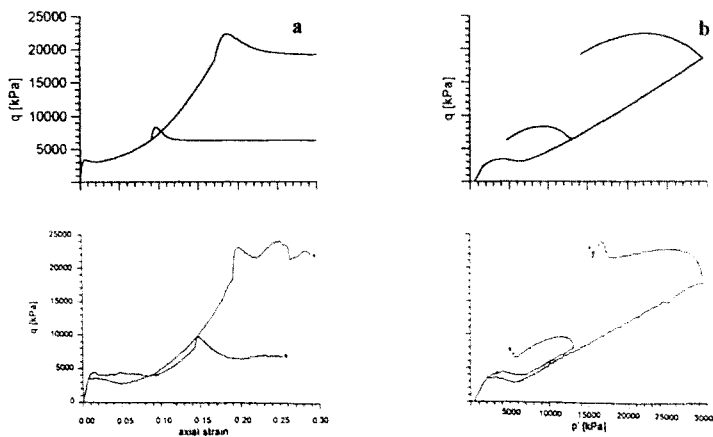


**FIG.13.** Undrained tests after  $K_0$  consolidation on Stevn's Klint chalk: calculated results (above) from Nova and Lagioia (1996) and experimental data from Leddra (1988). a) stress strain relationship b) stress path

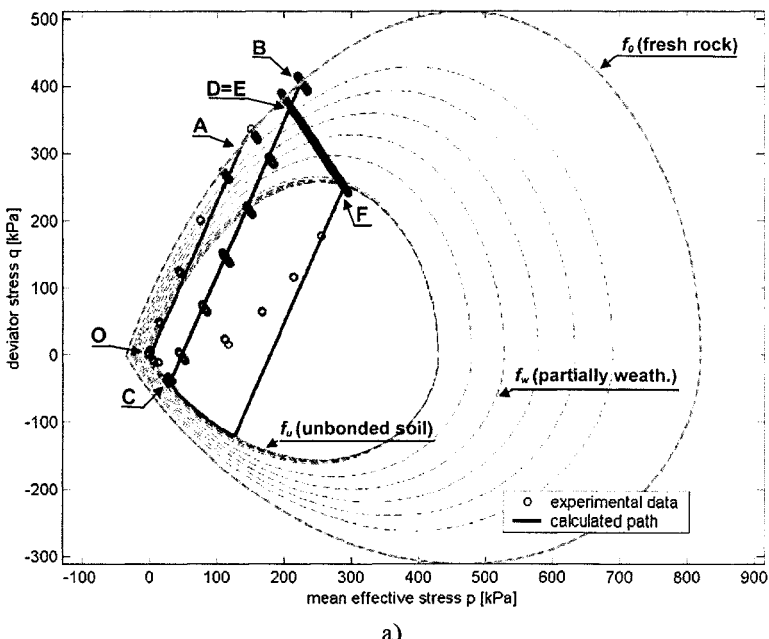
Experimental and calculated behaviour for drained tests at constant isotropic pressure are instead shown in Figures 9 and 10.

Similar results can be obtained for other soft rocks, such as different types of calcarenite (Lagioia and Nova (1995)), tuff and chalk (Nova and Lagioia (1996)).

Figures 11 and 12 show a comparison for experimental and calculated behaviour of Corinth marl (after Lagioia and Nova (1993) – data after Anagnostopoulos et al. ((1991). Figures 13 shows a comparison for experimental and calculated behaviour in undrained tests on chalk (after Nova and Lagioia (1996) – data after Leddra (1988)) after  $K_0$  consolidation. It is interesting to note how the model can reproduce the complicate effective stress path followed by the material element.

## MODELLING WEATHERING EFFECTS AND ASSOCIATED INSTABILITIES

The model has been recently refined (Nova (2000), Nova et al. (2003)), by keeping the same structure. A more realistic non-linear elastic law was introduced (Borja and Tamagnini (1998)). Degradation has been made to depend on volumetric and deviatoric plastic strains. A different expression (but similar shape) for plastic potential and loading function was chosen (Lagioia et al. (1996)). Most importantly the effects of weathering have been modelled by assuming that the cementation parameters  $p_i$  and  $p_m$  depend not only on plastic strains but also on non-mechanical variables, such as time, the degree of chemical attack (Nova and Castellanza (2001)) or temperature (Nova et al. (2004)).



a)

@Seismicisolation

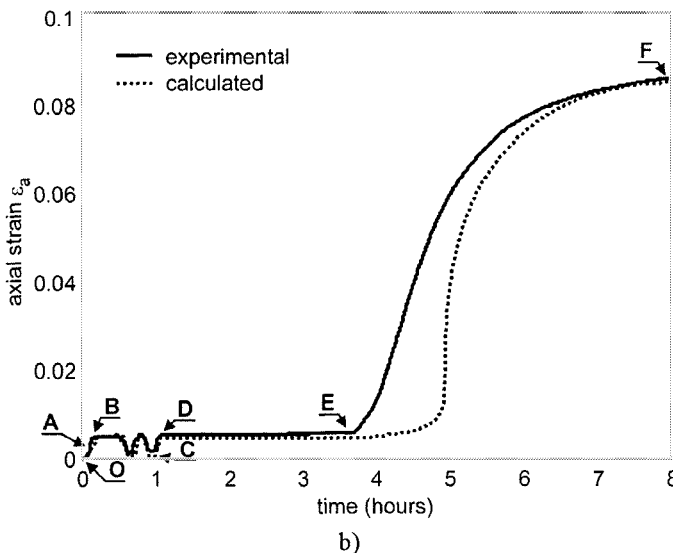


**FIG.14.** Lime cemented silica sand: oedometric loading followed by chemical attack at constant axial load and final unloading: a) stress path; b) variation of axial strain with time (after Nova et al. (2003)).

As an example, Figure 14 shows the experimental and the calculated behaviour of a specimen of lime cemented silica sand subject to oedometric loading, chemical degradation by seepage of acid at constant vertical stress, and unloading after full degradation.

It can be further shown that, with a convenient set of parameters, the model can describe unstable phenomena. These include compaction bands (Nova (2003), Castellanza and Nova (2003)) or even implosions under isotropic loading and the associated pore pressure build up when drainage is not allowed for (Arroyo et al. (2004)).

## CONCLUSIONS

Although relatively simple and characterised by a limited number of constitutive parameters, the model presented is capable of reproducing the observed behaviour of many different geomaterials: soils (gravel, sand, silt and clay) and soft rocks (calcarenite, tuff, chalk and marl). Clearly, the more complex the fabric of the material or the phenomena one wishes to describe, the larger is the number of parameters. The structure of the model is similar however when passing from 'simple' materials to more complex ones. Despite that, many interesting phenomena can be described. In particular several types of instability (loose sand liquefaction, drained and undrained shear bands, compaction bands in cemented soils, implosion under isotropic loading) are predicted by the model.

## APPENDIX I: NOTATION

*The following symbols are used in this paper:*

- $B_e$  = elastic logarithmic compressibility in isotropic compression
- $B_p$  = plastic logarithmic compressibility in isotropic compression
- $G$  = elastic shear modulus
- $J_{2\eta}$  = second invariant of stress ratio tensor
- $J_{3\eta}$  = third invariant of stress ratio tensor
- $K_0$  = coefficient of earth pressure at rest
- $L$  = elastic shear constant
- $b$  = ratio of stress differences
- $d_f$  = dilatancy at failure
- $e$  = void ratio
- $e_{ij}^P$  = plastic deviatoric strain tensor
- $f$  = loading function
- $g$  = plastic potential
- $p'$  = mean effective stress
- $p^*$  = modified mean effective stress
- $p_c$  = isotropic consolidation pressure of a virgin soil or size measure of the elastic domain for a bonded soil
- $p_{c0}$  = initial value of  $p_c$
- $p_k$  = generic hidden variable
- $p_g$  = dummy parameter of the plastic potential
- $p_m$  = hidden variable related to the strength of the bonds in compression tests
- $p_s$  = hidden variable equivalent to the isotropic consolidation pressure of a virgin soil
- $p_t$  = hidden variable related to the strength of the bonds in tension tests
- $q$  = deviator stress
- $s_{ij}$  = deviator stress tensor
- $v$  = specific volume
- $\Delta\sigma_z$  = vertical stress variation in hollow cylinder test
- $\Lambda$  = plastic multiplier
- $\alpha$  = proportionality constant
- $\beta$  = shape parameter of the yield function
- $\hat{\beta}$  = angle of inclination of major principal stress in the hollow cylinder test
- $\gamma$  = parameter linked to the characteristic state inclination
- $\delta_{hk}$  = Kronecker  $\delta$
- $\varepsilon_d$  = deviator strain
- $\varepsilon_d^P$  = plastic deviator strain
- $\varepsilon_{rs}^P$  = plastic strain tensor
- $\varepsilon_v$  = volumetric strain
- $\varepsilon_v^P$  = plastic volumetric strain
- $\varepsilon_1, \varepsilon_3$  = major and minor principal strains
- $\eta_f$  = stress ratio at failure
- $\eta_{ij}$  = stress ratio tensor

$\eta^*_{ij}$  = modified stress ratio tensor

$\zeta$  = hardening parameter linked to dilatancy

$\rho_t$  = hardening parameter controlling the rate of mechanical degradation

$\sigma'_{ij}$  = effective stress tensor

$\sigma_x'$ ,  $\sigma_y'$ ,  $\sigma_z'$  = effective stress component in horizontal (x,y) and vertical directions

$\phi'$  = friction angle

$\phi_{cv}'$  = friction angle at constant volume

$\psi$  = hardening parameter linked to dilatancy

$\tau_{0z}$  = shear stress in hollow cylinder test

## 1. REFERENCES

- Anagnostopoulos, A.G., N. Kalteziotis, G.k. Tsiambaos & M. Kavvadas (1991). Geotechnical properties of the Corinth Canal marls. *Geot. and Geol. Eng.*, 9, 1-26.
- Arroyo, M., Nova R. and Tsige M. (2004). "Microstructure and compactive instabilities of a stabilised residue" pending publication
- Butterfield, R. (1979). "A natural compression law for soils." *Géotechnique*, 29, 469-480.
- Borja, R. I., Tamagnini, C. (1998). Cam-Clay plasticity, part III: Extension of the infinitesimal model to include finite strains, *Mech. Cohes.-Frict. Mater.*, 155, 73-95.
- Castellanza, R. and Nova, R.(2003). "Compaction bands in oedometric tests on cemented granular soils" *Proc. Int. Symp. Prediction and Simulation Methods in Geomechanics*, Athens, F.Oka, I. Vardoulakis, A. Murakami, & T. Kodaka eds, 37-40
- Castro, G. (1975). Liquefaction and cyclic mobility of saturated sand *Journal of the Geotechnical Engineering Division ASCE* 101, GT6, 551-569
- Coop, M.R. & J.H. Atkinson (1993). The mechanics of cemented carbonate sand. *Géotechnique* 43.
- Desai , C., Somasundaram S. and Frantziskonis G. (1986). A hierarchical approach for constitutive modelling of geologic materials *Int. J. Num. Anal. Meth. Geomech.*, 10 (3), 225-257
- Drucker, D. C., Gibson R. E. and Henkel D. J. (1957). "Soil Mechanics and workhardening theories of plasticity" *Trans. ASCE*, 122, 338-346.
- Gens, A., Nova, R. (1993). "Conceptual bases for a constitutive model for bonded soils and weak rocks." *Proc. Geotechnical Engineering Hard Soils-Soft Rocks*, Athens, Anagnostopoulos et al. Eds., Balkema, Rotterdam, 485-494.
- Kavvadas, M., Anagnostopoulos,A. & Kalteziotis, N., (1993). A framework for the mechanical behaviour of cemented Corinth marl. *Proc. Geotechnical Engineering of Hard Soils-Soft Rocks*, Rotterdam, Balkema, 577-583.
- Imposimato, S. and Nova, R. (1998a). "An investigation on the uniqueness of the incremental response of elastoplastic models for virgin sand" *Mechanics of Cohesive Frictional Materials*, 3, 65-87
- Imposimato S. and Nova R. (1998b). "Instabilities of loose sand specimens in undrained tests" *Localisation and Bifurcation Theory for Soils and Rocks*, Adachi, Oka and Yashima editors, Balkema, 313-322
- Ishihara, K., Tatsuoka, F. and Yasuda, S. (1975). "Undrained deformation and liquefaction of sand under cyclic stresses" *Soils and Foundations* 15, 1, 29-44.
- Kim, M.K. and Lade, P.V. (1984). Modelling rock strength in three dimensions *Int. J. Rock Mech. & Mining Sc.* 21,1, 21-33
- Lade, P.V. (1977). "Elastoplastic stress-strain theory for cohesionless soil with curved yield surfaces" *Int. J. Solids and Structures*, 13, 1019-1035.
- Lade P. V. (1992). "Static instability and liquefaction of loose fine sandy slopes", *Jour. of Geot. Engrg.*, ASCE, Vol. 118, No 1, 51-71
- Lagioia, R. and Nova, R. (1993). "A constitutive model for soft rocks" *Proc. Int.Symp. Geotechnical Engineering of Hard Soils-Soft Rocks*, Athens, A. Anagnostopoulos et al. eds, Balkema, Rotterdam, 625-632

 @Seismicisolation

- Lagioia, R. and Nova, R. (1995). "An experimental and theoretical study of the behaviour of a calcarenous soil in triaxial compression." *Géotechnique*, 45(4), 633-648.
- Lagioia, R., Puzrin, A. M., Potts, D. M. (1996). "A new versatile expression for yield and plastic potential surfaces." *Comp. & Geotechnics*, 19, 171-191.
- Lanier, J. and Zitouni, Z. (1988). "Development of a data base using the Grenoble true triaxial apparatus" in Proc. Int. Conf. *Constitutive Equations for Granular non-cohesive soils*, Cleveland , A. Saada & G. Bianchini eds., Balkema, Rotterdam , 47-58.
- Leedra, M.J.(1988)."Deformation on Chalk through compaction and flow". PhD Thesis, Univ. of London.
- Leroueil, S. and Vaughan, P.R. (1990). "The general and congruent effects of structure in natural soils and weak rocks" *Géotechnique*, 40, 3, 467-488
- Luong M.P. (1980). "Phénomènes cycliques dans les sols pulvérulents" *Revue Française de Géotechnique*, 10, 39-53
- Nova, R. (1977). "On the hardening of soils" *Archiwum. Mechaniki. Stosowanej.* 29, 3, 445-458.
- Nova, R. (1986). "Soil models as a basis for modelling the behaviour of geophysical materials" *Acta Mechanica*, 64, 31-44.
- Nova, R. (1988). "Sinfonietta classica: an exercise on classical soil modelling" Proc. Symp. *Constitutive Equations for Granular non-cohesive soils*, Cleveland , A. Saada & G. Bianchini eds., Balkema, Rotterdam , 501-519.
- Nova, R. (1989). Liquefaction, stability, bifurcations of soil via strain-hardening plasticity. In E.Dembicki, G.Gudehus & Z. Sikora (eds) *Numerical Methods for Localisations and Bifurcations of granular bodies*, Proc. Int. Works. Gdansk, Technical University of Gdansk, 117-132
- Nova, R. (1992). "Mathematical modelling of natural and engineered geomaterials" general lecture 1st E.C.S.M. Munchen, *European J. Mech. A/Solids*, 11, Special issue, 135-154.
- Nova, R. (2000). "Modelling weathering effects on the mechanical behaviour of granite", in *Constitutive Modelling of Granular Materials*, D. Kolymbas editor, Springer, Berlin, 397-411
- Nova, R. (2003). "The failure concept in soil mechanics revisited" in *Bifurcations and Instabilities in Geomechanics*, J.F. Labuz & A. Drescher eds. , Balkema, Lisse, 3-16
- Nova, R. and Castellanza, R., (2001). "Modelling weathering effects on the mechanical behaviour of soft rocks" Golden Jubilee Indian Institute of Science, ICCE 2001, 1, 157-167
- Nova, R., Castellanza, R., Tamagnini, C. (2003). "A constitutive model for bonded geomaterials subject to mechanical and/or chemical degradation." *Int. J. Num. Anal. Meth. Geomech.*, 27(9),705-732
- Nova, R., Castellanza, R. and Tamagnini, C. (2004). A constitutive model for mechanical and thermal loading of bonded geomaterials based on the concept of plasticity with extended hardening, *Proc. NUMOG 9*, Ottawa, G.N.Pande & S. Pietruszczak editors, Swets & Zeitlinger, Lisse,

- Nova, R. and Imposimato, S. (1997). "Non-uniqueness of the incremental response of soil specimens under true-triaxial stress paths" Proc. *VI NUMOG*, Montreal, G.N. Pande and S. Pietruszczak eds, Balkema, 193-197
- Nova, R. and Lagioia, R. (1996). "Soft Rocks: Behaviour and Modelling" Keynote lecture, *Proc. Eurock '96*, Turin, Balkema 2000, 3, 1521-1540
- Nova, R. and Wood, D.M. (1979). "A constitutive model for sand in triaxial compression" *Int. J. Numerical Analytical Methods Geomechanics*, 3(3), 255-278
- Saada A. and Bianchini, G. eds. (1988). *Constitutive Equations for Granular non-cohesive soils*, Cleveland, Balkema, Rotterdam, pag 733.
- Schofield A.N. and Wroth C.P. *Critical State Soil Mechanics*, McGraw Hill
- Shao J. F., Henry J. P. (1991). Development of elastoplastic model for forcesrocks, *Int. J. of Plasticity*, 7, 1, 1-13.
- Vermeer, P. A. (1978). "A double hardening model for sand" *Géotechnique*. 28, 4, 413-433.

## CALIBRATION OF ELASTO-VISCOPLASTIC MODELS FOR COHESIVE SOILS

Fusao Oka<sup>1</sup>, Sayuri Kimoto<sup>2</sup>, and Toshihisa Adachi<sup>3</sup>

**ABSTRACT:** The aim of the present paper is to present a calibration method of an elasto-viscoplastic model for clay. The model discussed herein is an elasto-thermo-viscoplastic model for clay based on the overstress type of theory derived by the authors that can describe plasticity, rate sensitivity and temperature dependency. In the present paper, specification methods of material parameters for rate sensitivity and structural degradation are in particular discussed. In addition the model is validated by the comparison of simulated and experimental results.

### INTRODUCTION

In computational geomechanics and geotechnics, verification and validation of software code such as FE code for the numerical analysis are very important. In the verification and validation process, constitutive model calibration is essential, in which constitutive parameters included in models should be rationally determined by the material tests. Some of the parameters can be determined directly but several parameters need to be determined by the calibration of the model to the laboratory test results. In the present paper, calibration method of elasto-viscoplastic models for cohesive soil and the applicability of models are discussed. The elasto-viscoplastic model for cohesive soils considered here is the model that can describe dilatancy, rate sensitivity, temperature dependency, strain softening and degradation of structure. An elasto-viscoplastic model was derived based on the overstress type elasto-viscoplastic model for clay by Adachi and Oka (1982), and recently, that was extended to describe the effect of temperature by Yashima, Leroueil, Oka and Guntro (1998). Kimoto, Oka and Higo (2004) modified it in order to describe the degradation effect due to microstructure for both

<sup>1</sup>Professor, Dept. of Civil and Earth Resources Eng., Graduate School of Eng., Kyoto University, Kyoto 606-8501, Japan, E-mail: foka@nakisuna.kuciv.kyoto-u.ac.jp

<sup>2</sup>Research Associate, Dept. of Civil and Earth Resources Eng., Graduate School of Eng., Kyoto University, E-mail: kimoto@nakisuna.kuciv.kyoto-u.ac.jp

<sup>3</sup>Principal Director, Geo-Research Institute, Osaka, Japan

normally and overconsolidated clay. The method of determination of material parameters is presented and the applicability of the model is validated with the comparison of simulated results and experimental data.

## ELASTO-VISCOPLASTIC MODEL FOR CLAY

In the present study, the concept of Terzaghi's effective stress for water-saturated soil is used as

$$\sigma_{ij} = \sigma'_{ij} + u_w \delta_{ij} \quad (1)$$

where  $\sigma_{ij}$  is the total stress tensor,  $\sigma'_{ij}$  is the effective stress tensor,  $u_w$  is the pore water pressure, and  $\delta_{ij}$  is Kronecker's delta. It is assumed that the strain rate tensor consists of an elastic strain rate tensor and a viscoplastic strain rate tensor, so that

$$\dot{\varepsilon}_{ij} = \dot{\varepsilon}_{ij}^e + \dot{\varepsilon}_{ij}^{vp} \quad (2)$$

Elastic strain rate  $\dot{\varepsilon}_{ij}^e$  can be broken down into

$$\dot{\varepsilon}_{ij}^e = \dot{\varepsilon}_{ij}^e + \frac{1}{3} \dot{\varepsilon}_v^e \delta_{ij} = \frac{1}{2G} \dot{S}_{ij} + \frac{1}{3} \frac{\kappa}{1+e_0} \frac{\dot{\sigma}'_m}{\sigma'_m} \delta_{ij} \quad (3)$$

where  $\dot{\varepsilon}_{ij}^e$  is the deviatoric component of the elastic strain rate tensor and  $\dot{\varepsilon}_v^e$  is the elastic volumetric strain rate ( $\dot{\varepsilon}_v^e = \dot{\varepsilon}_{11}^e + \dot{\varepsilon}_{22}^e + \dot{\varepsilon}_{33}^e$ ).  $S_{ij}$  is the deviatoric stress tensor ( $S_{ij} = \sigma'_{ij} - \sigma'_m \delta_{ij}$ ), and the superimposed dot denotes the time differentiation, and  $\sigma'_m$  denotes the mean effective stress ( $\sigma'_m = \frac{1}{3} \sigma'_{kk}$ ).  $\kappa$  is the swelling index determined by the slope of the volumetric unloading curve on the natural logarithmic scale, and  $e_0$  is the initial void ratio.  $G$  is the elastic shear coefficient, which is assumed to be proportional to  $\sqrt{\sigma'_m}$  as

$$G = G_0 \sqrt{\frac{\sigma'_m}{\sigma'_{m0}}} \quad (4)$$

in which  $G_0$  is the value of  $G$  when  $\sigma'_m$  is the initial mean effective stress of  $\sigma'_{m0}$ .

## Overconsolidation (OC) Boundary Surface

In the constitutive model for overconsolidated soils proposed by Adachi and Oka (1984), it is assumed that an overconsolidation (OC) boundary surface exists which delineates the OC region ( $f_b < 0$ ) from the normal consolidated (NC) region ( $f_b \geq 0$ ). In previous papers (Adachi and Oka 1984; Oka 1992; Oka et al. 1999), a similar OC boundary surface was used in an elasto-plastic model for sand and overconsolidated clay. The OC boundary surface was introduced to control the value of  $M^*$  in the plastic potential function and the yield function.

$$f_b = \bar{\eta}_{(0)}^* + M_m^* \ln(\sigma'_m / \sigma'_{mb}) = 0 \quad (5)$$

where  $\bar{\eta}_{(0)}^*$  is the relative stress ratio defined by

$$\bar{\eta}_{(0)}^* = \left\{ (\eta_{ij}^* - \eta_{ij(0)}^*) (\eta_{ij}^* - \eta_{ij(0)}^*) \right\}^{1/2} \quad (6)$$

 @Seismicisolation

in which (0) denotes the initial state before deformation occurs.  $\eta_{ij}^*$  is the stress ratio tensor ( $\eta_{ij}^* = \frac{S_{ij}}{\sigma_m^*}$ ) and  $M_m^*$  is the value of  $\eta^* = \sqrt{\eta_{ij}^* \eta_{ji}^*}$  when the volumetric strain increment changes from compression to expansion.  $\sigma'_{mb}$  is the hardening parameter which controls the size of the surface. Regarding the structured soil, which has been affected by chemical bonding, secondary consolidation, etc., namely, the aging effect, the consolidation yield stress exceeds the largest stress that the soil has ever suffered. That is called quasi-overconsolidated soil. Therefore, it is appropriate to define the quasi-overconsolidation ratio as the ratio of consolidation yield stress  $\sigma'_{mbi}$  to the mean effective stress at the end of consolidation  $\sigma'_{m0}$ , that is,  $OCR^* = \sigma'_{mbi}/\sigma'_{m0}$ .

Originally, the hardening rule for the OC boundary surface was defined with respect to the viscoplastic volumetric strain as

$$\sigma'_{mb} = \sigma'_{mbi} \exp \left( \frac{1 + e_0}{\lambda - \kappa} \varepsilon_v^{vp} \right) \quad (7)$$

where  $\sigma'_{mbi}$  is the initial value of  $\sigma'_{mb}$ , which is defined as the isotropic consolidation yield stress.  $\varepsilon_v^{vp}$  is the viscoplastic volumetric strain,  $\lambda$  and  $\kappa$  are the compression and the swelling index which are determined by the slope of the volumetric loading and unloading, respectively, on the natural logarithmic scale, and  $e_0$  is the initial void ratio.

In order to describe the degradation of the material caused by structural changes, strain-softening with the viscoplastic strain is introduced (Kimoto et al. 2004) in addition to the hardening with the viscoplastic volumetric strain as

$$\sigma'_{mb} = \sigma'_{ma} \exp \left( \frac{1 + e_0}{\lambda - \kappa} \varepsilon_v^{vp} \right) \quad (8)$$

in which  $\sigma'_{ma}$  is assumed to decrease with an increasing viscoplastic strain as

$$\sigma'_{ma} = \sigma'_{maf} + (\sigma'_{mai} - \sigma'_{maf}) \exp(-\beta z) \quad (9)$$

where  $z$  is an accumulation of the second invariant of the viscoplastic strain rate.

$$z = \int_0^t \dot{z} dt \quad (10)$$

$$\dot{z} = \left( \dot{\varepsilon}_{ij}^{vp} \dot{\varepsilon}_{ij}^{vp} \right)^{\frac{1}{2}} \quad (11)$$

$\sigma'_{mai}$  is the value of  $\sigma'_{ma}$  when no viscoplastic deformation occurs, and it coincides with  $\sigma'_{mbi}$  in the original model.  $\sigma'_{maf}$  is the final values of  $\sigma'_{ma}$ , and determined from the difference between peak stress and residual stress.  $\beta$  is a parameter which denotes the degradation rate of  $\sigma'_{ma}$ . Hence, two independent parameters,  $\sigma'_{maf}$  and  $\beta$ , are introduced to describe the soil structures. The ratio of  $\sigma'_{maf}$  to  $\sigma'_{mai}$ , namely,

$$n = \sigma'_{maf}/\sigma'_{mai} \quad (12)$$

provides the degree for a possible collapse of the structure at the initial state.

## Static Yield Function

The mechanical behavior of clay at its static equilibrium state is assumed to be described by the original Cam-clay model (Adachi and Oka 1982). The following static yield function is used as

$$f_y = \bar{\eta}_{(0)}^* + \tilde{M}^* \ln \frac{\sigma'_m}{\sigma'_{my}} = 0 \quad (13)$$

$$\bar{\eta}_{(0)}^* = \left\{ \left( \eta_{ij}^* - \eta_{ij(0)}^* \right) \left( \eta_{ij}^* - \eta_{ij(0)}^* \right) \right\}^{1/2} \quad (14)$$

In the above equation,  $\sigma'_{my}$  denotes the mean effective stress in the static equilibrium state, where stress may be reached after an infinite period of time. Accordingly,  $f_y = 0$  represents the static state in which no viscoplastic deformation occurs. Considering volumetric strain hardening, the hardening rule of  $\sigma'_{my}$  was originally given as follows:

$$\sigma'_{my} = \sigma'_{myi} \exp \left( \frac{1 + e_0}{\lambda - \kappa} \varepsilon_v^{vp} \right) \quad (15)$$

In a similar way for OC boundary surface, strain-softening is defined in order to express the effect of a structural collapse through changes in  $\sigma'_{my}$  with the viscoplastic strain.

$$\sigma'_{my} = \{n + (1 - n) \exp(-\beta z)\} \sigma'_{myi} \exp \left( \frac{1 + e_0}{\lambda - \kappa} \varepsilon_v^{vp} \right) \quad (16)$$

The decrease in  $\sigma'_{my}$ , defined by Eq. 16, leads to the shrinking of the static yield function according to the structural degradation.

## Viscoplastic Potential Function

The viscoplastic potential function is given as follows:

$$f_p = \bar{\eta}_{(0)}^* + \tilde{M}^* \ln \frac{\sigma'_m}{\sigma'_{mp}} = 0 \quad (17)$$

where  $\tilde{M}^*$  is assumed to be constant in the NC region ,and varies with the current stress and  $\sigma'_{mc}$  in the OC region as

$$\tilde{M}^* = \begin{cases} M_m^* & : f_b \geq 0 \\ -\frac{\sqrt{\eta_{ij}^* \eta_{ij}^*}}{\ln(\sigma'_m / \sigma'_{mc})} & : f_b < 0 \end{cases} \quad (18)$$

where  $\sigma'_{mc}$  denotes the mean effective stress at the intersection of the overconsolidation boundary surface and the  $\sigma'_m$  axis as

$$\sigma'_{mc} = \sigma'_{mb} \exp \frac{\sqrt{\eta_{ij(0)}^* \eta_{ij(0)}^*}}{M_m^*} \quad (19)$$



In the case of isotropic consolidation,  $\sigma'_{mc}$  equals  $\sigma'_{mb}$ . The overconsolidation boundary surface,  $f_b = 0$ , the static yield surface,  $f_y = 0$ , and the viscoplastic potential surface  $f_p = 0$ , for  $\eta_{ij(0)}^* = 0$ , are illustrated in the  $\sigma'_m - \sqrt{S_{ij}S_{ij}}$  space in FIG. 1 for the NC region and in FIG. 2 for the OC region, respectively.  $\sigma'_{mb}$  and  $\sigma'^{(s)}_{my}$  decrease with an increasing viscoplastic strain. Although the inside of the static yield function is defined as the elastic region, the initial value of  $\sigma'^{(s)}_{myi}$ , which is included in parameter  $C_0$  introduced later, is assumed to be very small, so that the current stress state is always outside of the static yield function. The static yield function as well as the potential surface is transformed smoothly between the OC and the NC regions, so that calculations can be conducted continuously without interruption.

### Viscoplastic Flow Rule

Viscoplastic strain rate tensor  $\dot{\varepsilon}_{ij}^{vp}$  is given as the following equation based an overstress type of viscoplastic theory.

$$\dot{\varepsilon}_{ij}^{vp} = \gamma \langle \Phi_1(f_y) \rangle \frac{\partial f_p}{\partial \sigma'_{ij}} \quad (20)$$

where the symbol  $\langle \rangle$  is defined as

$$\langle \Phi_1(f_y) \rangle = \begin{cases} \Phi_1(f_y) & ; f_y > 0 \\ 0 & ; f_y \leq 0 \end{cases} \quad (21)$$

in which  $\Phi_1$  denotes a material function for rate sensitivity. In Eq. 21,  $\Phi_1$  is the function of  $f_y$  although Perzyna used normalized yield function (Perzyna, 1963). In the present study, since  $f_y$  is non dimensional, it is not necessary to use normalized yield function. Based on the experimental results of the strain-rate constant triaxial tests (Adachi and Oka 1982), material function  $\Phi_1$  is defined by an exponential function.

$$\begin{aligned} \gamma \Phi_1(f_y) &= C' \sigma'_m \exp \left\{ m' \left( \bar{\eta}_{(0)}^* + \tilde{M}^* \ln \frac{\sigma'_m}{\sigma'^{(s)}_{my}} \right) \right\} \\ &= C' \sigma'_m \exp \left( m' \tilde{M}^* \ln \frac{\sigma'_{mai}}{\sigma'^{(s)}_{myi}} \right) \exp \left\{ m' \left( \bar{\eta}_{(0)}^* + \tilde{M}^* \ln \frac{\sigma'_m}{\sigma'_{ma} \exp(A_3 \dot{\varepsilon}_v^{vp})} \right) \right\} \\ &= C_0 \sigma'_m \exp \left\{ m' \left( \bar{\eta}_{(0)}^* + \tilde{M}^* \ln \frac{\sigma'_m}{\sigma'_{ma} \exp(A_3 \dot{\varepsilon}_v^{vp})} \right) \right\} \end{aligned} \quad (22)$$

$$C_0 = C' \exp \left( m' \tilde{M}^* \ln \frac{\sigma'_{mai}}{\sigma'^{(s)}_{myi}} \right) \quad (23)$$

where,  $C_0$  is the viscoplastic parameter,  $A_3 = \frac{1+e_0}{\lambda-\kappa}$ . Substituting Eq. 22 into Eq. 20 gives the viscoplastic strain rate as

$$\dot{\varepsilon}_{ij}^{vp} = C_0 \sigma'_m \exp \left\{ m' \left( \bar{\eta}_{(0)}^* + \tilde{M}^* \ln \frac{\sigma'_m}{\sigma'_{mb}} \right) \right\} \frac{\partial f_p}{\partial \sigma'_{ij}} \quad (24)$$

Finally the viscoplastic deviatoric strain rate and the viscoplastic strain rate are obtained as follows:

$$\dot{\epsilon}_{ij}^{vp} = C_0 \exp \left\{ m' \left( \bar{\eta}_{(0)}^* + \tilde{M}^* \ln \frac{\sigma'_m}{\sigma'_{mb}} \right) \right\} \frac{\eta_{ij}^* - \eta_{ij(0)}^*}{\bar{\eta}_{(0)}^*} \quad (25)$$

$$\dot{\epsilon}_v^{vp} = C_0 \exp \left\{ m' \left( \bar{\eta}_{(0)}^* + \tilde{M}^* \ln \frac{\sigma'_m}{\sigma'_{mb}} \right) \right\} \left( \tilde{M}^* - \frac{\eta_{ij}^* (\eta_{ij}^* - \eta_{ij(0)}^*)}{\bar{\eta}_{(0)}^*} \right) \quad (26)$$

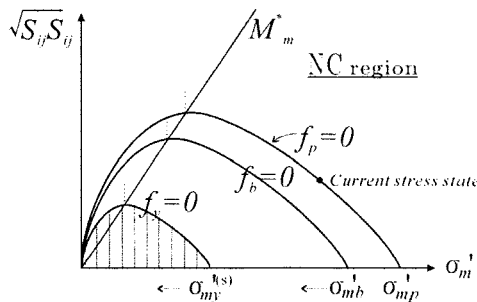


FIG. 1: OC Boundary Surface, Static Yield Surface, and Potential Surface in the NC Region

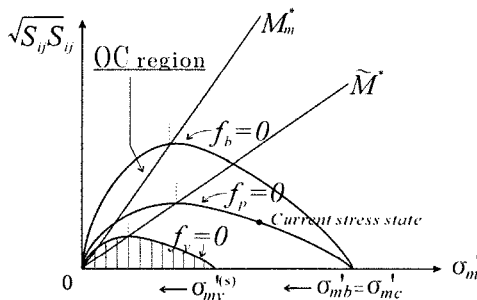


FIG. 2: OC Boundary Surface, Static Yield Surface, and Potential Surface in the OC Region

## DETERMINATION OF THE MATERIAL PARAMETERS

In the present study we will discuss about the calibration method of elasto-viscoplastic models, namely determination of material parameters. We will only consider the elasto-viscoplastic model for clay under monotonic loading conditions.

Given below are the ten material parameters for the proposed equations.

**@Seismicisolation**

- Initial void ratio  $e_0$ , compression index  $\lambda$ , and swelling index  $\kappa$
- Elastic shear modulus  $G_0$
- Compression yield stress  $\sigma'_{mbi}$
- Stress ratio at maximum compression  $M_m^*$
- Viscoplastic parameters  $m'$  and  $C_0$
- Structural parameters  $\sigma'_{maf}$  and  $\beta$

The procedure for determining these parameters is as follows. Initial void ratio  $e_0$  can be obtained from tests for physical properties. Compression index  $\lambda$  and swelling index  $\kappa$  are given by the slope of the isotropic consolidation and the swelling tests, respectively. Compression yield stress  $\sigma'_{mbi}$  is assumed to be determined from the yield point of the isotropic consolidation tests.

Elastic shear modulus  $G_0$  can be determined from the initial slope of the undrained triaxial compression tests as

$$G_0 = \frac{1}{3} \frac{\Delta q}{\Delta \varepsilon_{11}} \quad (27)$$

or the drained triaxial compression tests as

$$G_0 = \frac{1}{3} \frac{\Delta q}{\Delta e_{11}} \quad (28)$$

where  $\Delta q$  is the increment in the deviator stress, namely,  $q = \sigma'_{11} - \sigma'_{33}$ ,  $\Delta \varepsilon_{11}$  is the increment in the axial strain, and  $\Delta e_{11}$  is the increment in the deviatoric strain, namely,  $e_{11} = \varepsilon_{11} - \varepsilon_v/3$ .

Other material parameters are determined from undrained triaxial compression tests. The stress ratio at maximum compression  $M_m^*$  is defined as the stress ratio whereby maximum compression occurs in the drained compression tests. For clay, however, it has been assumed to equal the stress ratio at the critical state. Herein,  $M_m^*$  is determined from the stress ratio at the residual state in the undrained triaxial compression tests.

### Viscoplastic Parameters

Viscoplastic parameter  $m'$  can be determined from undrained triaxial compression tests with different strain rates. From Eq. 25, viscoplastic deviatoric strain rate  $\dot{\varepsilon}_{11}^{vp}$  in triaxial stress state is obtained as

$$\dot{\varepsilon}_{11}^{vp} = \sqrt{\frac{2}{3}} C_0 \exp \left\{ m' \left( \sqrt{\frac{2}{3}} \frac{q}{\sigma'_m} + \tilde{M}^* \ln \frac{\sigma'_m}{\sigma'_{mb}} \right) \right\} \quad (29)$$

Considering the undrained conditions, and assuming that the elastic strain rate is negligible, we obtain  $\dot{\varepsilon}_{11}^{vp} = \dot{\varepsilon}_{11}$ . When undrained triaxial tests with different strain rates  $\dot{\varepsilon}_{11}^{(1)}$  and  $\dot{\varepsilon}_{11}^{(2)}$  are performed, the following equations are obtained at the point where the mean

effective stress takes the same value in the stress path (see FIG. 3). Note that the volumetric viscoplastic strain takes the same value when the effective stress is the same, however, the deviatoric component of the viscoplastic strain at the point is different with the strain rate. We should take the point where the difference in an accumulation of the second invariant of the viscoplastic strain rate of  $z$  in Eq. 10, consequently, the difference in the value of  $\sigma'_{ma}$  in Eq. 9, is small.

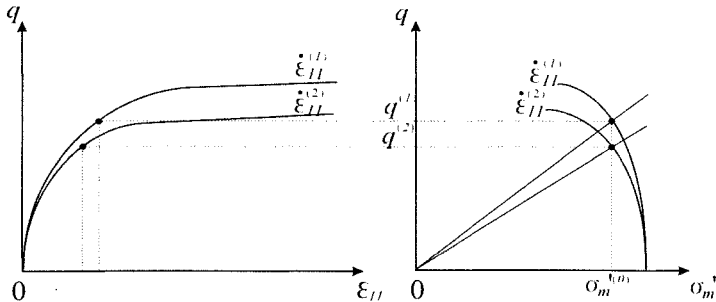


FIG. 3: Determination of Parameter  $m'$

$$\frac{\dot{\varepsilon}_{11}^{(1)}}{\dot{\varepsilon}_{11}^{(2)}} = \exp \left\{ m' \sqrt{\frac{2}{3}} \left( \left( \frac{q}{\sigma'_m} \right)^{(1)} - \left( \frac{q}{\sigma'_m} \right)^{(2)} \right) \right\} \quad (30)$$

$$m' = \sqrt{\frac{3}{2} \frac{\ln \dot{\varepsilon}_{11}^{(1)} - \ln \dot{\varepsilon}_{11}^{(2)}}{\left( \frac{q}{\sigma'_m} \right)^{(1)} - \left( \frac{q}{\sigma'_m} \right)^{(2)}}} \quad (31)$$

When  $m'$  is determined, viscoplastic parameter  $C_0$  is obtained from Eq. 29. The determination of structural parameters  $\sigma'_{maf}$  and  $\beta$  will be discussed in the next section.

Under isotropic conditions,  $\eta_{(0)}^*$  is zero. If  $\sigma'_{ma} = \sigma'_{mai} = \sigma'_m$  (current value of mean effective stress) at the initial state, the stress state is in the normally consolidated region;  $\tilde{M}^* = M^*$ . Hence,

$$\begin{aligned} \dot{\varepsilon}_{kk}^{vp} &= C' \exp \left[ m' \left( M^* \ln \frac{\sigma'_m}{\sigma'_{my}} \right) \right] = C_0 \exp \left[ m' \left( M^* \ln \frac{\sigma'_m}{\sigma'_{mb}} \right) \right] \\ &= C_0 \exp \left[ m' \left( M^* \ln \frac{\sigma'_m}{\sigma'_{ma}} - M^* A_3 \dot{\varepsilon}_{kk}^{vp} \right) \right] = C_0 \exp (-m' M^* A_3 \dot{\varepsilon}_{kk}^{vp}) \end{aligned} \quad (32)$$

where  $A_3 = \frac{1+\epsilon}{\lambda-\kappa}$ . When the initial value of viscoplastic volumetric strain  $\dot{\varepsilon}_{kk}^{vp} = 0$ ,  $\dot{\varepsilon}_{kk}^{vp} = C_0$ .

From discussed above, the viscoplastic volumetric strain rate is given by

$$\dot{\varepsilon}_{kk}^{vp} = C_0 \exp (-m' M^* A_3 \dot{\varepsilon}_{kk}^{vp}) \quad (33)$$

It is easily shown that the above differential equation has the following solution as

$$\varepsilon_{kk}^{vp} = \alpha \ln(t/t_{(0)}) + \varepsilon_{kk(0)}^{vp} \quad (34)$$

where  $\alpha = \frac{\lambda - \kappa}{m' M^*(1+e)}$ , and  $\varepsilon_{kk(0)}^{vp}$  is the value of  $\varepsilon_{kk}^{vp}$  at  $t = t_{(0)}$ .

This type of solution is the well-known relation between the viscoplastic strain and time during the secondary compression process and  $\alpha$  is the rate of secondary compression. This means that the viscoplastic parameters  $C_0$  and  $m'$  are related to the initial viscoplastic volumetric strain rate and the rate of secondary compression.

### Temperature-dependent Viscoplastic Parameter

Based on the experimental data by Boudali et al. (1994), Yashima et al. (1998) showed the following relation between consolidation yield stress  $\sigma'_p$  and temperature  $\theta$ :

$$\frac{\sigma'_p}{\sigma'_{pr}} = \left[ \frac{\theta_r}{\theta} \right]^A \quad (35)$$

in which  $\sigma'_{pr}$  is the value of  $\sigma'_p$  at the referential temperature  $\theta_r$  and  $A$  is the gradient of the line  $\log \sigma'_p - \log \theta$ .

If the stress ratio during one-dimensional compression is assumed to be constant and the initial hardening parameter  $\sigma_{my}^{(s)}$  is linearly proportional to the consolidation yield stress  $\sigma'_p$ , the temperature-dependent viscoplastic parameter  $C(\theta)$  is rewritten from Eq. 22 as

$$C(\theta) = C' \exp \left\{ m' \tilde{M}^* \left( -\ln \left[ \frac{\sigma'_p}{\sigma'_0} \right] \right) \right\} \quad (36)$$

Substituting Eq. 35 into Eq. 36 yields

Table 1: Material Parameters

Parameters	NC clay	OCR 2.0	OCR 5.9
Elastic shear modulus $G_0$ (kPa)	31600	22500	13000
Compression index $\lambda$		0.508	
Swelling index $\kappa$		0.0261	
Initial void ratio $e_0$		1.70	
Compression yield stress $\sigma'_{mbi}$ (kPa)		580	
Stress ratio at maximum compression $M_m^*$		1.09	
Viscoplastic parameter $m'$		18.5	
Viscoplastic parameter $C_0$ (1/s)	$1.3 \times 10^{-13}$	$4.0 \times 10^{-13}$	$1.0 \times 10^{-10}$

$$C(\theta) = C(\theta_r) \exp \left\{ m' \tilde{M}^* \left( -\ln \left[ \frac{\theta_r}{\theta} \right]^A \right) \right\}, \quad C(\theta_r) = C' \exp \left\{ m' \tilde{M}^* \left( -\ln \left[ \frac{\sigma'_{pr}}{\sigma'_0} \right] \right) \right\} \quad (37)$$

where  $\sigma'_0$  is preconsolidation stress. From Eq. 37, temperature dependency of viscoplastic parameter  $C$  is obtained as follows:

$$\frac{C(\theta)}{C(\theta_r)} = \left[ \frac{\theta}{\theta_r} \right]^B, \quad B = Am' \tilde{M}^* \quad (38)$$

in which coefficient of dilatancy  $\tilde{M}^*$  is a function of stress ratio in the OC region (see Eq. 18). However, thermo-viscoplastic parameter  $B$  is independently determined as material constant. This corresponds to the fact that Boudali et al. (1994) have found that  $m'$ , the viscoplastic parameter, is independent of the temperature.

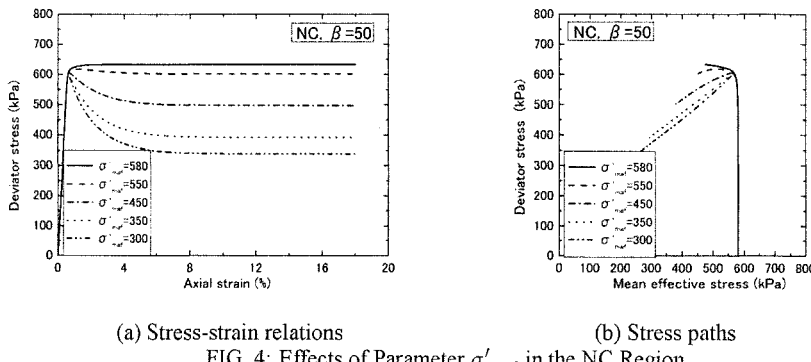


FIG. 4: Effects of Parameter  $\sigma'_{maf}$  in the NC Region

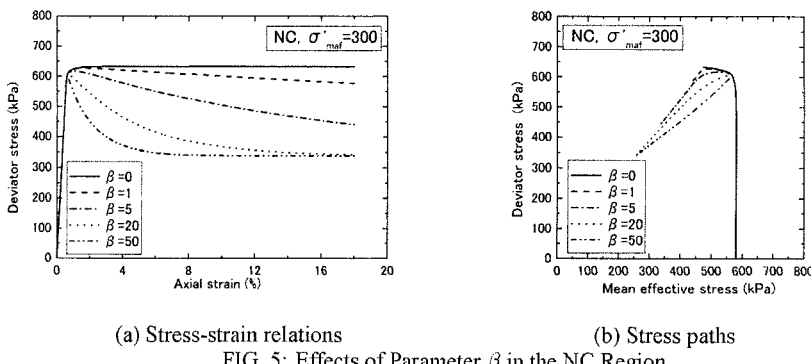
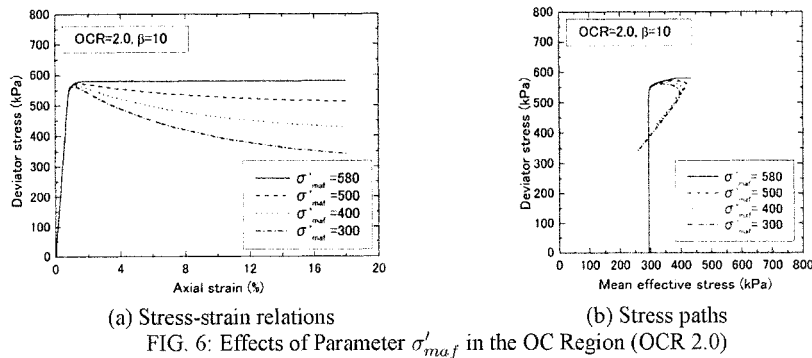
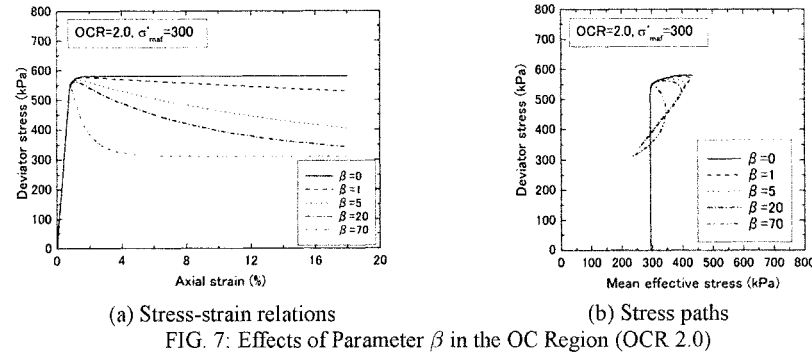


FIG. 5: Effects of Parameter  $\beta$  in the NC Region



(a) Stress-strain relations

(b) Stress paths

FIG. 6: Effects of Parameter  $\sigma'_{maf}$  in the OC Region (OCR 2.0)

(a) Stress-strain relations

(b) Stress paths

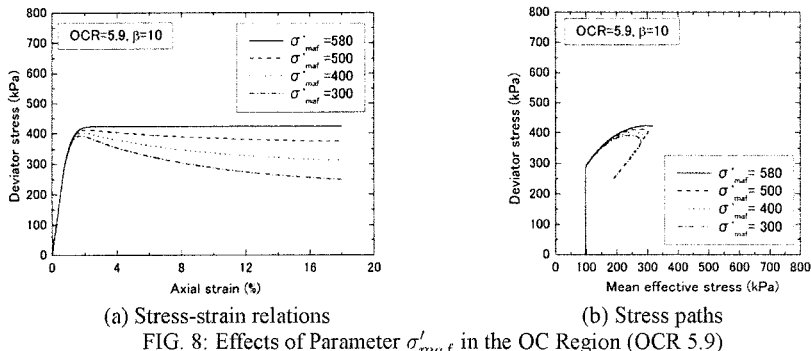
FIG. 7: Effects of Parameter  $\beta$  in the OC Region (OCR 2.0)

## PARAMETRIC STUDY OF THE STRUCTURAL PARAMETERS

Simulations of undrained triaxial tests are conducted to investigate the performance of the model including dilatancy characteristics and stress-strain relations in both NC and OC regions. In particular the effects of structural parameters  $\sigma'_{maf}$  and  $\beta$  are studied.

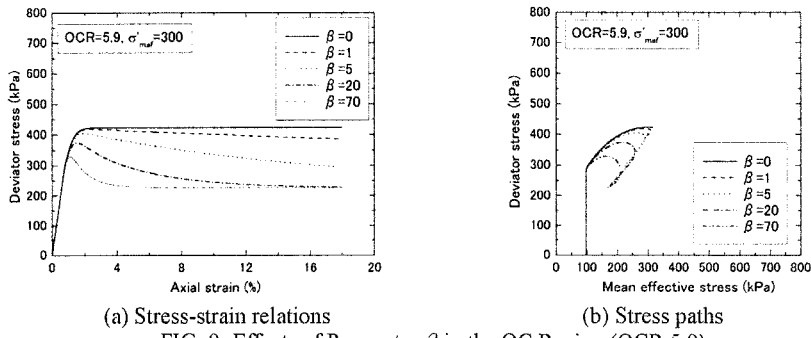
Numerical simulations of undrained triaxial compression tests are conducted using Runge-Kutta method, by giving incompressive strain rates under the triaxial stress state. An axial strain rate of  $\dot{\epsilon}_{11}=0.005\%/\text{min}$  is provided for all calculations.

The effects of structural parameters  $\sigma'_{maf}$  and  $\beta$  are firstly examined in the NC region. Parametric studies on the changes in  $\sigma'_{maf}$  are shown in FIG. 4.  $\beta$  is set to be 50 in all calculations. The remaining soil parameters are listed in Table 1. FIG. 4 (a) shows the relationships between the axial strain  $\epsilon_{11}$  and the deviator stress  $\sigma'_{11} - \sigma'_{33}$ , and FIG. 4 (b) shows the relationships between the mean effective stress  $\sigma'_m$  and the deviator stress. From FIG. 4, it is confirmed that parameter  $\sigma'_{maf}$  controls the degree of the decline in peak stress. In the original model, which corresponds to the case of  $\sigma'_{maf} = 580 (= \sigma'_{mas})$ , the stress state remains constant in a residual state. The smaller the value of  $\sigma'_{maf}$  becomes, the lower the residual stress becomes. FIG. 5 shows the



(a) Stress-strain relations

(b) Stress paths

FIG. 8: Effects of Parameter  $\sigma'_{maf}$  in the OC Region (OCR 5.9)

(a) Stress-strain relations

(b) Stress paths

FIG. 9: Effects of Parameter  $\beta$  in the OC Region (OCR 5.9)

effect of  $\beta$  in the NC region. The material parameters used in the calculations are the same as those listed in Table 1. In the calculations,  $\sigma'_{maf}$  is set to be 300 kPa. FIG. 5 confirms that  $\beta$  determines the rate of the degradation of strain-softening. The larger the  $\beta$  value becomes, the faster the stress state reaches the residual state. In other words, the rate of decrease in stress is large in small strain when the value of  $\beta$  is large, in contrast, the rate is large in large strain when the value of  $\beta$  is small.

Similarly parametric studies for  $\sigma'_{maf}$  and  $\beta$  are conducted in the overconsolidated regions of OCR=2.0 and 5.9. The material parameters for the overconsolidated soils are listed in Table 1. The parametric studies of  $\sigma'_{maf}$  and  $\beta$  for OCR=2.0 are shown in FIGS. 6 and 7, respectively. The effects of the structural parameters are similar to those obtained in the NC region. The parametric studies of the structural parameters for OCR=5.9 are shown in FIGS. 8 and 9, respectively. These results reveals that structural parameter  $\sigma'_{maf}$  provides the residual state of the soil, which is related to the degree of initial structure, while  $\beta$  controls the rate of collapse of the structure.

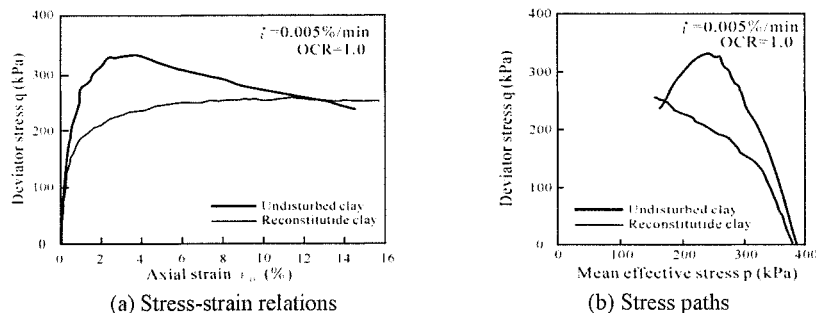


FIG. 10: Experiments of undrained triaxial tests for Kyuhoji clay (Yashima et al. 1999)

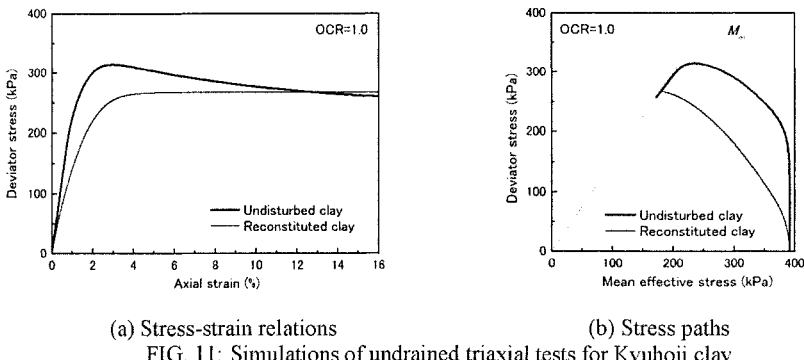


FIG. 11: Simulations of undrained triaxial tests for Kyuhoji clay

## APPLICATION TO EXPERIMENTAL DATA

The model is applied to Osaka Pleistocene clay, namely, Kyuhoji clay. That is sampled from the upper Pleistocene layer called Ma12, which is distributed widely in the western and eastern part of Osaka at a depth of 20-40 meters (Shigematsu 2002). These are marine clays containing diatoms, and exhibit sensitive behavior, which is due to the effect of structures formed during the sedimentation process.

FIG. 10 compares the undrained compression test results between undisturbed and reconstituted samples for Kyuhoji clay (Yashima et al. 1999). Both of undisturbed and reconstituted clays were sheared with an axial strain rate of  $0.005\%/\text{min}$  after isotropically consolidated with a confining pressure of 392 kPa, which is a little larger than the compression yield stress of 340 kPa. The initial void ratio of the undisturbed clay is larger than that of the reconstituted clay, specifically, 1.41 for the undisturbed clay and 1.02 for the reconstituted clay. The undisturbed clay exhibits larger strength and the deviator stress decreases after the peak stress in FIG. 10.

FIG. 11 shows the results of simulations. The temperature-dependency is not considered in the following simulations. The material parameters used in the simulations are shown in Table 2. The structural parameter  $\sigma'_{maf}$  is set to be 280 kPa for the undis-

Table 2: Material parameters for Kyuhoji clay

Parameters	Undisturbed	Reconstituted
Elastic shear modulus $G_0$ (kPa)	8333	6330
Compression index $\lambda$	0.327	
Swelling index $\kappa$	0.028	
Initial void ratio $e_0$	1.41	1.02
Compression yield stress $\sigma'_{mbi} (= \sigma'_{mai})$ (kPa)	392	
Stress ratio at maximum compression $M_m^*$	1.22	
Viscoplastic parameter $m'$	21.5	
Viscoplastic parameter $C_0$ (l/s)	$4.5 \times 10^{-11}$	$2.5 \times 10^{-8}$
Structural parameter $\sigma'_{maf}$ (kPa)	280	392
Structural parameter $\beta$	10	0

turbed clay, and  $\beta$  is set to be 10 for the undisturbed clay and 0 for reconstituted clay.  $\beta=0$  provides the original model which does not describe structural changes. The values of  $C_0$  contains  $\sigma'^{(s)}_{myi}$  concerning the degree of initial structures in the derivation (Eq. 23). Since the degree of the initial structure of the reconstituted clay is considered lower than the undisturbed clay, the larger value of  $C_0$  is given for the reconstituted clay. FIG. 11 confirms that the proposed model can describe the difference in the behavior between the high structured and the low structured soils.

## CONCLUSIONS

The calibration method for an elasto-viscoplastic constitutive model for cohesive soils is presented, and the effect of the viscoplastic parameters and the structural parameters is discussed in detail. It is shown that the viscoplastic parameter  $m'$  is related to the rate of secondary compression, and the viscoplastic parameter  $C_0$  describes the initial viscoplastic volumetric strain rate under isotropic consolidation. The parametric study of the structural parameters reveals that structural parameter  $\beta$  provides the residual state of the soil, and  $\sigma'_{maf}$  controls the rate of degradation of the soil structure. The application to the triaxial tests for Pleistocene clay indicates that the model can well describe the different behavior between structured and reconstituted clays.

**REFERENCES**

- Adachi, T. and Okano, M. (1974). "A constitutive equation for normally consolidated clay", *Soils and Foundations*, 14 (4), 55-73.
- Adachi, T. and Oka, F. (1982). "Constitutive equations for normally consolidated clay based on elasto-viscoplasticity", *Soils and Foundations*, 22 (4), 55-70.
- Adachi, T. and Oka, F. (1984). "Constitutive equations for sands and overconsolidated clays and assigned works for sand", *Proc. Int. Workshop on Constitutive Relations for soils* (ed. by Gudehus, G., Darve, F. and Vardoulakis, I.), 6-8 September 1982, Grenoble, Balkema, 141-157.
- Boudali, M., Leroueil, S. and Srinivasa Murthy, B.R. (1994), "Viscous behaviour of natural clays", *Proc. 13th ICSMFE*, New Delhi, 1, 411-416.
- Kimoto, S. (2002). "Constitutive models for geomaterials considering structural changes and anisotropy", Doctoral thesis, Kyoto University, Japan.
- Kimoto, S., Oka, F. and Higo, Y. (2004). "Strain localization analysis of elasto-viscoplastic soil considering structural degradation", *Computer Methods in Applied Mechanics and Engineering*, 193, 2845-2866.
- Oka, F. (1981). "Prediction of time-dependent behaviour of clay", *Proc. 10th Int. Conf. on Soil Mech. and Foundation Engrg.*, 15-19 June, Stockholm, Balkema, 1, 215-218.
- Oka, F. (1992). "A cyclic elasto-viscoplastic constitutive model for clay based on the non-linear-hardening rule", *Proc. 4th Int. Symp. on Numerical Models in Geomechanics* (ed. by Pande, G.N. and Pietruszczak, S.), 24-27 August, Swansea, UK, Balkema, 1, 105-114.
- Oka, F., Yashima, A., Tateishi, A., Taguchi, Y. and Yamashita, S. (1999). "A cyclic elasto-plastic constitutive model for sand considering a plastic-strain dependence of the shear modulus", *Géotechnique*, 49 (5), 661-680.
- Perzyna, P. (1963). "The constitutive equations for work-hardening and rate sensitive plastic materials", *Proc. Vibrational Problems*, Warsaw, 4 (3), 281-290.
- Shigematsu, H. (2002). "Study on the microstructure and mechanical behavior of natural sedimentary soils with aging effect", Doctoral thesis, Gifu University, Japan (in Japanese).
- Yashima, A., Leroueil, S., Oka, F. and Guntro, I. (1998). "Modelling temperature and strain rate dependent behavior of clays: one dimensional consolidation", *Soils and Foundations*, 38 (2), 63-73.
- Yashima, A., Shigematsu, H., Oka, F. and Nagaya, J. (1999). "Mechanical behavior and micro-structure of Osaka upper-most Pleistocene marine clay", *J. Geotech. Engrg.*, 624 (3-47), 217-229 (in Japanese).

## CALIBRATION OF A SIMPLE ANISOTROPIC PLASTICITY MODEL FOR SOFT CLAYS

Achilleas G. Papadimitriou<sup>1</sup>, Majid T. Manzari<sup>2</sup>, Yannis F. Dafalias<sup>3</sup>

**ABSTRACT:** This paper presents the calibration process of a recently proposed simple anisotropic plasticity model, which provides successful simulation of the rate-independent behavior of soft clays. The model is characterized by a non-associative flow rule, which is introduced by adopting a yield surface different than the plastic potential surface. Besides the isotropic hardening of the yield surface, both elliptical surfaces evolve according to a combined distortional and rotational hardening rule, simulating the evolving anisotropy. The model is simple enough to require merely three (3) constants more than those of the Modified Cam Clay model. Their calibration requires data from undrained triaxial tests and at least one constant stress-ratio test (e.g.  $K_0$  consolidation) with lateral stress measurements. For the sake of simplicity, two of these three constants are calibrated using analytical relations, and merely a single constant necessitates trial-and-error runs of the model. The paper presents the step-by-step calibration process for Boston Blue Clay and presents the model performance for triaxial shearing of the same clay, as well as the Lower Cromer Till.

### INTRODUCTION

The new model was proposed by Dafalias et al (2003) and builds upon the associative flow rule anisotropic model of Dafalias (1986, 1987). The latter constitutes probably the simplest possible energetic extension of the Modified Cam

<sup>1</sup> Dept. of Civil and Environmental Engineering, UC Davis, USA & Geotechnical Dept., School of Civil Engineering, National Technical University of Athens, HELLAS; <[apapad@civil.ntua.gr](mailto:apapad@civil.ntua.gr)>

<sup>2</sup> Dept. of Civil and Environmental Engineering, George Washington University, USA; <[manzari@gwu.edu](mailto:manzari@gwu.edu)>

<sup>3</sup> Dept. of Civil and Environmental Engineering, UC Davis, USA & Dept. of Mechanics, School of Applied Mathematical and Physical Sciences, National Technical University of Athens, HELLAS; <[yfdafalias@ucdavis.edu](mailto:yfdafalias@ucdavis.edu)>



Clay (MCC) model from isotropic to anisotropic response at the expense of merely two extra constants. Compared to the original model of Dafalias (1986, 1987), the new model has two major differences: (a) it is non-associative, since its yield surface is different from its plastic potential surface and (b) it is characterized by more elaborate combined distortional and rotational hardening rules for both surfaces. Besides their differences, the new model has only one extra constant compared to the original, but significantly better simulative abilities. For example, the new model can predict the softening response of soft clays in undrained triaxial compression following  $K_0$ -consolidation. The next section presents an outline of the constitutive equations of the new model in the triaxial stress-strain space, while the remaining sections of the paper focus on its calibration, with emphasis on the three extra constants compared to the MCC model.

## CONSTITUTIVE EQUATIONS

Based on the above, the new model employs the use of two (similarly shaped) elliptical surfaces, which are illustrated in Figure 1 for the special simplified case of the triaxial stress space  $p - q$ . In particular, the yield surface expression is given by:

$$f = (q - p\beta)^2 - (N^2 - \beta^2)p(p_o - p) = 0 \quad (1)$$

where  $\beta$  is the rotational hardening variable of the yield surface, and  $N$  a constant to be specified. The  $p_o$  represents the isotropic hardening variable, and is the value of  $p$  at  $\eta = q/p = \beta$ . The non-associated flow rule is introduced via the gradient to the second surface in Fig.1, named plastic potential surface, whose expression is:

$$g = (q - p\alpha)^2 - (M^2 - \alpha^2)p(p_a - p) = 0 \quad (2)$$

where  $M$  is the critical stress ratio,  $\alpha$  the stress anisotropy variable introducing the coupling of deviatoric and volumetric plastic strain rates. Note that  $p_a$  is the value of  $p$  at  $\eta = \alpha$ , a variable that is constantly adjusted so that Eq. (2) is always satisfied for the ever-current set of  $p, q$  values on the yield surface. Also note that the shape of the rotated and distorted ellipse for the plastic potential surface, Eq.(2), is a direct derivative of an energetic assumption by Dafalias (1986) on the plastic work rate expression, which differentiates this approach from earlier propositions of rotated ellipses. Furthermore, observe that  $M, \alpha$  and  $p_a$  substitute for  $N, \beta$  and  $p_o$ , respectively, in Eq. (1) to yield Eq. (2). Finally, notice that the associative flow rule ellipse of the MCC model is obtained by simply setting  $\alpha = 0$  and  $f = g$ .

The flow rule and dilatancy expressions follow straightforwardly from the calculation of  $\partial g / \partial p$  and  $\partial g / \partial q$  and their ratio based on Eq. (2), and read:

$$\dot{\epsilon}_v^p = \langle L \rangle p(M^2 - \eta^2); \quad \dot{\epsilon}_q^p = \langle L \rangle 2p(\eta - \alpha); \quad \psi = \frac{M^2 - \eta^2}{2(\eta - \alpha)} \quad (3)$$

where  $\dot{\epsilon}_v^p$  and  $\dot{\epsilon}_q^p$  are the hydrostatic (volumetric) and deviatoric plastic strain rates components,  $\langle \rangle$  are the Macauley brackets,  $\partial g / \partial p$  and  $\partial g / \partial q$  is what follows  $\langle L \rangle$  in the first two expressions, and  $L$  is the loading index (or plastic multiplier).

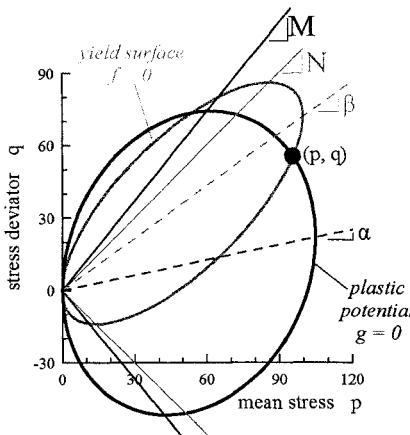


**FIG. 1. Model surfaces in triaxial stress space**

For the  $p_o$  the classical evolution law of critical state soil mechanics is used:

$$\dot{p}_o = \left( \frac{1+e_{in}}{\lambda - \kappa} \right) p_o \dot{\varepsilon}_v^p = <L> \left( \frac{1+e_{in}}{\lambda - \kappa} \right) \frac{\partial g}{\partial p} p_o = <L> \bar{p}_o \quad (4)$$

where  $e_{in}$  is the initial value of the void ratio  $e$  (the current value of  $e$  would be used instead, if logarithmic volumetric strain is considered), and  $\lambda, \kappa$  are the slopes of the normal consolidation and rebound lines, respectively, in the  $e - \ln p$  space.

For the evolution of  $\alpha$ , Dafalias et al (2003) proposed:

$$\dot{\alpha} = <L> \left( \frac{1+e_{in}}{\lambda - \kappa} \right) c \left( \frac{p}{p_o} \right)^2 p (\eta - x \alpha) = <L> \bar{\alpha} \quad (5)$$

where  $c$  is a dimensionless model constant controlling the pace of evolution of  $\alpha$ , and  $x$  another constant controlling the saturation level of  $\alpha$  at a given  $\eta$ , i.e. that  $\dot{\alpha} = 0$  when  $\alpha = \eta/x$ . Eq.(5) is a variation of the respective equation of Dafalias (1986), that eliminates a  $\partial g / \partial p$  multiplier allowing for evolution of anisotropy at critical state but at a reduced rate that is accomplished by introducing an exponent 2 for the  $(p/p_o)$  term.

Observe from Eq. (2) that the existence of real values of  $q$  necessitates that  $|\alpha| < M$ . Although the saturation value  $\eta/x$  of  $\alpha$  can rarely surpass  $M$  ( $x > 1$  as will be seen in the sequel), for extremely high values of  $c$  it is conceivable that at high values of  $\eta$  the  $\alpha$  may surpass  $M$ . If such case may occur, one must substitute  $M$  for  $\eta$  in Eq. (5) when  $\eta$  becomes larger than  $M$ . Notice that at critical state where  $\eta = M$ , the  $\alpha$  continues to evolve until it saturates at  $M/x$ , thus allowing for evolution of anisotropy in regards to the plastic potential.

For the evolution of  $\beta$ , Dafalias et al (2003) proposed:

$$\dot{\beta} = <L> \left( \frac{1+e_{in}}{\lambda - \kappa} \right) c \left( \frac{p}{p_o} \right)^2 \left| \frac{\partial g}{\partial p} \right| (\eta - \beta) = <L> \bar{\beta} \quad (6)$$

**@Seismicisolation**

where  $c$  is the same as in Eq. (5). The saturation level of  $\beta$  is  $\eta$  itself. Again, in order to avoid having  $\beta$  increasing above  $N$  (a case which may occur for unlikely very high values of  $c$ ), so that Eq. (1) yields real solution for  $q$ , one must substitute  $N$  for  $\eta$  in Eq. (6) when  $\eta > N$ .

Notice that at critical state, where  $\eta = M_c$  or  $\eta = -M_e$  for triaxial compression or extension respectively, the  $\beta$  does not evolve, since  $\partial g/\partial p=0$ . Furthermore, observe that the intersection of the yield surface with the critical state stress ratio  $M_c$  and  $M_e$  lines, occurs at different values of  $p$  when  $\beta \neq 0$ , thus, showing that the critical state line in  $e - \ln p$  space depends on anisotropy via  $\beta$ , and is different in compression from extension (recall that  $\beta$  does not evolve when  $\eta = M_c$  or  $-M_e$ ).

To fully define Eqs (3) through (6), one must define the loading index,  $L$ , which is a function of the plastic modulus  $K_p$  according to:

$$L = \frac{1}{K_p} \left( \frac{\partial f}{\partial p} \dot{p} + \frac{\partial f}{\partial q} \dot{q} \right) ; \quad K_p = - \left( \frac{\partial f}{\partial p_o} \bar{p}_o + \frac{\partial f}{\partial \beta} \bar{\beta} \right) \quad (7)$$

Note that the derivatives of  $f$  used in Eq. (7) can easily be computed from Eq. (1), while the  $\bar{p}_o$  and  $\bar{\beta}$  are defined in Eqs. (4) and (6). The constitutive modelling is complete by providing the standard isotropic hypoelastic incremental relations:

$$\dot{\varepsilon}_v^e = \frac{\kappa}{1+e_{in}} \frac{\dot{p}}{p} ; \quad \dot{\varepsilon}_q^e = \frac{\dot{q}}{3G} \quad (8)$$

with the elastic bulk modulus defined from  $K = p(1+e_{in})/\kappa$ , the elastic shear modulus  $G$  is expressed in terms of  $K$  and the elastic Poisson's ratio  $v$ .

## CALIBRATION OF CONSTANTS

Based on the constitutive equations presented in the previous section, the new model requires the calibration of seven (7) constants:

TABLE 1. Constants of new model

Constant	Description
$M$	Value of stress ratio $\eta = q/p$ at critical state (or $M_c$ and $M_e$ )
$\kappa$	Compressibility of overconsolidated OC clay
$\lambda$	Compressibility of normally consolidated NC clay
$v$	Elastic Poisson's ratio
$N$	Shape of the yield surface
$x$	Saturation limit of anisotropy (under paths with $\eta = q/p = \text{constant}$ )
$c$	Rate of evolution of anisotropy

As will be shown in detail in the section that follows, the calibration of these constants for clays requires data from relatively standard laboratory tests, namely:

- (a) One-dimensional ( $K_o$ ) or better isotropic consolidation tests to stresses significantly larger than the preconsolidation pressure with at least one unload-reload cycle using an oedometer or a triaxial device (for constants  $\kappa, \lambda$ )
- (b) Lateral stress measurements during one-dimensional ( $K_o$ ) compression and swelling reaching stresses significantly larger than the preconsolidation

pressure using either a computer controlled triaxial device or a lateral stress oedometer (for constants  $x, v$ )

- (c) Undrained triaxial compression ( $CK_o$ UC) and extension ( $CK_o$ UE) tests on normally  $K_o$ -consolidated clay (for constants  $M_c$  and  $M_e$ ,  $N$ ,  $c$ )

More specifically, the calibration process of these constants is presented herein with reference to (resedimented) Boston Blue Clay (BBC), a material exhaustively tested over the years in the eastern US (M.I.T. group of researchers).

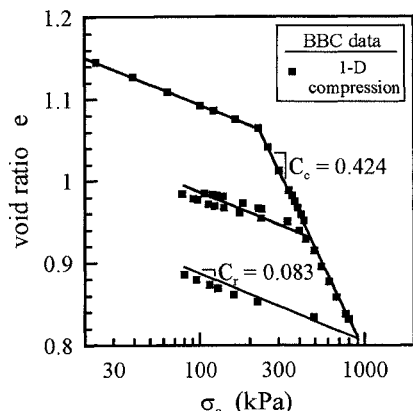
Figure 2 presents the response of this clay in an oedometer test during one-dimensional ( $K_o$ ) compression and swelling. Lacking lateral stress measurements in this test, plotting of the data is performed in terms of void ratio  $e - \log\sigma_a$ , where  $\sigma_a$  is the axial (vertical) stress. Given that  $\lambda$  and  $\kappa$  are defined as the slopes of the normal compression and swelling lines in the  $e - \ln\sigma_a$  space, the respective slopes in the  $e - \log\sigma_a$  space,  $C_c$  and  $C_r$  that are measured in Figure 2 are related to  $\lambda$  and  $\kappa$  as:  $\lambda = C_c/\ln 10 = 0.184$  and  $\kappa = C_r/\ln 10 = 0.036$ . Note that while this indirect estimation of  $\lambda$  is accurate, its respective for  $\kappa$  is only approximate given the relative increase of  $p/\sigma_a$  in swelling due to the increase of  $K_o$ . Hence, calibrating these constants on the basis of an isotropic consolidation test, if available, should be preferred.

Figure 3 presents the response of this clay in  $CK_o$ UC and  $CK_o$ UE tests on normally  $K_o$ -consolidated (resedimented) clay, i.e. following  $K_o$ -loading starting from slurry (gray line). The data are presented in terms of the effective stress path, normalized to the value of  $\sigma_{a,\max}$ , i.e. the maximum axial (vertical) stress of the preceding  $K_o$ -loading path. Given these tests,  $M_c$  and  $M_e$  are estimated directly as shown in the figure. Note that in the present case of BBC the measured  $M_c = 1.353$  and  $M_e = 0.932$  correspond to  $\varphi_c = \varphi_e = 33.5^\circ$ , according to:

$$M_c = \frac{6 \sin \phi_c}{3 - \sin \phi_c} \quad ; \quad M_e = \frac{6 \sin \phi_e}{3 + \sin \phi_e} \quad (9)$$

Observe that a unique value of  $M = M_c = M_e = 1.353$  is not advised for use, since it seriously overestimates the clay strength in extension ( $\varphi_e = 60.9^\circ$ ). Hence, when only a  $CK_o$ UC test is available, then  $M_e$  should be calibrated with caution, keeping in mind that  $M_{e,\min} \leq M_e < M_c$ , where  $M_{e,\min}$  is the value of  $M_e$  corresponding to  $\varphi_e = \varphi_c$ .

Figure 4 focuses on the  $K_o$  loading and unloading stress paths of this resedimented clay. Observe that the  $K_o$ -unloading stress path presented with a dashed gray line in this figure is the average curve that fits the initial data points of the triaxial compression and extension tests for  $OCR=1, 2, 4$  and  $8$  that are available for this clay. As an approximation, the initial part of this path is proposed for use in the calibration of the elastic Poisson's ratio  $v$  of the clay. This implies that upon unloading from  $K_o$  conditions, the clay response is assumed elastic, which requires that the initial part of this path lies within the yield surface. The new model achieves this requirement by having the yield surface aligned along the  $K_o$ -loading line (gray line), something that is achieved by Eq.(6), which terminates the rotation and distortion of the yield surface when  $\beta = \eta_{k_0}$ . Given this location of the yield surface, the stress path upon  $K_o$ -unloading lies within it (see also Figure 1).



**FIG. 2. Calibration of  $\lambda$  and  $\kappa$ , via  $C_c$  and  $C_r$  respectively**

In such a path,  $\dot{\varepsilon}_v^e / \dot{\varepsilon}_q^e = 3/2$ , which according to Eq.(8) gives:

$$\dot{q} = \frac{3(1-2\nu)}{(1+\nu)} \dot{p} \quad (10)$$

i.e. the slope of the initial part of the  $K_o$ -unloading stress path is a function of the elastic Poisson's ratio  $\nu$ . Hence, a value of  $\nu=0.24$  for BBC procures from Figure 4.

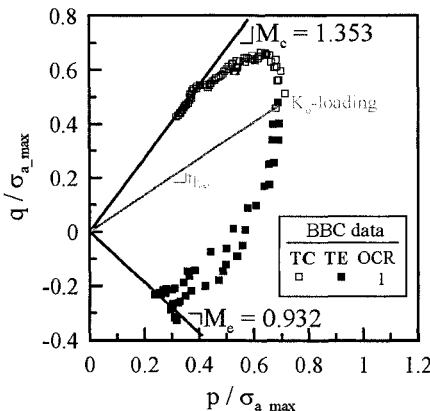
Figures 2 through 4 focused on the calibration of  $M$ ,  $\kappa$ ,  $\lambda$  and  $\nu$ , i.e. well-known geotechnical constants that comprise the set of constants of the MCC model. The remaining part of this section presents the calibration process of the extra three (3) constants,  $x$ ,  $N$  and  $c$ . For  $x$  and  $N$ , the use of closed-form analytical relations is proposed which makes their calibration easy and straightforward. The derivation of these relations is based on the fact the  $f=0$  function of Eq.(1) is homogeneous in  $p$ ,  $q$  and  $p_0$ , i.e. the yield surface remains geometrically similar to itself as  $p_0$  changes.

Specifically, for the estimation of constant  $x$ , the case of a drained path with  $\eta=\eta_k=\text{constant}$  is considered. Practically speaking, all consolidation paths starting from slurry have this characteristic. In such a path, eventually  $\dot{\alpha}=\dot{\beta}=0$ , i.e. the two surfaces cease to rotate and distort. This condition is being used for the calculation of the ratio of total strain rates  $\varepsilon=\dot{\varepsilon}_v^e / \dot{\varepsilon}_q^e$  based on Eqs (3) and (7), neglecting  $\dot{\varepsilon}_q^e$  and accounting for the foregoing value of  $\bar{p}_0$  and the analytical homogeneity of  $f=0$  in  $p$ ,  $q$  and  $p_0$  (Dafalias, 1986). After some algebra, this procedure yields:

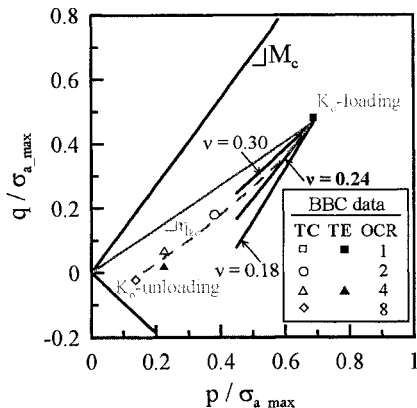
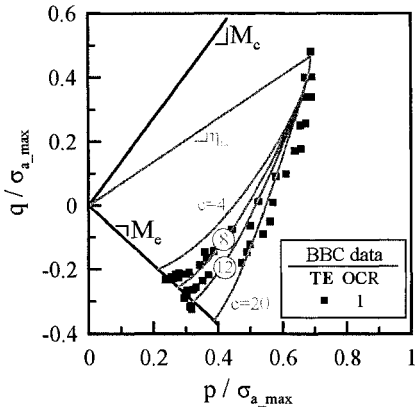
$$\psi = (1 - (\kappa/\lambda)) \varepsilon \quad (11)$$

where  $\kappa$  and  $\lambda$  the isotropic compressibility constants and  $\psi$  is the dilatancy of the model given by Eq.(3)<sub>3</sub>. Hence, Eq.(11) with Eq.(3)<sub>3</sub> may be rearranged to yield the saturated value of  $\alpha=\alpha_k=\text{constant}$ , according to (Dafalias 1986, Dafalias et al. 2002):

$$\alpha_k = \frac{\eta_k}{x} = \frac{\eta_k^2 + 2\varepsilon(1-(\kappa/\lambda))\eta_k - M_c^2}{2\varepsilon(1-(\kappa/\lambda))} \quad (12)$$



**FIG. 3. Calibration of  $M_c$  and  $M_e$**

FIG. 4. Calibration of  $v$ FIG. 5. Calibration of  $c$ 

Different paths with  $\eta_k = \text{constant}$  correspond to different  $\varepsilon$  values, which are not always *a priori* known. Of all possible such paths, the most frequently run is the  $K_0$ -loading path, for which  $\varepsilon = 3/2$  and  $\eta_k = \eta_{k0} = 3(1 - K_0)/(1 + 2K_0)$ , where  $K_0$  is the measured value of the earth coefficient at rest. Hence, having measured the  $K_0$  value, one may estimate the value of constant  $x$  using Eq.(12). Note that the thus estimated value of  $x$  is usually 10 – 20% larger than the accurate value of  $x$ , which may be estimated analytically if the restriction of  $\dot{\epsilon}_q^e = 0$  is lifted. By doing so, the closed-form relation for  $x$  (and  $a_k$ ) takes the following form:

$$\alpha_k = \frac{\eta_k}{x} = \frac{B\varepsilon\eta_k^3 + \eta_k^2 + [2(1 - (\kappa/\lambda)) - BM_c^2]\varepsilon\eta_k - M_c^2}{2\varepsilon(1 - (\kappa/\lambda))} ; \quad B = -\frac{2(1 + v)}{9(1 - 2v)} \frac{\kappa}{\lambda} \quad (13)$$

Observe that the exact solution for  $x$ , Eq.(13), degenerates to Eq.(12) by setting  $B=0$ , which corresponds to  $v=-1$  that materializes the  $\dot{\epsilon}_q^e = 0$  restriction. For example, for the case of the BBC, for  $\kappa=0.036$ ,  $\lambda=0.184$ ,  $M_c=1.353$ ,  $v=0.24$  and  $K_0=0.533$ , Eq.(13) for  $\varepsilon=3/2$  yields  $x=4$  (compare with  $x=6.2$ , from simplifying Eq.12). Hence, for given values of  $\kappa$ ,  $\lambda$ ,  $M_c$  and  $v$  (the MCC model constants), constant  $x$  is a unique increasing function of  $K_0$ . This flexibility allows the new model to be calibrated to whatever the measured value of  $K_0$ , unlike the MCC model, which is known for overestimating the  $K_0$  value.

Similarly, for the estimation of constant  $N$  the case of an undrained shearing path is considered. In such a path  $\dot{\epsilon}_v^e + \dot{\epsilon}_v^p = 0$ , which based on Eqs (3)<sub>1</sub>, (8)<sub>1</sub> and (7) with  $\beta=\text{constant}$ , and taking into account the analytical homogeneity of  $f=0$  yields the undrained effective stress path in the  $p-\eta$  space (Dafalias, 1986; Dafalias et al 2002):

$$\frac{p}{p_{in}} = \left( \frac{\eta_{in}^2 - 2\beta\eta_{in} + N^2}{\eta^2 - 2\beta\eta + N^2} \right)^{\frac{\kappa}{\lambda}} \quad (14)$$

where  $p_{in}$  and  $\eta_{in}$  are the initial values of  $p$  and  $\eta$  and  $N$  and  $\beta$  are the two quantities that enter the  $f=0$  relation, Eq.(1).

**@Seismicisolation**

As mentioned above, the derivation of Eq.(14) is based on the assumption of a non-rotating yield surface ( $\beta=\text{constant}$ ). Such a condition is realistic only when the  $\eta_{\text{in}}$  is not far from the final  $\eta$  of the effective stress path (e.g.  $2\eta_{\text{in}} > \text{final } \eta$ ). Practically, given the available tests for calibration of the model constants it is the CK<sub>o</sub>UC test on normally consolidated clay that is suitable for the purpose at hand. In this case, one has  $\eta_{\text{in}}=\beta=\eta_{\text{ko}}=3(1-K_o)/(1+2K_o)$  and  $p_{\text{in}}=p_{\text{ko}}$ , i.e. the  $p$  value after the end of the  $K_o$  consolidation. Given these conditions, the value of  $N$  in Eq.(14) quantifies how contractive the effective undrained stress path is. The proposed way of calibrating  $N$  via Eq.(14) is to provide the known end conditions of the effective stress path ( $p$ ,  $\eta$ ) and solve Eq.(14) for  $N$ . Specifically, one would set  $p=p_f$  and  $\eta=M_c$ , where  $p_f$  is the value of  $p$  when the test reaches critical failure and Eq.(14) yields:

$$\frac{p_f}{p_{\text{ko}}} = \left( \frac{N^2 - \eta_{\text{ko}}^2}{N^2 - 2\eta_{\text{ko}}M_c + M_c^2} \right)^{1-\kappa} \quad (15)$$

Hence, one merely needs to solve Eq.(15) for  $N$ , given data of a CK<sub>o</sub>UC test on normally consolidated clay. For the case of the BBC data (Figure 5), for which  $\kappa=0.036$ ,  $\lambda=0.184$ ,  $M_c=1.353$ ,  $K_o=0.533$  and  $p_f/p_{\text{ko}}=0.522$ , Eq.(15) yields  $N=0.91 < M_c$ . According to Eq.(14), for  $N < \eta < M_c$  the effective stress path for a CK<sub>o</sub>UC path shows softening, i.e. a desirable constitutive feature for normally consolidated clays. Nevertheless, if  $N < M_c$  the effective stress path for a CK<sub>o</sub>UE test could show small softening for  $-N > \eta > -M_c$ , something which is not usually measured after  $K_o$  conditions. Hence, as a practical rule, the use of Eq.(15) is suggested for  $N$ , which must be restricted to  $N \geq M_c$ . This restriction applies to the BBC data shown here, which do not show softening in extension (see Figure 3), leading to  $N=0.932 (=M_c)$ .

Finally, the calibration of constant  $c$  requires the execution of trial runs, having all other constants calibrated in advance. Observe that constant  $c$  quantifies the rate of rotation and distortion of the yield surface and the plastic potential in Eqs. (5) and (6). Hence, tests appropriate for its calibration are those that induce significant surface rotation, or in other words, tests for which the  $\eta_{\text{in}}$  is far from the final  $\eta$  of the effective stress path, and possibly of opposite sign. Practically, a CK<sub>o</sub>UE test on normally consolidated clay is very suitable for the purpose at hand. Hence, Figure 5 presents the CK<sub>o</sub>UE test data on normally consolidated BBC, along with a series of trial runs for  $c = 4, 8, 12$  and  $20$ . Observe that the higher the value of  $c$  the larger the predicted undrained strength in triaxial extension. For the BBC in particular,  $c=8$  appears most appropriate.

Experience has shown that constant  $c$  usually varies between  $c = 4$  and  $20$  for various clays. Moreover, it appears that its calibration on the basis of undrained triaxial extension is appropriate for non-triaxial undrained paths as well (e.g. plane strain compression). Yet, some caution should be taken for its use in drained shearing paths, for which the thus estimated value of  $c$  may be rather large. Nevertheless, drained failure is not critical for soft clays for which this new model is proposed, and furthermore very few of the clay data available in the literature contain drained shear testing. Hence, the foregoing calibration process should be considered as appropriate for any boundary value problem application involving soft clays.



## MODEL PERFORMANCE

Figures 6 and 7 show the comparison of simulations with triaxial test data for two clays and different OCRs, the Boston Blue Clay (BBC), as measured by Ladd and Varallyay (1965) and Sheahan (1991) and the Lower Cromer Till (LCT) from Gens (1982). Note that  $\epsilon_a$  in these Figures is the axial strain during shearing. The model simulations were performed using the model constants summarized in Table 2. Obviously, the constants for the BBC are those estimated above.

**TABLE 2. Model constants and values for two different clays**

Clay	$\lambda$	$\kappa$	$\nu$	$M_c$	$M_e$	N	x	c
BBC	0.184	0.036	0.24	1.353	0.932	0.932	4.00	8
LCT	0.140	0.020	0.20	1.200	0.910	0.960	1.62	20

As deduced from Figures 6 and 7, the model predicts successfully the response of normally  $K_0$ -consolidated clays, in both triaxial compression and extension, following accurate simulation of the preceding consolidation phase (see Fig.2). Furthermore, it is shown that it can also be used for simulating the response of overconsolidated clays (OCR up to 8), but with a lesser degree of accuracy. Nevertheless, on the whole, the predictive abilities of this model are considered satisfactory taking into account its simplicity, especially in terms of the small number of constants and how easily they are calibrated.

## ACKNOWLEDGEMENTS

Y. F. Dafalias would like to acknowledge partial support from NSF Grant CMS-02-01231. Similarly, M. T. Manzari acknowledges partial support from NSF Grant CMS-99-88557.

## REFERENCES

- Burland, J. B. (1965). "The yielding and dilation of clay." *Geotechnique* 15(2): 211-214.
- Dafalias, Y. F. (1986). "An anisotropic critical state soil plasticity model." *Mechanics Research Communications* 13(6): 341-347.
- Dafalias, Y. F. (1987). "An anisotropic critical state clay plasticity model." In C. S. Desai et al. (ed.), *Constitutive laws for engineering materials: Theory and Applications*, Proc., 2<sup>nd</sup> IC, I: 513-521. New York: Elsevier.
- Dafalias, Y. F., Manzari, M. T. & Akaishi M. (2002). "A simple anisotropic clay plasticity model." *Mechanics Research Communications* 29(4): 241-245
- Dafalias, Y. F., Papadimitriou, A. G. & Manzari, M. T. (2003). "Simple anisotropic plasticity model for soft clays." In P. A. Vermeer et al. (ed.), *Geotechnics of Soft Clays: Theory and Practice*, Proc., Intern. Workshop, 189-195
- Gens, A. 1982. Stress-strain and strength of a low plasticity clay. *Ph.D. Thesis*, Imperial College, London University, p. 856.
- Ladd, C.C. & Varallyay, J. 1965. The influence of the stress system on the behavior of saturated clays during undrained shear. *Research Report No. R65-11*, Dept. of Civil Engineering, MIT, Cambridge, MA

Sheahan, T.C. 1991. An experimental study of the time-dependent undrained shear behavior of resedimented clay using automated stress path equipment. *Sc.D Thesis*, MIT, Cambridge, MA

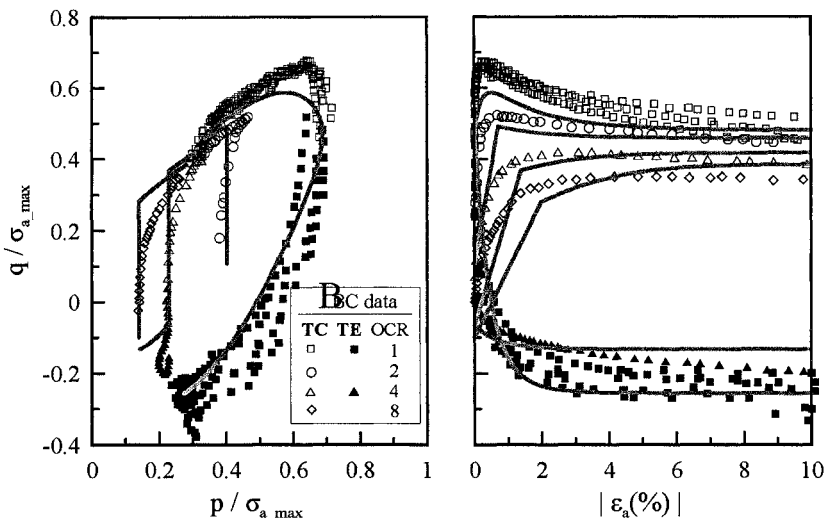


**FIG. 6. Simulations versus undrained triaxial data after  $K_0$ -consolidation on BBC (Ladd and Varallay 1965, Sheahan 1991)**

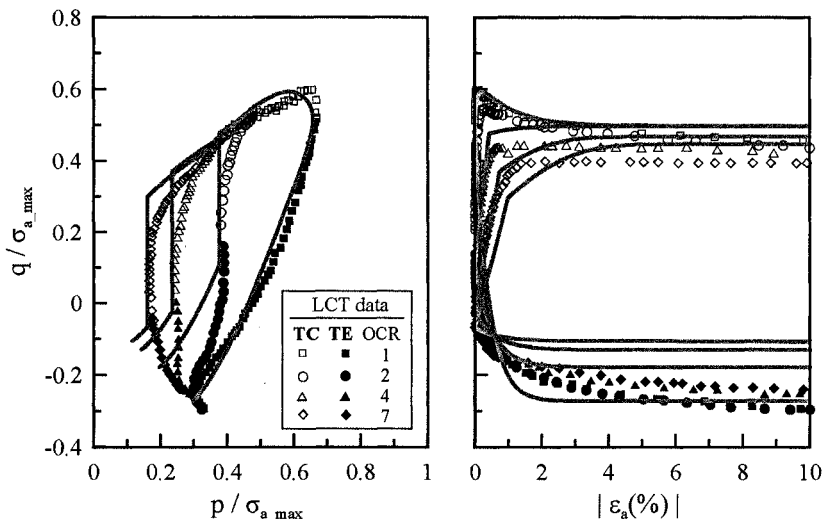


**FIG. 7. Simulations versus undrained triaxial data after  $K_0$ -consolidation on LCT (Gens 1982)**

## SELECTION OF MATERIAL PARAMETERS FOR SANDS USING THE MIT-S1 MODEL

Juan M. Pestana<sup>1</sup>, Maria Nikolinakou<sup>2</sup> & Andrew J. Whittle<sup>3</sup>  
Members ASCE

**ABSTRACT:** The MIT-S1 model describes the rate independent behavior of clays, sands and silts within a unified elasto-plastic formulation. The authors (Pestana et al., 2002a, b) have described in detail the selection of input parameters for this model for sands and clays. The current paper summarizes the proposed methodology for parameter selection for sands and illustrates this procedure for Toyoura sand, a very well documented reference material. This approach is compared with a more recent calibration of the model for Berlin sand that demonstrates some of the difficulties and compromises needed to select parameters in practical applications of this advanced constitutive model.

### INTRODUCTION

The use of numerical simulations to assess the performance of complex construction processes, such as deep excavations and staged constructions on soft soils, is quickly becoming the state-of-the-practice in geotechnical engineering practice. However, for many of these applications the description of the geomaterials and/or foundation soils is commonly based on relatively simple soil models. This fact is somewhat surprising given the great effort and advances in constitutive modeling for soils in the last three decades. Several factors contribute to this phenomenon and include: a) many models are not efficiently and robustly implemented in numerical tools, such as finite element programs, used for the analysis of boundary value problems and therefore they are only used to predict

---

<sup>1</sup> Associate Professor, Univ. of California, Berkeley, Dept. of Civil and Environmental Engineering, Berkeley, CA 94720

<sup>2</sup> Graduate Student, Dept. of Civil and Environmental Engineering, Massachusetts Institute of Technology, Cambridge, MA 02139.

<sup>3</sup> Professor, Dept. of Civil and Environmental Engineering, Massachusetts Institute of Technology, Cambridge, MA 02139.



"element level" results, and b) the lack of reliable experimental data necessary for calibration of the material parameters.

This paper focuses primarily on the selection of the MIT-S1 material parameters for two sands and illustrates some of the difficulties and compromises involved in the process. The MIT-S1 model has been implemented in several finite element programs (as a user-defined constitutive law) and has been used in simulations of various boundary value problems (e.g., Hsieh et al., 2003). Most recently, the model has been used to predict and interpret the performance of deep excavations for a well-documented section of the VZB project in Berlin (Nikolinakou et al., 2004a, b)

## SELECTION OF MATERIAL PARAMETERS

MIT-S1 is a generalized soil model based on the incrementally linearized theory of rate independent elasto-plasticity (e.g., Prévost, 1978) that was developed to predict the behavior of uncemented sands, clays and silts (Pestana, 1994; Pestana & Whittle, 1999). The model incorporates the void ratio as a separate state variable (in addition to the state of stresses) in order to simulate characteristic transitions of sand behavior from dilative to contractive response as the formation void ratio or the confining stress increases. The model also uses a new framework for describing the compression behavior of soils, based on the existence of the Limiting Compression Curve, LCC (Pestana and Whittle, 1995), which provides the means for unifying the behavior of clays and sands.

The model in its most general form has 16 material parameters, but only 13 are required to describe the behavior of freshly deposited, uncemented clean sands. Pestana et al. (2002) have detailed the selection of these parameters for Toyoura sand, a standard test sand whose behavior has been extensively documented in the Japanese literature over the last 25 years. Toyoura sand is a poorly graded, uniform sand consisting of sub-angular particles with mean diameter,  $D_{50} = 0.16\text{--}0.20$  mm. The maximum void ratio,  $e_{\max}$ , for this sand is 0.98 and the minimum,  $e_{\min}$ , is approximately  $0.60 \pm 0.01$ . This paper uses primarily undrained triaxial compression data presented by Ishihara (1993), high pressure drained compression tests by Miura and Yamanouchi (1975) and small strain measurements by Tatsuoka and Shibuya (1992).

Since there was no comparable database available for the Berlin sand, an extensive program of laboratory compression and triaxial shear tests were carried out at MIT to enable parameter selection. Berlin sand is a quartzitic sand, with mean particle size,  $D_{50}$  of  $0.38 \pm 0.01$  mm and formation void ratios ranging from  $e_{\max} = 0.59$  to  $e_{\min} = 0.39$  (tested according to DIN 18124, 1997). It should be noted that the range of formation densities for Berlin sand is quite small compared to a wide variety of sands reported in the literature (e.g., Pestana and Whittle, 1995). The test program included four high pressure 1-D CRS consolidation tests and a total of 35 triaxial shear tests performed on specimens prepared by moist tamping at void ratio,  $e_0 = 0.43\text{--}0.60$  and consolidated hydrostatically to confining pressures  $\sigma'_c = 100\text{--}800$  kPa. The first series of shear tests included undrained and drained shear tests performed on moist tamped specimens at similar void ratios and confining stresses (Glaserapp, 2002). A second series of tests performed by Becker (2002) used more refined testing procedures



including reduced friction end-platens and local strain measurements to enable more reliable interpretation of large strain critical state conditions and small strain stiffness properties.

Table 1 summarizes the MIT-S1 model input parameters and their physical meaning as well as final selected values of these parameters for Toyoura and Berlin sands. The 13 model input parameters can be broadly grouped into three sub-sets: 1) parameters that can be unambiguously obtained from the laboratory tests ( $\rho_c$ ,  $p'_{ref}/p_{at}$ ,  $\theta$ ,  $\phi'_{cs}$ ); 2) parameters that have relatively small ranges of input values and can be reasonably estimated based on prior empirical experience ( $K_{0NC}$ ,  $v'_0$ ,  $\omega$ ), and 3) parameters that require detailed interpretation of the laboratory data ( $C_b$ ,  $\phi'_{mr}$ ,  $p$ ,  $m$ ,  $\psi$ ,  $\omega_s$ ). Pestana and Whittle (1999) have proposed one procedure for parameter selection that makes efficient use of data from a limited number of laboratory tests. Selection of these parameters for Toyoura sand was previously detailed by Pestana et al. (2002).

TABLE No. 1 Summary of the selected MIT-S1 input parameters

Test Type	Parameter /Symbol	Physical contribution /meaning	Toyoura Sand	Berlin Sand
Hydrostatic or 1-D Compression Test	$\rho_c$	Compressibility of sands at large stresses (LCC regime)	0.37	0.34
	$p'_{ref}/p_{at}$	Reference stress at unit void ratio for the LCC	55	23.5
	$\theta$	Describes first loading curve in the transitional regime	0.20	0.25
$K_0$ – oedometer or $K_0$ – triaxial	$K_{0NC}$	$K_0$ in the LCC regime	0.49	0.50
	$v'_0$	Poisson's ratio at load reversal	0.23	0.28
	$\omega$	Non-linear Poisson's ratio. 1-D unloading stress path	1.00	1.00
Undrained/ Drained Triaxial Shear Tests:	$\phi'_{cs}$	Critical state friction angle in triaxial compression	31°	31°
	$\phi'_{mr}$	Controls peak friction angle as a function of formation density at low stresses	28.5°	12.5°
	$p$	Geometry of bounding surface. Undrained stress paths	2.45	2.7
	$m$	Small strain (< 0.1%) non-linearity in shear	0.55	0.42
	$\omega_s$	Rate of evolution of anisotropy Stress-strain curves	2.5	4.0
	$\psi$		50	10
Bender Elements	$C_b$	Small strain stiffness at load reversal	750	950

## COMPRESSION BEHAVIOR

The MIT-S1 model assumes that sand specimens compressed from different initial formation densities approach a unique response at high stress levels, referred to as the Limiting Compression Curve (LCC). Behavior in the LCC regime is characterized

@Seismicisolation

by a linear relationship in the log[e]-log[p] space, as shown in Figure 1.  $\rho_c$  describes the slope of the LCC curve,  $p'_{ref}$  is a reference mean effective stress at unit void ratio ( $e = 1$ ) and  $p_{at}$  is the atmospheric pressure (~100kPa). Figure 1a shows the selection of compression properties for Toyoura sand based on three high quality isotropic compression tests to high stresses. The measured response supports the LCC concept and the values for  $\rho_c$  and  $p'_{ref}/p_{at}$  can be directly determined from the graph. A third parameter,  $\theta$  controls the transition regime and describes the progressive particle breakage and subsequent rearrangement as the specimens are compressed into the LCC regime. The model predictions using  $\theta = 0.20$  provide a reasonable match to the measured behavior. Higher values cause a more gradual transition to the LCC regime (e.g.,  $\theta = 0.30$ , Fig. 1a) while lower values represent materials with well defined yield points (e.g.,  $\theta = 0.10$ , Fig. 1a).

A common shortcoming of the above mentioned procedure is the lack of experimental results from isotropic compression tests carried to high enough stresses into the LCC regime. An alternative approach is to infer these parameters from more common 1-D compression tests. Figure 1b shows data from four 1-D compression tests on Berlin sand from four different initial void ratios. Since there are no direct measurements of the lateral earth pressure coefficient in the LCC regime ( $K_{0NC}$ ), the current interpretation assumes  $K_{0NC} = 0.5$  which is consistent with empirical correlations assuming a large strain friction angle of 31° (equivalent to  $\phi'_{cs}$ , Table 1). Hendron (1963) shows experimental evidence supporting that  $K_0$  values converge to a common value in the LCC regime, irrespective of initial formation density. As a result, the slope of the  $K_0$ -LCC curve in a log[e]-log[ $\sigma'_{vref}$ ] space is identical as that of the I-LCC and therefore  $\rho_c$  can be determined readily from the graph. The MIT-S1 model specifies a spacing function that guarantees the robustness of the LCC concept and describes the location of the LCCs in a void ratio-mean effective stress according to the applied shear stress ratio (e.g., Isotropic [I-LCC] vs. 1-D [ $K_0$ -LCC] compression curves). This implies that the value of  $p'_{ref}$  can be easily determined from the value of  $\sigma'_{vref}$  (representing the reference vertical effective stress at a unity void ratio for the 1-D LCC) as follows:

$$\frac{p'_{ref}}{\sigma'_{vref}} = \left( \frac{1+2K_{0NC}}{3} \right) \left( 1 + \left( \frac{6}{a^2} \right) \left[ \frac{1-K_{0NC}}{1+2K_{0NC}} \right]^2 \right) \quad (1a)$$

$$\text{where } a^2 = 24 \cdot \sin^2 \phi'_{cs} / (3 - \sin^2 \phi'_{cs})^2 \leq 1 \quad (1b)$$

Substituting the values of  $K_{0NC} = 0.50$ ;  $\phi'_{cs} = 31^\circ$  and  $\sigma'_{vref}/p_{at} = 25.5$  for Berlin sand Fig. 1b) in equation 1a, we obtain  $p'_{ref}/\sigma'_{vref} \sim 0.92$  and  $p'_{ref}/p_{at} \sim 23.5$ . As a first approximation, it is useful to use  $p'_{ref} = \sigma'_{vref}$  which is commonly referred to as the Rutledge hypothesis as discussed by Pestana (1994). Pestana and Whittle (1995) suggest that the value of  $\theta$  obtained from 1-D compression tests using a constant value of  $K_0 = K_{0NC}$  is a very good approximation for medium dense soils but small differences between predicted and measured void ratios should be expected for looser or denser soils for which the  $K_0$  values changes during loading into the LCC regime.

**@Seismicisolation**

The computed compression curves assuming  $\theta = 0.25$  provide a reasonable match to the measured data for Berlin sand. According to correlations established between  $p'_{ref}$  and  $\theta$  and index properties such as particle size ( $D_{50}$ ), uniformity ( $C_u$ ) and angularity, the LCC parameters selected for Berlin sand are more consistent with properties expected for a sand with much more angular particles (Nikolinakou et al., 2004a). This observation echoes earlier findings of De Beer (1965) who suggested that Berlin sands are more sensitive to splitting than those of other similar sand deposits (such as Mol sand) and attributed this behavior to impurities in the particles.

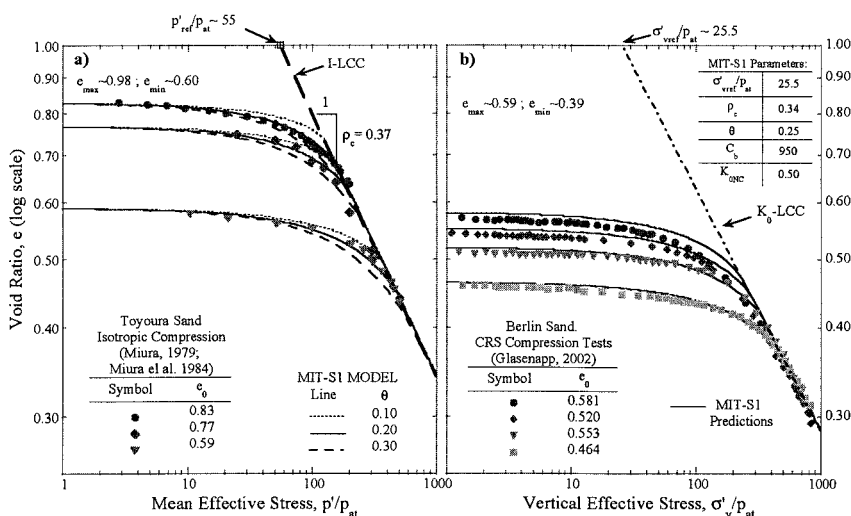


FIG. 1. Selection of material parameters for a) isotropic compression tests on Toyoura sand (Pestana et al., 2002) and b) one-dimensional compression tests on Berlin sand (Nikolinakou et al., 2004a)

The parameters,  $v'_0$  and  $\omega$  describe the elastic Poisson's ratio of the sand (i.e., at stress reversal) and its variation during unloading. Pestana and Whittle (1999) recommend selecting these parameters from stress paths measured 1-D unloading tests (e.g., from lateral stress oedometer tests) from the LCC regime. Figure 2 presents data of this type for Pennsylvania sand (Hendron, 1963), from which  $K_{ONC} \approx 0.49$  and  $v'_0 \approx 0.233$ . These same values were assumed for Toyoura sand (Pestana et al., 2002). For Berlin sand, Nikolinakou et al. (2004a) assumed  $K_{ONC} = 0.50$  and used high quality, small strain measurements from drained triaxial shear tests to estimate  $v'_0 = 0.28$ .

Figure 2, shows that the initial unloading stress ratio,  $K_0$ , is controlled primarily by the Poisson's ratio at reversal (note  $\omega = 0$ , implies a constant Poisson's ratio) while the values of  $K_0$  at larger OCR's is controlled by parameter  $\omega$ . A value of  $\omega \sim 1$  was

assumed based on recommendations of Pestana (1994) for both Toyoura and Berlin sand.

The input parameter  $C_b$  is a dimensionless property that defines the small strain volumetric stiffness (i.e.,  $K_{\max}$ ) and given the value of Poisson's ratio at reversal it also controls the value of the small strain shear stiffness (i.e.,  $G_{\max}$ ). Values of  $C_b$  for Toyoura sand were determined from high quality isotropic unloading tests and correlated well with estimated values of  $G_{\max}$ . For Berlin sands,  $C_b=950$  was selected based on data from both CIDC and CIUC triaxial shear tests using local strain measurements (Becker, 2002).

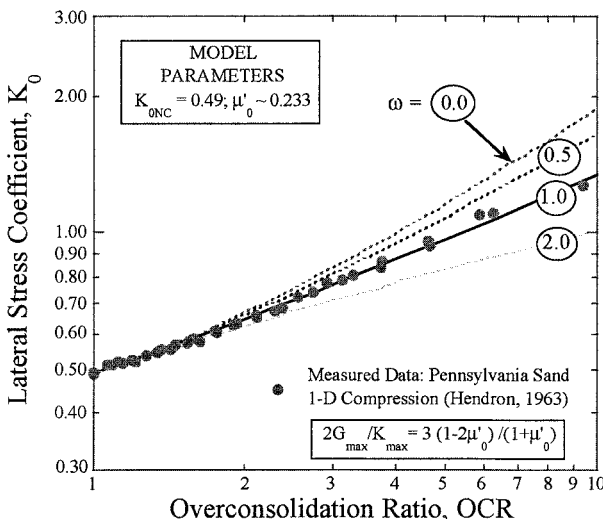


FIG. 2. Determination of parameters  $K_{0NC}$ ,  $\mu'_0$  and  $\omega$  from 1-D unloading response of Pennsylvania sand

## SHEAR RESPONSE

In the previous application of the MIT-S1 model for Toyoura sand, Pestana et al. (2002) proposed a procedure that will provide unambiguous estimation of the six input parameters that characterize shear behavior as follows: 1) the large strain friction angle,  $\phi'_{cs}$ , measured in either drained or undrained shear tests (assuming no localization of deformations or cavitation); 2) the peak friction angle measured in drained shear tests on dense specimens or the large strain stress conditions for undrained tests for two different values of void ratio (to enable selection of  $\phi'_{mr}$ ,  $p$ ); 3) the effective stress paths and stress-strain curves in undrained shearing to enable selection of parameters  $m$  and  $\psi$ ; and 4) the small strain non-linear stiffness to define  $\omega_s$ . This approach also minimizes the need to measure critical state conditions in the laboratory tests.

Figure 3 summarizes the determination of shear parameters for Toyoura sand based on undrained triaxial compression tests. From Figure 3a, it is possible to

@Seismicisolation

determine very precisely the value of  $\phi'_{cs}$ , and then a small parametric study on  $m$  is performed to obtain the best match with the undrained stress path. A value of  $m = 0.55$  is considered acceptable to Toyoura sand based on the densest specimen. Recent experience suggests that the determination of  $m$  is more sensitive if a more contractive specimen is used, but good agreement is obtained within the range of  $0.50 \pm 0.10$ . Pestana (1994) gives a closed-form solution for the large strain conditions corresponding to the critical state, Appendix A. The values of  $\phi'_{mr}$  and  $p$  describing the variation of the maximum aperture of the yield surface as a function of the current void ratio can be obtained by solving a system of equations designed to match the undrained shear stress values at large strains (provided no localization has taken place). Based on the two specimens at  $e = 0.735$  and  $0.833$ , this approach generates values of  $\phi'_{mr} = 28.5^\circ$  and  $p = 2.45$ . This method provides great results provided that large strain conditions are fully achieved. The parameter  $\omega_s$  controls the nonlinearity observed at small strains and requires high quality measurements at these values of strain ( $< 0.1\%$ ).

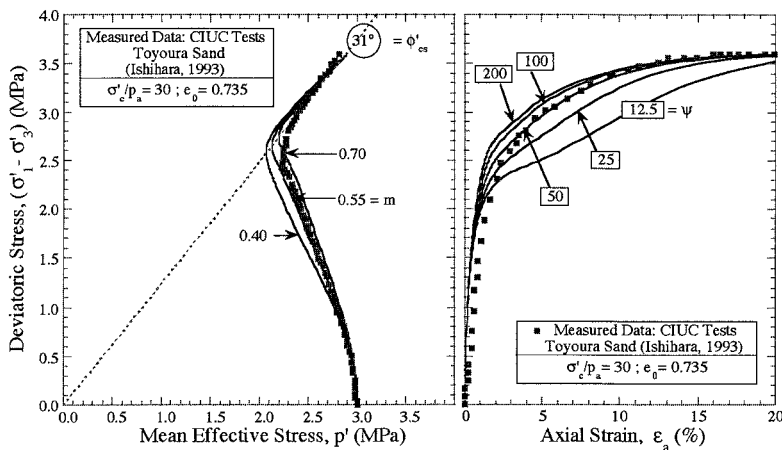


FIG. 3. Estimation of shear parameters for Toyoura sand based on undrained triaxial compression tests (after Pestana et al., 2002)

Finally, the rate of evolving anisotropy,  $\psi$ , is obtained by calibrating model predictions of the stress-strain curves in the intermediate strain range as shown in Figure 3b. It should be noted that the value of  $m$  affects slightly the stress-strain curves and  $\psi$  has a small effect on the effective stress path so it may be necessary to iterate once to obtain the optimal set of parameters.

For Berlin sand, it proved difficult to follow such a simple procedure due to uncertainties in the critical state and variability in the peak friction angles as shown in Figures 4 and 5. The peak friction angles measured CIDC shear tests, shown in Figure 5, are lower than would be expected for other quartzitic sands (at a similar range of confining pressures and void ratios) as noted by DeBeer (1965). Preliminary

@Seismicisolation

estimates indicated that the observed maximum friction angles can be simulated by combinations,  $p = 2 - 3$  and  $\phi'_{mr} = 8^\circ - 16^\circ$ . Although these values for  $p$  were consistent with prior data for other quartzitic sands, the range for  $\phi'_{mr}$  is much lower than expected (Pestana & Whittle, 1999).

The MIT-S1 model assumes there is a unique critical state condition for homogeneous shearing to large strains in the triaxial compression shear mode. The critical state was derived analytically by Pestana (1994) and is a function of the three input parameters,  $p$ ,  $\phi'_{mr}$  and  $m$  (i.e., the same parameters affecting predictions of the peak friction angle). In practice, critical state conditions are rarely achieved in laboratory shear tests on sands. Shear banding or strain localization commonly occurs in drained shear tests (where post peak strain softening occurs concurrently with dilative volumetric strains), while undrained shear tests often cavitate before reaching a steady state of deformation.

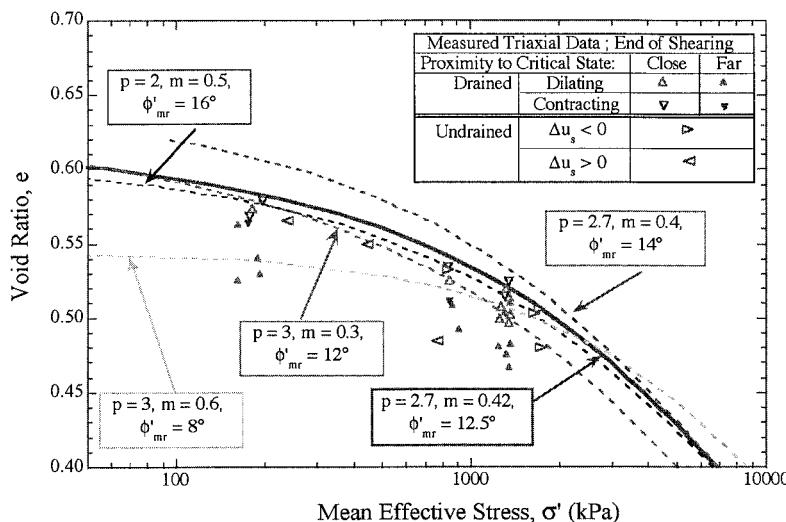


FIG. 4. Interpretation of critical state conditions from triaxial shear tests on Berlin sand (Nikolinakou et al., 2004a)

Figure 4 provides a symbolic interpretation of the final state of the triaxial shear tests on Berlin sand and their proximities to 'critical state conditions'. The arrowhead directions and size indicate the proximity of the critical state in each test based on a subjective interpretation of the data. The results show a broad band of possible locations for the critical state defined from combinations of drained tests that either contract or dilate towards critical state, and undrained tests that generate positive or negative shear induced pore pressures.

Figure 4 also illustrates the role of the model input parameters on prediction of the critical state for Berlin sand. The parameter,  $m$  controls the location of the critical state at high pressures ( $\sigma' > 1 \text{ MPa}$ ), while  $p$  and  $\phi'_{mr}$  both affect predictions in the lower stress range. The final parameter set reported in Table 1 provided the most consistent prediction of both the critical state conditions (Fig. 4) and peak friction angles in CIDC shear tests, as shown in Figure 5.

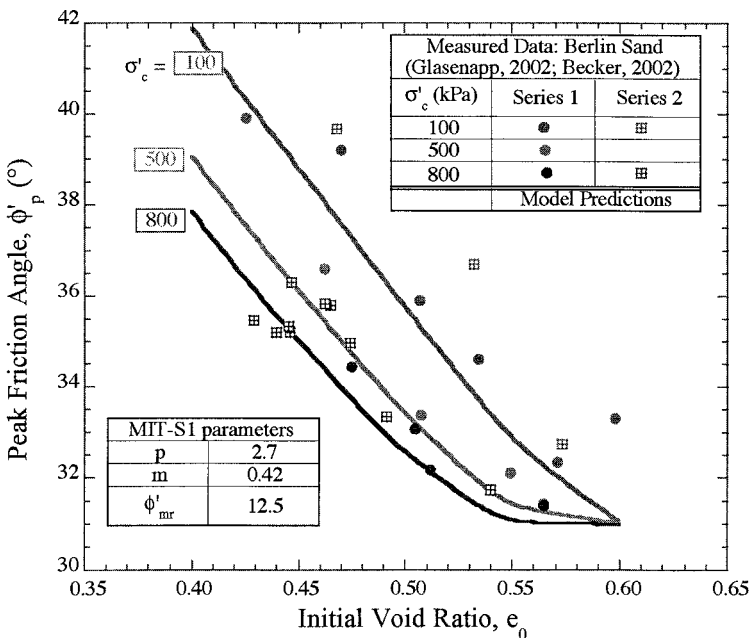


FIG. 5. Comparison of predicted and measured peak friction angles in drained triaxial shear tests (CIDC) on Berlin sand (Nikolinakou et al., 2004a).

In cases where values of the peak friction angle are available for the same confining stress but different void ratios it is possible to obtain a very close estimate of parameter  $p$  following the equation describing the maximum aperture of the yield surface at the origin as a function of void ratio proposed by Pestana (1994):

$$\left( \frac{\tan(90^\circ - \phi_m) - \tan(45^\circ - \phi_{cs}/2)}{\tan(90^\circ - \phi_{mr}) - \tan(45^\circ - \phi_{cs}/2)} \right) = e^p \quad (2)$$

Pestana (1994) shows that the variation of  $\phi'_m$  with respect to void ratio ( $e$ ) is nearly parallel to the observed peak friction angles,  $\phi_p$  as a function of void ratio at a constant confining pressure (cf. Figure 5). As a result, it is possible to use equation 2 using two representative points  $(e_1, \phi_{p1})$  and  $(e_2, \phi_{p2})$  and obtain the slope of the friction angle versus void ratio and easily get a first estimate of the value of  $p$ .

**@Seismicisolation**

Recent experience suggests  $p$  values in the range of  $p = 2.50 \pm 0.20$  for most sands. This reduces significantly the range of  $p$  that needs to be analyzed.

Parameter  $\phi'_{mr}$  represents a reference value arbitrarily selected at a unity void ratio. Nevertheless, there are sands with much lower formation void ratios than 1.0, such as the case for Berlin sand, and therefore values of  $\phi'_{mr}$  are expected to be lower than those obtained for Toyoura sand. Similarly, for sands with formation ratios larger than one, it is expected that values for  $\phi'_{mr}$  should be larger than those quoted for Toyoura sand. Perhaps a more representative value is the value of  $\phi'_m$  at the maximum formation void ratio,  $e_{max}$  for a specific sand. Using the values given in Table 1 and equation 2, it is possible to calculate the corresponding values of  $\phi'_m$  at  $e_{max}$  for Toyoura and Berlin sands as follows:

Sand	$e_{max}$	Selected: $\phi'_{mr}$	Selected: $p$	Inferred: $\phi'_m$ at $e_{max}$
Toyoura	0.98	28.5°	2.45	29.3
Berlin	0.59	12.5°	2.70	33.4

As can be seen the value of  $\phi'_m$  at the maximum formation void ratio is very close (within a few degrees) of the critical state friction angle and better reflects the specific formation characteristics for a given sand. Alternatively, if we assume as a first approximation that  $\phi'_m = \phi'_s$  at  $e = e_{max}$  and using an average value of  $p = 2.5$  for many sands, it is possible to have a first estimate of the value of  $\phi'_{mr}$  used by the MIT-S1 model.

Sand	$e_{max}$	Selected: $\phi'_m$ at $e_{max}$	Estimated : $p$	Inferred: $\phi'_{mr}$
Toyoura	0.98	31.0°	2.50	30.0°
Berlin	0.59	31.0°	2.50	12.0°

As can be seen from this simple exercise, the estimated values are very close to the final values selected by Pestana et al (2002) and Nikolinakou et al. (2004a) and simplify tremendously the selection process.

The parameter  $\omega_s$  controls the non-linearity in the stress-strain behavior at relatively small shear strains (less than 0.1%). This parameter has little influence on the overall predictions of stress-strain behavior (with shear strains in the range 1-10%). The final model input parameter,  $\psi$ , controls rotational hardening of the yield surface in MIT-S1 and hence, characterizes the evolution of anisotropic deformation and strength properties.  $\psi$  has been calibrated from the stress-strain response measured during undrained shearing to large strains. The value of  $\psi$  also has a secondary effect on the predictions of peak friction angle and on the strain required to mobilize the peak strength in CIDC tests. Figure 6 compares model predictions for  $\psi = 10$  and 25 with the measured shear stress-strain behavior from CIDC tests on Berlin sand consolidated to  $\sigma'_c = 800$ kPa from different formation void ratios. Although the results show that the model tends to underestimate the initial shear stiffness and peak shear resistance of the densest specimens (i.e.,  $e_0 = 0.462, 0.491$ ), the general trends in behavior are well described by the model with input parameters listed in Table 1.

Figure 7 compares the predicted and measured undrained effective stress paths and shear stress-strain behavior of dense specimens of Toyoura sand ( $e_i = 0.735$ ) at four different confining pressures,  $\sigma'_c \sim 0.1, 1.0, 2.0$  and  $3.0$  MPa. Good agreement is expected between model simulations for the CIUC tests at  $\sigma'_c = 3.0$  MPa, since this test is part of the database from which the input parameters were determined. The model predicts that all samples having the same pre-shear void ratio will have the same undrained strength at large strains.

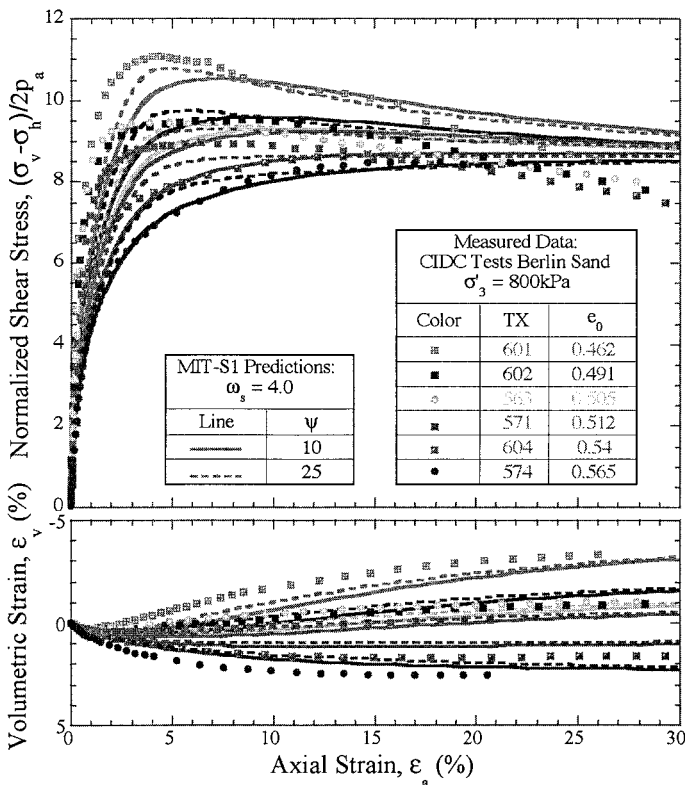


FIG. 6. Effect of parameter  $\psi$  on MIT-S1 model predictions of drained triaxial shear tests (CIDC) on Berlin sand (after Nikolinakou et al., 2004a)

The model accurately predicts the undrained stress paths and the transition from strongly dilative behavior experienced by specimens consolidated at low stresses (e.g., 0.1 to 1 MPa) to moderately contractive behavior at high stresses (e.g., positive pore pressures at confining stresses = 2.0- 3.0 MPa). Stress-strain curves and pore pressure-strain curves predicted by the model are in good agreement with measurements for tests at a confining pressure of 1.0 and 2.0 MPa and are in excellent agreement with the data at the lowest confining stress of 0.1 MPa.

For Toyoura sand, there is little uncertainty in the location of the critical state line reported from undrained triaxial compression shear tests reported by Ishihara (1993). Figure 8 shows excellent agreement between these data and MIT-S1 predictions using the parameters listed in Table 1. The critical state line, CSL, forms a non-linear locus over the range of the measured data (i.e.,  $0.3 \leq \sigma'/p_{at} \leq 30$ ) and highlights the limitations of the conventional linear relation in e-log $\sigma'$  space. At low stress levels, the slope of the CSL is very small, resulting in large changes in the undrained shear strength (at critical state) for small perturbations in void ratio. At larger stresses, the slope of the CSL increases and is parallel to the LCC at high pressures.

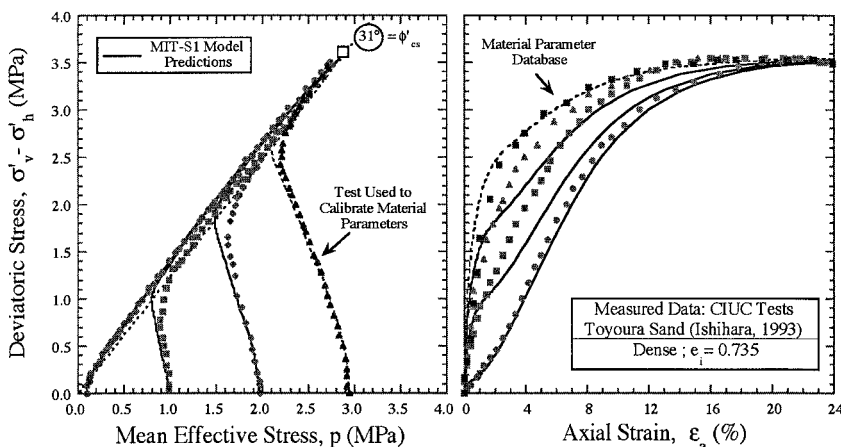


FIG. 7. Comparison of predicted response for CIUC tests on dense Toyoura sand

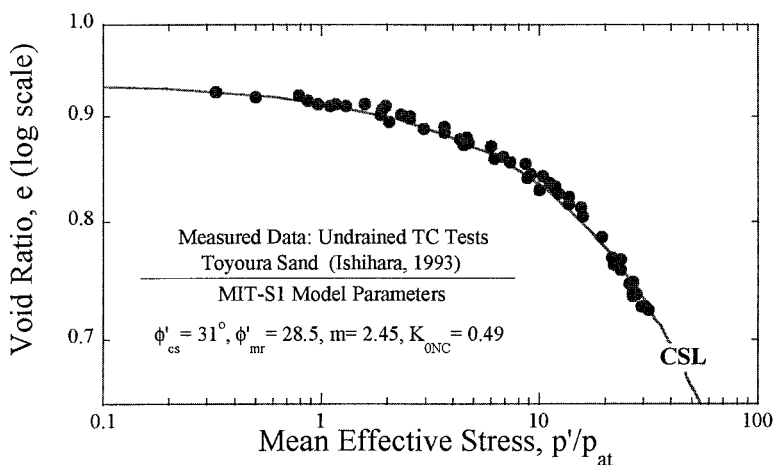


FIG. 8. Comparison of predicted and measured behavior at critical state for Toyoura sand determined from undrained tests.

**@Seismicisolation**

## CONCLUSIONS

This paper illustrates the selection of material parameters for the MIT-S1 model with particular application to the behavior of two clean, uncemented sands: Toyoura and Berlin sand. The 13 model input parameters can be broadly grouped into three subsets: 1) parameters that can be unambiguously obtained from the laboratory tests ( $\rho_c$ ,  $p'_{ref}/p_{at}$ ,  $\theta$ ,  $\phi'_{cs}$ ); 2) parameters that have relatively small ranges of input values and can be reasonably estimated based on prior empirical experience ( $K_{ONC}$ ,  $v'_0$ ,  $\omega$ ), and 3) parameters that require detailed interpretation of the laboratory data ( $C_b$ ,  $\phi'_{mr}$ ,  $p$ ,  $m$ ,  $\psi$ ,  $\omega_s$ ). Recent experience suggests smaller ranges for parameters  $p = 2.5 \pm 0.2$  and  $m = 0.5 \pm 0.2$  and presents guidelines to obtain a first approximation of the value of  $\phi'_{mr}$  based on (readily determined values of) the critical state friction angle,  $\phi'_{cs}$ , and the maximum void ratio,  $e_{max}$ .

The calibration of MIT-S1 has been showcased for Toyoura sand based on procedures presented by Pestana and Whittle (1999), enabling very good predictions the measured peak friction angles, critical state conditions, and effective stress-strain-strength properties measured in undrained and drained triaxial compression tests. The success of the model for Toyoura sand reflects the high quality of the published database on this reference material and the relatively small uncertainties in the location of the critical state line.

The Berlin sand has a very small range of formation void ratios and higher formation density than other apparently similar silicate sands reported in the literature. The selection of model input parameters for shear behavior has proved quite a challenge due to the uncertainty in the location of the critical state for shearing at large strains, and the variability in the measured peak friction angles from drained shear tests. The final set of model parameters for Berlin sand appear to achieve a very good compromise in describing the peak friction angles, critical state conditions, and effective stress-strain-strength behavior for both undrained and drained triaxial compression modes of shearing.

A comparison of the methodologies used for the two sands has provided insights for simplifying parameter selection in future studies.

## ACKNOWLEDGMENTS

The research on Toyoura sand has been documented in previous papers by the authors. The model application for Berlin sand is based on recent research at MIT that has been supported by grants from the NSF Western Europe (INT-0089508) program and DAAD. The lab tests were performed at the MIT geotechnical laboratory under the expert supervision of Dr John Germaine. Special thanks also to Ralf Glasenapp and Tim Becker for their meticulous experimental work.

## APPENDIX A: CRITICAL STATE LINE

The location of the Critical State Line predicted by MIT-S1 model in triaxial compression mode can be found analytically as a closed form function of the void ratio,  $e$ , as follows (Pestana, 1994):

$$\frac{\sigma'}{\sigma_r} = \left( \frac{a^2}{a^2 + b_1^2} \right) \left( \frac{c_a^2 - k_a^2}{c_a^2 - d_a^2} \right)^{1/m} (e)^{-1/p_c} \quad (A1)$$

where  $\sigma'$  is the mean effective stress, and  $e$  the void ratio.

The other terms in eqn. A1 can be written in terms of the material constants as follows:

$$a^2 = 24 \left( \frac{\sin \phi'_{cs}}{3 - \sin \phi'_{cs}} \right)^2 < 1 \quad (A2)$$

$$k_a^2 = (8 \sin^2 \phi'_{cs}) (3 + \sin^2 \phi'_{cs})^{-1} \quad (A3)$$

$$d_a^2 = \frac{2(1 - K_{0NC})^2}{(1 + K_{0NC} + K_{0NC}^2)} \quad (A4)$$

$$d^2 = d_a^2 + \left( 3 - \frac{d_a^2}{2} \right) \left( \frac{\eta_1^3}{3\sqrt{6}} \right) \quad (A5)$$

$$\eta_1 = 2\sqrt{6} \frac{\sin \phi'_{cs}}{3 - \sin \phi'_{cs}} \quad (A6)$$

The term  $b_1$  describes the orientation of the yield surface at the critical state condition and is a root of the following equation:

$$b_1^2 - 2\eta_1 b_1 + d^2 = 0 \quad (A7)$$

And

$$c_a^2 = (8 \sin^2 \phi'_{mr}) (3 + \sin^2 \phi'_{mr})^{-1} \quad (A8)$$

$$\text{where: } \tan \phi'_{mr} = \left( A + \left( \frac{1}{\tan \phi'_{mr}} - A \right) (e)^p \right)^{-1} \quad (A9)$$

$$\text{and } A = \tan(45^\circ - \phi'_{cs}/2) \quad (A10)$$

Hence, the critical state line in eqn (A1) is fully defined from the material input parameters  $\sigma'$ ,  $p_c$ ,  $m$ ,  $\phi'_{cs}$ ,  $\phi'_{mr}$ ,  $p$  and  $K_{0NC}$ .

## REFERENCES

- Becker, T. (2002) "Triaxialversuche mit reduzierter Endflächenreibung zur Untersuchung des Materialverhaltens von Berliner Sand," Diplomarbeit, Technische Universität Berlin, Fachgebeit für Grundbau und Bodenmechanik.
- De Beer, E.E. (1965) "Influence of the mean normal stress on the shearing strength of sand," *Proc. 6th ICSMFE*, Montreal, 1, 165-169.
- Glasenapp, R. (2002) "Triaxialversuche mit Berliner Sand," Diplomarbeit, Technische Universität Berlin, Fachgebeit für Grundbau und Bodenmechanik.
- Hendron, A.J. Jr. (1963) "The Behavior of Sand in One-Dimensional Compression," Ph.D. Thesis, University of Illinois, at Urbana, IL.
- Hsieh, Y-M., Whittle, A.J. & Yu, H-S. (2002) "Interpretation of pressuremeter tests in sand using an advanced soil model," *ASCE Journal of Geotechnical & Geoenvironmental Engineering*, 128(3), 274-278.
- Ishihara, K. (1993) "Liquefaction and Flow Failure During Earthquakes," *Géotechnique*, 43(3), 351-415.
- Miura, N. and Yamanouchi, T. (1975) "Effect of Water on the Behavior of a Quartz-Rich Sand Under High Stress," *Soils and Foundations*, 15(4), 23-34.
- Nikolinakou, M., Whittle, A.J. & Savidis, S. (2004a) "Selection of MIT-S1 parameters for Berlin sand," *Proc. Geotechnical Innovations*, Eds. R.B.J. Brinkgreve, H. Schad, H.F. Schweiger, & E. Willand, Verlag Glückauf, 599-608.
- Nikolinakou, M., Whittle, A.J., Savidis, S. & Schran, U. (2004b) "Modeling of Berlin sand and prediction of excavation performance for the VZB project," Draft paper in preparation.
- Pestana J.M. (1994) "A unified constitutive model for clays and sands", Sc.D. thesis, MIT, Cambridge, MA.
- Pestana, J.M. & Whittle, A.J. (1995) "Compression model for cohesionless soils," *Géotechnique*, 45(4), 611-633.
- Pestana, J.M. & Whittle A.J. (1999) "Formulation of a unified constitutive model for clays and sands," *International Journal for Numerical and Analytical Methods in Geomechanics*, 23, 1215-1243.
- Pestana, J.M., Whittle, A.J. & Salvati, L. (2002) "Evaluation of a constitutive model for clays and sands: Part I – Sand behavior," *International Journal for Numerical and Analytical Methods in Geomechanics*, 26, 1097-1121.
- Prévost, J.H. (1978) "Plasticity theory for soil stress-strain behavior," *ASCE, Journal of Engineering Mechanics Division*, 104 (EM5), 1177-1194.
- Tatsuoka, F. and Shibuya, S. (1992) "Deformation Characteristics of Soils and Rocks from Field and Laboratory Tests," *Proc. 9th Asian Regional Conf. on Soil Mech. and Found. Engrg.*, Bangkok, 2, 101-190.

## PARAMETERS FOR AVERAGE GULF CLAY AND PREDICTION OF PILE SET-UP IN THE GULF OF MEXICO

Andrew J. Whittle<sup>1</sup>, P.E., Member, ASCE and Twarath Sutabutr<sup>2</sup>

**ABSTRACT:** The MIT-E3 soil model has been applied in predictions of set-up for driven piles in soft clays for more than fifteen years. Site specific calibrations of model parameters have been performed for a series of offshore projects in the Gulf of Mexico (in water depths, 750m - 1200m), following a standardized suite of laboratory tests. This paper presents a synthesis of these model calibrations and shows that Pleistocene clay units in the Gulf of Mexico can be represented by the MIT-E3 model with input parameters corresponding to an Average Gulf Clay (AGC). Engineering properties of AGC are then compared with behavior for other high plasticity clays. Predictions of pile set-up can be performed using generic design charts developed for AGC.

### INTRODUCTION

The MIT-E3 soil model (Whittle, 1987) was developed to simulate the effective stress-strain-strength behavior of normally and moderately overconsolidated clays ( $1 \leq \text{OCR} \leq 4$ ). Although the model formulation is relatively complex, practical application of the model is made possible through a standardized procedure for parameter selection using results of laboratory tests. To date, this procedure has been used to calibrate parameters for more than 20 types of clay. The model has been used extensively in numerical analyses of practical geotechnical problems ranging from the performance of offshore friction piles (Aubeny, 1992; Whittle, 1992), to embankments on soft ground (Ladd et al., 1994; Zdravkovic et al., 2002) and deep excavations (Whittle et al., 1993; Jen, 1998; Hashash & Whittle, 2001) through integration of the constitutive equations in finite element programs.

The model has been particularly widely used in the prediction of pile set-up in clay in the design of large diameter, open-ended piles used to support offshore structures. The key assumption of these analyses is that the capacity of driven, friction piles is controlled by changes in the effective stresses and soil properties that occur during successive phases in the life of a pile. Set-up refers to the increase in shaft capacity that occurs after driving, due to dissipation of installation-induced excess pore pressures and concomitant increases in effective stresses within the soil. The predictions have been extensively validated with data from instrumented model

<sup>1</sup> Professor, Department of Civil and Environmental Engineering, Massachusetts Institute of Technology, Cambridge, MA 02139, ajwhitl@mit.edu

<sup>2</sup> Department of Mineral Resources, Royal Thai Government, Bangkok, Thailand



piles and pile shaft elements at a number of well documented on-shore test sites (e.g., Whittle & Sutabutr, 1999). The previous research (e.g., Azzouz et al., 1990; Whittle, 1992) has also shown that there are many soil properties that can affect predictions of soil stresses and pore pressures during undrained pile installation and subsequent consolidation. For example, small strain stiffness properties and post-peak strain softening (sensitivity) affect the radial extent and magnitude of the installation excess pore pressures, while the initial stress history (OCR) and radial compressibility (within the installation zone of disturbance) affect the subsequent dissipation. Given this complexity, the development of generalized solutions for predicting pore pressure dissipation and/or pile set-up is highly unlikely.

During the last 10 years, site specific calibrations of the MIT-E3 model have been developed for a series of five major projects in the Gulf of Mexico in water depths ranging from 750m – 1200m. The projects span a distance of more than 600km, include sites in the Garden Banks, Green Canyon, Mississippi Canyon and Viosca Knoll sectors of the Gulf. In each case, suites of laboratory triaxial shear tests were performed on specimens from selected units of the clay to enable MIT-E3 parameter selection and prediction of pile set-up. In reviewing data from these projects, Sutabutr (1999) found a relatively small range among each of the key model parameters and hence, proposed that the set-up can be predicted with reasonable accuracy using a single set of parameters corresponding to the behavior of Average Gulf Clay (AGC). This paper summarizes the parameter selection, the MIT-E3 predictions for AGC properties and proposes a design procedure for estimating pile set-up at deepwater sites in the Gulf of Mexico.

## PARAMETER SELECTION FOR MIT-E3 MODEL

The MIT-E3 formulation (Whittle & Kavvadas, 1994) is based on the theory of incrementally linearized elasto-plasticity and consists of three distinct components: a) an elasto-plastic model for normally consolidated clays; b) a perfectly hysteretic formulation and c) bounding surface plasticity. The model describes a number of important aspects of soil behavior which have been observed in laboratory tests on  $K_0$ -consolidated clays including: 1) small strain non-linearity following a reversal of load direction; 2) hysteretic behavior during unload-reload cycles of loading; 3) anisotropic stress-strain-strength properties associated with 1-D consolidation history and subsequent straining; 4) post-peak, strain softening in undrained shear tests in certain modes of shearing on normally and lightly overconsolidated clays; and 5) occurrence of irrecoverable plastic strains during cyclic loading and shearing of overconsolidated clays. The model also has a number of key restrictions: 1) it uses a rate independent formulation and hence, cannot model creep, relaxation or other strain rate dependent properties of the soil skeleton; and 2) it assumes normalized soil properties (e.g., the strength and stiffness are proportional to the confining pressure at a given overconsolidation ratio, OCR) and hence, does not describe complex aspects of soil behavior associated with cementation; and 3) its predictions become progressively less reliable for  $OCR > 4 - 8$ .

Whittle et al. (1994) detailed a procedure for selecting model input parameters from a suite of laboratory tests. Table 1 summarizes these input parameters, their physical meaning within the model formulation and laboratory tests from which they



can be obtained. Five of the fifteen input parameters can be obtained from 1-D consolidation tests (preferably performed in a CRS consolidometer) which include at least one cycle of unloading and reloading in the prescribed test procedure. Two of these parameters correspond to the conventional Virgin Consolidation Line (VCL;  $e_0$ ,  $\lambda$ ) used in other critical state soil models, while the other three define the non-linear stiffness in unloading ( $C$ ,  $n$ ) and irrecoverable plastic strain ( $h$ ) from the reload branch. An example model calibration from a CRS tests is shown in Figure 1.

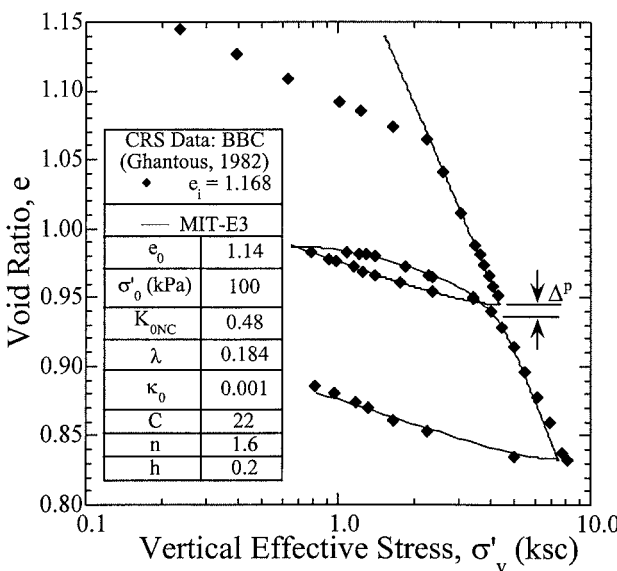


**FIG. 1. Calibration of MIT-E3 input parameters from 1-D consolidation test (Whittle et al. 1994)**

Another 8 parameters are obtained from a suite of three independent undrained triaxial shear tests on  $K_0$ -consolidated specimens. The model formulation assumes normalized soil properties and hence, these tests can be performed using SHANSEP type consolidation procedures (Ladd & Foott, 1974), where the specimens are loaded to stress levels typically up to two times the measured pre-consolidation pressures. Two calibration tests are needed at  $OCR = 1.0$ , one each in triaxial compression and extension modes of shearing ( $CK_0UC$  and  $CK_0UE$ , respectively), while a third compression test should be performed on a specimen consolidated at a specified  $OCR \approx 1.5 - 2.0$ . Among this group of parameters  $K_{0NC}$  and  $2G/K^*$  are derived from the consolidation branches of the tests, while  $\phi'_{TC}$  and  $\phi'_{TE}$  correspond to the friction angles measured for shearing to large shear strains. Of the remainder, two ( $c$ ,  $\gamma$ ) are derived from the measured effective stress paths and two from the shear stress-strain

\*  $2G/K = 3(1-2\nu')/(1+\nu')$ , where  $\nu'$  is the elastic Poisson's ratio at load reversal.

curves (pre-peak,  $\omega$ ; and post-peak,  $s_t$ ). Figure 2 illustrates the calibration of these model parameters from  $K_0$ -consolidated undrained triaxial shear tests.

The parameter  $\kappa_0$  controls the stiffness of clay that is encountered for shearing at very small strain levels or immediately after reversal of load direction. In principal,  $\kappa_0$ , can also be obtained from triaxial tests that are equipped to measure small strain stiffness either statically using local (on-specimen) strain measurements or indirectly from shear wave velocity measurements using bender elements. Alternatively,  $\kappa_0$  can be found from laboratory resonant column or in-situ shear wave velocity data.

The final model parameter,  $\psi_0$ , describes the rotation rate of the bounding yield surface for MIT-E3 and hence, controls the evolution of anisotropic properties for normally consolidated clays. Whittle et al. (1994) have shown that this parameter can be estimated from specially devised drained strain path consolidation tests (performed in a triaxial cell). Parametric studies have found that this parameter has little influence on model predictions and hence, a default value has been used in most practical applications of the model to date.

Table 1 contrasts the selected values of model input parameters for two reference materials; low plasticity (CL), sensitive ( $S_t = 3-7$ ) Boston Blue Clay and a high plasticity (CH), low sensitivity clay from the Empire test site in Louisiana. There is an extensive database of laboratory tests available on resedimented Boston Blue Clay, enabling very detailed validation of model predictions at the element level (Whittle et al., 1994), while parameters for Empire clay were based on laboratory tests performed by Lutz (1984). Whittle and Baligh (1988) have compared predictions of pile set-up with field measurements for a model pile shaft (PLS cell) reported by Azzouz & Morrison (1988) at both MIT and Empire tests sites.

## PROPERTIES OF HIGH PLASTICITY GULF OF MEXICO CLAYS

Geotechnical investigations from a series of five deepwater projects in the Gulf of Mexico (GOM) reported generalized soil profiles similar to those described by Quiros et al. (1983) and Doyle (1994) with two principal units:

- Upper Holocene deposits (generally less than 15m thick) with very high water contents,  $w_n > 100\%$  (often exceeding the liquid limit) and plasticity indices ranging from  $I_p = 60-85\%$ .
- Lower Pleistocene deposits that are predominately clay sediments with relatively low water content and plasticity index that decrease with depth. At 30m depth,  $w_n = 100\%$  and  $I_p = 60\%$ , while at 150m below mudline,  $w_n = 30\%$  and  $I_p = 40\%$ . The undrained shear strength typically increases linearly with depth, and the average sensitivity  $S_t \approx 2$ .

For long pipe pile foundations, the properties of the Pleistocene clays are of primary importance for set-up. In each project, model calibration test data were obtained on specimens ranging from 15m – 150m below mudline, avoiding units with significant slump features etc. Model input parameters for the Average Gulf Clay (AGC; Sutabutr, 1999), Table 1, are based on simple averaging of the site specific parameters from each of the five project locations. The following paragraphs compare model parameters and MIT-E3 predictions for AGC with the two reference soils (BBC, Empire) and with data from the five project sites.

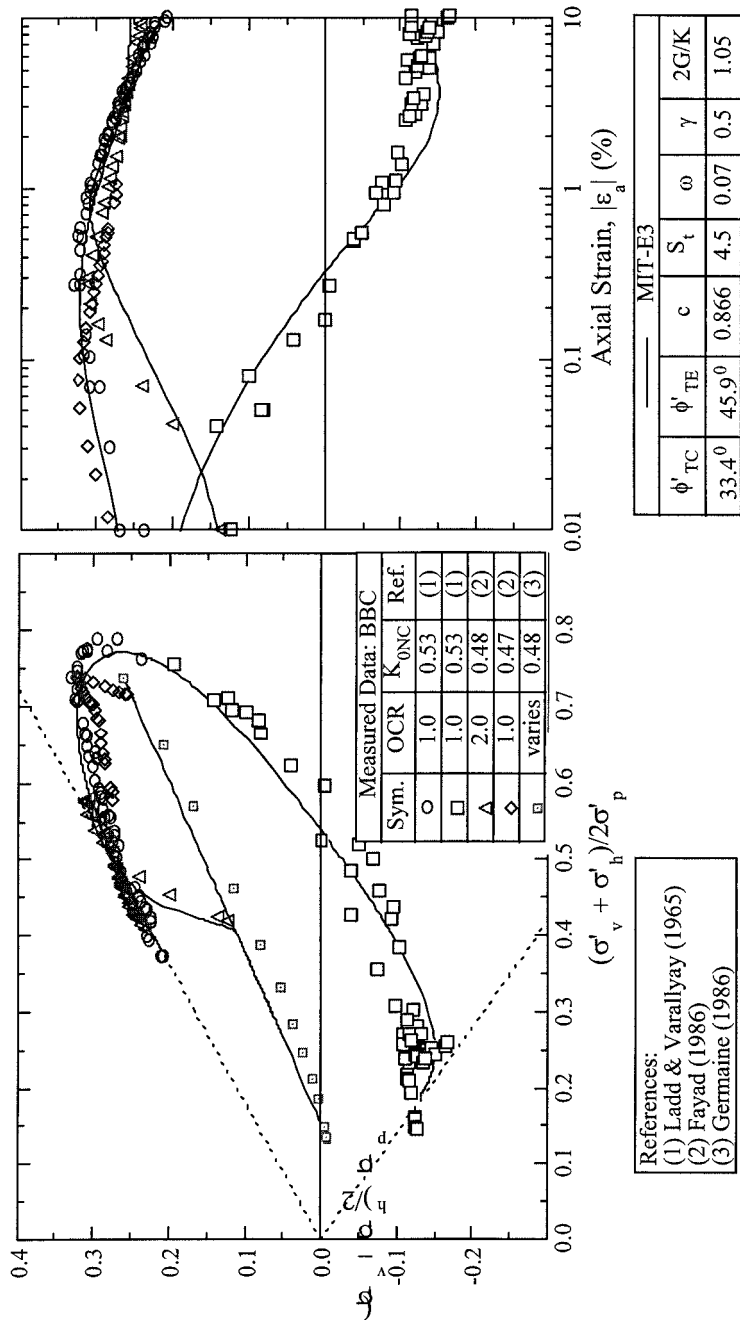


FIG. 2. Selection of MIT-E3 input parameters from undrained triaxial shear tests (Whittle et al., 1994)

**TABLE 1. Input Parameters for MIT-E3 Soil Model**

Test Type	Parameter/ Symbol	Physical contribution/meaning	Boston Blue Clay	Empire Clay	Average Gulf Clay AGC*
1-D Consolidation (Oedometer CRS etc.)	$e_0$	Void ratio at reference stress on virgin consolidation line	1.12	1.26	$1.492 \pm 0.36$
	$\lambda$	Compressibility of virgin normally consolidated clay	0.184	0.274	$0.282 \pm 0.082$
	C	Non-linear volumetric swelling behavior	22.0	24.0	$6.25 \pm 0.92$
	n		1.6	1.75	$1.53 \pm 0.04$
	h	Irrecoverable plastic strain	0.2	0.2	0.3
K <sub>0</sub> -oedometer or K <sub>0</sub> -triaxial	K <sub>DNC</sub>	K <sub>0</sub> for virgin normally consolidated clay	0.48	0.62	0.63
	2G/K	Ratio of elastic shear to bulk modulus (Poisson's ratio for initial unload)	1.05	0.86	$0.923 \pm 0.04$
Undrained Triaxial Shear Tests: OCR=1; CK <sub>0</sub> UC	$\phi_{TC}$	Critical state friction angles in triaxial compression and extension (large strain failure criterion)	33.4°	23.6°	$25.6^\circ \pm 1.2^\circ$
	$\phi_{TE}$		45.9°	21.6°	$27.8^\circ \pm 2.3^\circ$
	c	Undrained shear strength (geometry of bounding surface)	0.86	0.75	$0.785 \pm 0.03$
OCR=1; CK <sub>0</sub> UE OCR=2; CK <sub>0</sub> UC	s <sub>t</sub>	Amount of post-peak strain softening in undrained triaxial compression	4.5	3.0	$3.1 \pm 0.5$
	$\omega$	Non-linearity at small strains in undrained shear	0.07	0.20	$0.39 \pm 0.17$
Shear wave velocity <sup>1</sup>	$\gamma$	Shear induced pore pressure for OC clay	0.5	0.5	$0.5 \pm 0.1$
Drained Triaxial	$\kappa_0$	Small strain compressibility at load reversal	0.001	0.0035	$0.0065 \pm 0.002$
	$\psi_0$	Rate of evolution of anisotropy (rotation of bounding surface)	100.0	100.0	100.0

\* Standard deviation based on data from five project sites.

The parameters  $\lambda$ ,  $e_0$  characterize the compressibility of  $K_0$ -normally consolidated clay. Figure 3 shows one dimensional compression data from Constant Rate of Strain (CRS) and incremental oedometer tests from the 5 offshore sites. The selected virgin consolidation line (VCL;  $\lambda=0.282$ ,  $e_0=1.492$ ) of AGC provides a good representation of the average behavior from four of the five sites, where there is little variation in the interpreted VCL with depth. At site 1, the VCL varies substantially with depth, requiring a more detailed subdivision of the Pleistocene clay units. The Average Gulf Clay is much more compressible than resedimented BBC ( $\lambda = 0.184$ ,  $e_0 = 1.12$ ) but very similar to Empire clay ( $\lambda = 0.274$ ,  $e_0 = 1.26$ ).

The parameter  $\kappa_0$  controls the small strain stiffness of the clays. For each of the five offshore projects, the value of  $\kappa_0$  was obtained from resonant column tests that measured maximum shear modulus,  $G_{\max}/\sigma' v_0 \approx 150 \pm 50$ . In general, the interpreted small strain shear stiffness of AGC is lower than the Empire clay ( $G_{\max}/\sigma' v_0 = 200$ ) and much smaller than that for the low plasticity BBC ( $G_{\max}/\sigma' v_0 = 1100$ ).

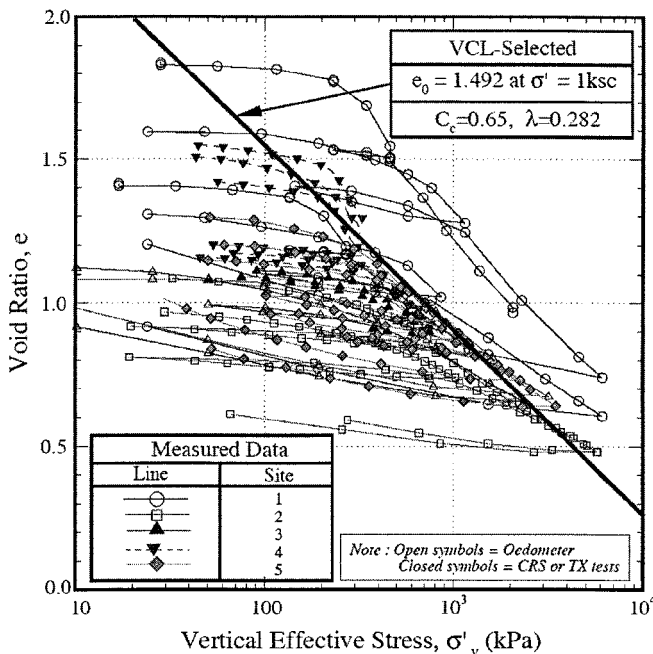


**FIG. 3. Representation of GOM compression data using AGC parameters**

The parameters  $C$  and  $n$  control the amount of recoverable strain on unloading and reloading. These parameters are important for predictions of pile set-up as they affect the radial compressibility of the soil close to the pile shaft. Unfortunately, the physical interpretation of these parameters cannot be decoupled from the selected value of  $\kappa_0$ .

However, observe differences in the one-dimensional swelling strain predicted for a specified amount of unloading as shown in Figure 4. For example, the strain obtained for swelling to stress level,  $\xi_v = 10$ , for the five offshore sites,  $\Delta\epsilon_v = 2.0 - 5.0\%$ . This is much lower than the strain recovered for Empire clay ( $\Delta\epsilon_v = 10\%$ , generating a much high value of C; Table 1) but quite comparable to BBC ( $\Delta\epsilon_v = 2\%$ ). This is quite a surprising result and may reflect differences in the mineralogy between the Empire clay and the GOM sites, or in their geological deposition histories.

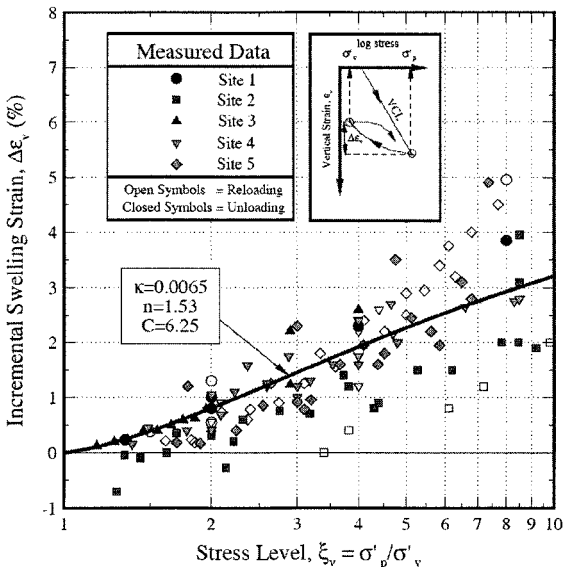
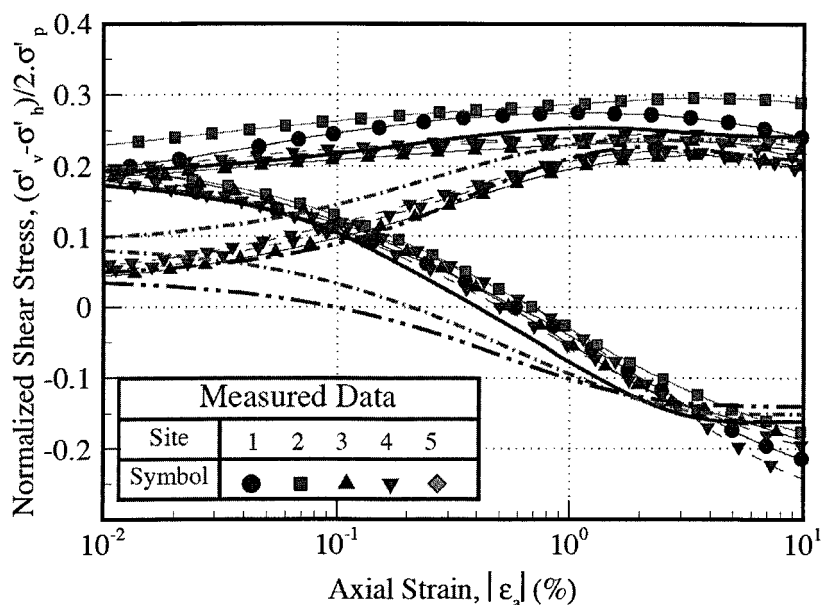
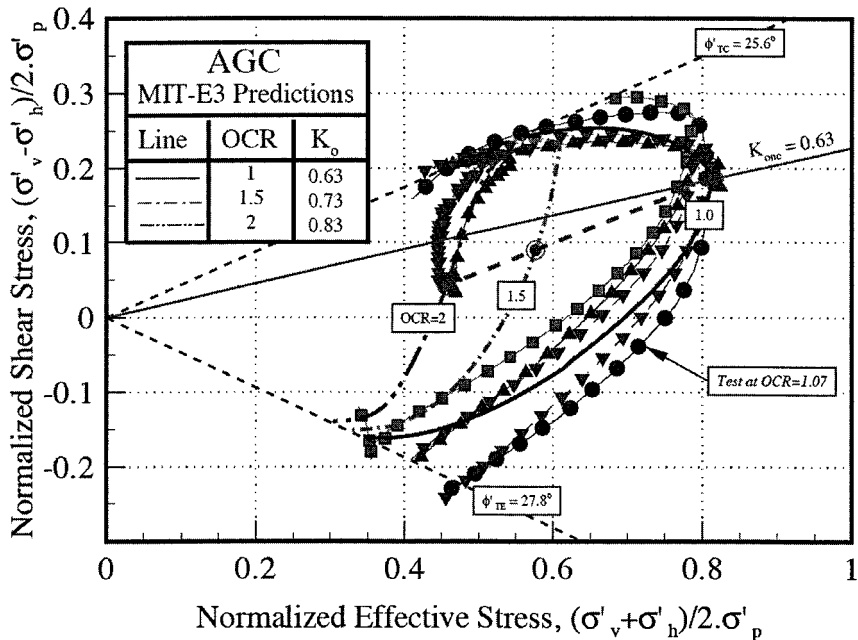
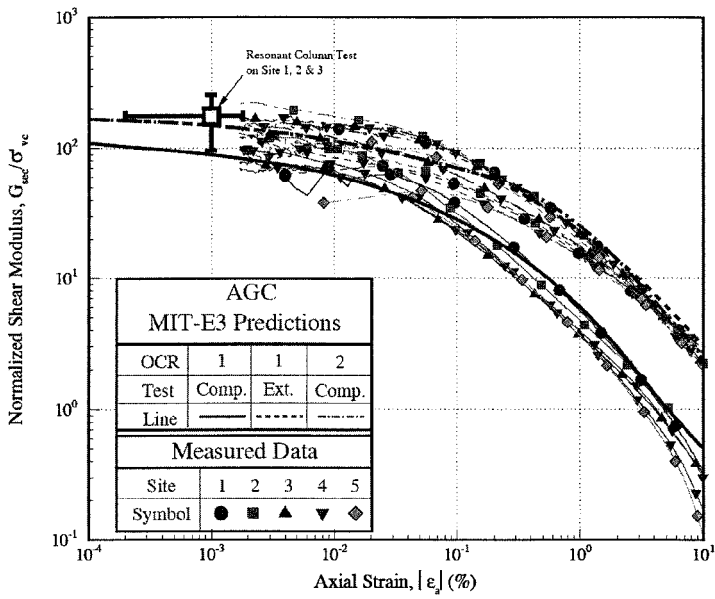


**FIG. 4. Comparison of measured 1-D swelling behavior for GOM clays with AGC representation**

The large strain friction angles of AGC are well defined from undrained compression tests ( $\phi'_{TC} = 25.6^\circ \pm 1.2^\circ$  from the five projects). However, it is often more difficult to obtain reliable friction angles from the extension tests ( $\phi'_{TE} = 27.8^\circ \pm 2.3^\circ$ ) due to experimental problems of sample necking. The AGC friction angles are generally higher than those selected for the high plasticity Empire clay. There is a very small range in the measured lateral stress ratio for  $K_0$ -normally consolidated GOM clays,  $K_{0NC} = 0.63 \pm 0.02$  and these data match earlier measurements for the Empire clay. The shape of the MIT-E3 yield surface is described by the parameter, c. Surprisingly, there is no correlation between the selected values of c and the soil plasticity (Table 1). This result reflects a limitation of the MIT-E3 model that has been investigated extensively by Pestana (1994).



@Seismicisolation



c) Secant modulus degradation

**FIG. 5. Comparison of measured undrained triaxial shear behavior for GOM clays with MIT-E3 model with AGC parameters**

Figures 5a-c compare the measured effective stress paths, shear stress strain response and secant shear modulus degradation from the five GOM sites with MIT-E3 predictions using the AGC parameters. It is clear that AGC provide a good first order representation of the measured data in the compression and extension shear modes. There is significant scatter in the measured undrained strength ratios in triaxial compression tests ( $s_{uTC}/\sigma'_p = 0.22 - 0.30$ ) at  $\text{OCR} = 1.0$ . The AGC predicts an average undrained strength ratio,  $s_{uTC}/\sigma'_p = 0.25$ , that is mobilized at an axial strain,  $\epsilon_{ap} = 1.5\%$  consistent with the data. These strength ratios are much lower than those measured for BBC and show minimal post-peak strain softening (cf. Fig. 2). The predicted undrained shear strength ratio in the extension mode ( $s_{uTE}/\sigma'_p = 0.16$ ) is consistent with the shear resistance measured at 5% axial strain, but tends to underestimate the measured large strain conditions (in part this is due to necking in the tests). The model gives excellent representation of the non-linear shear stiffness as a function of the shear strain level in both shear modes and at  $\text{OCR} = 2.0$  (Figs. 5b, c).

Figures 6a and b compare the AGC predictions with measured behavior from  $K_0$ -consolidated undrained Direct Simple Shear ( $CK_0\text{UDSS}$ ) tests on the GOM clays. These tests are routinely performed for the geotechnical characterization of the undrained shear strength profiles at the project sites. They provide a partial validation of model predictions at the element level (as the data are not used in parameter selection). The

results show excellent agreement between the computed and measured effective stress paths and shear stress-strain response, with undrained strength ratio,  $s_{uDSS}/\sigma'_p = 0.233$  at OCR = 1.0.

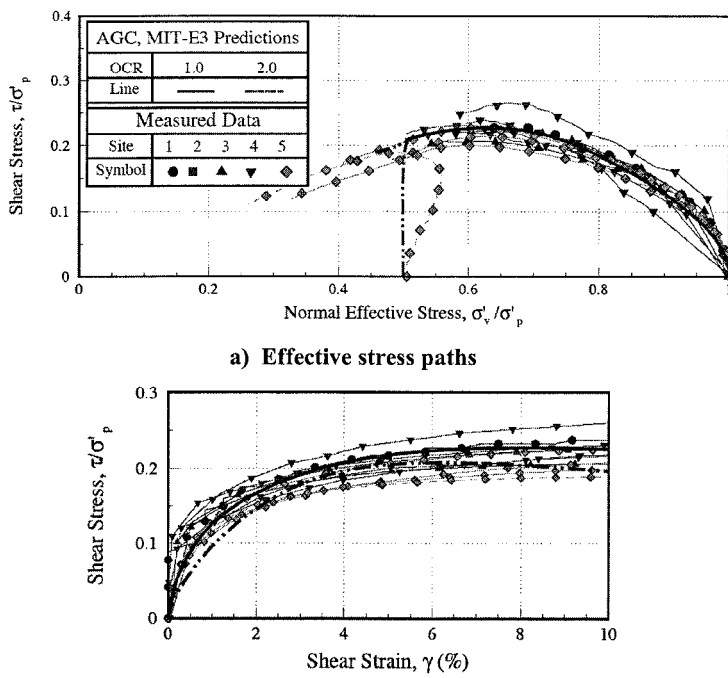


**FIG. 6. Comparison of predicted and measured behavior of GOM clays in  $K_0$ -consolidated undrained direct simple shear tests**

Figure 7 summarizes the predicted and measured undrained strength ratios as functions of OCR for each of the three standard shear modes. The MIT-E3 predictions with AGC parameters are in close agreement with the design strength relation proposed by Quiros et al. (1983) from three other sites in the Gulf of Mexico.

The results in Figures 3-7 provide solid evidence to support the use of AGC parameters to represent the effective stress strain strength properties of deepwater GOM clays.

## PREDICTIONS OF PILE SET-UP

### Methodology

Predictions of pile set-up are based on analyses which simulate the changes in effective stresses and soil properties occurring around a single pile during installation, subsequent equilibration of excess pore pressures, and undrained shear resistance of the

soil due to rapid axial loading of the pile shaft (Azzouz et al., 1990; Whittle, 1992). Pile installation is modeled using the framework of the Strain Path Method (SPM; Baligh, 1985), while changes in effective stresses and soil properties at all stages of the analysis are described by the MIT-E3 soil model with input parameters corresponding to Average Gulf Clay. The five project sites comprised clay deposits that were either normally consolidated or underconsolidated (due to excess pore pressures from shallow water flow). Predictions of set-up have been carried out assuming  $OCR \leq 2.0$  (Sutabutr, 1999).

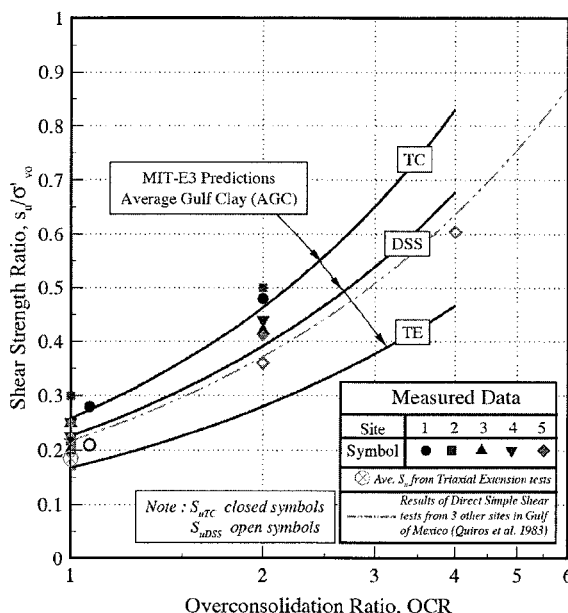


**FIG. 7 . Comparison of predicted and measured undrained shear strength ratios for GOM clays**

After installation, the analyses solve the dissipation of excess pore pressures around the pile shaft and set-up of effective stresses in the soil by non-linear finite element methods (based on work of Aubeny, 1992). These effective stress, coupled consolidation analyses (E-C) assume that pore water flow in the soil is controlled by D'Arcy's law, with constant (homogeneous) hydraulic conductivity,  $k$ . Hence, non-linearity is controlled exclusively by stiffness changes of the soil skeleton. For these assumptions, there is no unique definition of the time factor. Instead, a dimensionless time factor,  $T$ , is selected in order to normalize predictions of set-up times in normally and lightly overconsolidated clays (typically found offshore). Aubeny (1992) showed that the effective normalization is achieved using the following definition:

$$T = \frac{\sigma'_p k t}{\gamma_w R_{eq}^2} \quad (1)$$

where  $t$  is the time after probe installation,  $\sigma'_p$  is the vertical pre-consolidation pressure (measured in laboratory 1-D consolidation tests);  $R_{eq}$  is the equivalent radius\* of a closed-ended (i.e., solid cylindrical section) pile,  $\gamma_w$  is the unit weight of water and  $k$  is the hydraulic conductivity of the clay (either measured in laboratory CRS consolidation tests or backfigured from field dissipation measurements; Whittle et al., 2001).

Predictions of axial pile capacity are evaluated in terms of the limiting shear resistance acting at the surface of the pile based on the  $\rho$ -method of Azzouz et al. (1990). The limiting skin friction at any time,  $t$ , after pile installation is written as:

$$f_s(t) = \beta \sigma'_{v0} = K \rho \sigma'_{v0} \quad (2)$$

where  $K\sigma'_{v0} = \sigma'_r$  is the lateral effective stress acting on the pile shaft and  $\rho$  is the undrained strength ratio of the clay adjacent to the pile shaft. The parameters  $K$  and  $\rho$  can be further subdivided:

$$K = \left( \frac{K}{K_c} \right) K_c \quad \text{and} \quad \rho = \left( \frac{\rho}{\rho_c} \right) \rho_c \quad (3)$$

where  $K_c$  and  $\rho_c$  are the parameters at full set-up (i.e., after full dissipation of the installation pore pressures;  $t \rightarrow \infty$ ), while the terms in brackets describe the set-up response characteristics.

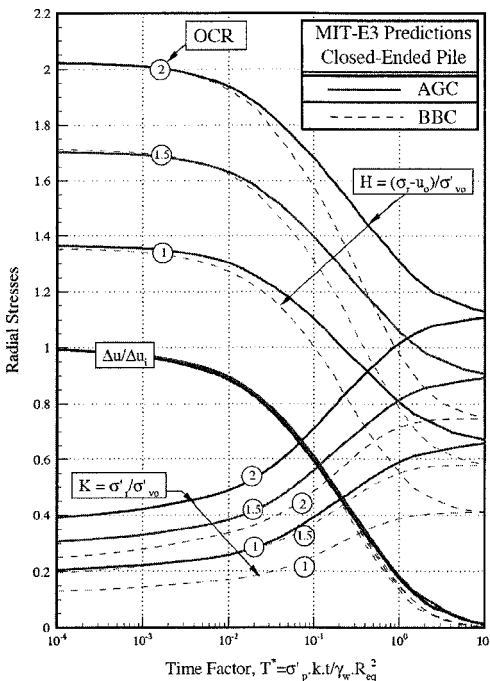
### Predictions for Average Gulf Clay

Figure 8 summarizes numerical predictions of set-up behavior at the shaft of a closed-ended pile (CEP) installed in  $K_0$ -consolidated AGC clay with OCR's = 1.0, 1.5 and 2.0 (corresponding to the full range of stress histories expected in the Gulf of Mexico clays). The results show the following:

- The predicted pore pressure dissipation curves,  $\Delta u / \Delta u_i$  (the subscript  $i$  refers to conditions at the end of pile installation, i.e.,  $T \rightarrow 0$ ) are practically independent of the initial OCR and are also very similar to results obtained for analyses of piles installed in BBC (actual dissipation times will depend on differences in  $\sigma'_p$  and  $k$ ).
- The initial radial effective stresses acting on the pile shaft (at the time of pile installation)  $K_i = 0.2 - 0.4$  are smaller than  $K_{0NC}$  (Table 1) for OCR's = 1.0 – 2.0. The radial stresses ( $K = \sigma'_r / \sigma'_{v0}$ ) increase monotonically during consolidation with final set-up conditions ranging from  $K_c = 0.66$  at  $OCR = 1.0$  to 1.11 at  $OCR = 2.0$ . The final set-up stresses are much higher for AGC than the reference results for BBC (at the same OCR).

\* For open-ended piles which penetrate in an unplugged mode,  $R_{eq} = \sqrt{(2Rw)}$ , where  $R$  is the pile radius and  $w$  the wall thickness.

- There is a substantial decay in total radial stress ( $H = [\sigma_r - u_0]/\sigma'_{v0}$ ) at the pile shaft for all OCR's, such that the final value of  $H/H_i$  for AGC varies from 0.48 at  $OCR = 1.0$  to 0.55 at  $OCR = 2.0$ . It is surprising that the predicted total radial stress at installation is similar for AGC and BBC (at all three OCR's). This result may reflect compensating effects of the different sensitivity and initial  $K_0$  of the two soils. However, it suggests that the total radial stress at installation is largely independent of soil type but is a function of initial OCR.



**FIG. 8. Predictions of set-up behavior for consolidation around closed-ended piles installed in AGC clay**

Sutabutr (1999) has performed a large number of set-up simulations for open-ended, pipe piles (OEP) with aspect ratios  $B/w = 50$  and  $100$  ( $B$  is the pile diameter and  $w$  the wall thickness). Figure 9 shows that the predictions of set-up behavior for these different pile geometries can be very well characterized for AGC by three parameters, the pore pressure ratio,  $\Delta u/\Delta u_i$ , the set-up of radial effective stress,  $K/K_c$  and the decay of total radial stress,  $H/H_i$ . The final set-up stress level,  $K_c$  is a function of the initial OCR and has some smaller dependence on the cross-sectional geometry of the pile as shown in Figure 10. This figure also confirms that the final set-up stresses for piles in AGC are comparable to  $K_{0NC}$  at  $OCR = 1$ , but are generally higher than the expected  $K_0$  conditions for  $OCR > 1.0$ . Values of  $K_c$  are 50% to 80% higher than comparable predictions for BBC (also shown on the same figure).

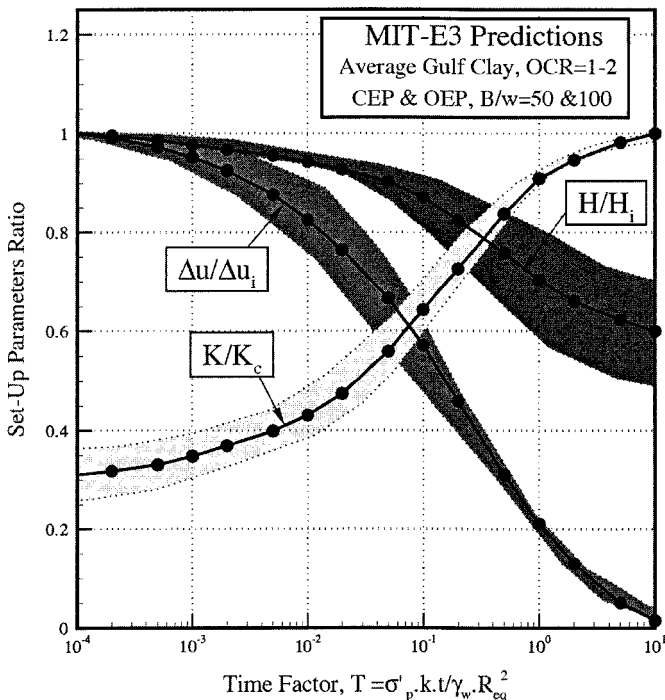


FIG. 9. Design chart showing normalized set-up behavior for AGC clay

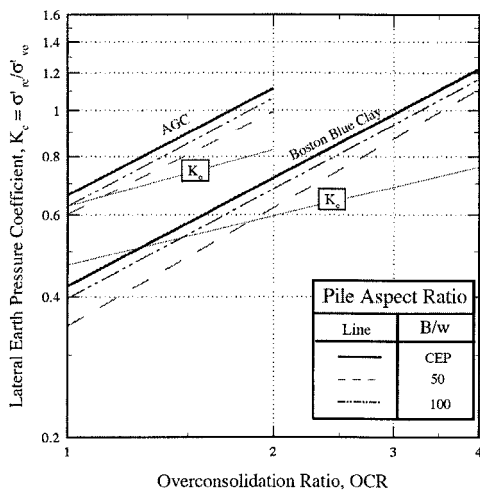
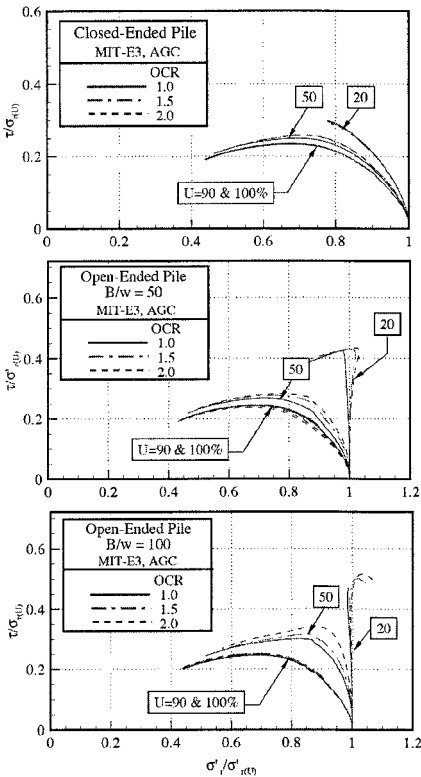


FIG. 10. Comparison of final set-up effective stress at pile shaft for AGC and BBC

@Seismicisolation



**FIG. 11. Model predictions of shear behavior for soil elements adjacent to pile shaft in AGC**

The shaft capacity in axial loading conditions is estimated from the undrained shear strength of soil elements adjacent to the pile. Figures 11a, b and c show the effective stress paths of these elements at selected stages of consolidation ( $U = 1 - [\Delta u / \Delta u_i] = 20, 50, 90$  and  $100\%$ ) for CEP and OEP pile geometries ( $B/w = 50, 100$ ) and OCR's = 1.0 – 2.0. In each case the stresses are normalized by the current radial effective stress at the time of pile loading  $\sigma'_{r,U}$ . These analyses correspond to an undrained direct simple shear mode and can be compared with previous predictions of  $CK_0$ UDSS tests in Figure 6a. The results show that the effective stress path is independent of the initial OCR at any selected stage of consolidation,  $U$ .

The results in Figure 10 are qualitatively similar to those presented previously by Azzouz et al. (1990) for BBC and Empire clays. The effects of slippage at the pile-soil interface can be neglected, as the computed stress obliquity  $\alpha'_p = \tan^{-1}(\tau/\sigma') \leq 25^\circ$  (Fig. 10) is smaller than the expected pile-AGC clay interface friction angle,  $\delta'$ .

The effective stress paths converge to a unique response, independent of the initial pile geometry, for pore pressure ratios,  $U > 90\%$ . This final response resembles very closely the normalized behavior seen in  $CK_0$ UDSS tests at  $OCR = 1.0$ , with a limiting undrained strength ratio,  $\rho_c = 0.23 - 0.25$  (where  $\rho = \tau/\sigma'_{ru}|_{max}$  at the selected  $U$ ). The undrained behavior at earlier stages of consolidation ( $U = 20\%, 50\%$ ), resembles the behavior of overconsolidated clays in DSS tests (cf. Fig. 6) and hence, the results in Figure 10 provide a clear picture of the predicted reconsolidation processes occurring around the pile shaft.

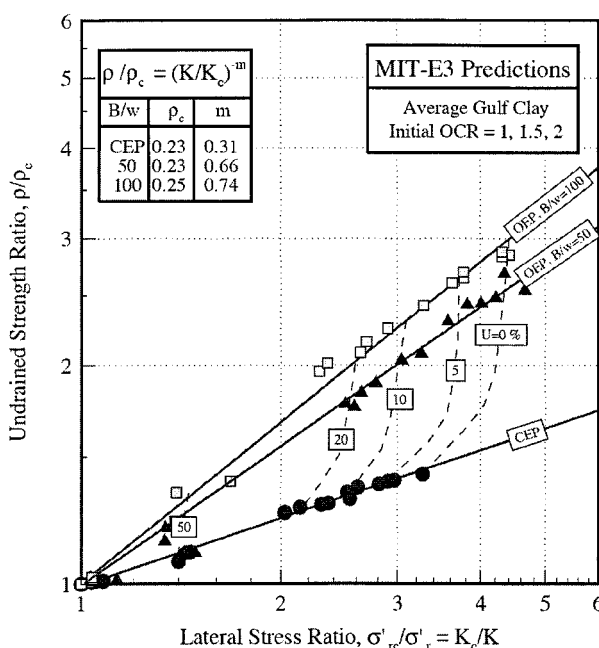


**FIG. 12. Design method for prediction of shaft capacity with partial set-up in AGC**

Figure 12 summarizes the predictions of the skin friction ratio,  $\rho$ , of the AGC adjacent to the pile shaft as functions of the radial effective stress build up,  $K/K_c$  (Fig. 9) and pile aspect ratio,  $B/w$ . For a specified pile aspect ratio,  $\rho$  can be computed from a power law relation:

$$\frac{\rho}{\rho_c} = \left( \frac{K}{K_c} \right)^{-m} \quad (4)$$

where  $\rho_c = 0.23 - 0.25$  and values of  $m$  are functions of the pile geometry shown in Fig. 12.

Hence, the limiting skin friction can be estimated for design purposes at any stage of pile set-up from the following relation:

$$f_s = \left( \frac{K}{K_c} \right)^{1-m} K_c \rho_c \sigma'_{vo} \quad (5)$$

where  $K/K_c$  is a normalized function of the dissipation time factor,  $T$  (Fig. 9) and values of  $K_c$  and  $m$  are shown in Figures 10 and 12, respectively.

## CONCLUSIONS

The MIT-E3 model has been extensively used in analyzing the set-up of driven pipe piles for offshore foundations – based on a series of well documented validations with field tests (e.g., Azzouz et al., 1990, Whittle, 1992; Whittle & Sutabutr, 1999). Throughout this work, the selection of input parameters for the model has followed a standardized procedure using a suite of laboratory 1-D consolidation and undrained triaxial shear tests. Site specific predictions for a series of five deep water projects in the Gulf of Mexico have found small ranges in most of the model parameters. This paper has shown that reasonable predictions of these laboratory data can be achieved by considering a single set of parameters corresponding to a synthetic “Average Gulf Clay” (AGC). The Authors have then proposed generic design charts to enable the prediction of pile set-up at deepwater sites using the MIT-E3 model with AGC parameters. This work demonstrates that relatively complex soil models can have an important role in geotechnical design.

## ACKNOWLEDGEMENTS

The Authors would like to thank their MIT colleague Dr John T. Germaine, who performed many of the tests on GOM clays. The original research was supported by Fugro-McClelland Marine Geosciences, Inc., (FMMG) Houston and a Joint Oil Industry Consortium comprising Amoco Worldwide Engineering & Construction, BP International Ltd., Chevron Petroleum Technology Company, Conoco Inc., Mobil Oil Corporation, and Shell E&P Technology.

## REFERENCES

- Aubeny, C.P. (1992). "Rational interpretation of in-situ tests in cohesive soils." Ph.D. Thesis, MIT, Cambridge, MA..
- Azzouz, A.S. & Morrison, M.J. (1988). "Field measurements on model pile in two clay deposits." *Journal of Geotechnical Engineering, ASCE*, 114(1), 104-121.
- Azzouz, A.S., Baligh, M.M. & Whittle, A.J. (1990). "Shaft resistance of friction piles in clay." *Journal of Geotechnical Engineering, ASCE*, 116(2), 205-221.
- Baligh, M.M. (1985). "Strain path method." *Journal of Geotechnical Engineering, ASCE*, 111(9), 1108-1136.
- Doyle, E. (1994). "Geotechnical Considerations for foundation design of the AUGER and MARS TLP's." *Proc. 7<sup>th</sup> Int. Conf. On the Behavior of Offshore Structures (BOSS'94)*, Ed. Chryssostimidis, C., Boston, MA, 1-22.
- Hashash, Y.M.A. & Whittle, A.J. (2002). "Load transfer mechanisms and arching in braced excavations in soft clay." *ASCE Journal of Geotechnical & Geoenvironmental Engineering*, 128(3), 187-197.
- Jen. L. (1998). "The design and performance of deep excavations in clay. Ph.D Thesis, MIT, Cambridge, MA,

- Ladd, C.C. & Foott, R. (1974). "New design procedure for stability of soft clays." *Journal of Geotechnical Engineering, ASCE*, 100(7), 763-786.
- Ladd, C.C., Whittle, A.J. & Legaspi, D.E. (1994). "Stress-deformation behavior of an embankment on Boston Blue Clay." *Vertical and Horizontal Deformations of Foundations and Embankments*, ASCE Geotechnical Special Publication No. 40(2), 1730-1759.
- Lutz, D.G. (1985). "Predictions of the axial capacity of friction piles in Empire clay by means of the Piezo-Lateral Stress Cell." SM Thesis, MIT, Cambridge, MA.
- Pestana, J.M. (1994). "A unified constitutive model for clays, sands and silts." Ph.D. Thesis, MIT, Cambridge, MA.
- Quiros, G.W., Young, A.G., Pelletier, J.H & Chan, J.H.C. (1983). "Shear strength interpretation for Gulf of Mexico clays." *Proc. Geotechnical Practice in Offshore Engrg.*, ASCE, Austin, TX, 144-165.
- Sutabutr, T. (1999) "Analysis and interpretation of tapered piezoprobe and application to offshore pile design." Ph.D. Thesis, MIT, Cambridge, MA.
- Whittle, A.J. (1987). "A constitutive model for overconsolidated clays with application to the cyclic loading of friction piles." Sc,D Thesis, MIT, Cambridge, MA.
- Whittle, A.J. (1992). "Assessment of an effective stress analysis for predicting the performance of driven piles in clays." *Advances in Underwater Technology, Ocean Science and Offshore Engineering Volume 28*, Offshore Site Investigation and Foundation Behavior, Society for Underwater Technology, London, 607-643.
- Whittle, A.J. & Baligh, M.M. (1988) "The behavior of piles supporting tension leg platforms, Results of Phases 3", Report submitted to Joint Oil Industry Consortium.
- Whittle, A.J., Hashash, Y.M.A. & Whitman, R.V. (1993). "Analysis of a deep excavation in Boston." *Journal of Geotechnical Engineering, ASCE*, 119(1), 69-91
- Whittle, A.J. & Kavvadas, M.J. (1994). "Formulation of the MIT-E3 constitutive model for overconsolidated clays." *Journal of Geotechnical Engineering, ASCE*, 120(1), 173-199.
- Whittle, A.J., DeGroot, D.J., Ladd, C.C. & Seah, T-H. (1994). "Model prediction of the anisotropic behavior of Boston Blue Clay." *Journal of Geotechnical Engineering, ASCE*, 120(1), 199-225.
- Whittle, A.J. & Sutabutr, T. (1999). "Prediction of pile set-up in clay." *Transportation Research Record*, 1663, pp. 33-41
- Whittle, A.J., Sutabutr, T., Germaine, J.T. & Varney, A. (2001). "Prediction and interpretation of pore pressure dissipation for a tapered piezoprobe." *Géotechnique*, 51(7), 601-617.
- Zdravkovic, L., Potts, D.M. & Hight, D.W. (2002) "The effect of strength anisotropy on the behavior of embankments on soft ground," 52(6), 447-457.

## HIERARCHICAL CRITICAL STATE MODELS

David Muir Wood<sup>1</sup>, Member, ASCE and Alessandro Gajo<sup>2</sup>

**ABSTRACT** The development of constitutive models that will actually be used by geotechnical engineers requires a combination of successful simulation and calibration with physical reasonableness and with a ring of familiarity. The models described here have therefore been developed hierarchically from concepts of strength and stiffness with which most practising engineers are familiar. Two lines of development have been followed: Mohr-Coulomb and Cam clay.

### INTRODUCTION

Geotechnical journals and conferences abound with constitutive models. The choice of model is to some extent a matter of mathematical aesthetics and subjective judgement. Some models have been so widely used that they are generally available in all numerical analysis programs intended for geotechnical application to geotechnical problems: isotropic elasticity; elastic-perfectly plastic Mohr-Coulomb; and Cam clay. Engineers are more likely to make use of models which can be clearly seen as incrementally different from models with which they have some familiarity than to make use of models which adopt a completely different language. The choice of model to be used for analysis is in the hands of the modeller. As in all modelling, *adequate complexity* should be sought. It is too easy to discover that key elements of response are obscured by unnecessary and detachable elements of the constitutive model.

The description of constitutive models in this paper concentrates on conditions that are accessible in the conventional triaxial apparatus. Geotechnical engineers have a familiarity with the triaxial apparatus: by presenting the models in this way there is a chance that some confidence in the concepts of constitutive modelling can be created. Compressive stresses and compressive strains are positive. We use stress components: mean effective stress  $p' = (\sigma'_a + 2\sigma'_r)/3$  and distortional stress  $q = \sigma'_a - \sigma'_r$ ; and corresponding strain increments: volumetric strain  $\delta\epsilon_p = \delta\epsilon_a + 2\delta\epsilon_r$  and distortional strain  $\delta\epsilon_q = 2(\delta\epsilon_a - \delta\epsilon_r)/3$  where  $\sigma'_a$ ,  $\sigma'_r$ ,

<sup>1</sup>Professor of Civil Engineering, University of Bristol, Bristol BS8 1TR, UK

<sup>2</sup>Associate Professor, University of Trento, 38050 Trento, Italy

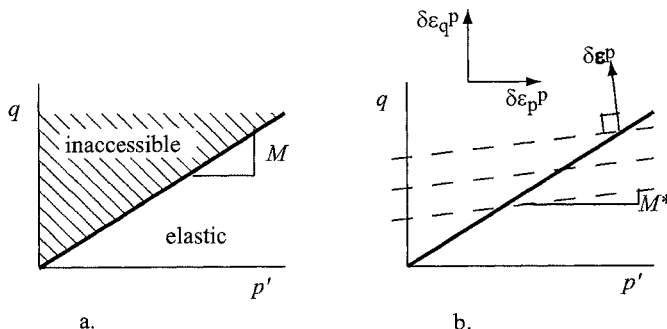


**FIG. 1: Elastic-perfectly plastic Mohr-Coulomb model (a) yield/failure locus; (b) plastic potentials**

$\delta\epsilon_a$ ,  $\delta\epsilon_r$  are axial and radial effective stress and axial and radial strain increment respectively.

Parts of this paper have appeared in Muir Wood (2004).

## MOHR-COULOMB MODELS

### Elastic-perfectly plastic Mohr-Coulomb model

Mohr-Coulomb failure is something which is familiar to *all* undergraduate civil engineers and this model is available in most finite element programs that might be used by practising civil engineers. There is a familiarity in some of the ingredients of the model. The strain increments that accompany any change in stress are assumed to be formed of elastic ( $\epsilon^e$ ) (recoverable) and plastic ( $\epsilon^p$ ) (irrecoverable) parts:  $\delta\epsilon = \delta\epsilon^e + \delta\epsilon^p$ . The elastic strain increment  $\delta\epsilon^e$  occurs whenever there is any change in stress  $\delta\sigma$ . The first ingredient of the model is therefore a description of the elastic behaviour which may be isotropic if appropriate.

There is a region of stress space bounded by a yield surface which can be reached elastically, without incurring any irrecoverable deformations (Fig 1). However, as soon as the boundary of this elastic region is reached then the material yields (or fails) at constant stress. For the Mohr-Coulomb model the yield function is (Fig 1a)

$$f(\sigma) = f(p', q) = q - Mp' \quad (1)$$

If  $f(p', q) < 0$  the soil is behaving elastically; if  $f(p', q) = 0$  the soil is yielding (failing) and generating plastic deformations. To have  $f(p', q) > 0$  is impossible: this defines an inaccessible region of the  $(p', q)$  stress plane.

We assume that there exists a plastic potential function such that the ratio of the two components of plastic strain is:

$$\frac{\delta\epsilon_p^p}{\delta\epsilon_q^p} = -M^* \quad (2)$$

@Seismicisolation

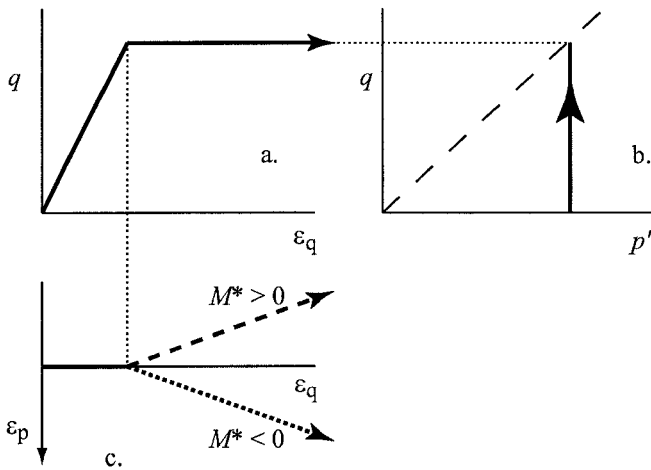


**FIG. 2:** Elastic-perfectly plastic Mohr-Coulomb model: (a) stress:strain response; (b) constant  $p'$  effective stress path; (c) volumetric strain, dependence on  $M^*$

where  $M^*$  is another soil property. For  $M^* = 0$  plastic deformation occurs at constant volume (zero dilatancy). Soils that contract when they are sheared plastically have negative angles of dilation:  $M^* < 0$  (Fig 2c); soils that expand have positive angles of dilation:  $M^* > 0$  (Fig 2c). It is generally found that for most real soils  $M^* < M$ . The plastic energy that is dissipated during an increment of plastic deformation is  $\delta W^p = (M - M^*)p'\delta\epsilon_q^p$ . If  $M^* = M$  there is no plastic energy dissipation which provides an unsatisfactory description of soil behaviour.

The link between strain increments and stress increments can be shown through the generation of stress response envelopes (Gudehus, 1979). For each of the strain increments of a rosette of increments of similar magnitude but different direction we can calculate the stress increment response (Fig 3). This stress response envelope consists of two parts. For elastic increments the response envelope takes the form of half of an ellipse (Fig 3). If the strain increment requires the soil to yield then the stress state has to lie on the yield locus (Fig 3). Not only is part of the stress plane inaccessible (anywhere implying a value of  $q/p' > M$ ), even for stress changes which lie along the boundary of the elastic region ( $\delta q/\delta p' = M$ ) there is an infinite number of possible causative strain increments and we cannot even tell whether the soil is behaving elastoplastically or purely elastically. The ambiguity in trying to work from stress increments to strain increments is emphasised.

Applied to the prefailure response of such a system, an elastic-perfectly plastic

@Seismicisolation

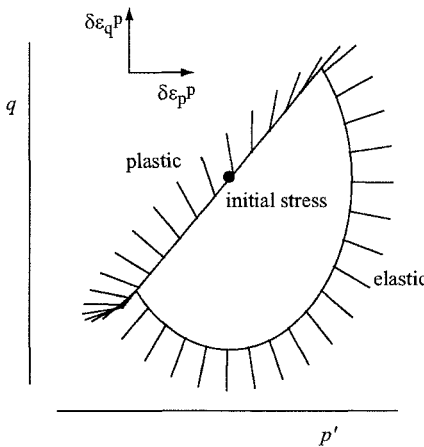


**FIG. 3:** Elastic-perfectly plastic Mohr-Coulomb model: stress response envelope (calculated with  $M = 1.2$ ,  $M^* = 0.2$  and initial stresses  $p' = 100$ ,  $q = Mp' = 120$ )

model shows a steady transition from the initial linear elastic response to the ultimate zero stiffness perfectly plastic collapse condition. For each individual element of soil, however, the elastic-perfectly plastic description looks unconvincing (Fig 4). The model can only at best describe the final failure condition together with some average stiffness corresponding to a stress state intermediate between the beginning and end of the test. Such an average stiffness will not give an accurate description of the behaviour at any soil element—no soil element will actually experience combinations of stress and strain which fall along this assumed notional linear elastic prefailure relationship. The volumetric response is also only crudely represented (Fig 4b).

#### Elastic-hardening plastic Mohr-Coulomb model

Hardening models are natural extensions of the perfectly plastic models. The additional feature is that the yield function is no longer merely a function of the stresses but also introduces a hardening parameter which characterises the current size of the yield surface. An extra hardening equation is then required to define the way in which this hardening parameter changes as plastic strains occur—or in other words the penalty in permanent deformation of the material which is necessary in order to increase the size of the elastic region and *harden* the material.

There are four ingredients of the hardening plastic model—three of these are common to the perfectly plastic models.

1. *Elastic properties:* Whenever the stresses change elastic strains will occur. Let us continue to assume isotropic elasticity.

**@Seismicisolation**

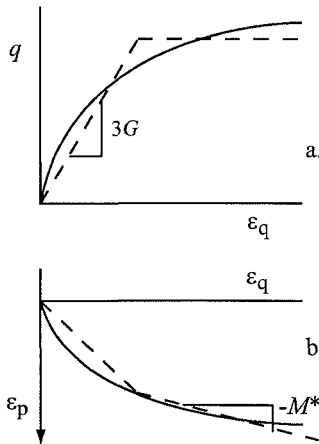


**FIG. 4: Elastic-perfectly plastic Mohr-Coulomb model compared with typical soil response in conventional drained triaxial compression test**

2. *Yield criterion:* The boundary of the region of elastic behaviour (Fig 5a) is not fixed but will depend on the history of loading of the soil. The yield criterion is now taken to be a generalisation of the yield criterion assumed for the perfectly plastic model

$$f(\sigma, \chi) = f(p', q, \eta_y) = q - \eta_y p' \quad (3)$$

where  $\eta_y$  indicates the current size of the yield locus (Fig 5a).

3. *Flow rule:* It is unsatisfactory to assume normality of plastic strain increment vectors to the current yield locus. Following Taylor's (1948) proposal of a link between dilatancy and mobilised friction in a shear box test, a stress-dilatancy equation can be proposed:

$$\frac{\delta \epsilon_p^p}{\delta \epsilon_q^p} = M - \frac{q}{p'} = M - \eta_y \quad (4)$$

where  $M$  is the critical state stress ratio at which constant volume shearing can occur. This flow rule generates the plastic potential curves plotted in Fig 5b.

4. *Hardening rule:* We will assume that the soil is a distortional hardening material so that the current size of the yield locus  $\eta_y$  depends only on the plastic distortional strain  $\epsilon_q^p$

$$\frac{\eta_y}{\eta_p} = \frac{\epsilon_q^p}{a + \epsilon_q^p} \quad (5)$$

where  $\eta_p$  is a limiting value of stress ratio and  $a$  is a soil constant.

The volumetric response depends on the relative values of  $\eta_p$  and  $M$  (Fig 6b). We cannot describe strain softening with this model. In practice, pre-peak response may be adequate since working loads are not intended to produce significant

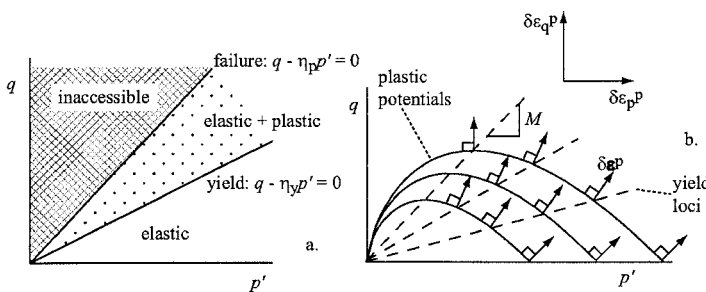


FIG. 5: Elastic-hardening plastic Mohr-Coulomb model: (a) yield locus and failure locus separating elastic, plastic and inaccessible regions of stress plane; (b) plastic potential curves (solid lines) and yield loci (dashed lines)

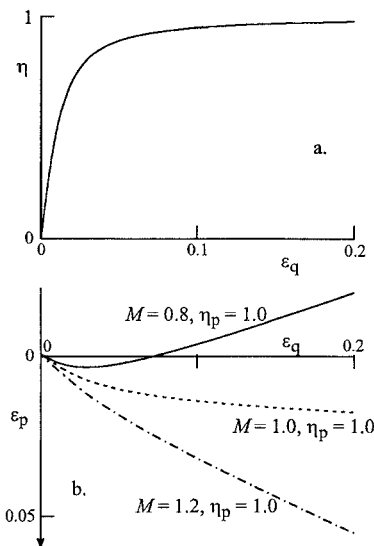
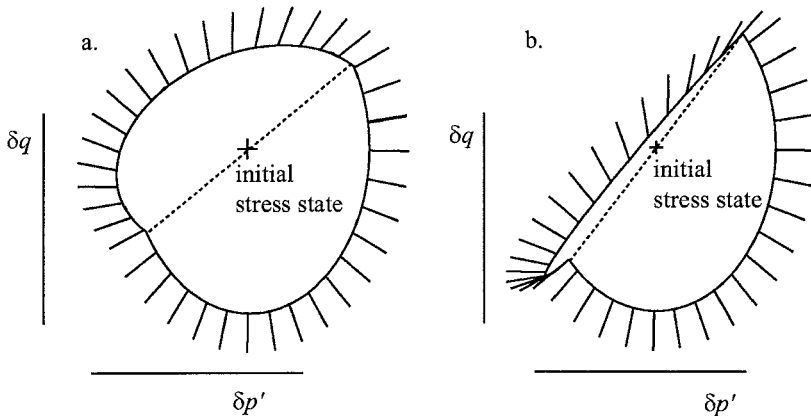


FIG. 6: Elastic-hardening plastic Mohr-Coulomb model: triaxial compression tests with constant mean effective stress: (a) stress:strain response and (b) volumetric response for different values of  $M$  and  $\eta_p$  ( $K = 5000$  kPa,  $\nu = 0.25$ ,  $a = 0.005$ ,  $p' = 100$  kPa)



**FIG. 7:** Elastic-hardening plastic Mohr-Coulomb model: stress response envelopes for (a)  $\eta_y = \eta = 0.8$  and (b)  $\eta_y = \eta = 1.3$  ( $K = 1500$  kPa,  $\nu = 0.3$ ,  $a = 0.01$ ,  $M = 1.2$ ,  $\eta_p = 1.5$ ,  $p'_i = 100$  kPa)

amounts of failure and we are interested in pre-failure response of our geotechnical structures. If much of the soil around a structure has been brought to failure then the overall deformations of the structure are likely to be unacceptably large.

Stress response envelopes are shown in Fig 7 for two different values of stress ratio. As the stress state approaches the peak stress ratio, the stress response envelope (which is composed of two separate elliptical sections for the elastic and elastic-plastic strain increments) becomes more and more distorted. The stress response envelope for the elastic-perfectly plastic model (Fig 3) is a degenerate version of the response envelope for the hardening model.

#### Mohr Coulomb model with strength dependent on state variable

This model is defective in not allowing softening. A switch to softening can be introduced when some designated peak stress ratio has been attained: this is the strategy adopted by Nova and Wood (1979). However, failure switches seem somewhat unsatisfactory from a physical point of view. A way in which both hardening and softening can be rather simply combined in a single model, which is again clearly a development from the Mohr-Coulomb family, has been described by Muir Wood, Belkheir and Liu (1994) and by Gajo and Muir Wood (1999a, b).

Strength of soils is linked with density (Fig 8b). If the density of a soil changes as it is sheared then the strength will change. Let us make the *current* peak strength  $\eta_p$  in the hardening model (5) a variable which is a function of the current state variable  $\psi$  combining information of density (through specific volume  $v$ ) and mean stress (Fig 8a). This model now homes in on a critical state condi-

@Seismicisolation

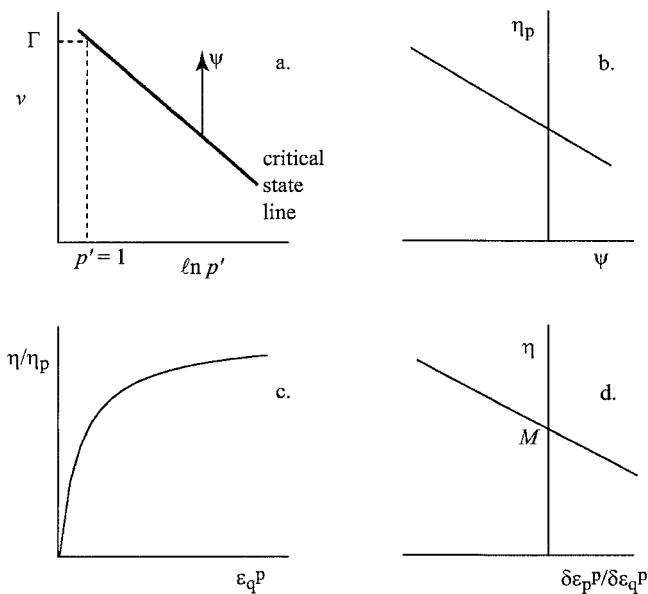


**FIG. 8:** (a) Definition of state variable  $\psi$ ; (b) link between current strength and state variable; (c) monotonic hyperbolic increase of mobilised strength towards current peak strength; (d) stress-dilatancy relationship or flow rule.

tion, heading always towards the current peak strength following the hyperbolic hardening law (Fig 8c) but this peak strength is changing as the soil compresses or dilates with shearing controlled by the stress-dilatancy relationship or flow rule (Fig 8d). Thus, even though the hardening law appears to be a simple hyperbolic monotonically increasing function of strain, the stress:strain response is able to introduce strain softening and the accompanying smooth transition between compression and dilation. The peak strength is thus a moving target which can only be attained at infinite distortional strain (it remains the asymptote of the hardening law) by which time it is identical with the critical state strength.

Typical stress-strain and volumetric strain responses calculated using this model are shown in Fig 9. The behaviour depends strongly on the initial value of state variable: a positive initial state variable indicates an initially loose material which tends to compress as it is sheared and shows little in the way of a peak strength; a negative initial state variable indicates an initially dense material which dilates as soon as the critical state stress ratio is exceeded on the initial loading and then shows a peak with subsequent strain softening. The stress response envelopes that are calculated (Fig 10) depend on whether the current state is pre-peak—in which case the response is similar to that shown for the hardening model (Fig

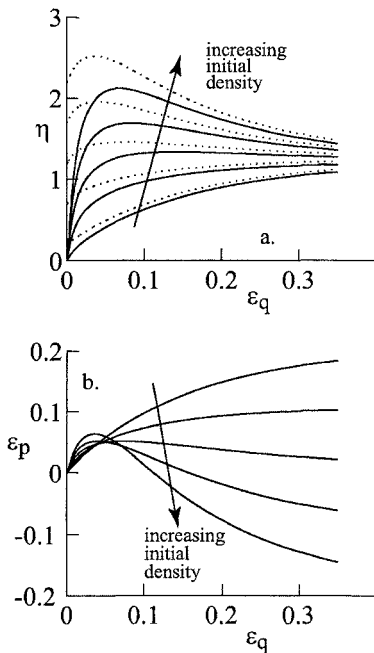


**FIG. 9:** Response of elastic-hardening plastic Mohr-Coulomb model with current strength dependent on state variable in conventional drained triaxial compression tests ( $\delta\sigma_r = 0$ ): (a) stress:strain response (dotted curves indicate variation in current peak strength; solid curves indicate mobilised strength) and (b) volumetric strain response dependent on initial density (initial value of state variable in range  $-0.5 \leq \psi_i \leq 0.5$ ,  $p'_i = 100$  kPa) ( $K = 1500$  kPa,  $\nu = 0.3$ ,  $M = 1.2$ ,  $a = 0.01$ ,  $k = 2$ )

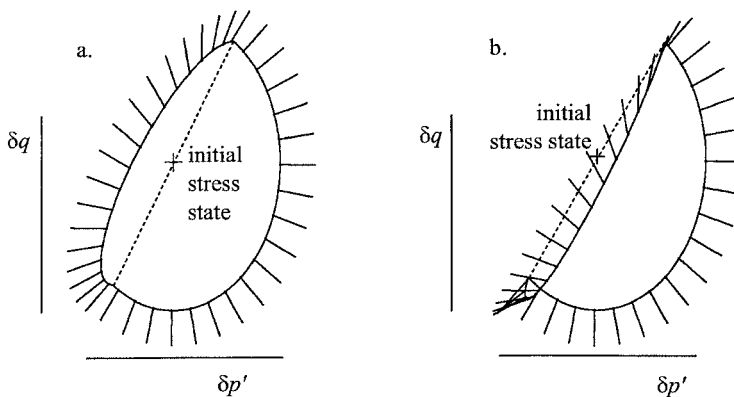


**FIG. 10:** Elastic-hardening plastic Mohr-Coulomb model with strength dependent on state variable: stress response envelopes (a) pre-peak (hardening  $\epsilon_q = 0.04$ ); (b) post-peak (softening  $\epsilon_q = 0.2$ ) (all constitutive parameters as in Fig 9,  $\psi_i = -0.5$ )

7)—or post-peak—in which case the response envelope is folded over on itself indicating that *all* strain increments lead to either elastic or plastic unloading—but all strain increments remain possible and the mapping from strain increment to stress increment is still uniquely defined.

#### Kinematic hardening Mohr-Coulomb model with strength dependent on state variable

Although we are describing some of the nonlinearity of stiffness and post-peak softening of sand we are not yet able to describe the nonlinearity and reversed plasticity that is observed when the direction of loading is reversed. Our model tells us that the behaviour will be purely elastic for all stress ratios lower than the previous maximum stress ratio. A simple way to overcome this shortcoming is to add kinematic hardening to the model so that the elastic region of high stiffness is carried round with the recent stress history (Fig 11). The boundary of this elastic region is of course *the* yield surface but in order to retain a hierarchical link with the previous model we describe the previous yield surface as a *bounding* surface and use the idea of bounding surface plasticity (Dafalias and Popov, 1975) to permit the plastic hardening stiffness to depend on the separation of the yield surface and bounding surface. By careful choice of the stiffness interpolation function we can make the stiffness vary continuously and smoothly from the elastic value to the fully plastic value as the stress state moves from within the kinematic yield surface towards the outer surface.

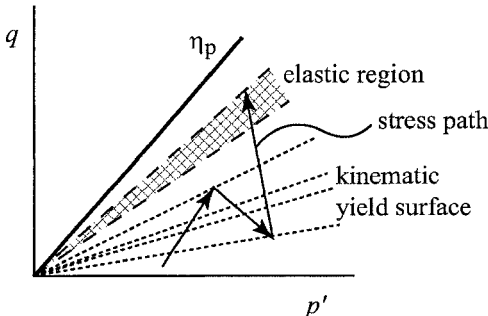


**FIG. 11: Kinematic hardening Mohr-Coulomb model**

This model, named Severn-Trent sand in its complete form (Gajo and Muir Wood, 1999), has been successfully calibrated against triaxial test data for Hostun sand (Fig 12). The effects of different initial density or stress level are automatically described using a single set of soil parameters. We ignore the practical problem of maintaining complete homogeneity within a sand sample which is undergoing softening and merely propose that the model is demonstrably able to describe the sort of softening that might develop within a localised shear band. More detailed analysis of the effects of localisation in sand samples is given by Gajo, Bigoni and Muir Wood (2004) again based on a model equivalent to Severn-Trent sand.

The use of the model to simulate cyclic undrained loading leading to eventual liquefaction is shown in Fig 13. The model fails after 25 cycles; the actual soil sample fails after 89 cycles. Number of cycles to liquefaction is not a particularly reliable parameter to use for model calibration—though there is an obvious significant difference between samples which liquefy in one or two cycles and those which, like the one shown in Fig 13, survive for many cycles. The important conclusion is that this model is able to reproduce an important aspect of soil response which is linked to the volume change characteristics of the soil.

### CAM CLAY

Historically it is reasonable to describe Cam clay as the first *hardening* plastic model that has become generally adopted for soils. It has formed a basis for much subsequent development of soil models. Originally developed in the early 1960s, models of the Cam clay form have been widely and successfully used for analysis of problems involving the loading of soft clays. For clays, an important aspect of the observed mechanical behaviour is the large change in volume that occurs during isotropic or one-dimensional compression. The irrecoverability of this volumetric response in clays suggests that a different mechanism of plastic deformation will be required. This could be achieved by adding extra yield mechanisms to the Mohr-Coulomb models; the volumetric hardening Cam clay model provides an

**@Seismicisolation**

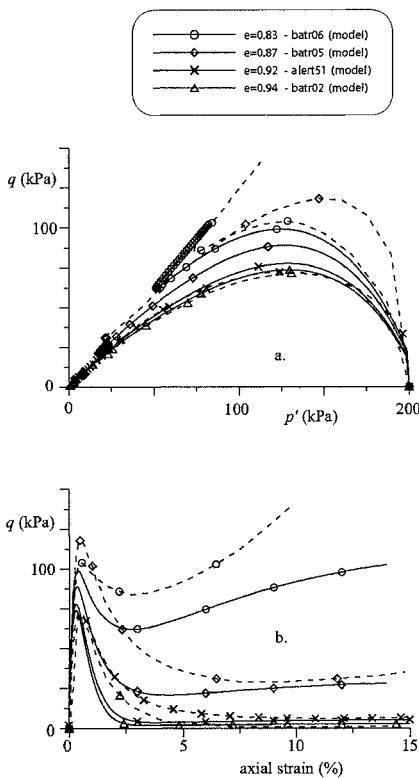


FIG. 12: Comparison of simulation and experiment: effects of initial density on triaxial undrained compression tests on Hostun sand with initial mean effective stress  $p'_i = 200$  kPa (Gajo and Muir Wood, 1999)

elegant alternative route. A detailed description of the Cam clay model and of the behaviour of soils—especially clays—seen against the patterns of behaviour that the Cam clay model reveals is given by Muir Wood (1990).

1. *Elastic properties:* We will assume that the elastic behaviour of the soil is isotropic and defined by two elastic parameters, bulk modulus  $K$  and shear modulus  $G$ . Results of oedometer tests are typically presented in semilogarithmic plots. It is logical then to use the average slope  $\kappa$  of an unload-reload line to characterise the elastic volumetric response (Fig 14), and convert this to an incremental relationship which implies that the bulk modulus  $K$  is not constant but is dependent on stress level (and on current packing)  $K = vp'/\kappa$ .

2. *Yield criterion:* In the triaxial stress plane ( $p', q$ ) the yield locus has an elliptical shape passing through the origin of the stress plane (Fig 14b). This

**@Seismicisolation**

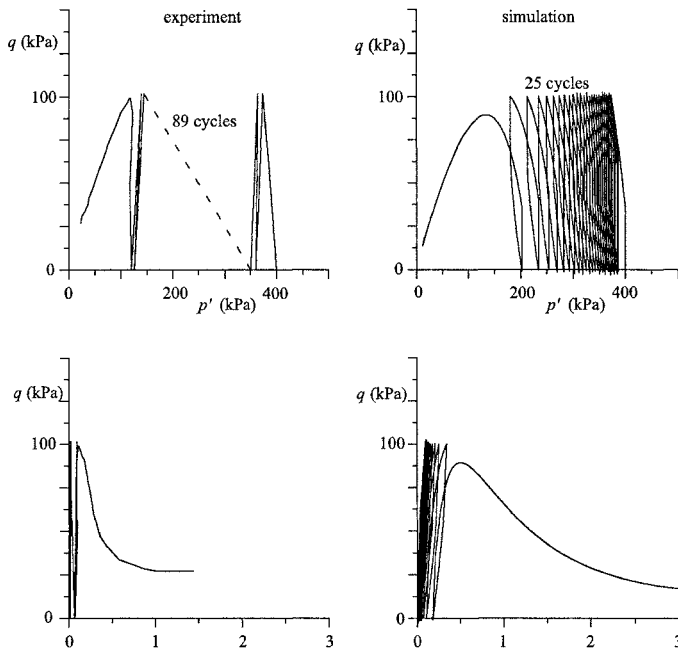


FIG. 13: Comparison of simulation and experiment: undrained cyclic loading of loose Hostun sand

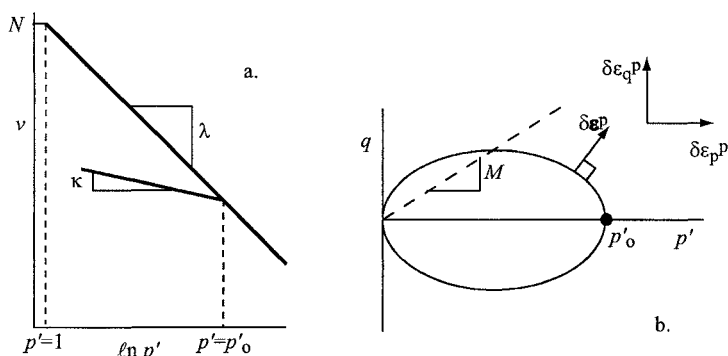


FIG. 14: Cam clay: (a) linear normal compression and unloading-reloading lines in semilogarithmic compression plane; (b) elliptical yield locus

@Seismicisolation

introduces two variables: the aspect ratio of the ellipse  $M$  which controls the shape of the ellipse, the ratio of the vertical ( $q$ ) axis to the horizontal ( $p'$ ) axis; and the size of the ellipse  $p'_o$  which is the hardening parameter for the Cam clay model.

3. *Flow rule:* It is assumed that Cam clay obeys the hypothesis of associated flow (normality) so that the plastic strain increment vector is assumed to be normal to the yield surface at the current stress state (Fig 14b).

4. *Hardening rule:* Cam clay is a volumetric hardening model in which it is assumed that the size of the yield locus  $p'_o$  depends only on the plastic volumetric strain:

$$\delta\epsilon_p^p = \frac{\lambda - \kappa}{v} \frac{\delta p'_o}{p'_o} \quad (6)$$

The Cam clay model yields stably with stress ratio  $\eta < M$ . In a typical compression test the deviator stress rises steadily towards the ultimate value (low overconsolidation ratio in Fig 15). A typical stress response envelope for this regime is shown in Fig 16a. The two elliptical segments are now tangential to each other for stress increments which imply neutral loading with the stress increment tangential to the yield locus. This is a consequence of the assumption of associated flow.

However, if the soil is yielding with stress ratio  $\eta > M$ , continuing shearing with  $\delta\epsilon_q^p > 0$  implies  $\delta\epsilon_p^p < 0$ ,  $\delta p'_o < 0$  and  $\delta q < 0$  which implies strain softening (high overconsolidation ratio in Fig 15). The stress ratio  $\eta = M$  is still an ultimate asymptote but the soil now approaches this stress ratio from above rather than from below. The stress response envelope (Fig 16b) is folded over on itself. All strain increments are possible and each strain increment implies an unambiguous stress increment. Stress changes which move inside the current yield locus can be associated with either purely elastic or with elastic plus plastic strains.

### Kinematic hardening ‘bubble’ Cam clay model

A kinematic hardening extension of a Cam clay-like model is illustrated in Fig 17b (Al-Tabbaa and Muir Wood, 1989). The elastic region is now confined to an elastic ‘bubble’ which floats around in stress space with the current stress state. Plastic strains occur whenever the ‘bubble’ moves but the plastic stiffness is controlled by the separation,  $b$ , of the ‘bubble’ and some outer ‘bounding’ surface and falls as the ‘bubble’ approaches this ‘bounding’ surface. A translation rule is introduced to describe the way in which the ‘bubble’ decides how much to change in size and how much to change in position as the stress engages with it. The ‘bubble’ has a size which is a fixed proportion  $R$  of the size of the ‘bounding’ surface. With appropriate formulation this model can be made to behave identically to Cam clay when the soil is being loaded with the ‘bubble’ in contact with the bounding surface (which then looks rather like the Cam clay yield surface—but is not actually a yield surface because it does not control the onset of development of plastic strains) (Fig 17a, b). There is thus a hierarchical development of the model, adding desirable features (smooth variation of stiffness,

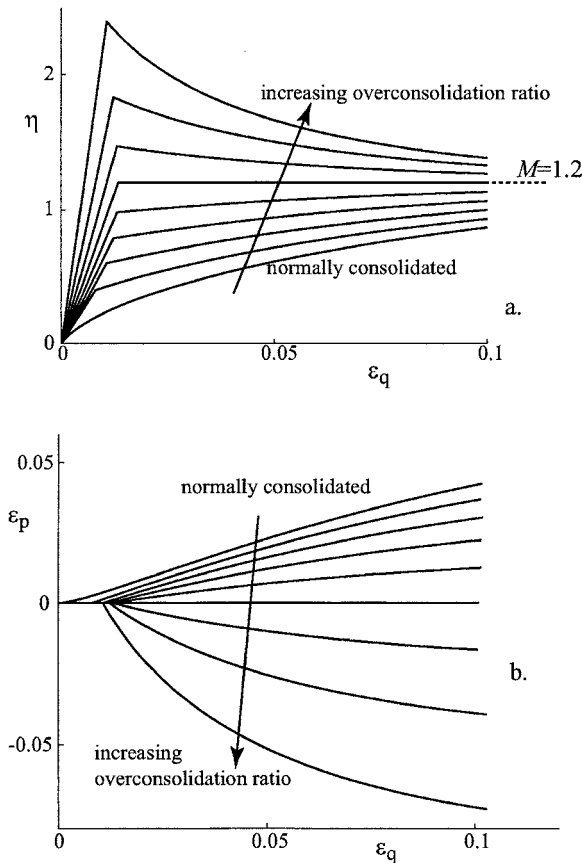


**FIG. 15:** Cam clay: (a) stress:strain and (b) volumetric strain response in drained triaxial compression tests with constant mean stress ( $\delta p' = 0$ ) ( $\kappa = 0.05$ ,  $G = 1500$  kPa,  $\lambda = 0.25$ ,  $M = 1.2$ ) (overconsolidation ratios  $p'_o/p'_i$  in range 1-5,  $p'_o = 100$  kPa)

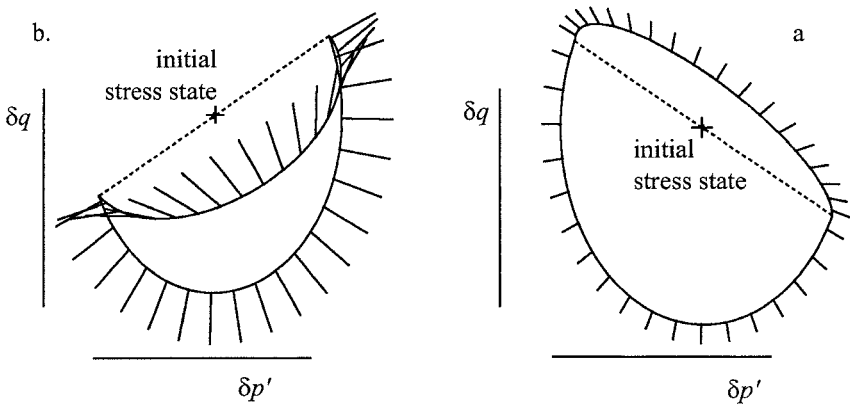


FIG. 16: Cam clay: stress response envelopes (a)  $\eta < M$ ,  $p'_i/p'_o = 0.75$ ; (b)  $\eta > M$ ,  $p'_i/p'_o = 0.25$  ( $\kappa = 0.1$ ,  $\nu = 0.3$ ,  $\lambda = 0.25$ ,  $M = 1.2$ ) ( $v_i = 2.5$ ,  $p'_o = 200$  kPa)

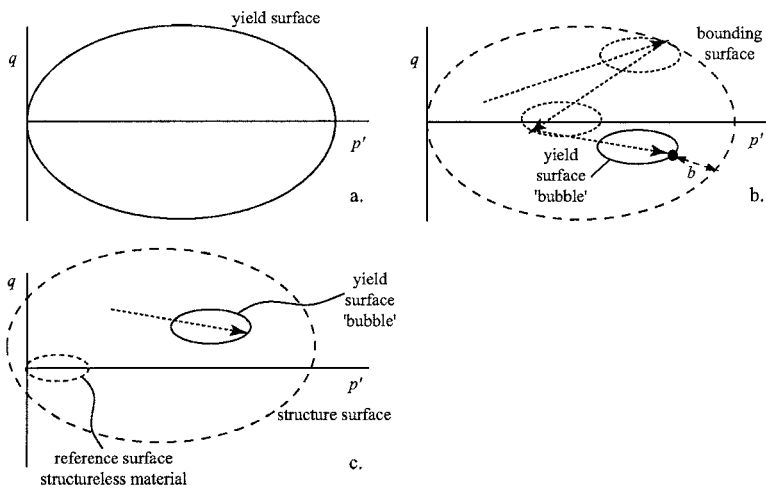
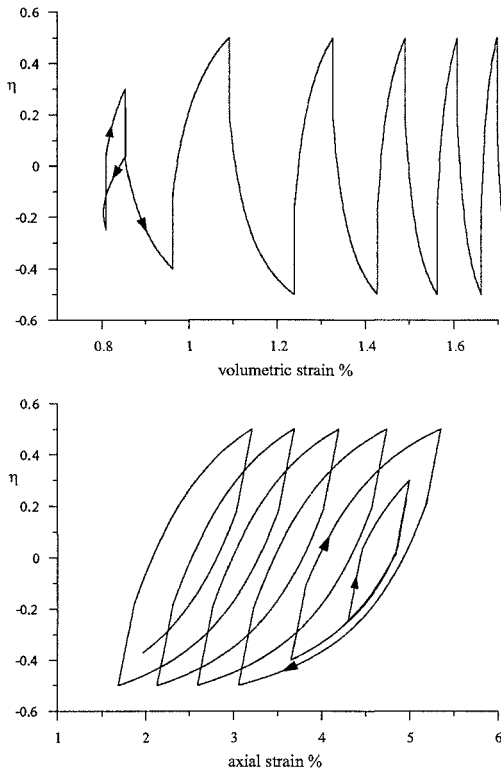


FIG. 17: (a) Cam clay; (b) kinematic hardening extension of Cam clay: 'bubble' bounds elastic region and moves with stress history; (c) addition of structure or bonding to kinematic hardening Cam clay model



**FIG. 18:** Kinematic hardening extension of Cam clay: response in cyclic triaxial test with constant mean effective stress  $p'$

plasticity on stress reversal) to an already somewhat familiar model, Cam clay. (Setting the size ratio of the ‘bubble’  $R = 1$  the model is identical to Cam clay.) Typical response of this ‘bubble’ model for a cyclic triaxial test is shown in Fig 18. There is a combination of hysteretic cyclic stress-strain response together with development of permanent strains.

#### Modelling cementation and structure: extension to ‘bubble’ model

We can add further effects in a similarly hierarchical way. Natural soils often contain a certain amount of structure which may also manifest itself as a bonding between particles which can be destroyed with mechanical or chemical damage. Quick clay slides occur because a change of pore water chemistry upsets the particle bonds leaving a metastable structure which can easily be destroyed. The bonded material can be described by a model in which the yield surface has an increased size as a result of the bonding. With plastic straining (or chemical

@Seismicisolation

weathering) the yield surface gradually shrinks to the yield surface, appropriate to the remoulded, structureless material. This approach is adopted as an extension of the ‘bubble’ kinematic extension of Cam clay by Rouainia and Muir Wood (2000), Gajo and Muir Wood (2001) and Callisto *et al.* (2002) to simulate the behaviour of natural clays damaged only by plastic straining (Fig 17). All features of the ‘bubble’ model are retained but in addition a measure of structure or bonding, characterised by a single scalar parameter  $r$ , is introduced. The ‘bounding’ surface is now called a ‘structure’ surface and has a size  $r$  times larger than a reference surface (Fig 17c). Structure is lost whenever plastic strains occur, according to a damage law, here assumed exponential:

$$\delta r = -\frac{k}{\lambda - \kappa} (r - 1)^\psi \delta \epsilon_d^p \quad (7)$$

where  $k$  and  $\psi$  are soil parameters controlling the rate of loss of structure. The damage plastic strain increment  $\delta \epsilon_d^p$  is assumed to be a combination of plastic volumetric and plastic distortional strain increments with an additional parameter being introduced to control their relative importance. It is assumed that the structure progressively disappears and  $r \rightarrow 1$  as any plastic deformation continues to increase. This appears logical because a structureless soil is one which has been so mechanically pummelled that it has no remaining bonds between particles. It may be that particular forms of laboratory testing (triaxial testing, for example) are not able to provide sufficient damage and that the evolution law (7) and definition of damage strain need to include some more subtle reference to the nature of the strain path: shearing with rotation of principal axes is likely to be especially damaging.

Given the scalar measure of structure  $r$  it would be perfectly feasible to introduce other evolution laws which relate its change (increase or decrease) to chemical environment or time or temperature effects. Since structure effects have been provided as an add-on to the ‘bubble’ model, models like that of Nova *et al.* (2003) can be obtained by simply setting the ‘bubble’ size ratio  $R = 1$ . Cam clay can be regained by in addition setting  $r = 1$ .

Comparison of observations and simulations for a series of stress probes on Bothkennar clay are shown in Fig 19 (Gajo and Muir Wood, 2001). The stress paths are normalised with respect to the current size of the reference surface. The paths head outwards until they meet the effects of damage collapsing towards them. If continued far enough most paths would eventually reach a critical state with  $r = 1$ . As for the softening sand model we note that in the presence of such softening tendencies it is to be expected that localisation may occur within a soil sample. The model is clearly able to describe softening linked with loss of structure: it may be difficult for this to occur homogeneously in practice.

## CALIBRATION OF MODELS

As a simple exercise in parameter selection, we will show how soil parameters might be selected to match the response observed in a single drained triaxial compression test on normally consolidated Weald clay (Fig 20).



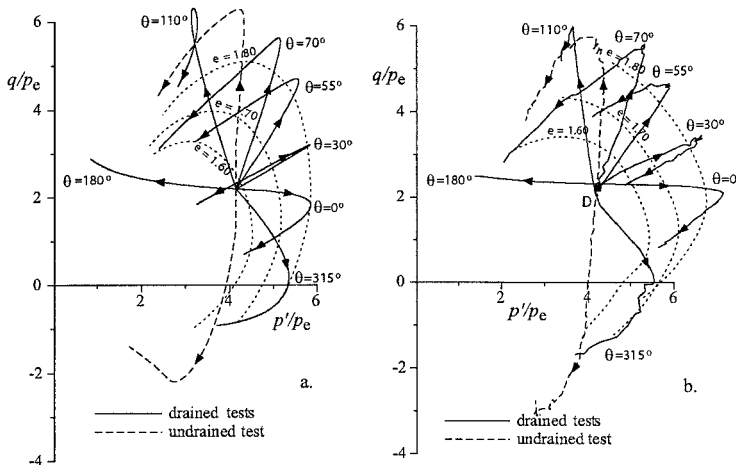


**FIG. 19:** Comparison between (a) simulated normalised large strain behaviour of undisturbed Bothkennar clay from triaxial stress paths and (b) experimental results by Smith *et al.* (1992) ( $p_e$  is Hvorslev equivalent pressure, representing the stress on the isotropic normal compression line for the structureless remoulded material at the current specific volume) (from Gajo and Muir Wood, 2001)

The most commonly required parameter selection is certainly the most subjective: the choice of parameters for an elastic-perfectly plastic Mohr-Coulomb model. One possible fitting is shown in Fig 20 (EPP). For the simulation shown:  $G = 1500$  kPa,  $K = 2800$  kPa,  $M = 0.8$  and  $M^* = -0.15$ . The value of Poisson's ratio is  $\nu = 0.273$ .

With a hardening plastic model—whether the extended Mohr-Coulomb model or Cam clay—it is quite possible, by trial and error, to obtain really quite a good match to both the stress:strain and the volumetric response of the soil in this test. The values of soil parameters used for the Mohr-Coulomb model (MCH in Fig 20) are:  $G = 3800$  kPa,  $K = 6000$  kPa,  $M = 0.91$ ,  $a = 0.015$  and  $\eta_p = 0.95$ . The value of Poisson's ratio implied by the elastic properties is  $\nu = 0.238$ . The elastic stiffnesses are higher because plastic strains occur right from the start of the test. For the Cam clay model (CC in Fig 20) the parameters giving a similar quality of fit are: elastic properties  $G = 3500$  kPa and  $\kappa = 0.015$ —implying an initial bulk modulus  $K = vp'/\kappa = 22632$  kPa and Poisson's ratio  $\nu = 0.426$ ; and plastic properties  $\lambda = 0.055$  and  $M = 0.9$ . The value of the intercept  $N$  on the normal compression line is  $N = 1.933$ . Whereas the values of shear modulus  $G$  are similar for these two hardening plastic models, Cam clay predicts a lot of plastic volumetric strain at the start of the test—the plastic strain increment, normal to the elliptical yield locus, indicates only plastic volumetric strain to

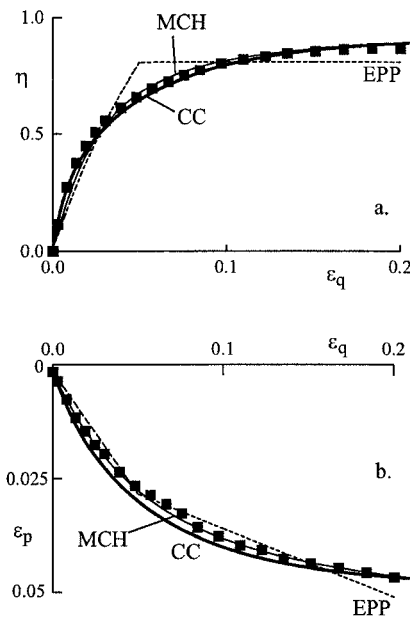


**FIG. 20:** Conventional drained triaxial compression test on Weald clay (data from Bishop and Henkel, 1962) and fitting of constitutive models (initial specific volume  $v_i = 1.64$ , confining pressure  $\sigma'_c = 207$  kPa (EPP: elastic-perfectly plastic Mohr-Coulomb model; MCH: extended (hardening) Mohr-Coulomb model; CC: Cam clay) (Muir Wood, 2004)

start with—and the elastic properties indicate near incompressibility ( $\nu \rightarrow 0.5$ ) in order to ensure that there is negligible additional elastic volumetric strain. The values of  $M$  are similar.

We cannot determine the optimum model by fitting data for a single test. As presented here, the Mohr-Coulomb models will not predict significant volumetric strain for stress paths which load the soil at more or less constant stress ratio. If we believe that such paths are going to be important in the behaviour of our geotechnical system then we need to ensure that we have data from special triaxial and other tests with which to calibrate our model. The more sets of data that we attempt to fit simultaneously the less likely it is that we will be able to achieve a fit as close as that shown in Fig 20.

Each test being used for calibration is a boundary value problem: the deduction of constitutive parameters from experimental observation is a deconvolution problem. How confident can we be that data sets obtained from one device actually

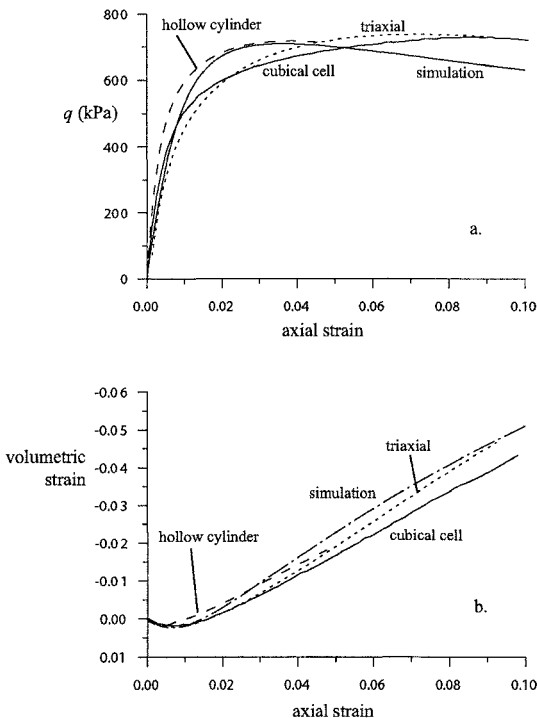


**FIG. 21:** Comparison of simulation (Severn-Trent sand) and observation (Hostun sand) for triaxial drained compression tests in different apparatus ( $e = 0.61$ ,  $\sigma'_r = 500$  kPa (Gajo and Muir Wood, 1999b)

reflect the ideal response of a single element? Fig 21 shows the range of data for a single axisymmetric triaxial test performed in three different apparatus, together with the optimum Severn-Trent sand simulation (Gajo and Muir Wood, 1999b). Constitutive modellers should not cast aspersions on the reliability of individual experiments but might expect a tolerance in matching observations as great as the spread of those observations.

For the models that have been briefly described here, most of the constitutive parameters are linked to well understood aspects of the behaviour of soils which are familiar to most engineers (ideas of strength and compressibility in Cam clay, for example). Perhaps this is an important part of the sales process needed to convince practising engineers of the potential value of adopting modestly unfamiliar models. However, the deformation range over which these parameters are determined will often be totally different from (much larger than) that which will be tolerable in engineering application. How important is this physical basis for

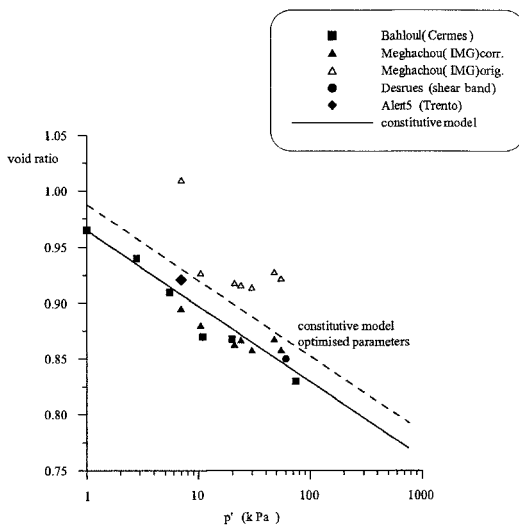


**FIG. 22:** Position of experimental critical state points and assumed position of critical state line for Hostun sand (Gajo and Muir Wood, 1999a)

constitutive modelling?

Data of critical states of Hostun sand are shown in Fig 22. Models such as Severn-Trent sand are very strongly influenced by the precise location of the critical state line. The figure shows three things: first, the data are inevitably scattered, but statistical methods can be used to optimise the fit; second, accurate determination of specific volumes in sand samples is not always easy—there are volume changes associated with the process of saturation which may be quite significant (compare the Meghachou original and corrected points); and third, the optimum fit of the model to a range of available data puts the critical state line slightly higher than the least squares fit—the sand seems to feel relatively denser in its stress:strain response than the critical state data would imply.

If we propose the importance of trying to ensure that the paths followed in our laboratory tests bear some resemblance to the range of significant paths that will be followed in our geotechnical system then we should also expect that the models being calibrated should be demonstrably successful over ranges of stress and strain which are going to be practically relevant and be less concerned about the detail of response over much more extensive territory. The stiffness characteristics of soils are so sensitive to the detail of history and stress path that using a constitutive model to extrapolate from inappropriate limited laboratory testing may not lead to reliable estimates of response of geotechnical systems—especially under working loads, far from failure, where the detail of rather small strains will be crucial.

@Seismicisolation

An alternative calibration strategy is then to attempt some algorithmic best overall fit to give greater objectivity to our parameter selection (see, for example, Muir Wood *et al.*, 1993). As part of this process, faced with data from tests of varying reliability, we may wish to weight differently the several sets of data. Visual fitting may introduce some unconscious bias. The values of soil parameters deduced from direct observation may be used as initial estimates with which to seed the optimisation process but we might be relaxed about the actual values which eventually emerge. For example, Muir Wood *et al.* (1993) show that the best fit of Cam clay to drained compression data for kaolin is obtained with a value of elastic volumetric compressibility  $\kappa$  which is considerably higher than that directly deduced from normal compression and unloading of the clay—implying a very low or even negative value of Poisson's ratio.

## CONCLUSION

The phrase *critical state models* covers a wide range of possibilities (Muir Wood, 2002). Two quite different routes through constitutive modelling have been explored here. The common feature is that both routes progress incrementally and hierarchically from well-known models in such a way that extra features can be easily extinguished by appropriate parameter selection. Both sets of models incorporate critical states. There are other hierarchical features that could be included: cementation or bonding could be readily added to the Mohr-Coulomb family; viscoplastic or other descriptions of rate effects could be readily added to either family.

Calibration of models shows that the fewer the available experimental data the less the certainty with which one out of a selection of available models can be chosen. On the other hand as more data come available the likelihood of inconsistencies increases. There may be some advantage in making use of an automatic algorithmic optimisation process; with appropriate weighting given to data of different qualities of origin; choosing data from stress and strain histories which are relevant to the intended application; and without too much concern for the relationship of the constitutive parameters thus deduced with their supposed physical origins.

## REFERENCES

- Al-Tabbaa, A and Muir Wood, D (1989) An experimentally based ‘bubble’ model for clay. *Numerical Models in Geomechanics NUMOG III* (eds S Pietruszczak and GN Pande) Elsevier Applied Science, London 91-99.
- Bishop, AW and Henkel, DJ (1962) *The measurement of soil properties in the triaxial test.* (2nd edition) Edward Arnold, London.
- Callisto, L, Gajo, A and Muir Wood, D (2002) Simulation of stress probe tests on natural and reconstituted Pisa clay. *Géotechnique* **52** (9) 649-666.
- Dafalias, YF and Popov, EP (1975) A model of nonlinear hardening materials for complex loading. *Acta Mechanica* **21** 173-192.
- Gajo, A, Bigoni, D and Muir Wood, D (2004) Multiple shear band development



- and related instabilities in granular materials. *Journal of Mathematics and Physics of Solids* (in press)
- Gajo, A and Muir Wood, D (1999a) Severn-Trent sand: a kinematic hardening constitutive model for sands: the  $q - p$  formulation. *Géotechnique* **49** (5) 595-614.
- Gajo, A and Muir Wood, D (1999b) A kinematic hardening constitutive model for sands: the multiaxial formulation. *International Journal for Numerical and Analytical Methods in Geomechanics* **23** (5) 925-965.
- Gajo, A and Muir Wood, D (2001) A new approach to anisotropic, bounding surface plasticity: general formulation and simulations of natural and reconstituted clay behaviour. *International Journal for Numerical and Analytical Methods in Geomechanics* **25** (3) 207-241.
- Gudehus, G (1979) A comparison of some constitutive laws for soils under radially symmetric loading and unloading. *Proc. 3rd Conf. Numerical methods in geomechanics*, Aachen (ed W Wittke) AA Balkema, Rotterdam 1309-1323.
- Muir Wood, D (1990) *Soil behaviour and critical state soil mechanics*. Cambridge University Press, Cambridge.
- Muir Wood, D (2002) Constitutive cladistics: the progeny of Critical State Soil Mechanics. *Constitutive and centrifuge modelling: two extremes* (ed S Springman) Swets & Zeitlinger, Lisse 35-58.
- Muir Wood, D (2004) *Geotechnical modelling* E&FN Spon, London.
- Muir Wood, D, Belkheir, K and Liu, D-F (1994) Strain-softening and state parameter for sand modelling. *Géotechnique* **44** (2) 335-339.
- Muir Wood, D, MacKenzie, NL and Chan, AHC (1993) Selection of parameters for numerical predictions. *Predictive soil mechanics (Proc. Wroth Memorial Symposium)* (eds GT Housby and AN Schofield) Thomas Telford, London 496-512.
- Nova, R, Castellanza, R and Tamagnini, C (2002) A constitutive model for bonded geomaterials subject to mechanical and/or chemical degradation. *International Journal for Numerical and Analytical Methods in Geomechanics* **27** (9) 705-732.
- Nova, R and Wood, DM (1979) A constitutive model for sand. *Int. J. for Numerical and Analytical Methods in Geomechanics* **3** (3) 255-278.
- Rouainia, M and Muir Wood, D (2000) A kinematic hardening constitutive model for natural clays with loss of structure. *Géotechnique* **50** (2) 153-164.
- Taylor, DW (1948) *Fundamentals of soil mechanics*. John Wiley, New York.

## CALIBRATION OF A GENERALIZED PLASTICITY MODEL AND ITS APPLICATION TO LIQUEFACTION ANALYSIS

Songtao Yang<sup>1</sup> and Hoe I. Ling<sup>2</sup>

**ABSTRACT:** The application of a modified version of generalized plasticity model to soil liquefaction analysis is demonstrated in this paper. Different from the original generalized plasticity model, this model considers pressure dependency and cyclic hardening behavior of sand. The model was calibrated against a fine sand (Nevada sand) at loose conditions. The constitutive model and analysis procedures were then validated against the VELACS centrifuge test results. The simulation showed good agreement with the experimental results.

### INTRODUCTION

It is well known that the sands respond differently to the change in confining pressure and void ratio. Experimental investigation has shown that the volume and angle of internal friction of a sand reduce considerably when sheared under high confining pressure, and increase markedly as the confining pressure decreases (e.g., Tatsuoka et al. 1986; Maeda and Miura 1999). The change in void ratio, such as loose or dense state, affects the stress-deformation behavior of sand.

Another significant property of sand is related to the densification and hardening behavior under repeated loadings (e.g., Silver and Seed 1971; Pradhan 1989). Following an increase in the number of cycles of loading, the stiffness increases while damping reduces, thus affecting the dynamic response of the soil structures.

Many attempts have been made to developed constitutive models that incorporate the pressure dependency (e.g., Been and Jefferies 1985; Tatsuoka et al. 1993; Li and Dafalias. 2000) and hardening behavior (e.g., Bouckovalas et al. 1986; Dobry and Petrakis 1990). In most of these works, classic plasticity theory was used with which the yield surface and plastic potential were defined explicitly.

Generalized plasticity theory allows a less complicated simulation of sand

<sup>1</sup> Graduate Research Assistant, Department of Civil Engineering and Engineering Mechanics, Columbia University, New York, NY 10027

<sup>2</sup> Associate Professor, Department of Civil Engineering and Engineering Mechanics, Columbia University, New York, NY 10027

behavior, with which the direction vectors are used instead of the definition of the yield surface and plastic potential. This theory was introduced and applied to geomaterials by Mroz and Zienkiewicz (1984), and was later extended by Zienkiewicz et al. (1985) and Pastor et al. (1990). However, Pastor-Zienkiewicz-Chan model (Pastor et al. 1990) does not simulate pressure dependency and densification behavior of sand under cyclic loading. In Pastor et. al (1993), densification was considered but the hardening effect was not simulated satisfactorily.

In Liu (2002) and Ling and Liu (2003), based on the work of Pastor et al. (1990), the generalized plasticity model was extended to include pressure dependency and densification behavior under monotonic and cyclic loadings, and the corresponding predictive capability was demonstrated by comparing the simulation of loose and dense sands with the triaxial test results under both drained and undrained conditions. This model is hereafter known as the “modified model”.

In this paper, the modified model was incorporated into a finite element program DIANA-Swandyne-II (Chan, 1988 and Chan, 1993), and the centrifugal test (Test 2 of Model No.1) conducted at RPI under VELCAS (Verification of Liquefaction Analysis by Centrifuge Studies) project (Arulanandan and Scott, 1993) was simulated and compared. The parameters of the modified model were obtained by calibrating with the response of Nevada sand obtained under triaxial compression tests.

## SALIENT FEATURES OF MODIFIED MODEL

The details of modified model are given in Ling and Liu (2003). Only salient features of the model is summarized as follow:

The elastic behavior is defined by the shear and bulk moduli ( $G_{\max}$  and  $K_{\max}$ ), which are modified to be dependent on the normalized mean effective stress with an exponent equal to 0.5:

$$G_{\max} = G_0(p'/p_a)^{0.5} \quad (1)$$

$$K_{\max} = K_0(p'/p_a)^{0.5} \quad (2)$$

where  $G_0$  and  $K_0$  are the shear and bulk moduli numbers, respectively;  $p'$  is the mean effective stress and  $p_a$  is the atmospheric pressure.

The stress-dilatancy relationship is expressed as

$$d_g = \frac{dH^p}{dH_s^p} = (1 - \Delta)(M_g - K) \quad (3)$$

where  $dH^p$  and  $dH_s^p$  are the incremental plastic volumetric and deviatoric strains, respectively.  $M_g$  is the slope of the critical state line on  $p'$ - $q$  plane,  $K = \frac{q}{p'}$  is the stress ratio, and  $\Delta$  is a model parameter.

The plastic flow direction under loading  $\mathbf{n}_{gl}$  is given in the triaxial space as

$$\mathbf{n}_{gL} = \left( \frac{d_g}{\sqrt{1 - d_g^2}}, \frac{1}{\sqrt{1 - d_g^2}} \right)^T \quad (4)$$

The non-associate flow rule is followed and the loading direction is expressed as

$$\mathbf{n} = \left( \frac{d_f}{\sqrt{1 - d_f^2}}, \frac{1}{\sqrt{1 - d_f^2}} \right)^T \quad (5)$$

where  $d_f = (1 - \Delta)(M_f - K)$  and  $M_f$  is a model parameter.

The plastic modulus under monotonic loading  $H_L$  is modified by, first, including a power term containing normalized mean effective stress

$$H_L = H_0(p'/p_a)^{0.5} H_f H_v H_s \quad (6)$$

where  $H_0$  is a constant;  $H_f$ ,  $H_v$ , and  $H_s$  are the plastic coefficients. Here,  $H_f$  and  $H_v$  are the same as the base model, while  $H_s$  is modified to

$$H_s = E_l \exp \frac{K_s \left( \frac{p'}{p_a} - 1 \right)}{E_0 f} \quad (7)$$

where  $f = \int dH_s$  is the accumulative plastic deviatoric strain;  $E_0$  and  $k_s$  are constants;  $E_l$  is a function of mean effective stress  $p'$  and stress ratio  $K = \frac{q}{p'}$ , expressed as

$$E_l = E_{l0} \frac{\frac{K_p}{K_{p0}} / M_g - 1}{\frac{K_{p0}}{K_{p0}} / M_g - 1} \quad (8)$$

where  $K_{p0}$  is the peak value of stress ratio ( $K_p$ ) at reference stress  $p_a$ . For isotropic compression test, the stress ratio  $K = 0.0$ , thus  $E_l$  remains constant. For very loose sand, at peak strength  $K = M_g$  and  $E_l = E_{l0}$ . For medium and dense sands, the peak strength is determined by the following equation

$$I = I_0 + \vartheta I \log_{10}(p'/p_a) \quad (9)$$

where  $I$  is the peak angle of internal friction,  $I_0$  is the peak angle of internal friction at atmospheric pressure and  $\vartheta I$  is the change of angle for a 10-fold increase in the pressure.

As to unloading plastic modulus, a power term of  $p'$  and a term  $H_{den}$  are introduced to consider densification and hardening behavior

$$H_u = H_{u0} (p'/p_a)^{0.5} \left( \frac{M_g}{K} \right)^{r_u} H_{den} \quad \text{for } \left| \frac{M_g}{K} \right| > 1$$

$$H_u = H_{u0} (p'/p_a)^{0.5} H_{den} \quad \text{for } \left| \frac{M_g}{K} \right| \leq 1 \quad (10)$$

$$H_{den} = \exp(-r_d H_{vo}^p) \quad (11)$$

where  $r_u$  is a constant;  $H_{vo}^p$  is the plastic volumetric strain at the instant of unloading or reloading that is either compressive or zero.

The reloading plastic modulus  $H_L$  is modified to account for the effects of mean effective stress and past stress history

$$H_L = H_0 (p'/p_a)^{0.5} H_f |H_v| H_s H_{DM} H_{den} \quad (12)$$

where  $H_f$ ,  $H_v$ ,  $H_s$  and  $H_{den}$  are the same as in equations (6) and (10). Here, a stress memory factor  $H_{DM}$  was introduced to account for the history of past events. Three normalized deviatoric stress tensors, at the last unloading, at the starting point of reloading and at the second point of reloading, were used to define  $H_{DM}$

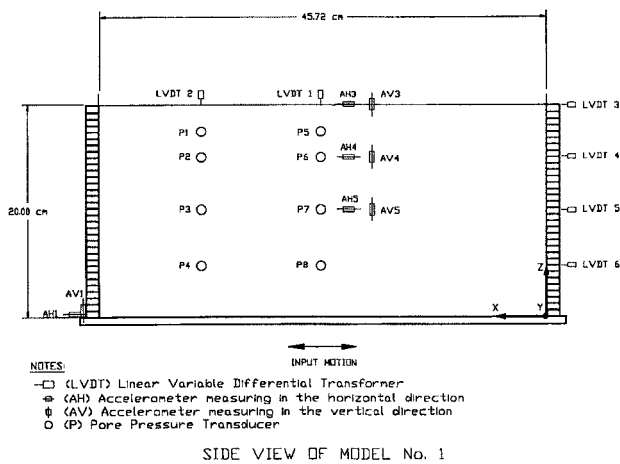
## DESCRIPTION OF VELACS CENTRIFUGE STUDIES

In VELACS project, nine different boundary value problems were studied by conducting dynamic centrifuge tests. A sketch of the laminar box and instrumentation for RPI Model No.1 is shown in Figure 1. The model consisted of a 20cm thick horizontal soil deposit (Nevada sand No. 120), which was placed in a laminar box at a relative density of about 40%. It was fully saturated with water, spun at a centrifuge acceleration of 50g, and was excited horizontally at the base with 20 cycles of a 100 Hz sinusoidal input, with variable amplitude and maximum peak acceleration of 11.75g. This corresponded to a sinusoidal wave with a frequency of 2 Hz and peak acceleration of 0.235g in the prototype.

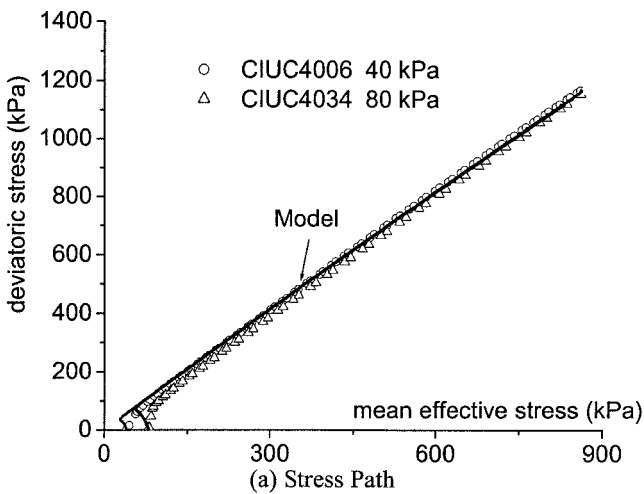
## CONSTITUTIVE MODEL CALIBRATION

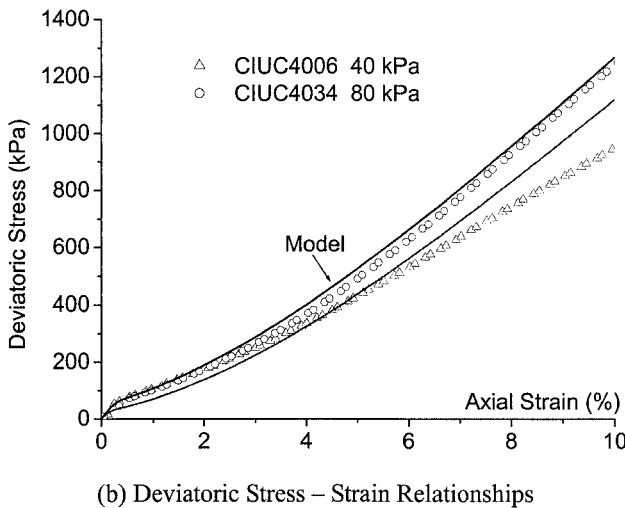
A total of 15 parameters are needed in characterizing the model under cyclic loading. To identify the parameters, three drained or undrained triaxial tests having the same initial density are recommended. Two of the tests should be monotonic that are of different initial confining pressures, and the other test should be conducted under cyclic loading. The procedures of calibration are given in Ling and Liu (2003).

In this paper, undrained triaxial monotonic tests CIUC4006, CIUC4051 and undrained triaxial cyclic test CY40114 for Nevada sand (Dr= 40%) conducted for the VELACS project (Arulmoli et al., 1992) are used for calibration. The parameters are:  $I_{p0} = 38^\circ$ ,  $\varphi = 25^\circ$ ,  $M_g = 1.25$ ,  $M_f = 1.18$ ,  $G_o = 2.5 \times 10^4$  kPa,  $K_o = 3.0 \times 10^4$  kPa,  $k_s = 0.01$ ,  $E_{10} = 2.8$ ,  $E_0 = 9.0$ ,  $\Delta = 0.45$ ,  $H_o = 2.0 \times 10^4$  kPa,  $H_{uo} = 4.0 \times 10^4$  kPa,  $r = 3.5$ ,  $r_u = 1.0$ ,  $r_d = 80.0$ . The comparisons between simulated and experimental results for monotonic and cyclic loadings are shown in Figures 2 and 3, respectively.



**FIG. 1. Configuration of Centrifuge Model No. 1 Conducted at RPI**





(b) Deviatoric Stress – Strain Relationships

**FIG. 2. Comparison of Simulated and Experimental Results for Monotonic Triaxial Compression Tests: (a) Stress Path, (b) Stress-Strain Relationships**

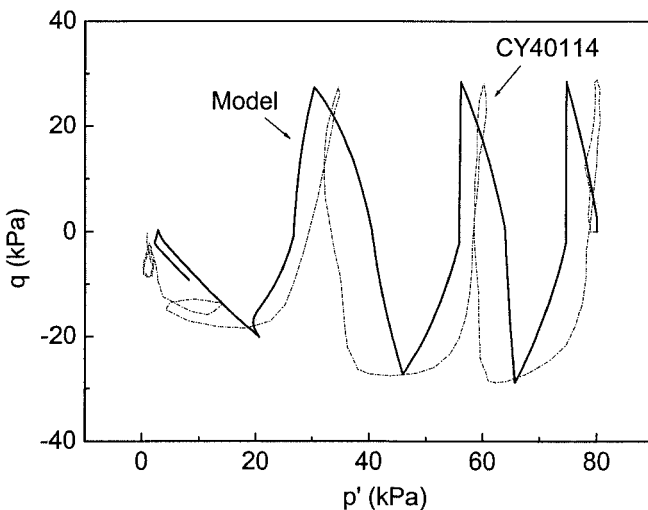


**FIG. 3. Comparison of Simulated and Experimental Results for Cyclic Triaxial Test**

## FINITE ELEMENT ANALYSIS

The modified model was incorporated into a finite element program Diana Swandyne-II (Chan, 1988 and Chan, 1993) by Liu (2002). It is a two-dimensional (plane strain and axisymmetric) program based on a fully coupled Biot dynamic equation with the u-p (skeleton displacement and pore pressure p) formulation (Zienkiewicz et al., 2000). The basic procedures for numerical analysis are given as follows:

Figure 4 shows the mesh composing of quadrilateral elements each having 8 solid and 4 fluid nodes. The experiment was simulated in the model scale and a gravity level of 50g. The laminar box was modeled using tied node features. The displacement degrees of freedom on the side boundary were tied to each other to have identical movement. The side fluid boundary is impermeable. The bottom fluid boundary is also impermeable with the solid nodes fixed to the input motion. The top of the model is traction free for the solid and has zero reference pressure for the fluid.

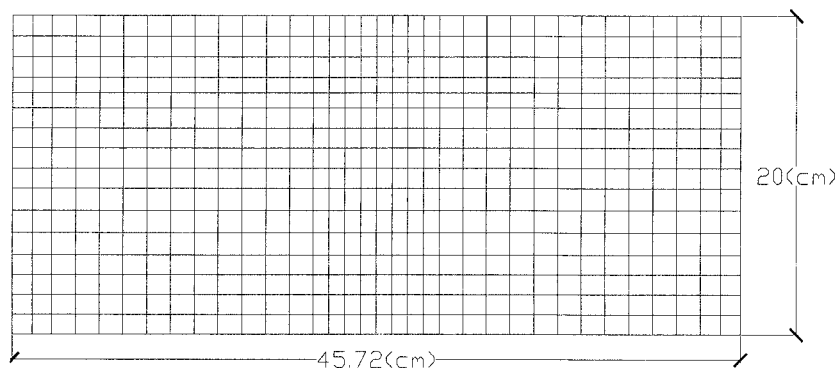


**FIG. 4. Finite Element Mesh**

The analysis procedure included static followed by dynamic and consolidation analyses. First, a static analysis using general power elastic model was performed to determine the initial stress state of the model. Then, a nonlinear dynamic analysis was performed for the sinusoidal shaking. Then, a consolidation analysis followed with an enlarging time steps to simulate the dissipation of excess pore pressure.

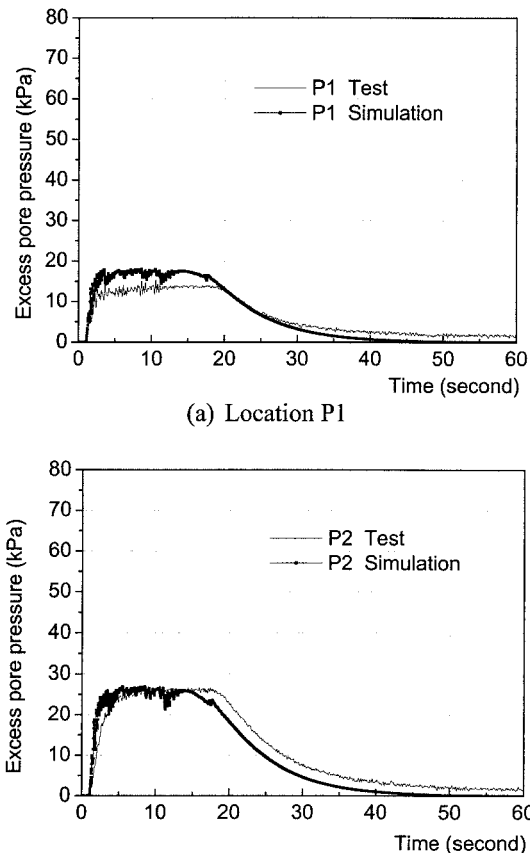
The coefficient of permeability of  $6.6 \times 10^{-5}$  m/s was used in the analyses. The time step for the dynamic and consolidation analyses were 0.0003325 and 0.00064 model seconds, respectively. A total of 1024 and 2000 steps were used for the dynamic and consolidation analyses. Rayleigh damping of 5% was applied at 100Hz. The time stepping parameters were  $E_1 = 0.6$ ,  $E_2 = 0.605$  for the solid phase and  $E_1 = 0.6$  for

the fluid phase. In the simulation, the horizontal input acceleration was obtained from the centrifuge model test, while the vertical acceleration was not considered.

## COMPARISON OF RESULTS

The comparison of excess pore pressures and horizontal accelerations between the analyses and experiments is made in Figures 5 and 6. The locations of transducers are referred to Figure 1. It is observed that the simulated results show good agreement with the experimental results, especially for the excess pore pressure that is very important in assessing liquefaction. The dissipation of excess pore water pressure was also well simulated.

The comparison of acceleration in general seems satisfactory. However, the response in the upper portion of the layer is stronger than the experimental results toward the later part of shaking.



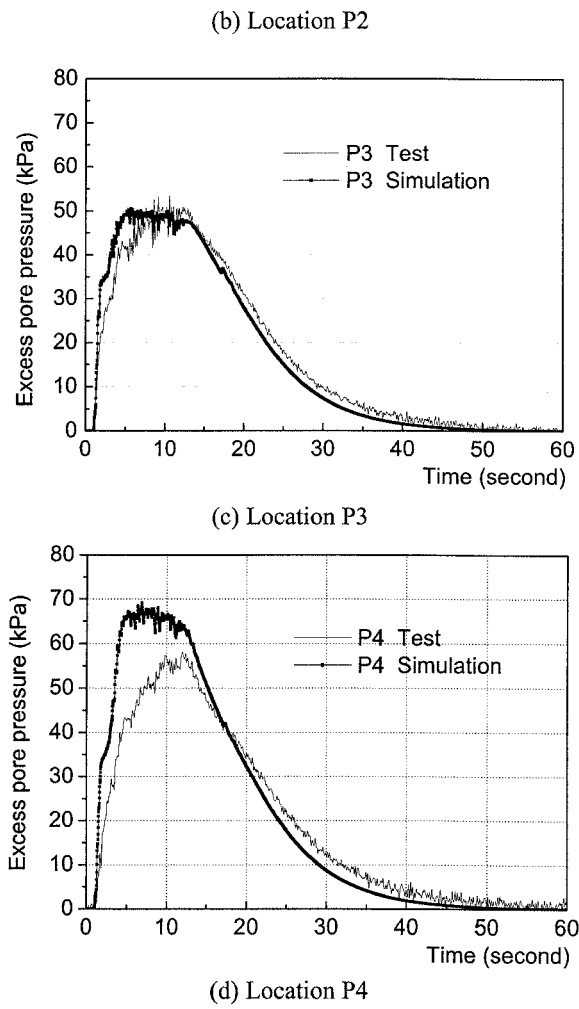


**FIG. 5. Comparison between Simulated and Experimental Results of Excess Pore Water Pressure (a) Location P1, (b) Location P2, (c) Location P3, and (d) Location P4**

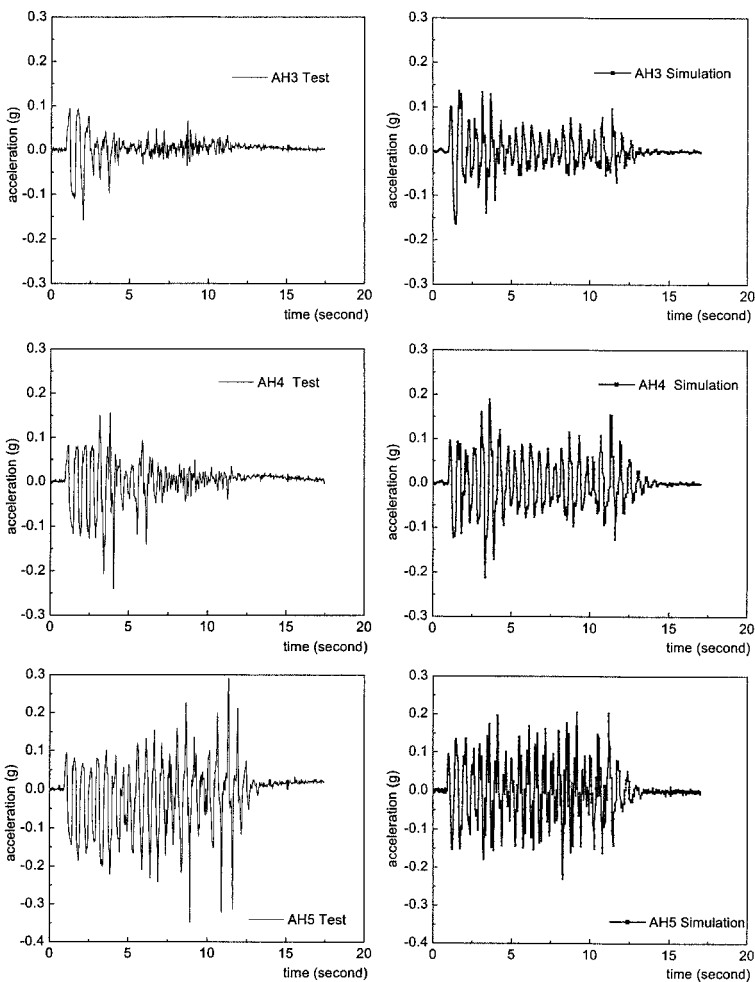


**FIG. 6. Comparison between Simulated and Experimental Results of Horizontal Acceleration: Locations H3, H4 and H5**

## CONCLUSIONS

The generalized plasticity model has been modified to include pressure-level dependency and also hardening under cyclic behavior. The model was calibrated against triaxial test results and then used for conducting liquefaction analysis by comparing the results with the centrifuge model. The analyses gave satisfactory agreement with the experimental results in terms of excess pore pressure and acceleration response.

The model presented in this paper though considers the pressure level dependency, it lacks capability to consider the effects of change in void ratio. Works are in progress by the authors to develop a different version of generalized plasticity model that considers both effects of pressure level dependency and change in void ratio.

## ACKNOWLEDGMENTS

The authors are supported by the National Science Foundation under Grant No. CMS-0092739 granted to the second author, with Dr. Clifford Astill followed by Dr. Juan Pestana, as Program Directors. Huabei Liu contributed to the development of modified model used in the analysis as part of the CMS-0092739.

## REFERENCES

- Arulanandan, K., and Scott, R.F., Eds. (1993). *Verification of Numerical Procedures for the Analysis of Soil Liquefaction Problems*. Balkema, Rotterdam, Netherlands.
- Been, K., and Jefferies, M. G. (1985). "A state parameter for sands." *Geotechnique*, 35(2), 99-112.
- Bouckovalas, G., Marr, W. A., and Christian, J. T. (1986). "Analyzing permanent drift due to cyclic loads." *J. Geotech. Eng.*, 112(6), 579-593.
- Chan, A. H. C (1988). A Unified Finite Element Solution to Static and Dynamic Geomechanics Problems. Ph.D. thesis, University College of Swansea, Wales.
- Chan, A. H. C. (1993). User Manual for DIANA-SWANDYNE II, Department of Civil Engineering, Glasgow University.
- Dobry, R., and Petrakis, E. (1990). "Micromechanics model to predict sand densification by cyclic straining." *J. Eng. Mech.*, 116(2), 288-308.
- Li, X.S. and Dafalias, Y.F. (2000). "Dilatancy of cohesionless soils", *Geotechnique* 50(4), 449-460.
- Ling, H.I. and Liu, H. (2003). "Pressure-level dependency and densification behavior of sand through a generalized plasticity model." *Journal of Engineering Mechanics*, ASCE, 129(8), 851-860.
- Liu, H. (2002). *Finite Element Simulation of The Response of Geosynthethic-Reinforced Soil Walls*, Ph.D. Thesis, Columbia University, New York, NY.
- Liu, H. and Ling, H.I. (2003). "A sand model based on generalized plasticity." in *Constitutive Modeling of Geomaterials: Selected Contributions from Frank L. DiMaggio Symposium*. Ling, H.I., Anandarajah, A., Manzari, M.T., Kaliakin, V.N., and Smyth, A., Editors, CRC Press, 40-46.

- Maeda, K., and Miura, K. (1999). "Confining stress dependency of mechanical properties of sands." *Soils Found.*, 39(1), 53-67.
- Mroz, Z., and Zienkiewicz, O. C. (1984). "Uniform formulation of constitutive equations for clay and sand." *Mechanics of Engineering Materials*, C. S. Desai and R. H. Gallagher, eds., Wiley, New York, 415-450.
- Pastor, M., Zienkiewicz, O. C., and Chan, A. H. C. (1990). "Generalized plasticity and the modeling of soil behavior." *Int. J. Numer. Analyt. Meth. Geomech.*, 14(3), 151-190.
- Pastor, M., Zienkiewicz, O. C., Xu, G. D., and Peraire, J. (1993). "Modeling of sand behavior: Cyclic loading, anisotropy and localization." *Modern Approaches to Plasticity*, D. Kolymbas, ed., Elsevier, New York, 469-492.
- Pradhan, T. B. S. (1989). "The behavior of sand subjected to monotonic and cyclic loadings." Ph.D. Thesis, Kyoto Univ., Japan.
- Silver, M. L., and Seed, H. B. (1971). "Deformation characteristics of sands under cyclic loading." *J. Soil Mech. Found. Div.*, ASCE, 97(8), 1081-1098.
- Tatsuoka, F., Sakamoto, M., Kawamura, T., and Fukushima, S. (1986). "Strength and deformation characteristics of sand in plane strain compression at extremely low pressures." *Soils Found.*, 26(1), 65-84.
- Tatsuoka, F., Siddiquee, M. S. A., Park, C. S., Sakamoto, M., and Abe, F. (1993). "Modelling stress-strain relations of sand." *Soils Found.*, 33(2), 60-81.
- Zienkiewicz, O. C., Leung, K. H., and Pastor, M. (1985). "Simple model for transient soil loading in earthquake analysis. I: Basic model and its application." *Int. J. Numer. Analyt. Meth. Geomech.*, 9(5), 453-476.
- Zienkiewicz, O.C., Chan, A.H.C., Pastor, M., Schrefler, B.A., and Shiomi, T. (1998). *Computational Geomechanics with Special Reference to Earthquake Engineering*, John Wiley & Sons, Ltd., Chichester, England.

# Subject Index

Page number refers to the first page of paper

- Algorithms, 310  
Anisotropy, 35, 415
- Calibration, 45, 184, 204, 310, 358, 400, 415, 483  
Clays, 35, 99, 333, 400, 415, 425, 440, 459  
Cohesive soils, 237, 400  
Computation, 400  
Consolidation, soils, 333  
Constitutive relations, 133
- Data analysis, 358
- Elasticity, 69  
Elastoplasticity, 35, 184, 237, 290, 358, 380, 425
- Finite difference method, 1  
Finite element method, 69  
Fractures, 159  
Fuzzy sets, 45
- Geomaterials, 133, 333, 358  
Granular materials, 257  
Gulf of Mexico, 440
- Hypoplasticity, 257
- Joints, 159
- Kinematics, 45
- Liquefaction, 159, 483  
Material properties, 290  
Mechanical properties, 69
- Optimization, 45
- Parameters, 69, 133, 237, 290, 310, 425, 440  
Plasticity, 45, 415, 483  
Predictions, 440
- Rocks, 184, 380
- Sand, 204, 333, 425, 483  
Simulation, 459  
Soft soils, 35, 380, 415, 440  
Softening, 35  
Soil deformation, 358  
Soil properties, 69, 99  
Soil structure, 99  
Soils, 159, 184, 257, 290, 310  
Soil-structure interaction, 1, 45  
Stress strain relations, 1, 69
- Time dependence, 237
- Viscoelasticity, 133, 237, 400  
Void ratio, 204

## Author Index

**Page number refers to the first page of paper**

- Adachi, Toshihisa, 400  
Andresen, Lars, 35
- Bao, Yu, 45  
Brinkgreve, Ronald B. J., 69
- Carter, John P., 99
- Dafalias, Yannis F., 415  
Darve, Félix A., 133  
Desai, Chandrakant S., 159  
Detournay, Christine, 184
- Gajo, Alessandro, 459  
Ge, Yu-Ning, 45
- Hart, Roger D., 184  
Herle, I., 257  
Hinokio, Masaya, 358
- Jefferies, Michael G., 204  
Jostad, Hans Petter, 35
- Kaliakin, Victor N., 237  
Kimoto, Sayuri, 400  
Kolymbas, D., 257
- Lade, Poul V., 1, 290  
Lambert, Cédric G., 133
- Ling, Hoe I., 483  
Liu, Martin D., 99
- Macari, Emir José, 310  
Manzari, Majid T., 415  
Matsuoka, Hajime, 333
- Nakai, Teruo, 358  
Nikolinakou, Maria, 425  
Nova, Roberto, 380
- Oka, Fusao, 400
- Papadimitriou, Achilleas G., 415  
Pestana, Juan M., 425
- Samarajiva, Prasad, 310  
Shuttle, Dawn A., 204  
Sture, Stein, 45  
Sun, De'An, 333  
Sutabutr, Twarath, 440
- Wathugala, Wije, 310  
Whittle, Andrew J., 425, 440  
Wood, David Muir, 459
- Yang, Songtao, 483  
Yao, Yang-Ping, 333